PORCINE ANTI-VIRAL IMMUNITY

EDITED BY: Anastasia N. Vlasova and John E. Butler
PUBLISHED IN: Frontiers in Immunology

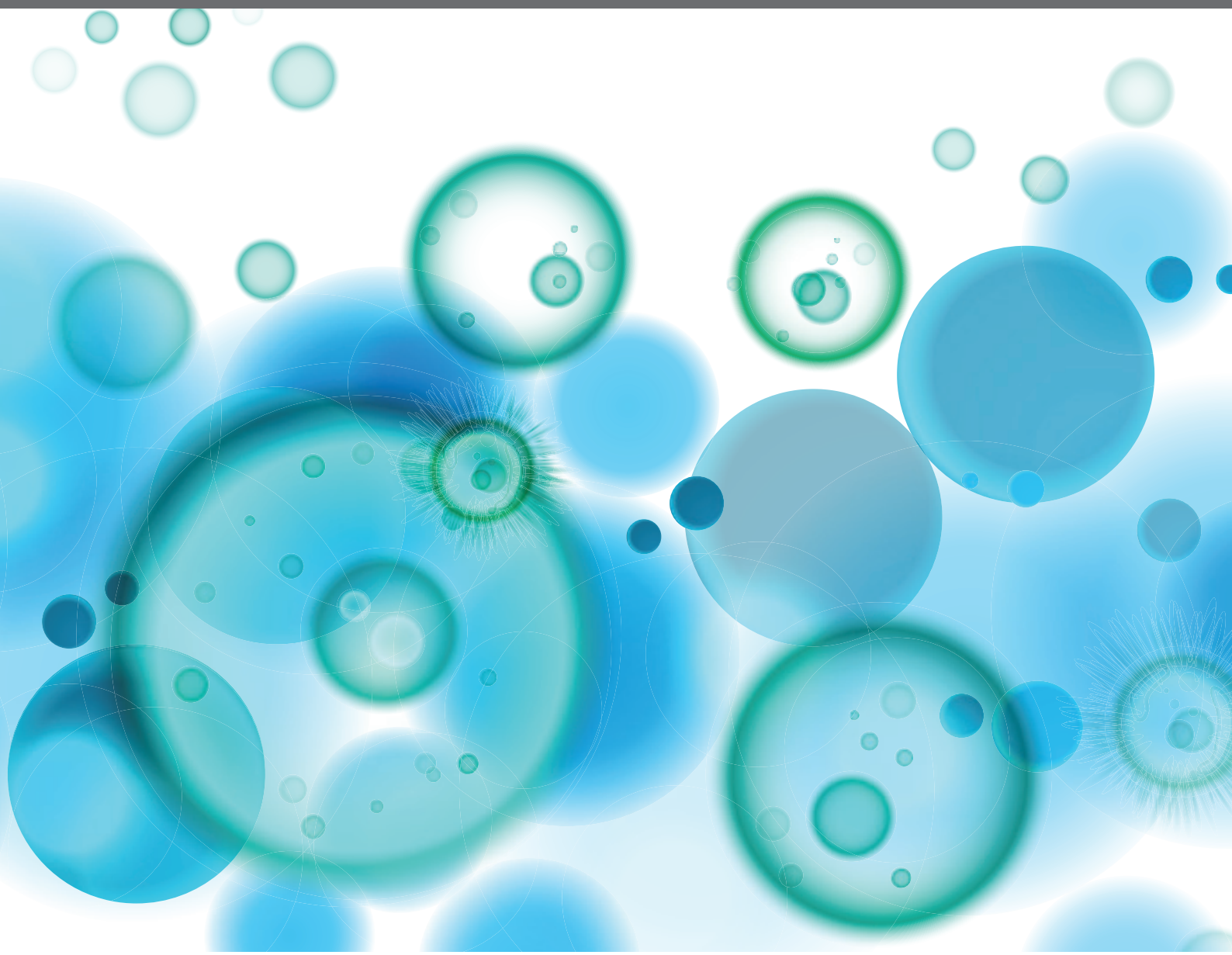

frontiers Research Topics

frontiers

ISSN 1664-8714
ISBN 978-2-88963-658-7
DOI 10.3389/978-2-88963-658-7

About Frontiers

Frontiers is more than just an open-access publisher of scholarly articles: it is a pioneering approach to the world of academia, radically improving the way scholarly research is managed. The grand vision of Frontiers is a world where all people have an equal opportunity to seek, share and generate knowledge. Frontiers provides immediate and permanent online open access to all its publications, but this alone is not enough to realize our grand goals.

Frontiers Journal Series

The Frontiers Journal Series is a multi-tier and interdisciplinary set of open-access, online journals, promising a paradigm shift from the current review, selection and dissemination processes in academic publishing. All Frontiers journals are driven by researchers for researchers; therefore, they constitute a service to the scholarly community. At the same time, the Frontiers Journal Series operates on a revolutionary invention, the tiered publishing system, initially addressing specific communities of scholars, and gradually climbing up to broader public understanding, thus serving the interests of the lay society, too.

Dedication to Quality

Each Frontiers article is a landmark of the highest quality, thanks to genuinely collaborative interactions between authors and review editors, who include some of the world's best academicians. Research must be certified by peers before entering a stream of knowledge that may eventually reach the public - and shape society; therefore, Frontiers only applies the most rigorous and unbiased reviews.
Frontiers revolutionizes research publishing by freely delivering the most outstanding research, evaluated with no bias from both the academic and social point of view. By applying the most advanced information technologies, Frontiers is catapulting scholarly publishing into a new generation.

What are Frontiers Research Topics?

Frontiers Research Topics are very popular trademarks of the Frontiers Journals Series: they are collections of at least ten articles, all centered on a particular subject. With their unique mix of varied contributions from Original Research to Review Articles, Frontiers Research Topics unify the most influential researchers, the latest key findings and historical advances in a hot research area! Find out more on how to host your own Frontiers Research Topic or contribute to one as an author by contacting the Frontiers Editorial Office: researchtopics@frontiersin.org

PORCINE ANTI-VIRAL IMMUNITY

Topic Editors:
Anastasia N. Vlasova, The Ohio State University, United States
John E. Butler, University of Iowa, United States

Citation: Vlasova, A. N., Butler, J. E., eds. (2020). Porcine Anti-Viral Immunity. Lausanne: Frontiers Media SA. doi: 10.3389/978-2-88963-658-7

Table of Contents

frontiers in Immunology

EDITORIAL
published: 06 March 2020
doi: 10.3389/fimmu.2020.00399

Editorial: Porcine Anti-Viral Immunity

Anastasia N. Vlasova[1]* *and John E. Butler*[2]*

[1] Food Animal Health Research Program, CFAES, Ohio Agricultural Research and Development Center, Department of Veterinary Preventive Medicine, The Ohio State University, Wooster, OH, United States, [2] Department of Microbiology and Immunology, Carver College of Medicine, University of Iowa, Iowa, IA, United States

Keywords: swine, viruses, immune response, vaccines, immune evasion, emerging

Editorial on the Research Topic

Porcine Anti-Viral Immunity

INTRODUCTION

The swine industry is an important part of agriculture in many countries, generating over $11 billion annually in the US alone. Viral diseases in pigs pose a serious risk for swine health and significantly impact the economy of the global swine industry. Pigs also serve as zoonotic reservoirs for viruses transmittable to humans and other species, including influenza A virus, Nipah virus, and hepatitis E virus (1). These problems are made worse by globalization and industrial livestock rearing (2, 3). Unlike bacterial pathogens, antibiotics do not protect against viral infections and cannot be used to control viral outbreaks or epidemics. Since viruses can alter their genome $>10^6$ times faster than their mammalian hosts (4), the latter would have succumbed to microbial infection were it not for their adaptive immune system that uses somatic gene rearrangement and mutation to counter the rapid diversification of microbes. Immediately following viral infection, neonatal survival depends on innate immunity and passive protection by lactogenic immune factors such as pathogen-specific antibodies, until an adaptive immune response can develop. Thus, intervention against these moving targets, depends on availability of effective maternal and neonatal vaccines and strict biosecurity measures.

Wide-spread porcine reproductive and respiratory syndrome virus (PRRSV) and swine influenza virus (SIV) represent major health challenges in the large US swine production systems and possibly worldwide. In the US alone, economic annual losses due to PRRSV are estimated to be 664 million U.S. dollar (USD) (5). While the exact costs associated with SIV and other endemic viruses, including rotavirus, are hard to evaluate, they are economically important due to their ubiquitous nature, which can reduce growth and increased morbidity (6). Emerging and re-emerging coronaviruses in pigs are quite often associated with diarrheal disease and high morbidity and mortality (7). The emergence of Seneca Valley virus (SVV) and increased incidence of SVV-associated vesicular disease alarmed the swine industry in several countries, including the US, Brazil, China, Thailand, and Colombia (8). Finally, a deadly swine disease, caused by African Swine Fever virus (ASFV), that has been plaguing Africa for decades, has now spread to south eastern Europe and Asia, and has severely impacted the world's largest swine industries in China (9).

In this special volume of Frontiers in Immunology, Comparative Immunology section, Lager and Buckley provide an overview of the importance of swine in the world food supply and a review of the major viral infection that threaten this species (Lager and Buckley). In introducing the topic of anti-viral immunity, we emphasize the genetic diversity of viruses, the virus life cycle and the pathology that viral infection can cause. A total of 12 articles are contained in this volume to which 86 researches have contributed.

OPEN ACCESS

Edited and reviewed by:
Falko Steinbach,
University of Surrey, United Kingdom

***Correspondence:**
Anastasia N. Vlasova
vlasova.1@osu.edu
John E. Butler
john-butler@uiowa.edu

Specialty section:
This article was submitted to Comparative Immunology, a section of the journal Frontiers in Immunology

Received: *10 January 2020*
Accepted: *20 February 2020*
Published: *06 March 2020*

Citation:
Vlasova AN and Butler JE (2020) Editorial: Porcine Anti-Viral Immunity. Front. Immunol. 11:399. doi: 10.3389/fimmu.2020.00399

NEWBORNS ARE MORE VULNERABLE TO VIRAL DISEASES

Despite the advantage of internal offspring development and the provision for passive immune protection, fetuses and neonates of higher vertebrates still remain vulnerable to environmental pathogens. Piglets *in utero* are protected from eukaryotic parasites and bacteria, but are vulnerable to viruses (including parvovirus, PRRSV, and porcine circovirus 2) since they are able to cross the placental barrier (10–12). These cause pathological injury and often fetal abortion. In a number of mammals, viruses infect the thymus and can also cause hypergammaglobulinemia. Butler et al. discuss the implication of thymic atrophy and apoptosis of thymocytes and hypergammaglobulinemia with regard to the persistence of PRRSV. However, apoptosis is also a host mechanisms used to eliminating virus-infected cells (13), but can also promote spread of the virus (14). Fernandes et al. demonstrated that SVV developed a 3C protease-dependent mechanism for late apoptosis that facilitates virus release from infected cells. Thus, the role and importance of virus-induced apoptosis awaits further research.

Since the adaptive immune system of fetal piglets is underdeveloped, the innate immune system is very important. Schäfer et al., emphasize its importance with the specific focus on porcine invariant natural killer T cells (iNKT) and their role in the pathogenesis of ASF and SI. They discuss iNKT age-dependence, levels and distribution in relationship to various porcine viral infections. One of the first host responses to viral infection is the production of interferons, which are needed to drive other elements of innate immunity and adaptive immunity. Likai et al. show how a porcine deltacoronavirus escapes from the immune system by suppressing IFN-α production, while Shi et al. describe a novel immune evasive mechanism that depends on PRRSV non-structural protein 1a which antagonizes TBK1-IRF3-IFN signaling. While the initial antibody response depends on broadly specific natural IgM antibodies, effective anti-viral immunity depends on an adaptive immune response that delivers IgG and IgA antibodies. Since adaptive immune responses depend on stimulation through the innate immune system, viruses that impair or interfere with the innate immune response, also impair adaptive immunity. Nedumpun et al. discuss how PRRSV-induced IL-1Ra downregulates innate immune responses, T lymphocyte differentiation and proliferation.

Piglets, unlike humans, but like the offspring of other artiodactyls and perissodactyls (horses), are especially dependent on lactogenic immunity since there is no transplacental transfer of passive antibodies in this group of mammals. Thus, providing ways to deliver anti-viral antibodies via colostrum/ milk is important. This topic is the focus of studies by Langel et al..

ANTI-VIRAL IMMUNITY AND VACCINE DEVELOPMENT

Antibodies can intercept and neutralize a virus before it infects additional cells and can prevent further infection by blocking the viral receptor; these are called virus neutralizing (VN) antibodies. Naturally, a critical step in viral vaccine design is the identification of viral epitopes targeted by effective VN antibodies. This become increasingly important in the case of PRRSV in which effective VN antibodies are slow to appear and current vaccines are of questionable efficacy. This is also an ongoing challenge in the case of ASFV which is rapidly spreading and for which no vaccine exists. Goldeck et al. describe a novel B cell cloning procedure to identify these epitopes on several strains of PRRSV. While VN antibodies can block or delay infection, the ultimate elimination of a virus is to kill the cells in which the virus replicates which is the job of cytotoxic T cells. Portions of the virus are displayed on infected cells. These are called a T cell epitope, i.e., a molecular structure that binds to the T cell receptor (TCR). In this volume, Pan et al. describe their efforts to identify such epitopes for their potential use in stimulating expansion of the cytotoxic T cells that recognize them.

Viral vaccines take various forms, the simplest being the use of killed virus. A more tedious procedure is to use only parts of the virus as the vaccine (subunit vaccines) that target the immune response to those viral epitopes that elicit VN antibodies. Killed viruses and subunit vaccines typically generate immediate responses that wane faster, making it imperative for long-lived mammals like humans, to receive booster vaccinations. A second approach to vaccine development is use of live attenuated virus that has been genetically modified or cell culture adapted and cannot produce a disease in the host but can still replicate. These are often more likely to stimulate virus-specific cytotoxic T cells and to induce longer term immunity. Sharma et al. developed a recombinant SVV strain using reverse genetics and tested its immunogenicity and protective efficacy in pigs. Toman et al. provide comparative data on four vaccines for PRRSV, two killed and two modified live.

We believe that veterinary immunovirology should place more emphasis on how each viral pathogen effects and/or avoids the host immune system and on the identification of viral epitopes that are effective targets of VN antibodies and T cell epitopes that can promote the action of cytotoxic T cells.

AUTHOR CONTRIBUTIONS

JB wrote the first draft and then both co-authors contributed equally to the final draft.

REFERENCES

1. Mandl JN, Ahmed R, Barreiro LB, Daszak P, Epstein JH, Virgin HW, et al. Reservoir host immune responses to emerging zoonotic viruses. *Cell.* (2015) 160:20–35. doi: 10.1016/j.cell.2014.12.003
2. Perry BD, Grace D, Sones K. Current drivers and future directions of global livestock disease dynamics. *Proc Natl Acad Sci USA*. (2013) 110:20871–7. doi: 10.1073/pnas.1012953108
3. McGlone JJ. The future of pork production in the world: towards sustainable, welfare-positive systems. *Animals.* (2013) 3:401–15. doi: 10.3390/ani3020401

4. Moelling K. What contemporary viruses tell us about evolution: a personal view. *Arch Virol.* (2013) 158:1833–48. doi: 10.1007/s00705-013-1679-6
5. Holtkamp DJ, Kliebenstein JB, Neumann EJ, Zimmerman JJ, Rotto HF, Yoder TK, et al. Assessment of the economic impact of porcine reproductive and respiratory syndrome virus on United States pork producers. *J Swine Health Prod.* (2013) 21:72–84. doi: 10.31274/ans_air-180814-28
6. Cornelison AS, Karriker LA, Williams NH, Haberl BJ, Stalder KJ, Schulz LL, et al. Impact of health challenges on pig growth performance, carcass characteristics, and net returns under commercial conditions. *Transl. Anim. Sci.* (2018) 2:50–61. doi: 10.1093/tas/txx005
7. Wang Q, Vlasova AN, Kenney SP, Saif LJ. Emerging and re-emerging coronaviruses in pigs. *Curr Opin Virol.* (2019) 34:39–49. doi: 10.1016/j.coviro.2018.12.001
8. Wang Z, Zhang X, Yan R, Yang P, Wu Y, Yang D, et al. Emergence of a novel recombinant Seneca Valley virus in Central China, (2018). *Emerg Microbes Infect.* (2018) 7:180. doi: 10.1038/s41426-018-0183-1
9. Lu G, Pan J, Zhang G. African swine fever virus in Asia: its rapid spread and potential threat to unaffected countries. *J Infect.* (2019) 80:350–71. doi: 10.1016/j.jinf.2019.11.011
10. Orzalli MH, Kagan JC. Apoptosis and necroptosis as host defense strategies to prevent viral infection. *Trends Cell Biol.* (2017) 27:800–9. doi: 10.1016/j.tcb.2017.05.007
11. Thomson BJ. Viruses and apoptosis. *Int J Exp Pathol.* (2001) 82:65–76. doi: 10.1111/j.1365-2613.2001.iep195.x
12. Gerber PF, Garrocho FM, Lana AM, Lobato ZI. Fetal infections and antibody profiles in pigs naturally infected with porcine circovirus type 2 (PCV2). *Can J Vet Res.* (2012) 76:38–44.
13. Brumm MC, Baysinger AK, Wills RW, Thaler RC. Effect of wean-to-finish management on pig performance. *J Anim Sci.* (2002) 80:309–15. doi: 10.2527/2002.802309x
14. Mengeling WL, Paul PS, Brown TT. Transplacental infection and embryonic death following maternal exposure to porcine parvovirus near the time of conception. *Arch Virol.* (1980) 65:55–62. doi: 10.1007/BF01340540

Conflict of Interest: The authors declare that the research was conducted in the absence of any commercial or financial relationships that could be construed as a potential conflict of interest.

frontiers in Immunology

ORIGINAL RESEARCH
published: 18 December 2018
doi: 10.3389/fimmu.2018.03023

Dual Regulation of Host TRAIP Post-translation and Nuclear/Plasma Distribution by Porcine Reproductive and Respiratory Syndrome Virus Non-structural Protein 1α Promotes Viral Proliferation

Peidian Shi[1†], Yanxin Su[1†], Ruiqiao Li[1], Lei Zhang[1], Chen Chen[1], Lilin Zhang[1], Kay Faaberg[2] and Jinhai Huang[1*]*

[1] School of Life Sciences, Tianjin University, Tianjin, China, [2] Agricultural Research Service, USDA, National Animal Disease Center, Ames, IA, United States

In this study, we show that porcine reproductive and respiratory syndrome virus (PRRSV) non-structural protein 1α (nsp1α) facilitates PRRSV escape from innate immune by modulating nuclear to cytoplasmic translocation and distribution ratio of TRAIP to promote virus proliferation. Mechanistically, TRAIP interacts with PRRSV nsp1α via its K205 site, while NSP1α decreases the SUMOylation and K48 ubiquitination independent of the TRAIP interaction K205 site. Modulation of the dual modification of TRAIP by PRRSV nsp1α results in over-enrichment of TRAIP in the cytoplasm. Enrichment of nsp1α-induced cytoplasmic TRAIP in turn leads to excessive K48 ubiquitination and degradation of serine/threonine-protein kinase (TBK1), thereby antagonizing TBK1-IRF3-IFN signaling. This study proposes a novel mechanism by which PRRSV utilizes host proteins to regulate innate immunity. Findings from this study provides novel perspective to advance our understanding in the pathogenesis of PRRSV.

Keywords: PRRSV, TRAIP, nsp1α, SUMOylation, IFN, TBK1

OPEN ACCESS

Edited by:
Anastasia N. Vlasova,
The Ohio State University,
United States

Reviewed by:
Jianzhong Zhu,
Yangzhou University, China
Scott P. Kenney,
The Ohio State University,
United States

***Correspondence:**
Kay Faaberg
kay.faaberg@ars.usda.gov
Jinhai Huang
jinhaih@tju.edu.cn

†These authors have contributed equally to this work

Specialty section:
This article was submitted to Viral Immunology, a section of the journal Frontiers in Immunology

Received: *21 September 2018*
Accepted: *06 December 2018*
Published: *18 December 2018*

Citation:
Shi P, Su Y, Li R, Zhang L, Chen C, Zhang L, Faaberg K and Huang J (2018) Dual Regulation of Host TRAIP Post-translation and Nuclear/Plasma Distribution by Porcine Reproductive and Respiratory Syndrome Virus Non-structural Protein 1α Promotes Viral Proliferation. Front. Immunol. 9:3023. doi: 10.3389/fimmu.2018.03023

INTRODUCTION

The host innate immune response, predominantly IFN-α and IFN-β, is the first line of defense against pathogens (1, 2). As multi-functional antiviral cytokines, type I interferons can be induced by virus infection (3). The viral RNA is recognized by cytosolic sensors, retinoic acid-inducible gene I (RIG-I) and melanoma differentiation-associated gene 5 protein (MDA5) (4). RIG-I and MDA-5 bind to the mitochondrial adapter protein MAVS/IPS-1, resulting in the activation of IκB kinase-ε (IKKε) or downstream signaling of TRAF family member-associated NF-kappa-B activator (TANK)-binding kinase 1 (TBK1), then phosphorylation of IRF-3, its entry nucleus and final induce IFN-β transcription (5, 6). However, porcine reproductive and respiratory syndrome virus (PRRSV) has developed a variety of strategies to avoid or suppress the host immune response, in particular the interferon (IFN)-mediated innate immune response.

PRRSV, the causative agent of PRRS, is a positive-strand RNA virus that belongs to the family *Arteriviridae* within the order *Nidovirales* (7). PRRSV infection often causes acute reproductive

failure in sows and dyspnea in piglets and substantial economic losses each year (8). Accumulating evidence has revealed that PRRSV results in persistent infection due partly to inhibition of the host innate immune response (9–11). The genome of PRRSV is approximately 15 kb and encodes 9 overlapping open reading frames (ORFs) encoding at least 8 structural proteins and 16 non-structural proteins (12, 13). PRRSV non-structural protein 1 (nsp1) contains two papain-like cysteine proteases, papain-like cysteine protease α (PCPα) and papain-like cysteine protease β (PCPβ), and self-cleaves into nsp1α and nsp1β subunits (14, 15). The nsp1α subunit is composed of three distinct functional motifs; a papain-like cysteine protease α motif (PCPα), a N-terminal zinc finger motif (ZF1), and a newly reported C-terminal zinc finger motif (ZF2) (16). PRRSV nsp1α has been reported to inhibit NF-κB activation by targeting linear ubiquitin chain complex (17) and block the transcription of type I interferon by the degradation of CREB-binding protein (CBP) (18). It has also been shown to contribute to PRRSV proliferation, while siRNAs which specifically target nsp1α significantly inhibit the replication of PRRSV in MARC-145 cells (19).

Protein post-translational modifications (PTMs) such as ubiquitination and SUMOylation play a key role in signal transduction pathways in cells (20, 21). The ubiquitination system utilizes the combination of ubiquitin molecules and their target proteins to form polyubiquitin chains (22–24). E3 ubiquitin ligase is a protein acting in the ubiquitination of a particular target protein (25). More recently it has been shown that the ubiquitin proteasome system can regulate the biological functions of tumor cells such as proliferation and metastasis by mediating the degradation of many tumor-related proteins (26, 27).

SUMO is a newly discovered ubiquitin-like molecule and can covalently conjugate proteins throughout the cell (28). At least three highly conserved SUMO proteins (SUMO1/2/3) exist in higher eukaryotic cells, and there is a high degree of homology between SUMO2 and SUMO3 (29). SUMOylation is a dynamic and reversible process catalyzed by SUMO-specific enzyme E1, E2, and E3 (30). The SUMO molecule is covalently linked to the substrate protein, regulating the target protein localization and the interaction of SUMO modified-proteins with their binding partners (31). Consequently, these changes in turn affect signaling mechanisms, which have been shown to regulate many cellular functions such as cell growth, proliferation, apoptosis, DNA repair, and cell survival (32–34).

TRAF-interacting protein (TRAIP), also known as RNF206 (RING-finger protein 206), was initially identified through its ability to bind TRAF1 and TRAF2 in yeast two-hybrid screening (35). TRAIP is indispensable, as mouse embryos fail to develop when TRAIP is knocked out in both mice and *Drosophila* (36, 37).TRAIP has been identified as an E3 ubiquitin ligase and a substrate of SUMOylation, which plays an important biological function. TRAIP is indispensable in the immune response, which negatively regulates TRAF2, tumor necrosis factor receptor 2 (TNFR2), CD30, and TNF mediated NF-κB activation (35, 38). As an E3 ubiquitin ligase, TRAIP directly binds to TBK1, which promotes TBK1 degradation via K48-linked ubiquitination in 293T cells (39).

In our research, the TRAIP gene was cloned from porcine peripheral blood mononuclear cells (PBMCs). The relationship between TRAIP and PRRSV replication was investigated. We verified that TRAIP contributed to the proliferation of PRRSV. The PCPα domain of nsp1α interacts with TRAIP. Interestingly, SUMOylation and self-ubiquitination of TRAIP was attenuated by PRRSV nsp1α. Changes in the dual modification of TRAIP affect its own proportional distribution in the nucleus and the cytoplasm. Functionally, the retention of TRAIP in the cytoplasm facilitates the ubiquitination of TBK1, resulting in the degradation of TBK1, thereby inhibiting the production of type I interferon. Therefore, our study revealed a new model of interaction between viral proteins and cellular hosts, one which aims to suppress type I interferon production, in order to promote PRRSV proliferation. As a crucial mechanism of PRRSV, achieving persistent infection and immunosuppression through nsp1α regulation of nuclear/plasma distribution and modification of TRAIP, our results provide a novel target pathway to develop antivirals against PRRSV.

MATERIALS AND METHODS

Ethics Statement

The protocol was reviewed and approved by the Tianjin University Institutional Animal Care and Use Committee (TJIACUC) (Protocol number: SYXK-Jin 2014-0004). All animal experiments were performed using BALB/c mice and maintained in individually ventilated cages at the Tianjin Laboratory Animals Center. This study was carried out in strict accordance with the recommendations in the Guide for the Care and Use of Laboratory Animals of the Tianjin government authority for the use of animals in experiments.

Cells, Virus, and Antibody

Porcine peripheral blood mononuclear cells (PBMCs) were isolated from pigs of the Tianjin Ninghe farm according to a previously described protocol (40). PRRSV-permissive PAM cell lines CRL2843-CD163 (3D4/21) and monoclonal antibodies against PRRSV nsp2 were kindly contributed by China Agricultural University. 3D4/21 cells were cultured in RPMI-1640 medium (Gibco, USA) supplemented with 10% (V/V) fetal bovine serum (FBS, Biological Industries) and antibiotic-antimycotic solution. Human embryonic kidney (HEK) 293T cells and HeLa cells were maintained in Dulbecco's modified Eagle's medium (DMEM, Gibco) with 10% FBS supplemented with an antibiotic-antimycotic mixture of 100 mg/ml streptomycin, 100 IU/ml penicillin and 50 U/ml amphotericin B. The cells were maintained in a humidified 5% CO_2 incubator at 37°C.The PRRSV-JXwn06 strain was used in our study and the titer was determined to be 104 PFU/ml as previously described (41).

Polyclonal antibody against TRAIP was prepared by immunizing BALB/c mice with recombinant His-TRAIP couple with mineral oil adjuvant as previously described (42). Monoclonal antibodies against PRRSV nsp1α and N protein were the gift of Prof. Shaobo Xiao of Huazhong Agricultural University and Jun Han of China Agricultural University,

respectively. Labeled antibodies used in the experiments were purchased from Cell Signaling Technology (CST, Danvers, MA, USA) and Applied Biological Materials Inc (ABM, Vancouver, Canada). An internal reference antibody and secondary antibodies were purchased from Invitrogen (Thermo Fisher Scientific, Waltham, MA, USA). Antibodies to β-actin and Histone H3 were purchased from TransGen (Beijing, China) and Santa Cruz Biotechnology (Santa Cruz, CA), respectively.

Cloning of the Complete Porcine TRAIP CDS

Total RNAs were extracted from PBMC cells using TRIzol reagent (TaKaRa, China). First-strand cDNA synthesis was carried out using reverse transcriptase (TaKaRa). TRAIP was synthesized using the specific primers based on the predicted TRAIP sequence (GenBank Accession Nos. XM_021068793.1) as shown in **Table 1**, and the amplified fragments were cloned into pGEM®-T Easy Vector (Transgen, Beijing).

Plasmid Construction

The pFLAG-CMV2-TRAIP, pMyc-CMV2-TRAIP, pHA-CMV2-TRAIP, and pEGFP-TRAIP eukaryotic expression vector was constructed, respectively. The specific primers pairs (**Table 1**), harboring common sequence with the vector, were used to amplify the TRAIP gene and ligated with pFlag-CMV2, pMyc-CMV2, pHA-CMV2, and pEGFP vector, respectively by using a one-step clong kit (Vazyme, Nanjing, China). The prokaryotic expression plasmid pet-28a-TRAIP was constructed using primers pet-28a-TRAIP-F and pet-28a-TRAIP-R (**Table 1**), to express the recombinant protein His-TRAIP.

Transcriptome Sequencing and Analysis

3D4/21 cells were grown on 6-well plates until the cell density was about 70∼80%, and then were inoculated 0.5 MOI PRRSV for 24 h. Virus-infected cells were washed twice with cold PBS and added 1 ml Trizol. The treated cells were sent to the Guangzhou GENE DENOVO Company for transcriptional sequencing. The obtained transcriptome data and a heatmap of differentially expressed genes was analyzed using an online website (https://software.broadinstitute.org/morpheus/).

Quantitative Reverse Transcription PCR (RT-qPCR)

First-strand cDNA was synthesized from purified RNAs of 3D4/21 cells or HEK293T cells using a First-Strand Synthesis System (Transgen, Beijing, China) according to the manufacturer's instructions. The relative gene expression was analyzed by qRT-PCR that was performed on an ABI 7500 Real-time PCR system (Applied Biosystems, Foster City, CA, USA). The comparative cycle threshold (CT) method was used to calculate the relative gene expression levels according to manufacturer's protocol (Applied Biosystem). All data presented was relatively quantitative, based on the mRNA level of the endogenous gene β-actin and analyzed using GraphPad Prism 6.0 software. All of the primers pairs used for quantitative real-time PCR are listed in **Table 2**.

Confocal Immunofluorescence

The procedure for confocal microscopy has been described previously (41). HeLa cells or 3D4/21 cells were seeded on 12-well plates until the cell density was about 30∼40%. Depending on the specific experiment, the cells were transfected with plasmid expressing TRAIP and/or nsp1α with different labels or empty vector (pFlag-CMV2, pMyc-CMV2, pHA-CMV2, or pEGFP vector) (0.5 μg). In order to detect endogenous immunofluorescence, 3D4/21 cells were infected with 0.5 MOI of PRRSV and incubated at 37°C. At 18 h post-transfection or infection, the cells were fixed with 4% paraformaldehyde for 15 min and then permeabilized with PBS containing 0.3% Triton X-100 for 10 min at room temperature. Then cells were blocked for 30 min with 1% bovine serum albumin (BSA) and incubated with primary antibodies (anti-Myc, anti-HA, anti-Flag) or anti-PRRSV nsp1α antibody (diluted at 1:200) at room temperature (RT) in a humid chamber followed by 10 min washing in PBS. Secondary antibodies (FITC-conjugated anti-mouse IgG or PE-conjugated anti-rabbit IgG) (diluted at 1: 200) were used and nuclear DNA was stained with 4′,6-diamidino-2-phenylindole (DAPI). Finally, the localization of TRAIP and nsp1α or TBK1 was observed with an Olympus confocal microscope. Images were taken at ×100 magnification.

Luciferase Assay

293T cells were seeded into 24-well plates and transfected with the TRAIP and/or nsp1α expression vectors, along with a luciferase reporter (IFNβ-Luc or ISRE-Luc) and the internal control LacZ. At 12 h post-transfection, the cells were infected with Sendai virus (SeV) at a MOI of 0.5. The lysed samples were prepared, and the luciferase activity was measured using the multimode microplate reader (Promega) according to the manufacturer's recommendations.

Western Blot Analyses

Transfected or virus-infected cells were washed twice with cold PBS and lyzed in RIPA buffer (Solarbio, Beijing, China) containing the proteinase inhibitors 20 nM phenylmethanesulfonyl fluoride [PMSF] or 2.5 mM desumoylation protease inhibitor N-Ethylmaleimide [NEM] (Sigma, USA).

Cell lysates were boiled in buffer for 10 min and separated with 12% SDS-PAGE. The separated proteins were transferred to the methanol-activated PVDF membrane (Millipore). Membranes were blocked with 5% non-fat dry milk in TBST (0.05% Tween-20) for 1 h and incubated with an antibody against PRRSV nsp1α (1:2,000), PRRSV N (1:5,000), TRAIP (1:500), β-actin (1:5,000) or labeled antibodies (1:5,000) for overnight at 4°C, followed by washing and incubation with HRP-conjugated antibody for 1 h at room temperature. Immunodetection was completed using Pierce ECL Western Bloting Substrate (Thermo Scientific).

Immunoprecipitation

For co-immunoprecipitation, cells were cultivated in 60 mm plates and transfected with Flag-TRAIP, Myc-nsp1α, or related expression plasmid. At 24 h post-transfection, the cells were lysed in 500 μL RIPA lysis buffer supplemented with protease inhibitor

TABLE 1 | Primers used for PCR amplification.

Primer name	Genbank number	Sequence of primer(5′-3′)
T-TRAIP-F	XM_021068793.1	GAGACCAGTCATGCCTATTCG
T-TRAIP-R		TGTTTTCACTAGGACAGGAAAC
pCMV-TRAIP-F	XM_021068793.1	ATTCGAATTTAAATCGGATCCATGCCTATTCGTGCTCTG
pCMV-TRAIP-R		ATCCTTCGCGGCCGCGGATCCCTAGGACAGGAAACTGT
pet-28a-TRAIP-F	XM_021068793.1	ACAGCAAATGGGTCGCGGATCCATGTATCGTGCAGCGGAT
pet-28a-TRAIP-R		GACGGAGCTCGAATTCGGATCCCAGACTTGTCTCCTCA
pCMV-TRAIP(1-177)-F	XM_021068793.1	CCAGTCGACTCTAGAGGATCCATGCCTATTCGTGCTCTGTGC
pCMV-TRAIP(1-177)-R		CAGGGATGCCACCCGGGATCCCTACCGCTGGCTCTGGAGTAGG
pCMV-TRAIP(1-395)-F	XM_021068793.1	CCAGTCGACTCTAGAGGATCCATGCCTATTCGTGCTCTGTGC
pCMV-TRAIP(1-395)-R		CAGGGATGCCACCCGGGATCCCTACCGGATGAAAACAGGGAAG
pCMV-TRAIP(54-472)-F	XM_021068793.1	ATTCGAATTTAAATCGGATCCATGCAAAAGAACCATTATCA
pCMV-TRAIP(54-472)-R		ATCCTTCGCGGCCGCGGATCCCTAGGACAGGAAACTGTCCAGC
pCMV-TRAIP(178-472)-F	XM_021068793.1	CCAGTCGACTCTAGAGGATCCATGCCTGAGGTGGAGGAAATGAT
pCMV-TRAIP(178-472)-R		CAGGGATGCCACCCGGGATCCCTAGGACAGGAAACTGTCCAGCT
pEGFP-TRAIP-F	XM_021068793.1	GTACCGCGGGCCCGGGATCCATGCCTATTCGTGCTCTG
pEGFP-TRAIP-R		TTATCTAGATCCGGTGGATCCGGACAGGAAACTGTCC
pCMV-nsp1-F	MF187956.1	CCAGTCGACTCTAGAGGATCCATGTCTGGGATACTTGATCGGTG
pCMV-nsp1- R		CAGGGATGCCACCCGGGATCCACCGTACCACTTATGACTGCCAA
pCMV-nsp1α-F	MF187956.1	CCAGTCGACTCTAGAGGATCCATGTCTGGGATACTTGATCGGTG
pCMV-nsp1α-R		CAGGGATGCCACCCGGGATCCCTACATAGCACACTCAAAAGGGC
pCMV-nsp1β-F	MF187956.1	CCAGTCGACTCTAGAGGATCCATGGCTGACGTCTATGACATTGGT
pCMV-nsp1β-R		CAGGGATGCCACCCGGGATCCCTAACCGTACCACTTATGACTGC
pCMV-nsp1α N(1-167)-F	MF187956.1	CCAGTCGACTCTAGAGGATCCATGTCTGGGATACTTGATCGGTG
pCMV-nsp1α N(1-167)-R		CAGGGATGCCACCCGGGATCCCTACCTCTGCGGGAGCGGCAA
pCMV-nsp1α N(67-180)-F	MF187956.1	CCAGTCGACTCTAGAGGATCCATGACTGTCGAGTGCTCCCCCG
pCMV-nsp1α N(67-180)-R		CAGGGATGCCACCCGGGATCCCTACATAGCACACTCAAAAGGGC

PMSF or NEM. The cell lysates were incubated with anti-Myc or anti-Flag labeled beads (Sigma, St. Louis, MO, USA) for 2 h or overnight at 4°C, followed by washing three times with lysis buffer for 10 min each and boiled for 5 min with protein loading buffer**.** Proteins bound to the beads were separated by SDS-PAGE and western blotting was performed as described above.

Flow Cytometry Analysis

3D4/21 cells were infected with PRRSV or transfected with the TRAIP plasmid. The cells were harvested at the indicated times, followed by washing with PBS twice and digested with trypsin. Pre-cooled 80% ethanol was added to the harvested cells for 1 h. Cells were washed with PBS twice and stained with anti-TRAIP antibody or anti-PRRSV nsp2, and incubated with goat anti-mouse IgG FITC conjugate (1:200) for 30 min. Fluorescence-activated cell sorting was performed on a FACS LSR II (BD Biosciences, San Jose, CA, USA). A total of 1×10^5 cells was analyzed per run.

RNA Interference

A small RNA interfering (siRNA) assay was performed to confirm the target gene of TRAIP (siTRAIP) and a negative control RNA (NC), synthesized by GenePharma (Shanghai, China) (**Table 3**). Briefly, 3D4/21 cells were seeded in 12-well plates (60–80% confluence) and transfected with siRNA1 (siTRAIP-1) or siRNA2 (siTRAIP-2) at a final concentration of 50 nmol/L using Lipofectamine3000 (Invitrogen). The cells were infected with 0.5 MOI PRRSV and harvested after 24 h. The gene expression levels were confirmed by quantitative real-time PCR (qRT-PCR) and western blotting.

TABLE 2 | Primers used for qRT-PCR amplification.

Primer name	Genbank number	Sequence of primer(5′-3′)
PRRSV-N-F	KX286735.1	GCCTCGTGTTGGGTGGCAGA
PRRSV-N-R		CACGGTCGCCCTAATTGAATAGG
TRAIP-F	XM_021068793.1	GGAAGCACATTCTCCCGTTCA
TRAIP-R		GGCGGATCATAGTCGTGTCAGTA
TNF-α-F	X57321	GAGATCAACCTGCCCGACT
TNF-α-R		CTTTCTAAACCAGAAGGACGTG
IFN-β-F	NM_001003923	GCAGTATTGATTATCCACGAGA
IFN-β-R		TCTGCCCATCAAGTTCCAC
NF-κB-F	X61498.1	CCCAGCCATTTGCACACCTCAC
NF-κB-R		TTCAGAATTGCCCGACCAGTTTTT
β-actin-F	DQ452569.1	GAATCCTGCGGCATCCACGA
β-actin-R		CTCGTCGTACTCCTGCTTGCT

Preparation of Nuclear and Cytoplasmic Extracts

HEK 293T cells were co-transfected with Myc-nsp1α and Flag-TRAIP (WT) or Flag-TRAIP (K205R) plasmids in the

TABLE 3 | Primers used in the small RNA interfering assay.

Primer name	Primer sequence (5′-3′)
Negative control	F:UUCUCCGAACGUGUCACGUTT
	R:ACGUGACACGUUCGGAGAATT
siTRAIP-1	F:GCACUAUAUGCUCCGACUUTT
	R:AAGUCGGAGCAUAUAGUGCTT
siTRAIP-2	F:GGAGGAGAGUGUCUUAGAUTT
	R:AUCUAAGACACUCUCCUCCTT

presence of the proteasome inhibitor MG132. Cytoplasmic and nuclear proteins were extracted using a Nuclear and Cytoplasmic Protein Extraction Kit (Beyotime Institute of Biotechnology, China) according to the manufacturer's instructions. Briefly, the treated cells were washed with PBS and collected. The cell pellet was completely suspended and dispersed with 200 μl cytoplasmic protein extraction reagent A. Next, 10 μl cytoplasmic protein extraction reagent B was added to the cell suspension on ice for 15 min. Cytoplasmic proteins are collected after centrifugation. Resuspend the nuclear pellet in 50 μl of ice cold nuclear extraction buffer. The nuclear fraction was collected after shaking and centrifugation. Abundance of TRAIP in the nucleus and cytoplasmic was detected by western blotting.

Statistical Analysis

Data were subjected to one-way analysis of variance (one-way ANOVA) and expressed as mean ± SEM. Pairwise multiple comparison was conducted to determine which group differed by two-way ANOVA followed by Bonferroni post-tests using Prism 6.0 (GraphPad Software Inc.). Results were considered statistically significant if $P < 0.05$.

RESULTS

Up-Regulation of TRAIP Accumulation in 3D4/21 by PRRSV

The RNA expression profiles of PRRSV-infected 3D4/21 were performed by high throughput RNA sequencing (RNA-Seq). A transcriptome analysis from 3D4/21 cells was performed to search for genes related to antiviral immunity that are significantly altered after PRRSV infection. The mRNA expression profiles of the E3 ubiquitin ligase family revealed an up-regulation of TRAIP in PRRSV-infected PAM cells (**Figure 1A**). To validate the results of the RNA-Seq data mining, 3D4/21 cells were inoculated with 0.5 MOI PRRSV for the indicated times. The dynamic expression of TRAIP in PRRSV-infected 3D4/21 cells was detected by qRT-PCR. The results showed that the mRNA level of TRAIP increased after PRRSV infection, especially at 12 h (**Figure 1B**). A similar increase of TRAIP protein in infected 3D4/21 cells was confirmed by western blotting (**Figure 1C**) and flow cytometry (**Figure 1D**). These data indicated that PRRSV infection led to an up-regulation of TRAIP. The changes in TRAIP expression levels suggests its potential involvement in the proliferation of PRRSV.

TRAIP Impact on PRRSV Proliferation

To investigate if the expression of TRAIP has an effect on PRRSV proliferation, a PRRSV-infected 3D4/21 cell model was developed. First, we constructed a eukaryotic expression vector (Flag-TRAIP) and designed siRNA sequences targeting TRAIP (**Table 3**). Western blot analysis revealed that the eukaryotic expression vector of TRAIP was successfully constructed (**Figure 2A**) and the expression of TRAIP was dramatically silenced by TRAIP siRNA1 (siTRAIP-1) or siRNA2 (siTRAIP-2), especially with siRNA2 (**Figure 2B**). Next, we attempted to detect the effects of TRAIP overexpression or interference on PRRSV proliferation. Compared to the control sample, the overexpression of TRAIP corresponded to an increase in PRRSV N gene mRNA (**Figure 2C**). The mRNA level of PRRSV N gene exhibited a downward trend in TRAIP siRNA transfected cells (**Figure 2D**). In line with that, the results of flow cytometry analysis further confirmed that TRAIP expression levels were consistent with PRRSV proliferation (**Figures 2E,F**). The results of western blotting also confirmed these findings (**Figure 2G**). Meanwhile, the virus titer was significantly higher in TRAIP plasmid transfected cells compared to the control (**Figure 2H**). These data indicate that the changes of cellular TRAIP is consistent with PRRSV proliferation, and TRAIP expression promotes PRRSV proliferation.

TRAIP Interacts With Nsp1α

We have found that changes in TRAIP expression levels induced by PRRSV infection appeared to be associated with early stage of PRRSV infection. Besides, TRAIP has been reported to be a gene involved in innate immunity (39). Therefore, we further explored whether there is an interaction between the TRAIP and PRRSV non-structural proteins nsp1, nsp4, nsp11, each of which is a major protein involved in inhibiting the IFN-β and NF-κB promoters (41, 43, 44). We first observed that Flag-tagged TRAIP interacted with Myc-nsp1 (**Supplementary Figure 1**), and the interaction between TRAIP and nsp1 was confirmed by co-immunoprecipitation (**Supplementary Figure 1a**). Immunofluorescence of both Myc-nsp1 and Flag-TRAIP showed that TRAIP and nsp1 co-localized around the nucleus at 18 h post-transfection (**Supplementary Figure 1b**). At the same time, we found that the TRAIP protein could also be localized to the cytoplasm as well as the nucleus. TRAIP has been shown to have the ability to shuttle between the nucleus and cytoplasm (39, 45). GFP labeled TRAIP protein was distributed in the cytoplasm as well as showing a punctate distribution in the nucleus (**Supplementary Figure 2a**). A similar distribution pattern of Myc-nsp1α was also observed (**Supplementary Figure 2b**).

In PRRSV-infected cells, the nsp1 protein is processed co-translationally into nsp1α and nsp1β. Therefore, we further examined whether nsp1α and/or nsp1β could interact with TRAIP. Co-immunoprecipitation analysis showed that TRAIP specifically interacts with nsp1α, but not nsp1β (**Figure 3A**). An indirect immunofluorescence assay revealed that Myc-nsp1α and Flag-TRAIP were colocalized both in the cytoplasm and nucleus of HeLa cells (**Figure 3B**) and 3D4/21 cells (**Figure 3C**). Similarly, colocalization of HA-TRAIP with nsp1α in PRRSV-infected 3D4/21 cells further confirmed the interaction between

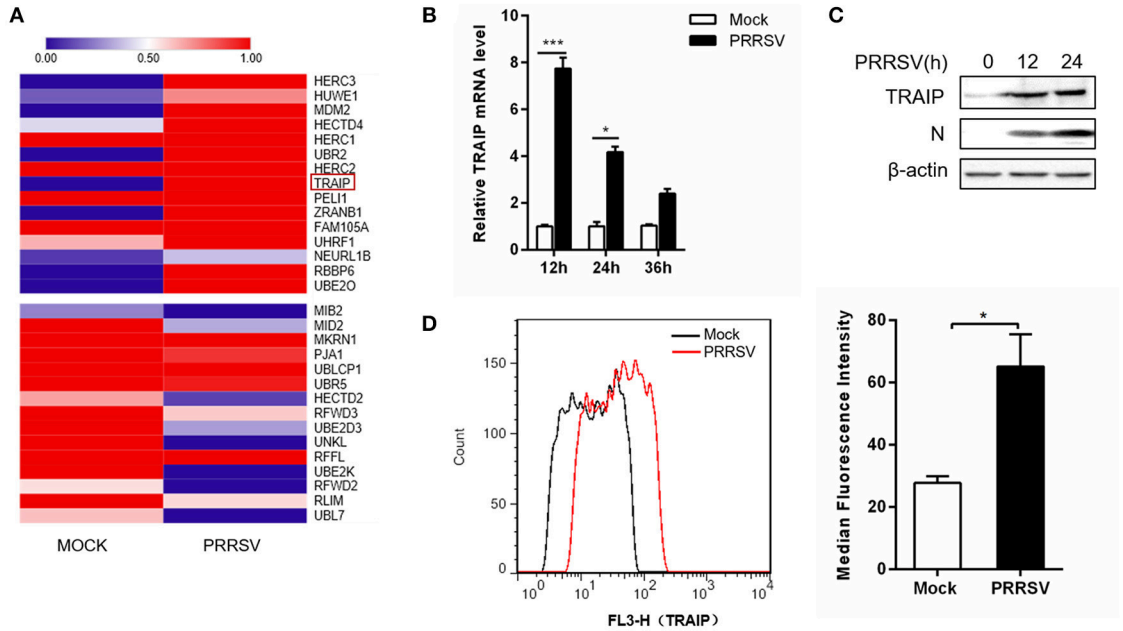

FIGURE 1 | TRAIP is upregulated in 3D4/21 by PRRSV. **(A)** The heatmap of ubiquitin-related differentially expressed genes analyses were generated using online websites (https://software.broadinstitute.org/morpheus/). Red bars indicate an upregulation in expression of at least 1x fold. **(B)** qRT-PCR analysis of TRAIP in 3D4/21 inoculated without or with 0.5 MOI PRRSV at the indicated times. **(C)** 3D4/21 were either mock-infected or infected with PRRSV at a 0.5 MOI for 12 or 24 h. The cells were then harvested to detect TRAIP by Western blotting using a mouse anti-TRAIP polyclonal antibody and cell lysates were then analyzed for expression of PRRSV structural protein (N) with anti-N MAb. **(D)** 3D4/21 cells were mock-infected or infected with 0.5 MOI PRRSV. Cells were collected at 12 h post-infection. Analysis of TRAIP protein expression levels by flow cytometry. $^{*}P < 0.05$, $^{***}P < 0.001$ (analysis of two-way ANOVA followed by Bonferroni post-test). Data are representative of three independent experiments.

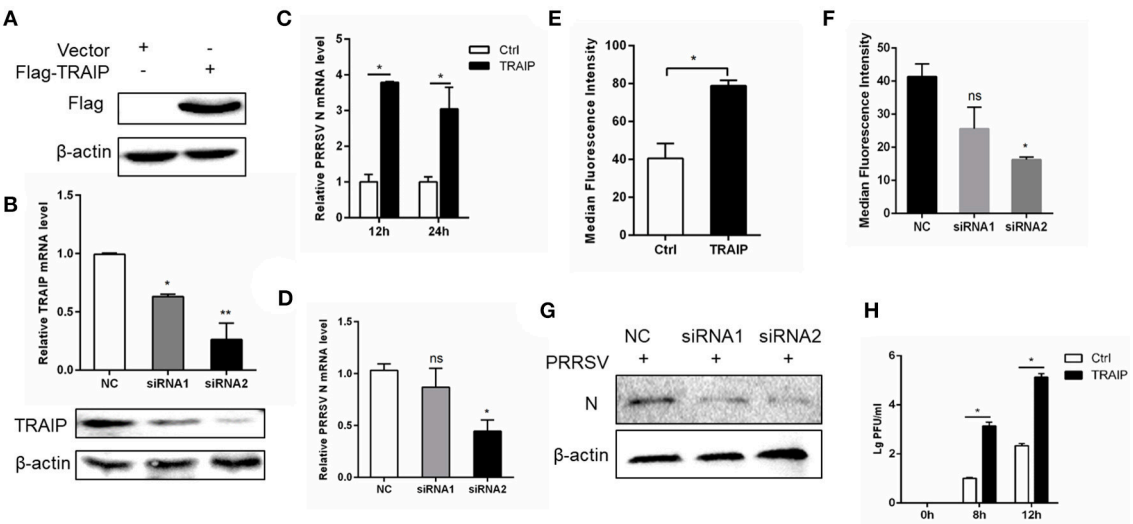

FIGURE 2 | TRAIP contributes to PRRSV proliferation. Flag-tagged TRAIP plasmid or negative control (NC) and siRNA1 (siTRAIP-1) or siRNA2 (siTRAIP-2) targeting TRAIP were transfected into 3D4/21 respectively at the indicated times **(A–D)**, after which the cells were infected with 0.5 MOI PRRSV and the cells were collected at 12 or 24 h post-infection. Flag-TRAIP was recognized by the anti-FLAG tag antibody **(A)** and siRNA interference effects were detected by TRAIP polyclonal immunoblotting and qRT-PCR at post-transfection 24 h **(B)**. The infected cells were collected at 12 h **(C–H)** or 24 h **(C)** post-infection, PRRSV N mRNA was detected by qRT-PCR, and PRRSV N was shown by WB analysis **(G)**. Analysis of PRRSV levels by flow cytometry detection of PRRSV N **(E,F)**. **(H)** PRRSV was inoculated after transfection with TRAIP and PRRSV load was tested by TCID50 after 8 or 12 h. $^{*}P < 0.05$, $^{**}P < 0.01$ (analysis of two-way ANOVA followed by Bonferroni post-test). Data are representative of three independent experiments.

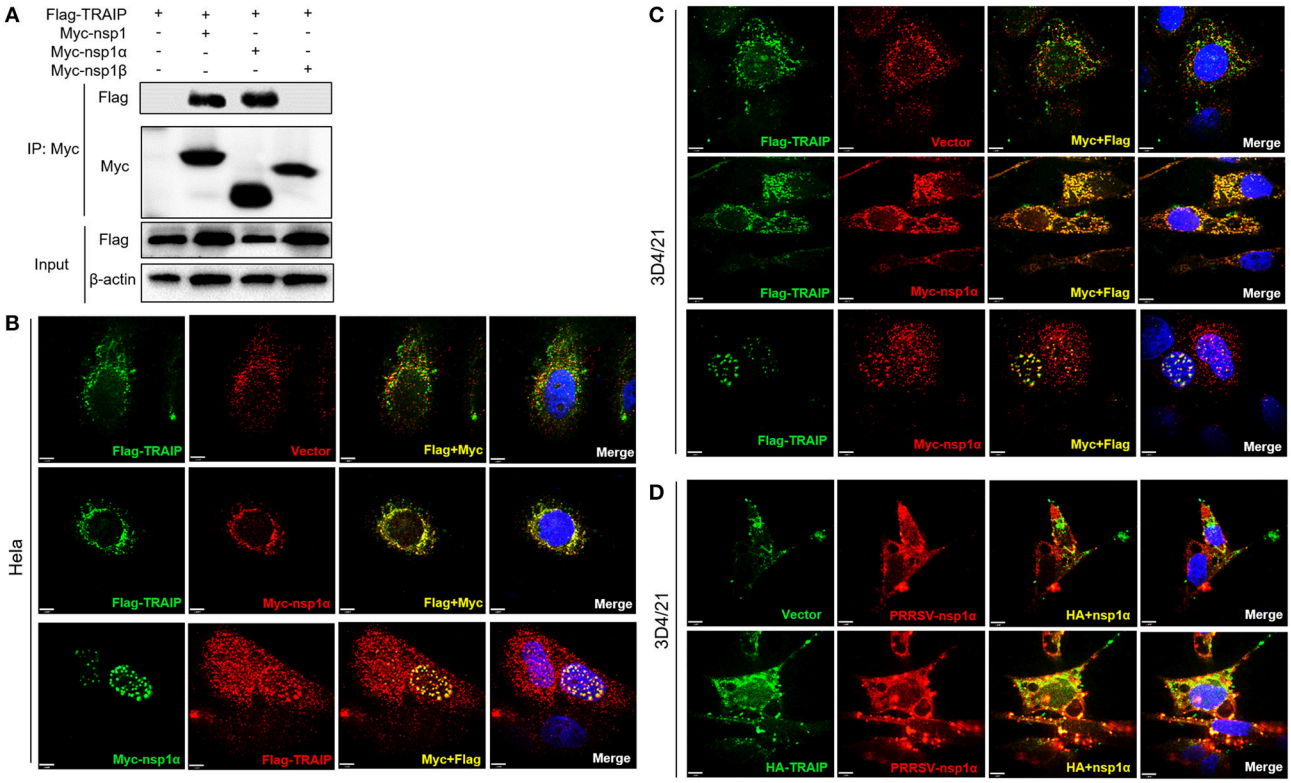

FIGURE 3 | TRAIP interacts with PRRSV-nsp1α. **(A)** HEK293 cells were first transfected with Flag-TRAIP and then co-transfected with Myc-nsp1, Myc-nsp1α, Myc-nsp1β, vector expressing plasmids. The cell lysates were then immunoprecipitated with an anti-Myc MAb and detected by Western blotting at 24 h post-transfection. **(B,C)** Co-localization of nsp1α protein with TRAIP in the cytoplasm and nucleus in HeLa cells and 3D4/21 cells. HeLa or 3D4/21 cells were seeded in 12-well plates and co-transfected with Flag-TRAIP and Myc-nsp1α expressing plasmid. At 18 h post-transfection, the cells were incubated with a rabbit anti-Myc mAb and a mouse anti-Flag antibody followed by FITC-conjugated anti-mouse IgG (green) and PE-conjugated anti-rabbit IgG (red) or FITC-conjugated anti-rabbit IgG (green) and PE-conjugated anti-mouse IgG (red). **(D)** Porcine TRAIP co-localize with PRRSV-nsp1α in PRRSV infection of 3D4/21 cells. Nuclei were stained with DAPI (blue). Cells were observed under a laser confocal imaging analysis system, scale bar: 7 μm.

TRAIP and nsp1α (**Figure 3D**). Taken together, our findings indicated TRAIP interacts with nsp1α.

Nsp1α Removes Sumo-Modification of TRAIP

Previous studies have shown that TRAIP is post-translationally modified by SUMO (46). Some viral proteins can also affect the SUMOylation of host cellular proteins to impact various intracellular activities (47, 48). Overexpression of PRRSV nsp1α weakened the SUMO modification of cells (**Supplementary Figure 3**). Next, the effect of nsp1α on TRAIP SUMO modification was detected using SUMO1 antibody or SUMO2/3 antibody. We found a pronounced TRAIP sumo-modified band appeared, especially the sumo1 modification, and was attenuated in the TRAIP and nsp1α co-expression groups (**Figures 4A,B**). At the same time, TRAIP expression is detected by western blotting using anti-Flag antibody and TRAIP antibody, respectively. Our results suggested that Flag-TRAIP or endogenous TRAIP is modified with SUMO moieties. However, SUMOylation of TRAIP is reduced when PPRSV nsp1α is overexpressed (**Figures 4C,D**). To more accurately detect the effect of nsp1α on sumoylated TRAIP, a co-immunoprecipitation assays was used. The co-immunoprecipitation results further confirmed the effect of nsp1α on the SUMOylation of TRAIP (**Figures 4E,F**). Taken together, these findings demonstrate that PRRSV nsp1α can significantly reduce the SUMO modification of TRAIP.

The LZ Domain of TRAIP Interacts With PCPα of Nsp1α

Previous experiments have verified the interaction of nsp1α with TRAIP. To further provide a molecular mechanism for this interaction, the domain of TRAIP was analyzed and different TRAIP truncations were constructed. Analysis showed that TRAIP consisted of a RING domain, putative coiled-coil domain and leucine zipper region (**Figure 5A**). The immunoprecipitation results indicated that Flag-TRAIP could be co-precipitated with Myc-nsp1α and the key to this interaction was the LZ domain (residues 201–280) (**Figure 5B**). Subsequently, to identify the critical domains of nsp1α that were responsible for TRAIP binding, we mapped the domains of PRRSV nsp1α and constructed the corresponding

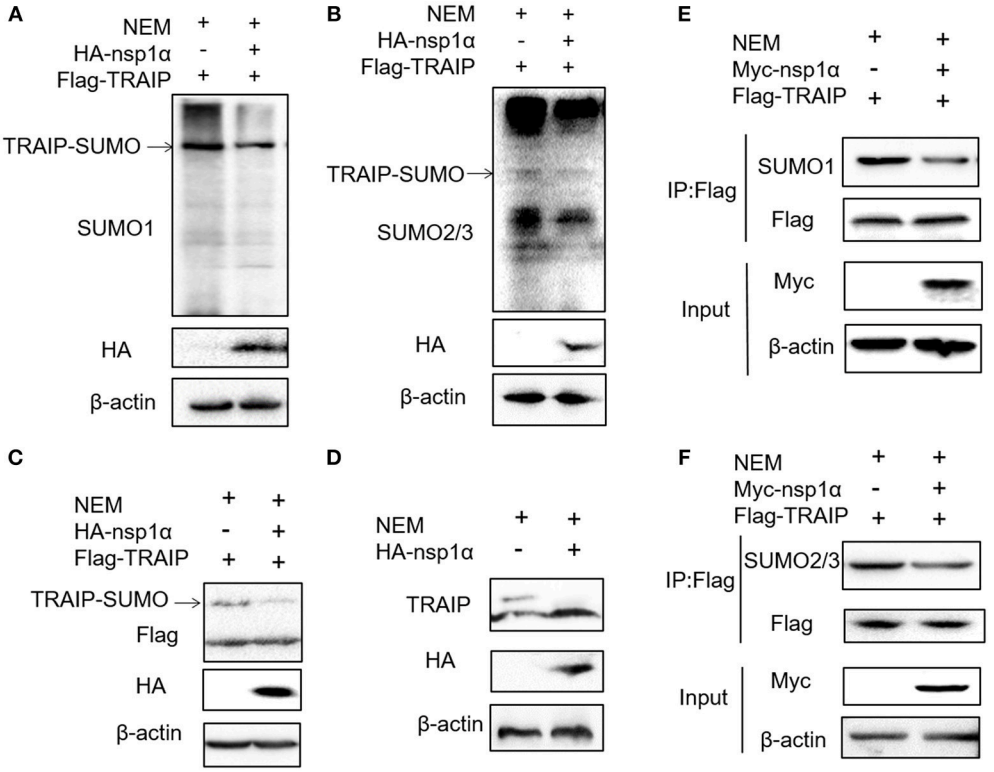

FIGURE 4 | Nsp1α removed SUMO-modification of TRAIP. HEK 293T cells were transfected with HA-nsp1α and Flag-TRAIP, and lyzed in RIPA buffer containing desumoylation protease inhibitor N-Ethylmaleimide [NEM] inhibition of deSUMOylation of TRAIP. The effect of nsp1α on TRAIP SUMO modification was detected using SUMO1 antibody **(A)** or SUMO2/3 antibody **(B)**. **(C)** HEK 293T cells were co-transfected with HA-nsp1α and Flag-TRAIP, and the effect of nsp1α on exogenous TRAIP SUMO-modification was detected by Western blotting. **(D)** HEK 293T cells were transfected with HA-nsp1α or vector and the effect of nsp1α on endogenous TRAIP SUMO modification was detected by WB. HEK 293T cells were cotransfected with Myc-nsp1α and Flag-TRAIP **(E,F)** and the effect of nsp1α on endogenous TRAIP SUMO modification was detected by co-immunoprecipitation.

truncated segments, which consisted of amino acids (aa) 1–167 (nsp1α-N), aa 67–180 (nsp1α-C) (**Figure 5C**). We next investigated the PCPα motif interacted with intact TRAIP (**Figure 5D**). All nsp1α segments were shown to interact when analyzed by immunoprecipitation. Together these results revealed that the PRRSV nsp1α and TRAIP interaction depended on the PCPα motif of nsp1α and LZ domain of TRAIP (**Figure 5E**).

The Effect of PRRSV Nsp1α on TRAIP SUMOylation Is Independent of the Interaction

Five SUMOylation sites in TRAIP (K80R, K127R, K205R, K247R, and K465R) have been identified in previous studies (46). In this study, the complete CDS of TRAIP was successfully amplified, and amino acid sequence alignment analysis was performed, indicating that TRAIP has high amino acid sequence identity with Homo sapiens and Mus musculus. It is worth noting that the TRAIP's SUMOylation sites are highly conserved (**Figure 6A**). We constructed TRAIP point mutations to determine whether the SUMOylation site was important for its association with nsp1α. Co-immunoprecipitation analysis indicated that the K205 residue of TRAIP was critical for the interaction (**Figure 6B**). Next, we sought to investigate the effect of nsp1α on the SUMOylation function of different TRAIP mutants. Surprisingly, nsp1α removed SUMO modifications of different mutants to a similar extent, including K205 (**Figures 6C,D**). Therefore, nsp1α reduces the SUMO modification of TRAIP independent of the interaction. It was hypothesized that nsp1α may affect the multi-step enzymatic process in SUMOylation or deSUMOylation.

Nsp1α Inhibits K48-Linked Polyubiquitination and Degradation of TRAIP

Recent analyses suggest an evolutionarily conserved and fundamental molecular interface between the SUMO and ubiquitin systems (49). Protein SUMOylation can influence its subsequent ubiquitination and degradation (50, 51). Studies have shown that TRAIP can be ubiquitinated, and SUMOylation of TRAIP affects its ubiquitination (46). So the next step, the role of nsp1α on TRAIP ubiquitination was investigated.

The results revealed that nsp1α inhibited the ubiquitination of TRAIP-WT, but not TRAIP-K205R (**Figure 7A**). Further

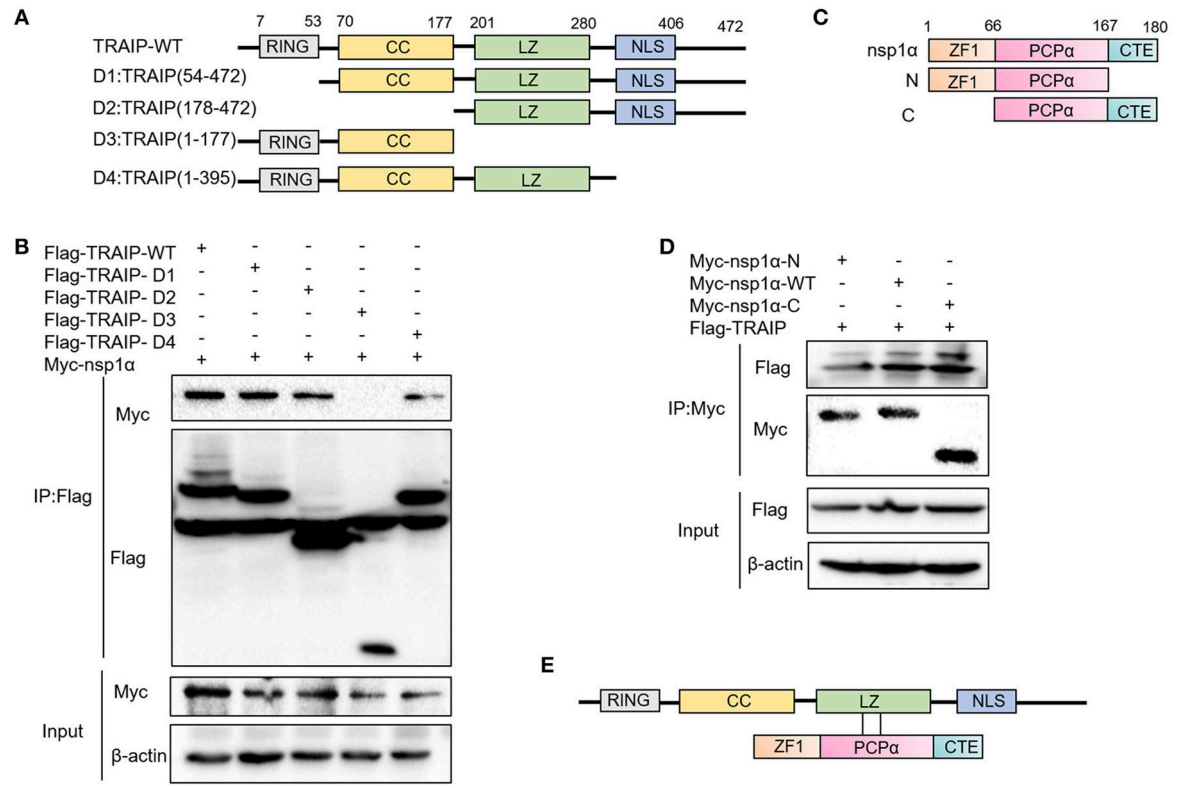

FIGURE 5 | The LZ domain of TRAIP interacts with PCPα of nsp1α. **(A)** Mapping of wild-type (WT) TRAIP and different key enzyme truncated of TRAIP. TRAIP is consisted of a RING domain, a Coiled coil (CC) domain, a Zipper domain, and nuclear localization signals (NLS). **(B)** HEK293T cells were co-transfected with Myc-nsp1α and different Flag-tag TRAIP deletion mutants plasmids. Cells were harvested and lysed, and immunoprecipited (IP) with Flag-conjugated beads. **(C)** Mapping of wild-type (WT) nsp1α and internal deletion mutants. Nsp1α is consisted of a papain-like cysteine protease α (PCPα) motif, an N-terminal zinc finger motif (ZF1), and the carboxyl-terminal extension (CTE). **(D)** Flag-TRAIP interacts with the PCP1α domain of nsp1α. **(E)** The model of TRAIP interacts with nsp1α was proposed.

analysis found that PRRSV nsp1α inhibited K48-linked polyubiquitination in TRAIP (**Figure 7B**). As shown in **Figure 7B**, mutation of lysine 205 to arginine did not affect its ubiquitination level, suggesting that K205 is not a ubiquitination site (lane 7 and lane 5). However, the nsp1α lost the ability to inhibit polyubiquitination of TRAIP-K205R mutant, indicating that nsp1α is dependent on K205 site to reduce the self-ubiquitination of TRAIP. Further analysis showed the K48 polyubiquitination of TRAIP was inhibited by deleting the LZ domain of TRAIP, indicating the presence of the K48 ubiquitination site in the LZ domain (**Figure 7C**). Next, changes in protein levels caused by nsp1α-induced ubiquitination regulation of TRAIP were verified. When the proteasome degradation of TRAIP was inhibited by MG132, the intracellular TRAIP protein content was not affected in overexpressed nsp1α cells, indicating that nsp1α does not affect the production of TRAIP protein (**Figure 7D**). However, nsp1α co-transfection can increase the protein stability of TRAIP in the absence of MG132 (**Figure 7E**). Taken together, nsp1α co-transfection can inhibit K48-linked self-ubiquitination of TRAIP possibly occupy or occlude the ubiquitination site in the LZ domain by changing the TRAIP spatial conformation, thereby inhibiting the degradation of TRAIP and maintaining TRAIP stability.

Nsp1α Decreased the Abundance of TRAIP in the Nucleus

As shown previously, SUMO modification played a key role in its nuclear import (52, 53). We therefore examined the effect of overexpression of nsp1α on the nuclear distribution of TRAIP. The results showed that the distribution of TRAIP in the nucleus was significantly reduced, while that in the cytoplasmic was increased conversely when nsp1α was overexpressed (**Figure 8A**). Similarly, nsp1α can also affect the distribution of TRAIP K205R mutant (**Figure 8B**). Detection of endogenous TRAIP protein distribution further validated the result (**Figure 8C**). To visually detect the distribution of TRAIP in the cytoplasm and nucleus, the TRAIP immunofluorescence was analyzed at the indicated time points (**Figure 8D**). Statistics showed PRRSV nsp1α significantly reduced the TRAIP content in the nucleus (**Figure 8E**). Collectively, these results suggest nsp1α alters the distribution in the nucleus and cytoplasm and reduces the abundance of TRAIP in the nucleus.

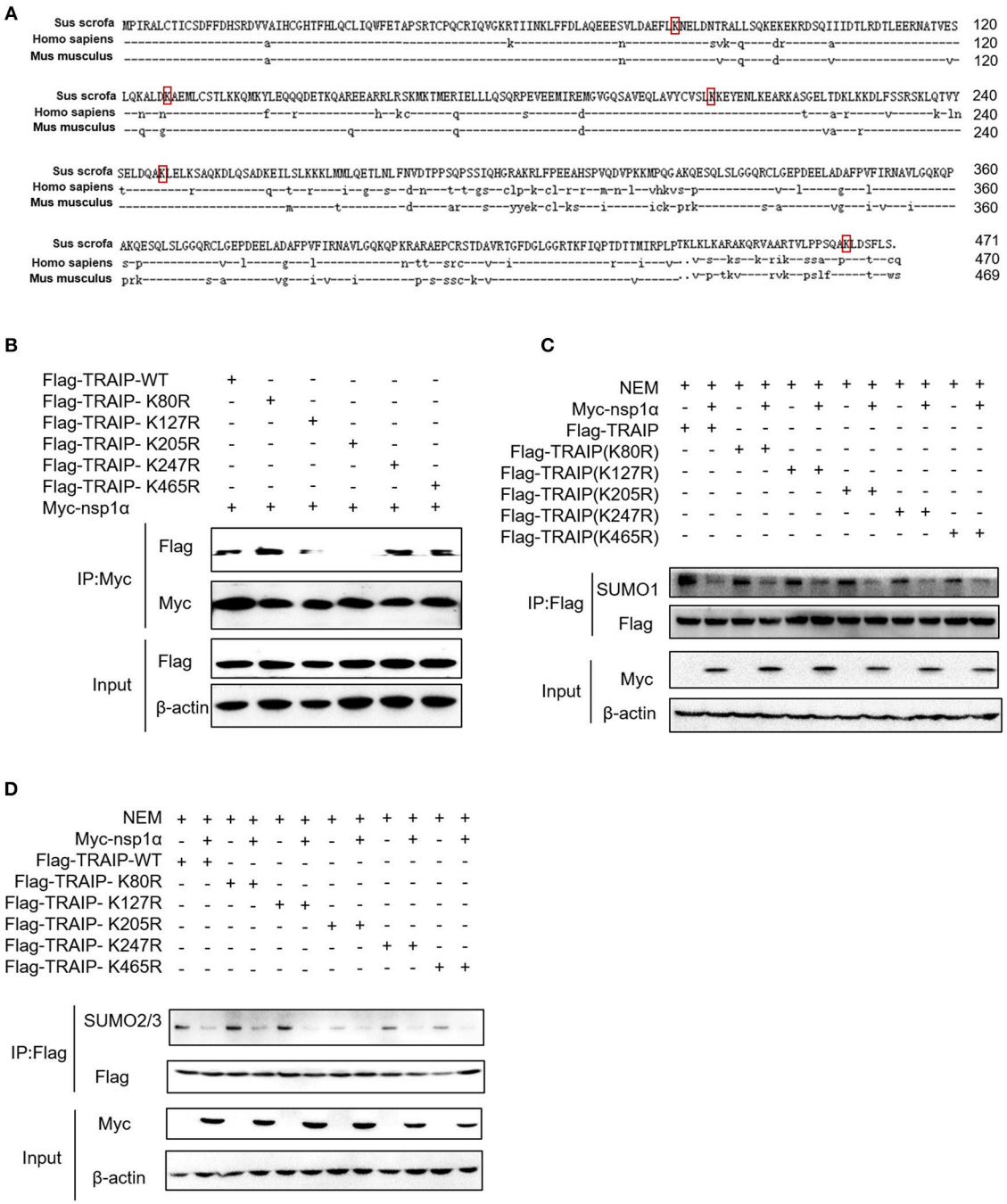

FIGURE 6 | The effect of nsp1α on SUMOylation of TRAIP is independent of their interaction. **(A)** Sequence comparison of TRAIP and homologs from other species. The TRAIP cDNA encoded an ORF with 471 amino acid-long protein, GeneBank Accession XM_021068793.1. Porcine TRAIP amino acid sequence was compared with those from Homo sapiens TRAIP (NM_005879.2), Mus musculus (NM_011634.3), respectively. **(B)** Coimmunoprecipitation analysis of TRAIP K205R SUMO site interacts with Myc-nsp1α in HEK293T cells. **(C,D)** HEK 293T cells were cotransfected with Myc-nsp1α and Flag-TRAIP or different point mutants, and the effect of nsp1α on endogenous TRAIP SUMO modification was detected by co-immunoprecipitation.

Nsp1α Expression Can Increase K48-Linked Ubiquitination of TBK1

We have shown that nsp1α regulated the distribution of TRAIP in the cytoplasm and nucleus by removing both the SUMO modification and K48-ubiquitination modifications of TRAIP. Previous research has found that TRAIP promoted TBK1 degradation via K48-linked ubiquitination (39) and this result was verified in this report (**Figure 9A**). It was

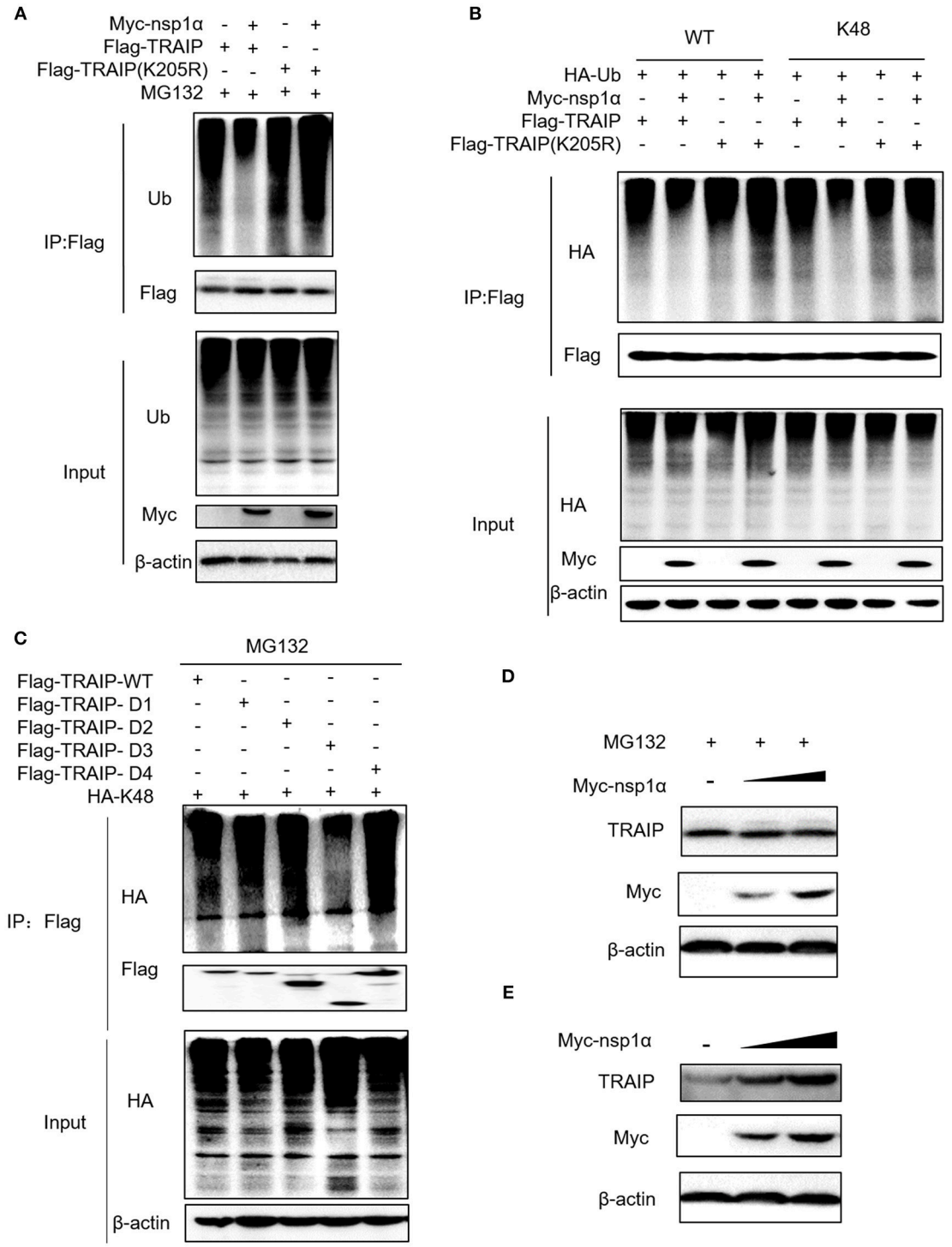

FIGURE 7 | Nsp1α inhibits K48-linked polyubiquitination and degradation of TRAIP. HEK 293T cells were co-transfected with Flag-TRAIP and Myc-nsp1α or vector supplemented 10 μM MG132 **(A)**. At 24 h post-transfection, the cell lysates were co-immunoprecipitated with an anti-Flag and probed with Ub antibody to detect ubiquitin levels of TRAIP respectively by Western blotting. **(B)** 293T cells were co-transfected with Flag-TRAIP or Flag-TRAIP (K205R), HA-Ub-WT, HA-Ub-K48 (ubiquitin mutants retaining a single lysine residue), and Myc-nsp1α or vector. At 24 h post-transfection, the cell lysates were precipitated with an anti-Flag MAb and further detected by Western blotting with an anti-HA MAb and an anti-Flag. **(C)** The K48 polyubiquitination of TRAIP was detected in different TRAIP deletion mutants. HEK 293T cells were transfected with Myc-nsp1α (0.5 or 1.0 μg) or vector **(D,E)**. TRAIP expression in total cellular protein and the protein stability of TRAIP in the absence of proteasome inhibitor MG132 (5 μM) was detected by Western blotting, respectively.

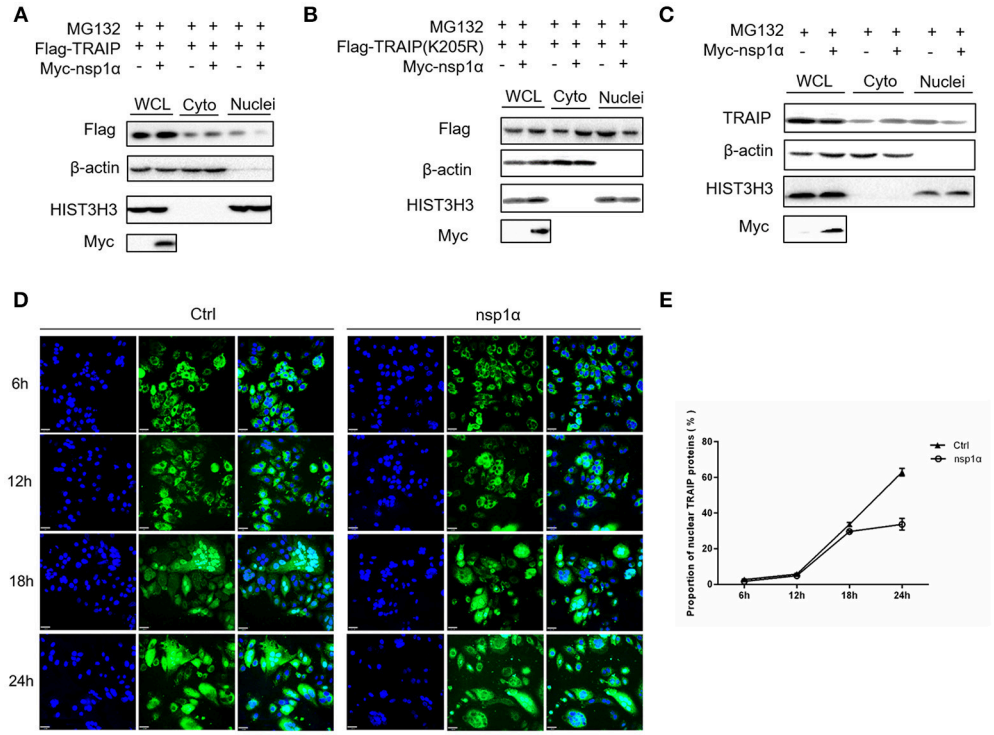

FIGURE 8 | Nsp1α decreased the abundance of TRAIP in the nucleus. HEK 293T cells were co-transfected with Myc-nsp1α and Flag-TRAIP (WT) **(A)** or Flag-TRAIP (K205R) **(B)**, in the presence of proteasome inhibitor MG132 (5 μM) and after 24 h, cytoplasmic protein and nucleoprotein were extracted and detected with anti-Flag mAb or anti-Myc antibody, respectively, by Western blotting. HIST3H3 was used as an internal loading control for nuclear protein load, and β-actin as the control for cytoplasmic protein load. **(C)** HEK 293T cells were transfected with Myc-nsp1α. At 24 h post-transfection, cytoplasmic protein and nucleoprotein were extracted and detected with TRAIP mAb or anti-Myc antibody. **(D)** Co-transfection of Flag-TRAIP with Myc-nsp1α or vector into HeLa cells. The cells were fixed and double-stained with a mouse anti-Flag antibody at the indicated times, followed by FITC-conjugated anti-mouse IgG (green). Nuclei were stained with DAPI (blue). Cells were observed under a laser confocal imaging analysis system, scale bar: 7 μm. **(E)** Statistical analysis of TRAIP distribution in cytoplasm and nucleus in HeLa cells was counted.

found Flag-TBK1 can interact with Myc-nsp1α and HA-TBK1 by immunoprecipitation (**Figure 9B**). The trimer complex of nsp1α with TRAIP and TBK1 was further confirmed in HeLa and 3D4/21 cells by immunofluorescence (**Figures 9C,D**). Furthermore, nsp1α promoted the K48-linked ubiquitination of TBK1 by TRAIP (**Figures 9E,F**). Therefore, it appeared that nsp1α increased TRAIP cytoplasmic abundance, leading to excessive TBK1 K48-linked ubiquitination.

Nsp1α Promotes the Inhibitory Effect of TRAIP on Interferon-Mediated Innate Immunity

Type I (IFN-α and β) are parts of the non-specific immune system and serve as the first line of defense (1). Studies have found that TRAIP plays an important role in RIG-I-mediated type I interferon response. In our work, the function of TRAIP in the interferon signaling pathway induced by PRRSV was also examined. The results demonstrated that TRAIP significantly inhibited the production of type I interferons (IFN-α, IFN-β) and inflammatory related factors (IL-1β, IL-6, TNF-α) (**Supplementary Figures 4a,b**). While expression of TRAIP was downregulated by siRNA, the mRNA levels of IFN-α, IFN-β, and inflammatory cytokines (IL-1β, IL-6, TNF-α) increased (**Supplementary Figures 4c–g**). Then, the role of PRRSV nsp1α and TRAIP in interferon-mediated innate immunity was examined. Nsp1α significantly enhanced TRAIP inhibition of IRF3 and IFN-β mRNA levels in SeV-stimulated interferon activation (**Figures 10A,B**). Consistently, the luciferase reporter system further confirmed that TRAIP inhibited IFN production together with PRRSV nsp1α, and the downregulation of the IFN-β and ISRE activation was remarkable in cells co-transfected with Myc-nsp1α and Flag-TRAIP (**Figures 10C,D**). The vesicular stomatitis virus (VSV-GFP) was used to further substantiate the presence of biologically active IFN. As shown in **Figure 10E**, TRAIP promoted VSV proliferation while co-expression of nsp1α. Next, the expression of TBK1 and phosphorylated IRF3 in the interferon signaling pathway were examined by western blotting. The results showed nsp1α enhanced the effect of TRAIP on TBK1 degradation and IRF3 activation (**Figure 10F**). Consistently, the additive effect disappeared when the K205R mutation of TRAIP was present. Collectively, these data together reflected the biological activity of the interaction of nsp1α with TRAIP in the regulation of antiviral innate immune responses.

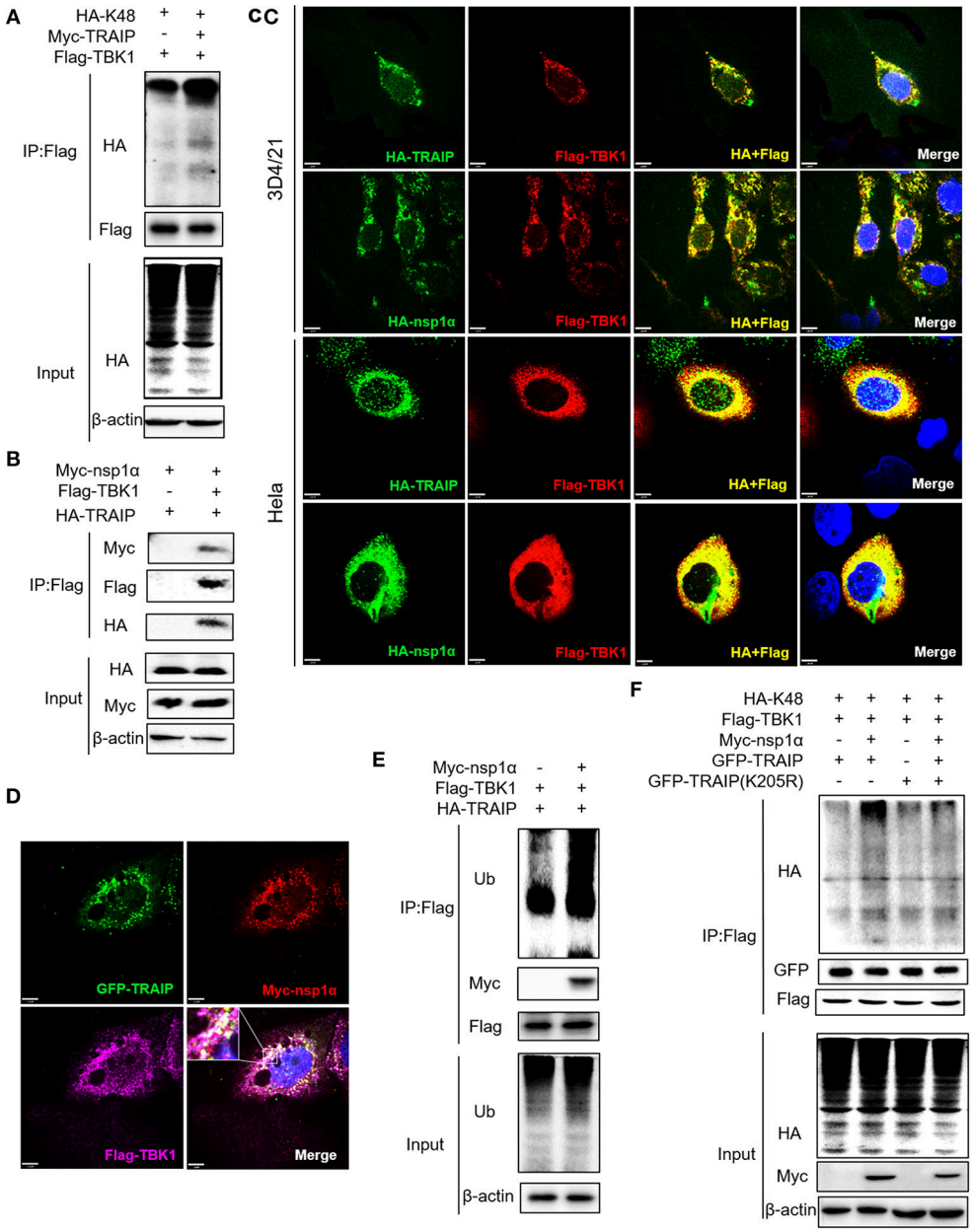

FIGURE 9 | Nsp1α forms trimer complex with TRAIP and TBK1. **(A,F)** Detection of Lys48 (K48)-linked polyubiquitination of TBK1. HEK 293T cells were transfected with Flag-TBK1, Myc-TRAIP, HA-K48, or Myc-empty vector **(A)** or HA-K48, GFP-TRAIP or GFP-TRAIP (K205R), Flag-TBK1, Myc-nsp1α, or Myc-empty vector **(F)**. At 24 h post-transfection, FLAG-immunoprecipitates were probed with HA antibodies to detect to Lys48 (K48)-linked polyubiquitination of TBK1. **(B)** HEK293T cells were co-transfected with Myc-nsp1α, HA-TRAIP, Flag-TBK1, or Flag-empty vector. FLAG immunoprecipitation (IP) was used to detect the interaction of TBK1, nsp1α, and TRAIP. **(C)** Immunofluorescence was used to detect the interaction between TBK1, nsp1α, and TRAIP in 3D4/21 and HeLa cells. **(D)** Co-transfection of GFP-TRAIP with Myc-nsp1α and Flag-TBK1 into HeLa cells. The cells were fixed and double-stained with a mouse anti-Myc antibody and a rabbit anti-Flag antibody and followed by PE-conjugated anti-mouse IgG (red) and IF647 goat anti-rabbit IgG. Nuclei were stained with DAPI (blue). Cells were observed under a laser confocal imaging analysis system, scale bar: 7 μm. **(E)** HEK 293T cells were transfected with Flag-TBK1, HA-TRAIP, or Myc-empty vector. At 24 h post-transfection, FLAG-immunoprecipitates were probed with Ub antibodies to detect polyubiquitination of TBK1.

DISCUSSION

Post-translational modifications (PTMs) of proteins are critical for controlling essential cellular processes. Both ubiquitination and SUMOylation are among the most common post-translational modifications. The ubiquitin molecule contains seven lysine sites (K6, K11, K27, K29, K33, K48, and K63). Target proteins linked by the K48 ubiquitin chain

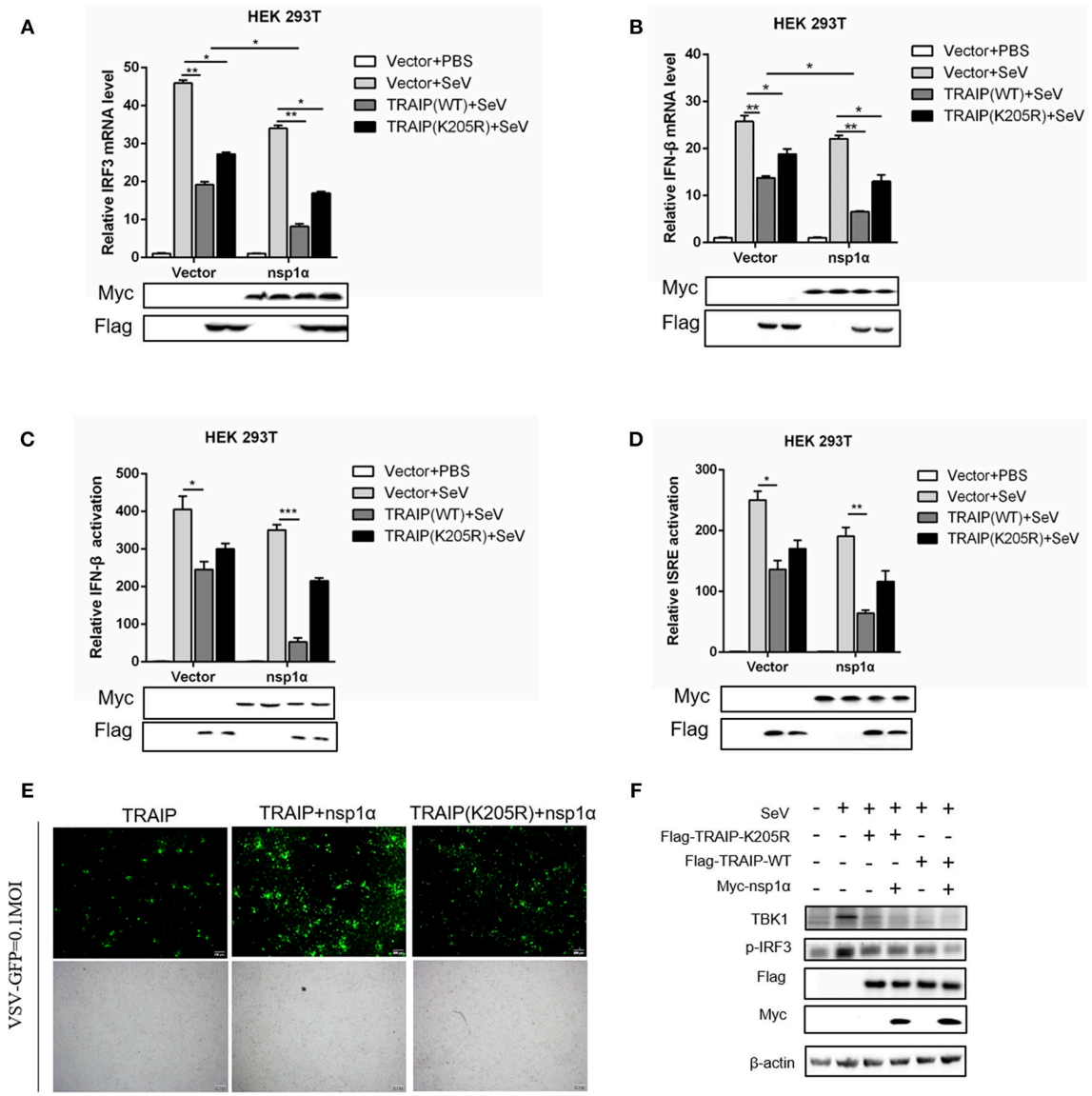

FIGURE 10 | The inhibitory effect of TRAIP and nsp1α on interferon-mediated innate immunity. **(A,B)** HEK293T were transfected with TRAIP or TRAIP(K205R)together with Myc-nsp1α or Myc-empty vector respectively and then infected with 0.1 MOI SeV for 12 h. Cells were harvested, mRNA expression of IRF3 **(A)** and IFN-β **(B)** were analyzed by qRT-PCR, and TBK1 and p-IRF3 were detected by Western blotting **(F)**. **(C,D)** HEK293T were transfected with TRAIP or TRAIP(K205R)and Myc-nsp1α or Myc-empty vector together with IFN-β reporter or ISRE reporter constructs for 18h and then infected with 0.1 MOI SeV before being lysed for luciferase assays. **(E)** HEK293T were transfected with TRAIP or TRAIP(K205R)together with Myc-nsp1α or Myc-empty vector and then infected with 0.1 MOI VSV-GFP, immunofluorescence microscopy imaging detected the proliferation of VSV.

can be recognized and degraded by the proteasome, and ubiquitin–protein ligases (E3s) play a crucial role in this process by recognizing target proteins. Ubiquitination changes the interaction between proteins, the stability and degradation of key proteins in signal pathways, thereby regulating natural immunity. SUMOylation is similar to the ubiquitination process, and reversibly modifies many proteins rather than perform proteasome-mediated degradation. SUMOylated proteins are more stable and SUMOylation modifications have extensive functions that are mainly reflected in their modified substrates. For example, TRAIP is a SUMO substrate and its activity is regulated by the SUMO machinery. SUMO-modified TRAIP has been reviewed in the regulation of protein localization and antagonism of ubiquitination. The SUMO modification of TRAIP guarantees its proper subcellular localization (46).

The virus employs multiple strategies to promote their own common proliferation in infected host cells. Viral proteins do not only participate in the regulation of the SUMOylation modification system, but also utilize the SUMOylation modification system to regulate other signaling pathways (54).

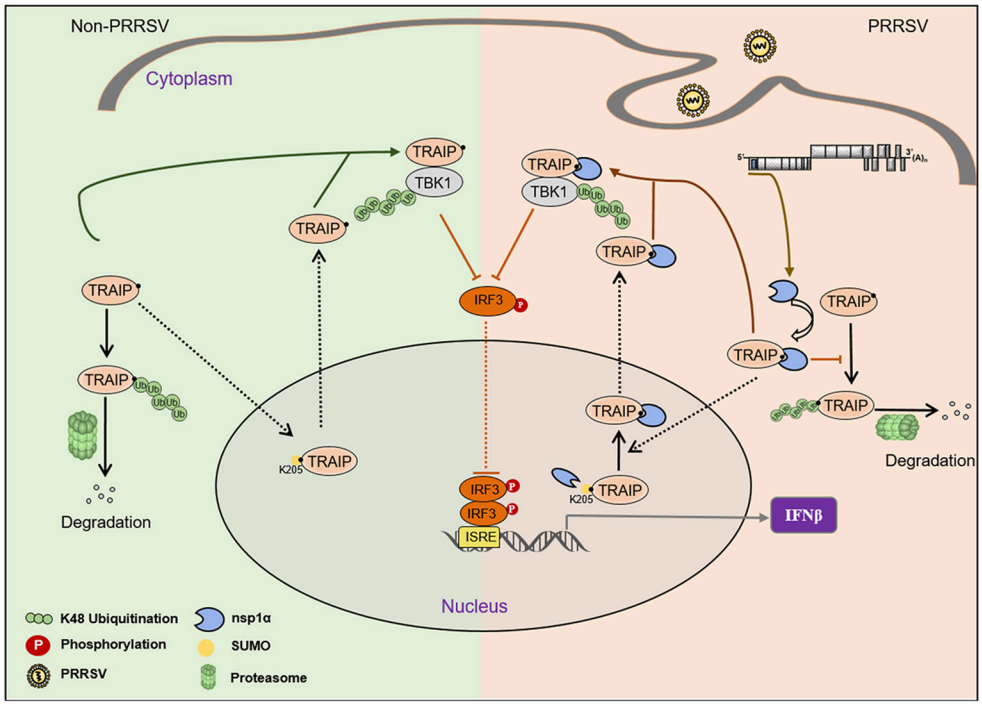

FIGURE 11 | Proposed model for the regulation of the interaction of PRRSV nsp1α with post-translational SUMO modification of TRAIP. Compared to non-PRRSV infection model, PRRSV-nsp1α alters the role of TRAIP in cellular life activities by modulating post-translational modifications of proteins. (I) PRRSV infection inhibits SUMOylation and self-ubiquitination of TRAIP, resulting in excessive enrichment of TRAIP in the cytoplasm. (II) Enrichment of cytoplasmic TRAIP leads to excessive K48 ubiquitination and degradation of TBK1, resulting in reduced phosphorylated IRF3 and type I interferon production.

In this study, the complete coding sequence (CDS) of TRAIP was cloned from porcine peripheral blood mononuclear cells (PBMC) and its amino acid sequence was highly homologous to *Homo sapiens*, including the RING domain and multiple SUMO sites. The SUMOylation and K48-linked polyubiquitination of TRAIP was attenuated by PRRSV nsp1α, thereby affecting intracellular localization of TRAIP and changing the distribution in the nucleus and cytoplasm. Consequently, these changes in turn affected the regulation of host immune signaling pathways. Our model for the regulation of the interaction of PRRSV nsp1α with post-translational modification of TRAIP is presented in **Figure 11**.

PRRSV is an important pathogen of swine. PRRSV-induced TRAIP transcription levels peak in early infection, which is consistent with the stage of high transcriptional expression levels of non-structural proteins during PRRSV replication and proliferation (55). Interestingly, we further observed that the morphology and subcellular localization of TRAIP was similar to nsp1α. What's more, PRRSV proliferation showed a trend of increasing in TRAIP overexpression in 3D4/21 cells.

There is crosstalk between SUMOylation and other post-translational modifications (56), and SUMOylation can compete with ubiquitination for substrate lysine residues to prevent proteasome degradation and ensure its stability (57, 58). However, some studies have shown that substrate proteins modified by SUMO as labeled molecules can recruit SUMO-targeted ubiquitin ligases (STUbL) to mediate subsequent ubiquitination degradation (50, 59, 60). Analysis revealed that most of SUMO-modified target molecules contained ψ-Lys-X-Glu (ψ representing an aliphatic amino acid, X being any amino acid) sites that specifically bind to SUMO (61). Subsequently, SUMO-linked TRAIP was verified and SUMO sites in TRAIP substrates have also been characterized (46). The LZ domain of TRAIP interacts with the PCPα domain of PRRSV nsp1α, and the K205 site in TRAIP was further confirmed as the key site. The specific mechanism of nsp1α control of TRAIP SUMO modification independent of the binding position. We hypothesized that nsp1α may affect the multi-step enzymatic process in SUMOylation or deSUMOylation. Interestingly, nsp1α not only inhibited SUMOylation but also reduced K48 ubiquitination of TRAIP. The K48 polyubiquitination of TRAIP was also inhibited by deleting the LZ domain of TRAIP, indicating that the ubiquitination sites in the LZ domain of TRAIP are crucial. Nsp1α may occupy or occlude the ubiquitination site in the LZ domain by changing the TRAIP spatial conformation, resulting in nsp1α inhibiting K48 ubiquitination of TRAIP and further stabilizing its structure.

Both nsp1α and TRAIP have been identified as nuclear shuttling proteins. The subcellular distribution of proteins is affected by the presence of nuclear localization signals (NLS) and nuclear export signals (NES) (62). Previous research has proposed that a nuclear export signal in PRRSV nsp1α is

necessary for type I IFN inhibition (62), and PRRSV nsp1α may enter the cell nucleus through interaction with cellular proteins (63). Our study suggests that TRAIP containing an NLS is a potential cellular molecule assisting nsp1α into the nucleus, and TRAIP may also enter the cytoplasm as a partner of nsp1α. Nsp1α increased the cytoplasmic abundance and stability of TRAIP, further promoting TBK1 degradation via K48-linked ubiquitination in 293T cells. In addition, nsp1α, which appears to act as a partner molecule, forms a ternary complex with TRAIP and TBK1 in the cytoplasm. Ubiquitination modification not only regulates a number of physiological functions within the cell, but is also involved in the regulation of a variety of viral replication and proliferation processes. E3 ubiquitin ligases have been reported to be involved in the regulation of protein stability in RIG-I signaling (64–66).

Overall, our study elucidates a unique novel mechanism by which PRRSV nsp1α resists innate immunity and promotes virus proliferation by modulating TRAIP protein nuclear:cytoplasmic ratio. As showed in **Figure 2**, TRAIP was identified as a protein that is overexpressed by PRRSV infection and favors virus proliferation. Mechanistically, nsp1α inhibits SUMOylation and self-ubiquitination of TRAIP, inducing over-enrichment of TRAIP in the cytoplasm. As a nuclear transport protein, TRAIP has immune regulation functions for life activities of the cell. Enrichment of nsp1α-induced TRAIP cytoplasm also leads to excessive K48 ubiquitination and degradation of TBK1, thus impairing type I interferon production. This study proposes a new mechanism for PRRSV dual regulation modification of host proteins to affect innate immunity. However, whether nsp1α regulates TRAIP through other patterns besides steric hindrance, such as enzyme regulation, is still unknown. The effects of PRRSV on TRAIP post-translational modification or nuclear ratio in the context of virus-infected cells require more data to prove. And the mechanism of PRRSV infection induced excessive transcription and expression of TRAIP also demands further exploration.

AUTHOR'S NOTE

Tumor necrosis factor (TNF) receptor associated factors (TRAF) interacting protein (TRAIP) is a particular host protein that exerts multiple functions in cell cycle progression, DNA damage response, and DNA repair pathways. Currently, the mechanism of action of TRAIP in PRRSV infection has never been reported. In this study, the relationship between TRAIP and porcine reproductive and respiratory syndrome virus replication (PRRSV) was investigated. Small ubiquitin-like modifier self-addition (SUMOylation) and self-ubiquitination of TRAIP was attenuated by PRRSV non-structural protein 1α (nsp1α), thereby affecting intracellular localization of TRAIP and changing the distribution in the nucleus and cytoplasm. As a cytoplasmic event, the cytoplasmic guiding effect of nsp1α on TRAIP promotes the ubiquitination and degradation of serine/threonine-protein kinase (TBK1). To sum up, a novel mechanism was presented by which PRRSV utilizes host proteins to regulate innate immunity. This study enriches the understanding of viral regulatory host protein post-translational modifications and interference with cell life processes.

AUTHOR CONTRIBUTIONS

JH conceived and designed the experiments. PS, YS, RL, CC, Liz, and LeZ performed the experiments. YS, PS, and KF analyzed the data. JH contributed reagents, materials, analysis tools. PS and JH wrote the paper.

FUNDING

This work was supported by the National Key Research and Development Program of China (2018YFD0500500), National Natural Science Foundation of China (31272540) and the underprop project of Tianjin Science and Technology Committee in China (16YFZCNC00640).

ACKNOWLEDGMENTS

We would like to thank Prof. Shaobo Xiao of Huazhong Agricultural University for gift of NSP1α monoclonal antibody.

SUPPLEMENTARY MATERIAL

The Supplementary Material for this article can be found online at: https://www.frontiersin.org/articles/10.3389/fimmu.2018.03023/full#supplementary-material

REFERENCES

1. Tanji T, Ip YT. Regulators of the Toll and Imd pathways in the Drosophila innate immune response. *Trends Immunol.* (2005) 26:193–8. doi: 10.1016/j.it.2005.02.006
2. Bourgeois C, Majer O, Frohner IE, Lesiakmarkowicz I, Hildering KS, Glaser W, et al. Conventional dendritic cells mount a type I IFN response against *Candida* spp. requiring novel phagosomal TLR7-mediated IFN-β signaling. *J Immunol.* (2011) 186, 3104–12. doi: 10.4049/jimmunol.1002599
3. Schoggins JW, Wilson SJ, Panis M, Murphy MY, Jones CT, Bieniasz P, et al. A diverse range of gene products are effectors of the type I interferon antiviral response. *Nature* (2011) 472:481–5. doi: 10.1038/nature09907
4. Loo YM, Fornek J, Crochet N, Bajwa G, Perwitasari O, Martinezsobrido L, et al. Distinct RIG-I and MDA5 signaling by RNA viruses in innate immunity. *J Virol.* (2008) 82:335–45. doi: 10.1128/JVI.01080-07
5. Thanos D, Maniatis T. Virus induction of human IFNβ gene expression requires the assembly of an enhanceosome. *Cell* (1995) 83:1091–100. doi: 10.1016/0092-8674(95)90136-1
6. Maniatis T, Falvo JV, Kim TH, Kim TK, Lin CH, Parekh BS, et al. Structure and function of the interferon-beta enhanceosome. *Cold Spring Harb Symp Quant Biol.* (1998) 63:609–20. doi: 10.1101/sqb.1998.63.609
7. Allende R, Laegreid WW, Kutish GF, Galeota JA, Wills RW, Osorio FA. Porcine reproductive and respiratory syndrome virus: description of persistence in individual pigs upon experimental infection. *J Virol.* (2000) 74:10834–7. doi: 10.1128/JVI.74.22.10834-10837.2000

8. Pejsak Z, Stadejek T, Markowska-Daniel I. Clinical signs and economic losses caused by porcine reproductive and respiratory syndrome virus in a large breeding farm. *Vet Microbiol.* (1997) 55:317. doi: 10.1016/S0378-1135(96)01326-0
9. Sang Y, Rowland RRR, Blecha F. Interaction between innate immunity and porcine reproductive and respiratory syndrome virus. *Anim Health Res Rev.* (2011) 12:149–67. doi: 10.1017/S1466252311000144
10. Robinson S. *Mechanisms of Immune Protection Against Porcine Reproductive and Respiratory Syndrome Virus (PRRSV).* Dissertations and Theses - Gradworks (2015).
11. Osorio FA, Galeota JA, Nelson E, Brodersen B, Doster A, Wills R, et al. Passive transfer of virus-specific antibodies confers protection against reproductive failure induced by a virulent strain of porcine reproductive and respiratory syndrome virus and establishes sterilizing immunity. *Virology* (2002) 302:9–20. doi: 10.1006/viro.2002.1612
12. Dea S, Gagnon CA, Mardassi H, Pirzadeh B, Rogan D. Current knowledge on the structural proteins of porcine reproductive and respiratory syndrome (PRRS) virus: comparison of the North American and European isolates. *Arch Virol.* (2000) 145:659–88. doi: 10.1007/s007050050662
13. Wootton S, Yoo D, Rogan D. Full-length sequence of a Canadian porcine reproductive and respiratory syndrome virus (PRRSV) isolate. *Arch Virol.* (2000) 145:2297–323. doi: 10.1007/s007050070022
14. Chen Z, Lawson S, Sun Z, Zhou X, Guan X, Christopher-Hennings J, et al. Identification of two auto-cleavage products of nonstructural protein 1 (nsp1) in porcine reproductive and respiratory syndrome virus infected cells: nsp1 function as interferon antagonist. *Virology* (2010) 398:87–97. doi: 10.1016/j.virol.2009.11.033
15. Xue F, Sun Y, Yan L, Zhao C, Chen J, Bartlam M, et al. The crystal structure of the PRRSV nonstructural protein nsp1{beta} reveals a novel metal. *J Virol.* (2010) 84:6461–71. doi: 10.1128/JVI.00301-10
16. Fang Y, Snijder EJ. The PRRSV replicase: exploring the multifunctionality of an intriguing set of nonstructural proteins. *Virus Res.* (2010) 154:61–76. doi: 10.1016/j.virusres.2010.07.030
17. Jing H, Fang L, Zhen D, Dang W, Hao W, Li G, et al. Porcine reproductive and respiratory syndrome virus nsp1α inhibits NF-κB activation by targeting the linear ubiquitin chain assembly complex. *J. Virol.* (2017) 91:e01911-16. doi: 10.1128/JVI.01911-16
18. Han M, Du Y, Song C, Yoo D. Degradation of CREB-binding protein and modulation of type I interferon induction by the zinc finger motif of the porcine reproductive and respiratory syndrome virus nsp1α subunit. *Virus Res.* (2013) 172:54–65. doi: 10.1016/j.virusres.2012.12.012
19. Shi X, Chang Y, Zhang X, Wang L, Li C, Jiang K, et al. Small interfering RNA targeting nonstructural protein1 α (nsp1α) of porcine reproductive and respiratory syndrome virus (PRRSV) can reduce the replication of PRRSV in MARC-145 cells. *Res Vet Sci.* (2015) 99:215–7. doi: 10.1016/j.rvsc.2015.01.015
20. Seo J, Lee KJ. Post-translational modifications and their biological functions: proteomic analysis and systematic approaches. *J Biochem Mol Biol.* (2004) 37:35–44. doi: 10.5483/BMBRep.2004.37.1.035
21. Choudhary C, Weinert BT, Nishida Y, Verdin E, Mann M. The growing landscape of lysine acetylation links metabolism and cell signalling. *Nat Rev Mol Cell Biol.* (2014) 15:536–50. doi: 10.1038/nrm3841
22. Wilkinson KD. Ubiquitination and deubiquitination: targeting of proteins for degradation by the proteasome. *Semin Cell Dev Biol.* (2000) 11:141–8. doi: 10.1006/scdb.2000.0164
23. Mueller DL. E3 ubiquitin ligases as T cell anergy factors. *Nat Immunol.* (2004) 5:883–90. doi: 10.1038/ni1106
24. Ikeda F, Dikic I. Atypical ubiquitin chains: new molecular signals. *EMBO Rep.* (2008) 9:536–42. doi: 10.1038/embor.2008.93
25. Spratt DE, Wu K, Kovacev J, Pan ZQ, Shaw GS. Selective recruitment of an E2∼ubiquitin complex by an E3 ubiquitin ligase. *J Biol Chem.* (2012) 287:17374–85. doi: 10.1074/jbc.M112.353748
26. Chen D, Dou QP. The ubiquitin-proteasome system as a prospective molecular target for cancer treatment and prevention. *Curr Protein Pept Sci.* (2010) 11:459–70. doi: 10.2174/138920310791824057
27. Li B, Dou QP. Bax degradation by the ubiquitin/proteasome-dependent pathway: involvement in tumor survival and progression. *Proc Natl Acad Sci USA.* (2000) 97:3850–5. doi: 10.1073/pnas.070047997
28. Denuc A, Marfany G. SUMO and ubiquitin paths converge. *Biochem Soc Trans.* (2010) 38:34–9. doi: 10.1042/BST0380034
29. Kerscher O, Felberbaum R, Hochstrasser M. Modification of proteins by ubiquitin and ubiquitin-like proteins. *Ann Rev Cell Dev Biol.* (2006) 22:159–80. doi: 10.1146/annurev.cellbio.22.010605.093503
30. Wang L, Wansleeben C, Zhao S, Pei M, Paschen W, Wei Y. SUMO2 is essential while SUMO3 is dispensable for mouse embryonic development. *EMBO Rep.* (2014) 15:878–85. doi: 10.15252/embr.201438534
31. Geissfriedlander R, Melchior F. Concepts in sumoylation: a decade on. *Nat Rev Mol Cell Biol.* (2007) 8:947–56. doi: 10.1038/nrm2293
32. Deyrieux A, Rosas-Acosta G, Ozbun M, Wilson V. Sumoylation dynamics during keratinocyte differentiation. *J Cell Sci.* (2007) 120:125. doi: 10.1242/jcs.03317
33. Gill G. Something about SUMO inhibits transcription. *Curr Opin Genet Dev.* (2005) 15:536–41. doi: 10.1016/j.gde.2005.07.004
34. Ihara M, Koyama H, Uchimura Y, Saitoh H, Kikuchi A. Noncovalent binding of small ubiquitin-related modifier (SUMO) protease to SUMO is necessary for enzymatic activities and cell growth. *J Biol Chem.* (2007) 282:16465–75. doi: 10.1074/jbc.M610723200
35. Lee SY, Sang YL, Choi Y. TRAF-interacting Protein (TRIP): a novel component of the Tumor Necrosis Factor Receptor (TNFR)- and CD30-TRAF signaling complexes that inhibits TRAF2-mediated NF-κB activation. *J Exp Med.* (1997) 185:1275–85. doi: 10.1084/jem.185.7.1275
36. Park ES, Choi S, Kim JM, Jeong Y, Choe J, Park CS, et al. Early embryonic lethality caused by targeted disruption of the TRAF-interacting protein (TRIP) gene. *Biochem Biophys Res Commun.* (2007) 363:971–7. doi: 10.1016/j.bbrc.2007.09.103
37. Merkle JA, Rickmyre JL, Garg A, Loggins EB, Jodoin JN, Lee E, et al. *no poles* encodes a predicted E3 ubiquitin ligase required for early embryonic development of *Drosophila*. *Development* (2009) 136:449–59. doi: 10.1242/dev.027599
38. Regamey A, Hohl D, Liu JW, Roger T, Kogerman P, Toftgard R, et al. The tumor suppressor CYLD interacts with TRIP and regulates negatively nuclear factor kappaB activation by tumor necrosis factor. *J Exp Med.* (2003) 198:1959–64. doi: 10.1084/jem.20031187
39. Zhang M, Wang L, Zhao X, Zhao K, Meng H, Zhao W, et al. TRAF-interacting protein (TRIP) negatively regulates IFN-β production and antiviral response by promoting proteasomal degradation of TANK-binding kinase 1. *J Exp Med.* (2012) 209:1703–11. doi: 10.1084/jem.20120024
40. Uddin MJ, Nurogyina PK, Islam MA, Tesfaye D, Tholen E, Looft C, et al. Expression dynamics of Toll-like receptors mRNA and cytokines in porcine peripheral blood mononuclear cells stimulated by bacterial lipopolysaccharide. *Vet Immunol Immunopathol.* (2012) 147:211–22. doi: 10.1016/j.vetimm.2012.04.020
41. Su Y, Shi P, Zhang L, Lu D, Zhao C, Li R, et al. The superimposed deubiquitination effect of OTULIN and Porcine Reproductive and Respiratory Syndrome Virus (PRRSV) Nsp11 promotes multiplication of PRRSV. *J Virol.* (2018) 92:e00175-18. doi: 10.1128/JVI.00175-18
42. Shi P, Zhang L, Wang J, Lu D, Li Y, Ren J, et al. Porcine FcεRI mediates porcine reproductive and respiratory syndrome virus multiplication and regulates the inflammatory reaction. *Virol Sin.* (2018) 33:249–60. doi: 10.1007/s12250-018-0032-3
43. Han M, Kim CY, Rowland RR, Fang Y, Kim D, Yoo D. Biogenesis of non-structural protein 1 (nsp1) and nsp1-mediated type I interferon modulation in arteriviruses. *Virology* (2014) 458–9:136–50. doi: 10.1016/j.virol.2014.04.028
44. Huang C, Zhang Q, Guo X, Yu Z, Xu A, Tang J, et al. Porcine reproductive and respiratory syndrome virus nonstructural protein 4 antagonizes IFN? Expression by targeting NEMO[J]. *J Virol.* (2014) 88:01396–14. doi: 10.1128/JVI.01396-14
45. Chapard C, Meraldi P, Gleich T, Bachmann D, Hohl D, Huber M. TRAIP is a regulator of the spindle assembly checkpoint. *J Cell Sci.* (2014) 127:5149–56. doi: 10.1242/jcs.152579
46. Park IS, Han YG, Chung HJ, Jung YW, Kim Y, Kim H. SUMOylation regulates nuclear localization and stability of TRAIP/RNF206. *Biochem Biophys Res Commun.* (2016) 470:881–7. doi: 10.1016/j.bbrc.2016.01.141
47. Chang TH, Toru K, Mayumi M, Steven J, Bradfute SB, Mike B, et al. Ebola zaire virus blocks type I interferon production by exploiting the

host SUMO modification machinery. *PLoS Pathog.* (2009) 5:e1000493. doi: 10.1371/journal.ppat.1000493
48. El Mchichi B, Regad T, Maroui MA, Rodriguez MS, Aminev A, Gerbaud S. SUMOylation promotes PML degradation during encephalomyocarditis virus infection. *J Virol.* (2010) 84:11634–45. doi: 10.1128/JVI.01321-10
49. Staudinger JL. The molecular interface between the SUMO and ubiquitin systems. In: *SUMO Regulation of Cellular Processes*. Cham: Springer (2017). p. 99–110. doi: 10.1007/978-3-319-50044-7_6
50. Burgess RC, Rahman S, Lisby M, Rothstein R, Zhao X. The Slx5-Slx8 complex affects sumoylation of DNA repair proteins and negatively regulates recombination. *Mol Cell Biol.* (2007) 27:6153–62. doi: 10.1128/MCB.00787-07
51. Mullen JR, Brill SJ. Activation of the Slx5–Slx8 ubiquitin ligase by Poly-small ubiquitin-like modifier conjugates. *J Biol Chem.* (2008) 283:19912–21. doi: 10.1074/jbc.M802690200
52. Stade K. A lack of SUMO conjugation affects cNLS-dependent nuclear protein import in yeast. *J Biol Chem*. (2002) 277:49554–61. doi: 10.1074/jbc.M207991200
53. Saracco SA, Miller MJ, Kurepa J, Vierstra RD. Genetic analysis of SUMOylation in Arabidopsis: conjugation of SUMO1 and SUMO2 to nuclear proteins is essential. *Plant Physiol.* (2007) 145:119–34. doi: 10.1104/pp.107.102285
54. Deyrieux AF, Wilson VG. Viral interplay with the host sumoylation system. *Adv Exp Med Biol.* (2017) 963:359–88. doi: 10.1007/978-3-319-50044-7_21
55. Han J. *Characterization of the Multidomain Nsp2 Replicase Protein of Porcine Reproductive and Respiratory Syndrome Virus.* Dissertations and Theses (2008).
56. Hendriks IA, D'Souza RC, Yang B, Verlaande VM, Mann M, Vertegaal AC. Uncovering global SUMOylation signaling networks in a site-specific manner. *Nat Struct Mol Biol.* (2014) 21:927–36. doi: 10.1038/nsmb.2890
57. Klenk C, Humrich J, Quitterer U, Lohse MJ. SUMO-1 controls the protein stability and the biological function of phosducin. *J Biol Chem.* (2006) 281:8357–64. doi: 10.1074/jbc.M513703200
58. Escobarramirez A, Vercoutteredouart AS, Mortuaire M, Huvent I, Hardivillé S, Hoedt E, et al. Modification by SUMOylation controls both the transcriptional activity and the stability of delta-lactoferrin. *PLoS ONE* (2015) 10:e0129965. doi: 10.1371/journal.pone.0129965
59. Ii T, Fung J, Mullen JR, Brill SJ. The yeast Slx5-Slx8 DNA integrity complex displays ubiquitin ligase activity. *Cell Cycle* (2007) 6:2800–9. doi: 10.4161/cc.6.22.4882
60. Ii T, Mullen JR, Slagle CE, Brill SJ. Stimulation of *in-vitro* sumoylation by Slx5-Slx8: evidence for a functional interaction with the SUMO pathway. *DNA Repair* (2007) 6:1679–91. doi: 10.1016/j.dnarep.2007.06.004
61. Rodriguez MS, Dargemont C, Hay RT. SUMO-1 conjugation *in vivo* requires both a consensus modification motif and nuclear targeting. *J Biol Chem.* (2001) 276:12654–9. doi: 10.1074/jbc.M009476200
62. Zhi C, Liu S, Sun W, Lei C, Yoo D, Feng L, et al. Nuclear export signal of PRRSV NSP1α is necessary for type I IFN inhibition. *Virology* (2016) 499:278–87. doi: 10.1016/j.virol.2016.07.008
63. Tijms MA, Snijder EJ. Equine arteritis virus non-structural protein 1, an essential factor for viral subgenomic mRNA synthesis, interacts with the cellular transcription co-factor p100. *J Gen Virol.* (2003) 84:2317–22. doi: 10.1099/vir.0.19297-0
64. Kawai T, Akira S. Regulation of innate immune signalling pathways by the tripartite motif (TRIM) family proteins. *EMBO Mol Med.* (2011) 3:513–27. doi: 10.1002/emmm.201100160
65. Nakhaei P, Mesplede T, Solis M, Sun Q, Zhao T, Yang L, et al. The E3 ubiquitin ligase Triad3A negatively regulates the RIG-I/MAVS signaling pathway by targeting TRAF3 for degradation. *Cytokine* (2008) 43:e1000650. doi: 10.1371/journal.ppat.1000650
66. Arimoto K, Takahashi H, Hishiki T, Konishi H, Fujita T, Shimotohno K. Negative regulation of the RIG-I signaling by the ubiquitin ligase RNF125. *Proc Natl Acad Sci USA.* (2007) 104:7500–5. doi: 10.1073/pnas.0611551104

Conflict of Interest Statement: The authors declare that the research was conducted in the absence of any commercial or financial relationships that could be construed as a potential conflict of interest.

frontiers in Immunology

ORIGINAL RESEARCH
published: 13 March 2019
doi: 10.3389/fimmu.2019.00363

Senecavirus A 3C Protease Mediates Host Cell Apoptosis Late in Infection

*Maureen H. V. Fernandes, Mayara F. Maggioli, Jaelin Otta, Lok R. Joshi, Steve Lawson and Diego G. Diel**

Animal Disease Research And Diagnostic Laboratory, Department of Veterinary and Biomedical Sciences, South Dakota State University, Brookings, SD, United States

Senecavirus A (SVA), an oncolytic picornavirus used for cancer treatment in humans, has recently emerged as a vesicular disease (VD)-causing agent in swine worldwide. Notably, SVA-induced VD is indistinguishable from foot-and-mouth disease (FMD) and other high-consequence VDs of pigs. Here we investigated the role of apoptosis on infection and replication of SVA. Given the critical role of the nuclear factor-kappa B (NF-κB) signaling pathway on modulation of cell death, we first assessed activation of NF-κB during SVA infection. Results here show that while early during infection SVA induces activation of NF-κB, as evidenced by nuclear translocation of NF-κB-p65 and NF-κB-mediated transcription, late in infection a cleaved product corresponding to the C-terminus of NF-κB-p65 is detected in infected cells, resulting in lower NF-κB transcriptional activity. Additionally, we assessed the potential role of SVA 3C protease ($3C^{pro}$) in SVA-induced host-cell apoptosis and cleavage of NF-κB-p65. Transient expression of SVA $3C^{pro}$ was associated with cleavage of NF-κB-p65 and Poly (ADP-ribose) polymerase (PARP), suggesting its involvement in virus-induced apoptosis. Most importantly, we showed that while cleavage of NF-κB-p65 is secondary to caspase activation, the proteolytic activity of SVA $3C^{pro}$ is essential for induction of apoptosis. Experiments using the pan-caspase inhibitor Z-VAD-FMK confirmed the relevance of late apoptosis for SVA infection, indicating that SVA induces apoptosis, presumably, as a mechanism to facilitate virus release and/or spread from infected cells. Together, these results suggest an important role of apoptosis for SVA infection biology.

Keywords: Senecavirus A, Seneca Valley virus, apoptosis, 3C protease, virus egress

OPEN ACCESS

Edited by:
Anastasia N. Vlasova, The Ohio State University, United States

Reviewed by:
Cheryl Dvorak, University of Minnesota Twin Cities, United States
Mads Gyrd-Hansen, University of Oxford, United Kingdom

****Correspondence:***
Diego G. Diel
diego.diel@sdstate.edu

Specialty section:
This article was submitted to Viral Immunology, a section of the journal Frontiers in Immunology

Received: *26 October 2018*
Accepted: *12 February 2019*
Published: *13 March 2019*

Citation:
Fernandes MHV, Maggioli MF, Otta J, Joshi LR, Lawson S and Diel DG (2019) Senecavirus A 3C Protease Mediates Host Cell Apoptosis Late in Infection. Front. Immunol. 10:363. doi: 10.3389/fimmu.2019.00363

INTRODUCTION

Senecavirus A (SVA) is a non-enveloped single-stranded positive-sense RNA virus of the genus *Senecavirus*, family *Picornaviridae* (1, 2). SVA was first detected as a cell culture contaminant in 2002 in the United States (US) (3), and subsequently identified as a novel picornavirus closely related to members of the genus *Cardiovirus* (1). The SVA genome is approximately 7.2 kb in length containing a single open reading frame (ORF) that encodes a 2181 aa polyprotein, which is cleaved into four structural proteins (VP1, VP2, VP3, and VP4) and eight non-structural proteins (L, 2A, 2B, 2C, 3A, 3B, 3C, and 3D) (1). Processing of the polyprotein into mature viral proteins is catalyzed by the non-structural protein $3C^{pro}$, a virus-encoded cysteine protease that contains a conserved His, Asp, Cys catalytic triad (1, 4). While the structural proteins of picornaviruses form the virus capsid and are involved in receptor binding and cell entry, non-structural proteins are mainly responsible for virus replication (5) and play important roles on virus-host interactions contributing to innate immune evasion, virus virulence and pathogenesis (6–28).

Since its identification, SVA has been associated with sporadic cases of vesicular disease in pigs in the US and Canada (29–31). However, after 2014, outbreaks of vesicular disease associated to SVA have been reported in major swine producing countries around the world (32–36). The lesions observed during these outbreaks include vesicles on the snout, oral mucosa and feet, involving the coronary bands, interdigital space, due claws, and/or sole (29, 31, 33, 34, 37, 38). This clinical presentation was also observed in experimentally infected animals (39–42). Importantly, SVA-induced disease is clinically indistinguishable from other high consequence vesicular diseases of swine, including foot-and-mouth-disease (FMD), swine vesicular disease (SVD), vesicular stomatitis (VS), and vesicular exanthema of swine (VES) (31, 43).

In addition to its relevance to animal health, SVA has been tested as an oncolytic agent for cancer treatment in humans (2, 44–47). Given the promising results in animal models, SVA was tested in phase I clinical trials, becoming the first oncolytic picornavirus to be tested in humans (47, 48). The main limitations to the broad use of SVA as an oncolytic agent in humans, however, are the development of neutralizing antibodies that result in rapid viral clearance from treated patients and the fact that the molecular basis of SVA's oncolytic activity remain unknown (49). A better understanding of the molecular SVA-host interactions and of the mechanism(s) underlying virus replication in susceptible cells may allow the development of improved SVA-based therapeutics for cancer treatment.

Picornaviruses modulate many host cellular pathways, including the host translation machinery, innate immune responses and cell survival or apoptosis. Foot-and-Mouth disease virus (FMDV), for example has been shown to inhibit nuclear factor kappa B- (NF-κB) (18) and interferon beta (IFN-β) signaling (28). Enteroviruses, on the other hand, were shown to take advantage of the host secretory autophagy pathway to enhance their transmissibility (50) and cardioviruses were shown to inhibit nucleocytoplasmic trafficking of host cell proteins (7). Another important cellular process that is targeted by several picornaviruses is programmed cell death, or apoptosis. Poliovirus has been shown to modulate apoptosis and is known to inhibit or induce host cell death during different phases of the infection (51, 52), while Coxsackievirus B3 (53), and Hepatitis A virus (54) are known to induce apoptosis. Recently, apoptosis was observed in lesions caused by FMDV in the tongue of experimentally infected pigs (55). These observations highlight the importance of modulation of host cell apoptosis for the infection biology of picornaviruses.

While apoptosis usually functions as a host defense mechanism that ensures killing of infected cells (56, 57), several viruses, including picornaviruses, have been shown to induce apoptosis to enable efficient virus transmission while avoiding overt inflammatory responses and activation of the immune system (58). Activation of apoptosis occurs mainly by two distinct pathways, the intrinsic and extrinsic pathways, which utilize executioner caspases (Casp–3, –6, and –7) to induce cell death (56, 59). Caspases are a family of serine proteases that mediate many features of apoptosis (57). These enzymes are maintained in the cell cytoplasm as inactive proenzymes comprising two subunits (large and small) and a variable amino terminal prodomain. Activation of the caspases requires loss of the prodomain through catalytic cleavage of a C-terminal aspartate residue and dimerization of the large and small subunits to form the active protease (57, 60). Apoptotic responses are usually initiated by activation of Casp-8 or Casp-9 (via tumor necrosis factor receptor or Fas, respectively), whose activity results in downstream activation of the effector Casp–3, –6, and –7 (57, 60). These effector enzymes cause cellular disassembly through cleavage of cell death substrates, including lamin, poly(ADP-ribose) polymerase (PARP) or the caspase-activated DNase/DNA fragmentation factor (CAD/DFF) complex (61–63). Additional substrates of the effector caspases include pro-survival transcription factors, such as NF-κB (64, 65). Collectively, the action of the caspases result in fragmentation of cellular DNA and cell death (57, 62, 63).

NF-κB is a ubiquitous transcription factor that modulates not only cell death but also innate immunity and inflammatory responses. This pathway seems to play critical roles in the picornaviral life cycle (8, 11, 14, 16, 18, 19, 22, 27, 66). Activation of the NF-κB signaling pathway by viruses is mediated by pattern recognition receptors (PRRs) which detect pathogen associated molecular patterns (PAMPs; including double-stranded RNA [dsRNA] and/or viral proteins) and initiate the signaling cascade that leads to host gene transcription (67, 68). In unstimulated cells, the NF-κB transcription factors (NF-κB-p50, -p52, -p65, RelB, or c-Rel) form homo- or heterodimers (69), that are sequestered by the NF-κB inhibitor alpha (NFκBIA/IκBα) in the cell cytoplasm (70). Once the pathway is activated, IκBα is phosphorylated by upstream IκB kinases (IKKα, IKKβ), triggering its proteasomal degradation and leading to translocation of NF-κB subunits to the nucleus, where they undergo additional post-translational modifications and modulate transcription of pro-inflammatory-, innate immunity-, and/or apoptosis-related genes (69). In this context, NF-κB seems to play an essential role in protecting host cells from picornavirus-induced apoptosis (71).

In the present study, we investigated the host apoptotic responses during SVA infection and dissected the interplay between the virus, host cell apoptosis and NF-κB signaling. Results here show that SVA induces apoptosis late in infection, which plays a critical role on the virus infection cycle, likely facilitating virus release from infected cells.

MATERIALS AND METHODS

Cells and Virus

Primary swine turbinate (STu) and NCI-H1299 non-small human lung carcinoma cell lines (ATCC® CRL-5803) were cultured at 37°C with 5% CO_2 in minimum essential medium (MEM, Corning®) or RPMI 1640 medium (Corning®) supplemented with 20 or 10% fetal bovine serum (FBS; Seradigm), respectively. Cell culture media was supplemented with 2 mM L-glutamine (Corning®), penicillin (100 IU/mL; Corning®), streptomycin (100 μg/mL; Corning®), and gentamicin (50 μg/ml; Corning®). Senecavirus A strain SD15-26 was isolated from a vesicular lesion from a finishing pig and

has been previously characterized (39). Low passage (passage 4) SVA stocks were prepared and titrated in H1299 cells, and used in all experiments involving SVA infection described here.

Plasmids

Luciferase reporter plasmids (pNF-κB-luciferase reporter, and pRL-TK control plasmids) are commercially available (Promega). The coding sequence of SVA $3C^{pro}$ was fused with Flag-tag (N-terminus fusion), chemically synthesized (GenScript), and cloned into the pcDNA3.1 expression plasmid (pcDNA-Flag-3C). Additionally, SVA $3C^{pro}$ was amplified from SVA strain SD15-26 by RT-PCR and cloned into the eukaryotic expression plasmid pET28a as a His-tag fusion protein (pET28-SVA-3C). SVA strain SD15-26 VP1 expressing plasmid (pcDNA-HA-VP1) was kindly provided by Dr. Steve Lawson (Department of Veterinary and Biomedical Sciences, South Dakota State University). Control plasmid pCMV-Flag-BAP is commercially available (Sigma). The plasmid pCMV-HA-NF-κB-p65 was constructed by standard cloning techniques. Briefly, porcine NF-κB-p65 coding sequence (GenBank NM_001114281) was PCR amplified from cDNA prepared from swine testicle (ST) cells and cloned in fusion with the HA epitope tag into the pCMV-HA-N expression vector (Clontech). Sequence identity of the expression plasmids generated here were confirmed by DNA sequencing.

Antibodies and Reagents

Antibodies against β-actin (clone C4), NF-κB-p65 (clone C-20; C-terminus), NF-κB-p65 (clone F-6), and IκBα (clone H4) were purchased from Santa Cruz Biotechnology. Antibodies against NF-κB-p65 (clone C22B4; N-terminus), IKKα (clone3G12), IKKβ (D30C6), cleaved caspase-3 (Asp175, clone 5A1E), and PARP (clone 46D11) were obtained from Cell Signaling. SVA VP1 and SVA VP2 mouse monoclonals and SVA whole virus antibodies were kindly provided by Dr. Steve Lawson (SDSU). Anti-Flag or anti-HA mouse monoclonal antibodies are commercially available (GenScript and Thermo Scientific, respectively). Anti-rabbit and/or anti-mouse secondary antibodies conjugated with Alexa Fluor® 594 and Alexa Fluor 488® were purchased from Life Technologies. IRDye 800CW-labeled anti mouse IgG and IRDye 680-labeledRD anti rabbit IgG secondary antibodies were purchased from Li-Cor Biosciences. Recombinant TNF-α was obtained from InvivoGen. Staurosporine was purchased from Cell Signaling and Z-VAD-FMK was obtained from Santa Cruz Biotechnology.

SVA $3C^{pro}$-Specific Rabbit Antibody Production

SVA $3C^{pro}$ was expressed using a prokaryotic expression system. SVA $3C^{pro}$ coding sequence (GenBank KX778101) was PCR amplified from cDNA of SVA SD15-26 and cloned into the bacterial expression plasmid pET-28a (EMD Millipore/Novagen). The recombinant protein was expressed in *Escherichia coli* strain BL-21 cells as a 6×His-tag fusion protein and purified using nickel-charged agarose resin (Qiagen) according to the manufacturer's instructions. Purified recombinant protein was used for polyclonal antibody production in rabbits.

One adult 12-week old rabbit was kept in an individual cage with food and water *ad libitum* throughout the study. The animal was immunized with 660 ng of SVA $3C^{pro}$ emulsified in water-in-oil (W/O) adjuvant (1:1; 1 mL:1 mL; Montanide™ ISA 50 V2, Seppic). The antigen was administered by three 0.5 mL subcutaneous injections and one 0.5 mL intramuscular injection. Two weeks post-primary immunization the animal received a booster immunization as above. Two weeks after the booster immunization the rabbit was euthanized and exsanguinated, and polyclonal serum containing SVA $3C^{pro}$-specific antibodies was isolated by centrifugation (at 2,000 × g for 15 min at 4°C). All animal procedures and protocols for antibody production were reviewed and approved by the South Dakota State University Institutional Animal Care and Use Committee (IACUC) under approval number 15-095A.

Terminal Deoxynucleotidyltransferase-Mediated dUTP-Biotin Nick-End Labeling (TUNEL)

Primary STu cells were cultured on glass cover slips and infected with SVA (MOI = 5) or mock-infected and then fixed at 12 h p.i. with 3.7% formaldehyde in PBS (pH 7.2) for 20 min. Positive control cells were treated with 0.1 μM staurosporine for 4 h and then fixed as above. Additionally, formaline-fixed paraffin-embedded (FFPE) tissue sections from a previous SVA pathogenesis experiment conducted in our laboratory (40) were subjected to TUNEL. Cell cultures or tissue samples were permeabilized and stained with an *in situ* cell death detection kit (TUNEL, Abcam) according to the manufacturer's instructions.

Histopathology

Formalin-fixed paraffin-embedded tissue sections (skin) from a previous SVA animal experiment were processed following standard histological procedures and stained with hematoxylin and eosin for histological examination. All animal procedures and protocols were reviewed and approved by the SDSU IACUC under approval number 16-002A.

In situ Hybridization

Formalin-fixed paraffin-embedded tissue sections (skin) were used to perform *in situ* hybridization (RNAScope®). ISH probe utilized was specific for the viral genome SVV (301-1345 region of VP1 gene, GenBank: EU271758.1, Advanced Cell Diagnostics, Inc.). The ISH was performed as previous described (72).

Flow Cytometry

Activation of caspase 3 and 7 (Casp-3/-7) was assessed by flow cytometry during SVA infection. Semi-confluent STu or H1299 cells were cultured in 12-well plates and infected with SVA (MOI = 5). At 2, 4, 5, 6, 7, 8, and 10 h p.i. the supernatant was removed and the cells trypsinized to dissociate the monolayer. Mock-infected cells and mock-infected cells treated with 0.3 μM staurosporine were used as negative and positive controls, respectively. After trypsinization, cells and supernatant were mixed and centrifuged at 1,500 × g for 5 min at 4°C. Activation of Casp-3/-7 was assessed using the CellEvent™ Caspase-3/7 Green Flow Cytometry Assay kit (Thermo Fisher Scientific)

according to manufacturer's protocol. The flow cytometry data were acquired with an Attune NxT flow cytometer (Thermo Fisher Scientific) and analyzed using FlowJo software (TreeStar).

To investigate activation of Casp-3/-7 in the context of NF-κB-p65 expression and SVA infection, STu cells were transfected with 1 μg of pCMV-HA-NF-κB-p65 or empty pCMV-HA plasmids (control) using Lipofectamine 3000 (Life Technologies) and subsequently infected with SVA (MOI = 5). Cells were collected at 4, 7, 8, and 10 h p.i. and processed for flow cytometry assessment of Casp-3/-7 activation as described above.

Growth Curve

SVA growth curves were performed in STu and H1299 cells. Cells were cultured in 12-well plates, inoculated with SVA (MOI = 5) and harvested at 2, 4, 8, 12, and 24 h p.i. Virus titers were determined on each time by limiting dilutions in H1299 cells. At 48 h p.i. cells were fixed (3.7% formaldehyde), permeabilized (0.2% Triton-X), and stained with an anti-SVA whole virus rabbit polyclonal antibody. Viral titers were determined by the Spearman and Karber's method (73) and expressed as tissue culture infectious dose 50 ($TCID_{50}$) per milliliter.

The effect of NF-κB pathway activation during SVA replication was assessed by overexpression of NF-κB-p65 in STu cells. For this, semi-confluent STu cells were plated in 12-well plates and transfected with 1 μg of pCMV-HA-NF-κB-p65 or empty pCMV-HA (control) per well using Lipofectamine 3000 (Life Technologies) as recommended by the manufacturer. At 24 h post-transfection, cells were infected with SVA (MOI = 0.1). After 1 h adsorption, the inoculum was removed and fresh media was added. The cells were harvested at 2, 4, 8, 12, and 24 h p.i. and virus titers determined as described above.

To assess the role of apoptosis on SVA infection cycle, multiple-step growth curves were performed in STu or H1299 cells. Cells were plated in 12-well plates and infected with SVA (MOI = 0.1). After 1 h adsorption, fresh media containing 30 μg/mL of Z-VAD-FMK, a pan-caspase inhibitor was added to the cells. Plain media was added to untreated control wells. Cells and supernatant were collected separately at 2, 4, 8, 12, and 24 h p.i. and subjected to virus titration. Additionally, the effect of apoptosis on SVA infection was assessed in STu cells infected with a high MOI. For this, cells were infected with SVA at an MOI = 5 and cells and supernatant collected separately at 8 h p.i. and subjected to virus titrations.

RNA Extraction and Quantitative Reverse-Transcription-PCR (RT-qPCR)

To determine transcription levels of NF-κB target genes during SVA infection we performed RT-qPCR. STu cells cultured in 6-well plates were infected with SVA (MOI = 5), collected at 2, 4, 8, and 12 h p.i., and cellular RNA extracted using TRIzol reagent (Invitrogen) according to manufacturer's protocol. RNA samples were treated with DNase (Ambion) and further cleaned using the RNeasy® Mini kit (QIAGEN). Mock infected cells were used as a negative control. Transcription levels of TNF-α, Caspase 8, FADD, BAX, BAK, BCL-2, XIAP, CXCL8, PTGS2, IRF1, and NF-κBIA genes were determined using RT-qPCR and TaqMan gene expression assays (Thermo Scientific). The housekeeping gene glyceraldehyde 3-phosphate dehydrogenase (GAPDH) was used as loading control. RT-qPCR reactions were performed using the RNA-to-Ct™ 1 Step-kit and TaqMan assays for each target gene. The amplification/detection reactions were performed in a 7500 Real Time PCR System (Applied Biosystems). Transcription of target gene was normalized to that of GAPDH and genome copy numbers were determined using the relative quantitation method. Data were analyzed and expressed as fold changes normalized to levels of RNA detected in mock infected cells.

Indirect Immunofluorescence (IFA)

Expression and activation of NF-κB-p65 was assessed during early stages of SVA infection by IFA. STu cells cultured in 24-wells plates were infected with SVA (MOI = 5). At 0, 2, and 4 h p.i. cells were fixed using 3.7% formaldehyde in PBS (pH 7.2) for 20 min. The cells were washed three times with PBS and permeabilized with 0.2% Triton X-100 in PBS for 10 min at room temperature (RT). Plates were incubated for 1 h at RT with an antibody specific for the C-terminus-NF-κB-p65 (1:250 in PBS/1% BSA) and for SVA (1:250 in PBS/1% BSA). After primary antibody incubation, cells were washed as above and incubated for 1 h at RT with appropriate secondary antibodies conjugated with Alexa Fluor 594 and/or 488 (1:250 in PBS/1% BSA). Cells were washed three times with PBS and nuclear stain was performed with DAPI (Thermo Scientific). Cells were visualized using a fluorescence microscope (Olympus CKX53, 40× magnification).

Expression and activation of NF-κB-p65 was also assessed during late stages of SVA infection by IFA. STu cells cultured in 24-well plates were infected with SVA (MOI = 1). At 7 and 8 h p.i. cells were fixed and IFA was performed as described above.

The effect of SVA $3C^{pro}$ on expression of NF-κB-p65 was assessed by IFA. H1299 cells were transfected with pcDNA-Flag-3C (100 μg) expression plasmid and subjected to IFA staining. C-terminus-NF-κB-p65 (1:250 in PBS/1% BSA) and Flag-Tag-specific antibodies (1:250 in PBS/1% BSA) were used as primary antibodies. All IFA steps were performed as described above.

Western Blots

The effect of SVA on apoptosis and NF-κB signaling pathway was investigated by western blots. Semi-confluent monolayers of STu cells cultured in 6-well plates were infected with SVA (MOI = 10) and harvested at 0.5, 1, 2, 3, 4, 8, and 12 h p.i. Mock-infected cells were used as negative controls. This experiment was also performed in H1299 cells, with samples collected at 4, 8, 12, and 24 h p.i. Mock-infected cells unstimulated or stimulated with 100 ng/mL of TNF-α were used as negative and positive controls, respectively. Cells were lysed with M-PER mammalian extraction reagent (Thermo Scientific) containing protease inhibitors (RPI). One hundred microgram whole cell protein extracts was resolved by SDS-PAGE in 10% acrylamide gels and transferred to nitrocellulose membranes. Blots were incubated with 5% non-fat dry milk in PBS overnight at 4°C and then probed with the antibodies indicated in the Figures, followed by incubation with appropriate Dye-light fluorescent conjugate secondary antibodies. The membranes were scanned with the Odyssey

infrared imaging system (Li-Cor). Densitometric analysis was performed using ImageJ® with expression levels of selected target proteins being normalized to those of the housekeeping gene β-actin.

The effect of SVA $3C^{pro}$ on apoptotic pathways was assessed under transient expression experiments. H1299 cells cultured in 6-wells plates were transfected with 2 μg of pcDNA-Flag-3C and harvested at 18 h post-transfection. Positive control cells were stimulated with TNF-α (100 ng/mL) for 1 h. In the experiments with catalytic dead mutants of SVA $3C^{pro}$, H1299 cells were transfected with 2 μg of pcDNA-Flag-3C, pcDNA-Flag-3C(H47D), or pcDNA-Flag-3C(C159R) and harvested 18 h post-transfection. Protein extracts and western blots were performed as described above.

To assess the expression of SVA $3C^{pro}$ during viral replication and its relationship with the cleavage of NF-κB-p65 and apoptosis, STu cells were infected with SVA (MOI = 10) and collected the total protein extract at 2, 4, 5, 6, 7, 8, and 12 h p.i. Western blot was performed as above, and the blots were probed with antibodies indicated in the Figures.

To determine the cleavage site of NF-κB-p65, semi-confluent H1299 cells were cultured in 6-well plates and co-transfected with an empty plasmid (negative control) or pcDNA-Flag-3C (2 μg/well) and either pCMV-HA-NF-κB-p65, pCMV-HA-NF-κB-p65(478R/479D), pCMV-HA-NF-κB-p65(482R/483D), pCMV-HA-NF-κB-p65(478R-483D), pCMV-HA-NF-κB-p65(444L-450R), pCMV-HA-NF-κB-p65(464V-467E), pCMV-HA-NF-κB-p65(444L-450R 478R-483D), or pCMV-HA-NF-κB-p65(464V-467E 478R-483D) (1 μg of each). Cells were harvested at 18 h post-transfection and protein extracts and western blots performed as described above. Antibodies used are indicated in **Figures 8B–D**.

To investigate if caspases or SVA $3C^{pro}$ were responsible for NF-κB-p65 cleavage, semi-confluent H1299 cells were cultured in 6-well plates and co-transfected with an empty plasmid (negative control) or pcDNA-Flag-3C (1 μg/well) and pCMV-HA-NF-κB-p65 (2 μg/well). At 3 h post-transfection, fresh media was added to negative controls and fresh media containing or not 150 μg/mL of Z-VAD-FMK was added to the cells transfected with pcDNA-Flag-3C and pCMV-HA-NF-κB-p65. Cells were harvested at 18 h post-transfection and protein extracts and western blots performed as described above. Antibodies used are indicated in **Figure 8E**.

Luciferase Reporter Assays

The effect of SVA on NF-κB-mediated transcription was investigated by luciferase reporter assays. To detect the ability of SVA to inhibit NF-κB activation, semi-confluent H1299 cells cultured in 24-well plates were co-transfected with the NF-κB-luciferase reporter plasmid (315 ng/well) and the control plasmid pRL-TK (35 ng/well) using Lipofectamine 3000 (Life Technologies) and infected with SVA (MOI = 5). SVA-infected cells were stimulated or not with TNF-α (100 ng/mL) at 2, 4, 8, or 12 h p.i. and incubated for 12 h post-TNF-α stimulation. Mock-infected cells were also stimulated with TNF-α for 12 h. The dual-luciferase reporter system (Promega) was used to determine the luciferase activity in each treatment condition following the manufacturer's instructions. Firefly luciferase activity was normalized to renilla luciferase activity and fold-changes calculated based on the levels of luciferase detected in mock-infected/non-stimulated cells.

The effect of SVA $3C^{pro}$ on NF-κB-mediated transcription was investigated by luciferase assays. H1299 cells were co-transfected with pNF-κB-luciferase reporter plasmid (315 ng/well), pRL-TK (35 ng), and either pcDNA-Flag-3C (550 ng/well), or control plasmids pCMV-Flag-BAP (550 ng/well) or pcDNA-HA-VP1 (550 ng/well). At 14 h post-transfection cells were stimulated with TNF-α, harvested at 12 h post-TNF-α-stimulation and the luciferase activity was determined as described above.

To assess whether the proteolytic activity of $3C^{pro}$ is required for its effect on NF-κB-mediated transcription, H1299 cells were co-transfected with pNF-κB-luciferase reporter plasmid (315 ng/well), pRL-TK (35 ng), and either pcDNA-Flag-3C (550 ng/well), pcDNA-Flag-3C(H47D) (550 ng/well), or pcDNA-Flag-3C(C159R) (550 ng/well) expression plasmids. At 14 h post-transfection, cells were stimulated with TNF-α, harvested at 12 h post-TNF-α-stimulation and the luciferase activity was determined as described above.

Site-Direct Mutagenesis

Mutations in the catalytic triad of SVA $3C^{pro}$ and in the porcine NF-κB-p65 were introduced in the SVA $3C^{pro}$- and NF-κB-p65-encoding plasmids using the Q5® Site-Directed Mutagenesis Kit (New England BioLabs® Inc.) according to the manufacturer's instructions. Site directed mutagenesis primers containing nucleotide substitutions targeting amino acids H47 and C159 leading to substitutions of H to D, or C to R on SVA $3C^{pro}$ were designed and used with the site-direct mutagenesis protocol to generate the mutant plasmids pcDNA-Flag-3C(H47D) and pcDNA-Flag-3C(C159R). NF-κB-p65-specific primers containing nucleotide substitutions targeting the putative SVA $3C^{pro}$ cleavage sites individually (478QL and 482QG) or simultaneously 478QLLNQG were designed and used with the site-direct mutagenesis protocol, resulting in plasmids pCMV-HA-NF-κB-p65(478R/479D), pCMV-HA-NF-κB-p65(482R/483D), and pCMV-HA-NF-κB-p65(478R-483D), respectively. Primers containing nucleotide substitutions targeting putative caspase cleavage sites in NF-κB-p65 coding sequence (444LQFDTDED and 464VFTD) were designed and used with site directed mutagenesis kit, resulting in plasmids pCMV-HA-NF-κB-p65(444L-450R) and pCMV-HA-NF-κB-p65(464V-467E). Double caspase and SVA $3C^{pro}$ cleavage site-mutants were also generated, resulting in plasmids pCMV-HA-NF-κB-p65(444L-450R 478R-483D) and pCMV-HA-NF-κB-p65(464V-467E 478R-483D). The sequences of each NF-κB-p65 mutant are indicated in **Figure 8E**. Correct nucleotide substitutions were confirmed by DNA sequencing.

Three-Dimensional Protein Structure Prediction

The SVA $3C^{pro}$ template-based protein structure modeling was performed using RaptorX web server (74). The best template

for SVA $3C^{pro}$ was the 2wv4A [Foot-and-Mouth disease virus 3C, p-value 1.48e-09 (75)]. SVA $3C^{pro}$ structure prediction was designed using the PyMOL Molecular Graphics System, version 2.0 Schrödinger, LLC.

Plaque Assay

Confluent primary STu cells cultured in 6-well plates were infected with serial 10-fold dilutions of SVA (titer $10^{7.88}$). After 1 h adsorption, the inoculum was removed and fresh 1%-agarose media containing or not 50 μg/mL of Z-VAD-FMK was used to overlay the cells. The agarose overlay was removed and cells were fixed at 24 h p.i. with 3.7% formaldehyde in PBS (pH 7.2) for 20 min. The cells were stained with 1% Crystal Violet solution for 20 min and washed four times with PBS. The area in mm^2 of each viral plaque was calculated using ImageJ®.

Statistical Analysis

The average of three independent experiments is presented where appropriate. Error bars represent standard error of the mean (±SEM). Statistical significance of the data was assessed using the *Students*' *t*-test, Mann-Whitney *U*-test or *Sidak's* multiple comparisons test. The level of statistical significance was defined as $p < 0.05$.

RESULTS

SVA Infection Induces Apoptosis *in vitro* and *in vivo*

Replication of SVA in primary STu cells induces cytopathic effect (CPE) characterized by cell rounding and plasma membrane blebbing (**Figure 1A**). Therefore, induction of apoptosis was investigated during SVA infection. Initially, TUNEL was performed in SVA-infected cells to detect exposed 3′-OH ends of DNA fragments, which are generated in response to apoptotic signals. As shown in **Figure 1B**, apoptotic nuclei were detected in SVA-infected cells and cells treated with staurosporine (a potent inducer of apoptosis) (arrows), suggesting induction of apoptosis during SVA infection.

To assess whether apoptosis occurs during viral infection in the swine host *in vivo*, paraffin-embedded skin sections collected from SVA-infected pigs on day 7 post-infection (p.i.), were subjected to TUNEL. Skin sections were obtained from characteristic SVA vesicular lesions (**Figure 1C**). Sequential skin sections were subjected to H&E staining, ISH to detect SVA RNA and TUNEL to detected apoptosis. As shown in **Figure 1D,** strong brown staining indicating the presence of apoptotic cells was detected by TUNEL (**Figure 1D**, middle panels), in an area that presented histological changes caused by SVA replication in the dermis and epidermis (**Figure 1D**, left panels), and that coincided with the ISH staining for SVA RNA (**Figure 1D**, right panels).

Since Casp-3/-7 are the main executioners of apoptosis, and are responsible for the proteolytic cleavage of many cellular proteins during cell death (57), we assessed their activation during SVA infection by flow cytometry. SVA induced activation of Casp-3/-7 from 7 h p.i. onward in STu cells, with an increasing number of cells containing active caspases detected until 10 h p.i. (**Figures 2A,B**). Notably, the frequency of live cells with active Casp-3/-7 representing cells in early stages of apoptosis were ∼4-fold higher at 8 h p.i. (25.56%; $p < 0.05$) than those detected at 7 h p.i. (6.29%, when compared to mock-infected cells) (**Figure 2B**). Interestingly, at 10 h p.i., the percentage of active Casp-3/-7 detected in Sytox-green positive cells, indicating late stages of apoptosis, reached 46.23% ($p < 0.01$ when compared to mock-infected cells). A significant increase in the frequency of cells presenting active Casp-3/-7 was also detected at 8–10 h p.i. (7.6–14.2%, $p < 0.01$ when compared to mock-infected cells) in SVA-infected H1299 cells (**Figure 2C**). Similar to the results in STu cells, the frequency of late-stage apoptotic cells (Casp-3/7 and Sytox positive cells) was markedly increased at 10 h p.i. in H1299 cells. These results demonstrate that Casp-3/-7 are activated between 7 and 10 h post-SVA infection, which corresponds to the time in which the virus completes one round/cycle of replication (**Figure 2D**). Together these results demonstrate that SVA infection induces apoptosis late during infection *in vitro* and in skin lesions in the natural swine host *in vivo*.

SVA Infection Modulates Expression of Pro-Inflammatory and Apoptosis Related Genes

NF-κB is one of the major players modulating host cell apoptosis and pro-inflammatory responses (76, 77). Thus, we assessed transcription of NF-κB-regulated genes during SVA infection. For this, STu cells were mock-infected or infected with SVA (MOI = 5) and total RNA was extracted during infection (2, 4, 8, and 12 h). As shown in **Figures 3A–F**, all pro- (Casp-8, FADD, BAX, and BAK) or anti-apoptotic (BCL-2 and XIAP) genes tested were down regulated at early time points post-SVA infection (2–4 h p.i.) ($p < 0.05$ when compared to mock-infected cells). Additionally, the pro-inflammatory NF-κB-regulated genes, including CXCL8, PTGS2, IRF1, NF-κBIA, and TNF-α were up-regulated during SVA infection (4–12 or 8–12 h p.i.) (**Figures 3G–K**). These results suggest modulation of NF-κB-regulated gene expression during SVA infection in primary STu cells.

Effect of SVA Infection on the NF-κB Signaling Pathway

Given the transcriptional changes and modulation of apoptotic pathway observed in SVA infected cells (**Figures 2** and **3**), we investigated activation of NF-κB signaling during SVA infection. Since NF-κB-p65 is one of the key NF-κB subunits, that is directly responsible for the transactivation of NF-κB target genes (78), expression and activation of NF-κB-p65 were assessed in SVA infected cells using IFA. As shown in **Figure 4**, at ∼2 h p.i. NF-κB-p65 translocated to the nucleus of cells, indicating activation of the NF-κB pathway following SVA infection.

Interestingly, at later times p.i. (7–8 h p.i.) on a low MOI experiment, many of the SVA-infected cells presented a marked decrease in expression of NF-κB-p65 (**Figure 5A**), suggesting

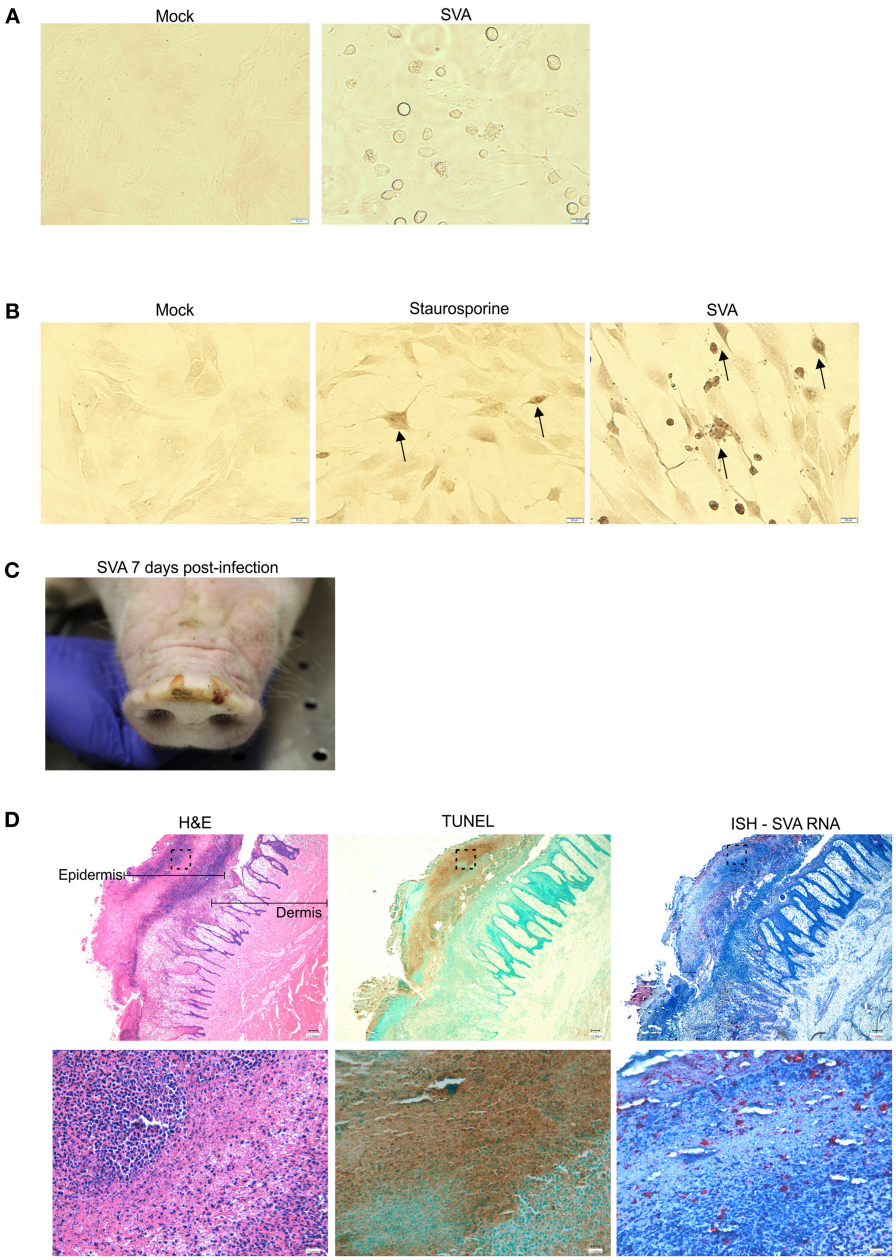

FIGURE 1 | SVA induces apoptosis *in vitro* and *in vivo* **(A)** Cytopathic effect (CPE) caused by SVA in cell culture. Mock-infected (left panel) or SVA-infected (MOI = 5, right panel) primary swine turbinate (STu) cells. 40× magnification. **(B)** TUNEL staining of mock-infected- (left panel), staurosporine-treated- (middle panel) and SVA infected (right panel, MOI = 5) STu cells. 40× magnification. The black arrows indicate apoptotic cells. **(C,D)** Apoptosis occurs during SVA infection in the swine host *in vivo*. Sequential paraffin-embedded skin lesions collected from SVA-infected pigs on day 7 post-infection **(C)** were subjected to hematoxylin and eosin staining (**D**, left panels), TUNEL (**D**, middle panels), and in situ hybridization for detection of SVA RNA (RNAScope®) (**D**, right panels). 4× (top panels) and 40× (bottom panels) magnifications. Areas highlighted in the top panels are represented in the bottom higher magnification images.

potential degradation or cleavage of the C-terminus region of this transcription factor. To assess whether the decreased levels of NF-κB-p65 observed in SVA-infected cells at late times p.i. occurred due to degradation or cleavage of the C-terminus of the molecule, expression of NF-κB-p65 was evaluated throughout the virus infection cycle using western blots. As shown in **Figure 5B**, similar levels of N- and C-terminus NF-κB-p65 were detected in SVA infected cells up to 4 h p.i., when compared to control mock-infected cells. At 8 h p.i., a marked decrease in the levels of NF-κB-p65 (∼70% compared to the average of mock cells) was observed in SVA-infected cells ($p < 0.05$; **Figure 5B**). Notably, accumulation of a cleaved product of ∼50

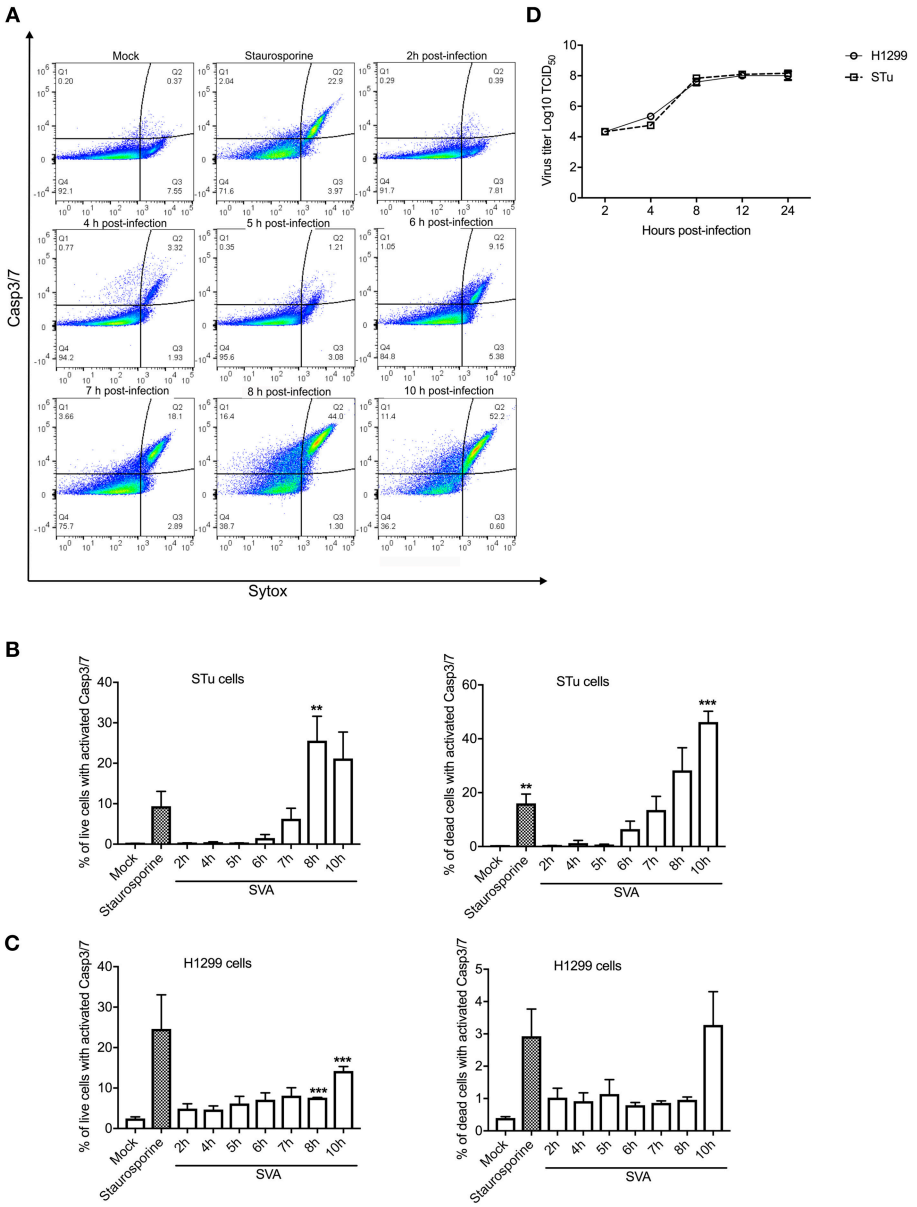

FIGURE 2 | Activation of caspases 3/7 (Casp-3/-7) during SVA infection. **(A)** Gating strategy used to determine percent of cells with active Caspase-3/7 and stained with Sytox-green during SVA infection. Caspase activation was determined using the CellEventTM Caspase-3/7 Green Flow Cytometry Assay kit. **(B**,**C)** Caspase-3/7 activation in STu or H1299-infected cells (MOI = 5) negative (left panel) or positively (right panel) stained with Sytox-green, representing live cells (early apoptotic cells), or dead cells (late apoptotic cells). The flow cytometry data were acquired with an Attune NxT flow cytometer and analyzed using FlowJo software. The results represent the average of three independent experiments in STu **(B)** or H1299 **(C)** cells. Error bars represent SEM calculated based on the results of the independent experiments; $^{**}p < 0.05$ and $^{***}p < 0.01$, compared to mock-infected cells. **(D)** Single-step growth curves of SVA (MOI = 5) in STu or H1299 cells. Cells were collected at indicated time points and virus titers expressed as $\log_{10}$ tissue culture infections dose 50 ($TCID_{50}$) per milliliter. The results represent the average of three independent experiments. Error bars represent SEM.

kDa, corresponding to N-terminus of NF-κB-p65 was detected at 8–12 h p.i. (**Figure 5B**). Similar results were observed in the human carcinoma cell line H1299 (**Figure 5C**).

NF-κB transcriptional activity was assessed during SVA infection using an NF-κB-luciferase reporter assay. A significant decrease in TNF-α-induced NF-κB-mediated luciferase activity was observed between 8 and 12 h post-SVA infection (**Figure 5D**). Collectively, these results demonstrate a fine modulation of NF-κB pathway during SVA infection. While early during infection the NF-κB pathway is activated, at later times p.i., SVA infection induces cleavage of NF-κB-p65, which results, in lower transcriptional activity of this important modulator of host cell inflammation and survival.

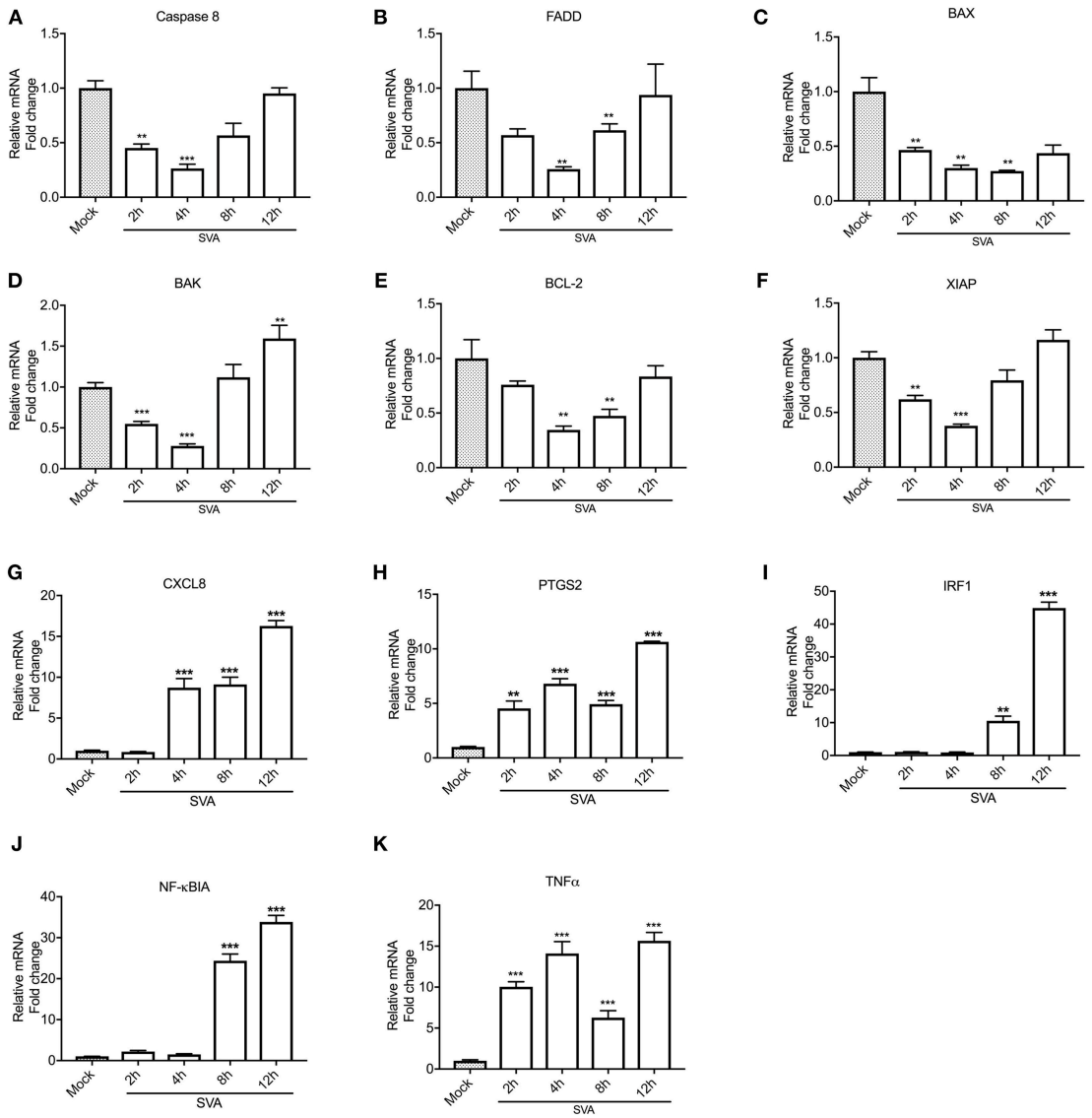

FIGURE 3 | Expression levels of select NF-κB target genes during SVA infection. Expression of pro-apoptotic (Caspase 8, FADD, BAX, and BAK), anti-apoptotic (BCL-2 and XIAP) and pro-inflammatory (CXCL8, PTGS2, IRF1, NFκBIA, and TNF-α) genes were assessed by RT-qPCR at different time points post-SVA infection in primary swine turbinate (STu) cells (2, 4, 8, and 12 h; MOI = 5). Expression levels of Caspase 8 **(A)**, FADD **(B)**, BAX **(C)**, BAK**(D)**, BCL-2 **(E)**, XIAP **(F)**, CXCL8 **(G)**, PTGS2 **(H)**, IRF1 **(I)**, NFκBIA **(J),** and TNF-α **(K)** were normalized to that of Glyceraldehyde 3-phosphate dehydrogenase (GAPDH). Mock-infected cells were used as negative control. The results were expressed as relative fold changes in mRNA levels compared to mock-infected cells. The results represent the average of three biological replicates. Error bars represent SEM, $^{**}p < 0.05$ and $^{***}p < 0.01$, compared to mock-infected cells.

Expression of SVA 3C^{pro} Is Associated With Apoptosis and Cleavage of NF-κB-p65

Next we sought to dissect the mechanisms underlying SVA-induced host-cell apoptosis and its link with cleavage of NF-κB-p65. First, we assessed the potential role of SVA non-structural protein 3C^{pro}, the main protease encoded by the virus (1), on apoptosis and cleavage of NF-κB-p65 using western blots. Expression of IKKα, IKKβ, IκBα, and NF-κB-p65 were investigated. Additionally, cleavage of PARP, a hallmark of host cell apoptosis (79), was also assessed in 3C^{pro} expressing cells. While expression of 3C^{pro} did not affect expression levels of the upstream NF-κB kinases (IKKα, IKKβ) (**Figure 6A**), a marked decrease in the levels of IκB-α and NF-κB-p65 were observed in 3C^{pro} expressing cells (**Figure 6A**). Accumulation of the cleaved 50 kDa-NF-κB product, observed in SVA-infected cells (**Figures 5B,C**), was also detected in 3C^{pro} expressing cells, when protein extracts were probed with the antibody against N-terminus NF-κB-p65 (**Figure 6A**). IFA experiments using an antibody specific for the C-terminus region of NF-κB-p65 confirmed decreased levels of C-terminus NF-κB-p65 in 3C^{pro} expressing cells (**Figure 6C**). Similar results were observed in primary STu cells (data not shown). Importantly, expression of SVA 3C^{pro} also resulted in cleavage of PARP (**Figure 6A**), suggesting that the viral

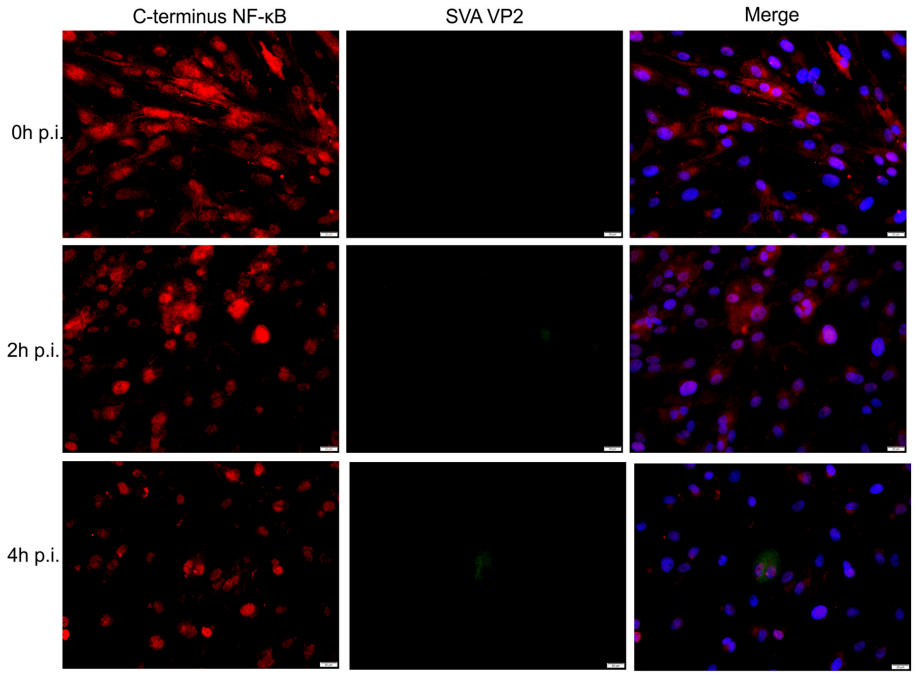

FIGURE 4 | Effect of SVA on expression of NF-κB-p65 in STu cells in early stages of infection. Primary swine turbinate (STu) cells were infected with SVA (MOI = 5) and stained with a SVA VP2 monoclonal antibody (middle panel; green—Alexa fluor 488) and a rabbit polyclonal antibody specific for C-terminus of NF-κB-p65 (left panel; red—Alexa fluor 594). The cell nuclei were stained with DAPI (right panel; blue). 40× magnification.

protease induces apoptosis when expressed outside the context of SVA infection.

The effect of SVA $3C^{pro}$ expression on cleavage of NF-κB-p65 and activation of apoptotic pathways in the context of SVA infection were investigated by western blots. Expression of SVA $3C^{pro}$ was first detected using a SVA $3C^{pro}$-specific rabbit polyclonal antibody at 5 h p.i., with increasing levels of the protein being detected up to 12 h p.i. (**Figure 6B**). Decreased levels of C-terminus NF-κB-p65 were observed after 7 h post-SVA infection (0.88) (**Figure 6B**). In addition, accumulation of the cleaved 50 kDa-NF-κB product was observed at 8 h p.i. (**Figure 6B**). Notably, a decrease in the levels of the full-length PARP was evident after 5 h p.i., with a cleaved product of the protein accumulating in infected cells after 8 h p.i. (**Figure 6B**). Detection of cleaved Casp-3 at 8–12 h p.i. confirmed induction of apoptosis late during SVA infection (**Figure 6B**).

The effect of $3C^{pro}$ expression on the transcriptional activity of NF-κB was investigated using a luciferase reporter assay. Expression of SVA $3C^{pro}$ in H1299 cells completely suppressed TNF-α-induced NF-κB-luciferase activity (**Figure 6D**) as evidenced by significantly decreased luciferase activity in SVA $3C^{pro}$-expressing cells (∼2.2-fold, $p < 0.05$) when compared to cells expressing either VP1- or BAP-control proteins (**Figure 6D**). These results indicate that expression of SVA $3C^{pro}$ results in reduced NF-κB-mediated transcription following stimulation of cells with TNF-α. Collectively, these findings suggest that expression of SVA $3C^{pro}$ could be associated with cleavage of NF-κB-p65 and induction of apoptosis in SVA infected cells.

The Protease Activity of $3C^{pro}$ Is Required for Induction of Apoptosis and Cleavage of NF-κB-p65

To assess whether the protease activity of SVA $3C^{pro}$ contributes to induction of apoptosis and/or cleavage of NF-κB-p65, we constructed two plasmids encoding for mutants of SVA $3C^{pro}$. The picornavirus $3C^{pro}$ contains a conserved catalytic triad (His, Asp, Cys) that is required for its protease activity (4, 80). To disrupt the catalytic triad and, consequently, the proteolytic activity of SVA $3C^{pro}$ we introduced a mutation at His 47 (H47D) or Cys 159 (C159R) using site-directed mutagenesis (**Figure 7A**). The effect of these mutations on apoptosis and cleavage of NF-κB-p65 were investigated in $3C^{pro}$-expressing cells. H1299 cells were transfected with plasmids encoding the wild type or each of the $3C^{pro}$ mutants (H47D or C159R) and total protein extracts were subjected to western blot analysis. Notably, while expression of the wild type SVA $3C^{pro}$ resulted in activation of Casp-3 and cleavage of NF-κB-p65, expression of the $3C^{pro}$ catalytic dead mutants H47D or C159R did not lead to Casp-3 activation nor NF-κB-p65 cleavage (**Figure 7B**).

The effect of SVA $3C^{pro}$ protease activity on NF-κB-mediated gene transcription was investigated using luciferase reporter assays. Notably, while expression of the wild type SVA $3C^{pro}$ markedly inhibited TNF-α-induced NF-κB-mediated luciferase activity ($p > 0.05$), expression of the $3C^{pro}$ mutants (H47D and C159R) did not inhibit TNF-α-induced NF-κB-mediated luciferase activity (**Figure 7C**). These results suggest that the protease activity of SVA $3C^{pro}$ may be the trigger that leads to

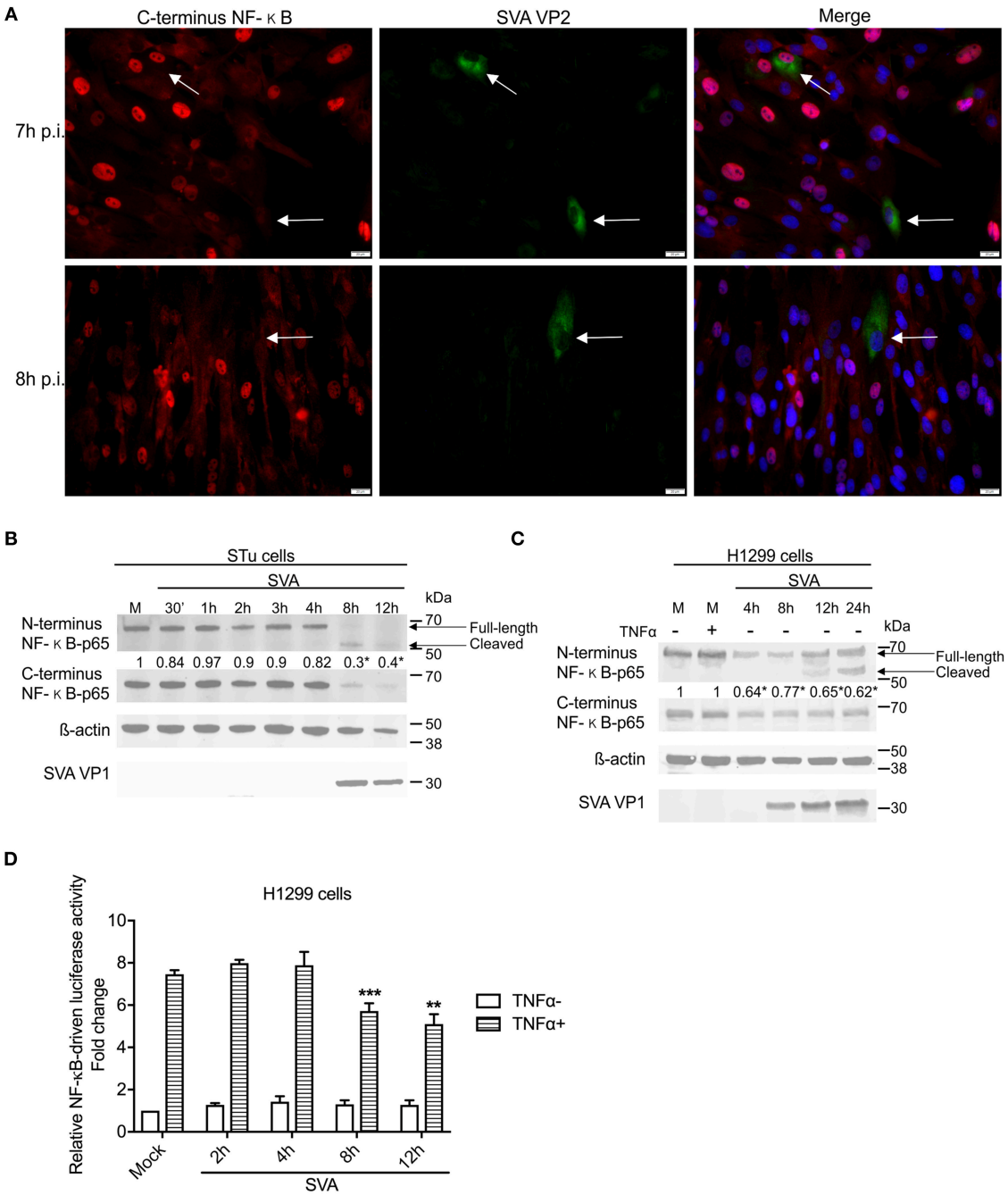

FIGURE 5 | NF-κB-p65 is cleaved during SVA infection. **(A)** Immunofluorescence of primary swine turbinate (STu) cells infected with SVA (MOI = 1) and stained with a monoclonal antibody specific for SVA VP2 (middle panel; green—Alexa fluor 488) and a rabbit polyclonal antibody specific for C-terminus of NF-κB-p65 (left panel; red—Alexa fluor 594). The cell nuclei were stained with DAPI (right panel; blue). 40× magnification. The white arrows indicate the cells infected with SVA. **(B,C)** Western blot analysis of primary STu or H1299 showing cleavage of NF-κB-p65 during SVA infection. Total protein extracts were analyzed by western blot using antibodies specific to N-terminus NF-κB-p65, C-terminus NF-κB-p65, SVA VP1, or β-actin. Densitometric analysis was performed to quantify the levels of C-terminus NF-κB-p65. The densitometry of C-terminus NF-κB-p65 bands were normalized to the β-actin control and expressed as relative densitometry to mock infected control cell (numbers on top of NF-κB-p65 blot; $^{*}p < 0.05$; compared to mock-infected cells). The results are representative of four independent experiments. **(D)** Luciferase reporter assays in H1299 cells during SVA infection. Cells were infected and stimulated with TNF-α at the indicated time points. Firefly luciferase activity was determined at 12 h post-TNF-α stimulation and normalized to the renilla luciferase activities. The results were expressed as relative fold changes in luciferase activity ($^{**}p < 0.05$ and $^{***}p < 0.01$, compared to mock-infected TNF-α-stimulated cells). Error bars represent SEM calculated based on the results of the three independent experiments.

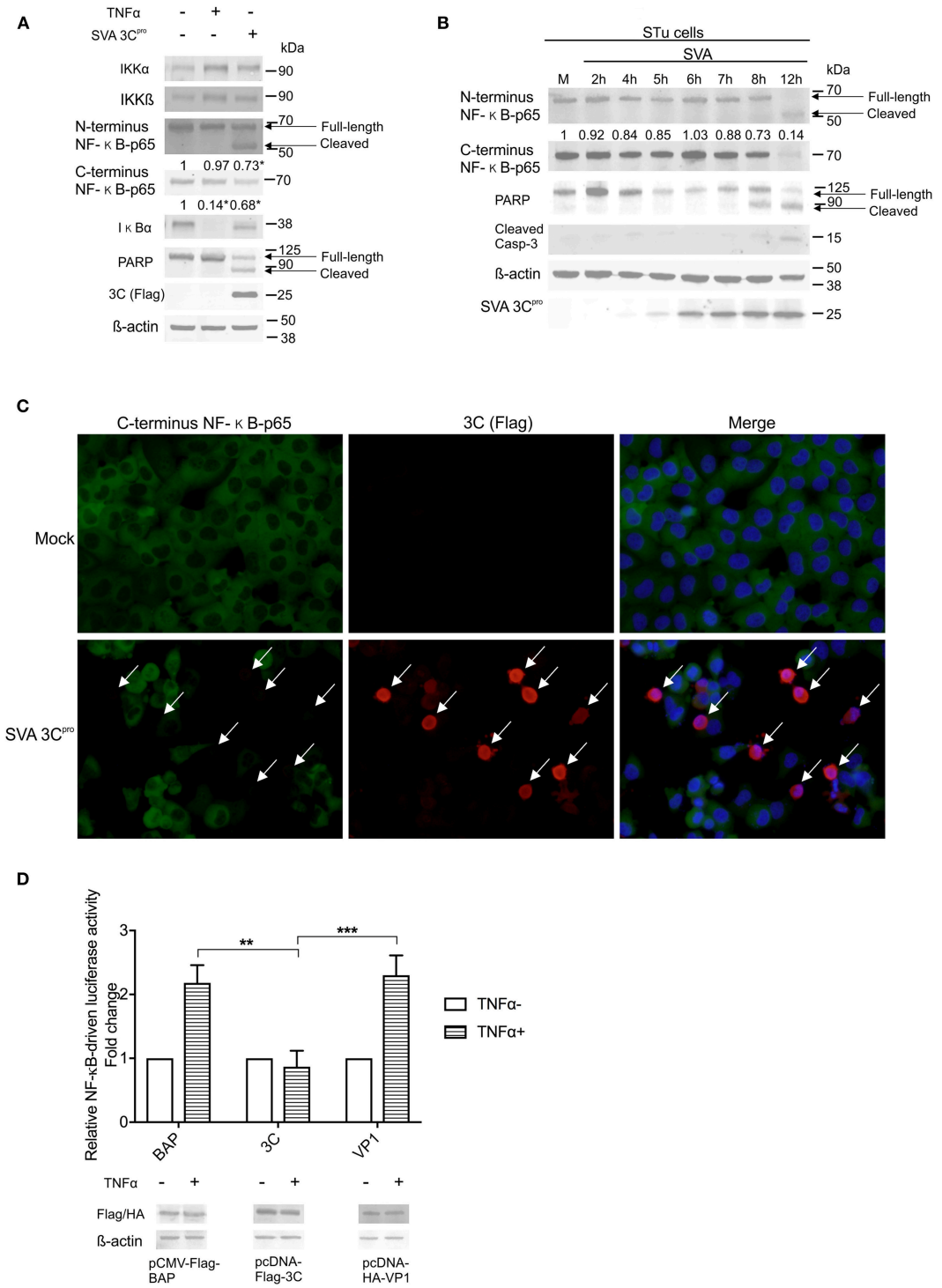

FIGURE 6 | Expression of SVA 3Cpro is associated with apoptosis and cleavage of NF-κB-p65. **(A)** Western blot analysis of H1299 cells transiently expressing SVA 3Cpro demonstrating cleavage of NF-κB-p65 and PARP. Non-transfected cells were stimulated or not with TNF-α for 1 h, and used as negative and positive controls, respectively. Total protein extracts were analyzed by western blots using antibodies indicated on the left. The results are representative of three independent experiments. **(B)** Western blot analysis of STu cells demonstrating cleavage of NF-κB-p65 and PARP during SVA infection. Total protein extracts were analyzed using antibodies indicated on the left. Densitometric analysis was performed to quantify the levels of C-terminus NF-κB-p65. The densitometry of C-terminus NF-κB-p65 bands were normalized to the β-actin control and expressed as relative densitometry to mock infected control cells. **(C)** Immunofluorescence staining showing decreased levels of NF-κB-p65 in in SVA 3Cpro expressing H1299 cells. Flag-tag antibody (red—Alexa fluor 594) and rabbit polyclonal antibodies specific for C-terminus NF-κB-p65 (green—Alexa fluor 488). The cell nuclei were stained with DAPI (blue). 40× magnification. The white arrows indicate the cells expressing

(Continued)

FIGURE 6 | SVA 3Cpro (red). **(D)** Luciferase reporter assays in H1299 cells expressing SVA 3Cpro. At 14 h post-transfection of luciferase and 3Cpro expressing plasmids, cells were stimulated with TNF-α for 12 h (TNFα+) or left unstimulated (TNF α-). Luciferase activity was determined, and firefly luciferase activity normalized to renilla luciferase activity. The results were expressed as relative fold changes in luciferase activity (**$p < 0.05$; ***$p < 0.01$; compared Flag-BAP and HA-VP1 expressing cells). Data shown represent the average of five independent experiments. Error bars represent SEM calculated based on the results of the independent experiments. Western blot showing expression of BAP, SVA 3Cpro, and VP1 in samples examined by luciferase assays (bottom panel).

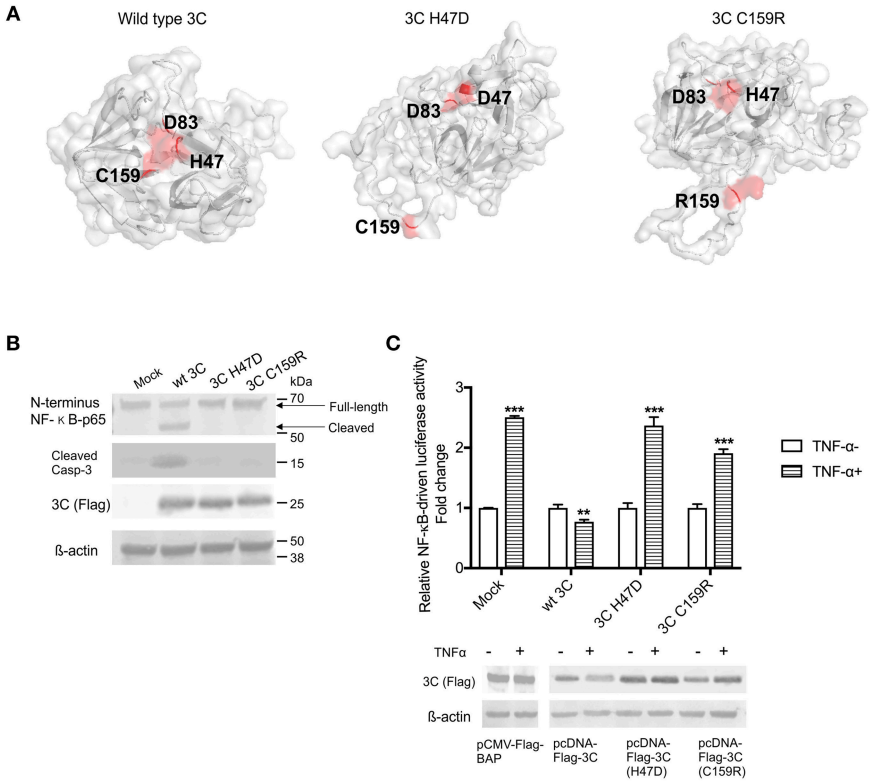

FIGURE 7 | The protease activity of $3C^{pro}$ is required for induction of apoptosis. **(A)** Three-dimensional protein structure prediction. The wild type SVA $3C^{pro}$ and the $3C^{pro}$ mutants (H47D and C159R) template-based protein structure models were determined using RaptorX web server (63). Red dots represent the aa present in the catalytic triad (H47, D83, and C159), or the point mutations H47D or C159R introduced in SVA $3C^{pro}$. **(B)** Western blot analysis of H1299- cells expressing SVA $3C^{pro}$ showing that mutations in the catalytic triad of the protease impairs its pro-apoptotic function. Protein extracts were analyzed by western blot using antibodies specific for N-terminus NF-κB-p65, cleaved Caspase 3, Flag-tag, and β-actin as loading protein control. The results are representative of three independent experiments. **(C)** Luciferase assay showing that SVA $3C^{pro}$ catalytic triad is important for its inhibitory effect on NF-κB-p65 transcriptional activity. H1299 cells were transfected with NF-κB-luciferase reporter plasmids and either wild type or mutant 3C-expressing plasmids. At 12 h post-transfection cells were stimulated with TNF-α for 12 h, and luciferase activity determined. Firefly luciferase activity was normalized to the renilla luciferase activity. The results were expressed as relative fold changes in luciferase activity (**$p < 0.05$ and ***$p < 0.01$, compared to BAP-expressing cells treated with TNF-α). Results shown represent the average of five independent experiments. Error bars represent SEM. Western blots showing expression of BAP, wild type $3C^{pro}$, 3C H47D, and 3C C159R in samples examined by luciferase assays (bottom panel).

host cell apoptosis and potentially to cleavage of NF-κB-p65 in host cells.

Assessing the Mechanism of NF-κB-p65 Cleavage

To dissect whether cleavage of NF-κB-p65 is directly mediated by SVA $3C^{pro}$ or whether it is secondary to caspase activation following $3C^{pro}$ expression, we generated a panel of plasmids encoding NF-κB-p65 proteins containing mutations on predicted cleavage sites for Casp-3/-6 (81) and/or for the SVA $3C^{pro}$ (**Figure 8A**). Two cleavage sites for $3C^{pro}$ (Q/L or Q/G, 478QL, and 482QG) (**Figure 8A**) and two cleavage sites for caspases (444LQFDTDED and 464VFTD) were identified in the transactivation domain (TAD) of NF-κB-p65 (**Figure 8A**). These predicted cleavage sites were mutated using site directed mutagenesis and resultant plasmids used in transient expression experiments. (**Figure 8A**). Cleavage of NF-κB-p65 was evaluated after transient co-expression of wild type- or mutant NF-κB-p65 proteins and the SVA $3C^{pro}$ by western blots. As shown in **Figure 8B**, all NF-κB-p65 constructs with mutations on predicted cleavage sites for SVA $3C^{pro}$ were cleaved when co-expressed with the viral protease. Notably, when the NF-κB-p65 containing mutations in the predicted cleavage sites for cellular caspases (444L-450R and 464V-467E) were co-expressed with $3C^{pro}$, NF-κB-p65 464-467E mutant was cleaved, while no cleavage of NF-κB-p65 444L-450R mutant was observed (**Figure 8C**).

This phenotype was confirmed in double NF-κB-p65 mutants, containing $3C^{pro}$- and Casp-cleavage site mutations. As shown in **Figure 8D**, when the mutation 444L-450R in the caspase cleavage site was introduced in NF-κB-p65 containing a mutation on the $3C^{pro}$ cleavage site (478R-483D), NF-κB-p65 was not cleaved (**Figure 8D**). Additionally, inhibition of caspases by incubation of cells with Z-VAD-FMK (a pan caspase inhibitor) prevented cleavage of NF-κB-p65 in cells expressing $3C^{pro}$ (**Figure 8E**). Together, these results show that NF-κB-p65 cleavage occurs at the caspase cleavage site (444LQFDTDED), suggesting that cleavage of NF-κB-p65 is mediated by caspases and not by the direct action of SVA $3C^{pro}$.

Link Between NF-κB-p65 and Apoptosis During SVA Infection

Given our results demonstrating the association between cleavage of NF-κB-p65, and host cell apoptosis late in SVA infection, we investigated the importance of this process on virus replication. First, we assessed the effect of NF-κB-p65 on SVA-induced apoptosis using a Casp-3/-7 flow cytometry-based assay in STu cells transiently expressing NF-κB-p65. Notably, expression of NF-κB-p65 resulted in markedly low activation of Casp-3/-7 following SVA infection when compared to cells transfected with an empty control plasmid (**Figure 9A**). Indeed, when NF-κB-p65 was expressed, caspase activation levels in SVA-infected- or staurosporine-treated cells were similar to those observed in mock-infected cells (**Figure 9A**). These results indicate that overexpression of NF-κB-p65 prevents SVA-induced apoptosis in STu cells.

Since expression of NF-κB-p65 led to reduced levels of apoptosis in SVA infected cells, we next assessed its effect on SVA replication. Expression of NF-κB-p65 in both STu or H1299 cells resulted in reduced viral yields as evidenced by significantly lower viral titers in cells expressing NF-κB-p65, when compared to cells transfected with the empty control plasmid ($p < 0.05$, STu; $p < 0.01$, H1299) (**Figures 9B,C**). Together these results suggest that Casp-mediated cleavage of NF-κB-p65 (**Figure 8**) and induction of host cell apoptosis late during SVA infection (**Figure 2**) might be critical for virus replication and/or release from infected cells.

Late Induction of Apoptosis Seems Essential for SVA Infection Cycle

Given our results demonstrating that overexpression of NF-κB-65 prevents SVA-induced apoptosis and results in lower viral yields from infected cells, we investigate the direct effect of apoptosis on SVA infection. For this, replication kinetics experiments were performed in cells treated or not with Z-VAD-FMK to directly inhibit caspase-mediated apoptosis (82). As shown in **Figures 10A** and **B**, viral yields were lower in both STu and H1299 cells when apoptosis was inhibited (Z-VAD-FMK^{+}).

Next, viral yields were evaluated in the supernatant or cell fraction of cell cultures treated with Z-VAD-FMK following high MOI SVA infection. Cells were infected with SVA (MOI = 5) and treated or not with apoptosis inhibitor (Z-VAD-FMK). While no differences in viral yields were detected in the cell fraction at 8 h p.i. (**Figure 10C**), significantly lower viral titers were detected in the supernatant of cells treated with Z-VAD-FMK when compared to control untreated cells. Additionally, the effect of apoptosis on SVA spread was assessed by plaque assays. As shown in **Figure 10D**, inhibition of apoptosis by Z-VAD-FMK decreased the ability of SVA to spread from cell-to-cell, as evidenced by markedly smaller viral plaques in cells treated with the apoptosis inhibitor ($p < 0.001$). Together these results suggest that induction of apoptosis late in SVA infection may be important for SVA release and/or spread from infected cells.

DISCUSSION

Programmed cell death or apoptosis is induced by infection with several picornaviruses (54, 55, 71, 83–85). Here, we demonstrated the occurrence of apoptosis at late times post-SVA infection and provided evidence that this process may contribute to virus release from infected cells. Notably, early in SVA infection, the apoptotic pathway is not activated, as evidenced by low Casp-3/-7 activity or lack of PARP cleavage in SVA infected cells (**Figures 2A**, **6B**). Suppression of apoptosis early in infection likely allows the virus to complete the replication cycle before cell death/lysis (86). Inhibition of apoptosis in early stages of infection has also been described for Coxsackievirus (87) and Enterovirus 71 (88). Similar to our results with SVA, poliovirus, the prototype of the *Picornaviridae* family (89), was shown to suppress host cell death at early stages of infection and to trigger apoptosis at late times p.i. (51, 52, 90). Induction of apoptosis late in infection is thought contribute to picornavirus release from infected cells (91). Results here showing reduced SVA titers in the supernatant of cells treated with apoptosis inhibitor Z-VAD-FMK are aligned with this hypothesis.

Given that cleavage of NF-κB-p65 was detected in SVA infected cells, we investigated the potential role of SVA viral protease $3C^{pro}$ on this function. The $3C^{pro}$ is the only protease encoded by SVA and it plays a critical role during virus replication by processing the polyprotein into mature proteins (1, 92). Additionally, $3C^{pro}$ is important in virus-host interactions and functions as a key modulator of viral immune evasion (8, 11, 14, 16, 21, 27, 91). When SVA $3C^{pro}$ was transiently expressed in cell culture *in vitro*, a cleaved fragment of NF-κB-p65 similar to the one observed in the SVA infected cells, was detected. SVA $3C^{pro}$ also inhibited TNF-α-induced NF-κB-mediated luciferase expression, suggesting that cleavage of NF-κB-p65 leads to a decreased trans-activating activity of this transcription factor. This was also observed in the context of SVA infection, with lower NF-κB-mediated luciferase activity detected at 8–12 h post-SVA infection. An important observation to note is the fact that cleavage of NF-κB-p65 is not complete in SVA infected cells. This is reflected in the luciferase activity (**Figure 5D**), which shows repression of NF-κB transcriptional activity, but not complete inhibition of the transcription factor. These observations would likely explain the detection of mRNA of NF-κB-target genes late in SVA infection.

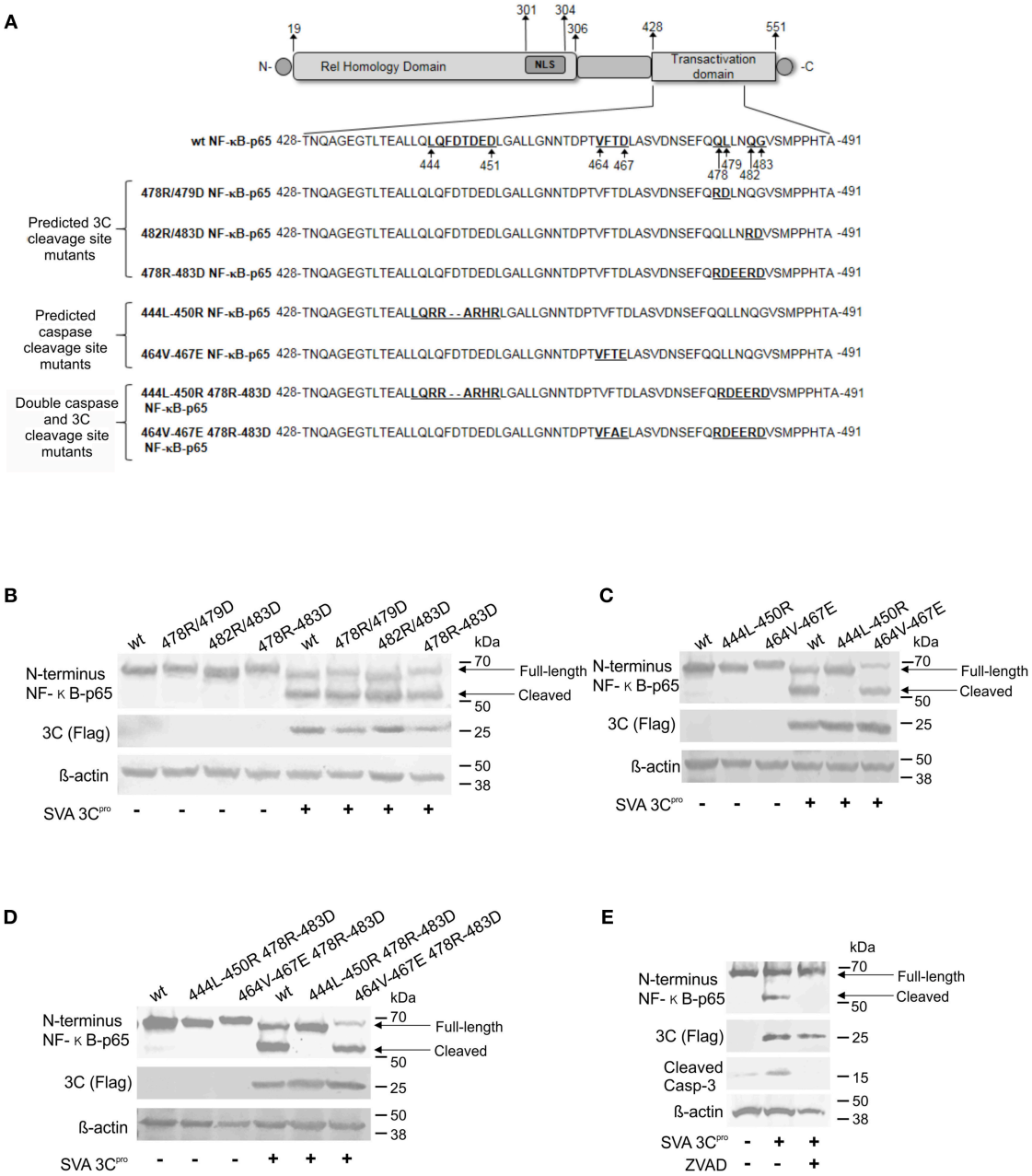

FIGURE 8 | Cleavage of NF-κB-p65 is mediated by caspases and not by the direct action of SVA 3C^{pro}. **(A)** Schematic representation of NF-κB-p65 protein depicting predicted cleavage sites for Casp-3/-6 (81) and/or SVA 3C^{pro} in the TAD. Western blot analysis of H1299 cells expressing wild type or mutant NF-κB-p65 proteins containing aa substitutions on SVA 3C predicted cleavage sites **(B)**, caspase predicted cleavage sites **(C)**, or double SVA 3C^{pro} and caspase predicted cleavage sites **(D)**. **(E)** Western blot to assess cleavage of NF-κB-p65 in SVA 3C^{pro}-expressing cells in the presence or absence of caspase inhibitor Z-VAD-FMK. Blots in **(B–E)** were probed with antibodies indicated on the left.

Additionally, transient expression of SVA 3C^{pro} led to cell membrane blebbing (data not shown) and cleavage of PARP, a key marker of cell death, suggesting that this viral protease is involved on host cell apoptosis (**Figure 6A**). This was also observed in the context of SVA infection, in which expression of SVA 3C^{pro} correlated with decreased levels of PARP and cleavage of NF-κB-p65. The ability of 3C^{pro} to induce apoptosis seems to be conserved in picornaviruses including Enterovirus 71 (93, 94), Poliovirus (95), Coxsackievirus B3 (96), and Hepatitis A virus (9).

The picornaviral 3C^{pro} contains a His-Asp-Cys catalytic triad (4, 80). This site, known as peptide-binding cleft, is located at the interface between two β-barrels (80), which is characteristic of serine proteases (97). The predicted catalytic triad of SVA 3C^{pro} consists of histidine 47 (H47), aspartate 83 (D83), and

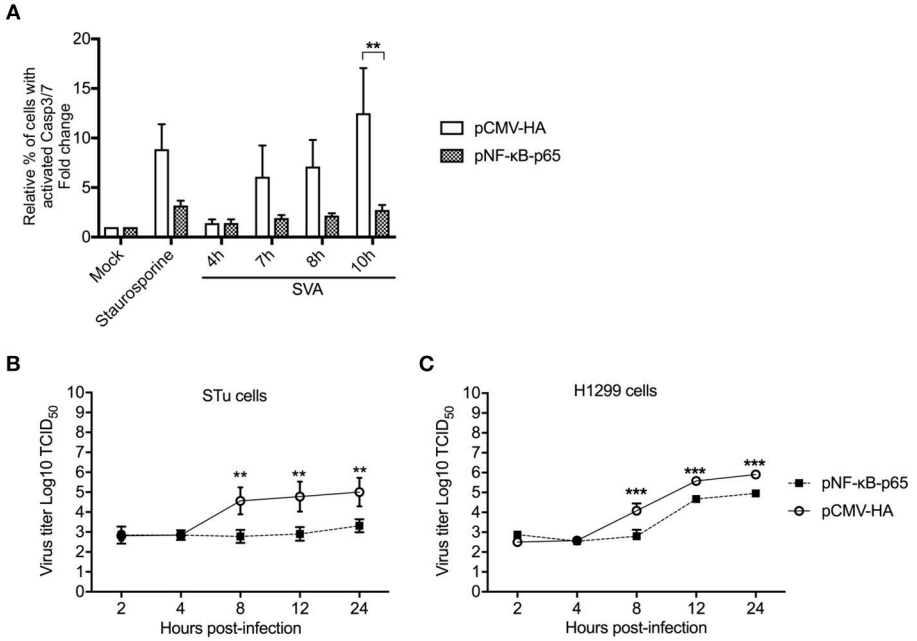

FIGURE 9 | Overexpression of NF-κB-p65 suppresses SVA-induced apoptosis and decreases SVA yields. **(A)** Flow cytometry analysis of STu cells showing that transient expression of NF-κB-p65 decreases apoptosis induced by SVA infection. Cells were stained with CellEvent™ Caspase-3/7 Green Flow Cytometry Assay kit. The flow cytometry data were acquired with an Attune NxT flow cytometer and analyzed using FlowJo software. The results were expressed as percent of cells with active Casp-3/-7. Error bars represent SEM; $^{**}p < 0.05$ compared to mock-infected cells; Sidak's multiple comparison test. **(B)**, **(C)** Replication kinetics of SVA in STu **(B)** or H1299 cells **(C)** transiently expressing NF-κB-p65. Cells were infected and harvested at indicated time points and virus titers determined by the Spearman and Karber's method and expressed as $\log_{10}$ tissue culture infections dose 50 ($TCID_{50}$) per milliliter. The results represent the average of three independent experiments. Error bars represent SEM ($^{**}p < 0.05$, $^{***}p < 0.01$; comparisons between each time point, Students' *t*-test).

cysteine 159 (C159). To assess the importance of the proteolytic function of SVA $3C^{pro}$ to its pro-apoptotic activity and inhibitory effect on the NF-κB pathway, we generated two 3C mutants containing single aa substitutions at H47 (H47D) and C159 (C159R) to disrupt the catalytic triad of the protein. Notably, while expression of wild type $3C^{pro}$ resulted in activation of caspases and cleavage of NF-κB-p65, mutations on the catalytic triad of $3C^{pro}$ (H47D and C159R) abolished these phenotypes, indicating that the protease activity of SVA $3C^{pro}$ is essential for its function on these pathways.

Cleavage of NF-κB-p65 has also been observed during infection with poliovirus (8) and FMDV (18), and this phenotype was attributed to the expression of $3C^{pro}$ or L^{pro} by these viruses, respectively. Initial results here, suggested that SVA $3C^{pro}$ could also be potentially be involved with this function. However, since cellular caspases are also able to cleave NF-κB-p65 (64, 65), we devised experiments to dissect the mechanism underlying SVA-induced cleavage of this important transcription factor. For this, NF-κB-p65-expressing plasmids containing single or double mutations in predicted cleavage sites for the SVA $3C^{pro}$ and/or effector caspases were generated by site directed mutagenesis (**Figure 8A**). Notably, results from co-transfection and caspase inhibition experiments suggest that cleavage of NF-κB-p65 occurs due to the activity of cellular caspases and not due to the direct action of SVA $3C^{pro}$ (**Figure 8E**). Our results show that NF-κB-p65 is cleaved at a Casp-3/-6 predicted cleavage site (444LQFDTDED) when host cell apoptotic pathways are activated by expression of SVA $3C^{pro}$ (**Figures 8B–D**). Although, previous studies with poliovirus suggest that cleavage of NF-κB-p65 is mediated by $3C^{pro}$ (8), our findings using mutant NF-κB-p65 expressing plasmids provide evidence that, for SVA, cleavage of this important pro-survival molecule is likely secondary to caspase activation.

Several studies demonstrated that caspase-mediated cleavage of NF-κB-p65 abrogates cell survival signaling, leading to host cell apoptosis (64, 65). Notably, infection with Human Immunodeficiency virus (HIV) and African Swine fever virus (ASFV) were shown to induce caspase-mediated cleavage of NF-κB-p65 resulting in enhanced viral replication (98), or induction of apoptosis after completion of the virus replication cycle (99), respectively. Here we demonstrated the relevance of caspase-mediated cleavage of NF-κB-p65 for SVA infection. Overexpression of NF-κB-p65 suppressed SVA-induced apoptosis (**Figure 9A**), and resulted in significantly lower viral yields from infected cells (**Figures 9B,C**). These results suggest that when high levels of NF-κB-p65 are present, caspase-mediated cleavage of NF-κB-p65 may be saturated resulting in decreased levels of viral-induced apoptosis. These findings highlight the relevance of late apoptosis for SVA infection. This was confirmed with experiments in which apoptosis was inhibited throughout the virus infection cycle using the pan-caspase inhibitor Z-VAD-FMK. Results from these experiments demonstrated lower viral yields from cells in which apoptosis was suppressed. These findings suggest that SVA

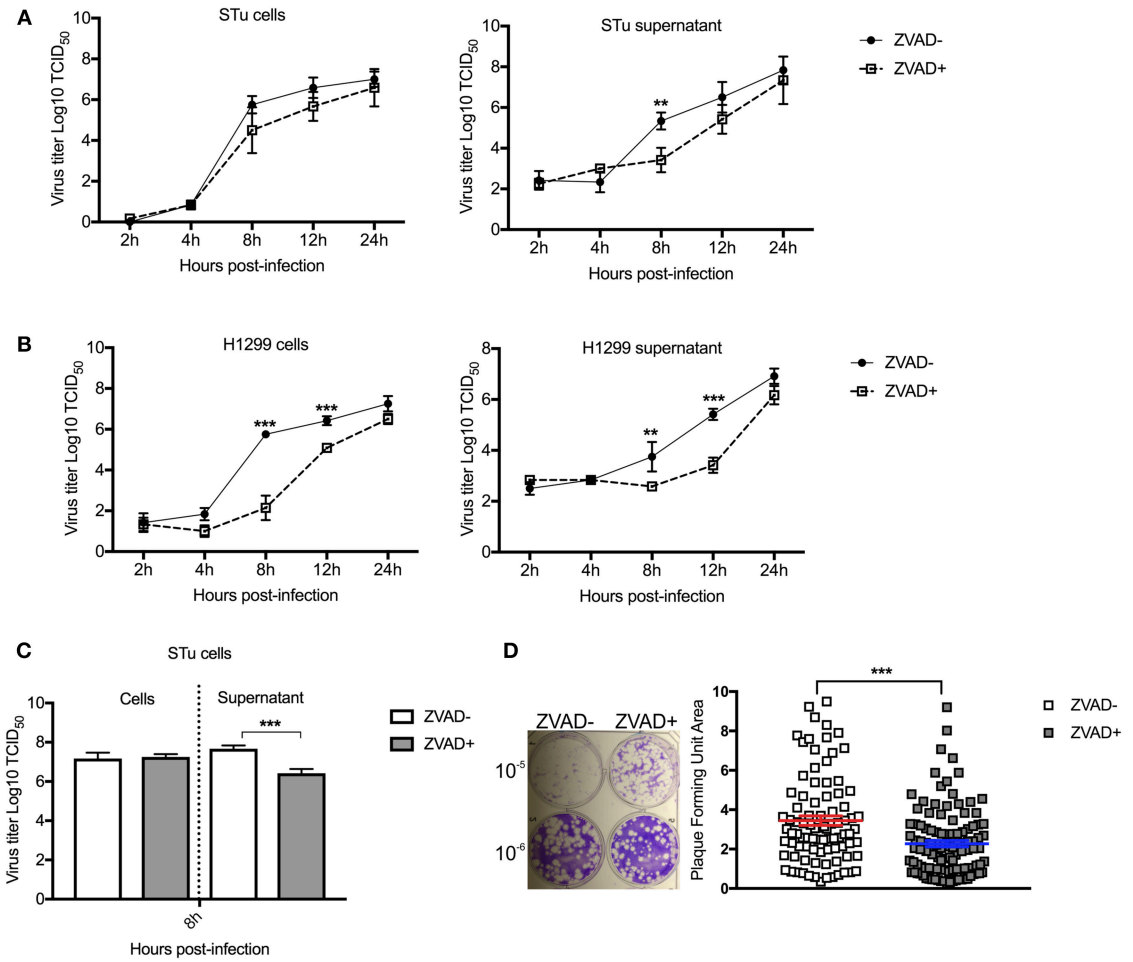

FIGURE 10 | Induction of apoptosis late in SVA infection is important for virus release and/or spread from infected cells. Multiple-step growth curves in STu **(A)** or H1299 **(B)** cells (MOI = 0.1), and single step growth curve STu **(C)** cells (MOI = 5) treated or not with Z-VAD-FMK, a pan-caspase inhibitor. Cells and supernatants were harvested separately at the indicated time points and subjected to virus titration. The virus titers were determined by the Spearman and Karber's method and expressed as $\log_{10}$ tissue culture infections dose 50 ($TCID_{50}$) per milliliter. Results represent the average of three independent experiments. Error bars represent SEM $^{**}p < 0.05$, $^{***}p < 0.01$; comparisons between each time point in the multiple-step growth curve; and $^{***}p < 0.01$; comparisons between the time point in the single-step growth curve. **(D)** Plaque assay in STu cells treated or not with Z-VAD-FMK showing reduced viral spread in cells in which apoptosis is inhibited. In the right panel, the graphic represents SVA plaque forming unit area of cells treated or not with Z-VAD-FMK (10^{-6} dilution). Plaque areas were determined with ImageJ software. Error bars represent SEM ($^{***}p < 0.01$; comparisons between treatments, Multiple *t*-tests).

induces apoptosis late in infection, presumably as a mechanism to facilitate virus release and/or spread from infected cells (**Figure 10C**). Indeed, the primary mode of spreading of non-enveloped viruses is cell lysis (100), and apoptosis could allow viruses to use cell remnants for viral transmission, while avoiding the host immune response (58).

In summary, results here show that SVA modulates important host cell pathways, including NF-κB and apoptosis, throughout the infection cycle. The proteolytic activity of SVA $3C^{pro}$ is essential to induction of apoptosis, however the precise function of the viral protease to this process remains unknown. Our data demonstrate that induction of apoptosis late in infection is a critical process for SVA infection *in vitro*. Results showing induction of apoptosis *in vivo* suggest that this event may also have direct implications on SVA infection and pathogenesis in the natural swine host.

BIOETHICS

All animal studies were carried out in accordance with the principles of the the Animal Welfare Act, the Public Health Service (PHS) Policy on Humane Care and Use of Laboratory Animals, and recommendations of the Guide for the Care and Use of Laboratory Animals. The protocols were approved by the SDSU IACUC (15-095A and 16-002A).

DATA AVAILABILITY

All datasets generated for this study are included in the manuscript and/or the supplementary files.

AUTHOR CONTRIBUTIONS

MF designed, performed, and analyzed the experiments and data. MM, JO, LJ, and SL developed reagents and helped with experiments. DD planned experiments, analyzed data, and secured funding. MF and DD wrote the manuscript.

FUNDING

This work was supported by the USDA National Institute of Food and Agriculture Hatch project SD00H517-14 and Multi-state project SD00R518-14. The South Dakota Governor's Office for Economic Development grant to the Center for Biologics Research and Commercialization (CBRC) funded the flow cytometer used in our study. MF is recipient of the MorriSTONE graduate scholarship, a kind gift provided by Pipestone Veterinary Service.

ACKNOWLEDGMENTS

We thank the SDSU functional genomics core facility for the use of critical instrumentation to conduct the experiments in this study.

REFERENCES

1. Hales LM, Knowles NJ, Reddy PS, Xu L, Hay C, Hallenbeck PL. Complete genome sequence analysis of Seneca Valley virus-001, a novel oncolytic picornavirus. *J Gen Virol.* (2008) 89:1265–75. doi: 10.1099/vir.0.83570-0
2. Venkataraman S, Reddy SP, Loo J, Idamakanti N, Hallenbeck PL, Reddy VS. Structure of Seneca Valley Virus-001: an oncolytic picornavirus representing a new genus. *Structure*. (2008) 16:1555–61. doi: 10.1016/j.str.2008.07.013
3. Knowles NJ, Hales LM, Jones BH, Landgraf JG, House JA, Skele KL, et al. Epidemiology of Seneca Valley Virus: identification and characterization of isolates from pigs in the United States. In: *XIVth Meeting of the European Study Group on Molecular Biology of Picornaviruses* (Saariselka), G2.
4. Birtley JR, Knox SR, Jaulent AM, Brick P, Leatherbarrow RJ, Curry S. Crystal structure of foot-and-mouth disease virus 3C protease: new insights into catalytic mechanism and cleavage specificity. *J Biol Chem.* (2005) 280:11520–7. doi: 10.1074/jbc.M413254200
5. Lin JY, Chen TC, Weng KF, Chang SC, Chen LL, Shih SR. Viral and host proteins involved in picornavirus life cycle. *J Biomed Sci.* (2009) 16:103. doi: 10.1186/1423-0127-16-103
6. Bacot-Davis VR, Palmenberg AC. Encephalomyocarditis virus Leader protein hinge domain is responsible for interactions with Ran GTPase. *Virology*. (2013) 443:177–85. doi: 10.1016/j.virol.2013.05.002
7. Ciomperlik JJ, Basta HA, Palmenberg AC. Cardiovirus leader proteins bind exportins: implications for virus replication and nucleocytoplasmic trafficking inhibition. *Virology*. (2016) 487:19–26. doi: 10.1016/j.virol.2015.10.001
8. Neznanov N, Chumakov KM, Neznanova L, Almasan A, Banerjee AK, Gudkov AV. Proteolytic cleavage of the p65-RelA subunit of NF-kappaB during poliovirus infection. *J Biol Chem.* (2005) 280:24153–8. doi: 10.1074/jbc.M502303200
9. Shubin AV, Demidyuk IV, Lunina NA, Komissarov AA, Roschina MP, Leonova OG, et al. Protease 3C of hepatitis A virus induces vacuolization of lysosomal/endosomal organelles and caspase-independent cell death. *BMC Cell Biol.* (2015) 16:4. doi: 10.1186/s12860-015-0050-z
10. Walker EJ, Younessi P, Fulcher AJ, McCuaig R, Thomas BJ, Bardin PG, et al. Rhinovirus 3C protease facilitates specific nucleoporin cleavage and mislocalisation of nuclear proteins in infected host cells. *PLoS ONE.* (2013) 8:e71316. doi: 10.1371/journal.pone.0071316
11. Wang D, Fang L, Li K, Zhong H, Fan J, Ouyang C, et al. Foot-and-mouth disease virus 3C protease cleaves NEMO to impair innate immune signaling. *J Virol.* (2012) 86:9311–22. doi: 10.1128/JVI.00722-12
12. Wang J, Wang Y, Liu J, Ding L, Zhang Q, Li X, et al. A critical role of N-myc and STAT interactor (Nmi) in foot-and-mouth disease virus (FMDV) 2C-induced apoptosis. *Virus Res.* (2012) 170:59–65. doi: 10.1016/j.virusres.2012.08.018
13. Wang ZY, Zhong T, Wang Y, Song FM, Yu XF, Xing LP, et al. Human enterovirus 68 interferes with the host cell cycle to facilitate viral production. *Front Cell Infect Microbiol.* (2017) 7:29. doi: 10.3389/fcimb.2017.00029
14. Xiang Z, Li L, Lei X, Zhou H, Zhou Z, He B, et al. Enterovirus 68 3C protease cleaves TRIF to attenuate antiviral responses mediated by toll-like receptor 3. *J Virol.* (2014) 88:6650–9. doi: 10.1128/JVI.03138-13
15. Yu J, Zhang L, Ren P, Zhong T, Li Z, Wang Z, et al. Enterovirus 71 mediates cell cycle arrest in S phase through non-structural protein 3D. *Cell Cycle*. (2015) 14:425–36. doi: 10.4161/15384101.2014.980631
16. Zaragoza C, Saura M, Padalko EY, Lopez-Rivera E, Lizarbe TR, Lamas S, et al. Viral protease cleavage of inhibitor of kappaBalpha triggers host cell apoptosis. *Proc Natl Acad Sci USA*. (2006) 103:19051–6. doi: 10.1073/pnas.0606019103
17. Zhang YZ, Gan X, Song J, Sun P, Song QQ, Li GQ, et al. [The 2A protease of enterovirus 71 cleaves nup62 to inhibit nuclear transport]. *Chinese J Virol.* (2013) 29:421–5. doi: 10.1016/51286-4579(02)01634-9
18. de Los Santos T, Diaz-San Segundo F, Grubman MJ. Degradation of nuclear factor kappa B during foot-and-mouth disease virus infection. *J Virol.* (2007) 81:12803–15. doi: 10.1128/JVI.01467-07
19. Zheng Z, Li H, Zhang Z, Meng J, Mao D, Bai B, et al. Enterovirus 71 2C protein inhibits TNF-α-mediated activation of NF-κB by suppressing IκB kinase phosphorylation. *J Immunol.* (2011) 187:2202–12. doi: 10.4049/jimmunol.1100285
20. Zhou Z, Mogensen MM, Powell PP, Curry S, Wileman T. Foot-and-mouth disease virus 3C protease induces fragmentation of the Golgi compartment and blocks intra-Golgi transport. *J Virol.* (2013) 87:11721–9. doi: 10.1128/JVI.01355-13
21. Xiang Z, Liu L, Lei X, Zhou Z, He B, Wang J. 3C protease of enterovirus D68 inhibits cellular defense mediated by interferon regulatory factor 7. *J Virol.* (2015) 90:1613–21. doi: 10.1128/JVI.02395-15
22. Du H, Yin P, Yang X, Zhang L, Jin Q, Zhu G. Enterovirus 71 2C protein inhibits NF-κB activation by binding to RelA(p65). *Sci Rep.* (2015) 5:14302. doi: 10.1038/srep14302
23. Feng Q, Langereis MA, Lork M, Nguyen M, Hato SV, Lanke K, et al. Enterovirus 2Apro Targets MDA5 and MAVS in infected cells. *J Virol.* (2014) 88:3369–78. doi: 10.1128/JVI.02712-13
24. Gladue DP, O'Donnell V, Baker-Bransetter R, Pacheco JM, Holinka LG, Arzt J, et al. Interaction of foot-and-mouth disease virus nonstructural protein 3A with host protein DCTN3 is important for viral virulence in cattle. *J Virol.* (2014) 88:2737–47. doi: 10.1128/JVI.03059-13
25. Hanson PJ, Ye X, Qiu Y, Zhang HM, Hemida MG, Wang F, et al. Cleavage of DAP5 by coxsackievirus B3 2A protease facilitates viral replication and enhances apoptosis by altering translation of IRES-containing genes. *Cell Death Differ.* (2016) 23:828–40. doi: 10.1038/cdd.2015.145
26. Harris KG, Coyne CB. Unc93b induces apoptotic cell death and is cleaved by host and enteroviral proteases. *PLoS ONE.* (2015) 10:e0141383. doi: 10.1371/journal.pone.0141383
27. Huang L, Liu Q, Zhang L, Zhang Q, Hu L, Li C, et al. Encephalomyocarditis virus 3C protease relieves TRAF family member-associated NF-κB Activator (TANK) inhibitory effect on TRAF6-mediated NF-κB signaling through cleavage of TANK. *J Biol Chem.* (2015) 290:27618–32. doi: 10.1074/jbc.M115.660761
28. Li D, Lei C, Xu Z, Yang F, Liu H, Zhu Z, et al. Foot-and-mouth disease virus non-structural protein 3A inhibits the interferon-β signaling pathway. *Sci Rep.* (2016) 6:21888. doi: 10.1038/srep21888
29. Bracht AJ, O'Hearn ES, Fabian AW, Barrette RW, Sayed A. Real-time reverse transcription PCR assay for detection of Senecavirus A in

swine vesicular diagnostic specimens. *PLoS ONE*. (2016) 11:e0146211. doi: 10.1371/journal.pone.0146211
30. Singh K, Corner S, Clark S, Sherba G, Fredrickson R. Seneca Valley virus and vesicular lesions in a pig with idiopathic vesicular disease. *J Vet Sci Technol.* (2012) 3:123. doi: 10.4172/2157-7579.1000123
31. Pasma T, Davidson S, Shaw SL. Idiopathic vesicular disease in swine in Manitoba. *Can Vet J.* (2008) 49:84–5.
32. Wu Q, Zhao X, Bai Y, Sun B, Xie Q, Ma J. the first identification and complete genome of *Senecavirus A* affecting pig with idiopathic vesicular disease in China. *Transbound Emerg Dis.* (2017) 64:1633–40. doi: 10.1111/tbed.12557
33. Canning P, Canon A, Bates JL, Gerardy K, Linhares DCL, Pi∼Neyro PE, et al. Neonatal mortality, vesicular lesions and lameness associated with Senecavirus A in a U.S. Sow Farm. *Transbound Emerg Dis.* (2016) 63:373–8. doi: 10.1111/tbed.12516
34. Joshi LR, Mohr KA, Clement T, Hain KS, Myers B, Yaros J, et al. Detection of the emerging picornavirus Senecavirus A in pigs, mice, and houseflies. *J Clin Microbiol.* (2016) 54:1536–45. doi: 10.1128/JCM.03390-15
35. Saeng-chuto K, Stott CJ, Wegner M, Kaewprommal P, Piriyapongsa J, Nilubol D. The full-length genome characterization, genetic diversity and evolutionary analyses of Senecavirus A isolated in Thailand in 2016. *Infect Genet Evol.* (2018) 64:32–45. doi: 10.1016/J.MEEGID.2018.06.011
36. Sun D, Vannucci F, Knutson TP, Corzo C, Marthaler DG. Emergence and whole-genome sequence of Senecavirus A in Colombia. *Transbound Emerg Dis.* (2017) 64:1346–9. doi: 10.1111/tbed.12669
37. Leme RA, Zotti E, Alcântara BK, Oliveira M V, Freitas LA, Alfieri AF, et al. Senecavirus A: an emerging vesicular infection in brazilian pig herds. *Transbound Emerg Dis.* (2015) 62:603–11. doi: 10.1111/tbed.12430
38. Vannucci FA, Linhares DCL, Barcellos DESN, Lam HC, Collins J, Marthaler D. Identification and complete genome of seneca valley virus in vesicular fluid and sera of pigs affected with idiopathic vesicular disease, Brazil. *Transbound Emerg Dis.* (2015) 62:589–93. doi: 10.1111/tbed.12410
39. Joshi LR, Fernandes MHV, Clement T, Lawson S, Pillatzki A, Resende TP, et al. Pathogenesis of Senecavirus A infection in finishing pigs. *J Gen Virol.* (2016) 97:3267–9. doi: 10.1099/jgv.0.000631
40. Fernandes MHV, Maggioli MF, Joshi LR, Clement T, Faccin TC, Rauh R, et al. Pathogenicity and cross-reactive immune responses of a historical and a contemporary Senecavirus A strains in pigs. *Virology*. (2018) 522:147–57. doi: 10.1016/J.VIROL.2018.06.003
41. Maggioli MF, Lawson S, de Lima M, Joshi LR, Faccin TC, Bauermann FV, et al. Adaptive immune responses following Senecavirus A infection in pigs. *J Virol.* (2018) 92:e01717-17. doi: 10.1128/JVI.01717-17
42. Montiel N, Buckley A, Guo B, Kulshreshtha V, VanGeelen A, Hoang H, et al. Vesicular disease in 9-week-old pigs experimentally infected with Senecavirus A. *Emerg Infect Dis.* (2016) 22:1246–8. doi: 10.3201/eid2207.151863
43. Alexandersen S, Zhang Z, Donaldson AI. Aspects of the persistence of foot-and-mouth disease virus in animals–the carrier problem. *Microbes Infect.* (2002) 4:1099–110.
44. Reddy PS, Burroughs KD, Hales LM, Ganesh S, Jones BH, Idamakanti N, et al. Seneca Valley virus, a systemically deliverable oncolytic picornavirus, and the treatment of neuroendocrine cancers. *J Natl Cancer Inst.* (2007) 99:1623–33. doi: 10.1093/jnci/djm198
45. Poirier JT, Dobromilskaya I, Moriarty WF, Peacock CD, Hann CL, Rudin CM. Selective tropism of Seneca Valley virus for variant subtype small cell lung cancer. *J Natl Cancer Inst.* (2013) 105:1059–65. doi: 10.1093/jnci/djt130
46. Liu Z, Zhao X, Mao H, Baxter PA, Huang Y, Yu L, et al. Intravenous injection of oncolytic picornavirus SVV-001 prolongs animal survival in a panel of primary tumor–based orthotopic xenograft mouse models of pediatric glioma. *Neuro Oncol.* (2013) 15:1173–85. doi: 10.1093/neuonc/not065
47. Rudin CM, Poirier JT, Senzer NN, Stephenson J, Loesch D, Burroughs KD, et al. Phase I Clinical Study of Seneca Valley Virus (SVV-001), a replication-competent picornavirus, in advanced solid tumors with neuroendocrine features. *Clin Cancer Res.* (2011) 17:888–95. doi: 10.1158/1078-0432.CCR-10-1706
48. Burke MJ, Ahern C, Weigel BJ, Poirier JT, Rudin CM, Chen Y, et al. Phase I trial of Seneca Valley Virus (NTX-010) in children with relapsed/refractory solid tumors: a report of the Children's Oncology Group. *Pediatr Blood Cancer*. (2015) 62:743–50. doi: 10.1002/pbc.25269
49. Burke MJ. Oncolytic Seneca Valley Virus: past perspectives and future directions. *Oncol Virother.* (2016) 5:81–9. doi: 10.2147/OV.S96915
50. Mutsafi Y, Altan-Bonnet N. Enterovirus transmission by secretory autophagy. *Viruses*. (2018) 10:139. doi: 10.3390/v10030139
51. Belov GA, Romanova LI, Tolskaya EA, Kolesnikova MS, Lazebnik YA, Agol VI. The major apoptotic pathway activated and suppressed by poliovirus. *J Virol.* (2003) 77:45–56. doi: 10.1128/JVI.77.1.45-56.2003
52. Brisac C, Téoulé F, Autret A, Pelletier I, Colbère-Garapin F, Brenner C, et al. Calcium flux between the endoplasmic reticulum and mitochondrion contributes to poliovirus-induced apoptosis. *J Virol.* (2010) 84:12226–35. doi: 10.1128/JVI.00994-10
53. Chi J, Yu S, Liu C, Zhao X, Zhong J, Liang Y, et al. Nox4-dependent ROS production is involved in CVB3-induced myocardial apoptosis. *Biochem Biophys Res Commun.* (2018) 503:1641–4. doi: 10.1016/J.BBRC.2018.07.093
54. Brack K, Frings W, Dotzauer A, Vallbracht A. A Cytopathogenic, apoptosis-inducing variant of hepatitis A virus. *J Virol*. (1998) 72:3370–6.
55. Yamada M, Fukai K, Morioka K, Nishi T, Yamazoe R, Kitano R, et al. Early pathogenesis of the foot-and-mouth disease virus O/JPN/2010 in experimentally infected pigs. *J Vet Med Sci.* (2018) 80:689–700. doi: 10.1292/jvms.17-0683
56. Elmore S. Apoptosis: a review of programmed cell death. *Toxicol Pathol.* (2007) 35:495–516. doi: 10.1080/01926230701320337
57. Cohen GM. Caspases: the executioners of apoptosis. *Biochem J.* (1997) 326(Pt 1):1–16.
58. Thomson BJ. Viruses and apoptosis. *Int J Exp Pathol.* (2001) 82:65–76. doi: 10.1111/J.1365-2613.2001.IEP0082-0065-X
59. Jin Z, El-Deiry WS. Overview of cell death signaling pathways. *Cancer Biol Ther.* (2005) 4:147–71. doi: 10.4161/cbt.4.2.1508
60. Nicholson DW, Thornberry NA. Caspases: killer proteases. *Trends Biochem Sci.* (1997) 22:299–306.
61. Lazebnik YA, Kaufmann SH, Desnoyers S, Poirier GG, Earnshaw WC. Cleavage of poly(ADP-ribose) polymerase by a proteinase with properties like ICE. *Nature*. (1994) 371:346–7. doi: 10.1038/371346a0
62. Oberhammer FA, Hochegger K, Fröschl G, Tiefenbacher R, Pavelka M. Chromatin condensation during apoptosis is accompanied by degradation of lamin A+B, without enhanced activation of cdc2 kinase. *J Cell Biol.* (1994) 126:827–37.
63. Liu X, Zou H, Slaughter C, Wang X. DFF, a heterodimeric protein that functions downstream of caspase-3 to trigger DNA fragmentation during apoptosis. *Cell*. (1997) 89:175–84.
64. Kang KH, Lee KH, Kim MY, Choi KH. Caspase-3-mediated cleavage of the NF-κB Subunit p65 at the NH_2 terminus potentiates naphthoquinone analog-induced apoptosis. (2001) *J Biol Chem.* 276:24638–44. doi: 10.1074/jbc.M101291200
65. Kim HS, Chang I, Kim JY, Choi KH, Lee MS. Caspase-Mediated p65 cleavage promotes TRAIL-induced apoptosis. *Cancer Res.* (2005) 65:6111–9. doi: 10.1158/0008-5472.CAN-05-0472
66. Li Q, Zheng Z, Liu Y, Zhang Z, Liu Q, Meng J, et al. 2C Proteins of enteroviruses suppress IKKβ phosphorylation by recruiting protein phosphatase 1. *J Virol.* (2016) 90:5141–51. doi: 10.1128/JVI.03021-15
67. Silverman N, Maniatis T. NF-kappaB signaling pathways in mammalian and insect innate immunity. *Genes Dev*. (2001) 15:2321–42. doi: 10.1101/gad.909001
68. Collins SE, Mossman KL. Danger, diversity and priming in innate antiviral immunity. *Cytokine Growth Factor Rev*. (2014) 25:525–31. doi: 10.1016/j.cytogfr.2014.07.002
69. Ghosh S, Dass JFP. Study of pathway cross-talk interactions with NF-κB leading to its activation via ubiquitination or phosphorylation: a brief review. *Gene*. (2016) 584:97–109. doi: 10.1016/j.gene.2016.03.008
70. Ling J, Kumar R. Crosstalk between NFkB and glucocorticoid signaling: a potential target of breast cancer therapy. *Cancer Lett.* (2012) 322:119–26. doi: 10.1016/j.canlet.2012.02.033
71. Schwarz EM, Cornel Badorff, Hiura TS, Wessely R, Badorff A, Verma IM, et al. NF-B-mediated inhibition of apoptosis is required for encephalomyocarditis virus virulence: a mechanism of resistance in p50 knockout mice. *J Virol.* (1998) 72:5654–60.
72. Resende TP, Marthaler DG, Vannucci FA. A novel RNA-based in situ hybridization to detect Seneca Valley virus in neonatal piglets and

sows affected with vesicular disease. *PLoS ONE*. (2017) 12:e0173190. doi: 10.1371/journal.pone.0173190
73. Hierholzer JC, Killington RA. Virus isolation and quantitation. In: Mahy BWJ, Kangro HO, editors. *Virology Methods Manual*. San Diego, CA: Academic Press (1996). p. 25–47.
74. Källberg M, Wang H, Wang S, Peng J, Wang Z, Lu H, et al. Template-based protein structure modeling using the RaptorX web server. *Nat Protoc.* (2012) 7:1511–22. doi: 10.1038/nprot.2012.085
75. Zunszain PA, Knox SR, Sweeney TR, Yang J, Roqué-Rosell N, Belsham GJ, et al. Insights into cleavage specificity from the crystal structure of foot-and-mouth disease virus 3C protease complexed with a peptide substrate. *J Mol Biol.* (2009) 395:375–89. doi: 10.1016/j.jmb.2009.10.048
76. Fan Y, Dutta J, Gupta N, Fan G, Gélinas C. Regulation of programmed cell death by NF-κB and its role in tumorigenesis and therapy. *Adv Exp Med Biol.* (2008) 615:223–50. doi: 10.1007/978-1-4020-6554-5_11
77. Lawrence T. The nuclear factor NF-kappaB pathway in inflammation. *Cold Spring Harb Perspect Biol.* (2009) 1:a001651. doi: 10.1101/cshperspect.a001651
78. Wan F, Lenardo MJ. Specification of DNA binding activity of NF-kappaB proteins. *Cold Spring Harb Perspect Biol.* (2009) 1:a000067. doi: 10.1101/cshperspect.a000067
79. Chaitanya GV, Steven AJ, Babu PP. PARP-1 cleavage fragments: signatures of cell-death proteases in neurodegeneration. *Cell Commun Signal.* (2010) 8:31. doi: 10.1186/1478-811X-8-31
80. Mosimann SC, Cherney MM, Sia S, Plotch S, James MN. Refined X-ray crystallographic structure of the poliovirus 3C gene product. *J Mol Biol.* (1997) 273:1032–47. doi: 10.1006/jmbi.1997.1306
81. Levkau B, Scatena M, Giachelli CM, Ross R, Raines EW. Apoptosis overrides survival signals through a caspase-mediated dominant-negative NF-κB loop. *Nat Cell Biol.* (1999) 1:227–33. doi: 10.1038/12050
82. Ni HM, McGill MR, Chao X, Woolbright BL, Jaeschke H, Ding WX. Caspase inhibition prevents tumor necrosis factor-α-induced apoptosis and promotes necrotic cell death in mouse hepatocytes *in vivo* and *in vitro*. *Am J Pathol.* (2016) 186:2623–36. doi: 10.1016/j.ajpath.2016.06.009
83. Peng JM, Liang SM, Liang CM. VP1 of foot-and-mouth disease virus induces apoptosis via the Akt signaling pathway. *J Biol Chem.* (2004) 279:52168–74. doi: 10.1074/jbc.M403686200
84. Deszcz L, Gaudernak E, Kuechler E, Seipelt J. Apoptotic events induced by human rhinovirus infection. *J Gen Virol.* (2005) 86(Pt 5):1379–89. doi: 10.1099/vir.0.80754-0
85. Lou Jelachich M, Lipton HL. Theiler's murine encephalomyelitis virus induces apoptosis in gamma interferon-activated M1 differentiated myelomonocytic cells through a mechanism involving tumor necrosis factor alpha (TNF-) and TNF-related apoptosis-inducing ligand. *J Virol.* (2001) 75:5930–8. doi: 10.1128/JVI.75.13.5930-5938.2001
86. Kaminskyy V, Zhivotovsky B. To kill or be killed: how viruses interact with the cell death machinery. *J Intern Med.* (2010) 267:473–82. doi: 10.1111/j.1365-2796.2010.02222.x
87. Salako MA, Carter MJ, Kass GEN. Coxsackievirus protein 2BC blocks host cell apoptosis by inhibiting caspase-3. *J Biol Chem.* (2006) 281:16296–304. doi: 10.1074/jbc.M510662200
88. Shi W, Li X, Hou X, Peng H, Jiang Q, Shi M, et al. Differential apoptosis gene expressions of rhabdomyosarcoma cells in response to enterovirus 71 infection. *BMC Infect Dis.* (2012) 12:327. doi: 10.1186/1471-2334-12-327
89. Melnick JL. The discovery of the enteroviruses and the classification of poliovirus among them. *Biologicals*. (1993) 21:305–9. doi: 10.1006/biol.1993.1088
90. Tolskaya EA, Romanova LI, Kolesnikova MS, Ivannikova TA, Smirnova EA, Raikhlin NT, et al. Apoptosis-inducing and apoptosis-preventing functions of poliovirus. *J Virol.* (1995) 69:1181–9.
91. Sun D, Chen S, Cheng A, Wang M. Roles of the picornaviral 3C proteinase in the viral life cycle and host cells. *Viruses*. (2016) 8:82. doi: 10.3390/v8030082
92. Palmenberg AC. Picornaviral processing: some new ideas. *J Cell Biochem.* (1987) 33:191–8. doi: 10.1002/jcb.240330306
93. Li J, Yao Y, Chen Y, Xu X, Lin Y, Yang Z, et al. Enterovirus 71 3C promotes apoptosis through cleavage of PinX1, a telomere binding protein. *J Virol.* (2017) 91:e02016–16. doi: 10.1128/JVI.02016-16
94. Li ML, Hsu TA, Chen TC, Chang SC, Lee JC, Chen CC, et al. The 3C protease activity of enterovirus 71 induces human neural cell apoptosis. *Virology*. (2002) 293:386–95. doi: 10.1006/viro.2001.1310
95. Barco A, Feduchi E, Carrasco L. Poliovirus protease 3Cpro kills cells by apoptosis. *Virology*. (2000) 266:352–60. doi: 10.1006/VIRO.1999.0043
96. Chau DHW, Yuan J, Zhang H, Cheung P, Lim T, Liu Z, et al. Coxsackievirus B3 proteases 2A and 3C induce apoptotic cell death through mitochondrial injury and cleavage of eIF4GI but not DAP5/p97/NAT1. *Apoptosis*. (2007) 12:513–24. doi: 10.1007/s10495-006-0013-0
97. Barrett AJ, Rawlings ND. Evolutionary lines of cysteine peptidases. *Biol Chem.* (2001) 382:727–33. doi: 10.1515/BC.2001.088
98. Vallé I, Tait SWG, Powell PP. African swine fever virus infection of porcine aortic endothelial cells leads to inhibition of inflammatory responses, activation of the thrombotic state, and apoptosis. *J Virol.* (2001) 75:10372–82. doi: 10.1128/JVI.75.21.10372-10382.2001
99. Coiras M, López-Huertas MR, Mateos E, Alcamí J. Caspase-3-mediated cleavage of p65/RelA results in a carboxy-terminal fragment that inhibits IkappaBalpha and enhances HIV-1 replication in human T lymphocytes. *Retrovirology*. (2008) 5:109. doi: 10.1186/1742-4690-5-109
100. Bird SW, Kirkegaard K. Escape of non-enveloped virus from intact cells. *Virology*. (2015) 479–480:444–9. doi: 10.1016/j.virol.2015.03.044

Conflict of Interest Statement: The authors declare that the research was conducted in the absence of any commercial or financial relationships that could be construed as a potential conflict of interest.

frontiers in Immunology

ORIGINAL RESEARCH
published: 26 March 2019
doi: 10.3389/fimmu.2019.00579

Negative Immunomodulatory Effects of Type 2 Porcine Reproductive and Respiratory Syndrome Virus-Induced Interleukin-1 Receptor Antagonist on Porcine Innate and Adaptive Immune Functions

Teerawut Nedumpun[1], *Navapon Techakriengkrai*[2,3], *Roongroje Thanawongnuwech*[3,4] *and Sanipa Suradhat*[2,3]*

[1] Interdisciplinary Program in Medical Microbiology, Graduate School, Chulalongkorn University, Bangkok, Thailand,
[2] Department of Veterinary Microbiology, Faculty of Veterinary Science, Chulalongkorn University, Bangkok, Thailand,
[3] Center of Excellence in Emerging Infectious Diseases in Animals, Chulalongkorn University (CU-EIDAs), Bangkok, Thailand,
[4] Department of Veterinary Pathology, Faculty of Veterinary Science, Chulalongkorn University, Bangkok, Thailand

OPEN ACCESS

Edited by:
John E. Butler,
University of Iowa, United States

Reviewed by:
Jesus Hernandez,
Centro de Investigación en Alimentación y Desarrollo (CIAD), Mexico
Suzie Hingley-Wilson,
University of Surrey, United Kingdom

***Correspondence:**
Sanipa Suradhat
sanipa.s@chula.ac.th

Specialty section:
This article was submitted to Comparative Immunology, a section of the journal Frontiers in Immunology

Received: 16 October 2018
Accepted: 04 March 2019
Published: 26 March 2019

Citation:
Nedumpun T, Techakriengkrai N, Thanawongnuwech R and Suradhat S (2019) Negative Immunomodulatory Effects of Type 2 Porcine Reproductive and Respiratory Syndrome Virus-Induced Interleukin-1 Receptor Antagonist on Porcine Innate and Adaptive Immune Functions. Front. Immunol. 10:579. doi: 10.3389/fimmu.2019.00579

Impaired innate and adaptive immune responses are evidenced throughout the course of PRRSV infection. We previously reported that interleukin-1 receptor antagonist (IL-1Ra) was involved in PRRSV-induced immunosuppression during an early phase of infection. However, the exact mechanism associated with PRRSV-induced IL-1Ra immunomodulation remains unknown. To explore the immunomodulatory properties of PRRSV-induced IL-1Ra on porcine immune functions, monocyte-derived dendritic cells (MoDC) and leukocytes were cultured with type 2 PRRSV, and the immunological role of IL-1Ra was assessed by addition of anti-porcine IL-1Ra Ab. The results demonstrated that PRRSV-induced IL-1Ra reduced phagocytosis, surface expression of MHC II (SLA-DR) and CD86, as well as downregulation of *IFNA* and *IL1* gene expression in the MoDC culture system. Interestingly, IL-1Ra secreted by the PRRSV-infected MoDC also inhibited T lymphocyte differentiation and proliferation, but not IFN-γ production. Although PRRSV-induced IL-1Ra was not directly linked to IL-10 production, it contributed to the differentiation of regulatory T lymphocytes (Treg) within the culture system. Taken together, our results demonstrated that PRRSV-induced IL-1Ra downregulates innate immune functions, T lymphocyte differentiation and proliferation, and influences collectively with IL-10 in the Treg induction. The immunomodulatory roles of IL-1Ra elucidated in this study increase our understanding of the immunobiology of PRRSV.

Keywords: type 2 PRRSV, pig, immunomodulatory effect, IL-1Ra, interleukin-1 receptor antagonist, innate and adaptive immune response

INTRODUCTION

Porcine Reproductive and Respiratory Syndrome Virus (PRRSV) is one of the major pathogens affecting the pig production industry worldwide. PRRSV is an enveloped, positive-stranded RNA virus, which belongs to the genus *Porartevirus*, family *Arteriviridae* and order *Nidovirales* (1). PRRSV can be classified into two genotypes; type 1 (EU) and type 2 (US) (2), but rapid evolutionary rate often leads to the emergence of PRRSV strain variants (3, 4). Most PRRSV strains have the capacity to impair host immunity, leading to generalized immunosuppression in infected pigs (5). Consequently, PRRSV infection usually increases the severity of other concomitantly infected pathogens (6).

Innate immunity is recognized as a key modulator for induction of efficient anti-viral immune responses (7, 8). However, previous studies strongly evidenced that PRRSV primarily infects innate immune cells, such as macrophage and non-conventional dendritic cells (DC), and suppresses their functions (9–11). PRRSV inhibits maturation of antigen presenting cells (APC) and decreases levels of both MHC II (SLA-DR) and co-stimulatory molecule (CD80 and CD86) expression (12, 13). Moreover, enhanced expression of programed cell death-ligand 1 (PD-L1) on PRRSV-infected APC supported induction of cell apoptosis and regulatory T lymphocyte (Treg) differentiation (14, 15). During an early phase of PRRSV infection, production of type I IFN and pro-inflammatory cytokines (IL-1, IL-6, and TNF-α) was drastically suppressed, leading to uncontrolled viral replication (16, 17). It has been suggested that PRRSV-induced suppression of innate immunity potentially causes poor adaptive immune responses (18), characterized by attenuated T lymphocyte proliferation, and poor induction of PRRSV-specific IFN-γ-producing cells (19, 20) together with delayed neutralizing antibody responses (21).

The negative immunomodulatory mechanism induced by type 2 PRRSV has been linked to the induction of interleukin-10 (IL-10), which in turn provides an immunological niche for Treg expansion (18, 22). However, the immunosuppressive effect of PRSSV might not be solely associated with the induction of IL-10 and Treg as these factors develop slowly, ∼1 week after the suppression of innate immunity (23, 24). Moreover, levels of IL-10 and Treg induction were different among the PRRSV strains (25).

Recently, interleukin-1 receptor antagonist (IL-1Ra) induced by PRRSV was suggested to play an important role during the early phase of PRRSV infection as increased levels of IL-1Ra were observed both *in vitro* and in PRRSV-infected pigs (26). Although effect of IL-1Ra on porcine immune responses remains elusive, several evidences have been shown in both human and mouse models. IL-1Ra competitively binds to IL-1 receptor (IL-1R), and subsequently inhibits IL-1-induced signaling cascades (27). Interestingly, APC maturation and induction of type I IFN, IL-1, and TNF-α were shown to be modulated by IL-1Ra production (27–29). Blocking the IL-1R signaling pathway could inhibit antigen-specific T lymphocyte activation and proliferation (29, 30). In addition, immunomodulatory effects of IL-1Ra were also reported in the progression of some infectious diseases. Increased level of IL-1Ra production induced by *Yesinia pestis* could suppress pro-inflammatory cytokine production, resulting in prolonged bacterial survival during the early stage of infection (31). Likewise, human immunodeficiency virus (HIV)-induced IL-1Ra production weakens inflammatory processes through inhibition of IL-1 synthesis in human monocytes (32). Altogether, these evidences strongly indicate that IL-1Ra represents a key immunomodulator during an early phase of immune responses. In this study, the impact of PRRSV-induced IL-1Ra on porcine innate and adaptive immune functions were investigated.

MATERIALS AND METHODS

Viruses and Cells

Type 2 PRRSV strain 01NP1 (33) and classical swine fever virus (CSFV) were kindly provided by Chulalongkorn University Veterinary Diagnostic Laboratory (CU-VDL; Bangkok, Thailand). PRRSV and CSFV were cultured and titrated in MARC-145 (CU-VDL) and SK6 (CU-VDL) cell lines, respectively. Mock-infected cell lysates were prepared from MARC-145 (for PRRSV) and SK6 (for CSFV) cells, respectively. All viruses and mock-infected cell lysates were stored at −80°C until needed.

Antibodies

Anti-PRRSV N mAb (SDOW-17, IgG) was purchased from RTI (SD, USA). Anti-porcine SLA-DR mAb (1053H2-18, IgG2a), anti-porcine CD3-FITC mAb (BB23-8E6, IgG2b), biotinylated anti-porcine CD4 mAb (74-12-4, IgG2b), and anti-porcine CD8-PE mAb (76-2-11, IgG2a) were purchased from Southern Biotech (Birmingham, AL, USA). Biotinylated anti-porcine IFN-γ mAb (P2C11) was purchased from BD Biosciences (San Jose, CA, USA). Anti-porcine IL-10 mAb (945A4C437B1, IgG1) was purchased from Biosource (Camarillo, CA, USA). Anti-human FOXP3 mAb-APC (236A/E7, IgG1) was purchased from eBioscience (SanDiego, CA, USA). Anti-porcine CD25 mAb (K231.3B2, IgG1), goat anti-mouse IgG1-FITC and goat anti-mouse IgG2a-FITC were purchased from AbD Serotec (Kidlington, UK). Anti-human CD86-PEcy7 mAb (IT2.2, IgG1), anti-BrdU-FITC (3D4, IgG1), streptavidin-APC and streptavidin-PEcy7 were purchased from BioLegend® (San Diego, CA, USA). Goat anti-mouse IgG1-Alexaflur 647 and streptavidin-PE were purchased from ThermoFisher Scientific (Invitrogen, Carlsbad, CA, USA).

Isolation of Porcine Leukocytes and Generation of Monocyte-Derived Dendritic Cells (MoDC)

Crossbred, PRRSV-seronegative pigs were previously immunized with CSFV-modified live vaccine (MLV) (COGLAPEST®, Ceva Santé Animale, Libourne, France) at 4 and 7 weeks of age. At 16 weeks of age, porcine peripheral blood mononuclear cells (PBMC) were isolated from heparinized whole blood by density gradient centrifugation, using LymphoSep™ (MP Biomedicals, California, USA) according to the manufacturer's procedure. MoDC were generated as previously described (34).

Briefly, the PBMC were resuspended at 5 x 10^6 cells/mL in Iscove's Modified Dulbecco's Media (IMDM) (GIBCO, Carlsbad, CA, USA), and incubated at 37°C and 5% CO_2 for 2 h. Non-adherent cells, referred as peripheral blood lymphocytes (PBL), were collected and stored at 5 × 10^7 cells/mL in liquid nitrogen until needed. The remaining adherent cells were cultured with 10 ng/mL porcine recombinant IL-4 (R&D system, Minneapolis, MN, USA) and 25 ng/mL porcine recombinant GM-CSF (R&D system) for 7 days. For downstream experiments, PBMC, PBL, and MoDC were plated in complete RPMI, containing advanced RPMI (GIBCO), 10% FBS (GIBCO), 2 mM L-glutamine (GIBCO), antibiotic/antimycotic solution (GIBCO), 25 mM HEPES (GIBCO), and 50 μM β-mercaptoethanol (Sigma Chemical Co., St. Loius, USA).

In vitro IL-1Ra Neutralization Assay

On MoDC

MoDC (1 × 10^6 cells/200 μl/well) were incubated with 0.1 m.o.i. of type 2 PRRSV or mock (MARC-145 cell lysate) in 24-well plates at 37°C and 5% CO_2. In some experimental conditions, cells were pre-treated with final concentration of 10 ng/mL polyclonal goat anti-porcine IL-1Ra antibody (R&D system, clone AF780) or polyclonal goat IgG isotype control antibody (R&D system) at 2 h post-inoculation to neutralize PRRSV-induced IL-1Ra which was then cultured for another 22 h. To determine the effect of PRRSV-induced IL-1Ra on MoDC phagocytic activity, the antibody pre-treated MoDC (2 × 10^6 cell) were further incubated with inactivated *E. coli*-FITC (ThermoFisher Scientific) in complete RPMI at a MoDC:*E. coli* ratio of 1:50 for 10 min at 37°C. Immediately after, cold PBSA was added to stop the phagocytic activity. The cell pellet was washed twice with PBSA and subjected to flow cytometric analyses. To measure the effect of PRRSV-induced IL-1Ra on MoDC maturation and cytokine gene expression, 1 μg/mL of LPS (Sigma Chemical Co.) was added into each respective well at 24 h post-inoculation, and cultured for another 24 h. Afterward, the cells were harvested and subjected to immunofluorescent staining and mRNA extraction.

On T Lymphocyte Responses

The supernatants from mock or PRRSV-infected MoDC at 24 h post-inoculation were incubated with 10 ng/mL of either anti-porcine IL-1Ra or isotype control antibodies for 2 h for IL-1Ra neutralization. Then, PBMC or PBL (2 × 10^6 cells/well) were incubated with 200 μL of these antibody pre-treated supernatants prior to performing downstream functional assays. To determine the effects of PRRSV-induced IL-1Ra on T lymphocyte differentiation, the supernatant-treated PBMC were inoculated with 0.1 m.o.i. of CSFV or mock (SK6 cell lysate) at 37°C and 5% CO_2. The cell pellets were collected at 0, 12, 24, 48, and 72 h post-inoculation for mRNA extraction.

To determine effects of PRRSV-induced IL-1Ra on IFN-γ production and proliferation, the pre-treated PBL or PBMC were incubated with 1 μg/mL PHA (Sigma Chemical Co.), DMSO (Sigma Chemical Co.), 0.1 m.o.i. of CSFV or mock (SK6 cell lysate) for 48 (IFN-γ production) or 96 h (proliferation). For the proliferation assay, the cells were cultured with 10 μM Bromodeoxyuridine (BrdU, BioLegend®) prior to incubation with indicated treatments. The cells were harvested and subjected to immunofluorescent staining and flow cytometric analyses.

On IL-10-Producing Cells and Treg

PBMC (2 × 10^6 cells/well) were inoculated with 0.1 m.o.i. of type 2 PRRSV or mock (MARC-145 cell lysate) in 24-well plates at 37°C and 5% CO_2 for 2 h. The cultures were subsequently treated with anti-porcine IL-1Ra or isotype control antibodies (10 ng/mL) and incubated for another 46 h. The cells were harvested and subjected to immunofluorescent staining for IL-10-producing T lymphocytes and Treg.

IL-1Ra ELISA

PBMC (2 × 10^6 cells/well) or MoDC (1 × 10^6 cells/well) were cultured with 0.1 m.o.i. of type 2 PRRSV or mock (MARC-145 cell lysate) in 24-well plates at 37°C and 5% CO_2 for 48 h. The culture supernatants were collected and measured for the level of PRRSV-induced IL-1Ra by porcine IL-1Ra ELISA (CUSABIO, Wuhan, China).

Immunofluorescent Staining and Flow Cytometric Analyses

To confirm PRRSV infection, PBMC and MoDC were stained and permeabilized with 1:100 anti-PRRSV N mAb (SDOW-17) diluted in Reagent B (Leucoperm, AbD serotec) in the dark at the 4°C for 30 min followed by PBSA washing. Subsequently, 1:100 of goat anti-mouse IgG1-FITC mAb diluted in PBSA supplemented with 0.5% BSA and 0.1% sodium azide, referred as the FACS buffer, were added and incubated in the dark at 4°C for 30 min. The stained cells were subjected to flow cytometric analyses.

After performing the neutralization assays, the cells (1 × 10^6 cells/well) were harvested and transferred into 96-well round-bottom plates and then washed twice with FACs buffer. For immunofluorescent staining of surface molecules including SLA-DR, CD86, CD3, CD4, CD8, and CD25, primary mAbs at indicated concentration; 1:100 of anti-SLA-DR, 1:50 of anti-CD86-PEcy7, 1:50 of anti-CD3-FITC, 1:50 of biotinylated anti-CD4, 1:50 of anti-CD8-PE, or 1:100 of anti-CD25 mAbs, diluted in FACS buffer at final volume 50 μL/reaction, were added and further incubated in the dark at 4°C for 30 min. For secondary staining, 1:500 of streptavidin-PE, 1:500 of streptavidin-PEcy7, 1:100 of goat anti-mouse IgG1-FITC or 1:100 of goat anti-mouse IgG2a-FITC, diluted in FACS buffer was added to the cells and incubated in the dark at 4°C for 30 min.

For intracellular staining, the cells were then fixed and permeabilized with 50% reagent A (Leucoperm, Serotec), diluted in FACS buffer, for 30 min. For primary staining, 1:100 of anti-BrdU-FITC, 1:100 of biotinylated anti-IFN-γ, 1:100 of IL-10 (IgG1) or 1:20 of anti-FOXP3-APC mAbs, diluted in Reagent B (Leucoperm, Serotec) was added to the cells and further incubated in the dark at 4°C for 45 min. For secondary staining, 1:500 of streptavidin-APC or 1:100 of goat anti-mouse IgG1-Alexaflur 647, diluted in FACS buffer was added to the cells and incubated in the dark at 4°C for 30 min.

Cells, stained with the different isotype controls, were used to set the background cut-off of the study. The fluorescent minus

one (FMO) staining samples were also performed during the establishment and validation of the assay. The cells were gated at least 1×10^5 cell/events for each analysis. Flow cytometric analyses were performed using FC 500 MPL (Beckman Coulter, CA, USA).

Quantitative Polymerase Chain Reaction (qPCR)

Total mRNAs were isolated from the cells (2×10^6 cells/reaction) by using the total mRNA extraction kit (Biotechrabbit, Germany) according to the manufacturer's instruction. The extracted mRNAs were assayed by NanoDrop (Thermo scientific, USA) and converted to cDNA using a cDNA synthesis kit (Invitrogen, USA). Levels of porcine *IFNA, IL1, IL6, TBET, GATA3, RORGT, FOXP3,* and *GAPDH* expression were quantified by SYBR green-based qPCR using the specific primer sets shown in **Table 1**. qPCR reaction was carried out as previously described (26, 35–37). Ct values of each gene were normalized against the housekeeping gene; *GAPDH*. Differences in Ct values between the treatment groups were analyzed by the formula $2^{-\Delta\Delta Ct}$.

Statistical Analyses

Data were analyzed using student *t*-test or analysis of variance (ANOVA) followed by Tukey's multiple comparison tests. All statistical analyses were performed using GraphPad Prism for Windows (GraphPad Software Incorporated, San Diego, CA, USA).

RESULTS

PRRSV-Induced IL-1Ra Impaired Phagocytic Activity, Maturation and Innate Cytokine Productions

To investigate the role of PRRSV-induced IL-1Ra on porcine innate immune functions, MoDC were infected with type 2 PRRSV or mock (MARC-145 cell lysate) and subsequently

TABLE 1 | Sequences of the qPCR primers.

Gene	NCBI Accession no.	Primer sequence (5′ > 3′)	Product size (bp)	References
IFNA	XM_003480507.3	F: CTG-GAG-GAG-GAC-TCC-AT R: GAG-TCT-GTC-TTG-CAG-GTT	268	(26)
IL1B	NM_214055.1	F: AAC-GTG-CAA-TGA-TGA-CTT-TG R: CAC-TTC-TCT-CTT-CAA-GTC-CC	292	(26)
IL6	JQ839263.1	F: AGA-ACT-CAT-TAA-GTA-CAT-CCT-CG R: AGA-TTG-GAA-GCA-TCC-GTC	180	(34)
TBET	XM_003132081.4	F: TCA-ATC-CTA-CTG-CCC-ACT-AC R: TTA-GGA-GAC-TCT-GGG-TGA-AC	151	(35)
GATA3	XM_022745494.1	F: ACA-GAC-CCC-TGA-CCA-TGA-AG R: GGA-GAT-GTG-GCT-GAG-AGA-GG	193	(35)
FOXP3	XM_021079539.1	F: CTC-CTA-CTC-CCT-GCT-GGC-AAA-T R: TAC-AAT-ACA-GCA-GGA-ACC-CTT-GTC-A	283	(24)
GAPDH	XM_005658673.2	F: AAG-TGG-ACA-TTG-TCG-CCA-TC R: TCA-CAA-ACA-TGG-GGG-CAT-C	318	(24)

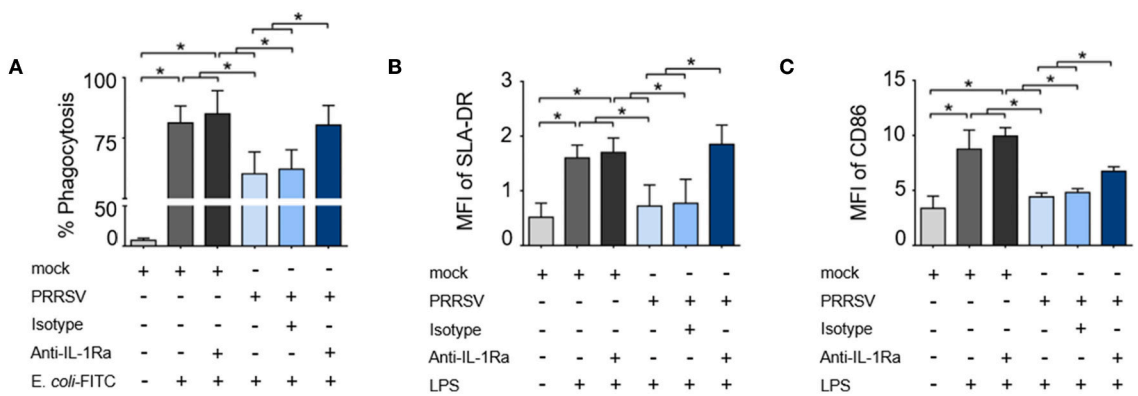

FIGURE 1 | PRRSV-induced IL-1Ra inhibited porcine innate immune functions. PRRSV-induced IL-1Ra inhibited **(A)** phagocytic activity, **(B)** SLA-DR and **(C)** CD86 expression. MoDC were cultured with type 2 PRRSV or mock, in the presence of anti-IL-1Ra Ab. LPS was added into the culture and further incubated for 24 h. ± indicates presence/absence of indicated treatment within the culture. Data represents mean ± SD from 5 pigs. Statistical significance was analyzed using ANOVA followed by Tukey's test. * indicates significant difference at $p < 0.05$.

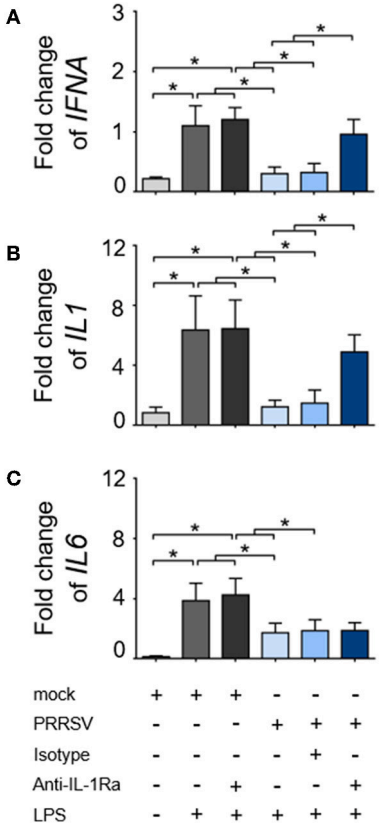

FIGURE 2 | PRRSV-induced IL-1Ra inhibited **(A)** *IFNA* and **(B)** *IL1*, **(C)** but not *IL6* expression. MoDC were cultured with type 2 PRRSV or mock, in the presence of anti-IL-1Ra Ab. LPS was added into the culture and further incubated for 24 h. ± indicates presence/absence of indicated treatment within the culture. Data represents mean ± SD from 5 pigs. Statistical significance was analyzed using ANOVA followed by Tukey's test. * indicates significant difference at $p < 0.05$.

cultured with anti-porcine IL-1Ra Ab. Antibody preincubation had no effect on the numbers of PRRSV-infected cells (**Supplementary Figure 1A**). Significant IL-1Ra production was observed in the supernatants of PRRSV-infected MoDC as confirmed by ELISA (**Supplementary Figure 1B**). PRRSV infection significantly decreased phagocytic activity of MoDC, which could be restored by the neutralization of IL-1Ra (**Figure 1A** and **Supplementary Figure 2A**). Addition of anti-IL-1Ra Ab alone did not affect the phagocytic activity of MoDC. Next, we investigated the effect of PRRSV-induced IL-1Ra on MoDC maturation. Consistent with previous findings (38–40), SLA-DR and CD86 expressions on LPS-induced MoDC were significantly decreased by PRRSV. The blockade of IL-1Ra in the culture increased SLA-DR (MHC II) and restored CD86 expression (**Figures 1B,C** and **Supplementary Figures 2B,C**).

As downregulation of *IFNA*, *IL1,* and *IL6* expression was always reported to precede the IL-10 induction during the course of PRRSV infection (17, 41–43), we hypothesized that these effects were mediated by PRRSV-induced IL-1Ra. In response to LPS stimulation, the expressions of *IFNA*, *IL1,* and *IL6* genes in the cultured MoDC were significantly increased and PRRSV abolished these innate cytokine gene expressions (**Figures 2A–C**). Neutralization of IL-1Ra restored *IFNA* and *IL1* gene expressions up to the levels observed in the control treatments (mock). However, neutralization of IL-1Ra appeared to have little effect on the level of *IL6* gene expression (**Figures 2A–C**) suggesting that PRRSV downregulated *IL6* by a different mechanism. Altogether, these findings indicated that PRRSV inhibited several key functions of APC, including phagocytic activity, antigen processing and presentation and certain pro-inflammatory cytokine production through IL-1Ra production.

PRRSV-Induced IL-1Ra Altered Expressions of Helper T Lymphocyte Transcriptional Factors During CSFV Reactivation

Development of porcine specific T lymphocyte lineages, namely Th1, Th2, and Treg, are specifically induced by constitutive expression of the transcription factors (TF); T-bet, GATA3, and FOXP3, respectively (36). It was previously reported that PRRSV infection interfered with host specific immune responses against other viral infections, including classical swine fever (CSFV) (44–46). Consequently, we investigated the immunomodulatory effect of PRRSV-induced IL-1Ra on the expression of major transcriptional factors during the recalled antigen (CSFV) responses. First, we confirmed that CSFV infection did not upregulate *IL1RA* gene expression in the CSFV-primed PBMC throughout the observation period (**Figure 3A**). Consistent with previous findings (47, 48), restimulation of CSFV-primed PBMCs with the same antigen significantly upregulated *TBET* expression indicating a shift of Th polarization toward Th1 (**Figure 3B**). Addition of the supernatant from PRRSV-infected MoDC decreased levels of CSFV-induced *TBET* and *GATA3* gene expression. The IL-1Ra neutralization was shown to restore or even increase the expressions of *TBET* and *GATA3* compared with CSFV restimulation alone (**Figures 3C,D**). Whereas, CSFV had no effect on *FOXP3* expression, the presence of supernatant of PRRSV-infected MoDC drastically upregulated transcriptional *FOXP3* at 48 and 72 h in CSFV-restimulated cells (**Figures 3B**,**E**). However, neutralization of IL-1Ra had no effect on the level of *FOXP3* expression (**Figure 3E**), suggesting Treg are differentiated by other mechanisms. Altogether, these results demonstrated the immunomodulatory effects of PRRSV-induced IL-1Ra on the antigen-specific Th differentiation.

PRRSV-Induced IL-1Ra Inhibited Lymphocyte Proliferation, but Not IFN-γ Production

To investigate the effect of PRRSV-induced IL-1Ra on T lymphocyte proliferation, the supernatants obtained from PRRSV-infected MoDC were pretreated with anti-IL-1Ra Ab, and then added into PHA- or CSFV-stimulated BrdU-cultured porcine PBL or PBMC. Lymphocytes were further gated into $CD4^+$ (putative T helper lymphocytes), $CD8^+$ (putative cytotoxic T lymphocytes) and $CD4^+CD8^+$ (putative memory

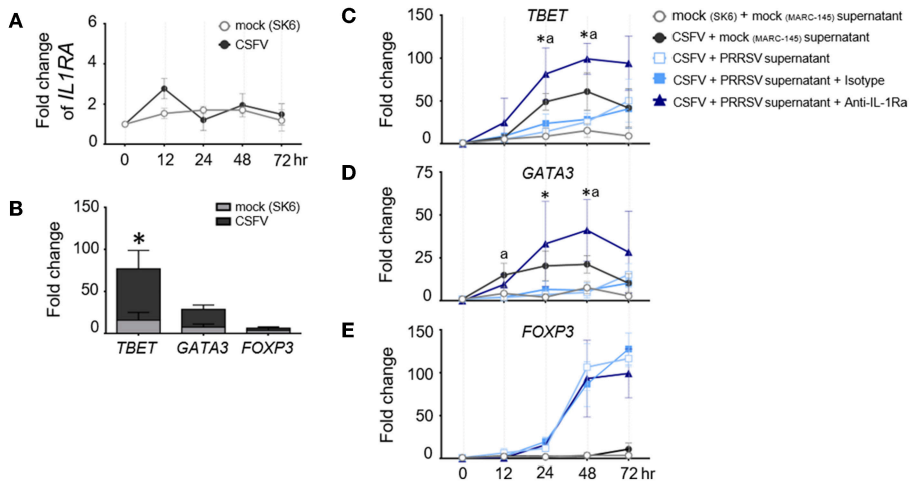

FIGURE 3 | PRRSV-induced IL-1Ra altered the expression of helper T lymphocyte transcriptional factors during the recalled antigen test. **(A)** CSFV had no effect on *IL1RA* gene expression. **(B)** Upon activation with the recalled antigen, CSFV, strong upregulation of *TBET* was observed in the CSFV-primed PBMC. *indicates significant difference levels at $p < 0.05$. **(C–E)** The levels of transcriptional factor gene expression in the CSFV-primed PBMC, upon reactivation with the recalled antigen. PRRSV-induced IL-1Ra decreased expressions of **(C)** *TBET* and **(D)** *GATA3*, **(E)** but not *FOXP3* gene expressions. The supernatants from type 2 PRRSV- or mock (MARC-145 cell lysate)-infected MoDC were pretreated with anti-IL-1Ra Ab for 2 h prior to addition into the culture system. PBMC obtained from CSFV-immunized pigs were *in vitro* reactivated with CSFV or mock (SK6 cell lysate), in the presence of pretreated supernatants. Data represents mean ± SD from 5 pigs. Statistical significances were analyzed using *t* test **(A)** ANOVA followed by Tukey's test **(B–E)**. [a] indicates significant difference between mock-infected cell supernatant (black circle) and PRRSV-infected cell supernatants (close and open light blue squares) at $p < 0.05$. * indicates significant difference between addition of anti-IL-1Ra Ab (dark blue triangle) and PRRSV-infected cell supernatants (close and open light blue squares) at $p < 0.05$.

T lymphocytes) subpopulations (**Supplementary Figures 3A,B**). Addition of PHA resulted in robust proliferation of $CD4^+$, $CD8^+$, and $CD4^+CD8^+$ subpopulations. Addition of anti-IL-1Ra Ab or isotype control did not affect PHA-stimulated cellular proliferation. On the contrary, the presence of PRRSV-infected MoDC supernatant significantly reduced the numbers of proliferating $CD4^+$, $CD8^+$, and $CD4^+CD8^+$ cells in the PHA-stimulated cultures, and these effects could be abrogated by addition of anti-IL-1Ra Ab (**Figures 4A–C** and **Supplementary Figure 3A**). The results indicated that PRRSV-induced IL-1Ra was involved in suppression of PHA-induced T lymphocyte proliferation.

Next, we examined the effect of PRRSV-induced IL-1Ra on antigen-specific T cell proliferation. Consistent with the above findings, the presence of CSFV induced antigen-specific proliferation of $CD4^+$, $CD8^+$, and $CD4^+CD8^+$ subpopulations from the CSFV-primed pigs. The CSFV-specific lymphocyte proliferation was significantly reduced in the presence of the supernatant obtained from the PRRSV-infected MoDC, whereas addition of anti-IL-1Ra Ab could restore the CSFV-specific lymphocyte proliferation (**Figures 4D–F** and **Supplementary Figure 3B**). The findings suggested the negative effect of PRRSV-induced IL-1Ra on porcine antigen-specific lymphocyte proliferation.

We further examined the effect of PRRSV-induced IL-1Ra on T lymphocyte effector function by enumerating the number of IFN-γ-producing T lymphocytes. Addition of supernatant from PRRSV-infected MoDC significantly reduced the numbers of PHA-activated and CSFV-specific IFN-γ-producing T lymphocytes (**Figures 5A,B** and **Supplementary Figures 5A,B**). Addition of anti-IL-1Ra Ab into PHA-induced PBMC could only partially restore the numbers of IFN-γ-producing T lymphocytes (**Figure 5A** and **Supplementary Figure 5A**). Similarly, addition of anti-IL-1Ra Ab did not restore the numbers of CSFV-specific IFN-γ-producing cells in the culture system (**Figure 5B** and **Supplementary Figure 5B**). Together, our data demonstrated that the presence of PRRSV-induced IL-1Ra in the culture system significantly inhibited mitogen-induced and virus-specific lymphocyte proliferation. However, the negative effect of PRRSV-induced IL-1Ra on IFN-γ produced by T lymphocytes was not significant.

PRRSV-Induced IL-1Ra Was Involved in the Induction of Treg, but Not IL-10-Producing T Lymphocytes

As shown earlier, strong upregulation of *FOXP3* was observed in the presence of PRRSV-infected MoDC supernatant. To further investigate the role of PRRSV-induced IL-1Ra on IL-10 production and induction of Treg, PBMC were infected with PRRSV or mock, and in the presence or absence of anti-IL-1Ra Ab. Similarly to MoDC, PRRSV infection significantly induced IL-1Ra production in the cultured PBMC (**Supplementary Figures 4A,B**). In agreement with previous findings (23, 49, 50), PRRSV enhanced the numbers of IL-10-producing T lymphocytes and Treg (**Figures 6A,B** and **Supplementary Figures 6A,B**). Addition of anti-IL-1Ra Ab had little effect on the reduction of IL-10-producing T lymphocytes (**Figure 6A** and **Supplementary Figure 6A**). IL-1Ra neutralization significantly decreased the numbers of Treg,

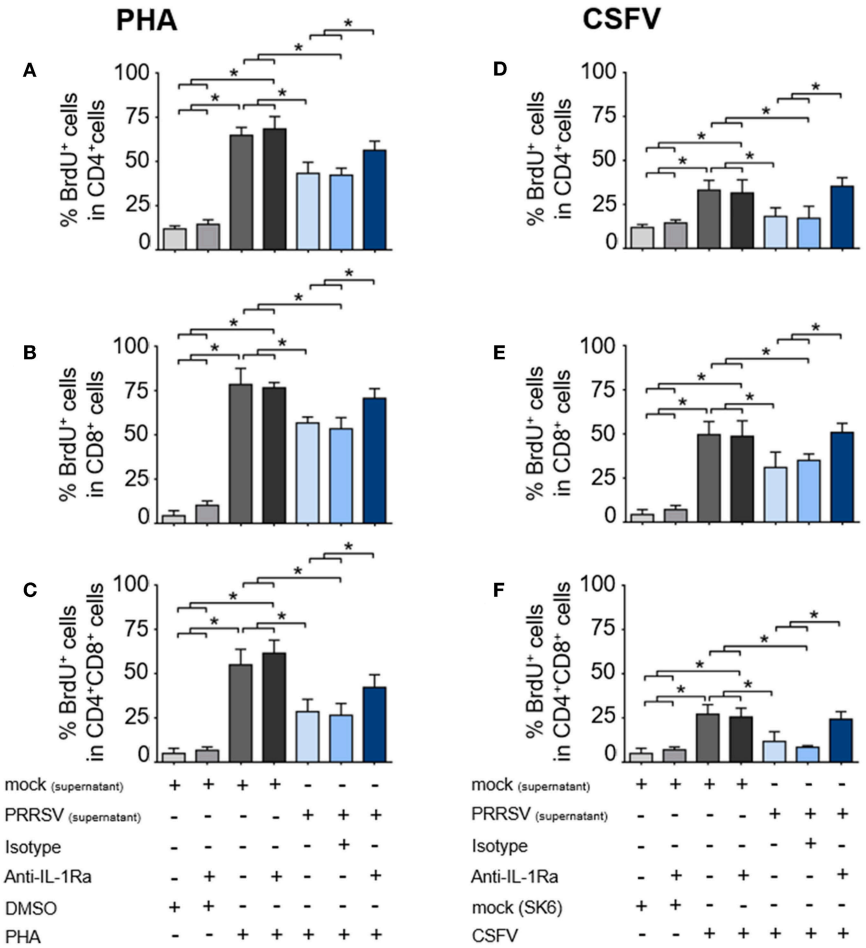

FIGURE 4 | PRRSV-induced IL-1Ra inhibited lymphocyte proliferation. PRRSV-induced IL-1Ra inhibited PHA-induced proliferation of the **(A)** $CD4^+$, **(B)** $CD8^+$, and **(C)** $CD4^+CD8^+$ subpopulations. PRRSV-induced IL-1Ra inhibited CSFV-specific proliferations of the **(D)** $CD4^+$, **(E)** $CD8^+$, and **(F)** $CD4^+CD8^+$ subpopulations. The supernatants obtained from type 2 PRRSV or mock (MARC-145 cell lysate) were pretreated with anti-IL-1Ra Ab for 2 h prior to addition into the culture. PBL or PBMC were culture with PHA, CSFV or controls for 96 h, in the presence of the pretreated supernatants. ± indicates presence/absence of indicated treatment within the culture. Data represents mean ± SD from 5 pigs. Statistical significance was analyzed using ANOVA followed by Tukey's test. * indicates significant difference at $p < 0.05$.

although not to the level of uninfected PBMC (**Figure 6B** and **Supplementary Figure 6B**). These findings indicated that PRRSV-induced IL-1Ra might not be directly involved in the development of IL-10-producing T lymphocytes, but could partly play a role in Treg induction under our studied conditions.

DISCUSSION

Interleukin-1 receptor antagonist (IL-1Ra) is known as an early inhibitory cytokine, which potentially participates in PRRSV-induced immunosuppression during the early phase of infection (26). As several reports showed that IL-1Ra is a potent negative immunomodulator of both innate and adaptive immune functions (51–53), the present study extended the characterization of the negative immunomodulatory effects of PRRSV-induced IL-1Ra on several aspects of porcine immune functions.

Porcine dendritic cell (DC) populations, i.e., conventional DC (cDC) and non-conventional DC, exhibit different PRRSV susceptibility. Several studies strongly indicated that PRRSV could not infect both cDC1 and cDC2 populations (54–56). It should be emphasized that this study utilized MoDC, a non-conventional DC, and that the observed PRRSV infectivity in porcine MoDC was consistent with the previous reports (10, 57). The immunomodulatory effects of PRRSV-induced IL-1Ra in the cDC population remains to be elucidated. In addition, variation in PRRSV infectivity of porcine myeloid cells might be related to the PRRSV strains used in the studies (58, 59).

The inhibition of phagocytic activity and APC maturation by PRRSV-induced IL-1Ra strongly supported the role of IL-1Ra in PRRSV immunopathogenesis. These findings were in agreement with the previous studies in human and mouse models reporting the suppressive effects of exogenous IL-1Ra on Fc-dependent phagocytosis (60), and APC maturation (52). Our observations that PRRSV-induced IL-1Ra downregulated *IFNA*

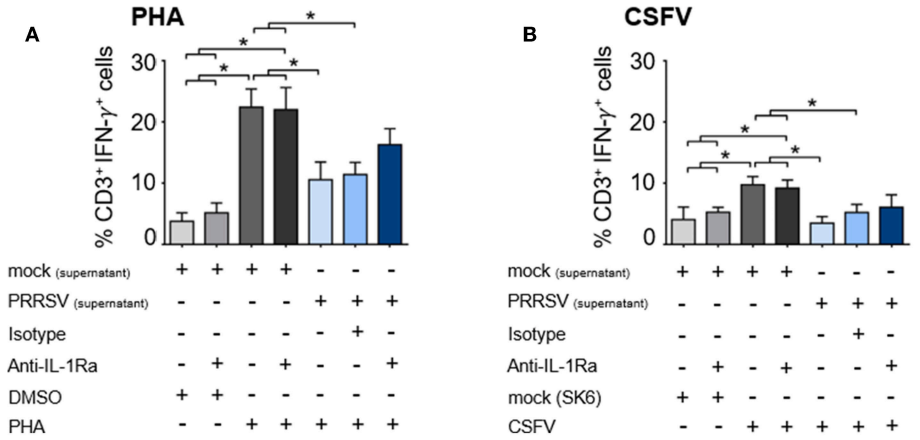

FIGURE 5 | PRRSV-induced IL-1Ra was not involved in suppression of IFN-γ-producing T lymphocytes in both **(A)** polyclonal and **(B)** recalled CSFV responses. The supernatants obtained from type 2 PRRSV or mock (MARC-145 cell lysate) were pretreated with anti-IL-1Ra Ab for 2 h prior to addition into the culture. PBL or PBMC were cultured with PHA, CSFV or controls for 48 h, in the presence of the pretreated supernatants. ± indicates presence/absence of indicated treatment within the culture. Data represents mean ± SD from 5 pigs. Statistical significance was analyzed using ANOVA followed by Tukey's test. * indicates significant difference at $p < 0.05$.

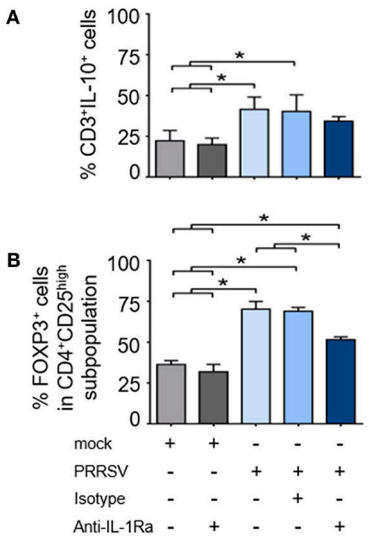

FIGURE 6 | PRRSV-induced IL-1Ra was partially involved in regulatory T lymphocyte (Treg) induction. PRRSV-induced IL-1Ra decreased numbers of **(A)** Treg, **(B)** but not IL-10-producing T lymphocytes. PBMC were cultured in the presence of type 2 PRRSV or mock. Subsequently, anti-IL-1Ra Ab was added into the culture and further incubated for 48 h. ± indicates presence/absence of indicated treatment within the culture. Data represents mean ± SD from 5 pigs. Statistical significance was analyzed using ANOVA followed by Tukey's test. * indicates significant difference at $p < 0.05$.

and *IL1* gene expression were in agreement with previously published data on the inhibitory effects of IL-1Ra on type I IFN and pro-inflammatory cytokine productions in macrophages and DC (28, 61). Interestingly, suppression of *IL6* gene expression by PRRSV was not dependent with IL-1Ra under our experimental conditions. It must be pointed out that in experimental models of acute-phase response (62), IL-1Ra could not prevent excessive IL-6 production within local injury. Hence, our results suggested that other mechanisms besides IL-1Ra mediate PRRSV-suppressed IL-6 production.

PRRSV infection has long been shown to cause a negative impact on host immunity against other pathogens, including CSFV (44, 45). Differentiation into porcine T helper 1 (Th1) and T helper 2 (Th2) lymphocyte lineages requires specific expression of transcription factors (TF), TBET and GATA3, respectively (63, 64). Here, we demonstrated that PRRSV-induced IL-1Ra interfered with antigen-specific Th1/Th2 response by the downregulation of *TBET* and *GATA3* expressions. Supporting our findings, blocking of IL-1R signaling pathway inhibited Th1 and Th2 differentiations (53, 65). Surprisingly, IL-1Ra neutralization resulted in a higher level of *TBET* and *GATA3* expressions than those from the cells cultured with CSFV alone suggesting that a basal level of IL-1Ra is requested to balance the Th differentiation (66–68). Suppression of T lymphocyte differentiation by PRRSV-induced IL-1Ra most likely contributed to the observed negative impact of PRRSV on CSFV-specific immune responses in pigs (44, 45). We also demonstrated that PRRSV-induced IL-1Ra significantly suppressed mitogen- as well as antigen-dependent lymphocyte proliferation. The effect of PRRSV-induced IL-1Ra on T lymphocyte proliferation was quite expected as signaling via IL-1R was shown to be a prerequisite for induction of T helper lymphocyte (Th) proliferation (53). Moreover, blocking IL-1R activation with exogenous IL-1Ra could inhibit DNA replication, resulting in a reduction of T lymphocyte expansion (69, 70). Altogether, our findings suggested that the poor adaptive immune response, usually observed in PRRSV infected pigs, is in part due to the inhibition of T lymphocyte differentiation and proliferation by PRRSV-induced IL-1Ra.

The effector function of Th lymphocyte responses is attributable to specific types of cytokine production (71, 72). IFN-γ produced by Th1 lymphocytes can facilitate phagocytosis,

antigen processing and presentation, antiviral stage of affected cells, and activation of effector cytotoxic T lymphocytes (CTL) (73). Delayed PRRSV-specific IFN-γ-secreting T lymphocyte response is usually observed during PRRSV infection (19, 74). However, transcriptomic analysis of PRRSV-immunized pigs revealed that the IFN-γ pathway was essential for activation of anti-viral defense mechanism (75). On the other hand, IL-10, a potent inhibitory cytokine, is known as one of the major PRRSV-induced immunosuppressive mechanisms (22, 49, 50). Consistent with previous findings, we demonstrated that PRRSV infection suppressed IFN-γ and increased IL-10-producing T lymphocytes. Although IL-1R signaling was also reported to play an important role in T lymphocyte effector function (53, 76), neutralization of IL-1Ra had no effect on both IFN-γ and IL-10 production in the cultured T cell populations. These observations convincingly pointed out that PRRSV-induced IL-1Ra might not be directly involved in T lymphocyte effector functions, but rather may interfere with T cell induction phase as observed through alteration of TF gene and cellular proliferation. The findings also suggested that other undefined immunomodulatory mechanisms might be responsible for these observations. A possible mechanism is via IL-10, as it directly interferes with IFN-γ production in memory T lymphocytes (77, 78). Although IL-10 production by other leukocyte populations was not determined in this study, previous reports evidenced the secretion of IL-10 from PRRSV-infected macrophages and DC (9, 50). Collectively, IL-10 produced by various leukocyte subpopulations may help promote IL-1Ra production as IL-10 can enhance production of IL-1Ra by recruitment of NF-κB to IL-1Ra promotor in monocytes and macrophages (79). It is likely that both IL-1Ra and IL-10 act synergistically in PRRSV-induced immunosuppression.

Induction of Treg, the inhibitory Th lymphocytes, is one of the PRRSV-induced negative immunomodulatory mechanisms (49, 80, 81). Development and function of Treg are distinct among Th lymphocyte lineages (82). Although expression of FOXP3 plays an important role during Treg differentiation and development, FOXP3 *per se* is not sufficient to maintain Treg phenotype and their functions (83). Other costimulatory regulators including PD-L1, CTLA-4, IL-2, IL-10, and TGF-β, collectively contribute to stable Treg phenotype and suppressive activities (84, 85), neutralization of IL-1Ra did not modulate PRRSV-induced *FOXP3* gene expression in the cultured PBMC (**Figure 3E**), but it could partially reduce the induction of PRRSV-induced $FOXP3^{+}CD4^{+}CD25^{high}$ subpopulation (**Figure 6B**). It is possible that PRRSV-induced IL-1Ra does not help to promote Treg development, but potentially participates in maintaining Treg characteristics in the culture system. The finding on effects of PRRSV-induced IL-1Ra on Treg induction is intriguing. Previously, it was clearly demonstrated that IL-10 was responsible for induction of PRRSV-specific Treg (22). Apart from IL-10, PRRSV-induced TGF-β production is also involved in differentiation of inducible Treg (80, 86–89). There were some studies reporting that IL-1Ra could enhance TGF-β production in leukocytes and somatic cells (90, 91). This finding could strengthen our hypothesis on the role of PRRSV-induced IL-1Ra in the maintenance of Treg population.

Several key questions remain unanswered but need to be deeply investigated in order to fully characterize the roles of IL-1Ra in PRRSV immunopathogenesis. First, what is the precise molecular mechanism(s) of PRRSV-induced IL-1Ra in the infected cell? Second, what is the effect of PRRSV-induced IL-1Ra on IL-10 production, and vice versa, in myeloid cell population? Is it possible that both cytokines act synergistically to provide an immunological niche promoting Treg? Furthermore, in the context of PRRSV vaccine development, promising strategies based on the reduction of both induced IL-1Ra and IL-10 should also be explored. Although our observations on the negative immunomodulatory effects of PRRSV-induced IL-1Ra were obtained using *in vitro* assays, these circumstances are likely relevant to PRRSV-induced immunosuppression in the infected pigs in regard to impaired innate cytokine production (16, 92), prolonged PRRSV-specific T helper and CTL induction (93), and enhanced PRRSV-specific Treg population (22, 24, 94). In contrast, highly pathogenic (HP)-PRRSV infection, which is deficient in its ability for IL-1Ra induction (26), causes robust innate cytokine production in an early phase of infection (95). These findings support our notion that IL-1Ra is, in part, responsible for negative immune responses in the PRRSV-infected pigs.

In conclusion, this study highlighted the negative immunomodulatory effects of PRRSV-induced IL-1Ra on both porcine innate and adaptive immune functions. Our findings clearly demonstrated the inhibitory effects of PRRSV-induced IL-1Ra on APC functions, including phagocytosis and maturation, as well as interfering with the induction phase of T lymphocyte responses. Furthermore, IL-1Ra could help to maintain PRRSV-specific Treg population. This study confirms the role of IL-1Ra as a key immunosuppressor during the course of PRRSV infection.

DATA AVAILABILITY

The datasets generated for this study are available on request to the corresponding author.

ETHICS STATEMENT

Animal care and use protocols for this study followed the *Ethical Principles and Guidelines for the Use of Animals*, National Research Council of Thailand, and the *Guide for the Care and Use of Laboratory Animals*, National Research Council, USA. All methods and animal studies were approved by Chulalongkorn University Animal Care and Use Committee, Chulalongkorn University (Animal Use Protocol No. 1631029).

AUTHOR CONTRIBUTIONS

TN, NT, RT, and SS designed research studies. TN and NT performed experiments, acquired data, analyzed data. TN, NT, and SS drafted the manuscript.

FUNDING

This work was supported by The Royal Golden Jubilee Ph.D. Program (TN PHD58K0106), and The 90th Anniversary of Chulalongkorn University fund (Ratchadaphisek Somphot endowment fund; TN, GCUGR1125602028D) and The Thailand Research Fund (RTA 6080012).

ACKNOWLEDGMENTS

The authors are grateful to the staffs of the Veterinary Diagnostic Laboratory (CU-VDL) and Department of Veterinary Microbiology at the Faculty of Veterinary Science, Chulalongkorn University (CUVET) for their technical assistance. We would like to thank Dr. Matthew D. Wegner, Dr. Alain Jacquet, Dr. Rangsima Reantragoon, and Dr. Jin Cui for kind assistance during manuscript preparation.

SUPPLEMENTARY MATERIAL

The Supplementary Material for this article can be found online at: https://www.frontiersin.org/articles/10.3389/fimmu.2019.00579/full#supplementary-material

REFERENCES

1. Kuhn JH, Lauck M, Bailey AL, Shchetinin AM, Vishnevskaya TV, Bao Y, et al. Reorganization and expansion of the nidoviral family Arteriviridae. *Arch Virol.* (2016) 161:755–68. doi: 10.1007/s00705-015-2672-z
2. Brar MS, Shi M, Hui RK, Leung FC. Genomic evolution of porcine reproductive and respiratory syndrome virus (PRRSV) isolates revealed by deep sequencing. *PLoS ONE.* (2014) 9:e88807. doi: 10.1371/journal.pone.0088807
3. Rowland RR, Steffen M, Ackerman T, Benfield DA. The evolution of porcine reproductive and respiratory syndrome virus: quasispecies and emergence of a virus subpopulation during infection of pigs with VR-2332. *Virology.* (1999) 259:262–6. doi: 10.1006/viro.1999.9789
4. Goldberg TL, Lowe JF, Milburn SM, Firkins LD. Quasispecies variation of porcine reproductive and respiratory syndrome virus during natural infection. *Virology.* (2003) 317:197–207. doi: 10.1016/j.virol.2003.07.009
5. Kimman TG, Cornelissen LA, Moormann RJ, Rebel JM, Stockhofe-Zurwieden N. Challenges for porcine reproductive and respiratory syndrome virus (PRRSV) vaccinology. *Vaccine.* (2009) 27:3704–18. doi: 10.1016/j.vaccine.2009.04.022
6. Jung K, Renukaradhya GJ, Alekseev KP, Fang Y, Tang Y, Saif LJ. Porcine reproductive and respiratory syndrome virus modifies innate immunity and alters disease outcome in pigs subsequently infected with porcine respiratory coronavirus: implications for respiratory viral co-infections. *J Gen Virol.* (2009) 90:2713–23. doi: 10.1099/vir.0.014001-0
7. Iwasaki A, Pillai PS. Innate immunity to influenza virus infection. *Nat Rev Immunol.* (2014) 14:315–28. doi: 10.1038/nri3665
8. Iwasaki A, Medzhitov R. Control of adaptive immunity by the innate immune system. *Nat Immunol.* (2015) 16:343–53. doi: 10.1038/ni.3123
9. Sang Y, Rowland RR, Blecha F. Interaction between innate immunity and porcine reproductive and respiratory syndrome virus. *Anim Health Res Rev.* (2011) 12:149–67. doi: 10.1017/S1466252311000144
10. Singleton H, Graham SP, Bodman-Smith KB, Frossard JP, Steinbach F. Establishing porcine monocyte-derived macrophage and dendritic cell systems for studying the interaction with PRRSV-1. *Front Microbiol.* (2016) 7:832. doi: 10.3389/fmicb.2016.00832
11. Ke H, Yoo D. The viral innate immune antagonism and an alternative vaccine design for PRRS virus. *Vet Microbiol.* (2017) 209:75–89. doi: 10.1016/j.vetmic.2017.03.014
12. Park JY, Kim HS, Seo SH. Characterization of interaction between porcine reproductive and respiratory syndrome virus and porcine dendritic cells. *J Microbiol Biotechnol.* (2008) 18:1709–16.
13. Rodriguez-Gomez IM, Gomez-Laguna J, Carrasco L. Impact of PRRSV on activation and viability of antigen presenting cells. *World J Virol.* (2013) 2:146–51. doi: 10.5501/wjv.v2.i4.146
14. Richmond O, Cecere TE, Erdogan E, Meng XJ, Pineyro P, Subramaniam S, et al. PD-L1 expression is increased in monocyte derived dendritic cells in response to porcine circovirus type 2 and porcine reproductive and respiratory syndrome virus infections. *Vet Immunol Immunopathol.* (2015) 168:24–9. doi: 10.1016/j.vetimm.2015.09.013
15. Richmond O, Cecere TE, Erdogan E, Meng XJ, Pineyro P, Subramaniam S, et al. The PD-L1/CD86 ratio is increased in dendritic cells co-infected with porcine circovirus type 2 and porcine reproductive and respiratory syndrome virus, and the PD-L1/PD-1 axis is associated with anergy, apoptosis, and the induction of regulatory T-cells in porcine lymphocytes. *Vet Microbiol.* (2015) 180:223–9. doi: 10.1016/j.vetmic.2015.09.014
16. van Reeth K, Nauwynck H. Proinflammatory cytokines and viral respiratory disease in pigs. *Vet Res.* (2000) 31:187–213. doi: 10.1051/vetres:2000113
17. Wang R, Zhang YJ. Antagonizing interferon-mediated immune response by porcine reproductive and respiratory syndrome virus. *Biomed Res Int.* (2014) 2014:315470. doi: 10.1155/2014/315470
18. Lunney JK, Fang Y, Ladinig A, Chen N, Li Y, Rowland B, et al. Porcine reproductive and respiratory syndrome virus (PRRSV): pathogenesis and interaction with the immune system. *Annu Rev Anim Biosci.* (2016) 4:129–54. doi: 10.1146/annurev-animal-022114-111025
19. Meier WA, Galeota J, Osorio FA, Husmann RJ, Schnitzlein WM, Zuckermann FA. Gradual development of the interferon-gamma response of swine to porcine reproductive and respiratory syndrome virus infection or vaccination. *Virology.* (2003) 309:18–31. doi: 10.1016/S0042-6822(03)00009-6
20. Butler JE, Lager KM, Golde W, Faaberg KS, Sinkora M, Loving C, et al. Porcine reproductive and respiratory syndrome (PRRS): an immune dysregulatory pandemic. *Immunol Res.* (2014) 59:81–108. doi: 10.1007/s12026-014-8549-5
21. Lopez OJ, Osorio FA. Role of neutralizing antibodies in PRRSV protective immunity. *Vet Immunol Immunopathol.* (2004) 102:155–63. doi: 10.1016/j.vetimm.2004.09.005
22. Wongyanin P, Buranapraditkul S, Yoo D, Thanawongnuwech R, Roth JA, Suradhat S. Role of porcine reproductive and respiratory syndrome virus nucleocapsid protein in induction of interleukin-10 and regulatory T-lymphocytes (Treg). *J Gen Virol.* (2012) 93:1236–46. doi: 10.1099/vir.0.040287-0
23. Chung HK, Chae C. Expression of interleukin-10 and interleukin-12 in piglets experimentally infected with porcine reproductive and respiratory syndrome virus (PRRSV). *J Comp Pathol.* (2003) 129:205–12. doi: 10.1016/S0021-9975(03)00036-7
24. Wongyanin P, Buranapraditkun S, Chokeshai-Usaha K, Thanawonguwech R, Suradhat S. Induction of inducible CD4+CD25+Foxp3+ regulatory T lymphocytes by porcine reproductive and respiratory syndrome virus (PRRSV). *Vet Immunol Immunopathol.* (2010) 133:170–82. doi: 10.1016/j.vetimm.2009.07.012
25. Charerntantanakul W, Platt R, Roth JA. Effects of porcine reproductive and respiratory syndrome virus-infected antigen-presenting cells on T cell activation and antiviral cytokine production. *Viral Immunol.* (2006) 19:646–61. doi: 10.1089/vim.2006.19.646
26. Nedumpun T, Wongyanin P, Sirisereewan C, Ritprajak P, Palaga T, Thanawongnuwech R, et al. Interleukin-1 receptor antagonist: an early immunomodulatory cytokine induced by porcine reproductive and respiratory syndrome virus. *J Gen Virol.* (2017) 98:77–88. doi: 10.1099/jgv.0.000665

27. Arend WP, Malyak M, Guthridge CJ, Gabay C. Interleukin-1 receptor antagonist: role in biology. *Annu Rev Immunol.* (1998) 16:27–55. doi: 10.1146/annurev.immunol.16.1.27
28. Marsh CB, Moore SA, Pope HA, Wewers MD. IL-1ra suppresses endotoxin-induced IL-1 beta and TNF-alpha release from mononuclear phagocytes. *Am J Physiol.* (1994) 267:L39–45. doi: 10.1152/ajplung.1994.267.1.L39
29. Sims JE, Smith DE. The IL-1 family: regulators of immunity. *Nat Rev Immunol.* (2010) 10:89–102. doi: 10.1038/nri2691
30. Matsuki T, Nakae S, Sudo K, Horai R, Iwakura Y. Abnormal T cell activation caused by the imbalance of the IL-1/IL-1R antagonist system is responsible for the development of experimental autoimmune encephalomyelitis. *Int Immunol.* (2006) 18:399–407. doi: 10.1093/intimm/dxh379
31. Sivaraman V, Pechous RD, Stasulli NM, Eichelberger KR, Miao EA, Goldman WE. Yersinia pestis activates both IL-1beta and IL-1 receptor antagonist to modulate lung inflammation during pneumonic plague. *PLoS Pathog.* (2015) 11:e1004688. doi: 10.1371/journal.ppat.1004688
32. Zavala F, Rimaniol AC, Boussin F, Dormont D, Bach JF, Descamps-Latscha B. HIV predominantly induces IL-1 receptor antagonist over IL-1 synthesis in human primary monocytes. *J Immunol.* (1995) 155:2784–93.
33. Thanawongnuwech R, Amonsin A, Tatsanakit A, Damrongwatanapokin S. Genetics and geographical variation of porcine reproductive and respiratory syndrome virus (PRRSV) in Thailand. *Vet Microbiol.* (2004) 101:9–21. doi: 10.1016/j.vetmic.2004.03.005
34. Nedumpun T, Ritprajak P, Suradhat S. Generation of potent porcine monocyte-derived dendritic cells (MoDCs) by modified culture protocol. *Vet Immunol Immunopathol.* (2016) 182:63–8. doi: 10.1016/j.vetimm.2016.10.002
35. Obremski K. The effect of *in vivo* exposure to zearalenone on cytokine secretion by Th1 and Th2 lymphocytes in porcine Peyer's patches after *in vitro* stimulation with LPS. *Pol J Vet Sci.* (2014) 17:625–32. doi: 10.2478/pjvs-2014-0093
36. Kiros TG, van Kessel J, Babiuk LA, Gerdts V. Induction, regulation and physiological role of IL-17 secreting helper T-cells isolated from PBMC, thymus, and lung lymphocytes of young pigs. *Vet Immunol Immunopathol.* (2011) 144:448–54. doi: 10.1016/j.vetimm.2011.08.021
37. Mounsey KE, Murray HC, Bielefeldt-Ohmann H, Pasay C, Holt DC, Currie BJ, et al. Prospective study in a porcine model of sarcoptes scabiei indicates the association of Th2 and Th17 pathways with the clinical severity of scabies. *PLoS Negl Trop Dis.* (2015) 9:98–115. doi: 10.1371/journal.pntd.0003498
38. Chang HC, Peng YT, Chang HL, Chaung HC, Chung WB. Phenotypic and functional modulation of bone marrow-derived dendritic cells by porcine reproductive and respiratory syndrome virus. *Vet Microbiol.* (2008) 129:281–93. doi: 10.1016/j.vetmic.2007.12.002
39. Gimeno M, Darwich L, Diaz I, de la Torre E, Pujols J, Martin M, et al. Cytokine profiles and phenotype regulation of antigen presenting cells by genotype-I porcine reproductive and respiratory syndrome virus isolates. *Vet Res.* (2011) 42:9. doi: 10.1186/1297-9716-42-9
40. Pineyro PE, Subramaniam S, Kenney SP, Heffron CL, Gimenez-Lirola LG, Meng XJ. Modulation of proinflammatory cytokines in monocyte-derived dendritic cells by porcine reproductive and respiratory syndrome virus through interaction with the porcine intercellular-adhesion-molecule-3-grabbing nonintegrin. *Viral Immunol.* (2016) 29:546–56. doi: 10.1089/vim.2016.0104
41. Lopez-Fuertes L, Campos E, Domenech N, Ezquerra A, Castro JM, Dominguez J, et al. Porcine reproductive and respiratory syndrome (PRRS) virus down-modulates TNF-alpha production in infected macrophages. *Virus Res.* (2000) 69:41–6. doi: 10.1016/S0168-1702(00)00172-6
42. Van Gucht S, Labarque G, Van Reeth K. The combination of PRRS virus and bacterial endotoxin as a model for multifactorial respiratory disease in pigs. *Vet Immunol Immunopathol.* (2004) 102:165–78. doi: 10.1016/j.vetimm.2004.09.006
43. Zhou Y, Bai J, Li Y, Wang X, Wang X, Jiang P. Suppression of immune responses in pigs by nonstructural protein 1 of porcine reproductive and respiratory syndrome virus. *Can J Vet Res.* (2012) 76:255–60.
44. Li H, Yang H. Infection of porcine reproductive and respiratory syndrome virus suppresses the antibody response to classical swine fever virus vaccination. *Vet Microbiol.* (2003) 95:295–301. doi: 10.1016/S0378-1135(03)00158-5
45. Suradhat S, Kesdangsakonwut S, Sada W, Buranapraditkun S, Wongsawang S, Thanawongnuwech R. Negative impact of porcine reproductive and respiratory syndrome virus infection on the efficacy of classical swine fever vaccine. *Vaccine.* (2006) 24:2634–42. doi: 10.1016/j.vaccine.2005.12.010
46. Rahe MC, Murtaugh MP. Mechanisms of adaptive immunity to porcine reproductive and respiratory syndrome virus. *Viruses.* (2017) 9:148. doi: 10.3390/v9060148
47. Franzoni G, Kurkure NV, Edgar DS, Everett HE, Gerner W, Bodman-Smith KB, et al. Assessment of the phenotype and functionality of porcine CD8 T cell responses following vaccination with live attenuated classical swine fever virus (CSFV) and virulent CSFV challenge. *Clin Vaccine Immunol.* (2013) 20:1604–16. doi: 10.1128/CVI.00415-13
48. Summerfield A, Ruggli N. Immune responses against classical swine fever virus: between ignorance and lunacy. *Front Vet Sci.* (2015) 2:10. doi: 10.3389/fvets.2015.00010
49. Suradhat S, Thanawongnuwech R, Poovorawan Y. Upregulation of IL-10 gene expression in porcine peripheral blood mononuclear cells by porcine reproductive and respiratory syndrome virus. *J Gen Virol.* (2003) 84:453–9. doi: 10.1099/vir.0.18698-0
50. Song S, Bi J, Wang D, Fang L, Zhang L, Li F, et al. Porcine reproductive and respiratory syndrome virus infection activates IL-10 production through NF-kappaB and p38 MAPK pathways in porcine alveolar macrophages. *Dev Comp Immunol.* (2013) 39:265–72. doi: 10.1016/j.dci.2012.10.001
51. Granowitz EV, Clark BD, Vannier E, Callahan MV, Dinarello CA. Effect of interleukin-1 (IL-1) blockade on cytokine synthesis: I. IL-1 receptor antagonist inhibits IL-1-induced cytokine synthesis and blocks the binding of IL-1 to its type II receptor on human monocytes. *Blood.* (1992) 79:2356–63.
52. Iizasa H, Yoneyama H, Mukaida N, Katakoka Y, Naito M, Yoshida N, et al. Exacerbation of granuloma formation in IL-1 receptor antagonist-deficient mice with impaired dendritic cell maturation associated with Th2 cytokine production. *J Immunol.* (2005) 174:3273–80. doi: 10.4049/jimmunol.174.6.3273
53. Ben-Sasson SZ, Hu-Li J, Quiel J, Cauchetaux S, Ratner M, Shapira I, et al. IL-1 acts directly on CD4 T cells to enhance their antigen-driven expansion and differentiation. *Proc Natl Acad Sci USA.* (2009) 106:7119–24. doi: 10.1073/pnas.0902745106
54. Bordet E, Blanc F, Tiret M, Crisci E, Bouguyon E, Renson P, et al. Porcine reproductive and respiratory syndrome virus type 1.3 lena triggers conventional dendritic cells 1 activation and T helper 1 immune response without infecting dendritic cells. *Front Immunol.* (2018) 9:2299. doi: 10.3389/fimmu.2018.02299
55. Resendiz M, Valenzuela O, Hernandez J. Response of the cDC1 and cDC2 subtypes of tracheal dendritic cells to porcine reproductive and respiratory syndrome virus. *Vet Microbiol.* (2018) 223:27–33. doi: 10.1016/j.vetmic.2018.07.012
56. Puebla-Clark L, Parra-Sanchez H, Resendiz M, Valenzuela O, Hernandez J. Tonsil conventional dendritic cells are not infected by porcine reproductive and respiratory syndrome virus. *Virology.* (2019) 529:65–72. doi: 10.1016/j.virol.2019.01.012
57. Silva-Campa E, Cordoba L, Fraile L, Flores-Mendoza L, Montoya M, Hernandez J. European genotype of porcine reproductive and respiratory syndrome (PRRSV) infects monocyte-derived dendritic cells but does not induce Treg cells. *Virology.* (2010) 396:264–71. doi: 10.1016/j.virol.2009.10.024
58. Frydas IS, Verbeeck M, Cao J, Nauwynck HJ. Replication characteristics of porcine reproductive and respiratory syndrome virus (PRRSV) European subtype 1 (Lelystad) and subtype 3 (Lena) strains in nasal mucosa and cells of the monocytic lineage: indications for the use of new receptors of PRRSV (Lena). *Vet Res.* (2013) 44:73. doi: 10.1186/1297-9716-44-73
59. Garcia-Nicolas O, Baumann A, Vielle NJ, Gomez-Laguna J, Quereda JJ, Pallares FJ, et al. Virulence and genotype-associated infectivity of interferon-treated macrophages by porcine reproductive and respiratory syndrome viruses. *Virus Res.* (2014) 179:204–11. doi: 10.1016/j.virusres.2013.08.009
60. Coopamah MD, Freedman J, Semple JW. Anti-D initially stimulates an Fc-dependent leukocyte oxidative burst and subsequently suppresses erythrophagocytosis via interleukin-1 receptor antagonist. *Blood.* (2003) 102:2862–7. doi: 10.1182/blood-2003-04-1029

61. Mayer-Barber KD, Andrade BB, Oland SD, Amaral EP, Barber DL, Gonzales J, et al. Host-directed therapy of tuberculosis based on interleukin-1 and type I interferon crosstalk. *Nature.* (2014) 511:99–103. doi: 10.1038/nature13489
62. Gabay C, Gigley J, Sipe J, Arend WP, Fantuzzi G. Production of IL-1 receptor antagonist by hepatocytes is regulated as an acute-phase protein *in vivo*. *Eur J Immunol.* (2001) 31:490–9. doi: 10.1002/1521-4141(200102)31:2<490::AID-IMMU490>3.0.CO;2-H
63. Gu W, Li CS, Yin WP, Hou XM, Zhang J, Zhang D, et al. Expression imbalance of transcription factors GATA-3 and T-bet in post-resuscitation myocardial immune dysfunction in a porcine model of cardiac arrest. *Resuscitation.* (2013) 84:848–53. doi: 10.1016/j.resuscitation.2012.11.023
64. Rodriguez-Gomez IM, Talker SC, Kaser T, Stadler M, Hammer SE, Saalmuller A, et al. Expression of T-bet, Eomesodermin and GATA-3 in porcine alphabeta T cells. *Dev Comp Immunol.* (2016) 60:115–26. doi: 10.1016/j.dci.2016.02.022
65. Nakahara T, Moroi Y, Uchi H, Furue M. Differential role of MAPK signaling in human dendritic cell maturation and Th1/Th2 engagement. *J Dermatol Sci.* (2006) 42:1–11. doi: 10.1016/j.jdermsci.2005.11.004
66. Arend WP. The balance between IL-1 and IL-1Ra in disease. *Cytokine Growth Factor Rev.* (2002) 13:323–40. doi: 10.1016/S1359-6101(02)00020-5
67. Santarlasci V, Cosmi L, Maggi L, Liotta F, Annunziato F. IL-1 and T helper immune responses. *Front Immunol.* (2013) 4:182. doi: 10.3389/fimmu.2013.00182
68. Ikeda S, Saijo S, Murayama MA, Shimizu K, Akitsu A, Iwakura Y. Excess IL-1 signaling enhances the development of Th17 cells by downregulating TGF-beta-induced Foxp3 expression. *J Immunol.* (2014) 192:1449–58. doi: 10.4049/jimmunol.1300387
69. Conti P, Reale M, Barbacane RC, Panara MR, Bongrazio M, Dempsey RA, et al. Reduced mitogen stimulation of DNA synthesis in human lymphocytes by a human recombinant interleukin-1 receptor antagonist. *Immunol Lett.* (1991) 28:19–25. doi: 10.1016/0165-2478(91)90122-Q
70. Rambaldi A, Torcia M, Bettoni S, Vannier E, Barbui T, Shaw AR, et al. Modulation of cell proliferation and cytokine production in acute myeloblastic leukemia by interleukin-1 receptor antagonist and lack of its expression by leukemic cells. *Blood.* (1991) 78:3248–53.
71. Lanzavecchia A, Sallusto F. Dynamics of T lymphocyte responses: intermediates, effectors, and memory cells. *Science.* (2000) 290:92–7. doi: 10.1126/science.290.5489.92
72. Olsen Saraiva Camara N, Lepique AP, Basso AS. Lymphocyte differentiation and effector functions. *Clin Dev Immunol.* (2012) 2012:510603. doi: 10.1155/2012/510603
73. Schroder K, Hertzog PJ, Ravasi T, Hume DA. Interferon-gamma: an overview of signals, mechanisms and functions. *J Leukoc Biol.* (2004) 75:163–89. doi: 10.1189/jlb.0603252
74. Dwivedi V, Manickam C, Binjawadagi B, Linhares D, Murtaugh MP, Renukaradhya GJ. Evaluation of immune responses to porcine reproductive and respiratory syndrome virus in pigs during early stage of infection under farm conditions. *Virol J.* (2012) 9:45. doi: 10.1186/1743-422X-9-45
75. Islam MA, Grosse-Brinkhaus C, Proll MJ, Uddin MJ, Aqter Rony S, Tesfaye D, et al. PBMC transcriptome profiles identifies potential candidate genes and functional networks controlling the innate and the adaptive immune response to PRRSV vaccine in Pietrain pig. *PLoS ONE.* (2017) 12:e0171828. doi: 10.1371/journal.pone.0171828
76. Ben-Sasson SZ, Hogg A, Hu-Li J, Wingfield P, Chen X, Crank M, et al. IL-1 enhances expansion, effector function, tissue localization, and memory response of antigen-specific CD8 T cells. *J Exp Med.* (2013) 210:491–502. doi: 10.1084/jem.20122006
77. Ito S, Ansari P, Sakatsume M, Dickensheets H, Vazquez N, Donnelly RP, et al. Interleukin-10 inhibits expression of both interferon alpha- and interferon gamma- induced genes by suppressing tyrosine phosphorylation of STAT1. *Blood.* (1999) 93:1456–63.
78. Naundorf S, Schroder M, Hoflich C, Suman N, Volk HD, Grutz G. IL-10 interferes directly with TCR-induced IFN-gamma but not IL-17 production in memory T cells. *Eur J Immunol.* (2009) 39:1066–77. doi: 10.1002/eji.200838773
79. Tamassia N, Castellucci M, Rossato M, Gasperini S, Bosisio D, Giacomelli M, et al. Uncovering an IL-10-dependent NF-kappaB recruitment to the IL-1ra promoter that is impaired in STAT3 functionally defective patients. *FASEB J.* (2010) 24:1365–75. doi: 10.1096/fj.09-145573
80. Silva-Campa E, Flores-Mendoza L, Resendiz M, Pinelli-Saavedra A, Mata-Haro V, Mwangi W, et al. Induction of T helper 3 regulatory cells by dendritic cells infected with porcine reproductive and respiratory syndrome virus. *Virology.* (2009) 387:373–9. doi: 10.1016/j.virol.2009.02.033
81. Loving CL, Osorio FA, Murtaugh MP, Zuckermann FA. Innate and adaptive immunity against porcine reproductive and respiratory syndrome virus. *Vet Immunol Immunopathol.* (2015) 167:1–14. doi: 10.1016/j.vetimm.2015.07.003
82. Tanoue T, Atarashi K, Honda K. Development and maintenance of intestinal regulatory T cells. *Nat Rev Immunol.* (2016) 16:295–309. doi: 10.1038/nri.2016.36
83. Ohkura N, Kitagawa Y, Sakaguchi S. Development and maintenance of regulatory T cells. *Immunity.* (2013) 38:414–23. doi: 10.1016/j.immuni.2013.03.002
84. Lin W, Haribhai D, Relland LM, Truong N, Carlson MR, Williams CB, et al. Regulatory T cell development in the absence of functional Foxp3. *Nat Immunol.* (2007) 8:359–68. doi: 10.1038/ni1445
85. Francisco LM, Salinas VH, Brown KE, Vanguri VK, Freeman GJ, Kuchroo VK, et al. PD-L1 regulates the development, maintenance, and function of induced regulatory T cells. *J Exp Med.* (2009) 206:3015–29. doi: 10.1084/jem.20090847
86. Fu S, Zhang N, Yopp AC, Chen D, Mao M, Chen D, et al. TGF-beta induces Foxp3 $^{+}$T-regulatory cells from CD4^{+} CD25 - precursors. *Am J Transl.* (2004) 4:1614–27. doi: 10.1111/j.1600-6143.2004.00566.x
87. Chen W, Konkel JE. TGF-beta and 'adaptive' Foxp3^{+} regulatory T cells. *J Mol Cell Biol.* (2010) 2:30–6. doi: 10.1093/jmcb/mjp004
88. Sang Y, Brichalli W, Rowland RR, Blecha F. Genome-wide analysis of antiviral signature genes in porcine macrophages at different activation statuses. *PLoS ONE.* (2014) 9:e87613. doi: 10.1371/journal.pone.0087613
89. Fan B, Liu X, Bai J, Li Y, Zhang Q, Jiang P. The 15N and 46R residues of highly pathogenic porcine reproductive and respiratory syndrome virus nucleocapsid protein enhance regulatory t lymphocytes proliferation. *PLoS ONE.* (2015) 10:e0138772. doi: 10.1371/journal.pone.0138772
90. Yue TL, Wang XK, Olson B, Feuerstein G. Interleukin-1 beta (IL-1 beta) induces transforming growth factor-β, (TGF-beta 1) production by rat aortic smooth muscle cells. *Biochem Biophys Res Commun.* (1994) 204:1186–92. doi: 10.1006/bbrc.1994.2588
91. Danis VA, Millington M, Hyland VJ, Grennan D. Cytokine production by normal human monocytes: inter-subject variation and relationship to an IL-1 receptor antagonist (IL-1Ra) gene polymorphism. *Clin Exp Immunol.* (1995) 99:303–10. doi: 10.1111/j.1365-2249.1995.tb05549.x
92. van Gucht S, van Reeth K, Pensaert M. Interaction between porcine reproductive-respiratory syndrome virus and bacterial endotoxin in the lungs of pigs: potentiation of cytokine production and respiratory disease. *J Clin Microbiol.* (2003) 41:960–6. doi: 10.1128/JCM.41.3.960-966.2003
93. Zhang SL, Han J, Li F, Gao SY, Liu L, Ma YB, et al. Advance in immunology and immune evasion of PRRSV. *Bing Du Xue Bao.* (2012) 28:689–98.
94. Silva-Campa E, Mata-Haro V, Mateu E, Hernandez J. Porcine reproductive and respiratory syndrome virus induces CD4^{+}CD8^{+}CD25^{+}Foxp3^{+} regulatory T cells (Tregs). *Virology.* (2012) 430:73–80. doi: 10.1016/j.virol.2012.04.009
95. Liu Y, Shi W, Zhou E, Wang S, Hu S, Cai X, et al. Dynamic changes in inflammatory cytokines in pigs infected with highly pathogenic porcine reproductive and respiratory syndrome virus. *Clin Vaccine Immunol.* (2010) 17:1439–45. doi: 10.1128/CVI.00517-09

Conflict of Interest Statement: The authors declare that the research was conducted in the absence of any commercial or financial relationships that could be construed as a potential conflict of interest.

frontiers in Immunology

ORIGINAL RESEARCH
published: 27 March 2019
doi: 10.3389/fimmu.2019.00572

Establishment of Systems to Enable Isolation of Porcine Monoclonal Antibodies Broadly Neutralizing the Porcine Reproductive and Respiratory Syndrome Virus

David Goldeck[1†], Dana M. Perry[1,2†], Jack W. P. Hayes[1,2†], Luke P. M. Johnson[1,3], Jordan E. Young[4], Parimal Roychoudhury[1,5], Elle L. McLuskey[1,6], Katy Moffat[1], Arjen Q. Bakker[7], Mark J. Kwakkenbos[7], Jean-Pierre Frossard[8], Raymond R. R. Rowland[9], Michael P. Murtaugh[4‡] and Simon P. Graham[1,3]*

[1] The Pirbright Institute, Pirbright, United Kingdom, [2] School of Biosciences and Medicine, Faculty of Health and Medical Sciences, University of Surrey, Guildford, United Kingdom, [3] School of Veterinary Science , Faculty of Health and Medical Sciences, University of Surrey, Guildford, United Kingdom, [4] College of Veterinary Medicine, University of Minnesota, St. Paul, MN, United States, [5] College of Veterinary Science and Animal Husbandry, Central Agricultural University, Aizawl, India, [6] Faculty of Health and Medical Sciences, University of Surrey, Guildford, United Kingdom, [7] AIMM Therapeutics, Amsterdam, Netherlands, [8] Department of Virology, Animal and Plant Health Agency, Addlestone, United Kingdom, [9] College of Veterinary Medicine, Kansas State University, Manhattan, KS, United States

OPEN ACCESS

Edited by:
John E. Butler,
University of Iowa, United States

Reviewed by:
Serge Muyldermans,
Vrije University Brussel, Belgium
Matt Reynolds,
University of Wisconsin-Madison, United States

***Correspondence:**
Simon P. Graham
simon.graham@pirbright.ac.uk

[†]These authors have contributed equally to this work

[‡]Deceased

Specialty section:
This article was submitted to Comparative Immunology, a section of the journal Frontiers in Immunology

Received: 10 January 2019
Accepted: 04 March 2019
Published: 27 March 2019

Citation:
Goldeck D, Perry DM, Hayes JWP, Johnson LPM, Young JE, Roychoudhury P, McLuskey EL, Moffat K, Bakker AQ, Kwakkenbos MJ, Frossard J-P, Rowland RRR, Murtaugh MP and Graham SP (2019) Establishment of Systems to Enable Isolation of Porcine Monoclonal Antibodies Broadly Neutralizing the Porcine Reproductive and Respiratory Syndrome Virus. Front. Immunol. 10:572. doi: 10.3389/fimmu.2019.00572

The rapid evolution of porcine reproductive and respiratory syndrome viruses (PRRSV) poses a major challenge to effective disease control since available vaccines show variable efficacy against divergent strains. Knowledge of the antigenic targets of virus-neutralizing antibodies that confer protection against heterologous PRRSV strains would be a catalyst for the development of next-generation vaccines. Key to discovering these epitopes is the isolation of neutralizing monoclonal antibodies (mAbs) from immune pigs. To address this need, we sought to establish systems to enable the isolation of PRRSV neutralizing porcine mAbs. We experimentally produced a cohort of immune pigs by sequential challenge infection with four heterologous PRRSV strains spanning PRRSV-1 subtypes and PRRSV species. Whilst priming with PRRSV-1 subtype 1 did not confer full protection against a subsequent infection with a PRRSV-1 subtype 3 strain, animals were protected against a subsequent PRRSV-2 infection. The infection protocol resulted in high serum neutralizing antibody titers against PRRSV-1 Olot/91 and significant neutralization of heterologous PRRSV-1/-2 strains. Enriched memory B cells isolated at the termination of the study were genetically programmed by transduction with a retroviral vector expressing the Bcl-6 transcription factor and the anti-apoptotic Bcl-xL protein, a technology we demonstrated efficiently converts porcine memory B cells into proliferating antibody-secreting cells. Pools of transduced memory B cells were cultured and supernatants containing PRRSV-specific antibodies identified by flow cytometric staining of infected MARC-145 cells and *in vitro* neutralization of PRRSV-1. Collectively, these data suggest that this experimental system may be further exploited to produce a panel of PRRSV-specific mAbs, which will contribute both to our understanding of the antibody response to PRRSV and allow epitopes to be resolved that may ultimately guide the design of immunogens to induce cross-protective immunity.

Keywords: porcine reproductive and respiratory syndrome virus, B cell, antibody, heterologous protection, genetic programming

INTRODUCTION

Porcine reproductive and respiratory syndrome (PRRS) is the most important infectious disease affecting the global pig industry. PRRS viruses (PRRSV) are a major threat to both animal welfare and food security, as demonstrated by the pig high fever disease outbreak that rapidly spread across Southeast Asia with devastating consequences (1). Annual losses to PRRSV in the USA and Europe are estimated to exceed US$600 million and €1.5 billion, respectively (2, 3). PRRSV exists as two genetically and antigenically distinct species, PRRSV-1 and -2, which are both rapidly evolving. The emergence of highly pathogenic strains from both species (1, 4, 5) and the failure of current live attenuated vaccines to provide broad protection against an ever-expanding diversity of viral strains pose significant challenges to effective disease control world-wide. There is therefore an urgent requirement to explore alternative approaches to vaccine development to combat PRRSV. Neutralizing antibodies (nAbs) confer protection against PRRSV (6) and recent studies have shown antibody responses can neutralize a wide diversity of PRRSV strains (7–11). An improved understanding of conserved antigenic targets of nAbs would enable the design of novel vaccines.

Identification of the epitopes recognized by broadly nAbs is an area of intense recent research in the context of a number of highly variable human viruses. Central to this are methods to generate and analyze the specificity of naturally occurring monoclonal antibodies (mAbs). Recent advances in methodologies to analyze antigen-specific B cells and their immunoglobulin genes are now providing large numbers of human mAbs for potential application in the design of novel immunogens. One approach with the potential to be applied to veterinary species, including the pig, involves the use of a retroviral vector to constitutively express the B cell lymphoma-6 (Bcl-6) transcription factor and the anti-apoptotic B cell lymphoma-extra large protein 1 (Bcl-xL) in memory B cells (12). With co-stimulation, transduced cells are converted into proliferating, antibody-secreting cells, amenable to cloning and analysis of their specificity in culture supernatants. This approach has been successfully deployed to isolate human mAbs capable of broadly neutralizing human parechovirus (13), respiratory syncytial virus (RSV) (12) and influenza A viruses (14), which are being used to support vaccine development (15). Additionally, the human RSV-specific mAb MEDI8897 (D25) is currently under clinical investigation as a potential passive RSV vaccine for infants (16). This approach has also been successfully used to immortalize B cells from rabbits, mice, rats, llamas, and non-human primates (12, 17).

The induction of nAbs recognizing the diverse array of PRRSV in the field is a clear and important goal for vaccine development research. We report here important first steps with the experimental induction of broad cross-protection and high titer PRRSV-neutralizing antibody responses in pigs and the adaptation of a technological system to enable the isolation of PRRSV-specific/neutralizing porcine mAbs.

MATERIALS AND METHODS

Viruses

PRRSV-1 subtype 3 SU1-Bel and subtype 1 215-06 strains were propagated in porcine alveolar macrophages (5). PRRSV-2 strains KS06-72109 (18), KS62 (10), VR2332 (ATCC, USA), and the attenuated PRRSV-1 subtype 1 strains Olot/91 (19) and Porcillis (MSD Animal Health) were propagated in MARC-145 cells.

Experimental PRRSV Infection of Pigs

Animal work was approved by The Pirbright Institute Animal Welfare and Ethics Committee and conducted in accordance with the UK Animals (Scientific Procedures) Act 1986. Ethical endpoints were in place and were not reached. A sequential heterologous infection study was carried out using six 12-weeks-old, PRRSV naïve, Large White/Landrace cross, female pigs. Animals were inoculated intranasally and intramuscularly with 10^6 $TCID_{50}$ of PRRSV-1 Olot/91. The pigs were then sequentially challenged at 35 day intervals by similar inoculation with 10^5 $TCID_{50}$ of PRRSV-1 SU1-Bel (day 35), PRRSV-1 215-06 (day 70) and PRRSV-2 KS06-72109 (day 105). Pigs were finally challenged with 10^7 $TCID_{50}$ PRRSV-1 Olot/91 (day 140) and the study terminated 7 days later (day 147). Clinical signs and rectal temperatures were measured daily and blood samples collected at weekly intervals. Serum samples were stored at −80°C for subsequent analysis and heparinized blood used for isolation of peripheral blood mononuclear cells (PBMCs), which were cryopreserved in 10% DMSO in FBS.

PRRSV Detection by Quantitative RT-PCR

RNA was isolated from serum using the QIAamp Viral RNA Mini Kit (Qiagen, Crawley, UK) and PRRSV RNA measured by reverse transcription quantitative PCR (RT-qPCR; VetMAX™ PRRSV EU & NA RT-PCR kit, Thermo Fisher Scientific, Loughborough, UK). To determine the utility of this kit to detect the PRRSV challenge strains, RNA was extracted from aliquots of PRRSV-1 Olot/91, 215-06 and SU1-Bel, and PRRSV-2 KS06-72109 stocks and specific detection by the PRRSV-1 and PRRSV-2 primer/probes confirmed (data not shown).

Detection of PRRSV-Specific and Neutralizing Antibody Responses In Serum

PRRSV nucleoprotein-specific serum antibody responses were determined by ELISA (PrioCHECK Porcine PRRSV Ab Strip Kit, Thermo Fisher Scientific). PRRSV-nAb titers were assessed by incubating serial 2-fold dilutions of heat-inactivated sera with 400 $TCID_{50}$ of PRRSV for 1 h at 37°C. Virus-serum mixtures were added to MARC-145 cells (1.5×10^4 cells/well) and after 72 h incubation, infection was assessed by immunofluorescence using a Cytation5 Cell Imaging Multi-Mode Reader (BioTek, Swindon, UK). nAb titers were calculated as $\log_2$ of the reciprocal serum dilution that fully neutralized viral replication in 50% of the wells (ND_{50}).

Enrichment of Porcine B Cell Populations From PBMC Using Magnetic- and Fluorescence-Activated Cell sorting

In a pilot study, B cells from uninfected pigs were enriched by magnetic-based cell sorting (MACSorting) for $CD21^+$ cells. PBMC were suspended in 25 μl/10^6 PBMC of CD21-PE mAb (Clone BB6-11C9-6, Cambridge Bioscience, Cambridge, UK). Cells were incubated at room temperature for 15 min in the dark, washed once in 2%FBS/PBS and re-suspended in 10 μl/10^7 PBMC of anti-PE microbeads (Miltenyi Biotec, Bisley, UK). Cells were incubated, washed and re-suspended in 500 μl/10^8 PBMC of 2%FBS/PBS with 5 mM EDTA (MACS buffer). Five hundred microliter of MACS buffer was then used to equilibrate the MACS MS column held within a MiniMACS magnet (Miltenyi Biotec). A volume containing $\leq 1 \times 10^7$ labeled/2×10^8 total PBMC was added to the column via a 70 μm cell strainer (Thermo Fisher Scientific), and washed three times with 500 μl MACS buffer. The column was removed from the magnet, $CD21^+$ cells eluted with 3 ml 2%FBS/PBS and washed once in 2%FBS/PBS. Aliquots were taken post-labeling pre-enrichment and from the $CD21^-$ and $CD21^+$ fractions post-enrichment to assess CD21-PE labeling and enrichment. Enriched $CD21^+$ B cells were labeled in 25 μl/10^6 cells with Zombie Aqua Fixable Viability Dye (BioLegend, London, UK), biotinylated IgM (Fc) polyclonal Ab (pAb) (Cambridge Bioscience), FITC-conjugated IgA (Fc) pAb (Cambridge Bioscience), and FITC-conjugated IgG (Fc) pAb (Cambridge Bioscience) by incubation at room temperature in the dark for 15 min. All antibodies were titrated to optimal concentrations before use. Cells were washed and Brilliant Violet 421-conjugated streptavidin (BioLegend) was added 25 μl/10^6 cells and incubated as above. Cells were then re-suspended in 100 μl/10^6 cells IMDM with GlutaMAX (Fisher Scientific) supplemented with 2% FBS. After cells were distinguished from debris based on their FSC-A and SSC-A and singlets selected based on FSC-A and FSC-H, $Zombie^-CD21^+IgM^+IgG/IgA^-$ and $Zombie^-CD21^+IgM^-IgG/IgA^+$, were FACSorted using a BD FACSAria III cell sorter (BD Biosciences, Oxford, UK) into tubes pre-rinsed in FBS and containing 1 ml IMDM supplemented with 40% FBS. Memory B cells were enriched from previously cryopreserved PBMC from the PRRSV-hyperimmune pigs by staining with Zombie Near Infrared Fixable Viability Dye (BioLegend), biotinylated IgM pAb/streptavidin-Brilliant Violet 421, IgG-FITC pAb, IgA-FITC pAb, and IgLκ and IgLλ mAbs (clones clone 27.2.1 and 27.7.1, Celtic Diagnostics, Dublin, Ireland)/anti-mouse IgG1-Alexa Fluor 647 (Sigma, Poole, UK) and FACSorting of live IgL^+IgM^-IgG/IgA^+ B-cells using a BD FACSAria Fusion cell sorter (BD Biosciences).

Transduction of Enriched Memory B cells

MACSorted and FACSorted B cells were suspended in IMDM supplemented with 100 U/ml penicillin, 100 μg/ml streptomycin and 10% FBS (all Fisher Scientific; cIMDM) and plated 5×10^5 cells/well in a 24-well tissue culture plate containing 50 ng/ml (final concentration) recombinant murine IL-21 Fc fusion protein (IL-21; AIMM Therapeutics) and 5×10^4 L cells expressing human CD40 ligand (CD40L-L cells; AIMM Therapeutics) irradiated with 50 Gy of X-rays (RS2000 Biological Irradiator, Rad Source, Suwanee, USA). After 36 h culture at 37°C, B cells were harvested, washed in serum-free IMDM and transferred to 24-well non-tissue culture treated plates pre-coated with 30 μg/ml RetroNectin (Takara-Bio, Tokyo, Japan) and blocked with 2% bovine serum albumin. An equal volume of retroviral vector encoding human *Bcl-6*, human *Bcl-xL*, and *GFP* (12) was added, the plate centrifuged ($754 \times g$, 45 min, room temperature) and incubated overnight at 37°C. B cells were transferred to 24-well tissue culture plates containing CD40L-L cells and IL-21 as described above. Transduced B cells were passaged every 3–4 days and transduced cell growth monitored by volumetric flow cytometry (MACSQuant Analyzer, Miltenyi Biotec). The retroviral vector containing Bcl-6 and Bcl-xL have been generated by a for-profit company, AIMM Therapeutics, which makes the plasmids available. Obtaining the plasmids requires an MTA (http://www.aimmtherapeutics.com/partnering/academic-collaboration/) that includes financial obligations.

Assessment of Antibody Secretion by Bcl-6/Bcl-xL Transduced Porcine B Cells

MultiScreen-IP 96-well filter plates (Merck Millipore, Hertfordshire, UK) were prepared by prewetting with 15 μl/well of 35% ethanol, for 1 min, and rinsed three times with 150 μl PBS. 100 μl/well of porcine IgLκ and IgLλ mAbs at 10 μg/ml in sterile carbonate bicarbonate coating buffer (Sigma) was added and incubated at 4°C overnight. Coating antibody was decanted, wells washed thrice with IMDM, and the membrane was blocked by adding cIMDM and incubated for 2 h at 37°C. A log dilution series of transduced B cells (200, 20, and 2 cells) in cIMDM with IL-21 were added to triplicate wells before incubation for 20 h at 37°C. Wells were washed with water and 0.05% Tween20 (Sigma) in PBS (wash buffer). 100 μl/well of anti-pig IgG (H&L)-horseradish peroxidase conjugate (Cambridge Bioscience) diluted 1:5,000 in PBS was added and incubated (3 h, room temperature). The plate was washed five times with wash buffer before addition of AEC substrate solution (Thermo Fisher Scientific) and incubation (1 h, room temperature). Plates were washed with water and the membrane dried before spots were counted using an ELISpot reader (AID ELISpot System Classic, AID, Strassberg, Germany).

Screening of Antibodies From Bcl-6/Bcl-xL Transduced Porcine B Cell Culture Supernatants

"Minipool" cultures of 10–50 transduced B cells were established in 96 well flat-bottom tissue culture plates supplemented by addition of 4×10^3 irradiated CD40L-L cells and 50 ng/ml IL-21 twice weekly. Supernatants were harvested after 14 days culture and the antibody concentrations were assessed by IgG and IgA ELISA (Cambridge Biosciences). Supernatants were screened by intracytoplasmic staining of PRRSV-1 Olot/91-infected MARC-145 cells (20). Following secondary labeling with biotinylated IgG (H&L) pAb (Cambridge Biosciences)/streptavidin-Brilliant Violet 421 or Alexa Fluor 647-conjugated IgG mAb (Cohesion

Biosciences, London, UK), cells were analyzed by flow cytometry. Supernatants which stained infected cells were subsequently retested by staining both uninfected and infected cells. Selected supernatants were also simultaneously screened for PRRSV-specific reactivity by staining a mixture of infected and uninfected cells, the latter of which had previously been labeled with 10 μM Tag-it Violet Proliferation and Cell Tracking Dye (BioLegend) (21). Supernatants were additionally screened for neutralizing activity against PRRSV-1 Olot/91 as described above.

Data Analysis

Flow cytometry data was analyzed using FCS Express 6 (De Novo Software, Glendale, CA, USA), and GraphPad Prism 7.03 (GraphPad Software, La Jolla, CA, USA) was used for graphical and statistical analysis of data. One-way ANOVAs were conducted to compare changes in rectal temperatures, viral RNAemia, N-protein specific Ab and PRRSV-1 Olot/91 nAb titers over time, and, to compare nAb titers against different PRRSV strains. Two-way ANOVAs were conducted to compare the retroviral transduction and outgrowth of different porcine B cell populations as well as the assessment of their antibody secretion by ELISpot assay.

RESULTS

Outcome of Heterologous PRRSV Challenge Infections and Kinetics of Antibody Responses

Rectal temperatures and PRRSV RNA in serum were monitored longitudinally following the sequential challenges with heterologous strains spanning PRRSV-1 subtypes and PRRSV species (**Figures 1A,B**). Recovery from infection with the attenuated PRRSV-1 subtype 1 Olot/91 did not confer protection against challenge with the PRRSV-1 subtype 3 SU1-Bel strain. Following SU1-Bel challenge, animals experienced significantly elevated temperatures for 3 days (days 41–43; $p < 0.05$) and significant PRRSV RNAemia on days 42 and 49 ($p < 0.01$). However, following recovery from SU1-Bel infection, animals were protected against a subsequent infection with the low virulence PRRSV-1 215-06 strain and then the moderately virulent PRRSV-2 KS06-72109 strain. Assessment of PRRSV N protein-specific antibodies revealed a relatively steady increase in responses across the duration of the study. N-protein specific antibody responses were significant compared to pre-infection levels from day 42 ($p < 0.05$), however, anamnestic responses following each challenge did not achieve statistical significance (**Figure 1C**). PRRSV-1 Olot/91 nAbs were similarly assessed and titers were significantly elevated from day 42 ($p < 0.05$) and showed a significant increase in titers following the SU1-Bel challenge infection ($p < 0.05$). There was no anamnestic response after the 216-06 challenge but titers rose again after the KS06 challenge, albeit without statistical significance (**Figure 1D**). To assess the breadth of the serum nAb response, the neutralization of a panel of PRRSV strains (**Figure 1E**) was conducted on day 147 sera (**Figure 1F**). nAb titers were measurable against both homologous and heterologous PRRSV-1 and−2 strains. The highest nAb titers were observed against PRRSV-1 Olot/91 which were significantly greater than those against PRRSV-1 Porcillis and PRRSV-2 strains KS06-72109 and KS62 ($p < 0.05$). The next highest nAb titers were against the heterologous PRRSV-1 Porcillis and PRRSV-2 VR2332 strains ($p < 0.05$) and lowest titers were seen against PRRSV-2 KS06-7210 and KS62.

Assessment of the Genetic Programming of Porcine B cells

In the absence of definitive discriminatory markers, porcine memory B cells were enriched by sorting on the expression of class-switched B cell receptors (BcR). Since there was a risk that BcR labeling could induce cell-cycle arrest, a pilot experiment was conducted in which B cells were sorted based on the expression of (1) CD21, (2) IgM-BcR, or (3) IgA/IgG-BcR and transduced with the Bcl-6/Bcl-xL/GFP retroviral vector (**Figure 2A**). All three populations of transduced B cells proliferated with a steady increase in GFP expressing B cells between day 0 and 21 post-transduction ($p < 0.01$). Transduction efficiency was comparable (∼30–50%) between the populations with all cultures approaching 100% GFP^+ transduced cells by day 20 (**Figure 2B**). To assess antibody secretion, transduced B cells were incubated in ELISpot plates coated with anti-IgL and development of spots revealed the majority of B cells from transduced cultures were actively secreting antibodies ($p < 0.01$; **Figure 2C**).

Screening Transduced Memory B Cells From Immune Pigs for PRRSV-Specific Antibodies

Transduced B cells from the PRRSV-hyperimmune pigs seeded in minipool cultures were first screened after 2 weeks culture and shown to contain ∼850 ng/ml of IgG and IgA (**Figure 3A**). Supernatants were next screened by intracytoplasmic staining of PRRSV-1 Olot/91 infected MARC-145 cells. Whilst the large majority of supernatants did not stain infected cells, there were a number that showed varying degrees of staining (**Figure 3B**), suggesting the presence of virus-specific antibodies. Forty eight pools were rescreened by parallel staining of infected and uninfected cells and a proportion of supernatants showed evidence of specific labeling of infected cells, all of which were confirmed as IgG specific (**Figure 3C**). With a view to improving screening throughput, a third test was performed using a pool of infected and Tag-it Violet-labeled uninfected cells allowing for correction of non-specific binding within single samples (**Figure 3D**). B cell minipools 351, 629, and 649 showed specific labeling of the infected population whereas minipool 783 stained both infected and uninfected cells. Finally supernatants were screened for neutralization of Olot/91 and more than 20 minipools showed evidence of virus neutralization, with three, including minipool 783 demonstrating complete neutralization (**Figure 3E**).

DISCUSSION

The aim of this study was to establish systems that would allow the isolation of PRRSV-neutralizing mAbs from pigs

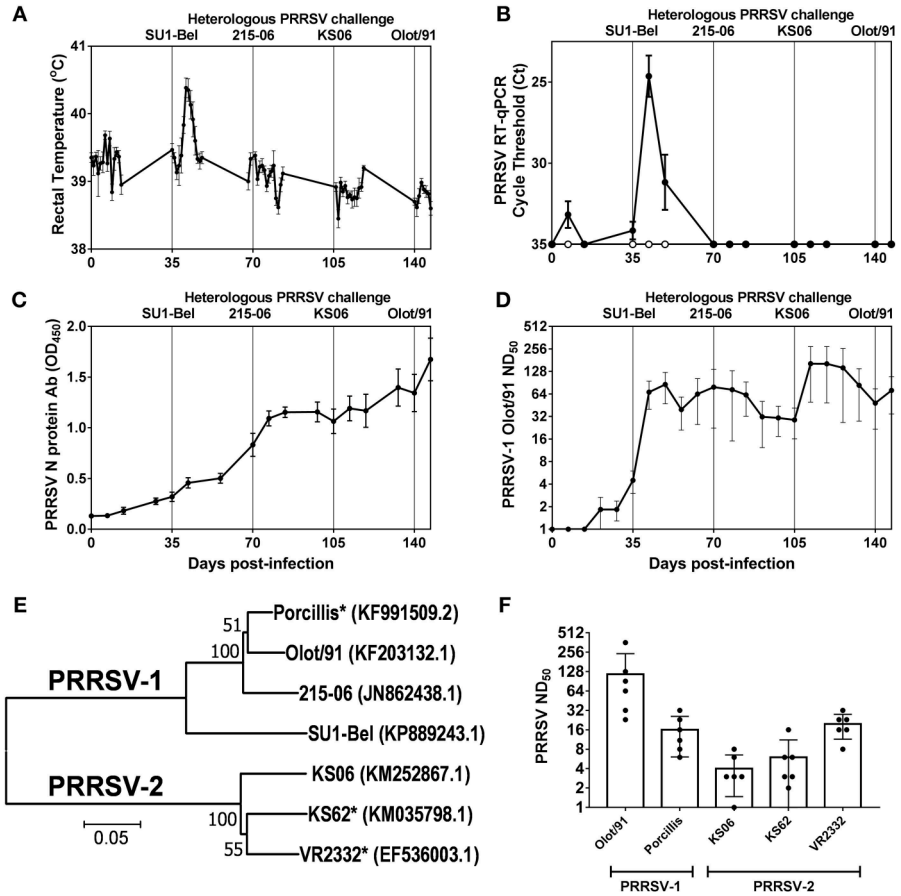

FIGURE 1 | Outcome of sequential heterologous PRRSV challenge infection and kinetics of antibody responses. Six pigs were experimentally challenged by inoculation of PRRSV-1 Olot/91, SU1-Bel, 215-06, PRRSV-2 KS06-72109 (KS06), and PRRSV-1 Olot/91 at 35 day intervals. Protection against PRRSV challenges was assessed by measurement of rectal temperatures **(A)** and detection of PRRSV-1 (closed symbols) and PRRSV-2 (open symbols) RNA in serum samples **(B)**. PRRSV N protein-specific **(C)** and PRRSV-1 Olot/91-neutralizing antibodies **(D)** were measured longitudinally in serum samples. PRRSV-neutralizing serum antibodies were assessed against heterologous PRRSV-1 and−2 strains. Phylogenetic relationships between the challenge strains and heterologous strains (indicated by *) were assessed based on ORF5 sequences **(E)** and neutralizing titers determined **(F)**.

displaying broadly nAb responses. The first step toward this goal was the sequential infection of naïve pigs with heterologous PRRSV strains, to promote the maturation and expansion of B cells recognizing conserved neutralizing epitopes. Priming the immune system with PRRSV-1 subtype 1 Olot/91 failed to provide clinical and virological protection against the divergent subtype 3 SU1-Bel strain, which confirms earlier reports of limited cross-protection between these subtypes (22–24). However, since PRRSV-1-nAb titers were still rising at the point of SU1-Bel challenge it could be speculated that by extending the time interval beyond 35 days we could have observed greater cross-protection. However, following recovery from SU1-Bel infection, animals were protected against the subsequent challenge infections. The cross-protection against PRRSV-2 KS06 is significant since cross-protection between PRRSV species has rarely been reported (25, 26). Assessment of PRRSV-2 nAbs at the point of KS06 challenge did not show detectable titers (data not shown). However, significant nAb titers against both homologous and heterologous PRRSV-1 and−2 strains were measurable at later time-points and it may be speculated that cross-reactive B cell responses were expanded upon KS06 challenge. However, dissecting this polyclonal response is required to confirm whether such broadly reactive antibodies exist in these animals. It is well described that animals can clear PRRSV infection and be immune to reinfection in the absence of measurable nAb titers, suggesting that cross-protection may also be mediated by non-neutralizing antibody or cell-mediated responses (27–30). Non-neutralizing antibody effector functions, such as antibody dependent cell-mediated cytotoxicity, antibody-dependent complement-mediated cytotoxicity, and antibody-dependent complement-mediated virolysis, may be play roles in PRRSV immunity. Whilst the only two published studies did not provide evidence for these effector functions against PRRSV-1 (31, 32), there is still merit in evaluating non-neutralizing antibody function using the sera from these animals. Cryo-banked longitudinal PBMC samples from these animals could

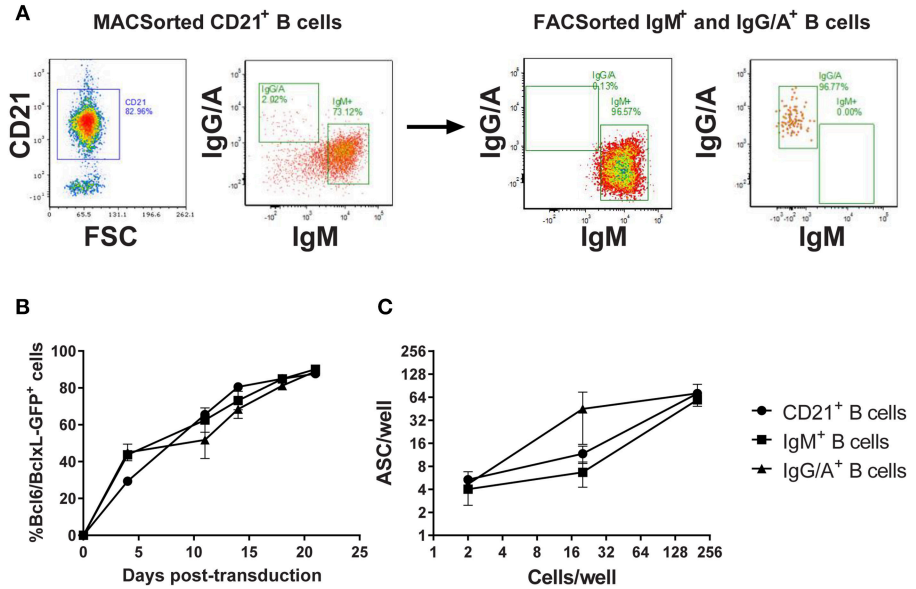

FIGURE 2 | Assessment of Bcl-6/Bcl-xL retroviral transduction of porcine B cell populations. $CD21^+$ B cells were enriched by MACSorting and populations of naïve/non-class switched B cells (IgM^+) and class-switched B cells (IgG/A^+) isolated by FACSorting **(A)**. Representative dot plots showing CD21, IgM, and IgG/A BcR staining before and after sorting are presented. $CD21^+$ B cells, IgM^+ B cells, and IgG/A^+ B cells were transduced with the retroviral vector expressing Bcl-6/Bcl-xL/GFP and cultured with IL-21 and irradiated CD40L-L cells. Transduced cell outgrowth was tracked by assessment of % cells expressing GFP **(B)**. Active antibody secretion from transduced $CD21^+$, IgM^+, and IgG/A^+ B cell cultures was confirmed by ELISpot assay **(C)**.

be used to assess T cell responses and their cross-reactivity against PRRSV-2.

The genetic programming of memory B cells is a highly effective platform technology to isolate monoclonal antibodies in a range of species (12, 17). Pilot experiments conducted with porcine B cell populations demonstrated that the system was working to expectation in this new species. The transduction efficiency for porcine B cells ranged from 30 to 50%, which is mid-range, compared to 80% for lapine B cells and 15% for camelid B cells (17). These transduction efficiencies are important to ensure a significant portion of the memory B cell repertoire is available for downstream study. Initial screening of 960 transduced B cell minipool cultures established from a single animal, provided strong evidence that PRRSV-specific B cells could be isolated using this technology. Intracytoplasmic staining of PRRSV-infected cells provided an unbiased approach to detect virus specific antibodies in transduced B cell culture supernatants. However, the screen was limited by the PRRSV strain selected. A recent study extended the fluorescent cell barcoding approach we trialed to individually labeling six populations of cells transfected with viral antigen variants (21). This allowed a quick and high-throughput approach to determine the breadth of antibody specificities. Retention of BcR expression on transduced B cells means that baiting with fluorescently labeled antigen (12) may be used to enrich for PRRSV-specific B cells, thereby significantly reducing the requirement for high-throughput screening. As proof-of-concept, we have shown that PRRSV-2 nsp7 tetramers detect rare specific B cell populations from immune pigs (33). However, the complexity of the nAb response to PRRSV and our limited understanding means that baiting with fluorescently tagged PRRSV virions (34) may provide a better approach. PRRSV-1 and−2 labeled with different dyes could allow for enrichment of mono- and pan-species specific B cells recognizing epitopes on the virion surface.

That few PRRSV-neutralizing minipool supernatants were identified is perhaps to be expected given the low serum nAb titers relative to many other virus infections. The logical next step would be to clone the B cells from these cultures to isolate mAbs which could be screened for neutralizing activity of PRRSV-1 and -2. A proteomic study revealed that PRRSV virions incorporate a variety of simian proteins after replication in MARC-145 cells (35). This raises the intriguing possibility that cross-neutralization of PRRSV strains may, in part, be mediated by antibodies recognizing simian antigens. This may also explain why minipool 783 contained antibodies that bound both infected and uninfected MARC-145 cells. To exclude this possibility, it will be important to assess neutralization in the context of both MARC-145 and macrophage infection. Sequence analysis of IGH and IGL genes would enable both their expression as recombinant mAbs and an assessment of their divergence from putative germ line predecessors (36). The longitudinal collection of PBMC from these pigs would allow a retrospective sequence based analysis of the antibody repertoire that could provide further insights into the evolution of PRRSV-nAbs (37).

There is a dire need to explore new approaches to PRRS vaccine development. We believe we have initiated an innovative approach to improve our understanding of the

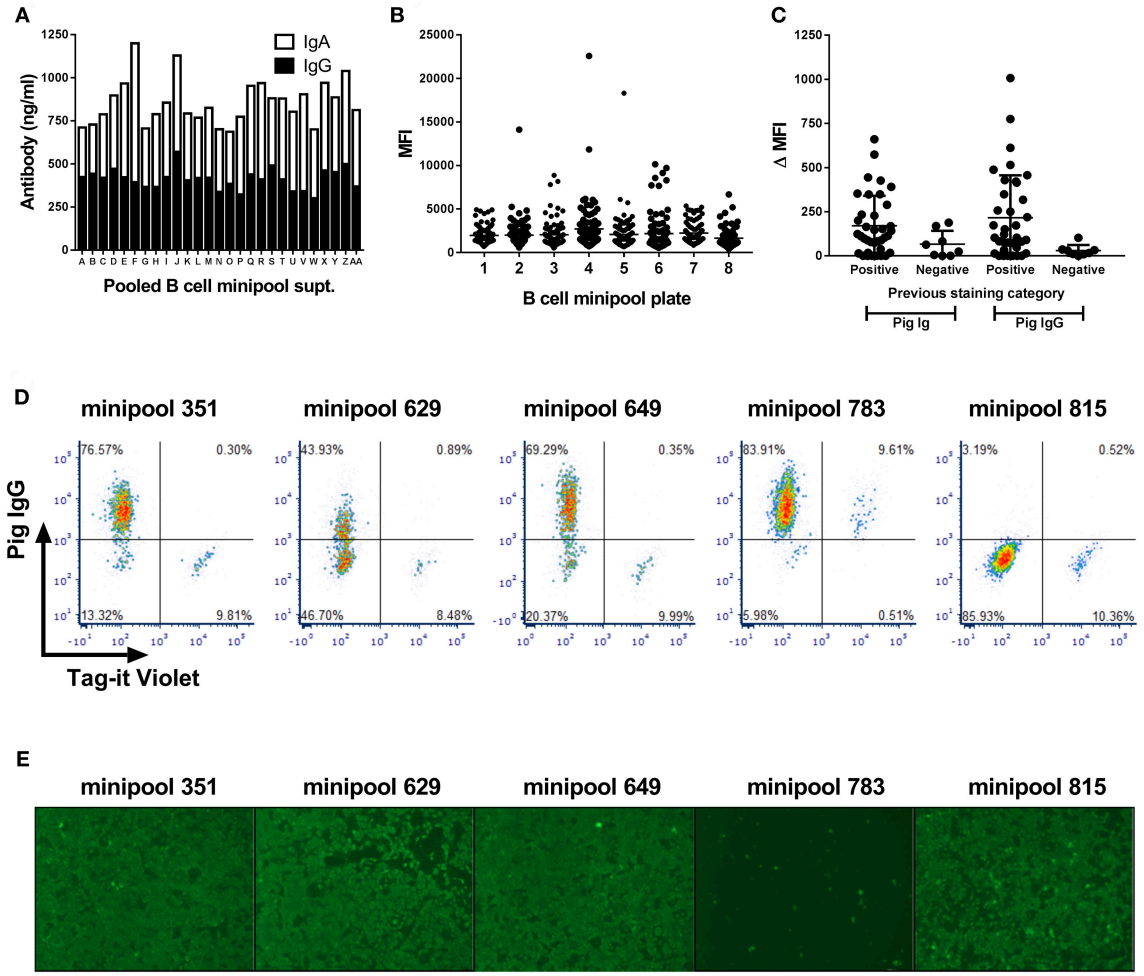

FIGURE 3 | Screening of Bcl-6/Bcl-xL transduced B cell cultures for PRRSV-specific antibodies. Antibody concentrations in pooled supernatants from 768 minipool transduced B cell cultures from a single pig **(A)**. Following two week culture, supernatants were pooled and screened by IgG and IgA ELISA. Median fluorescence intensity (MFI) of PRRSV-infected MARC-145 cells stained using the 768 transduced B cell minipool culture supernatants **(B)**. Each data point represents an individual minipool B cell supernatant. Flow cytometric staining of PRRSV-1 infected and uninfected cells by selected B cell minipool supernatants **(C)**. Staining was assessed using a pan-porcine Ig secondary antibody (Pig Ig) and a porcine IgG specific secondary antibody (Pig IgG) and data presented by subtraction of the MFI of uninfected cells from the MFI of infected cells (ΔMFI). Each data point represents an individual minipool B cell supernatant and bars represent mean ± SD. Supernatants from five selected minipool B cell cultures were re-screened for PRRSV-specific antibodies by staining of mixture of PRRSV-1 infected cells and uninfected cells pre-labeled with Tag-It Violet **(D)**. Assessment of PRRSV-1 neutralization by these selected transduced B cell minipool supernatants **(E)**. Neutralization of PRRSV-1 Olot/91 was assessed by immunofluorescence staining.

PRRSV-specific nAb response and isolate neutralizing mAbs. Using these neutralizing mAbs to resolve the epitopes they bind will underpin the future structure-based rational design of new PRRSV immunogens. Experimental passive immunization studies utilizing immune sera containing PRRSV-nAbs has demonstrated this to be an effective strategy (6, 11, 38). The accelerated discovery of human mAbs has meant that passive immunization strategies, for diseases where effective vaccines are lacking, is the subject of renewed interest. In addition to administration of recombinant mAbs produced in bioreactors, there are promising results being obtained by administration of vectors expressing recombinant mAbs (39–42). These vectors include mRNA, DNA and adenoviruses, which offer advantages in delivering mAbs that are difficult to produce and provide extended pharmacokinetics. Gene-based passive immunization of PRRSV-neutralizing mAbs could offer a novel, cost-effective tool in PRRS control. Our approach is also broadly applicable to the study of antibody responses to other swine pathogens. This includes bacteria (43) and as such could support vaccine development that would reduce the usage of antimicrobials in pig production. Demonstration that the genetic programming of memory B cells is effective in the pig, added to the list of species (rabbits, mice, rats, llamas, and non-human primates) previously studied (12, 17), further supports the application of this approach to other livestock or companion animal species.

DATA AVAILABILITY

All datasets generated for this study are included in the manuscript and/or the supplementary files.

DEDICATION

With great sorrow we mourn the passing of Dr. Michael P. Murtaugh on September 25, 2018, following complications from pancreatic cancer. Over his 33-year scientific career at the University of Minnesota, Mike made immense contributions to porcine immunology and swine diseases. He is most widely known for his significant advancements in the understanding of porcine reproductive and respiratory syndrome virus (PRRSV) evolution, pathogenesis and immunology. Mike also made extensive contributions to our fundamental understanding of the porcine immune system, antiviral immunity, molecular virology, and viral evolution, authoring over 225 peer-reviewed journal articles. His work will continue to impact the US and global swine industry for decades to come. Mike served as a mentor for over 30 Master's and PhD students, was on the editorial board of over a dozen academic journals, and successfully completed nearly 160 sponsored projects. Mike will be remembered for his dry sense of humor, caring heart, and his ability to ask difficult, yet poignant, questions that made even the sharpest grad student or post-doc sweat. He will be greatly missed.

AUTHOR CONTRIBUTIONS

SG, AB, MK, J-PF, RR, and MM contributed to the conception and design of the study. DG, DP, JH, LJ, JY, PR, EM, and KM performed the study and analysis. DG, DP, JH, and SG wrote the first draft of the manuscript. All authors contributed to manuscript revision, read and approved the submitted version.

FUNDING

This study was supported by a European PRRS Research Award from Boehringer Ingelheim Animal Health, and UK Biotechnology and Biological Sciences Research Council (BBSRC) awards BBS/E/I/00002035, BBS/E/I/00007031 and BBS/E/I/00007039. The funders had no role in study design, data collection and interpretation, or the decision to submit the work for publication.

ACKNOWLEDGMENTS

The authors gratefully acknowledge Julian Seago, Rachel Nash, and the Animal Services Team, The Pirbright Institute, and Margarita Garcia-Durán and Maria Jose Rodriguez, Ingenasa, Spain, for their assistance and collaboration.

REFERENCES

1. Zhou L, Yang H. Porcine reproductive and respiratory syndrome in China. *Virus Res.* (2010) 154:31–7. doi: 10.1016/j.virusres.2010.07.016
2. Holtkamp DJ, Neumann EJ, Mowrer C, Haley, C. Assessment of the economic impact of porcine reproductive and respiratory syndrome virus on United States pork producers. *J Swine Health Prod.* (2013). 21:72–84.
3. Paz XD. *PRRS Cost for the European Swine Industry.* (2015). Avaliable online at: https://www.pig333.com/articles/prrs-cost-for-the-european-swine-industry_10069/ (Accessed December 10, 2018.
4. Karniychuk UU, Geldhof M, Vanhee M, Van Doorsselaere J, Saveleva TA, Nauwynck HJ. Pathogenesis and antigenic characterization of a new East European subtype 3 porcine reproductive and respiratory syndrome virus isolate. *BMC Vet Res.* (2010) 6:30. doi: 10.1186/1746-6148-6-30
5. Morgan SB, Graham SP, Salguero FJ, Sanchez Cordon PJ, Mokhtar H, Rebel JM, et al. Increased pathogenicity of European porcine reproductive and respiratory syndrome virus is associated with enhanced adaptive responses and viral clearance. *Vet Microbiol.* (2013) 163:13–22. doi: 10.1016/j.vetmic.2012.11.024
6. Lopez OJ, Oliveira MF, Garcia EA, Kwon BJ, Doster A, Osorio FA. Protection against porcine reproductive and respiratory syndrome virus (PRRSV) infection through passive transfer of PRRSV-neutralizing antibodies is dose dependent. *Clin Vaccine Immunol.* (2007) 14:269–75. doi: 10.1128/CVI.00304-06
7. Martinez-Lobo FJ, Diez-Fuertes F, Simarro I, Castro JM, Prieto C. Porcine reproductive and respiratory syndrome virus isolates differ in their susceptibility to neutralization. *Vaccine.* (2011) 29:6928–40. doi: 10.1016/j.vaccine.2011.07.076
8. Kim WI, Kim JJ, Cha SH, Wu WH, Cooper V, Evans R, et al. Significance of genetic variation of PRRSV ORF5 in virus neutralization and molecular determinants corresponding to cross neutralization among PRRS viruses. *Vet Microbiol.* (2013) 162:10–22. doi: 10.1016/j.vetmic.2012.08.005
9. Robinson SR, Li J, Nelson EA, Murtaugh MP. Broadly neutralizing antibodies against the rapidly evolving porcine reproductive and respiratory syndrome virus. *Virus Res.* (2015) 203:56–65. doi: 10.1016/j.virusres.2015.03.016
10. Trible BR, Popescu LN, Monday N, Calvert JG, Rowland RR. A single amino Acid deletion in the matrix protein of porcine reproductive and respiratory syndrome virus confers resistance to a polyclonal Swine antibody with broadly neutralizing activity. *J Virol.* (2015) 89:6515–20. doi: 10.1128/JVI.03287-14
11. Robinson SR, Rahe MC, Gray DK, Martins KV, Murtaugh MP. Porcine reproductive and respiratory syndrome virus neutralizing antibodies provide *in vivo* cross-protection to PRRSV1 and PRRSV2 viral challenge. *Virus Res.* (2018) 248:13–23. doi: 10.1016/j.virusres.2018.01.015
12. Kwakkenbos MJ, Diehl SA, Yasuda E, Bakker AQ, Van Geelen CMM, Lukens MV, et al. Generation of stable monoclonal antibody-producing B cell receptor-positive human memory B cells by genetic programming. *Nat Med.* (2010) 16:123–8. doi: 10.1038/nm.2071
13. Westerhuis BM, Benschop KS, Koen G, Claassen YB, Wagner K, Bakker AQ, et al. Human memory B cells producing potent cross-neutralizing antibodies against human par echovirus: implications for prevalence, treatment, and diagnosis. *J Virol.* (2015) 89:7457–64. doi: 10.1128/JVI.01079-15
14. Friesen RHE, Lee PS, Stoop EJM, Hoffman RMB, Ekiert DC, Bhabha G, et al. A common solution to group 2 influenza virus neutralization. *Proc Natl Acad Sci USA.* (2014) 111:445–50. doi: 10.1073/pnas.1319058110
15. Mclellan JS, Chen M, Joyce MG, Sastry M, Stewart-Jones GBE, Yang Y, et al. Structure-based design of a fusion glycoprotein vaccine for respiratory syncytial virus. *Science.* (2013) 342:592–8. doi: 10.1126/science.1243283
16. Domachowske JB, Khan AA, Esser MT, Jensen K, Takas T, Villafana T, et al. Safety, tolerability and pharmacokinetics of MEDI8897, an extended half-life single-dose respiratory syncytial virus prefusion f-targeting monoclonal antibody administered as a single dose to healthy preterm infants. *Pediatr Infect Dis J.* (2018) 37:886–92. doi: 10.1097/INF.0000000000001916
17. Kwakkenbos MJ, Van Helden PM, Beaumont T, Spits H. Stable long-term cultures of self-renewing B cells and their applications. *Immunol Rev.* (2016) 270:65–77. doi: 10.1111/imr.12395

18. Hess AS, Islam Z, Hess MK, Rowland RR, Lunney JK, Doeschl-Wilson A, et al. Comparison of host genetic factors influencing pig response to infection with two North American isolates of porcine reproductive and respiratory syndrome virus. *Genet Sel Evol.* (2016) 48:43. doi: 10.1186/s12711-016-0222-0
19. Mokhtar H, Eck M, Morgan SB, Essler SE, Frossard JP, Ruggli N, et al. Proteome-wide screening of the European porcine reproductive and respiratory syndrome virus reveals a broad range of T cell antigen reactivity. *Vaccine.* (2014) 32:6828–37. doi: 10.1016/j.vaccine.2014.04.054
20. Singleton H, Graham SP, Bodman-Smith KB, Frossard JP, Steinbach F. Establishing porcine monocyte-derived macrophage and dendritic cell systems for studying the interaction with PRRSV-1. *Front Microbiol.* (2016) 7:832. doi: 10.3389/fmicb.2016.00832
21. Merat SJ, Van De Berg D, Bru C, Yasuda E, Breij E, Kootstra N, et al. Multiplex flow cytometry-based assay to study the breadth of antibody responses against E1E2 glycoproteins of hepatitis C virus. *J Immunol Methods.* (2018) 454:15–26. doi: 10.1016/j.jim.2017.07.015
22. Trus I, Bonckaert C, Van Der Meulen K, Nauwynck HJ. Efficacy of an attenuated European subtype 1 porcine reproductive and respiratory syndrome virus (PRRSV) vaccine in pigs upon challenge with the East European subtype 3 PRRSV strain Lena. *Vaccine.* (2014) 32:2995–3003. doi: 10.1016/j.vaccine.2014.03.077
23. Bonckaert C, Van Der Meulen K, Rodriguez-Ballara I, Pedrazuela Sanz R, Martinez MF, Nauwynck HJ. Modified-live PRRSV subtype 1 vaccine UNISTRAIN((R)) PRRS provides a partial clinical and virological protection upon challenge with East European subtype 3 PRRSV strain Lena. *Porcine Health Manag.* (2016) 2:12. doi: 10.1186/s40813-016-0029-y
24. Renson P, Fablet C, Le Dimna M, Mahe S, Touzain F, Blanchard Y, et al. Preparation for emergence of an Eastern European porcine reproductive and respiratory syndrome virus (PRRSV) strain in Western Europe: immunization with modified live virus vaccines or a field strain confers partial protection. *Vet Microbiol.* (2017) 204:133–40. doi: 10.1016/j.vetmic.2017.04.021
25. Jeong J, Kim S, Park C, Park KH, Kang I, Park SJ, et al. Commercial porcine reproductive and respiratory syndrome virus (PRRSV)-2 modified live virus vaccine against heterologous single and dual Korean PRRSV-1 and PRRSV-2 challenge. *Vet Rec.* (2018) 182:485. doi: 10.1136/vr.104397
26. Jeong J, Park C, Oh T, Park KH, Yang S, Kang I, et al. Cross-protection of a modified-live porcine reproductive and respiratory syndrome virus (PRRSV)-2 vaccine against a heterologous PRRSV-1 challenge in late-term pregnancy gilts. *Vet Microbiol.* (2018) 223:119–25. doi: 10.1016/j.vetmic.2018.08.008
27. Murtaugh MP, Genzow M. Immunological solutions for treatment and prevention of porcine reproductive and respiratory syndrome (PRRS). *Vaccine.* (2011) 29:8192–204. doi: 10.1016/j.vaccine.2011.09.013
28. Loving CL, Osorio FA, Murtaugh MP, Zuckermann FA. Innate and adaptive immunity against porcine reproductive and respiratory syndrome virus. *Vet Immunol Immunopathol.* (2015) 167:1–14. doi: 10.1016/j.vetimm.2015.07.003
29. Mokhtar H, Pedrera M, Frossard JP, Biffar L, Hammer SE, Kvisgaard LK, et al. The non-structural protein 5 and matrix protein are antigenic targets of T cell immunity to genotype 1 porcine reproductive and respiratory syndrome viruses. Front Immunol. (2016) 7:40. doi: 10.3389/fimmu.2016.00040
30. Rahe MC, Murtaugh MP. Mechanisms of adaptive immunity to porcine reproductive and respiratory syndrome virus. Viruses. (2017) 9:E148. doi: 10.3390/v9060148
31. Costers S, Delputte PL, Nauwynck HJ. Porcine reproductive and respiratory syndrome virus-infected alveolar macrophages contain no detectable levels of viral proteins in their plasma membrane and are protected against antibody-dependent, complement-mediated cell lysis. J Gen Virol. (2006) 87:2341–51. doi: 10.1099/vir.0.81808-0
32. Cao J, Grauwet K, Vermeulen B, Devriendt B, Jiang P, Favoreel H, et al. Suppression of NK cell-mediated cytotoxicity against PRRSV-infected porcine alveolar macrophages *in vitro*. Vet Microbiol. (2013) 164:261–9. doi: 10.1016/j.vetmic.2013.03.001
33. Rahe MC, Gustafson KL, Murtaugh MP. B cell tetramer development for veterinary vaccinology. Viral Immunol. (2018) 31:1–10. doi: 10.1089/vim.2017.0073
34. Zhang S, Tan HC, Ooi EE. Visualizing dengue virus through Alexa Fluor labeling. *J Vis Exp.* (2011) 167:e3168. doi: 10.3791/3168
35. Zhang C, Xue C, Li Y, Kong Q, Ren X, Li X, et al. Profiling of cellular proteins in porcine reproductive and respiratory syndrome virus virions by proteomics analysis. Virol J. (2010) 7:242. doi: 10.1186/1743-422X-7-242
36. Prabakaran P, Chen W, Dimitrov DS. The antibody germline/maturation hypothesis, elicitation of broadly neutralizing antibodies against HIV-1 and cord blood IgM repertoires. Front *Immunol.* (2014) 5:398. doi: 10.3389/fimmu.2014.00398
37. Miho E, Yermanos A, Weber CR, Berger CT, Reddy ST, Greiff V. Computational strategies for dissecting the high-dimensional complexity of adaptive immune repertoires. Front Immunol. (2018) 9:224. doi: 10.3389/fimmu.2018.00224
38. Osorio FA, Galeota JA, Nelson E, Brodersen B, Doster A, Wills R, et al. Passive transfer of virus-specific antibodies confers protection against reproductive failure induced by a virulent strain of porcine reproductive and respiratory syndrome virus and establishes sterilizing immunity. Virology. (2002) 302:9–20. doi: 10.1006/viro.2002.1612
39. Wohlbold TJ, Chromikova V, Tan GS, Meade P, Amanat F, Comella P, et al. Hemagglutinin stalk- and neuraminidase-specific monoclonal antibodies protect against lethal H10N8 influenza virus infection in mice. J Virol. (2016) 90:851–61. doi: 10.1128/JVI.02275-15
40. Welles HC, Jennewein MF, Mason RD, Narpala S, Wang L, Cheng C, et al. Vectored delivery of anti-SIV envelope targeting me via AAV8 protects rhesus macaques from repeated limiting dose intrarectal swarm SIVsmE660 challenge. PLoS Pathog. (2018) 14:e1007395. doi: 10.1371/journal.ppat.1007395
41. Yamazaki T, Nagashima M, Ninomiya D, Ainai A, Fujimoto A, Ichimonji I, et al. Neutralizing antibodies induced by gene-based hydrodynamic injection have a therapeutic effect in lethal influenza infection. Front Immunol. (2018) 9:47. doi: 10.3389/fimmu.2018.00047
42. Schlake T, Thess A, Thran M, Jordan I. mRNA as novel technology for passive immunotherapy. Cell Mol Life Sci. (2019) 76:301–28. doi: 10.1007/s00018-018-2935-4
43. Hazenbos WL, Kajihara KK, Vandlen R, Morisaki JH, Lehar SM, Kwakkenbos MJ, et al. Novel staphylococcal glycosyltransferases SdgA and SdgB mediate immunogenicity and protection of virulence-associated cell wall proteins. PLoS Pathog. (2013) 9:e1003653. doi: 10.1371/journal.ppat.1003653

Conflict of Interest Statement: AB and MK are employed by AIMM Therapeutics.

The remaining authors declare that the research was conducted in the absence of any commercial or financial relationships that could be construed as a potential conflict of interest.

frontiers in Immunology

ORIGINAL RESEARCH
published: 24 April 2019
doi: 10.3389/fimmu.2019.00727

Stage of Gestation at Porcine Epidemic Diarrhea Virus Infection of Pregnant Swine Impacts Maternal Immunity and Lactogenic Immune Protection of Neonatal Suckling Piglets

*Stephanie N. Langel[1], Francine C. Paim[1], Moyasar A. Alhamo[1], Alexandra Buckley[2], Albert Van Geelen[2], Kelly M. Lager[2], Anastasia N. Vlasova[1] and Linda J. Saif[1]**

[1] Food Animal Health Research Program, Department of Veterinary Preventive Medicine, Ohio Agricultural Research and Development Center, College of Food, Agriculture and Environmental Sciences, College of Veterinary Medicine, The Ohio State University, Wooster, OH, United States, [2] National Animal Disease Center, Agricultural Research Service, USDA, Ames, IA, United States

OPEN ACCESS

Edited by:
Falko Steinbach,
University of Surrey, United Kingdom

Reviewed by:
Jesus Hernandez,
Centro de Investigación en Alimentación y Desarrollo (CIAD), Mexico
Martin Faldyna,
Veterinary Research Institute (VRI), Czechia

***Correspondence:**
Linda J. Saif
saif.2@osu.edu

Specialty section:
This article was submitted to Comparative Immunology, a section of the journal Frontiers in Immunology

Received: 21 November 2018
Accepted: 18 March 2019
Published: 24 April 2019

Citation:
Langel SN, Paim FC, Alhamo MA, Buckley A, Van Geelen A, Lager KM, Vlasova AN and Saif LJ (2019) Stage of Gestation at Porcine Epidemic Diarrhea Virus Infection of Pregnant Swine Impacts Maternal Immunity and Lactogenic Immune Protection of Neonatal Suckling Piglets. Front. Immunol. 10:727. doi: 10.3389/fimmu.2019.00727

During pregnancy, the maternal immune response changes dramatically over the course of gestation. This has implications for generation of lactogenic immunity and subsequent protection in suckling neonates against enteric viral infections. For example, porcine epidemic diarrhea virus (PEDV) is an alphacoronavirus that causes acute diarrhea in neonatal piglets. Due to the high virulence of PEDV and the naïve, immature immune system of neonatal suckling piglets, passive lactogenic immunity to PEDV induced during pregnancy, via the gut-mammary gland (MG)-secretory IgA (sIgA) axis, is critical for piglet protection. However, the anti-PEDV immune response during pregnancy and stage of gestation required to optimally stimulate the gut-MG-sIgA axis is undefined. We hypothesize that there is a gestational window in which non-lethal PEDV infection of pregnant gilts influences maximum lymphocyte mucosal trafficking to the MG, resulting in optimal passive lactogenic protection in suckling piglets. To understand how the stages of gestation affect maternal immune responses to PEDV, three groups of gilts were orally infected with PEDV in the first, second or third trimester. Control (mock) gilts were inoculated with medium in the third trimester. To determine if lactogenic immunity correlated with protection, all piglets were PEDV-challenged at 3–5 days postpartum. PEDV infection of gilts at different stages of gestation significantly affected multiple maternal systemic immune parameters prepartum, including cytokines, B cells, PEDV antibodies (Abs), and PEDV antibody secreting cells (ASCs). Pregnant second trimester gilts had significantly higher levels of circulating PEDV IgA and IgG Abs and ASCs and PEDV virus neutralizing (VN) Abs post PEDV infection. Coinciding with the significantly higher PEDV Ab responses in second trimester gilts, the survival rate of their PEDV-challenged piglets was 100%, compared with 87.2, 55.9, and 5.7% for first, third, and mock litters, respectively. Additionally, piglet survival positively correlated with PEDV

IgA Abs and ASCs and VN Abs in milk and PEDV IgA and IgG Abs in piglet serum. Our findings have implications for gestational timing of oral attenuated PEDV maternal vaccines, whereby PEDV intestinal infection in the second trimester optimally stimulated the gut-MG-sIgA axis resulting in 100% lactogenic immune protection in suckling piglets.

Keywords: swine, PEDV, pregnancy, lactogenic immunity, gut-mammary-secretory IgA axis

INTRODUCTION

Diarrheal diseases in young animals account for an estimated multi-million dollar loss to the livestock industry annually due to the livestock industry annually due to mortality, reduced weight gain, treatment costs, and trade sanctions on exporting animal products from infected countries (1, 2). For example, porcine epidemic diarrhea virus (PEDV) is a highly virulent re-emerging enteric coronavirus that causes acute diarrhea, dehydration, and death in neonatal piglets (3). It has killed over 8.5 million piglets since its emergence in the US in 2013. In adult pigs, PEDV causes watery diarrhea, depression, and anorexia as well as agalactia and reduced reproductive performance (1–3). Lactogenic immunity remains the most promising and effective way to protect neonatal suckling piglets from enteric diseases like PEDV (4, 5). This is dependent on trafficking of pathogen-specific IgA^+ plasmablasts to the mammary gland (MG) and accumulation of secretory IgA (sIgA) antibodies (Abs) in milk, defined as the gut-MG-sIgA axis (6–8). Understanding the regulation of mucosal homing receptor and chemokine expression is critical to generate sufficient lactogenic immunity for piglet protection. For example, chemokine receptor (CCR)10, a lymphocyte gut homing marker, is required for IgA^+ plasmablast recruitment to the MG in mice and humans (9–11). Additionally, an increase in lymphocyte migration to the MG in swine at the end of gestation and during lactation coincides with an increase in $\alpha_4\beta_7$ integrin, another lymphocyte gut homing marker, on B cells (12). Identifying factors that influence lymphocyte migration and the gut-MG-sIgA axis may lead to improved PEDV vaccine regimens in gestating swine, boosting overall herd immunity and health and industry productivity.

Maternal vaccination that increases the amount of passively transferred protective Abs in milk, induced via the gut-MG-sIgA axis, is the strategy used to protect suckling piglets from PEDV immediately after birth (4, 5). For example, in swine, high rates of protection against another porcine enteric alphacoronavirus, transmissible gastroenteritis virus (TGEV) in piglets is achieved when pregnant sows are orally infected with live virulent virus (5–7, 13–15). The increased rate of protection was associated with high titers of IgA Abs in colostrum and milk. This demonstrates that enteric viral infection stimulates the intestinal mucosa influencing lactogenic immunity via the gut-MG-sIgA axis (4, 5). This model system can be used in the context of PEDV, as similar maternal vaccination strategies are needed for initiation of the gut-MG-sIgA axis and piglet protection (4, 12, 16, 17). We showed previously in third trimester pregnant gilts that administering a higher dose of virulent PEDV increased virus neutralizing (VN) Ab titers in colostrum/milk and piglet protection compared with a lower dose (4). Despite this, field reports demonstrate incomplete and variable protection in orally PEDV-infected gestating swine (4). Furthermore, the optimal stage of gestation to initiate the gut-MG-sIgA axis by means of natural infection or oral vaccination in naïve pregnant swine to generate protective lactogenic immunity is unknown.

Pregnancy modulates immunological processes that change over the course of gestation (18). For example, during the first trimester of gestation, levels of innate and proinflammatory factors increase, facilitating embryo implantation (19, 20). As pregnancy progresses, inflammatory cytokines decrease and regulatory cells and cytokines increase to support fetal growth and development to prevent rejection of the fetus (21–24). In the third trimester of gestation, the immunoregulatory environment is retained until immediately prior to parturition when proinflammatory and tissue repair factors increase, promoting the contraction of the uterus and expulsion of the fetus and placenta (18). The ability of pregnancy to differentially modulate the immune response explains why the severity of illness and efficacy of vaccination is dependent on stage of gestation. For example, the risk and severity of influenza (25), malaria (26), and listeria (27) is higher for women in their third trimester than other gestational stages. Additionally, in women vaccinated with the trivalent inactivated influenza vaccine, seroconversion rates were higher in late third trimester compared with first trimester-vaccinated women (28). Due to the differences in immune responses at different stages of pregnancy, it is important to consider stage of gestation when designing vaccines aimed to increase lactogenic immunity and passive transfer of protective Abs in colostrum/milk from mother to neonate.

In this study, we infected pregnant first parity gilts in their first, second and third trimesters of gestation with PEDV to determine the impact of stage of gestation on generation of maternal B-cell immunity, the gut-MG-sIgA axis and lactogenic immune protection in PEDV challenged piglets. Our goal was to identify innate and adaptive immune factors during pregnancy that influence lymphocyte trafficking, in addition to immune correlates of lactogenic immune protection in neonatal suckling piglets. Understanding the impact of stage of gestation at PEDV infection or exposure on maternal immunity will allow more precise maternal vaccination protocols to target the time when the animal is most immunologically responsive. Optimizing vaccine efficacy for gestating and lactating animals will enhance lactogenic immunity in neonates and decrease morbidity and mortality associated with neonatal enteric disease.

RESULTS

Overall Summary of Results and Significance for the Major Immune and PEDV Protection Parameters Assessed

An overall summary of the statistically significant results (**Table 1**) illustrates that PEDV infection of gilts at different stages of gestation (**Figure 1**) affects multiple maternal systemic immune parameters prepartum, including natural killer (NK) cells, cytokines, B cells, and PEDV Abs and antibody secreting cells (ASCs). In addition, significant postpartum effects on lactogenic immune parameters in colostrum and milk were observed including significantly increased PEDV IgA (colostrum and milk) and IgG (colostrum only) ASCs and PEDV IgA Abs and VN Abs in PEDV-infected second trimester gilts (**Table 1**). Notably several gilt [PEDV IgA (colostrum and milk) and IgG (colostrum only) ASCs, Abs, and VN Abs] and piglet (serum PEDV IgA and IgG Abs) parameters were positively correlated with piglet survival rates (**Table 2**), demonstrating the association between IgA ASCs and Abs and VN Abs and lactogenic immune protection of suckling neonates. The detailed results for each parameter are described in the following sections.

Third Trimester Gilts Had Significantly Higher PEDV RNA Shedding Titers and More Severe PEDV-Induced Diarrhea

Third trimester gilts had significantly higher PEDV RNA shedding titers at PID 2 compared with second trimester gilts (**Figure 2A**). Additionally, second trimester gilts had delayed onset of PEDV RNA shedding compared with first and third trimester gilts. Fecal consistency scores at PID 4 were significantly higher in third compared with second and first trimester gilts and third trimester gilts were the only treatment

TABLE 1 | Overall summary of results and significance for the major immune and PEDV protection parameters assessed.

Parameter	Result	Immune response, site	Significance
I. MATERNAL IMMUNITY (PREPARTUM)			
Gilt blood natural killer (NK) cell frequency and activity	1st trimester gilts had significantly higher mean NK cell frequencies and cytotoxic activity	Innate, systemic	NK cell frequency/activity in blood may modulate PEDV specific B cell response in 1st trimester gilts
Gilt serum transforming growth factor (TGF)-β concentration	2nd trimester gilts had significantly higher mean concentrations of serum TGF-β	T regulatory cytokine, systemic	Elevated serum TGF-β in 2nd trimester gilts may enhance PEDV B cell/antibody (Ab) responses
Gilt blood $\alpha4^+\beta7^+$ B cell frequency	2nd and 3rd trimester gilts had significantly higher mean frequencies of blood $\alpha4^+\beta7^+$ B cells	B cell, systemic	Increased circulating frequencies of $\alpha4^+\beta7^+$ B cells in 2nd/3rd trimester gilts may facilitate trafficking to the mammary gland
Gilt blood $CD2^-CD21^+$ B cell frequency	2nd and 3rd trimester gilts had significantly higher mean frequencies of blood $CD2^-CD21^+$ (activated and/or primed) B cells	B cell, systemic	Circulating frequencies of $CD2^-CD21^+$ B cells increase with gestational stage and may influence B cell activation/survival
Gilt blood PEDV IgA and IgG antibody secreting cells (ASCs)	2nd trimester gilts had significantly higher blood mean PEDV IgA and IgG ASCs	B cell, systemic	Increased blood PEDV IgA and IgG ASCs in 2nd trimester gilts is associated with ASC trafficking to the mammary gland
Gilt blood PEDV IgA, IgG, and virus neutralization (VN) Abs	2nd trimester gilts had significantly higher mean serum PEDV IgA, IgG and VN Abs	B cell/Abs, systemic	Increased serum PEDV IgA, IgG, and VN Ab in 2nd trimester gilts is associated with Ab accumulation in colostrum/milk
II. LACTOGENIC IMMUNITY (POSTPARTUM)			
Gilt colostrum/milk PEDV IgA and IgG ASCs	2nd trimester gilts had significantly higher mean PEDV IgA (in colostrum/milk) and IgG (in colostrum) ASCs	B cell, colostrum/milk	Increased PEDV IgA (colostrum/milk) and IgG ASCs (colostrum) in 2nd trimester gilts is correlated with lactogenic immune protection in piglets
Gilt colostrum/milk PEDV IgA and VN Abs	2nd trimester gilts had significantly higher mean colostrum/milk PEDV IgA and VN Abs	B cell/Abs, colostrum/milk	Increased colostrum/milk PEDV IgA and VN Abs in 2nd trimester gilts is correlated with lactogenic immune protection in piglets
III. PIGLET PROTECTION (POSTPARTUM)			
Piglet survival rate	2nd trimester litters had 100% survival rate	Piglet PEDV protection	Piglet survival rates were positively correlated with PEDV IgA ASCs and Abs and VN Abs in milk
Piglet PEDV RNA shedding titers and fecal consistency	2nd trimester litters had significantly lower mean PEDV RNA shedding titers and fecal consistency	Piglet PEDV protection, intestine	Increased lactogenic immune protection decreased viral shedding and diarrhea in 2nd trimester litters
Piglet serum IgA and IgG Abs	2nd trimester litters had significantly higher mean serum PEDV IgA and IgG Ab titers	B cell/Abs, systemic	Increased piglet serum IgA and IgG Abs positively correlated with survival rates

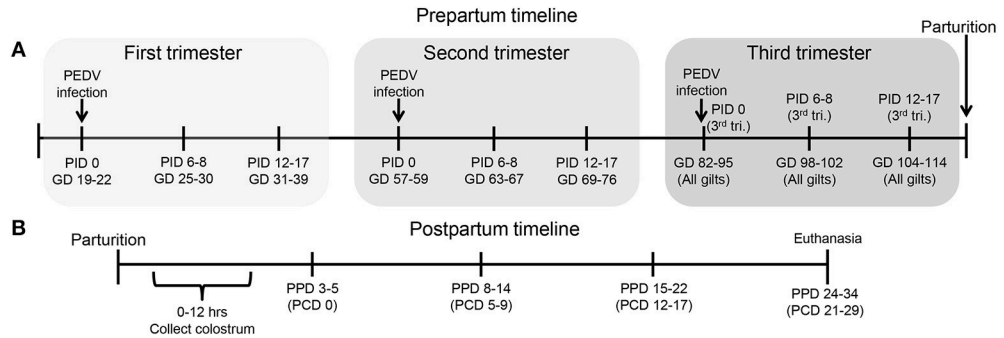

FIGURE 1 | Schematic diagram of the experimental design showing gilt porcine epidemic diarrhea virus (PEDV) infection and sample time points at post infection day (PID) 0, 6–8, 12–17 and gestation day (GD) 82–95, 98–102, and 104–114, **(B)** piglet PEDV challenge at 3–5 postpartum day (PPD) and sample time points at PPD 3–5 (PCD [post challenge day] 0), PPD 8–14 (PCD 5–9), PPD 15–22 (PCD 12–17), and PPD 24–34 (PCD 21–29).

TABLE 2 | Spearman's non-parametric correlations between piglet survival rate and numbers of PEDV IgA and IgG antibody secreting cells (ASCs) and log_{10}-transformed PEDV IgA, IgG, and virus neutralizing (VN) antibody (Ab) titers in colostrum, postpartum day (PPD) 3–5 milk, PPD 8–14 milk, and PPD 15–22 milk in first, second, and third trimester PEDV-infected gilts.

		PEDV IgA ASCs	PEDV IgG ASCs	PEDV IgA Abs	PEDV IgG Abs	PEDV VN Abs
Colostrum	*r*	0.71	0.76	0.83	0.29	0.60
	P-value	0.0097	0.01	0.0005	0.33	0.03
PPD 3-5 milk	*r*	0.61	0.55	0.38	0.50	0.56
	P-value	0.04	0.051	0.22	0.10	0.06
PPD 8-14 milk	*r*	0.77	0.55	0.73	0.17	0.68
	P-value	0.0019	0.07	0.0067	0.59	0.02
PPD 12-22 milk	*r*	0.44	0.42	0.32	−0.50	0.61
	P-value	0.15	0.20	0.33	0.10	0.048

*$P < 0.05$, **$P < 0.01$, ***$P < 0.001$.

group with clinical diarrhea (mean fecal consistency score of >1) (**Figure 2B**).

Stage of Gestation Modulated Innate Immune Parameters

Circulating NK cell frequencies were significantly higher in first trimester gilts at PID 0 compared with second or third trimester gilts (**Figure 3A**). At PID 6-8, peripheral NK cell activity was significantly higher in first compared with second and third trimester gilts (**Figure 3B**). Mean concentrations of serum IL-12, a cytokine essential for NK cell activation (29) and IL-22, a cytokine produced by subsets of T and NK cells (30–32), were numerically higher at PID 0 in first compared with second and third trimester gilts (**Figures 3C,D**). It is unlikely changes in serum cytokine concentrations were due to T cells as the frequency of circulating $CD4^+$ or $CD8^+$ cells did not significantly differ between treatment groups (data not shown). Third trimester gilts had numerically higher mean concentrations of serum proinflammatory cytokines tumor necrosis factor (TNF)-α, interferon (IFN)-α and IL-17 at PID 12–17 compared with first and second trimester gilts (**Figures S3A–C**). This time point corresponds to gestation day (GD) 104–114 in third trimester gilts, suggesting innate, and proinflammatory cytokines increase immediately prior to parturition in swine, as demonstrated in human pregnancy (33–36). Additionally, third trimester gilts had numerically higher mean serum concentrations of T-helper cell type-1 (Th1) cytokine IFN-γ while first trimester gilts had numerically higher mean serum Th2 and T regulatory cytokines IL-4 and IL-10, respectively, compared with second and third trimester gilts at PID 6–8 (**Figures 3SD–F**).

Second Trimester Gilts Had Significantly Higher Circulating PEDV Specific IgA and IgG ASCs, PEDV IgA Abs, and Concentrations of Serum Cytokine Transforming Growth Factor (TGF)-β

Maternal B-cell immune responses were measured at PID 0, 6–8, and 12–17 in first, second and third trimester gilts. Second trimester gilts had significantly higher circulating PEDV IgA and IgG ASCs at PID 12–17 compared with first and third trimester gilts (**Figures 4A,B**). Additionally, numbers of circulating PEDV IgA ASCs were consistently higher than PEDV IgG ASCs in first, second and third trimester gilts at PID 6–8 and 12–17 (**Figures 4A,B**). PEDV IgA Ab titers were significantly higher in second trimester gilts at PID 6–8 compared with first trimester gilts (**Figure 4C**). Serum TGF-β, a cytokine important for IgA class-switching (37), was significantly higher at PID 0 and remained numerically higher at PID 6–8 and 12–17 in second compared with first and third trimester gilts (**Figure 4D**). Serum IL-6, a cytokine essential for Ab production (38), was numerically higher at PID 0 and 6–8 in second trimester compared with first and third trimester gilts (**Figure 4E**). No significant differences were observed for serum PEDV IgG or VN Ab titers within the first 2 weeks post-PEDV infection but there was a trend for higher mean titers in second trimester gilts (**Figures S4A,B**).

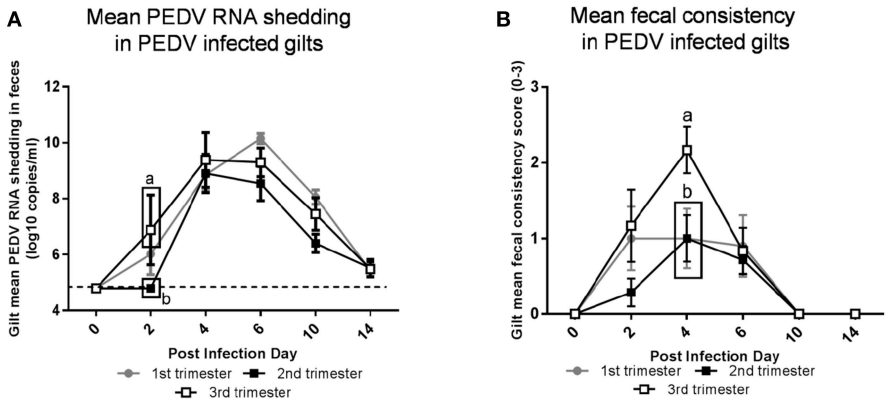

FIGURE 2 | Third trimester gilts had significantly higher porcine epidemic diarrhea virus (PEDV) RNA shedding titers at post infection day (PID) 2 compared with second trimester gilts and significantly greater PEDV-induced diarrhea at PID 4 compared with first and second trimester gilts. **(A)** PEDV RNA shedding titers were determined by real time quantitative polymerase chain reaction (qRT-PCR) and expressed as $\log_{10}$ copies/ml. **(B)** Diarrhea was determined by fecal consistency score >1 (fecal consistency was scored as follows: 0, normal; 1, pasty/semiliquid; 2, liquid; 3, watery). PEDV RNA shedding titers and fecal consistency scores were measured at PID 0, 2, 4, 6, 10, and 14. Different letters indicate significant differences among treatment groups at the same time point (mean ± SEM). Statistical analysis was performed using the two-way ANOVA with repeated measures and Bonferroni's correction for multiple comparisons.

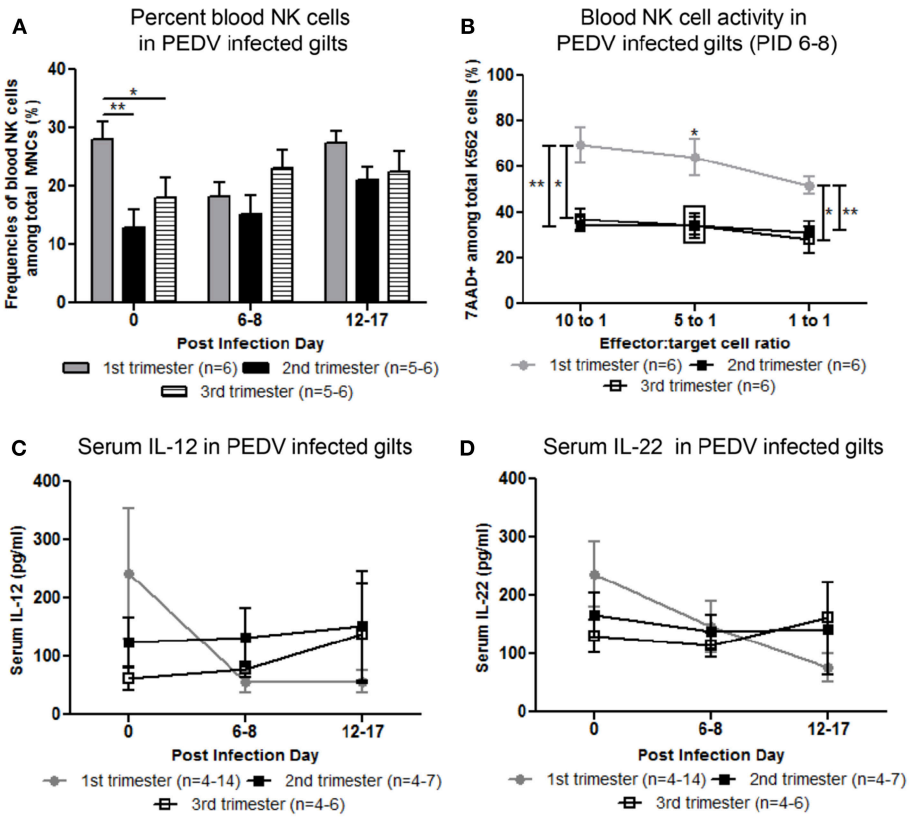

FIGURE 3 | Peripheral natural killer (NK) cell frequency and function and serum interleukin (IL)-12 and IL-22 concentrations were increased in first compared with second and third trimester gilts. **(A)** Peripheral blood mononuclear cells (PBMCs) were isolated and NK cell ($CD3^-$, $CD172^-$, $CD8^+$) frequencies were determined by flow cytometry at post infection day (PID) 0, 6–8, and 12–17. **(B)** PBMCs and CFSE-stained K562 tumor cells were used as effector and target cells, respectively, and co-cultured at 10:1 5:1 and 1:1 ratios to assess NK cell cytotoxic function at PID 6–8. **(C)** Serum cytokine concentrations (pg/ml) of IL-12 and **(D)** IL-22 were measured at PID 0, 6–8, and 12–17. Asterisks indicate significant differences among treatment groups (mean ± SEM). Statistical analysis was performed using the Student's *t*-test **(B)** or two-way ANOVA with repeated measures and Bonferroni's correction for multiple comparisons **(A,C,D)**. $^*P < 0.05$, $^{**}P < 0.01$.

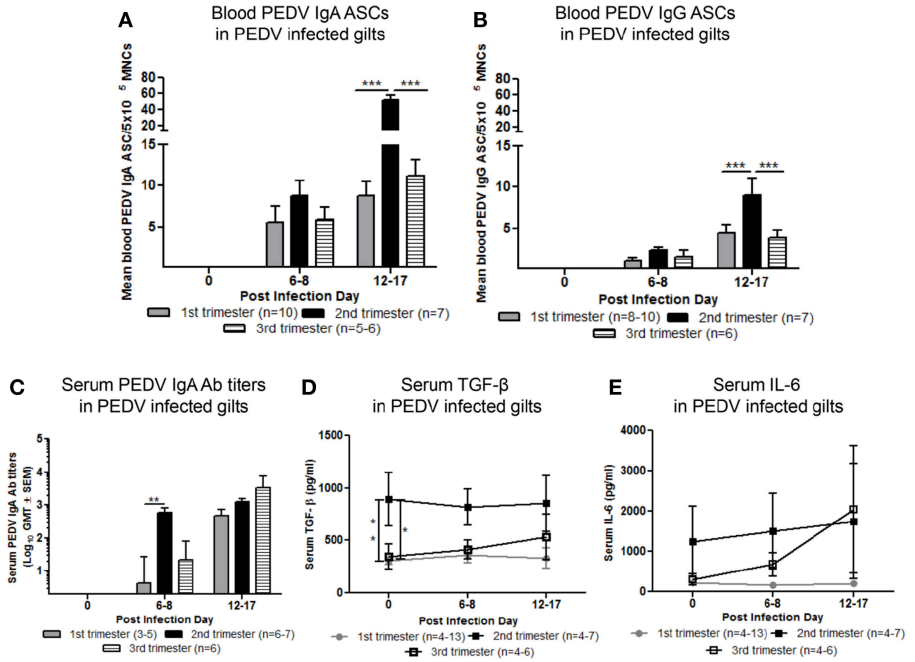

FIGURE 4 | Second trimester gilts had significantly increased circulating PEDV specific IgA and IgG antibody secreting cells (ASCs) at post infection day (PID) 12–17, PEDV specific IgA antibodies (Abs) at PID 6–8 and concentrations of transforming growth factor (TGF)-β at PID 0 compared with first and third trimester gilts. **(A)** Peripheral blood mononuclear cells (PBMCs) were isolated and added to PEDV ELISPOT plates to determine the PEDV specific IgA and **(B)** IgG ASCs. **(C)** Serum PEDV IgA Ab titers and cytokine concentrations (pg/ml) of **(D)** TGF-β and **(E)** interleukin (IL)-6 were determined by ELISA. Gilts were sampled at PID 0, 6–8, and 12–17. Asterisks indicate significant differences among treatment groups at the same time point (mean ± SEM). Statistical analysis was performed using the two-way ANOVA with repeated measures and Bonferroni's correction for multiple comparisons. $^{*}P < 0.05$, $^{**}P < 0.01$, $^{***}P < 0.001$.

Second Trimester Gilts Maintained Significantly Higher Levels of PEDV Specific ASCs and Abs Throughout Gestation

To standardize ASC and Ab responses among gilt treatment groups at uniform GDs, circulating PEDV IgA and IgG ASCs, Abs and VN Abs were compared at GD 82–95, 98–102, and 104–114 in first, second, and third trimester PEDV-infected gilts and third trimester mock gilts. Second trimester gilts had significantly higher circulating PEDV IgA and IgG ASCs at GD 82–95 and 98–102 and compared with first and third trimester gilts (**Figures 5A,B**). PEDV IgA ASCs were consistently higher than PEDV IgG ASCs in blood in first, second and third trimester gilts at GD 82–95, 98–102, and 104–114 (**Figures 5A,B**). Additionally, circulating PEDV IgA and IgG ASCs in first and second trimester gilts continually decreased in the 3 weeks prior to parturition, demonstrating parturition related or time post-infection effect on circulating PEDV IgA and IgG ASCs. This was not observed in third trimester gilts whose elevated numbers of PEDV IgA (numerically) and IgG (significantly) ASCs at GD 104–114 (**Figures 5A,B**) corresponded with PEDV RNA shedding in the feces at PID 6–8 and 12–17 (**Figure 2A**). Second trimester gilts had significantly higher serum PEDV IgA Ab titers compared with first trimester gilts at GD 82–95, 98–102, and 104–114 and third trimester gilts at GD 82–95 and 98–102 (**Figure 5C**). Serum PEDV IgG Ab titers were significantly higher in second compared with first trimester gilts at GD 82–95 and 104–114 and third trimester gilts at GD 82–95 and 98–102 (**Figure 5D**). Similarly, PEDV VN Ab titers were significantly higher in second compared with first trimester gilts at all time points but only significantly higher than third trimester gilts at GD 82–95 and 98–102 (**Figure 5E**).

Stage of Gestation Modulated Phenotypes of Gut Homing Circulating B Lymphocytes Prepartum

Mean frequencies of circulating $\alpha4^{+}\beta7^{+}$ (gut homing phenotype) B lymphocytes in second and third trimester gilts were significantly higher compared with first trimester gilts at PID 0 and 6–8 (**Figure 6A**). Additionally, first trimester gilts had a delayed increase in $\alpha4^{+}\beta7^{+}$ B lymphocyte frequencies in blood post PEDV infection (**Figure 6A**). Frequencies of $\alpha4^{+}\beta7^{+}$ B lymphocytes were standardized among gilt treatment groups at uniform GDs in late pregnancy (**Figure 6B**). Third trimester gilts had numerically elevated frequencies of circulating $\alpha4^{+}\beta7^{+}$ B lymphocytes (**Figure 6B**) at GD 98–102 and 104–114 corresponding with PEDV RNA shedding in the feces at PID 6–8 and 12–17 (**Figure 2A**). The mean frequencies of circulating chemokine receptor type 10 ($CCR10^{+}$) B lymphocytes were also measured post PEDV infection (**Figure 6C**) and standardized

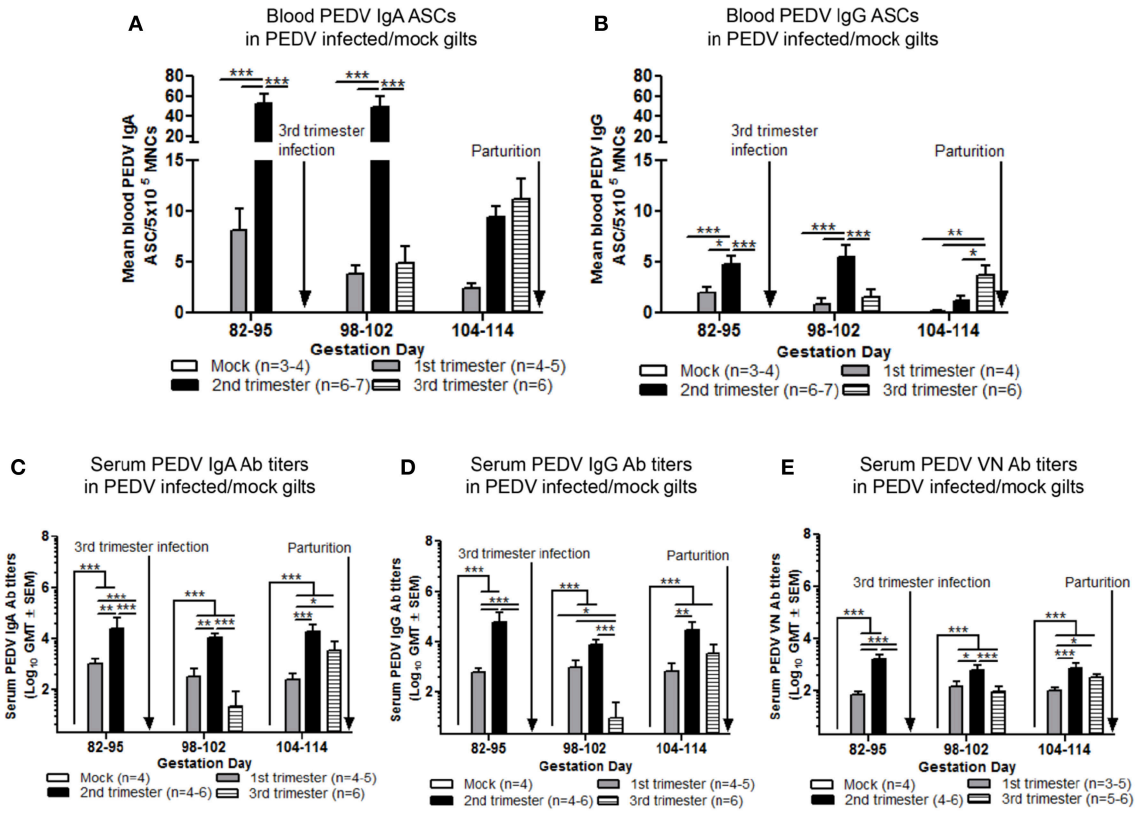

FIGURE 5 | Second trimester gilts maintained elevated circulating PEDV specific IgA and IgG antibody secreting cells (ASCs) and serum PEDV specific IgA, IgG and virus neutralizing (VN) antibodies (Abs) in late pregnancy. **(A)** Peripheral blood mononuclear cells (PBMCs) were isolated and added to PEDV ELISPOT plates to determine the PEDV specific IgA and **(B)** IgG ASCs. **(C)** Serum PEDV IgA and **(D)** IgG Abs were determined by ELISA while **(E)** serum PEDV VN Ab responses were determined by VN Ab assay. Gilts were sampled at gestation day (GD) 82–95, 98–102, and 104–114. Asterisks indicate significant differences among treatment groups at the same time point (mean ± SEM). Statistical analysis was performed using the two-way ANOVA with repeated measures and Bonferroni's correction for multiple comparisons. $^{*}P < 0.05$, $^{**}P < 0.01$, $^{***}P < 0.001$.

among gilt treatment groups at uniform GDs in late pregnancy (**Figure 6D**). No statistical differences among treatment groups were observed at PID 0, 6–8 or 12–17 (**Figure 6C**). However, third trimester gilts had significantly higher frequencies of circulating $CCR10^{+}$ B lymphocytes at GD 98–102 (PID 6–8) compared with second and first trimester and mock gilts (**Figure 6D**). The increase in circulating $CCR10^{+}$ B lymphocytes at GD 98–102 corresponded to peak PEDV RNA shedding titers at PID 6–8 (**Figure 2A**) in third trimester gilts. Additionally, significantly higher frequencies of activated B lymphocytes [$CD2^{-}CD21^{+}$ (39)] were observed in the blood of second and third compared with first trimester gilts at PID 0, 6–8, and 12–17 (**Figure 6E**).

Second Trimester PEDV-Infected Gilts Provided Optimum Lactogenic Immune Protection Resulting in 100% Piglet Protection

To determine the effect of stage of gestation at time of PEDV infection on lactogenic immune protection, piglets were challenged with PEDV at 3–5 days of age. The number of viable piglets born were not statistically significant between treatment groups (**Figure S5**). Second trimester PEDV infection of gilts resulted in 100% survival of PEDV challenged piglets (**Figure 7A**). First trimester gilts provided intermediate protection (87.2% survival) while third trimester gilts provided the least amount of protection (55.9% survival) among PEDV-infected gilts. Mock piglet's survival rate (5.7%) was significantly lower than all other treatment groups. Comparison of piglet weight gain revealed second trimester litters gained significantly more weight than all other treatment groups starting at post challenge day (PCD) 4 and lasting throughout the experiment (**Figure 7B**). First trimester litters had significantly higher normalized weights than third trimester litters at PCD 6, 7, and 9, but were similar thereafter. Mock litters were stunted (decreased or no weight gain) from PCD 1–7 and had the lowest normalized weights throughout the study. Lactogenic immune protection coincided with decreased PEDV RNA shedding titers where mean peak titers were 6.1 ± 0.2 $\log_{10}$ copies/ml, 7.8 ± 0.3 $\log_{10}$ copies/ml, 9.1 ± 0.3 $\log_{10}$ copies/ml, and 10.1 ±.2 $\log_{10}$ copies/ml for second, first, third, and mock litters, respectively (**Figure 7C**). Corresponding to increased weight gain and decreased PEDV RNA shedding titers, diarrhea scores were

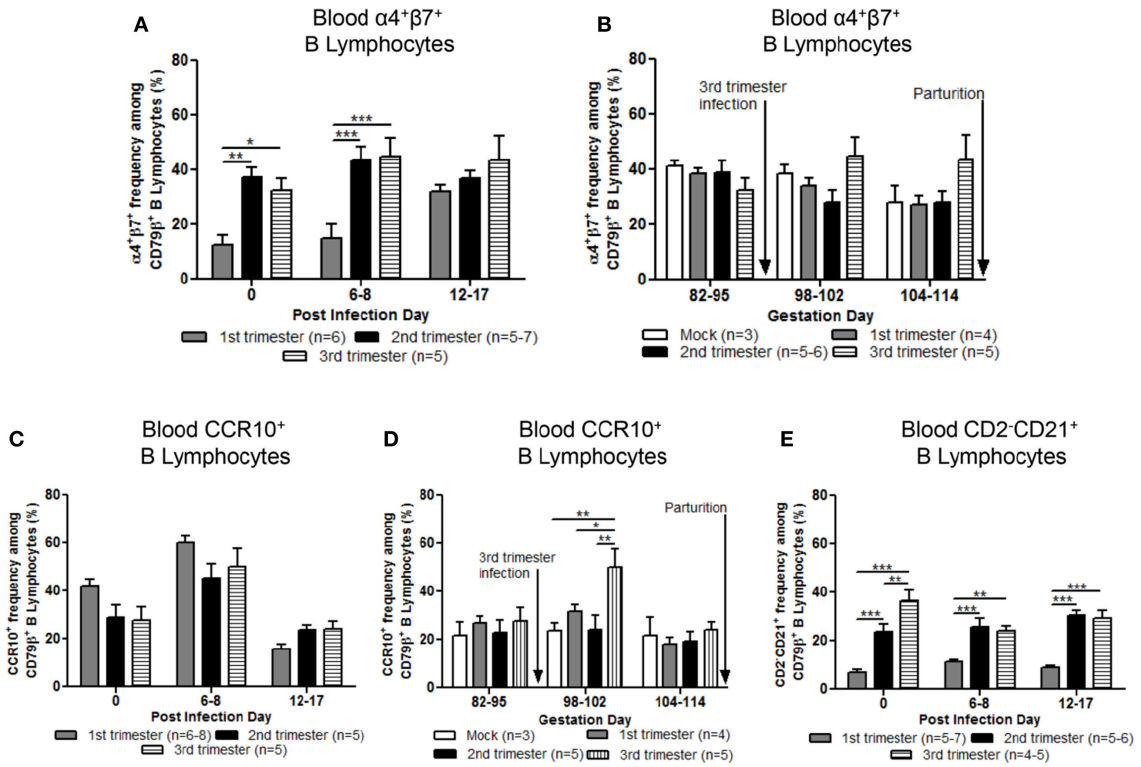

FIGURE 6 | Stage of gestation modulated circulating frequencies of B cell phenotypes prepartum**.** Peripheral blood mononuclear cells (MNCs) were isolated and analyzed at post infection day (PID) 0, 6–8 and 12–17 and gestation day (GD) 82–95, 98–102, and 104–114 for mean frequencies of $\alpha4^{+}\beta7^{+}$ **(A,B)** and chemokine receptor type 10 ($CCR10^{+}$) **(C,D)** B cells. Additionally, **(E)** primed and/or activated B lymphocytes ($CD2^{-}CD21^{+}$) were analyzed at PID 0, 6–8, and 12–17. Asterisks indicate significant differences among treatment groups at the same time point (mean ± SEM). Statistical analysis was performed using the two-way ANOVA with repeated measures and Bonferroni's correction for multiple comparisons. $^{*}P < 0.05$, $^{**}P < 0.01$, $^{***}P < 0.001$.

significantly lower in second trimester litters throughout the study (**Figure 7D**). While first trimester litters had diarrhea, it was delayed and significantly lower than third trimester litters at PCD 2–5. Mock litters had diarrhea immediately at PCD 1, lasting through PCD 11 and diarrhea scores were significantly higher than all other treatment groups. Gilt mean PEDV RNA shedding titers and fecal consistency scores were measured post piglet challenge. Mock gilt PEDV RNA shedding titers were significantly higher at PCD 2–7 than first, second and third trimester PEDV-infected gilts and remained numerically higher until PCD 17 (**Figure S6A**). Additionally, first trimester gilt PEDV RNA shedding titers peaked at PCD 4, earlier compared with second and third trimester gilts (**Figure S6A**). Mock gilt fecal consistency scores were significantly higher at PCD 5–11 compared with first, second and third trimester PEDV-infected gilts (**Figure S6B**). Diarrhea was not observed in previously PEDV-infected gilts post piglet challenge (**Figure S6B**).

Second Trimester Litters Had the Highest Titers of Circulating PEDV IgA and IgG Abs Positively Correlating With Survival Rate Protection Post PEDV Challenge

We evaluated the serum titers of piglet PEDV IgA and IgG Abs. Second trimester litters had significantly higher titers of circulating PEDV IgA Abs (**Figure 8A**) compared with first trimester litters at PCD 5–9 and PEDV IgG Abs at PCD 5–9 and 12–17 (**Figure 8B**). Additionally, compared with third trimester litters, second trimester litters had higher titers of PEDV IgA Abs at PCD 0 and 5–9 (**Figure 8A**) and PEDV IgG Abs at PCD 0 (**Figure 8B**). First trimester litters had significantly higher PEDV IgA and IgG Ab titers at PCD 0 compared with third trimester litters (**Figures 8A,B**). Lastly, circulating PEDV IgA and IgG Abs at PCD 0 were positively correlated with survival rates post piglet PEDV challenge (**Figures 8C,D**).

Piglet Survival Rates Post PEDV Challenge Correlated With Increased PEDV IgA ASCs and Abs and VN Abs in Milk

In colostrum, PEDV IgA and IgG ASCs were significantly higher in second compared with first and third trimester gilts (**Figures 9A,B**). However, in milk only PEDV IgA ASCs were significantly higher at postpartum day (PPD) 8–14/PCD 5–9 in second trimester gilts compared with all other treatment groups (**Figure 9A**). While PEDV IgA ASCs were maintained at high numbers in milk throughout lactation, milk PEDV IgG ASCs decreased significantly throughout the study (**Figures 9A,B**). Similar to ASCs, PEDV IgA and IgG Abs were significantly higher in the colostrum of second compared with first (IgA and IgG) and

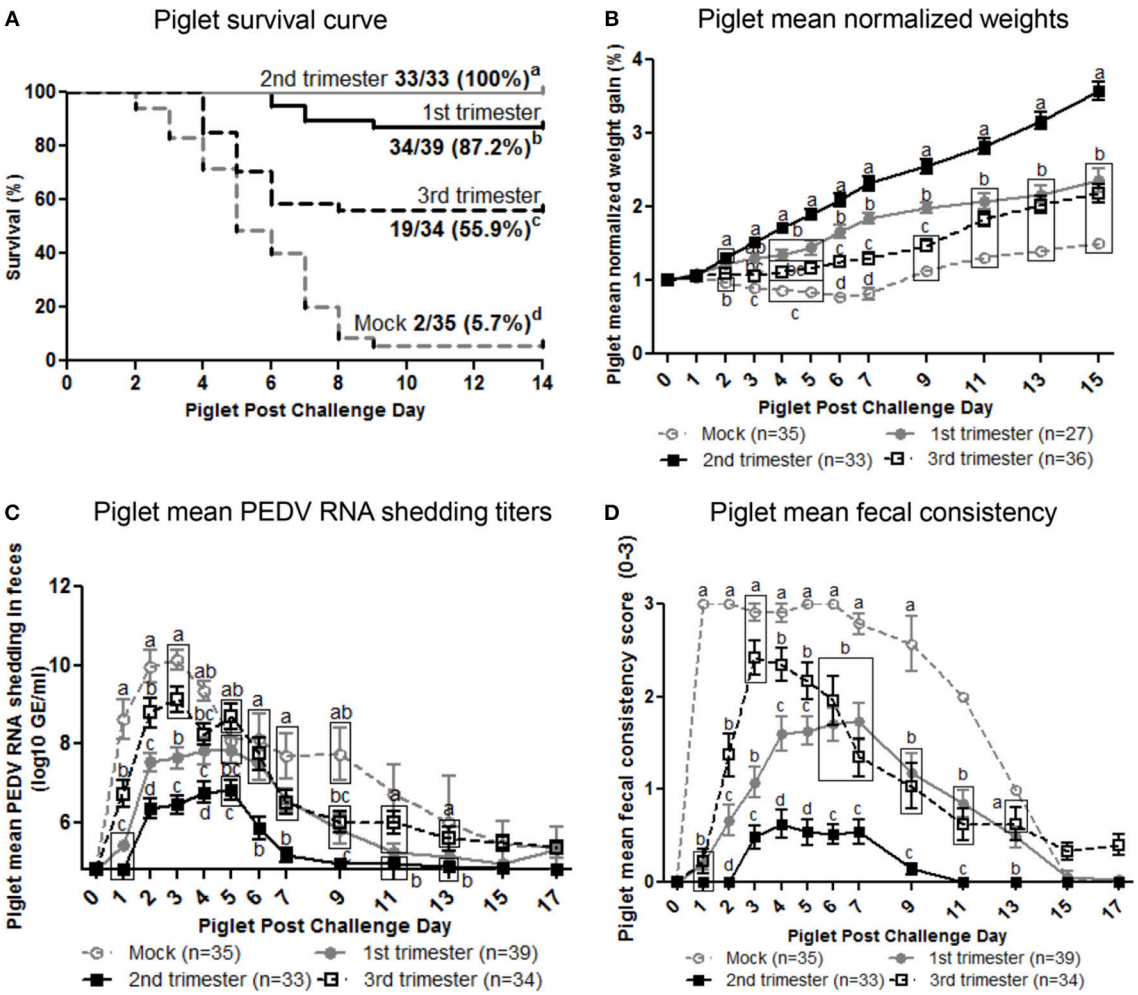

FIGURE 7 | Second trimester PEDV-infected gilts provided optimum lactogenic immune protection compared with first and third trimester and mock gilts. **(A)** Kaplan-Meier survival curve of first, second and third trimester and mock litters at post challenge day (PCD) 0–14. **(B)** Normalized weight gain of first, second and third trimester PEDV-infected and mock litters at PCD 0–15. Weights were normalized by dividing the daily weight (lbs.) by PCD 0 weight (lbs.). **(C)** Piglet PEDV RNA shedding titers were determined by real time quantitative polymerase chain reaction (qRT-PCR) and expressed as $\log_{10}$ copies/ml. **(D)** Piglet diarrhea was determined by fecal consistency score >1 (fecal consistency was scored as follows: 0, normal; 1, pasty/semiliquid; 2, liquid; 3, watery). Piglet diarrhea scores and PEDV RNA shedding titers were measured at PCD 1–7, 9, 11, 13, 15, and 17. Different letters indicate significant differences among treatment groups at the same time point (mean ± SEM). Statistical analysis was performed using the two-way ANOVA with repeated measures and Bonferroni's correction for multiple comparisons.

third trimester (IgA) gilts (**Figures 9C,D**). Additionally, PEDV VN Ab titers were significantly higher in colostrum in second compared with third trimester gilts (**Figure 9E**). After PEDV piglet challenge (PPD 8–14/PCD 5–9), PEDV IgA Ab titers in milk were significantly higher in second compared with third trimester gilts while PEDV IgG Ab titers were significantly higher in second compared with first trimester gilts (**Figures 9C,D**). Lastly, PEDV VN Ab titers were significantly higher in milk at PPD 8–14/PCD 5–9 compared with first and third trimester gilts (**Figure 9E**). We observed a significant correlation between PEDV IgA and IgG ASCs, and IgA and VN Abs in colostrum and piglet survival (**Table 2**). However, in mid and late lactation milk, only PEDV IgA ASCs, and IgA and VN Abs were significantly correlated with piglet survival. No significant ($P <$ 0.05) correlations were observed between milk IgG ASCs or Abs and piglet survival (**Table 2**). These correlations are consistent with our hypothesis that IgA ASC and Ab titers in milk are responsible for lactogenic immune protection in neonatal piglets against PEDV challenge.

PEDV Antibody$^+$ Cells Increased in the MG Post PEDV Challenge

Third trimester gilts had lower mean numbers of PEDV Ab$^+$ cells in the MG (2.7 ± 0.7) per microscopic field (30×) compared with second (6.1 ± 3.2) and first (6.9 ± 1.4) trimester gilts at GD 104–114 (**Figure S7**). There were no PEDV Ab$^+$ cells in the MG of mock gilts prepartum (GD 104–114). This suggests that while not significantly different, the mean numbers of PEDV Ab$^+$ cells

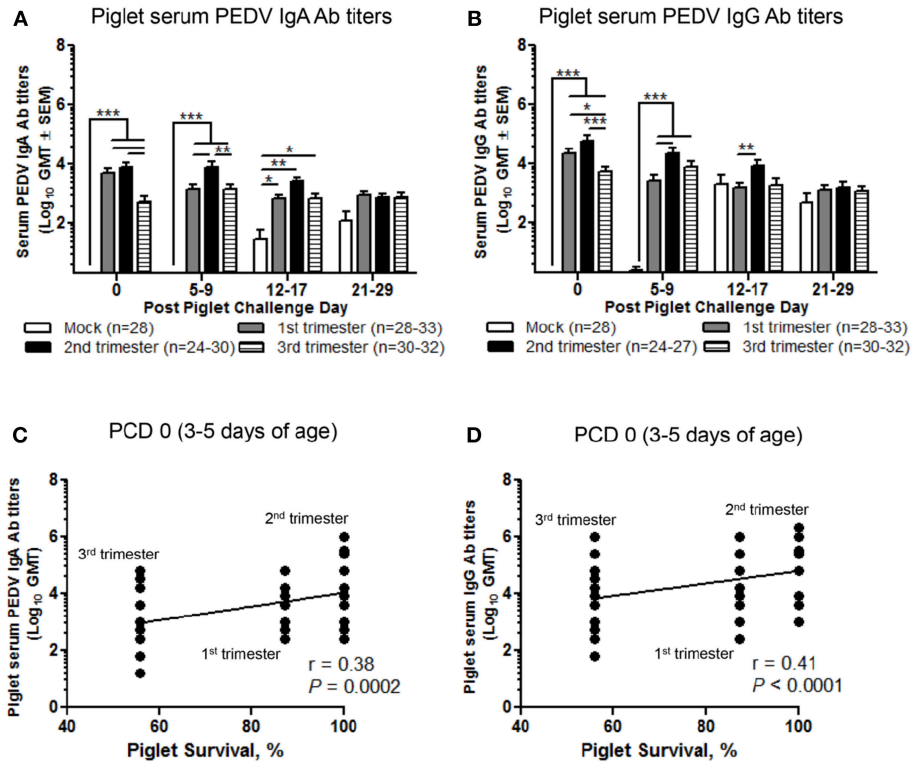

FIGURE 8 | Second trimester litters had the highest peak titers of circulating PEDV IgA and IgG antibodies (Abs) correlating with piglet protection post PEDV challenge. **(A)** Serum PEDV IgA and **(B)** IgG Ab responses were determined by PEDV ELISA assay. Piglet survival rates were significantly positively correlated with circulating PEDV **(C)** IgA and **(D)** IgG Abs at post challenge day (PCD) 0. Piglets were sampled at PCD 0, 5–9, 12–17, and 21–29. Asterisks indicate significant differences among treatment groups at the same time point (mean ± SEM). Statistical analysis was performed using the two-way ANOVA with repeated measures and Bonferroni's correction for multiple comparisons **(A,B)** or Spearman's non-parametric correlation **(C,D)**. $^{*}P < 0.05$, $^{**}P < 0.01$, $^{***}P < 0.001$.

in the MG may be reflective of levels of PEDV ASCs and Abs in colostrum. For example, third trimester gilts had the lowest mean number of PEDV Ab^{+} cells per microscopic field in the MG prepartum coinciding with the lowest mean numbers of IgA and IgG ASCs and mean titers of PEDV IgA and VN Abs in colostrum. PEDV Ab^{+} cells were also observed in the lactating MG at PCD 5–9. First, second and third trimester PEDV-infected gilts had significantly higher numbers of PEDV Ab^{+} cells per microscopic field in the MG compared with mock gilts post piglet challenge (**Figure S7**).

PEDV Exposure Post Piglet Challenge Differentially Affects MG, Spleen, Mesenteric Lymph Node, and Ileum ASC Responses of Gilts

The highest mean numbers of PEDV IgA ASCs were in the ileum while the highest mean numbers of PEDV IgG ASCs were in spleen and ileum (**Figures S8A,B**). Second trimester gilt mean numbers of IgA and IgG ASCs were significantly higher in the ileum than third and first trimester gilts, respectively. However, mock gilts had similar or higher mean numbers of IgA and IgG ASC in the spleen, mesenteric lymph node (MLN), and ileum compared with first, second, and third trimester gilts (**Figures S8A,B**), corresponding to higher PEDV RNA shedding titers in feces and PEDV-induced diarrhea of mock gilts (**Figures S6A,B**). Due to the high mortality rate of mock litters (**Figure 7A**), the MGs of mock gilts regressed rapidly post piglet challenge (40). There was not enough MG tissue left at PCD 21–29 to collect MG MNCs for ASC analysis.

DISCUSSION

Diarrheal disease represents a major global health burden and is the leading cause of morbidity and mortality in young children and animals. Specifically, the emergence of PEDV in the US in 2013 led to over 8.5 million piglet deaths and an estimated multi-million-dollar loss to the US swine industry (3, 41). Maternal vaccination that enhances passively transferred protective Abs in milk, induced via the gut-MG-sIgA axis, is the major strategy to protect neonatal suckling piglets immediately after birth (4, 5). However, due to the biological and immunological differences at each stage of pregnancy (18), the optimum time to induce maternal immunity and the gut-MG-sIgA axis was previously undefined. Here, we evaluated the impact of stage of gestation at PEDV infection on the maternal immune response, the generation of PEDV-specific ASCs and Abs in serum and milk

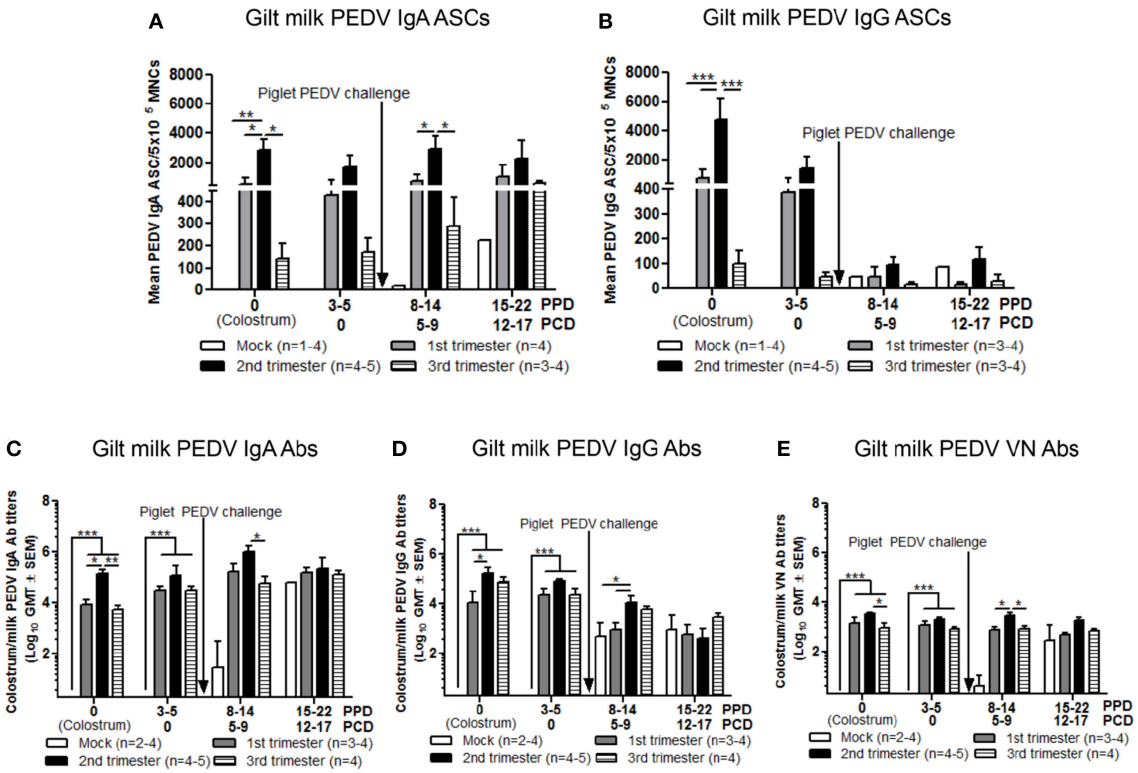

FIGURE 9 | Second trimester gilts had significantly increased circulating PEDV specific IgA and IgG antibody secreting cells (ASCs), PEDV IgA and IgG antibodies (Abs) and PEDV virus neutralizing (VN) Abs in colostrum/milk. **(A)** Milk mononuclear cells (MNCs) were isolated and added to PEDV ELISPOT plates to determine the PEDV specific IgA and **(B)** IgG ASCs. Whey PEDV **(C)** IgA and **(D)** IgG Abs were determined by ELISA while **(E)** whey PEDV VN Ab responses were determined by VN Ab assay. Gilts were sampled at postpartum day (PPD) 0, 3–5 (post challenge day [PCD] 0), 8–14 (PCD 5–9), and 15–22 (PCD 12–17). Asterisks indicate significant differences among treatment groups at the same time point (mean ± SEM). Statistical analysis was performed using the two-way ANOVA with repeated measures and Bonferroni's correction for multiple comparisons. $^{*}P < 0.05$, $^{**}P < 0.01$, $^{***}P < 0.001$.

and the protective effects of lactogenic immunity on PEDV-challenged piglets.

A major finding of our study is that PEDV infection in the second trimester was the optimum stage of gestation to generate the highest maternal immune responses in blood and milk correlating to 100% lactogenic immune protection in PEDV challenged suckling piglets (**Table 1**). For example, second trimester gilts had the highest peak levels of circulating PEDV IgA and IgG ASCs and Abs and VN Abs prior to parturition. Interestingly, this coincided with higher serum cytokine concentrations of TGF-β (significantly) and IL-6 (numerically) at PID 0 in second trimester gilts. TGF-β a cytokine produced by multiple lineages of leukocytes and stromal cells (42), is required for IgA class switch recombination (43) and IgA^{+} B cell survival in the lamina propria (44). Additionally, IL-6 promotes Ab production by increasing B cell helper capacity of $CD4^{+}$ T cells (38). Our data support previous research demonstrating increased serum TGF-β in women during the second trimester (45) correlating with increased Ab titers (46). The increased serum TGF-β and IL-6 at PEDV infection in second trimester gilts likely contributed to the enhanced anti-PEDV maternal immune responses.

Despite being PEDV-infected 5 weeks earlier, first trimester gilts generated a lower maternal immune response during gestation compared with second trimester gilts (**Table 1**). This suggests stage of gestation dependent differences in immune parameters may contribute to differential induction of the humoral immune response during PEDV infection (47, 48). The increase in NK cell frequencies at PID 0 in first compared with second and third trimester gilts (first trimester, GD 19–22; second trimester, GD 57–59; and third trimester, GD 96–97) is in agreement with previous studies reporting increased numbers of cytotoxic peripheral NK cells in first trimester women and swine (49–51). Furthermore, the significantly higher circulating NK cell cytotoxicity at PID 6–8 coincided with enhanced mean concentrations of serum IL-12 and IL-22, NK cell activation, and proliferation cytokines, at PID 0 in first trimester gilts (29, 52–54). Increased peripheral and decidual NK cell frequencies and lytic activity during the first trimester are thought to support maternal tissue remodeling during embryo implantation in swine and humans (20, 51, 55, 56). Additionally, NK cells are known to modulate B cell immunity (57, 58). Therefore, the unique immune environment during the first trimester may impact B cell responses to PEDV infection in pregnant gilts. Future

studies investigating the effects of NK cells on the maternal immune response during an enteric viral infection in gilts are warranted.

We also hypothesized that stage of gestation would impact B cell phenotypes pre and post PEDV infection. For example, lymphocyte $\alpha4^+\beta7^+$ integrin is a mucosal adhesion molecule responsible for cellular migration in the intestinal mucosa and lymphoid tissue by interacting with its receptor mucosal addressin cellular adhesion molecule 1 (MAdCAM-1) (59–62). Circulating $\alpha4\beta7^+$ lymphocytes reflect the intestinal tissue in which they were primed (63) and may influence the gut-MG-sIgA axis. The significantly higher frequencies of $\alpha4^+\beta7^+$ B cells at PID 0 and 6–8 in second and third trimester, compared with first trimester gilts (**Table 1**), coincides with increased concentrations of immune modulating pregnancy-associated hormones in swine, like estrone, estrone sulfate, 17β-estradiol (E2), and E2 sulfate (64). For example, trafficking of IgA^+ lymphoblasts to the MG in ovariectomized female mice was enhanced after E2 administration (65). Additionally, E2 in combination with progesterone administration in ovariectomized female mice resulted in increased L-selectin and α4-dependent adhesion of NK cells to mucosal tissues (60). Additionally, we observed differential effects of gestational stage on $CD2^-CD21^+$ (primed and/or activated) B cell frequencies in blood. The significant increase in circulating $CD2^-CD21^+$ B cell frequencies at PID 6–8 and 12–17 in second and third trimester compared with first trimester gilts is similar to the trend observed for $\alpha4\beta7^+$ B cell frequencies later in pregnancy (**Table 1**). The increasing concentrations of pregnancy-associated hormones as pregnancy progresses could modulate circulating frequencies of $CD2^-CD21^+$ B cells, contributing to the differential immune responses observed in this study. Future studies treating ovariectomized swine with exogenous E2 or progesterone are needed to decipher the *in vivo* effects of pregnancy associated hormones on mucosal lymphocyte trafficking, B cell activation and ASC and Ab production.

To our knowledge, this is the first study to demonstrate an effect of stage of gestation at time of enteric viral infection on the gut-MG-sIgA axis and immune protection in suckling piglets. In our study, second trimester gilts provided greater passive lactogenic immune protection (100%) compared with first (87.2%) and third (55.9%) trimester and mock gilts (5.7%). The increased levels of protection were significantly correlated with PEDV IgA ASCs and Abs and VN Abs in colostrum and milk (**Tables 1**, **2**). These results are in agreement with previous work done with TGEV-infected pregnant swine. For example, high rates of protection against TGEV in piglets were achieved when pregnant sows were orally infected (6, 7, 13) with live virulent virus (14, 15). The increased rate of protection was associated with high titers of IgA Abs in colostrum and milk induced via the gut-MG-sIgA axis (66). Additionally, PEDV IgA and IgG Ab titers in piglet serum at PCD 0 correlated with piglet protection against PEDV challenge. In our study, we experimentally infected gilts with the same dose and strain of PEDV and controlled for parity and lack of prior TGEV-exposure. Therefore, we were able to observe correlates of immunity where second trimester gilts provided optimal protection in PEDV challenged suckling piglets correlating with levels of colostrum and milk PEDV IgA ASCs and Abs and VN Abs and piglet serum IgA and IgG Abs (**Table 1**). Experimental infection studies of gilts/sows with controlled PEDV doses and timing of piglet challenge post parturition are important for determining correlates of lactogenic immune protection against PEDV.

Lastly, we observed significantly higher PEDV RNA shedding titers at PID 2 and diarrhea scores at PID 4 in third trimester gilts. This suggests factors involved in intestinal homeostasis are impacted by the hormonal changes during the third trimester. For example, circulating E2 and porcine growth hormone concentrations increase in the third trimester prior to parturition (64). There is growing evidence that hormones dynamically influence the gut microbiome (67). Coincidently, the gut microbial environment during pregnancy changes dramatically from the first to third trimesters in humans (68, 69) and swine (70) resulting in decreased bacterial community richness. Additionally, studies of PEDV-infected pregnant sows revealed a significant decrease of observed bacterial species compared with healthy pregnant sows (71). Although the gut microbiome was not examined in this study, it is possible that pregnancy hormone-induced effects on the gut microbiome during late pregnancy in combination with PEDV infection resulted in increased gut dysbiosis in third trimester pregnant gilts. Future studies investigating the impact of the microbiome during pregnancy on PEDV pathogenesis and the gut-MG-sIgA axis are warranted.

Previous research investigating stage of gestation at vaccination on the immune response in pregnant women reached conclusions similar to ours. Women vaccinated with the tetanus-diphtheria-acellular pertussis (Tdap) vaccine in the second and/or early third trimester had a higher concentration and avidity of anti-Tdap Abs in maternal blood and increased transplacental anti-Tdap Ab transfer compared with women immunized in the mid to late third trimester (72–74). This is in agreement with our results, demonstrating that second trimester PEDV infection yields the highest titer of PEDV IgA, IgG, and VN Abs in serum and colostrum/milk. More research is needed in humans and livestock to better understand maternal immunity and to design the most effective maternal vaccines to passively protect suckling neonates and prevent neonatal morbidity and mortality.

In summary, a comparison of PEDV infection at different stages of gestation demonstrated that first, second and third trimester gilt immune responses vary greatly in magnitude of their immune response and association with lactogenic immune protection. We conclude that second trimester gilts have the greatest capacity to generate a robust anti-PEDV humoral immune response prior to parturition, resulting in the highest amount of lactogenic immune protection against PEDV challenge in neonatal suckling piglets. Additionally, piglet protection against PEDV challenge is correlated with PEDV IgA ASC, IgA Abs, and VN Abs in milk and PEDV IgA and IgG Abs in piglet serum (**Tables 1**, **2**). Our results provide novel insights and identify possible predictors of maternal vaccine efficacy for passive protection of suckling piglets. Finally, pregnancy should not be evaluated as a single event and development of a successful attenuated PEDV vaccine requires consideration of stage of gestation at the time of vaccination.

MATERIALS AND METHODS

Virus

The wild-type PC22A strain of PEDV was used for gilt infection and piglet challenge at a dose of 1×10^5 plaque forming units (PFU) diluted in Minimal Essential Media [MEM (Life Technologies, Carlsbad, CA)]. Briefly, PC22A was isolated and cultured in Vero cells as described previously (75, 76). Cells were grown in growth medium containing Dulbecco's Modified Eagle's Medium [DMEM (Life Technologies, Carlsbad, CA)] supplemented with 5% fetal bovine serum (Life Technologies, Carlsbad, CA) and 1% antibiotic-antimycotic (Life Technologies, Carlsbad, CA). Virus was grown in Vero cells in maintenance medium containing DMEM supplemented with 10 μg/ml trypsin (Life Technologies, Carlsbad, CA), 0.3% tryptose phosphate broth (Sigma Aldrich, St. Louis, MO), and 1% antibiotic-antimycotic. Cells were kept in a humidified incubator at 37°C and 5% CO_2. PC22A was passaged three times in Vero cells before passaging once for generation of inoculum in a gnotobiotic pig. The virulence of pig passaged PC22A was confirmed in adult and neonatal pigs (4, 77, 78). Cell-culture adapted PC22A was used as a positive control in the VN Ab assay.

Experimental Design

All animal experiments were approved by the Institutional Animal Care and Use Committee at The Ohio State University. All pigs were maintained, sampled, and euthanized humanely. First parity PEDV, porcine deltacoronavirus (PDCoV) and TGEV seronegative pregnant gilts (Landrace × Yorkshire × Duroc cross-bred) were acquired from either Wilson Farms (Elkhorn, WI) or The Ohio State University swine center facility and randomly assigned to one of four treatment groups: PEDV-infected (1) first trimester (GD 19–22) ($n = 10$); (2) second trimester (GD 57–59) ($n = 7$); or (3) third trimester (GD 96–97) ($n = 6$) or MEM-infected third trimester control [GD 96–97 ($n = 4$)] (**Figure 1A**). Second and third trimester gilts arrived at our facilities at GD 49–51 and 89–92, respectively, and acclimated for 1 week prior to PEDV infection. First trimester gilts were housed and PEDV-infected at the National Animal Disease Center, USDA-ARS, in Ames, Iowa and then four gilts were shipped to our facilities at GD 93 after they were determined to be fecal shedding negative by real-time quantitative polymerase chain reaction (RT-qPCR). Gilt fecal samples were collected, and clinical signs observed on PID 0, 2, 4, 6, 10, and 14. Fecal consistency was scored as follows: 0, solid; 1, pasty; 2, semi-liquid; 3, liquid, respectively. A fecal consistency score of >1 was considered as diarrhea (4, 77). Blood samples were collected post-PEDV infection at PID 0, 6–8 and 12–17 and also prior to parturition at GD 82–95, 98–102, and 104–114 for serum and mononuclear cell (MNC) isolation. All gilts farrowed naturally in our facilities at GD 114 (± 3) and colostrum was collected within 12 h of parturition. Piglets were orally PEDV-challenged at 3–5 days of age (mean ± SD challenge day for first trimester litters = 4.0 ± 0.82, second trimester litters = 4.4 ± 0.96, third trimester litters = 4.2 ± 0.82 and mock litters = 3.7 ± 0.96). Gilt and piglet serum were collected on PCD 0, 5–9, 12–17, and 21–29. All colostrum and milk samples were collected after administration of 2cc oxytocin intramuscularly (IM) at PPD 0, 3–5, 8–14, and 15–22 (**Figure 1B**). Gilt MG biopsies were collected at GD 104–114 and PPD 8–14. Piglet fecal samples were collected and clinical signs and body weights were recorded daily on PCD 0–7 and every other day through PCD 15–17. All animals were euthanized at PCD 21–29. Upon euthanasia, gilt blood, ileum, MG, MLN, and spleen tissues were collected for MNC isolation. Piglet blood was collected and the serum separated for immunologic assays.

PEDV RNA Quantification by RT-qPCR

To determine PEDV RNA shedding titers, two rectal swabs were suspended in 4 mL MEM as described previously (78). Viral RNA was extracted from 50 μl of fecal supernatants following centrifugation (2,000 × g for 30 min at 4°C) using the MagMAX Viral RNA Isolation Kit (Applied Biosystems, Foster City, CA) according to the manufacturer's instructions. Titers of viral RNA shed in feces were determined by TaqMan RT-qPCR using the Onestep RT-PCR Kit (QIAGEN, Valencia, CA) (78). The detection limit was 10 copies per 20 μL of reaction, corresponding to 4.8 $\log_{10}$ copies/mL of original fecal samples.

Isolation of MNCs in Blood, Spleen, MLN, and Ileum

Blood, spleen, MLN, and ileum were collected aseptically at euthanasia and processed for MNC isolation as described previously (79). The isolated cells were resuspended in enriched RPMI [E-RPMI (Roswell Park Memorial Institute)] medium containing 8% fetal bovine serum, 2 mM l-glutamine, 1 mM sodium pyruvate, 0.1 mM non-essential amino acids, 20 mM HEPES (*N*-2-hydroxy- ethylpiperazine-*N*−2-ethanesulfonic acid), and 1% antibiotic-antimycotic (Life Technologies, Carlsbad, CA) and used for assays. The viability of MNCs was determined by trypan blue exclusion. Briefly, MNCs were diluted two-fold in 0.4% trypan blue before visualizing using an automated cell counter (Cellometer, Nexcelom, Lawrence, MA). The viability (%) was calculated as [1.00–(number of blue cells/numbers of total cells)] × 100.

Isolation of MNCs From the MG Tissue

The MG was collected aseptically at euthanasia and placed in ice-cold wash medium (RPMI 1640 with 10 mM HEPES, 200 g of gentamicin per ml, and 20 g of ampicillin per ml [Life Technologies, Carlsbad, CA]). Tissue was minced and pressed through stainless steel 80-mesh screens of a cell collector (Cellecter; E-C Apparatus Corp., St. Petersburg, FL.) to obtain single-cell suspensions and then pooled. A 90% Percoll solution (Sigma Aldrich, St. Louis, MO) was added to the MG cell suspensions and centrifuged at 1,200 × g for 30 min at 4°C. Cell pellets were resuspended in 43% Percoll, underlaid with 70% Percoll, and centrifuged at 1,200 × g for 30 min at 4°C. The MNC were collected from the 43-to-70% interface and washed with wash medium. Cells were filtered through a 70 μM pore filter and resuspended in E-RPMI. The viability of MNCs was determined by trypan blue exclusion.

Detection of Cytokines in Serum by ELISA

Serum samples were processed and analyzed for proinflammatory (TNF-α, IL-6, IL-17, IL-22), innate (IFN-α) and Th1 (IL-12, IFN-γ), Th2 (IL-4), and T regulatory (IL-10 and TGF-β) cytokines as described previously with some modifications (80, 81). Briefly, Nunc Maxisorp 96-well plates were coated with anti-porcine IL-4 (2 μg/ml, clone A155B16F2), anti-porcine IL-10 (4 μg/ml, clone 945A4C437B1), anti-porcine IFN-γ (1.5 μg/ml, clone A151D5B8), anti-porcine TGF-β (1.5 μg/ml, clone 55B16F2) (Thermo Fisher Scientific, Waltham, MA), anti-porcine IL-6 (0.75 μg/ml, goat polyclonal Ab), anti-porcine IL-12 (0.75 μg/ml, goat polyclonal Ab), anti-porcine IFN-α (2.5 μg/ml, clone K9) (R&D systems, Minneapolis, MN), anti-porcine TNF-α (1.5 μg/ml, goat polyclonal Ab), anti-porcine IL-17 (1.5 μg/ml, rabbit polyclonal Ab), and anti-porcine IL-22 (1.5 μg/ml, rabbit polyclonal Ab) (Kingfisher Biotech, Saint Paul, MN) overnight at 37°C for IFN-α or 4°C for all other cytokines. Biotinylated anti-porcine IL-4 (0.5 μg/ml, clone A155B15C6), anti-porcine IL-10 (1 μg/ml, clone 945A1A926C2), anti-porcine IFN-γ (0.5 μg/ml, clone A151D13C5), anti-TGF-β (0.4 μg/ml, TGF-β-1 Multispecies Ab Pair CHC1683) (Thermo Fisher Scientific, Waltham, MA), anti-porcine IL-6 (0.1 μg/ml, goat polyclonal IgG), anti-porcine IL-12 (0.2 μg/ml, goat polyclonal IgG), anti-porcine IFN-α (3.75 μg/ml, clone F17) (R&D systems, Minneapolis, MN), anti-porcine TNF-α (0.4 μg/ml, goat polyclonal Ab), anti-porcine IL-17 (1 μg/ml, rabbit polyclonal Ab) or anti-porcine IL-22 (1 μg/ml, rabbit polyclonal Ab) (Kingfisher Biotech, Saint Paul, MN) were used for detection. Porcine IFN-α detection Ab was biotinylated using a commercial kit as described previously (81). Plates were developed and cytokine concentrations were calculated as described previously (80). Sensitivities for these cytokine ELISA assays were 1 pg/ml for IL-4, IL-12, and IFN-α, 4 pg/ml for TNF-α, IL-17, and IL-22, 8 pg/ml for TGF-β, and 16 pg/ml for IL-6, IL-10, and IFN-γ.

Colostrum/Milk Processing for Whey and Isolation of MNCs

Colostrum/milk was collected aseptically after gilts were given 2cc oxytocin (VetOne, Boise, ID) IM to facilitate collection of mammary secretions. Colostrum/milk was placed immediately on ice. Samples were filtered through a 70 μM pore filter and centrifuged at 1,800 × g for 30 min at 4°C to separate fat, skim milk, and cell pellet portions. Fat was removed utilizing sterile plain-tipped applicators (Fisher Scientific, Hampton, NH). Skim milk was collected, centrifuged at 28,000 × g for 1 h at 4°C to separate the whey that was then stored at −20°C until tested. The cell pellet portion was resuspended in a 90% Percoll solution and centrifuged at 1,200 × g for 30 min at 4°C. Cell pellets were resuspended in 43% Percoll, underlaid with 70% Percoll, and centrifuged at 1,200 × g for 30 min at 4°C. The MNC were collected from the 43-to-70% interface and washed with wash medium. Cells were filtered through a 70 μM pore filter and resuspended in E-RPMI. The viability of the MNC preparation was determined by trypan blue exclusion.

NK Cell Cytotoxicity Assay

Blood MNC and K562 cells were used as effector and target cells, respectively. Effector: target cell ratios of 10:1, 5:1, and 1:1 were used and the assay was done as described previously (82).

Flow Cytometry to Assess NK Cell Frequencies

To determine the frequencies of NK cells, $CD3^-$, $CD172^-$, $CD8^+$ MNCs were identified. Briefly, 100 μl of peripheral blood mononuclear cells (PBMCs) at 1×10^7 cells/ml were stained with anti-porcine CD3 (clone PPT3, Southern Biotech), anti-porcine SWC3a [CD172 human analog (clone 74-22-15, Southern Biotech)] and anti-porcine CD8 (clone 76-2-11, Southern Biotech) monoclonal Abs (mAbs) for 15 min at 4°C. Subsequently cells were washed and incubated with streptavidin APC (BD Biosciences, San Jose, CA, USA) secondary Ab. Appropriate isotype matched control Abs were included. Acquisition of 50,000 events and analyses were done using the Accuri C6 flow cytometer (BD Biosciences). The gating strategy is depicted in **Figure S1**.

PEDV Plaque Reduction VN Assay

A plaque reduction VN assay was performed as described previously (83) with modifications. Serum and whey were inactivated at 56°C for 30 min prior to testing for PEDV neutralizing Abs. Serial 4-fold dilutions of test sera or whey were mixed with 70 PFU and 140 PFU PEDV PC22A cell-culture adapted strain, respectively. The serum/whey-virus mixtures (290 μl/well) were incubated for 1.5 h at 37°C with gentle rocking and then duplicate samples were infected onto 2–3 day confluent Vero cell monolayers in 6-well plates. Plates were incubated at 56°C for 1 h, lightly rocking every 15 min. Subsequently, the inoculum was removed, cells were washed twice with sterile PBS [1X pH 7.4 (Sigma Aldrich, St. Louis, MO)] and overlaid with 0.75% low melting point agarose (SeaPlaque, Lonza, Riverside, PA) in serum free media supplemented with tryptose phosphate broth and trypsin as described for PEDV cultivation (75). Plates were incubated at 37°C for 3 days and then stained with 0.001% neutral red solution (Sigma Aldrich, St. Louis, MO). Plaques were counted and the VN titers were determined by calculating the reciprocal of the highest dilution of a serum/whey sample showing an 80% reduction in the number of plaques compared with seronegative control serum/whey.

PEDV Whole Virus Ab ELISA

Cell culture adapted PC22A was propagated on 2–3-day-old Vero cells in polystyrene roller bottles (Fischer Scientific, Hampton, NH) until the cells demonstrated 90–95% cytopathic effects (CPE). Roller bottles were subjected to two freeze-thaw cycles at −80°C before collecting the supernatant and centrifuging at 3,000× g for 10 min at 4°C to remove Vero cell debris. The supernatant was overlayed onto 3 ml sucrose [35% in TNC buffer (50 mM Tris at pH 7.4, 150 mM NaCl, 10 mM $CaCl_2$, 0.02% NaN_3)] and centrifuged at 112,700 × g for 2 h at 4°C. The viral pellet was resuspended in TNC buffer, centrifuged at 107,200 × g for 2 h at 4°C and washed twice with sterile PBS (1X pH 7.4). Then the viral pellet was inactivated by using binary ethylenimine (BEI) as previously described (84). The semipurified inactivated virus was resuspended in PBS

(1X pH 7.4) at a dilution of 1:3 of the original supernatant volume and stored at −80°C. At the time of testing, PEDV or mock antigen solution was further diluted 1:4 and added (60 μl per well) to uncoated polystyrene plates (Fisher Scientific, Hampton, NH) in alternating wells. Plates were incubated for 4 h at 37°C or overnight at 4°C. Plates were washed 5X with PBS-T wash solution (PBS 1X, 0.1% Tween-20 [Fisher Scientific, Hampton NH], pH 7.4). General Block ELISA blocking solution (Immunochemistry Technologies, Bloomington, MN) was added (200 μl per well) and plates were stored at 4°C overnight. After incubation, plates were washed twice with PBS-T and samples were added. All samples were serially diluted starting at 1:4 and added (50 μl per well) in duplicate to coated plates. Positive and negative controls (Ab-positive and -negative experimental samples) were included per plate for each sample type. Plates were incubated at room temperature (RT) for 1.5 h and washed 5X with PBS-T. Primary Abs were added (100 μl per well) diluted in PBS-T to detect IgA Ab [peroxidase-conjugated goat anti-pig IgA (Bio-Rad, Hercules, CA)] and IgG [biotin-conjugated goat anti-pig IgG (Seracare, Milford, MA)] in serum (1:4,000 and 1:20,000, respectively) and milk/intestinal samples (1:20,000). IgA plates were incubated at RT for 1.5 h and IgG at 37°C for 1 hr. For IgG plates, peroxidase-conjugated streptavidin [1:10,000 (Roche, Basel, Switzerland)] was added (100 μl per well) and incubated at RT for 1 h. For both IgA and IgG, plates were washed twice with PBS-T and the reaction was visualized for all plates by adding 100 μl of 3,3′,5,5′-tetramethylbenzidine (TMB) substrate with H_2O_2 membrane peroxidase substrate system (Seracare, Milford, MA). Plates were incubated at RT for 5 min and stopped by addition of 100 μl stop solution (1 M sulfuric acid) to each well. Reactions were measured as optical density at 450 nm using an ELISA plate reader (Spectramax 340pc, Molecular Devices, San Jose, CA). The ELISA Ab titer was expressed as the reciprocal of the highest dilution that had a corrected A_{450} value (sample absorbance in the virus-coated well minus sample absorbance in the mock antigen-coated well) greater than the cut-off value (mean corrected A_{450} value of negative controls plus 3 standard deviations). Samples negative at a dilution of 1:4 were assigned a titer of 1:2 for the calculation of geometric mean titers (GMTs).

PEDV Antibody Secreting Cell ELISPOT

To detect PEDV ASCs, PEDV PC22A, and mock-infected, acetone-fixed Vero cells in 96-well plates were used similar to methods used to detect TGEV ASC (85, 86). Briefly, after infected Vero cells (at 95–100% confluency) showed 90–95% CPE, cells were fixed with 80% acetone for 15 min, allowed to dry for 1–2 h and stored at −20°C. Mock-infected cell monolayers served as negative controls. Plates were thawed and rehydrated in sterile PBS for 15 min at RT. Serial dilutions of MNCs (5×10^5, 5×10^4, 5×10^3, and 5×10^2) were added to duplicate wells (100 μl per well) of fixed PEDV PC22A and mock-infected cell monolayers. Plates were centrifuged at 120× g, for 5 min at RT and incubated at 37°C with 5% CO_2 for 12–14 h. After incubation, the plates were washed 5X with PBS-T. ASCs were detected by incubating plates with HRP-conjugated anti-pig IgA [1:4,000 (Bio-Rad, Hercules)] or biotinylated anti-pig IgG [1:20,000 (Seracare, Milford, MA)]. All Abs were added at 100 μl per well. Plates incubated with Abs to IgA were incubated at RT for 1.5 h and for Abs to IgG at 37°C for 1 h. For IgG plates, peroxidase-conjugated streptavidin [1:10,000 (Roche, Basel, Switzerland)] was added (100 μl per well) and incubated at RT for 1 h. The reaction was visualized for all plates by adding 100 μl TMB substrate with H_2O_2 membrane peroxidase substrate system (Seracare, Milford, MA). Spots were detected and counted using a light microscope. Counts were averaged from duplicate wells and expressed relative to 5×10^5 MNC.

Histopathologic Analysis and Evaluation of PEDV Ab$^+$ Cells in the MG

To evaluate PEDV Ab$^+$ cells in the MG, 5 cm biopsies were collected using a 12 gauge × 10 cm semi-automatic needle (Bard Peripheral Vascular, Tempe, AZ) and fixed in 10% neutral buffered formalin. Sections were trimmed, processed, and embedded in paraffin. Sections were cut (3.5 μm thick) and processed for antigen retrieval (0.05% pronase E treatment [Sigma Aldrich, St. Louis, MO]). For detection of PEDV Ab$^+$ cells, a PEDV viral suspension sandwich immunohistochemistry (IHC) method was developed. Semipurified inactivated PEDV antigen, as described previously for PEDV Ab ELISA plates, was added to tissue sections and incubated overnight at 4°C. A mAb to the N protein of a highly virulent US PEDV strain [PC22A-like (PEDV 72-111-25 IgM G-14, kindly provided by Steven Lawson and Eric Nelson, Department of Veterinary and Biomedical Sciences, South Dakota State University)] was added to tissue sections and incubated overnight at 4°C. Supersensitive Polymer-HRP IHC Detection System (Biogenex, Fremont, CA) was used as a secondary Ab and substrate prior to hematoxylin and eosin (H&E) staining. Microscopic imagines (30× magnification) were obtained using a fluorescence microscope (Olympus IX70-S1F2). Mean numbers of PEDV Ab$^+$ cells were evaluated by measuring at least 3 different microscopic fields at (30× magnification) for each sample time point (GD 104–114 and PCD 5–9) from first, second and third PEDV-infected or mock gilts.

Flow Cytometry to Assess Lymphocytes and Homing Marker Integrin and Receptor Frequencies

Procedures for flow cytometry staining (including buffers used) were performed as described previously with minor modifications (87). Briefly, 100 μl of MNCs at 1×10^7 cells/ml were stained with anti-porcine CD21-PE (clone BB6-11C9.6, Southern Biotech) and anti-porcine CD2 (clone MSA4, VMRD) monoclonal Abs (mAbs) to determine B cell subsets (88). To determine expression of α4 integrin, β7 integrin and CCR10, cells were stained with porcine cross-reactive anti-human α4 integrin (clone HP2/1, Abcam, Cambridge, MA), anti-mouse β7 integrin (clone FIB27, BD Biosciences), and anti-mouse CCR10 (clone 248918, R&D Systems) mAbs. Additionally, to determine expression of IgA, cells were stained with anti-porcine IgA (clone K61 1B4, Bio-Rad) mAb.

After washing, cells were stained with appropriate secondary antibodies. For intracellular CD79β staining, stained cells were permeabilized with Cytofix/Cytoperm (BD Biosciences), washed with Perm/Wash Buffer (BD Biosciences), and stained with porcine cross-reactive anti-mouse CD79β-FITC Ab (clone AT1072, Bio-Rad) mAb. Additionally, $CD4^+$ (anti-porcine CD4, clone 74-12-4, Southern Biotech) and $CD8^+$ (anti-porcine CD8, clone 76-2-11, Southern Biotech) T cells were assessed within the $CD3^+$ (anti-porcine CD3, clone PPT3, Southern Biotech) MNC population (T lymphocytes). Appropriate isotype matched control antibodies were included. Acquisition of 50,000 events and analyses were done using the Accuri C6 flow cytometer (BD Biosciences, San Jose, CA, USA). The gating strategy for T and B cell phenotypes are depicted in **Figures S1, S2**.

Statistics

PEDV RNA shedding titers, fecal consistency scores, normalized weights, frequencies of blood MNC populations in flow cytometry, mean concentrations of serum cytokines, PEDV IgA and IgG ASCs, log-transformed PEDV IgA, IgG and VN Ab titers and PEDV Ab^+ cells in the MG were analyzed by a two-way analysis of variance (ANOVA-general linear model), followed by Bonferroni's posttest. NK cell activity in blood and PEDV IgA and IgG ASCs in MG, spleen, MLN, and ileum tissues were compared among groups with the Mann-Whitney (non-parametric) test. The log-rank (Mantel-Cox) test was used for comparison of survival curves amongst treatment groups. Statistical significance was assessed at $P \leq 0.05$ for all comparisons. All statistical analyses were performed with GraphPad Prism 5 (GraphPad Software, Inc., CA).

ETHICS STATEMENT

Studies were approved by the Institutional Animal Care and Use Committee (IACUC) and performed on gestating and lactating gilts and piglets aged 0–5 weeks, in accordance with USDA and OSU IACUC guidelines.

AUTHOR CONTRIBUTIONS

LS, KL, and SL contributed conception and design of the study. SL conducted the experiments, analyzed the data, and wrote the manuscript. LS and AG supervised the work and contributed critical analysis to the results. FP, MA, AB, and AVG assisted with daily animal work, collected and processed samples and conducted RT-qPCR experiments and analysis. MA and SL conducted IHC experiments and analysis. All authors contributed to manuscript revision, read, and approved the submitted version.

FUNDING

This work was supported by USDA NADC ARS grant #60054098, AFRI NIFA Fellows Program/USDA National Institute of Food and Agriculture grant #60046830, and federal and state funds appropriated to the Ohio Agricultural Research and Development Center, The Ohio State University.

ACKNOWLEDGMENTS

The authors thank Dr. Qiuhong Wang for providing the wild-type PC22A strain of PEDV, Drs. E. Nelson and S. Lawson, South Dakota State University for MAb (72-111-25), Marcia Lee and Drs. Ayako Miyazaki and Sayaka Takanashi for their technical assistance, Dr. Juliette Hanson for surgical and veterinary clinical assistance, Dennis Hartzler, Sara Tallmadge, Megan Strother, Ronna Wood and Jeffrey Ogg for animal care and assistance, and Drs. Prosper Boyaka and Qiuhong Wang for their critical review of the manuscript.

SUPPLEMENTARY MATERIAL

The Supplementary Material for this article can be found online at: https://www.frontiersin.org/articles/10.3389/fimmu.2019.00727/full#supplementary-material

REFERENCES

1. Olanratmanee E-o, Kunavongkrit A, Tummaruk P. Impact of porcine epidemic diarrhea virus infection at different periods of pregnancy on subsequent reproductive performance in gilts and sows. *Anim Reprod Sci*. (2010) 122:42–51. doi: 10.1016/j.anireprosci.2010.07.004
2. Pijpers A, van Nieuwstadt AP, Terpstra C, Verheijden JH. Porcine epidemic diarrhoea virus as a cause of persistent diarrhoea in a herd of breeding and finishing pigs. *Vet Rec*. (1993) 132:129–31. doi: 10.1136/vr.132.6.129
3. Saif LJ, Pensaert MB, Sestak K, Yeo SG, Jung K. Coronaviruses. In: Zimmerman JJ, Karriker LA, Ramirez A, Schwartz KJ, Stevenson, GW, editors. *Diseases of Swine*. Hoboken, NJ: Wiley-Blackwell (2012).
4. Langel SN, Paim FC, Lager KM, Vlasova AN, Saif LJ. Lactogenic immunity and vaccines for porcine epidemic diarrhea virus (PEDV): historical and current concepts. *Virus Res*. (2016) 226:93–107.doi: 10.1016/j.virusres.2016.05.016
5. Chattha KS, Roth JA, Saif LJ. Strategies for design and application of enteric viral vaccines. *Annu Rev Anim Biosci*. (2015) 3:375–95. doi: 10.1146/annurev-animal-022114-111038
6. Bohl EH, Saif LJ. Passive immunity in transmissible gastroenteritis of swine: immunoglobulin characteristics of antibodies in milk after inoculating virus by different routes. *Infect Immun*. (1975) 11:23–32.
7. Bohl EH, Gupta RK, Olquin MV, Saif LJ. Antibody responses in serum, colostrum, and milk of swine after infection or vaccination with transmissible gastroenteritis virus. *Infect Immun*. (1972) 6:289–301.
8. Fink K. Origin and function of circulating plasmablasts during acute viral infections. *Front Immunol*. (2012) 3:78. doi: 10.3389/fimmu.2012.00078
9. Kunkel EJ, Kim CH, Lazarus NH, Vierra MA, Soler D, Bowman EP, et al. CCR10 expression is a common feature of circulating and mucosal epithelial tissue IgA Ab-secreting cells. *J Clin Invest*. (2003) 111:1001–10. doi: 10.1172/JCI17244
10. Hu S, Yang K, Yang J, Li M, Xiong N. Critical roles of chemokine receptor CCR10 in regulating memory IgA responses in intestines. *Proc Natl Acad Sci USA*. (2011) 108:E1035–44. doi: 10.1073/pnas.1100156108
11. Berri M, Meurens F, Lefevre F, Chevaleyre C, Zanello G, Gerdts V, et al. Molecular cloning and functional characterization of porcine CCL28: possible involvement in homing of IgA antibody secreting cells into the mammary gland. *Mol Immunol*. (2008) 45:271–7. doi: 10.1016/j.molimm.2007.04.026
12. Bourges D, Meurens F, Berri M, Chevaleyre C, Zanello G, Levast B, et al. New insights into the dual recruitment of IgA+ B cells in the developing mammary gland. *Mol Immunol*. (2008) 45:3354–62. doi: 10.1016/j.molimm.2008.04.017
13. Saif LJ, Bohl EH, Gupta RK. Isolation of porcine immunoglobulins and determination of the immunoglobulin classes of transmissible gastroenteritis viral antibodies. *Infect Immun*. (1972) 6:600–9.

14. Saif LJ. Enteric viral infections of pigs and strategies for induction of mucosal immunity. *Adv Vet Med*. (1999) 41:429–46. doi: 10.1016/S0065-3519(99)80033-0
15. Moxley RA, Olson LD. Clinical evaluation of transmissible gastroenteritis virus vaccines and vaccination procedures for inducing lactogenic immunity in sows. *Am J Vet Res*. (1989) 50:111–8.
16. Macpherson AJ, McCoy KD, Johansen FE, Brandtzaeg P. The immune geography of IgA induction and function. *Mucosal Immunol*. (2008) 1:11–22. doi: 10.1038/mi.2007.6
17. van der Feltz MJ, de Groot N, Bayley JP, Lee SH, Verbeet MP, de Boer HA. Lymphocyte homing and Ig secretion in the murine mammary gland. *Scand J Immunol*. (2001) 54:292–300. doi: 10.1046/j.1365-3083.2001.00933.x
18. Mor G, Cardenas I. The immune system in pregnancy: a unique complexity. *Am J Reprod Immunol*. (2010) 63:425–33. doi: 10.1111/j.1600-0897.2010.00836.x
19. Guzeloglu-Kayisli O, Kayisli UA, Taylor HS. The role of growth factors and cytokines during implantation: endocrine and paracrine interactions. *Semin Reprod Med*. (2009) 27:62–79. doi: 10.1055/s-0028-1108011
20. Hanna J, Goldman-Wohl D, Hamani Y, Avraham I, Greenfield C, Natanson-Yaron S, et al. Decidual NK cells regulate key developmental processes at the human fetal-maternal interface. *Nat Med*. (2006) 12:1065–74. doi: 10.1038/nm1452
21. Santner-Nanan B, Peek MJ, Khanam R, Richarts L, Zhu EB. Nanan R, et al. Systemic increase in the ratio between Foxp3+ and IL-17-producing CD4+ T cells in healthy pregnancy but not in preeclampsia. *J Immunol*. (2009) 183:7023–30. doi: 10.4049/jimmunol.0901154
22. Somerset DA, Zheng Y, Kilby MD, Sansom DM, Drayson MT. Normal human pregnancy is associated with an elevation in the immune suppressive CD25(+) CD4(+) regulatory T-cell subset. *Immunology*. (2004) 112:38–43. doi: 10.1111/j.1365-2567.2004.01869.x
23. Krishnan L, Guilbert LJ, Russell AS, Wegmann TG, Mosmann TR, Belosevic M. Pregnancy impairs resistance of C57BL/6 mice to Leishmania major infection and causes decreased antigen-specific IFN-gamma response and increased production of T helper 2 cytokines. *J Immunol*. (1996) 156:644–52.
24. Lin H, Mosmann TR, Guilbert L, Tuntipopipat S, Wegmann TG. Synthesis of T helper 2-type cytokines at the maternal-fetal interface. *J Immunol*. (1993) 151:4562–73.
25. Siston AM, Rasmussen SA, Honein MA, Fry AM, Seib K, Callaghan WM, et al. Pandemic 2009 influenza A(H1N1) virus illness among pregnant women in the United States. *JAMA*. (2010) 303:1517–25. doi: 10.1001/jama.2010.479
26. Adam I, Khamis AH, Elbashir MI. Prevalence and risk factors for Plasmodium falciparum malaria in pregnant women of eastern Sudan. *Malaria J*. (2005) 4:18–18. doi: 10.1186/1475-2875-4-18
27. Lamont RF, Sobel J, Mazaki-Tovi S, Kusanovic JP, Vaisbuch E, Kim SK, et al. Listeriosis in human pregnancy: a systematic review. *J Perinatal Med*. (2011) 39:227–36. doi: 10.1515/JPM.2011.035
28. Sperling RS, Engel SM, Wallenstein S, Kraus TA, Garrido J, Singh T, et al. Immunogenicity of trivalent inactivated influenza vaccination received during pregnancy or postpartum. *Obstet Gynecol*. (2012) 119:631–9. doi: 10.1097/AOG.0b013e318244ed20
29. Ferlazzo G, Pack M, Thomas D, Paludan C, Schmid D, Strowig T, et al. Distinct roles of IL-12 and IL-15 in human natural killer cell activation by dendritic cells from secondary lymphoid organs. *Proc Natl Acad Sci USA*. (2004) 101:16606–11. doi: 10.1073/pnas.0407522101
30. Male V, Hughes T, McClory S, Colucci F, Caligiuri MA, Moffett A. Immature NK cells, capable of producing IL-22, are present in human uterine mucosa. *J Immunol*. (2010) 185:3913–8. doi: 10.4049/jimmunol.1001637
31. Colonna M. Interleukin-22-producing natural killer cells and lymphoid tissue inducer-like cells in mucosal immunity. *Immunity*. (2009) 31:15–23. doi: 10.1016/j.immuni.2009.06.008
32. Rutz S, Eidenschenk C, Ouyang W. IL-22, not simply a Th17 cytokine. *Immunol Rev*. (2013) 252:116–32. doi: 10.1111/imr.12027
33. Chard T, Craig PH, Menabawey M, Lee C. Alpha interferon in human pregnancy. *Br J Obstet Gynaecol*. (1986) 93:1145–9. doi: 10.1111/j.1471-0528.1986.tb08635.x
34. Kirwan JP, Hauguel-De Mouzon S, Lepercq J, Challier JC, Huston-Presley L, Friedman JE, et al. TNF-alpha is a predictor of insulin resistance in human pregnancy. *Diabetes*. (2002) 51:2207–13. doi: 10.2337/diabetes.51.7.2207
35. Azizieh FY, Raghupathy RG. Tumor necrosis factor-alpha and pregnancy complications: a prospective study. *Med Princ Pract*. (2015) 24:165–70. doi: 10.1159/000369363
36. Martinez-Garcia EA, Chavez-Robles B, Sanchez-Hernandez PE, Nunez-Atahualpa L, Martin-Maquez BT, Munoz-Gomez A, et al. IL-17 increased in the third trimester in healthy women with term labor. *Am J Reprod Immunol*. (2011) 65:99–103. doi: 10.1111/j.1600-0897.2010.00893.x
37. Cerutti A. The regulation of IgA class switching. *Nat Rev Immunol*. (2008) 8:421–34. doi: 10.1038/nri2322
38. Dienz O, Eaton SM, Bond JP, Neveu W, Moquin D, Noubade R, et al. The induction of antibody production by IL-6 is indirectly mediated by IL-21 produced by CD4(+) T cells. *J Exp Med*. (2009) 206:69–78. doi: 10.1084/jem.20081571
39. Sinkora M, Stepanova K, Butler JE, Francis D, Santiago-Mateo K, Potockova H, et al. Ileal Peyer's patches are not necessary for systemic B cell development and maintenance and do not contribute significantly to the overall B cell pool in swine. *J Immunol*. (2011) 187:5150–61. doi: 10.4049/jimmunol.1101879
40. Kim SW, Easter RA, Hurley WL. The regression of unsuckled mammary glands during lactation in sows: the influence of lactation stage, dietary nutrients, and litter size. *J Anim Sci*. (2001) 79:2659–68. doi: 10.2527/2001.79102659x
41. Paarlberg PL. Updated estimated economic welfare impacts of porcine epidemic diarrhea virus (PEDv). In: *Working Paper #14-4*. Purdue University (2014).
42. Li MO, Wan YY, Sanjabi S, Robertson AK, Flavell RA. Transforming growth factor-beta regulation of immune responses. *Annu Rev Immunol*. (2006) 24:99–146. doi: 10.1146/annurev.immunol.24.021605.090737
43. GrimaldiSonoda E, Matsumoto R, Hitoshi Y, Ishii T, Sugimoto M, Araki S, et al. Transforming growth factor beta induces IgA production and acts additively with interleukin 5 for IgA production. *J Exp Med*. (1989) 170:1415–20. doi: 10.1084/jem.170.4.1415
44. Cong Y, Feng T, Fujihashi K, Schoeb TR, Elson CO. A dominant, coordinated T regulatory cell-IgA response to the intestinal microbiota. *Proc Natl Acad Sci USA*. (2009) 106:19256–61. doi: 10.1073/pnas.0812681106
45. Singh M, Orazulike NC, Ashmore J, Konje JC. Changes in maternal serum transforming growth factor beta-1 during pregnancy: a cross-sectional study. *Biomed Res Int*. (2013) 2013:318464. doi: 10.1155/2013/318464
46. Wegmann TG, Lin H, Guilbert L, Mosmann TR. Bidirectional cytokine interactions in the maternal-fetal relationship: is successful pregnancy a TH2 phenomenon? *Immunol Today*. (1993) 14:353–6. doi: 10.1016/0167-5699(93)90235-D
47. Robinson DP, Klein SL. Pregnancy and pregnancy-associated hormones alter immune responses and disease pathogenesis. *Horm Behav*. (2012) 62:263–71. doi: 10.1016/j.yhbeh.2012.02.023
48. Kraus TA, Engel SM, Sperling RS, Kellerman L, Lo Y, Wallenstein S, et al. Characterizing the pregnancy immune phenotype: results of the viral immunity and pregnancy (VIP) study. *J Clin Immunol*. (2012) 32:300–11. doi: 10.1007/s10875-011-9627-2
49. Watanabe M, Iwatani Y, Kaneda T, Hidaka Y, Mitsuda N, Morimoto Y, et al. Changes in T, B, and NK lymphocyte subsets during and after normal pregnancy. *Am J Reprod Immunol*. (1997) 37:368–77. doi: 10.1111/j.1600-0897.1997.tb00246.x
50. Hidaka Y, Amino N, Iwatani Y, Kaneda T, Mitsuda N, Morimoto Y, et al. Changes in natural killer cell activity in normal pregnant and postpartum women: increases in the first trimester and postpartum period and decrease in late pregnancy. *J Reprod Immunol*. (1991) 20:73–83. doi: 10.1016/0165-0378(91)90024-K
51. Yu Z, Croy BA, Chapeau C, King GJ. Elevated endometrial natural killer cell activity during early porcine pregnancy is conceptus-mediated. *J Reprod Immunol*. (1993) 24:153–64. doi: 10.1016/0165-0378(93)90017-C
52. Gately MK, Renzetti LM, Magram J, Stern AS, Adorini L, Gubler U, et al. The interleukin-12/interleukin-12-receptor system: role in normal and pathologic immune responses. *Annu Rev Immunol*. (1998) 16:495–521. doi: 10.1146/annurev.immunol.16.1.495
53. Cella M, Fuchs A, Vermi W, Facchetti F, Otero K, Lennerz JKM, et al. A human NK cell subset provides an innate source of IL-22 for mucosal immunity. *Nature*. (2009) 457:722–5. doi: 10.1038/nature07537
54. Parks OB, Pociask DA, Hodzic Z, Kolls JK, Good M. Interleukin-22 signaling in the regulation of intestinal health and disease.

Front Cell Dev Biol. (2016) 3:85. doi: 10.3389/fcell.2015.00085
55. Fujiwara H. Do circulating blood cells contribute to maternal tissue remodeling and embryo-maternal cross-talk around the implantation period? *Mol Hum Reprod*. (2009) 15:335–43. doi: 10.1093/molehr/gap027
56. Engelhardt H, Croy BA, King GJ. Evaluation of natural killer cell recruitment to embryonic attachment sites during early porcine pregnancy. *Biol Reprod*. (2002) 66:1185–92. doi: 10.1095/biolreprod66.4.1185
57. Rydyznski CE, Cranert SA, Zhou JQ, Xu H, Kleinstein SH, Singh H, et al. Affinity maturation is impaired by natural killer cell suppression of germinal centers. *Cell Rep*. (2018) 24:3367–73.e4. doi: 10.1016/j.celrep.2018.08.075
58. Rydyznski C, Daniels KA, Karmele EP, Brooks TR, Mahl SE, Moran MT, et al. Generation of cellular immune memory and B-cell immunity is impaired by natural killer cells. *Nat Commun.* (2015) 6:6375. doi: 10.1038/ncomms7375
59. Berlin C, Berg EL, Briskin MJ, Andrew DP, Kilshaw PJ, Holzmann B, et al. Alpha 4 beta 7 integrin mediates lymphocyte binding to the mucosal vascular addressin MAdCAM-1. *Cell*. (1993) 74:185–95. doi: 10.092-8674(93)90305-A
60. Wagner N, Lohler J, Kunkel EJ, Ley K, Leung E, Krissansen G, et al. Critical role for beta7 integrins in formation of the gut-associated lymphoid tissue. *Nature*. (1996) 382:366–70. doi: 10.1038/382366a0
61. Williams MB, Butcher EC. Homing of naive and memory T lymphocyte subsets to Peyer's patches, lymph nodes, and spleen. *J Immunol*. (1997) 159:1746–52.
62. Briskin M, Winsor-Hines D, Shyjan A, Cochran N, Bloom S, Wilson J, et al. Human mucosal addressin cell adhesion molecule-1 is preferentially expressed in intestinal tract and associated lymphoid tissue. *Am J Pathol*. (1997) 151:97–110.
63. Rott LS, Rose JR, Bass D, Williams MB, Greenberg HB, Butcher EC. Expression of mucosal homing receptor alpha4beta7 by circulating CD4+ cells with memory for intestinal rotavirus. *J Clin Invest*. (1997) 100:1204–8. doi: 10.1172/jci119633
64. DeHoff MH, Stoner CS, Bazer FW, Collier RJ, Kraeling RR, Buonomo FC. Temporal changes in steroids, prolactin and growth hormone in pregnant and pseudopregnant gilts during mammogenesis and lactogenesis. *Domestic Anim Endocrinol.* (1986) 3:95–105. doi: 10.1016/0739-7240(86)90016-0
65. Weisz-Carrington P, Roux ME, McWilliams M, Phillips-Quagliata JM, Lamm ME. Hormonal induction of the secretory immune system in the mammary gland. *Proc Natl Acad Sci USA*. (1978) 75:2928–32. doi: 10.1073/pnas.75.6.2928
66. Saif LJ. Enteric coronaviruses. In: Saif L, Heckert J, editors. *Viral Diarrhea of Man and Animals*. Bocal Raton, FL: CRC Press (1990).
67. Neuman H, Debelius JW, Knight R, Koren O. Microbial endocrinology: the interplay between the microbiota and the endocrine system. *FEMS Microbiol Rev*. (2015) 39:509–21. doi: 10.1093/femsre/fuu010
68. Koren O, Goodrich JK, Cullender TC, Spor A, Laitinen K, Backhed HK, et al. Host remodeling of the gut microbiome and metabolic changes during pregnancy. *Cell*. (2012) 150:470–80. doi: 10.1016/j.cell.2012.07.008
69. Collado MC, Isolauri E, Laitinen K, Salminen S. Distinct composition of gut microbiota during pregnancy in overweight and normal-weight women. *Am J Clin Nutr*. (2008) 88:894–9. doi: 10.1093/ajcn/88.4.894
70. Kong XF, Ji YJ, Li HW, Zhu Q, Blachier F, Geng MM, et al. Colonic luminal microbiota and bacterial metabolite composition in pregnant Huanjiang mini-pigs: effects of food composition at different times of pregnancy. *Sci Rep*. (2016) 6:37224. doi: 10.1038/srep37224
71. Song D, Peng Q, Chen Y, Zhou X, Zhang F, Li A, et al. Altered gut microbiota profiles in sows and neonatal piglets associated with porcine epidemic diarrhea virus infection. *Sci Rep*. (2017) 7:17439. doi: 10.1038/s41598-017-17830-z
72. Abu Raya B, Bamberger E, Almog M, Peri R, Srugo I, Kessel A. Immunization of pregnant women against pertussis: the effect of timing on antibody avidity. *Vaccine*. (2015) 33:1948–52. doi: 10.1016/j.vaccine.2015.02.059
73. Abu Raya B, Srugo I, Kessel A, Peterman M, Bader D, Gonen R, et al. The effect of timing of maternal tetanus, diphtheria, and acellular pertussis (Tdap) immunization during pregnancy on newborn pertussis antibody levels – A prospective study. *Vaccine*. (2014) 32:5787–93. doi: 10.1016/j.vaccine.2014.08.038
74. Eberhardt CS, Blanchard-Rohner G, Lemaitre B, Boukrid M, Combescure C, Othenin-Girard V, et al. Maternal immunization earlier in pregnancy maximizes antibody transfer and expected infant seropositivity against pertussis. *Clin Infect Dis*. (2016) 62:829–36. doi: 10.1093/cid/ciw027
75. Oka T, Saif LJ, Marthaler D, Esseili MA, Meulia T, Lin CM, et al. Cell culture isolation and sequence analysis of genetically diverse US porcine epidemic diarrhea virus strains including a novel strain with a large deletion in the spike gene. *Vet Microbiol*. (2014) 173:258–69. doi: 10.1016/j.vetmic.2014.08.012
76. Lin C M, Hou Y, Marthaler DG, Gao X, Liu X, Zheng L, et al. Attenuation of an original US porcine epidemic diarrhea virus strain PC22A via serial cell culture passage. *Vet Microbiol*. (2017) 201:62–71. doi: 10.1016/j.vetmic.2017.01.015
77. Liu X, Lin CM, Annamalai T, Gao X, Lu Z, Esseili MA, et al. Determination of the infectious titer and virulence of an original US porcine epidemic diarrhea virus PC22A strain. *Vet Res*. (2015) 46:109. doi: 10.1186/s13567-015-0249-1
78. Jung K, Wang Q, Scheuer KA, Lu Z, Zhang Y, Saif LJ. Pathology of US porcine epidemic diarrhea virus strain PC21A in gnotobiotic pigs. *Emerg Infect Dis*. (2014) 20:662–5. doi: 10.3201/eid2004.131685
79. Yuan L, Ward LA, Rosen BI, To TL, Saif LJ. Systematic and intestinal antibody-secreting cell responses and correlates of protective immunity to human rotavirus in a gnotobiotic pig model of disease. *J Virol*. (1996) 70:3075–83.
80. Azevedo MS, Yuan L, Pouly S, Gonzales AM, Jeong KI, Nguyen TV, et al. Cytokine responses in gnotobiotic pigs after infection with virulent or attenuated human rotavirus. *J Virol*. (2006) 80:372–82. doi: 10.1128/JVI.80.1.372-382.2006
81. Chattha KS, Vlasova AN, Kandasamy S, Rajashekara G, Saif LJ. Divergent immunomodulating effects of probiotics on T cell responses to oral attenuated human rotavirus vaccine and virulent human rotavirus infection in a neonatal gnotobiotic piglet disease model. *J Immunol*. (2013) 191:2446–56. doi: 10.4049/jimmunol.1300678
82. Vlasova AN, Paim FC, Kandasamy S, Alhamo MA, Fischer DD, Langel SN, et al. Protein malnutrition modifies innate immunity and gene expression by intestinal epithelial cells and human rotavirus infection in neonatal gnotobiotic pigs. *mSphere*. (2017) 2:2. doi: 10.1128/mSphere.00046-17
83. Annamalai T, Lin CM, Gao X, Liu X, Lu Z, Saif LJ, et al. Cross protective immune responses in nursing piglets infected with a US spike-insertion deletion porcine epidemic diarrhea virus strain and challenged with an original US PEDV strain. *Vet Res*. (2017) 48:61. doi: 10.1186/s13567-017-0469-7
84. Yuan L, Kang SY, Ward LA, To TL, Saif LJ. Antibody-secreting cell responses and protective immunity assessed in gnotobiotic pigs inoculated orally or intramuscularly with inactivated human rotavirus. *J Virol*. (1998) 72:330–8.
85. VanCott JL, Brim TA, Lunney JK, Saif LJ. Contribution of antibody-secreting cells induced in mucosal lymphoid tissues of pigs inoculated with respiratory or enteric strains of coronavirus to immunity against enteric coronavirus challenge. *J Immunol*. (1994) 152:3980–90.
86. VanCott JL, Brim TA, Simkins RA, Saif LJ. Isotype-specific antibody-secreting cells to transmissible gastroenteritis virus and porcine respiratory coronavirus in gut- and bronchus-associated lymphoid tissues of suckling pigs. *J Immunol*. (1993) 150:3990–4000.
87. Vlasova AN, Chattha KS, Kandasamy S, Siegismund CS, Saif LJ. Prenatally acquired vitamin A deficiency alters innate immune responses to human rotavirus in a gnotobiotic pig model. *J Immunol*. (2013) 190:4742–53. doi: 10.4049/jimmunol.1203575
88. Sinkora M, Stepanova K, Sinkorova J. Different anti-CD21 antibodies can be used to discriminate developmentally and functionally different subsets of B lymphocytes in circulation of pigs. *Dev Comp Immunol*. (2013) 39:409–18. doi: 10.1016/j.dci.2012.10.010

Conflict of Interest Statement: The authors declare that the research was conducted in the absence of any commercial or financial relationships that could be construed as a potential conflict of interest.

frontiers in Immunology

ORIGINAL RESEARCH
published: 09 May 2019
doi: 10.3389/fimmu.2019.01024

Porcine Deltacoronavirus Nucleocapsid Protein Suppressed IFN-β Production by Interfering Porcine RIG-I dsRNA-Binding and K63-Linked Polyubiquitination

*Ji Likai, Li Shasha, Zhu Wenxian, Ma Jingjiao, Sun Jianhe, Wang Hengan and Yan Yaxian**

Shanghai Key Laboratory of Veterinary Biotechnology, School of Agriculture and Biology, Shanghai Jiao Tong University, Shanghai, China

Porcine deltacoronavirus (PDCoV) is a newly detected porcine coronavirus causing serious vomiting and diarrhea in piglets, especially newborn piglets. There has been an outbreak of PDCoV in worldwide since 2014, causing significant economic losses in the pig industry. The interferon (IFN)-mediated antiviral response is an important component of virus-host interactions and plays an essential role in inhibiting virus infection. However, the mechanism of PDCoV escaping the porcine immune surveillance is unclear. In the present study, we demonstrated that the PDCoV nucleocapsid (N) protein antagonizes porcine IFN-β production after vesicular stomatitis virus (VSV) infection or poly(I:C) stimulation. PDCoV N protein also suppressed the activation of porcine IFN-β promoter when it was stimulated by porcine RLR signaling molecules. PDCoV N protein targeted porcine retinoic acid-inducible gene I (pRIG-I) and porcine TNF receptor associated factor 3 (pTRAF3) by directly interacting with them. The N-terminal region (1–246 aa) of PDCoV N protein was important for interacting with pRIG-I and interfere its function. We confirmed that PDCoV N antagonizes IFN-β production by associating with pRIG-I to impede it from binding double-stranded RNA. Furthermore, porcine Riplet (pRiplet) was an important activator for pRIG-I by mediating the K63-linked polyubiquitination. However, PDCoV N protein restrained the pRiplet binding pRIG-I to inhibit pRIG-I K63-linked polyubiquitination. Taken together, our results revealed a novel mechanism by which PDCoV N protein interferes with the early activation of pRIG-I in the host antiviral response. The novel findings provide a new insight into PDCoV on evading the host innate immune response and may provide new therapeutic targets and more efficacious vaccines strategies for PDCoV infections.

Keywords: PDCoV, nucleocapsid protein, porcine RIG-I, IFN-β, ubiquitination

OPEN ACCESS

Edited by:
John E. Butler,
University of Iowa, United States

Reviewed by:
M. Suresh,
University of Wisconsin-Madison, United States
Hui Hu,
Henan Agricultural University, China
Guiqing Peng,
Huazhong Agricultural University, China

****Correspondence:***
Yan Yaxian
yanyaxian@sjtu.edu.cn

Specialty section:
This article was submitted to Viral Immunology, a section of the journal Frontiers in Immunology

Received: *08 November 2018*
Accepted: *23 April 2019*
Published: *09 May 2019*

Citation:
Likai J, Shasha L, Wenxian Z, Jingjiao M, Jianhe S, Hengan W and Yaxian Y (2019) Porcine Deltacoronavirus Nucleocapsid Protein Suppressed IFN-β Production by Interfering Porcine RIG-I dsRNA-Binding and K63-Linked Polyubiquitination. Front. Immunol. 10:1024. doi: 10.3389/fimmu.2019.01024

INTRODUCTION

Porcine deltacoronavirus (PDCoV), a newly detected porcine coronavirus, as well as porcine transmissible gastroenteritis virus (TGEV), porcine rotavirus (PRV), and porcine epidemic diarrhea virus (PEDV) are the major pathogens of the porcine epidemic diarrhea disease. They cause microscopic intestinal lesions leading to serious diarrhea and often dehydration to death (1, 2).

PDCoV as a pathogen was identified in 2012 in Hong Kong (3). Until now PDCoV strains have been isolated from a few regions and countries, including the United States, China, South Korea, Laos, and Thailand (4–7). PDCoV is an enveloped, single-stranded, positive-sense RNA virus with the genome length of approximately 25 kb. The genome arrangements are in the order of 5′ untranslated region (UTR), open reading frame 1a/1b (ORF1a/1b), spike (S), envelope (E), membrane (M), accessory protein 6 (NS6), nucleocapsid (N), accessory protein 7 (NS7), accessory protein 7a (NS7a), and 3′ UTR (8, 9). PDCoV has only been found infectious in swine until now. However, PDCoV could use the aminopeptidase N (APN) of mammalian and avian species to efficiently infect cells of an unusual abroad species range, including humans and chickens (10).

The host innate immune response serves as the first line of defense to resist pathogenic microorganism infection and replication. The viral pathogen is sensed by pattern recognition receptors (PRRs) of the infected host cells to induce an antiviral response. The retinoic acid-inducible gene-1 (RIG-I)-like receptors (RLRs) are a major member of host PRRs, including three homologous protein, RIG-I, melanoma differentiation associated gene 5 (MDA5), and DExH-box helicase 58 (DHX58/LGP2) (11). RIG-I and MDA5 were the activators of interferon production post RNA virus infection or the double-stranded RNA (dsRNA) analog polyinosine and polycytidilic acid (poly(I:C)) (12). RIG-I also resides in an autorepression state in normal physiological status cells by covering its N-terminal tandem caspase activation and recruitment domains (CARDs), which are necessary for interaction with mitochondrial antiviral signaling protein (MAVS, also known as IPS-1/VISA/Cardif) (13–15). The Riplet, also known as ring finger protein 135 (RNF135), is a necessary E3 ligase for releasing RIG-I autorepression by K63-linked polyubiquitination (16). The tripartite motif containing 25 (TRIM25) is another key E3 ligase for RIG-I activation by mediating the K63-linked polyubiquitination of RIG-I N-terminal CARDs (17). However, MDA5 does not adopt an auto-repression state in the ligand-free state (11). MDA5 also interacts with MAVS via CARDs to active the type I interferon signaling pathway. The MAVS as the polymeric signaling scaffold could recruit and activate the signaling proteins including tumor necrosis factor receptor associated factor 2 (TRAF2), TRAF3, TRAF5, TRAF6, and associated serine kinases (TBK1 and the IKK family) (18, 19). The activation of TBK1 could activate master transcription factors IRF3 and NF-κB translocation into the cell nucleus, and then induce the antiviral genes' production, including IFN-β and major antiviral cytokines (20). Type I IFNs are secreted and bind to the cell surface receptors of both virus-infected and non-infected neighbor cells to induce interferon-stimulating genes (ISGs) for antivirals by activating the JAK-STAT pathway.

However, viruses take on a variety of tactics to escape the host innate immune surveillance during the infection and replication. AIV NS1 protein also could both interact with human TRIM25 and Riplet to suppress RIG-I activation (21). NS1 proteins from human but not swine or avian influenza virus strain were able to interact with human Riplet in a species-specific manner (22). West Nile virus NS1 also antagonizes IFN-β production by inhibiting RIG-I and MDA5 K63-linked polyubiquitination (22). Coronavirus nucleocapsid proteins play the most fundamental role in packaging the viral genome and viral assembly with a similar topological structure (23). When the coronavirus infects the host cells, the N protein is also abundantly produced to regulate the host cell cycle, cell stress responses, immune system interference, and signal transduction (24). Severe acute respiratory syndromes (SARS) and middle east respiratory syndrome (MERS) coronavirus N protein could counteract with human TRIM25 to suppress RIG-I activation (25). PEDV N protein suppressed IFN-β and NF-κB activation by sequestering the formation of human TBK1 and IRF3 complex in HEK293T cells (26). However, PEDV N protein could activate the NF-κB and up-regulate the IL-8 expression in porcine intestinal epithelial cell (IEC), which is the target host cell of PEDV (27, 28). The other important porcine coronavirus, TGEV infection could prominently promote NF-κB activation and IFN-β production through RLR signaling in PK-15 cells (29). PDCoV infection could suppress porcine RIG-I-mediated IFN-β production in LLC-PK1 cells (30). PDCoV Nsp5 and NS6 were confirmed as the important regulatory viral proteins to inhibit the IFN-β production (31, 32). However, the function of other viral proteins of PDCoV, especially the viral structure protein (S, E, M, N), has remained unclear. PDCoV N protein could change expression levels of many host immune proteins in the N-expressing PK-15 (PK-PDCoV-N) cells, such as HSP70 (33). However, it remains unclear whether PDCoV N protein is an antagonist in the porcine type I interferon signaling pathway and how to regulate the antiviral signaling pathway in porcine cells.

In this study, we confirmed and explained the mechanism by which PDCoV N protein antagonizes porcine IFN-β production. The results indicated that PDCoV N protein could directly target the porcine RIG-I and block its early activation by interfering its association with dsRNA and pRiplet- mediated K63-linked polyubiquitination.

MATERIALS AND METHODS

Cell Culture and Virus

HEK293T cells (ATCC®CRL-3216™) and PK-15 cells (ATCC®CCL-33™) were obtained from the China Center for Type Culture Collection and maintained at 37°C in 5% CO_2 in Dulbecco's Modified Ea-gle's medium (Gibco, USA) supplemented with 10% heat-inactivated fetal bovine se-rum (FBS) (Gibco, USA). The porcine jejunum intestinal cells (IPEC-J2) were obtained from the China Center for Type Culture Collection and maintained at 37°C in 5% CO_2 in Roswell Park Memorial Institute (RPMI) 1,640 medium (Gibco, USA) with 10% heat-inactivated FBS (Gibco, USA). The recombinant VSV-GFP virus was generously provided by Dr. Sun Tao, Shanghai Jiao Tong University, China.

Plasmids and Quantitative RT-PCR (qRT-PCR)

Total RNA was extracted by TRIZOL (Invitrogen). Then, 1 μg of RNA was used to synthesize cDNA using the ReverTra

Ace qPCR RT reverse transcription (RT) master mix with genomic DNA (gDNA) remover (Toyobo, Osaka, Japan). The cDNA of PK-15 cells or PDCoV-positive sample were used as the templates to perform in 50 μL amplification reaction containing 2 μL of cDNA, 2 μL of forward and reverse primers (10 pmol), 10 μL 5× PrimeSTAR GXLBuffer, 4 μL 2.5 nM dNTPs, 1 μL PrimeSTAR® GXL DNA Polymerase (TAKARA, Japan), and 29 μL ddH_2O. The reaction procedure was 98°C for 3 min, followed by 36 cycles at 98°C for 15 s, 60°C for 30 s and 72°C for 1 min, and finally 72°C for 5 min. And then the full length or mutant coding sequence of porcine RLR signaling molecules were con-structed into the pcDNA3.1-Flag or pcDNA3.1-HA plasmid by ClonExpress®II One Step Cloning Kit (Vazyme, China), including porcine *RIG-I* (*pRIG-I*) (NM_213804.2), three *pRIG-I* mutants: the 2′CARD, a middle helicase domain (HEL), and the internal repressor domain (RD). porcine *MDA5* (*pMDA5*) (MF358967.1), porcine *MAVS* (*pMAVS*) (NM_001097429.1), porcine *TBK1* (*pTBK1*) (NM_001105292.1), porcine *TRAF3* (*pTRAF3*) (XM_021081629.1), porcine *IRF3* (*pIRF3*) (NM_213770.1), porcine *TRIM25* (*pTRIM25*) (XM_005656971.3), and porcine *Riplet* (*pRiplet*) (XM_003131735.4). The full-length coding sequence (CDS) of PDCoV-N was constructed into the pcDNA3.1-HA or pcDNA3.1-Myc plasmid vector. All the PCR primers are provided in **Supplementary Table 1**. The pGL3-pIFN-β-Luc and pGL3-pNF-κB-Luc plasmid were constructed according a previous study (34). HA-tagged ubiquitin (Ub) and Ub mutants (K48R, K63R, K48, K63) plasmids were kindly provided by Dr. Yuan Congli, Shanghai Jiao Tong University, China.

Quantitative RT-PCR (qRT-PCR) was performed using SYBR green Supermix (ABI-7500, Life, USA). The primer sequences are shown in **Supplementary Table 1**. The relative gene expression levels were calculated using the $2^{-\Delta\Delta CT}$ method.

Dual-Luciferase Reporter Gene Assay

PK-15 or IPEC-J2 cells were grown in 24-well plates. In selected experiments, the recombination or empty expression plasmids were cotransfected with the pGL3-pIFN-β-Luc and pRL-TK (an internal control for the normalization of the transfection efficiency) using Lipofectamine 2000 (InvivoGen, USA). After transfection for 24 h, poly(I:C) or VSV-GFP virus were transfected or infected for 16 h. The cells were then lysed, and the firefly luciferase and Renilla luciferase activities were measured using the Dual-Luciferase reporter assay system (Promega, USA). Data were shown as the relative firefly luciferase activities normalized to the Renilla luciferase activities from three independently conducted experiments.

Western Blotting and Co-immunoprecipitation (Co-IP) Assay

HEK293T or PK-15 cells were transfected empty or recombinant plasmid. At 28 h post-transfection, the cells were harvested by adding lysis buffer (50 mM Tris-HCl (pH 7.4), 150 mM NaCl, 1% NP-40, 10% glycerin, 0.1% SDS, and 2 mM Na_2EDTA) for 30 min at 4°C supplemented with a protease inhibitor cocktail, phenylmethylsulphonyl fluoride (PMSF), and a phosphatase inhibitor cocktail. The lysates were subjected to SDS-PAGE and electroblotted onto a polyvinylidene difluoride membrane (Bio-Rad, USA). The membranes were then analyzed for the expression proteins by immunoblotting using mouse Flag, Myc, β-actin, and rabbit HA antibodies, respectively. The β-actin or β-Tublin monoclonal antibody was used to detect the expression of β-actin or β-Tublin to confirm equal protein sample loading.

HEK293T or PK-15 cells in 10-cm culture dishes were cotransfected with the recombination expression plasmid or an empty vector for 28 h. The cells were lysed on ice for 20 min in 600 μl of lysis buffer (50 mM Tris-HCl (pH 7.4), 150 mM NaCl, 1% NP-40, 10% glycerin, 0.1% SDS, and 2 mM Na_2EDTA) containing a protease inhibitor mixture plus the protease inhibitor PMSF. The cell lysates were then immunoprecipitated at 4°C with mouse anti-FLAG or anti-HA affinity gel (Biotool, USA) or mouse Myc monoclonal Ab with protein A+G agarose beads (Beyotime, China). The immunoprecipitants were washed four times with the protein lyse buffer and then subjected to western blotting analysis.

pRIG-I and dose-dependent PDCoV N expression plasmid or empty plasmid was cotransfected into the HEK293T cells for 28 h. Then, the dsRNA binding assay was implemented as described in a previous report (31).

Indirect Immunofluorescence Assay (IFA)

PK-15 cells were seeded onto microscope coverslips, placed into 12-well plates, and allowed to reach approximately 80% confluence. At 24 h post transfection, the cells were fixed with 4% paraformaldehyde for 10 min and then permeabilized with methyl alcohol for 10 min at room temperature. After three washes with TBST, the cells were blocked with TBST containing 5% bovine serum albumin (BSA) for 1 h and then incubated separately with a mouse Flag monoclonal antibody against Flag-tagged protein (1:1000) or a rabbit HA polyclonal antibody against the HA-tagged PDCoV N protein (1:1000) for 1 h. The cells were then treated with Alexa Fluor 488-labeled anti-mouse secondary antibody or Alexa Fluor 555-labeled anti-rabbit secondary antibody for 1 h at room temperature and subsequently treated with 4′, 6-diamidino-2-phenylindole (DAPI) for 15 min at room temperature. The antibody and DAPI used in the present study were purchased from Beyotime in China. Fluorescent images were visualized and examined using a confocal laser scanning microscope (Fluoview ver. 3.1; Olympus, Japan).

Ubiquitin Assay

To analyze the ubiquitination of porcine RIG-I, PK-15 or HEK-293T cells were cotransfected with Flag-RIG-I, HA-Ub, or HA-Ub mutants (K48R, K63R, K48, K63) and Myc-PDCoV-N for 28 h. The cells were washed twice in PBS supplemented with 10 mM NEM and lysed with 1% SDS lysis buffer (25 mM Tris-HCl, pH 7.4, 150 mM NaCl, 1% NP-40, 0.5% sodium deoxycholate, and 1% SDS) containing the protease inhibitor PMSF and 10 mM NEM. The mouse Flag-affinity gel was pretreated three times with 1 x TBS, and then the cell lysates were added and incubated for 3 h at 4°C. After washing them three times with 1xTBS,

the immunoprecipitants were boiled at 100°C for 10 min and subjected to western blotting analysis.

Statistical Analysis

Data are expressed as the mean ± standard deviation (SD) of three independent experiments. Student's *t*-tests were performed. Values of $p < 0.05$ were considered statistically significant and $p < 0.01$ were considered statistically highly significant.

RESULTS

PDCoV N Protein Suppressed Poly(I:C) and VSV Induced IFN-β Production

To explore whether PDCoV N protein antagonizes the production of pIFN-β, PK-15 cells were cotransfected empty vector, or PDCoV-N expression plasmid (pcDNA3.1-HA-PDCoV-N) with the reporter plasmid (pGL3-pIFN-β) and pRL-TK (as internal control) for 18 h, and then infected with VSV-GFP (a recombinant VSV strain) or treated with poly(I:C) for 16 h. The cells were lysed for the dual-luciferase reporter assays. The results showed that the VSV-GFP or poly(I:C) induced porcine IFN-β-luc promoter activation was significantly suppressed by PDCoV-N protein in PK-15 cells (**Figures 1A,C**). However, the porcine NF-κB-Luc promoter activation was not inhibited by PDCoV-N protein in PK-15 cells, when infected with VSV-GFP virus (**Figure 1B**). To further prove that PDCoV N protein inhibits porcine IFN-β production, PK-15 cells were transfected with PDCoV-N expression or empty vector plasmid for 24 h and then transfected or non-transfected with poly(I:C) for 12 h. Total RNA was extracted from cells to detect the expression level of porcine IFN-β and several interferon-induced genes (ISGs) by real-time quantitative polymerase chain reaction (qRT-PCR). The results showed that PDCoV N overexpression could significantly suppress poly(I:C)-induced porcine *IFNB1* (*pIFNB1*), porcine *OAS1* (*pOAS1*), and porcine *ISG15* (*pISG15*) mRNA expression in PK-15 cells (**Figure 1D**). The results indicated that PDCoV N protein suppressed porcine IFN-β production. IFN-β could significantly inhibit the VSV replication in infected host cells. Hence, to further confirm the porcine IFN-β protein production decreased by PDCoV N protein, VSV-GFP viruses were used to infect PK-15 cells. The results showed that poly(I:C) could significantly suppress the VSV-GFP replication in PK-15 cells (**Figure 1E**). In accordance with the results of dual luciferase assays and qRT-PCR described above, the expression of PDCoV N protein could restore the proliferation of VSV-GFP virus in ploy(I:C)-treated PK-15 cells (**Figure 1E**). These data suggested that PDCoV N protein was an antagonist of porcine IFN-β.

PDCoV N Protein Suppressed the Porcine RLR Signaling Pathway

In the present study, we found PDCoV N protein was an antagonist of porcine IFN-β production (**Figure 1**). Therefore, to determine whether PDCoV N protein could block the porcine RLR-mediated type I IFN signaling pathway, we constructed several key porcine RLR (pRLR) signaling molecules from PK-15 cells, including pRIG-I, pRIG-IN (a pRIG-I mutant, only the 2′-CARD domain of pRIG-I (pRIG-IN)), pMDA5, pMAVS, pTBK1, and pIRF3. To investigate the function of PDCoV N protein in the porcine RLR pathway, PK-15 cells were co-transfected the key signaling molecules with the PDCoV N expression or empty vector plasmid, together with the pGL3-pIFN-β and pRL-TK. Compared with the empty vector, the overexpression of the porcine signaling molecules could clearly activate the pIFN-β promoter activation (**Figure 2**). However, the activation of the pIFN-β promoter induced by those signaling molecules was significantly inhibited by PDCoV N protein (**Figure 2**). The function of PDCoV N was confirmed by the consistent results in the IPEC-J2 cells (**Supplementary Figure 1**). These results indicated that the PDCoV N protein could suppress the porcine IFN-β by inhibiting the porcine RLR signaling pathway.

PDCoV N Protein Interacted With Porcine RIG-I/TRAF3 Protein

To find the porcine RLR signaling molecular target of PDCoV N protein, the HEK293T cells were co-transfected with PDCoV N expression plasmid and several pRLR signaling molecules, pRIG-I, pMDA5, pMAVS, pTBK1, pTRAF3, or pIRF3, respectively. The whole cell lysates (WCLs) were immunoprecipitated with the anti-Flag affinity gel at 28 h post transfection. The results showed that pRIG-I and pTRAF3 were clearly coprecipitated with PDCoV N protein (**Figures 3A,B**). In addition, consistent results were presented, when the precipitation of pRIG-I or pTRAF3 with HA-PDCoV-N was analyzed by HA-affinity gel (**Figures 3C,D**). These results suggested that PDCoV N protein could directly interact with pRIG-I and pTRAF3. To further confirm the direct interaction between PDCoV N and pRIG-I in porcine cells, PK-15 cells were used to co-transfect the pRIG-I or pTRAF3 and PDCoV N expression plasmid. Indirect immunofluorescence assay (IFA) was performed at 24 h post transfection. The results showed that the PDCoV N protein and pRIG-I or pTRAF3 were co-localized in the cytoplasm in PK-15 cells (**Figure 3E**). All the data indicated that pRIG-I and pTRAF3 were the major targets of PDCoV N protein in the pRLR signaling pathway. RIG-I are the key cytoplasmic pathogen recognition receptors to recognize the RNA viruses. The activation of RIG-I was a prerequisite of IFN-β production by RLR signaling pathway. However, in the present study, PDCoV N protein could significantly block the pRIG-I-induced pIFN-β promoter activation (**Figure 2A**). Hence, pRIG-I was the main object in the following study. To investigate the interaction between PDCoV N protein and pRIG-I, two truncated mutants of PDCoV N protein(aa 1 to 246, and 168-342) were constructed and cotransfected with Flag-pRIG-I into HEK293T cells. The Co-IP results showed that the PDCoV N(1-246aa), but not another truncated region, could clearly coprecipitated with pRIG-I (**Figure 3F**). PDCoV N(1-246aa) was also significantly arrested pRIG-I induced porcine IFN-β promoter activation in PK-15 and IPEC-J2 cells (**Figure 3G** and **Supplementary Figure 2**). These results indicated that the N-terminal region was important for PDCoV N protein to interact with pRIG-I and interfere its function.

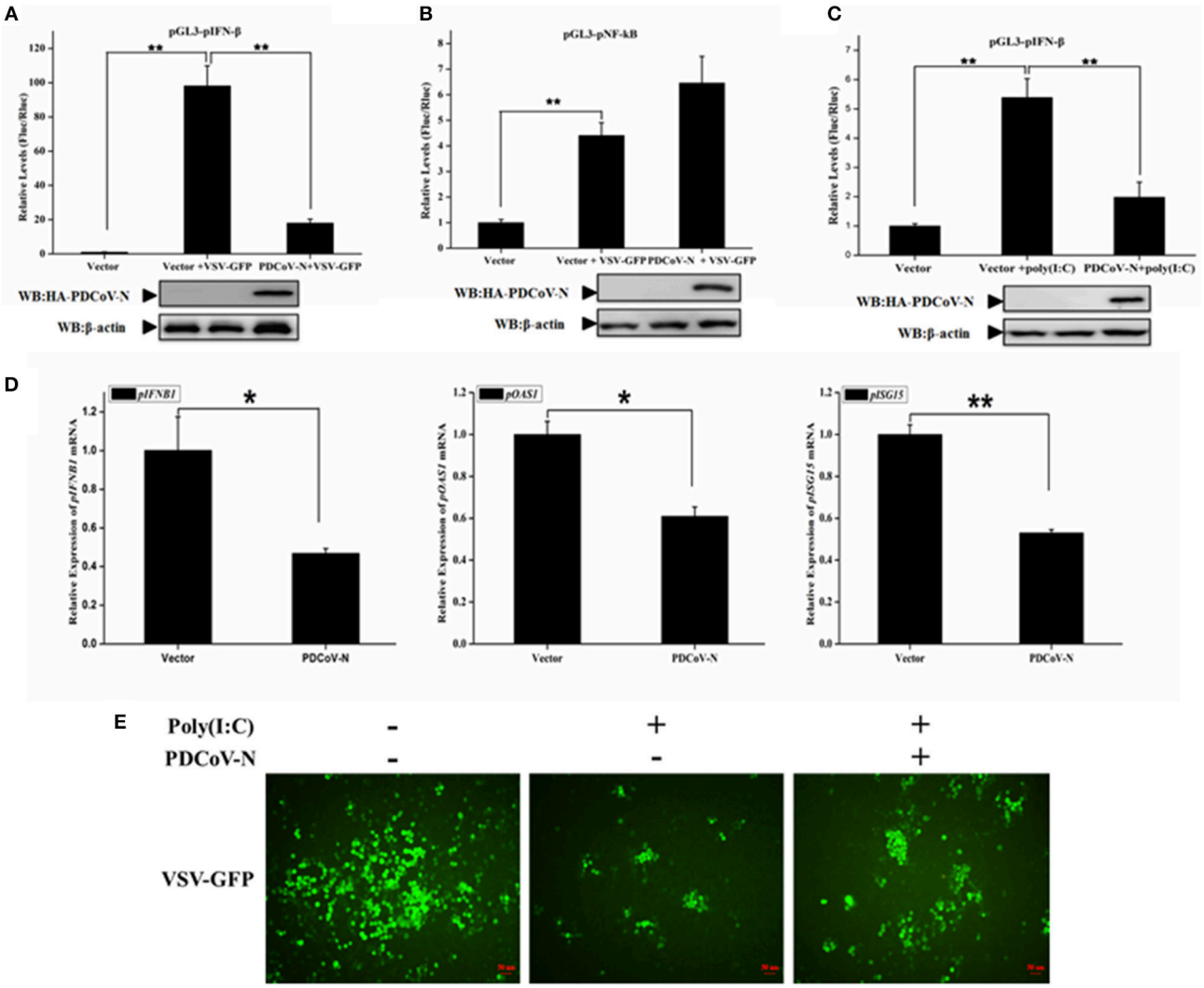

FIGURE 1 | PDCoV N protein inhibited porcine IFN-β and ISGs expression. **(A–C)** PK-15 cells cultured in 24-well plates were transfected with porcine IFN-β-Luc (pGL3-pIFN-β) or porcine NF-κB-Luc (pGL3-pNF-κB) plasmid and pRL-TK plasmid with PDCoV N expression plasmid (pcDNA3.1-HA-PDCoV-N). At 18 h after transfection, cells were treated or untreated with VSV-GFP or Poly(I:C) (LMW). The cells were then subjected to dual-luciferase assays at 16 h post-treatment. The relative firefly luciferase activity was relative to that of an empty vector control. The *Renilla reniformis* luciferase activity was used to normalize. The expression of PDCoV N protein was detected by western blot with HA antibody. β-actin was detected as the loading control. **(D,E)** PK-15 cells cultured in 12-well plates were transfected with pcDNA3.1-HA-PDCoV-N or empty plasmid for 24 h, and then transfected with Poly(I:C) (LMW). **(D)** After 16 h post transfection, the cells were lysed by TRZOL to extract the total RNA. The qRT-PCR was used to detect the relative expression of porcine ISGs mRNA. **(E)** At 12 h post transfection, the VSV-GFP (MOI = 0.1) infected the PK-15 cells for another 16 h. The GFP was detected by fluorescence microscope. $^{*}p < 0.05$; $^{**}p < 0.01$.

PDCoV N Protein Suppressed Porcine RIG-I Activation

Previous researchers have reported that PDCoV NS6 inhibited IFN-β production by suppressing the double-stranded RNA (dsRNA) binding human RIG-I and MDA5 in HEK293T cells (31). In the present study, PDCoV N protein was proved as a directly pRIG-I binding protein (**Figure 3**). It is unclear whether PDCoV N could compete with porcine RIG-I to bind dsRNA. To verify this assumption, the poly(I:C) binding assay was performed. pRIG-I or PDCoV-N was eukaryotic expressed by transfection in HEK293T cells, respectively. After 28 h, the WCLs were immunoprecipitated with poly(I:C) (dsRNA) or poly(C) (ssRNA) beads. The results showed that PDCoV-N and pRIG-I could bind to the poly(I:C)-beads (**Figure 4A**). However, only PDCoV N protein could bind to the poly(C)-beads (**Figure 4B**). pRIG-I and dose-increased PDCoV-N expression plasmid were cotransfected in HEK293T cells. After 28 h, the WCLs were immunoprecipitated with poly(I:C)-beads. The results showed that the PDCoV N protein could decrease the binding of dsRNA and pRIG-I in a dose-dependent manner (**Figure 3D**). The results indicated that PDCoV N protein could compete the binding of dsRNA with pRIG-I.

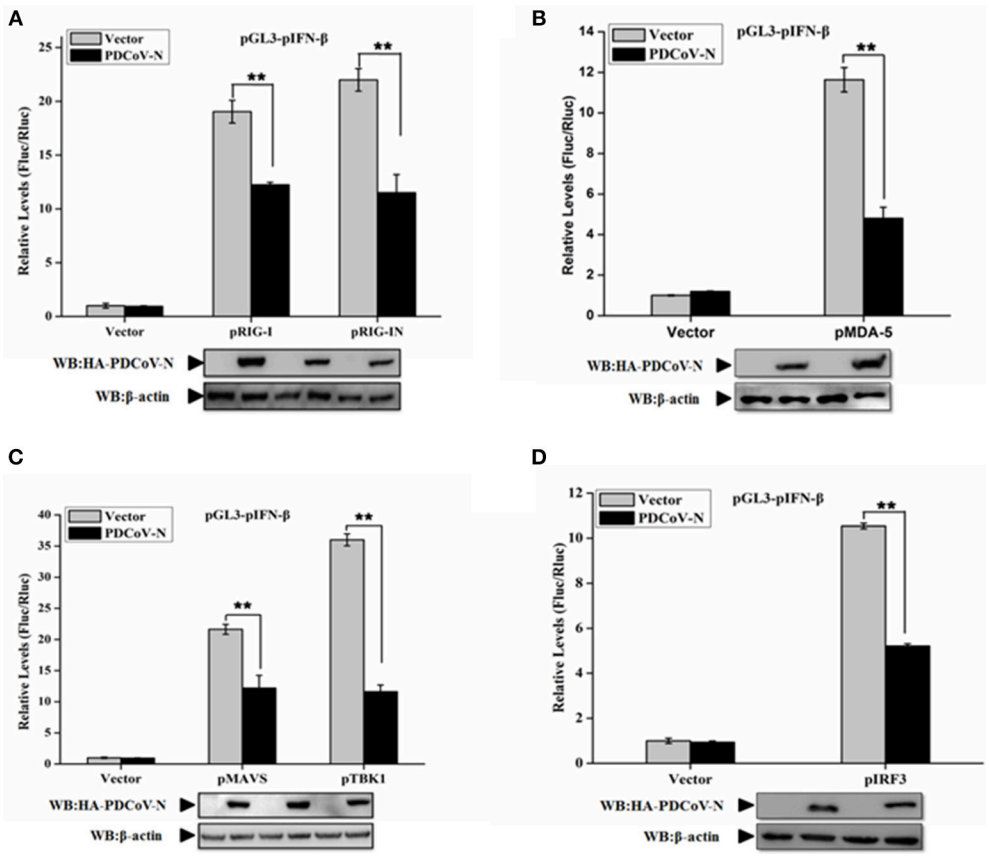

FIGURE 2 | PDCoV N protein inhibited porcine IFN-β promoter activation by the porcine RLR signaling pathway. PK-15 cells were cotransfected with pGL3-pIFN-β,pRL-TL, and pcDNA3.1-HA-PDCoV-N along with constructed expression porcine RIG-I/RIG-IN (pRIG-I/pRIG-IN) **(A)**, porcine MDA5 (pMDA5) **(B)**, porcine MAVS (pMAVS) **(C)**, porcine TBK1 (pTBK1) **(C),** or porcine IRF3 (pIRF3) **(D)**. Dual-luciferase assays were performed at 24 h post transfection. The relative firefly luciferase activity was relative to that of an empty vector control. The *Renilla reniformis* luciferase activity was used to normalize. Western blot was used to detect the protein expression of PDCoV N with HA antibody. The β-actin was as the loading control protein. All the experiments were independently performed three times. $^{**}p < 0.01$.

However, in our previous study, we also found PDCoV N protein could directly interact with porcine RIG-I without dsRNA (**Figures 3A,B**). This indicated that PDCoV N protein may have other functions in regulated porcine RIG-I. Previous finding indicated that viral protein could also inhibit RIG-I activation by suppressing its polyubiquitination (21, 22, 25). To explore the role of PDCoV N protein in pRIG-I ubiquitination, pRIG-I expression plasmid were cotransfected with HA-tagged ubiquitin (Ub) and PDCoV N or empty plasmid in PK-15 or HEK293T cells for 28 h. The porcine RIG-I was purification by Flag affinity gel. Then, the polyubiquitination levels of pRIG-I were examined by western blot. The results showed that the polyubiquitination of pRIG-I was significantly increased, and the polyubiquitination were remarkably decreased by PDCoV N protein both in HA-tagged ubiquitin transfected PK-15 or HEK293T cells (**Figures 5A,B**). To further study which formation of pRIG-I linked-polyubiquitination was suppressed by PDCoV N protein, the ubiquitin K48R or K63R (HA-Ub-K48R or HA-Ub-K63R) mutant expression plasmid was used to co-transfect with porcine RIG-I together with PDCoV-N expression or empty plasmid in HEK293T cells. The results showed that PDCoV N protein could decrease the pRIG-I K48R but not K63R-induced polyubiquitination (**Figure 5C**). To further verify the results, the ubiquitin K63 or K48 (HA-Ub-K48 or HA-Ub-K63) only expression mutant plasmid was used to do the same experiments. PDCoV N protein could significantly decrease the pRIG-I K63-linked polyubiquitination, but not the K48-linked polyubiquitination (**Figure 5D**). All the results indicated that PDCoV N protein could suppress the pRIG-I polyubiquitination, especially the K63-linked polyubiquitination.

PDCoV N Could Not Interact With Porcine Riplet and TRIM25

TRIM25 and Riplet protein were the two important regulated K63-polyubiquitinations of human RIG-I activation. To further explore the mechanism of PDCoV-N suppression of pRIG-I K63-polyubiquitination, porcine TRIM25 (pTRIM25) and Riplet (pRiplet) were mainly analyzed. pTRIM25 and pRiplet have only 77.93 and 67.38% identity to human TRIM25 (hTRIM25) and Riplet (hRiplet) by amino acids sequence

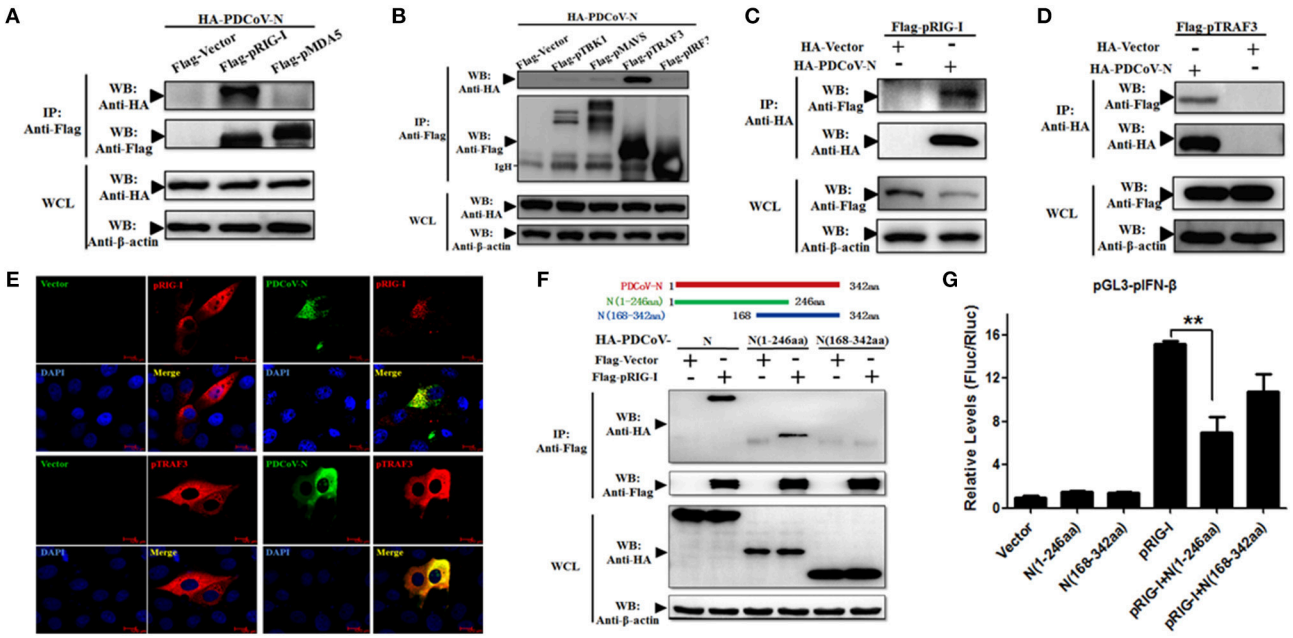

FIGURE 3 | PDCoV N interacts with both pRIG-I and pTRAF3. HEK293T cells were co-transfected with HA-tagged PDCoV-N and Flag-tagged pRIG-I **(A–C)**, Flag-tagged pMDA5 **(A)**, Flag-tagged TBK1 **(B)**, Flag-tagged pMAVS **(B)**, Flag-tagged pTRAF3 **(B,D)** or Flag-tagged pIRF3 **(B)**, respectively. After 28 h of transfection, cells were lysed for co-immunoprecipitation (Co-IP) assay with anti-Flag (IP: Anti-Flag) or anti-HA (IP: Anti-HA) affinity gel. The WCLs and immunoprecipitants were detected by western blot with anti-Flag, anti-HA or anti-β-action antibody. **(E)** PK-15 cells were cotransfected with HA-tagged PDCoV-N and Flag-tagged empty plasmid as control or Flag-tagged pRIG-I, respectively. At 24 h after transfection, cells were fixed for IFA to detect the PDCoV-N (green) and pRIG-I (Red) with anti-HA and anti-Flag antibodies, respectively. 4′, 6-diamidino-2-phenylindole (DAPI, blue) stained the cell nuclei. Fluorescent images were acquired with a confocal laser scanning microscope (scar bar: 10 μm). **(F)** Schematic representation of PDCoV N protein fragments used for Co-IP analyses (up). HEK293T cells were cotransfected with Flag-tagged pRIG-I and HA-tagged full-length or truncated fragments of the PDCoV N protein. After 28 h of transfection, cells were lysed for Co-IP assay with anti-Flag affinity gel. The WCLs and immunoprecipitants were detected by western blot with anti-Flag, anti-HA, or anti-β-action antibody. **(G)** PK-15 cells were cotransfected with pGL3-pIFN-β, pRL-TL, and pcDNA3.1-Flag-pRIG-I alone or together with PDCoV N truncated fragments, respectively. Dual-luciferase assays were performed at 24 h post transfection. All the experiments were independently performed three times. $^{**}p < 0.01$.

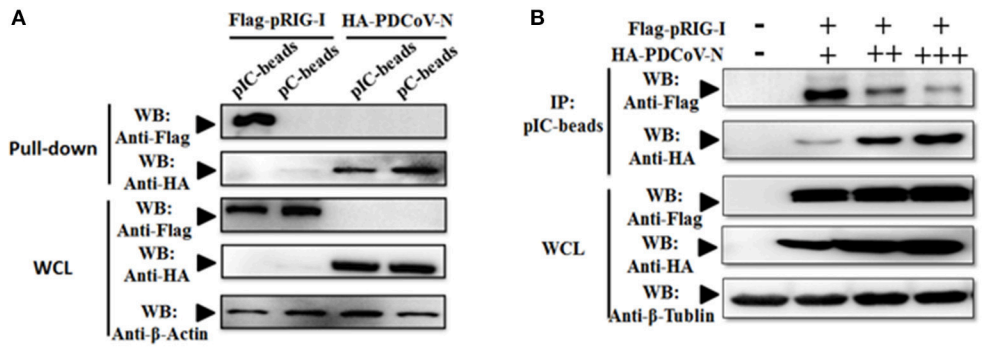

FIGURE 4 | PDCoV-N suppressed the porcine RIG-I-binding dsRNA. **(A)** HEK293T cells were transfected with Flag-tagged pRIG-I or HA-tagged PDCoV expression plasmid. Cells were lysed for Co-IP by poly(I:C) (pIC) or poly(C)(pC)-beads at 28 h post-transfection. Western blot was used to detect the protein. **(B)** HEK293T cells were cotransfected with Flag-tagged pRIG-I with different dose HA-tagged PDCoV expression plasmid. After 28 h of transfection, the cells were lysed for immunoprecipitation by poly(I:C)-beads. Western blot was used to detect the immunoprecipitants and WCLs protein.

analysis, respectively (**Figure 6A**). The pTRIM25 or pRiplet expression plasmid was constructed and expressed in PK-15 cells (**Figure 6B**). To explore the function of pTRIM25 or pRiplet in pRIG-I induced IFN-β production, the pTRIM25, or pRiplet was cotransfected with pRIG-I and pGL3-pIFN-β-Luc and pRL-TK-Luc plasmid in PK-15 cells for 28 h. The results showed that pRiplet could significantly promote pRIG-I-induced pIFN-β-Luc activation (**Figure 6C**). However, pTRIM25 could not influence pRIG-I-induced pIFN-β-Luc activation (**Figure 6C**). The consistent results were observed in the IPEC-J2 cells (**Supplementary Figure 3A**). The results showed that pRiplet was the more important protein in activating pRIG-I. To

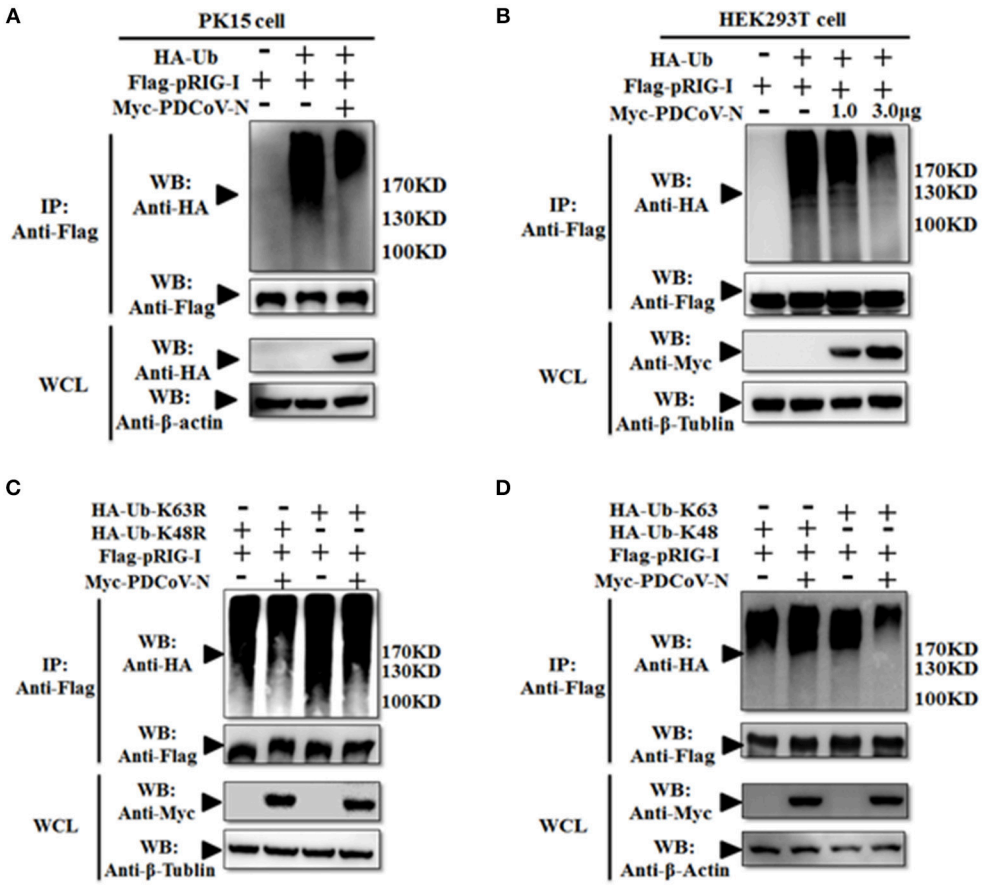

FIGURE 5 | PDCoV N protein inhibited the pRIG-I K63-linked polyubiquitination. **(A,B)** HEK293T or PK-15 were cotransfected with Flag-tagged pRIG-I and Myc-tagged PDCoV N or empty control plasmid with HA-tagged ubiquitin (HA-Ub) or empty control plasmid. **(C,D)** HEK293T cells were cotransfected Flag-tagged pRIG-I and Myc-tagged PDCoV N or empty control plasmid with HA-Ub K48R, K63R, K48 only, or K63 only mutant plasmid or empty control plasmid, respectively. After 28 h of transfection, the cells were lysed for Co-IP by Flag-affinity gel. Western blot was used to detect the immunoprecipitants and WCLs protein.

determine whether PDCoV N protein could influence the pRiplet-induced pRIG-I-induced pIFN-β production, pRIG-I and pRiplet were co-transfected with pGL3-pIFN-β-Luc, pRL-TK-Luc, and PDCoV N or empty plasmid for 28 h in PK-15 cells. The PDCoV N protein was detected in the WCLs by western blot (**Figure 6D**). The results showed that PDCoV N protein could prominently inhibit pIFN-β-Luc activation which is induced by pRiplet-promoted pRIG-I (**Figure 6D**). The consistent results were confirmed in the IPEC-J2 cells (**Supplementary Figure 3B**).

TRIM25 and Riplet were also the targets of a virus to suppress the type I IFN signaling pathway (21, 25). The interactions between PDCoV N protein and pTRIM25 or pRiplet are explored in the present study. The PDCoV N and pTRIM25 or pRiplet expression plasmid were co-transfected in the HEK293T cells for Co-IP analysis. The results showed that PDCoV N protein was neither coprecipitated with pTRIM25 nor pRiplet by HA-tagged affinity gel (**Figures 6E,G**). The pTRIM25 or pRiplet was also undetectable in anti-Myc immunoprecipitation (**Figures 6F,H**). The results demonstrated that PDCoV N protein could not directly interact with pTRIM25 or pRiplet.

PDCoV N Protein Interfered pRiplet Induced pRIG-I K63-Linked Polyubiquitination

To explore the mechanism of PDCoV N protein-repressed porcine Riplet-induced pRIG-I activation, first, pRiplet and pRIG-I plasmid were cotransfected in HEK293T cells for 28 h to analyze their relationship by Co-IP assay. The results showed that pRiplet could directly interact with pRIG-I (**Figures 7A,B**). Then, three pRIG-I mutants expression plasmids (only contain the 2′CARD, HEL, or RD domain) or empty plasmid was co-transfected with pRiplet expression plasmid in HEK293T cells (**Figure 7C**). The Co-IP results showed that pRiplet bound to the HEL and RD domain but not the 2′CARD domain (**Figure 7D**). Further analysis found that pRIG-I ubiquitination or K63-linked polyubiquitination was remarkably increased when the cells were cotransfected with pRiplet (**Figures 7D,E**). However, the PDCoV N protein expression could significantly decrease the pRiplet-induced pRIG-I ubiquitination and K63-linked polyubiquitination (**Figures 7C,D**).

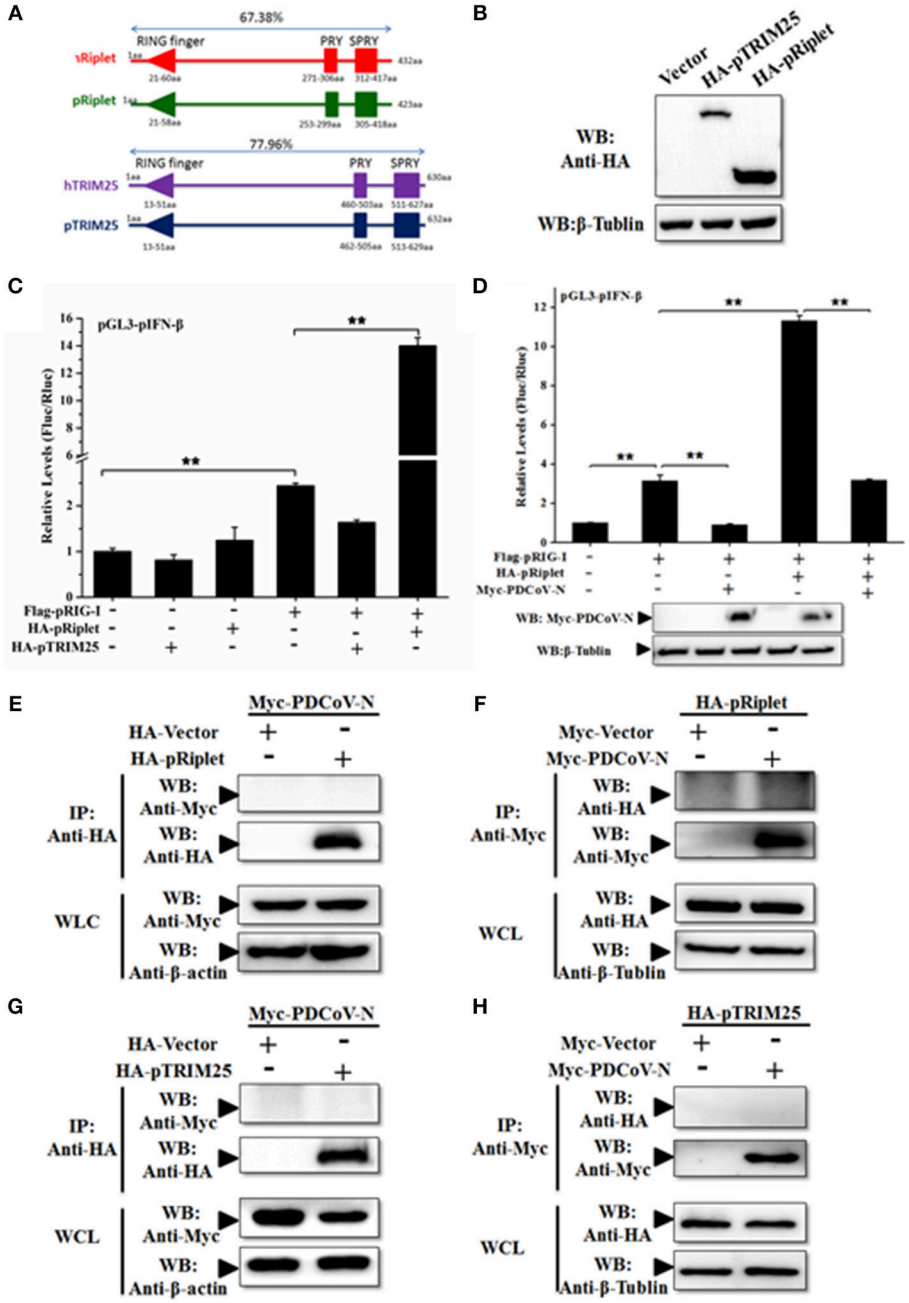

FIGURE 6 | PDCoV N repressed porcine Riplet-induced pRIG-I activation. **(A)** The sequence alignment of porcine TRIM25 (pTRIM25) and Riplet (pRiplet) with human TRIM25 (hTRIM25) and Riplet (hRiplet), respectively, by Clustal Omega (https://www.ebi.ac.uk/Tools/msa/clustalo/). **(B)** HEK293T cells were transfected with the HA-tagged pTRIM25 or HA-tagged pRiplet expression plasmid. After 28 h of transfected, the WCLs were detected with anti-HA antibody by western blot. **(C)** PK-15 cells were co-transfected with pRIG-I, pGL3-pIFN-β, and pRL-TK plasmid with pTRIM25 or pRiplet, the empty plasmid as the control. Dual-luciferase assays were performed at 24 h post transfection. **(D)** PK-15 cells were co-transfected with pRIG-I, pGL3-pIFN-β, and pRL-TK plasmid with pRiplet and Myc-PDCoV-N, the empty plasmid as the control. Dual-luciferase assays were performed at 24 h post transfection. All the experiments were independently performed three times. **(E,G)** HEK293T cells were cotransfected with HA-tagged pRiplet or HA-tagged pTRIM25 or HA-empty plasmid as the control with Myc-tagged PDCoV-N expression plasmid, respectively. **(F,H)** HEK293T cells were co-transfected with Myc-tagged PDCoV (Myc-PDCoV-N) or Myc-empty plasmid as the control expression plasmid with HA-tagged pRiplet **(F)** or HA-tagged pTRIM25 **(H)** plasmid, respectively. After 28 h of transfection, the cells were lysed for Co-IP with anti-Myc monoclonal antibody (IP: Anti-Myc). Western blot was used to detect the immunoprecipitants and WCLs protein. $^{**}p < 0.01$.

To further understand the mechanism of PDCoV N protein-binding pRIG-I, three pRIG-I mutants expression plasmids or empty plasmid was co-transfected with PDCoV N expression plasmid in HEK293T cells for 28 h. The Co-IP results showed that PDCoV N protein could bind to both the HEL and RD domain but not the 2′CARD domain (**Figure 7F**). The binding domains

were consistent with pRiplet (**Figure 7D**). This suggested that PDCoV N might interfere the binding between pRIG-I and pRiplet. To confirm the assumption, the pRiplet and pRIG-I were cotransfected with increasing doses of PDCoV N expression plasmid in HEK293T cells. The Co-IP results showed that with the PDCoV N protein increasing, the pRiplet binding pRIG-I was significantly decreased in the coprecipitates (**Figure 7H**). All above results proved that PDCoV N protein could interfere with pRiplet binding pRIG-I to inhibit the pRiplet-mediated pRIG-I K63-polyubiquitination.

DISCUSSION

Innate immunity is the first line to defend against virus infections, especially the production of IFNs and ISGs. Viruses also have diverse means to evade the host innate immune response. PDCoV infection suppressing IFN-β production has also been reported (30). Research has indicated that PDCoV non-structure protein 5 (Nsp5) encoded a 3C-like protease, which has lyase activity, to interrupt the IFN-β signaling pathway by decomposing human NEMO in HEK293T cells (32). PDCoV Nsp5 also could cleavage the signal transducer and activator of human transcription 2 (STAT2), an essential component of transcription factor complex ISGF3, to antagonize IFN-β signaling in HEK293T cells (35). PDCoV accessory protein 6 (NS6) was proved as another IFN-β antagonist by interfering with the binding of human RIG-I/MDA5 to double-stranded RNA in HEK293T cells (31). In the present study, we found that PDCoV N is another antagonist of porcine IFN-β production induced by poly(I:C), VSV, and porcine RLR-signaling molecules (**Figures 1**, **2** and **Supplementary Figure 1**).

Although TGEV N protein has no effect on IFN-β production, coronavirus N protein as an antagonist of the RLR-mediated IFN-β signaling pathway has been confirmed in PEDV, SARS-CoV, MHV, and MERS-CoV (25, 26, 36, 37). However, previous reports have indicated that the different coronavirus N protein as an IFN antagonist intervened with the RLR signaling pathway by targeting different signaling proteins. SARS-CoV N protein antagonized IFN-β in the initial signaling pathway (38). The protein activator of protein kinase R (PACT) is a cellular dsRNA-binding protein potentiating IFN production by binding to RIG-I and MDA5 (39, 40). The mouse hepatitis virus (MHV) and SARS-CoV N protein could interact with PACT to suppress the dsRNA translocated to RIG-I and MDA5 (36). The PEDV N protein was found to interact with human TBK1 and IKKε to inhibit the human TBK1/IRF3 complex confirmed to suppress IFN-β production (26). In the present study, we proved that PDCoV N directly interacts with pRIG-I and pTRAF3 (**Figure 3**), which is different from the previously reported coronavirus N protein, such as PEDV, SARS-CoV, MERS-CoV, and MHV.C-terminal region of SARS-CoV nucleocapsid protein was critical for antagonizing IFN-β response (38). However, the N-terminal region was necessary for PDCoV N protein to inhibit porcine IFN-β response by targeting pRIG-I (**Figures 3F,G**). Furthermore, we also found that PDCoV N protein significantly inhibited the porcine IRF3 induced IFN-β promoter activation. However, the PDCoV N protein was showed not interacting with porcine IRF3 protein, suggesting another target signal molecule of PDCoV N protein may exist in the downstream of porcine IRF3.

RIG-I and MDA5 contain three similar structures: 2′CARDs, HEL, and C-terminal domain (CTD) (15). RIG-I and MDA5 sense distinct RNAs depending on their different C-terminal structures. The C-terminal structure of human RIG-I contains a conservative internal repressor domain (RD), but this is not found in MDA5 (15). In the present study, we found that PDCoV N protein could directly interact with porcine RIG-I but not porcine MDA5. In addition, the RD domain was important for PDCoV N protein interacting with porcine RIG-I (**Figure 6F**). This may explain why PDCoV N protein specifically binds to porcine RIG-I.

Viral nucleic acids as pathogen associated molecular pattern are sensed by the host pattern recognition receptors after a viral infection. RIG-I and MDA5 are the major members of intracytoplasmic pathogenic molecular pattern recognition receptors that sense the intracellular viral RNA. Hence, one mechanism of the RNA virus escaping from host immune surveillance is to protect its ssRNA or dsRNA not to be recognized by RIG-I and MDA5. The MERS 4a protein is a dsRNA-binding protein that interacts with PACT in an RNA-dependent manner but not with RIG-I or MDA5, which suppresses the PACT-induced activation of RIG-I and MDA5 (41). PDCoV accessory protein 6 (NS6) could not bind dsRNA or ssRNA. However, eukaryotic-expression of PDCoV NS6 in HEK293T cells has been found to directly interact with human RIG-I and MDA5, and suppresses the host recognition of dsRNA (31). In the present study, PDCoV N protein was proven as a new member competing with porcine RIG-I binding dsRNA (**Figure 4B**). This is a mechanism of PDCoV N protein suppressing porcine IFN-β induction (**Figure 8**). It is noteworthy that the NS6 protein must be synthesized in infection cells, unlike the N protein, which can come from the parent virus itself. Therefore, we propose a hypothesis that there may be a synergistic effect between PDCoV N protein and NS6 protein. In the early stage of virus infection, especially before the synthesis of NS6 protein, the competitive binding dsRNA of PDCoV N protein inhibits the activation of pRIG-I. With the synthesis and expression of NS6 protein, the function of PDCoV N protein is replaced by NS6, which is conducive to N protein binding the viral gRNA to complete the assembly of progeny virus.

In addition, PDCoV N protein could inhibit porcine RIG-I or MDA5-induced pIFN-β promoter activation. The results indicated that PDCoV N protein may have another function to regulate the porcine RIG-I activation or suppress the downstream signaling transduction. TRAFs have an important role in signal transduction to regulate the immune and inflammatory responses. The C-terminal domain of TRAFs mediates its oligomerization and the association with upstream or downstream effector protein. TRAF3 has been considered the important signaling molecule as the bridge between MAVS and TBK1 (19). SARS-CoV papain-like protease could negatively regulate IRF3 activation by interacting with the STING-TRAF3-TBK1 complex (42). SARS-CoV M protein could suppress the TBK1/IKKε-dependent activation of IRF3/IRF7

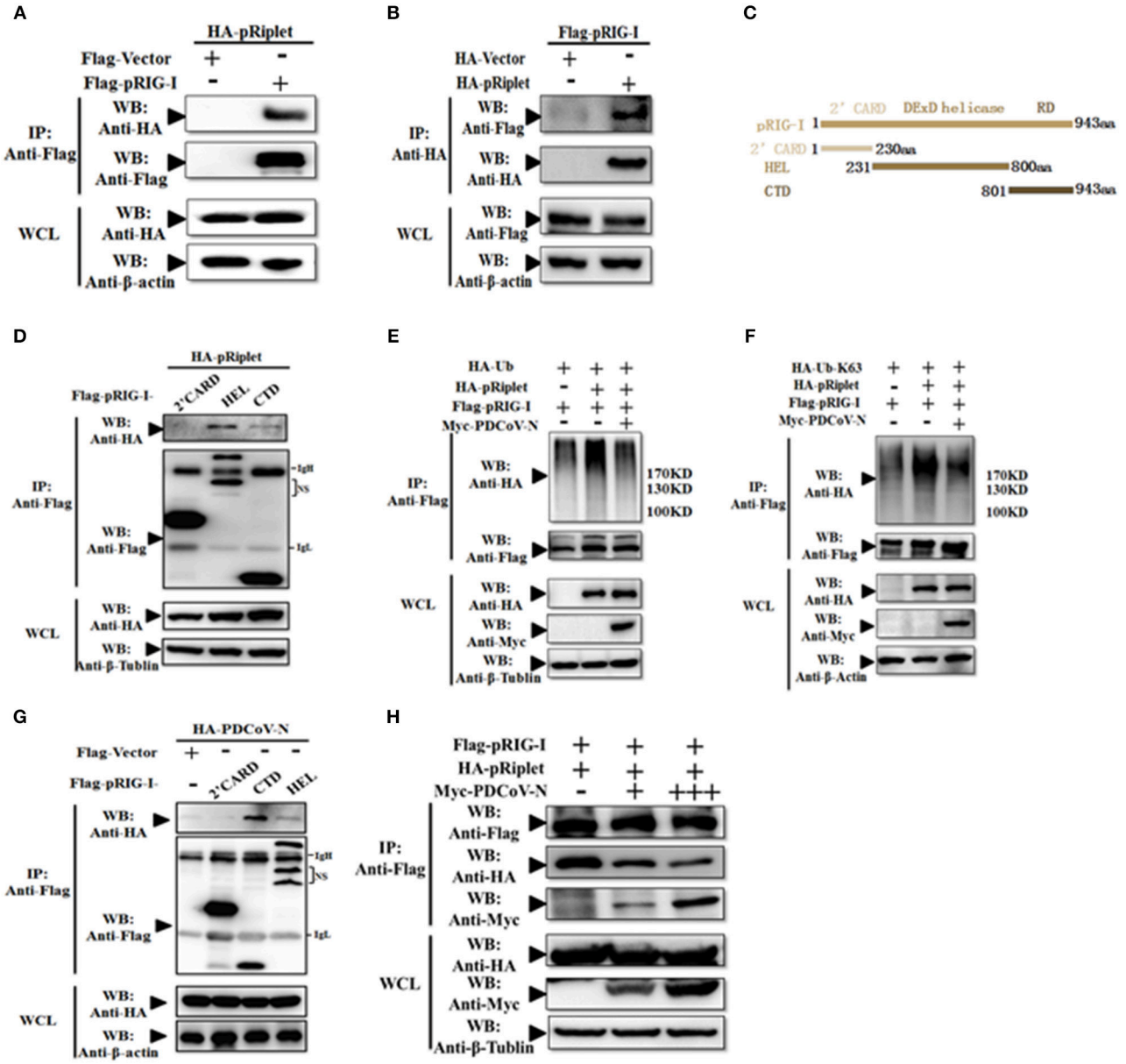

FIGURE 7 | PDCoV N protein inhibited pRiplet-induced pRIG-I K63-polyubiquitination. **(A,B)** HEK293T cells were co-transfected with HA-tagged pRiplet or Flag-tagged pRIG-I or empty plasmid as the control with Flag-tagged pRIG-I or HA-tagged PDCoV-N expression plasmid, respectively. After 28 h of transfection, the cells were lysed for Co-IP by Flag-affinity gel or HA-affinity gel. **(C)** Schematic representation of porcine RIG-I fragments used for Co-IP analyses. **(D,G)** HEK293T cells were co-transfected with HA-tagged pRiplet **(D)** or HA-tagged PDCoV-N **(G)** with three porcine RIG-I fragments (Flag-pRIG-I-2′CARD, Flag-pRIG-I-HEL, Flag-pRIG-I-CTD), or expression plasmid, respectively. After 28 h of transfection, the cells were lysed for Co-IP by Flag-affinity gel. **(E,F)** HEK293T cells were co-transfected with Flag-tagged pRIG-I and HA-Ub or HA-Ub-K63 with Myc-tagged PDCoV-N or HA-tagged pRiplet or empty control plasmid, respectively. After 28 h of transfection, the cells were lysed for Co-IP by Flag-affinity gel. **(H)** HEK293T cells were co-transfected with HA-tagged pRiplet and Flag-tagged pRIG-I with Myc-tagged PDCoV-N or empty plasmid as the control expression plasmid, respectively. After 28 h of transfection, the cells were lysed for Co-IP by Flag-affinity gel. Western blot was used to detect the immunoprecipitants and WCLs protein.

by preventing the formation of TRAF3/TANK/TBK1/IKKε complex (43). The C-terminal effector domain of AIV NS1 also interacts with the TRAF3 protein to decrease its K63-linked polyubiquitination and disrupt the formation of the MAVS/TRAF3 complex (44). In the present study, we confirmed that PDCoV N protein also directly interacted with porcine TRAF3 (**Figure 3**). The mechanism of PDCoV N protein targeting porcine TRAF3 to mediate the type I interferon signaling pathway is unclear and is currently being explored by our team.

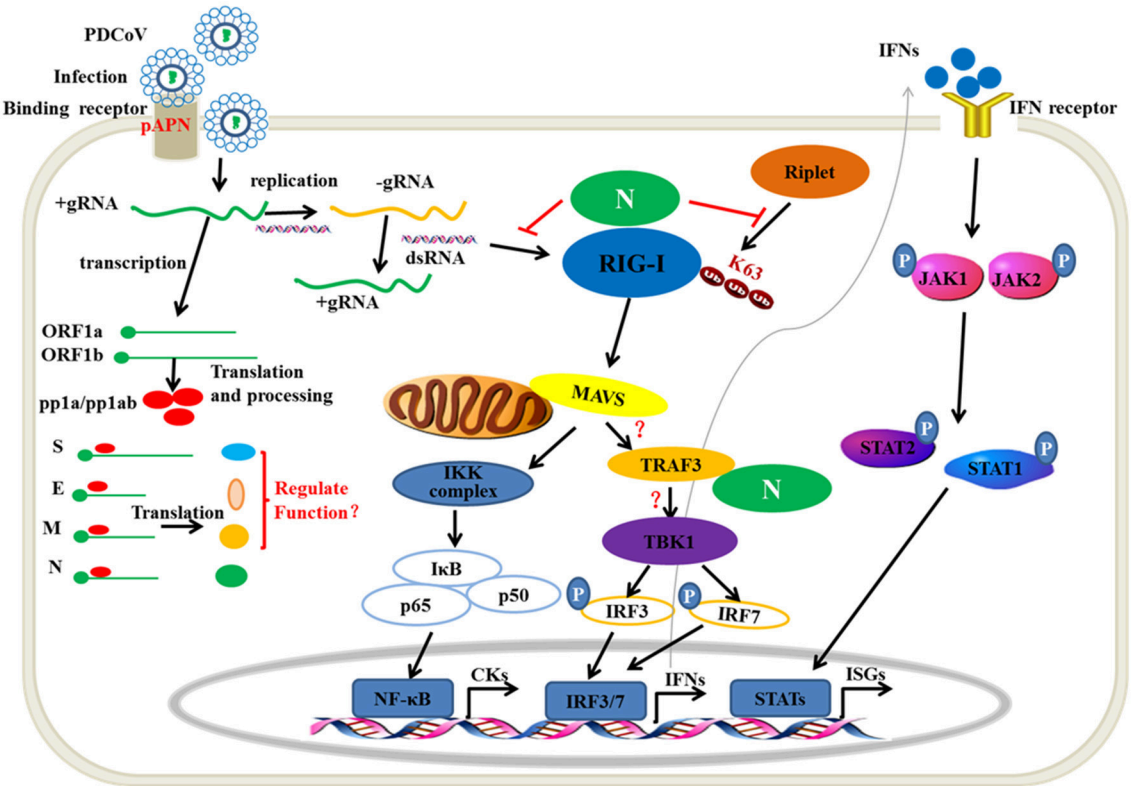

FIGURE 8 | The mechanism of PDCoV N protein interfered with the type I IFN response. PDCoV infect the host cells by attaching to the celluar receptor porcine APN. In the cytoplasm, PDCoV release the viral genomic RNA and then complete the transcription and replication process. The ssRNA as well as dsRNA as replicative intermediate are sensed by porcine innate nucleic acids sensors in the cytoplasm to induce the IFNs production, such as porcine RIG-I. The E3 ubiquitin ligase Riplet is shown to active RIG-I by K63-linked polyubiqutination. Activation of JAK-STAT pathway by IFNs binding its receptor induces the production of ISGs, such as *OAS1*, *ISG15*. In the present, PDCoV N protein can block the porcine RIG-I dsRNA-binding and interferes with porcine Riplet-mediated porcine RIG-I K63-linked polyubiquitination to restrain the type I IFN response. PDCoV N protein also interacts with porcine TRAF3. However, the mechanism of the association is unclear. The other viral structure proteins are unclear in regulating type I IFN response.

Ubiquitination is an important posttranslational modification in regulating the activation of signaling molecules. The E3 ubiquitin ligases TRIM25, TRIM4, and Riplet were proven to catalyze the K63-linked polyubiquitination of RIG-I in CARDs and CTD, respectively (17, 45–47). Suppressing the ubiquitin ligases binding with its target protein is another means of virus interfering with the host IFN-β production. AIV NS1 protein also could suppress RIG-I activation by species-specific interaction with TRIM25 or Riplet (21). The West Nile virus NS1 also antagonizes IFN-β production by inhibiting RIG-I and MDA5 K63-linked polyubiquitination (22). The SARS-CoV N protein directly interacts with human TRIM25 to suppress the RIG-I K63-linked polyubiquitination (25). The MERS-CoV N protein has a similar function as SARS-CoV N to inhibit RIG-I activation (25). However, we found that PDCoV N protein neither interacts with pTRIM25 nor pRiplet (**Figures 5D–G**). In the present study, we also found that pTRIM25 could not promote the activation of pRIG-I induced IFN-β promoter (**Figure 6C**). It indicated that the role of homologous proteins among different species might be different in regulating the activation of RLR signaling pathway. This may be an important reason for coronavirus N protein interaction with different proteins to regulate the host innate immunity in different hosts.

The mechanism of Riplet-mediated RIG-I activation remains unclear. hRiplet could promote the K63-linked polyubiquitination of the RIG-I CARD domain, which was indispensable for interaction between Riplet and RIG-I (34, 48). However, hRiplet was also found mainly interacting with the RIG-I RD domain and promoting the RD domain K63-linked polyubiquitination to release RIG-I autorepression (16, 47). In the present study, we found that pRiplet, as the homologous gene of hRiplet, could directly interact with pRIG-I, which was dispensable for the HEL and RD domain but not the CARD domain (**Figure 7**). pRilet mediated pRIG-I activation by increasing the pRIG-I K63-linked polyubiquitination. However, PDCoV N protein could suppress the pRiplet-mediated pRIG-I activation to induce IFN-β production. Further exploration demonstrated that PDCoV N protein blocked the pRIG-I K63-linked polyubiquitination by interfering pRiplet binding to pRIG-I (**Figure 8**). Two theories of the interfering binding mechanism might exist: First, because of the same target domains of PDCoV N protein and pRiplet binding pRIG-I, they may be

competitively binding pRIG-I. On the other hand, we found that pRiplet mainly binds to the HEL domain of pRIG-I (**Figure 7D**), while PDCoV N protein mainly binds to the CTD of pRIG-I (**Figure 7G**). The human RIG-I CTD could interact with the HEL and CARD domain to self-repression (15). Hence, another reason is that the protein conformation of pRIG-I might be changed after binding to PDCoV N protein, which leading the pRiplet could not interact with pRIG-I. To our knowledge, this is the first time that coronavirus N protein has been reported to interfere the host immune system by directly targeting host RIG-I. These results provide insight into a novel mechanism of PDCoV inhibiting the host antiviral response.

AUTHOR CONTRIBUTIONS

YY, SJ, and JL conceived and designed the experiments. JL, LS, and ZW performed the experiments and analyzed data. JL, MJ, and WH wrote the manuscript. All authors reviewed, revised, and approved the final manuscript.

FUNDING

This work was supported by funding from Shanghai Agriculture Applied Technology Development Program (No. T20170110), National Natural Science Foundation of China (No. 31571932 and 31772744).

ACKNOWLEDGMENTS

Authors highly appreciate Dr. Sun Tao, Dr. Yuan Congli for providing virus and plasmids described in Section Materials and Methods.

SUPPLEMENTARY MATERIAL

The Supplementary Material for this article can be found online at: https://www.frontiersin.org/articles/10.3389/fimmu.2019.01024/full#supplementary-material

REFERENCES

1. Zhang JQ. Porcine deltacoronavirus: overview of infection dynamics, diagnostic methods, prevalence and genetic evolution. *Virus Res.* (2016) 226:71–84. doi: 10.1016/j.virusres.2016.05.028
2. Xu Z, Zhong H, Zhou Q, Du Y, Chen L, Zhang Y, et al. A highly pathogenic strain of porcine deltacoronavirus caused watery diarrhea in newborn piglets. *Virologica Sinica.* (2018) 33:131–41. doi: 10.1007/s12250-018-0003-8
3. Woo PC, Lau SK, Lam CS, Lau CC, Tsang AK, Lau JH, et al. Discovery of seven novel Mammalian and avian coronaviruses in the genus deltacoronavirus supports bat coronaviruses as the gene source of alphacoronavirus and betacoronavirus and avian coronaviruses as the gene source of gammacoronavirus and deltacoronavirus. *J Virol.* (2012) 86:3995–4008. doi: 10.1128/JVI.06540-11
4. Dong N, Fang L, Yang H, Liu H, Du T, Fang P, et al. Isolation, genomic characterization, and pathogenicity of a Chinese porcine deltacoronavirus strain CHN-HN-2014. *Veter Microbiol.* (2016) 196:98–106. doi: 10.1016/j.vetmic.2016.10.022
5. Hu H, Jung K, Vlasova AN, Chepngeno J, Lu Z, Wang Q, et al. Isolation and characterization of porcine deltacoronavirus from pigs with diarrhea in the United States. *J Clini Microbiol.* (2015) 53:1537–48. doi: 10.1128/JCM.00031-15
6. Lorsirigool A, Saeng-chuto K, Temeeyasen G, Madapong A, Tripipat T, Wegner M, et al. The first detection and full-length genome sequence of porcine deltacoronavirus isolated in Lao PDR. *Arch Virol.* (2016) 161:2909–11. doi: 10.1007/s00705-016-2983-8
7. Saeng-Chuto K, Lorsirigool A, Temeeyasen G, Vui DT, Stott CJ, Madapong A, et al. Different lineage of porcine deltacoronavirus in Thailand, Vietnam and Lao PDR in 2015. *Transbound Emerg Dis.* (2017) 64:3–10. doi: 10.1111/tbed.12585
8. Fang PX, Fang LR, Liu XR, Hong YY, Wang YL, Dong N, et al. Identification and subcellular localization of porcine deltacoronavirus accessory protein NS6. *Virology.* (2016) 499:170–7. doi: 10.1016/j.virol.2016.09.015
9. Fang PX, Fang LR, Hong YY, Liu XR, Dong N, Ma PP, et al. Discovery of a novel accessory protein NS7a encoded by porcine deltacoronavirus. *J Gen Virol.* (2017) 98:173–8. doi: 10.1099/jgv.0.000690
10. Li WT, Hulswit RJG, Kenney SP, Widjaja I, Jung K, Alhamo MA, et al. Broad receptor engagement of an emerging global coronavirus may potentiate its diverse cross-species transmissibility. *Proc Natl Acad Sci USA.* (2018) 115:E5135–43. doi: 10.1073/pnas.1802879115
11. Bruns AM, Horvath CM. LGP2 synergy with MDA5 in RLR-mediated RNA recognition and antiviral signaling. *Cytokine.* (2015) 74:198–206. doi: 10.1016/j.cyto.2015.02.010
12. Yoneyama M, Kikuchi M, Matsumoto K, Imaizumi T, Miyagishi M, Taira K, et al. Shared and unique functions of the DExD/H-box helicases RIG-I, MDA5, and LGP2 in antiviral innate immunity. *J Immunol.* (2005) 175:2851–8. doi: 10.4049/jimmunol.175.5.2851
13. Kawai T, Takahashi K, Sato S, Coban C, Kumar H, Kato H, et al. IPS-1, an adaptor triggering RIG-I- and Mda5-mediated type I interferon induction. *Nat Immunol.* (2005) 6:981–8. doi: 10.1038/ni1243
14. Sun QM, Sun LJ, Liu HH, Chen X, Seth RB, Forman J, et al. The specific and essential role of MAVS in antiviral innate immune responses. *Immunity.* (2006) 24:633–42. doi: 10.1016/j.immuni.2006.04.004
15. Saito T, Hirai R, Loo YM, Owen D, Johnson CL, Sinha SC, et al. Regulation of innate antiviral defenses through a shared repressor domain in RIG-I and LGP2. *Proc Natl Acad Sci USA.* (2007) 104:582–7. doi: 10.1073/pnas.0606699104
16. Oshiumi H, Miyashita M, Matsumoto M, Seya T. A distinct role of Riplet-mediated K63-Linked polyubiquitination of the RIG-I repressor domain in human antiviral innate immune responses. *PLoS Pathog.* (2013) 9:e1003533. doi: 10.1371/journal.ppat.1003533
17. Gack MU, Shin YC, Joo CH, Urano T, Liang C, Sun LJ, et al. TRIM25 RING-finger E3 ubiquitin ligase is essential for RIG-I-mediated antiviral activity. *Nature.* (2007) 446:916–12. doi: 10.1038/nature05732
18. Liu S, Chen J, Cai X, Wu J, Chen X, Wu YT, et al. MAVS recruits multiple ubiquitin E3 ligases to activate antiviral signaling cascades. *eLife.* (2013) 2:e00785. doi: 10.7554/eLife.00785
19. Paz S, Vilasco M, Werden SJ, Arguello M, Joseph-Pillai D, Zhao T, et al. A functional C-terminal TRAF3-binding site in MAVS participates in positive and negative regulation of the IFN antiviral response. *Cell Res.* (2011) 21:895–910. doi: 10.1038/cr.2011.2
20. Honda K, Takaoka A, Taniguchi T. Type I interferon [corrected] gene induction by the interferon regulatory factor family of transcription factors. *Immunity.* (2006) 25:349–60. doi: 10.1016/j.immuni.2006.08.009
21. Rajsbaum R, Albrecht RA, Wang MK, Maharaj NP, Versteeg GA, Nistal-Villan E, et al. Species-specific inhibition of RIG-I ubiquitination and IFN induction by the influenza A virus NS1 protein. *PLoS Pathog.* (2012) 8:e1003059. doi: 10.1371/journal.ppat.1003059
22. Zhang HL, Ye HQ, Liu SQ, Deng CL, Li XD, Shi PY, et al. West nile virus NS1 antagonizes interferon beta production by targeting RIG-I and MDA5. *J Virol.* (2017) 91:e02396–16. doi: 10.1128/JVI.02396-16

23. Ma YL, Tong XH, Xu XL, Li XM, Lou ZY, Rao ZH. Structures of the N- and C-terminal domains of MHV-A59 nucleocapsid protein corroborate a conserved RNA-protein binding mechanism in coronavirus. *Protein Cell*. (2010) 1:688–97. doi: 10.1007/s13238-010-0079-x
24. McBride R, van Zyl M, Fielding BC. The coronavirus nucleocapsid is a multifunctional protein. *Viruses-Basel*. (2014) 6:2991–3018. doi: 10.3390/v6082991
25. Hu Y, Li W, Gao T, Cui Y, Jin Y, Li P, et al. The severe acute respiratory syndrome coronavirus nucleocapsid inhibits type I interferon production by interfering with TRIM25-mediated RIG-I ubiquitination. *J Virol*. (2017) 91: e02143–16. doi: 10.1128/JVI.02143-16
26. Ding Z, Fang LR, Jing HY, Zeng SL, Wang D, Liu LZ, et al. Porcine epidemic diarrhea virus nucleocapsid protein antagonizes beta interferon production by sequestering the interaction between IRF3 and TBK1. *J Virol*. (2014) 88:8936–45. doi: 10.1128/Jvi.00700-14
27. Xu X, Zhang H, Zhang Q, Huang Y, Dong J, Liang Y, et al. Porcine epidemic diarrhea virus N protein prolongs S-phase cell cycle, induces endoplasmic reticulum stress, and up-regulates interleukin-8 expression. *Veter Microbiol*. (2013) 164:212–1. doi: 10.1016/j.vetmic.2013.01.034
28. Cao L, Ge X, Gao Y, Ren Y, Ren X, Li G. Porcine epidemic diarrhea virus infection induces NF-κB activation through the TLR2, TLR3, and TLR9 pathways in porcine intestinal epithelial cells. *J Gen Virol*. (2015) 96:1757. doi: 10.1099/vir.0.000133
29. Ding Z, An K, Xie L, Wu W, Zhang R, Wang D, et al. Transmissible gastroenteritis virus infection induces NF-κB activation through RLR-mediated signaling. *Virology*. (2017) 507:170. doi: 10.1016/j.virol.2017.04.024
30. Luo JY, Fang LR, Dong N, Fang PX, Ding Z, Wang D, et al. Porcine deltacoronavirus (PDCoV) infection suppresses RIG-I-mediated interferon-beta production. *Virology*. (2016) 495:10–7. doi: 10.1016/j.virol.2016.04.025
31. Fang P, Fang L, Ren J, Hong Y, Liu X, Zhao Y, et al. Porcine deltacoronavirus accessory protein NS6 antagonizes interferon beta production by interfering with the binding of RIG-I/MDA5 to double-stranded RNA. *J Virol*. (2018) 92:e00712–18. doi: 10.1128/JVI.00712-18
32. Zhu XY, Fang LR, Wang D, Yang YT, Chen JY, Ye X, et al. Porcine deltacoronavirus Nsp5 inhibits interferon-beta production through the cleavage of NEMO. *Virology*. (2017) 502:33–8. doi: 10.1016/j.virol.2016.12.005
33. Lee S, Lee C. Functional characterization and proteomic analysis of the nucleocapsid protein of porcine deltacoronavirus. *Virus Res*. (2015) 208:136–45. doi: 10.1016/j.virusres.2015.06.013
34. Shi Y, Yuan B, Zhu W, Zhang R, Li L, Hao X, et al. Ube2D3 and Ube2N are essential for RIG-I-mediated MAVS aggregation in antiviral innate immunity. *Nat Comm*. (2017) 8:15138. doi: 10.1038/ncomms15138
35. Zhu XY, Wang D, Zhou JW, Pan T, Chen JY, Yang YT, et al. Porcine deltacoronavirus Nsp5 antagonizes type I interferon signaling by cleaving STAT2. *J Virol*. (2017) 91:e00003–17. doi: 10.1128/JVI.00003-17
36. Ding Z, Fang L, Yuan S, Zhao L, Wang X, Long S, et al. The nucleocapsid proteins of mouse hepatitis virus and severe acute respiratory syndrome coronavirus share the same IFN-beta antagonizing mechanism: attenuation of PACT-mediated RIG-I/ MDA5 activation. *Oncotarget*. (2017) 8:49655–70. doi: 10.18632/oncotarget.17912
37. Zhou YR, Wu W, Xie LL, Wang D, Ke QY, Hou ZZ, et al. Cellular RNA helicase DDX1 is involved in trasmissible gastroenteritis virus Nsp 14-induced interferon-beta production. *Front Immunol*. (2017) 8:940. doi: 10.3389/fimmu.2017.00940
38. Lu X, Pan J, Tao J, Guo D. SARS-CoV nucleocapsid protein antagonizes IFN-beta response by targeting initial step of IFN-beta induction pathway, and its C-terminal region is critical for the antagonism. *Virus Genes*. (2011) 42:37–45. doi: 10.1007/s11262-010-0544-x
39. Lui PY, Wong LR, Ho TH, Au SWN, Chan CP, Kok KH, et al. PACT Facilitates RNA-induced activation of MDA5 by promoting MDA5 oligomerization. *J Immunol*. (2017) 199:1846–55. doi: 10.4049/jimmunol.1601493
40. Kok KH, Lui PY, Ng MHJ, Siu KL, Au SWN, Jin DY. The double-stranded RNA-binding protein PACT functions as a cellular activator of RIG-I to facilitate innate antiviral response. *Cell Host Microbe*. (2011) 9:299–309. doi: 10.1016/j.chom.2011.03.007
41. Siu KL, Yeung ML, Kok KH, Yuen KS, Kew C, Lui PY, et al. Middle east respiratory syndrome coronavirus 4a protein is a double-stranded RNA-binding protein that suppresses PACT-induced activation of RIG-I and MDA5 in the innate antiviral response. *J Virol*. (2014) 88:4866–76. doi: 10.1128/JVI.03649-13
42. Chen XJ, Yang XX, Zheng Y, Yang YD, Xing YL, Chen ZB. SARS coronavirus papain-like protease inhibits the type I interferon signaling pathway through interaction with the STING-TRAF3-TBK1 complex. *Protein Cell*. (2014) 5:369–81. doi: 10.1007/s13238-014-0026-3
43. Siu KL, Kok KH, Ng MHJ, Poon VKM, Yuen KY, Zheng BJ, et al. Severe acute respiratory syndrome coronavirus M protein inhibits type I interferon production by impeding the formation of TRAF3 center dot TANK center dot TBK1/IKK epsilon Complex. *J Biol Chem*. (2009) 284:16202–9. doi: 10.1074/jbc.M109.008227
44. Wei Q, Wei X, Guo K, Li Y, Lin X, Zhong Z, et al. The C-terminal effector domain of non-structural protein 1 of influenza A virus blocks IFN-β production by targeting TNF receptor-associated factor 3. *Front Immunol*. (2017) 8:779. doi: 10.3389/fimmu.2017.00779
45. Yan J, Li Q, Mao AP, Hu MM, Shu HB. TRIM4 modulates type I interferon induction and cellular antiviral response by targeting RIG-I for K63-linked ubiquitination. *J Mol Cell Biol*. (2014) 6:154–63. doi: 10.1093/jmcb/mju005
46. Oshiumi H, Miyashita M, Inoue N, Okabe M, Matsumoto M, Seya T. The ubiquitin ligase riplet is essential for RIG-I-dependent innate immune responses to RNA virus infection. *Cell Host Microbe*. (2010) 8:496–509. doi: 10.1016/j.chom.2010.11.008
47. Oshiumi H, Matsumoto M, Hatakeyama S, Seya T. Riplet/RNF135, a RING finger protein, ubiquitinates RIG-I to promote interferon-beta induction during the early phase of viral infection. *J Biol Chem*. (2009) 284:807–17. doi: 10.1074/jbc.M804259200
48. Gao D, Yang YK, Wang RP, Zhou X, Diao FC, Li MD, et al. REUL is a novel E3 ubiquitin ligase and stimulator of retinoic-acid-inducible gene-I. *PloS ONE*. (2009) 4:e5760. doi: 10.1371/journal.pone.0005760

Conflict of Interest Statement: The authors declare that the research was conducted in the absence of any commercial or financial relationships that could be construed as a potential conflict of interest.

frontiers in Immunology

HYPOTHESIS AND THEORY
published: 15 May 2019
doi: 10.3389/fimmu.2019.01077

Perturbation of Thymocyte Development Underlies the PRRS Pandemic: A Testable Hypothesis

John E. Butler[1], Marek Sinkora[2], Gang Wang[3], Katerina Stepanova[2], Yuming Li[3] and Xuehui Cai[3]*

[1] Carver College of Medicine, University of Iowa, Iowa, IA, United States, [2] Laboratory of Gnotobiology, Institute of Microbiology of the Czech Academy of Sciences, Prague, Czechia, [3] State Key Laboratory of Veterinary Biotechnology, Harbin Veterinary Research Institute, Chinese Academy of Agricultural Sciences, Harbin, China

Porcine reproductive and respiratory syndrome virus (PRRSV) causes immune dysregulation during the Critical Window of Immunological Development. We hypothesize that thymocyte development is altered by infected thymic antigen presenting cells (TAPCs) in the fetal/neonatal thymus that interact with double-positive thymocytes causing an acute deficiency of T cells that produces "holes" in the T cell repertoire allowing for poor recognition of PRRSV and other neonatal pathogens. The deficiency may be the result of random elimination of PRRSV-specific T cells or the generation of T cells that accept PRRSV epitopes as self-antigens. Loss of helper T cells for virus neutralizing (VN) epitopes can result in the failure of selection for B cells in lymph node germinal centers capable of producing high affinity VN antibodies. Generation of cytotoxic and regulatory T cells may also be impaired. Similar to infections with LDV, LCMV, MCMV, HIV-1 and trypanosomes, the host responds to the deficiency of pathogen-specific T cells and perhaps regulatory T cells, by "last ditch" polyclonal B cell activation. In colostrum-deprived PRRSV-infected isolator piglets, this results in hypergammaglobulinemia, which we believe to be a "red herring" that detracts attention from the thymic atrophy story, but leads to our second independent hypothesis. Since hypergammaglobulinemia has not been reported in PRRSV-infected conventionally-reared piglets, we hypothesize that this is due to the down-regulatory effect of passive maternal IgG and cytokines in porcine colostrum, especially TGFβ which stimulates development of regulatory T cells (Tregs).

Keywords: hypergammaglobulinemia, PRRS virus, T cell repertoire, thymic atrophy, hypothesis

OPEN ACCESS

Edited by:
Nicolas Bertho, INRA Biologie, Épidémiologie et Analyse de Risque en Santé Animale (BIOEPAR), France

Reviewed by:
Artur Summerfield, Institute of Virology and Immunology (IVI), Switzerland
John C. Schwartz, Pirbright Institute (BBSRC), United Kingdom

****Correspondence:***
John E. Butler
john-butler@uiowa.edu

Specialty section:
This article was submitted to Comparative Immunology, a section of the journal Frontiers in Immunology

Received: *27 November 2018*
Accepted: *26 April 2019*
Published: *15 May 2019*

Citation:
Butler JE, Sinkora M, Wang G, Stepanova K, Li Y and Cai X (2019) Perturbation of Thymocyte Development Underlies the PRRS Pandemic: A Testable Hypothesis. Front. Immunol. 10:1077. doi: 10.3389/fimmu.2019.01077

BACKGROUND AND HYPOTHESIS

Porcine reproductive and respiratory syndrome (PRRS) is a major threat to swine health and global pork production. It is considered responsible for an annual 660 million dollar loss to the pork industry in the USA alone with proportionally similar loses in other countries (1; Lager this volume). The disease is a pandemic and ∼25 years of research has yet to clearly define the immune pathology that allows the virus to persist in young pigs for up to 150 dpi (1).

Therefore, we believe it is time to offer a testable hypothesis to explain the immune pathogenesis and persistence of PRRS in the belief that combating the PRRS pandemic and engineering vaccines depend on identifying the cause of the immune dysregulation. We believe that attenuated viral vaccines will have limited success unless they prevent infection of thymic antigen presenting cells (TAPCs) during the period in which the T cell repertoire is being developed.

PRRS is caused by a member of the Arteriviridae, order Nidoviralies, which includes lactate dehydrogenase elevating virus in mice (LDV), equine arterivirus (EAV), and simian hemorrhagic fever disease (SHFV). The virus is trophic for macrophages and dendritic cells, whereon, CD163 serve as a receptor (2) and when deleted, prevents macrophages infection (3). As indicated by the name, Porcine reproductive and respiratory syndrome virus (PRRSV) causes both fetal abortion and respiratory disease. Neonates are especially susceptible to viral and bacterial pathogens, because they encounter them during a critical period in development. The situation with PRRS is made more difficult in Class III Artiodactyls like swine (4, 5) because the virus can cross the placenta but protective maternal antibodies or cytotoxic T cells (CTLs) cannot. The mechanism of placental transfer of the virus is unclear, but may involve infected macrophages as is the case with LDV (6). Transfer may be facilitated by virus-induced apoptosis at the maternal-fetal interface (7). In any case, the primary target in fetuses is the thymus (8). Not surprisingly, fetal piglets develop the same features of immune dysregulation as seen in isolator piglets (9, 10). In contrast to piglets, infected adult swine make effective VN antibodies and can eliminate the infection (11) and VN antibodies from convalescent sows experimentally administered to piglets provide sterilizing immunity (12). These observation indicate that PRRS is a fetal/ newborn disease that strikes during the Critical Window of Immunological Development (13).

Early reports on PRRS showed that PRRSV-infected fetal and newborn piglets had increased susceptibility to secondary pathogens (14–17). More recent observations support this view (18–21). Co-infection studies using swine influenza (SIV), porcine circovirus Type 2 (PCV-2), *Salmonella choleraesuis*, *Mycoplasma hyopneumoniae,* and *Streptococcus suis* all result in prolonged fever and respiratory distress in PRRSV-infected piglets compared to controls infected with these pathogens alone. Twenty of 22 PRRS piglets co-infected with *S. suis* died, but only 5 of 23 infected with *S. suis* (22). Anti-PRRSV antibodies can be detected 6–14 dpi (22, 23) but VN antibodies do not appear before 28 dpi or later (24, 25), reminiscent of lymphocyte choriomeningitis virus (LCMV) infections in mice (26). Thus, the lack of VN antibodies when they are most needed, is one feature of this persistent viral disease. These observations collectively suggest that PRRSV infection induces immune suppression, i.e., neonatal immune dysregulation. This seems consistent with the acute lymphopenia after infection (27–30) although this can also occurs in many infectious diseases as monocytes and lymphocytes translocate from blood to hard tissue sites.

Some features of immune dysregulation are exaggerated in piglets reared in isolator units that are denied access to maternal colostrum and a natural gut flora. These piglets develop severe hypergammaglobulinemia, exhibit lymph node hyperplasia, develop lung lesions while autoantibodies appear and immune complexes are deposited in their kidneys and vasculature (9). **Figure 1** shows that IgG levels are elevated ∼20-fold and IgA and IgM levels are elevated 10-fold in PRRSV-infected piglets vs. littermates infected with SIV and PCV-2. While data on serum Ig levels in conventionally-reared piglets is limited, there are no reports of hypergammaglobulinemia. In any case, comparison of conventionally-reared piglets with isolator piglets indicates that IgG, IgM, and IgA levels in serum during hypergammaglobulinemia are circa 2-fold higher than in conventionally-reared piglets (**Figure 1**, note double arrows). Colonization with benign *E. coli* does not reduce the degree of hypergammaglobulinemia (**Figure 1**) yet the same benign *E. coli* stimulates development of their adaptive immune system (31).

Consistent with hypergammaglobulinemia in isolator piglets, PRRSV strongly stimulates B cell activity resulting in swift differentiation of naive $CD2^{+}CD21^{+}$ B cells to $CD2^{+}CD21^{-}$ antibody-forming cells (AFC) seemingly by-passing the presence of primed $CD2^{-}CD21^{+}$ B cells [**Figure 2**; (34)]. This decrease in $CD21^{+}$ B cells has also been observed in PRRSV-infected conventional piglets (25, 28, 29). In isolator piglets this results in a 5-fold increase in circulating B cells and high levels of Ig producing cells in secondary lymphoid tissues compared to infection with SIV and PCV-2. This increase is especially notable 3 weeks after infection and is inversely correlated with a shift from $CD4^{+}CD8^{-}$ αβ T cells to double positive (DP) T cells (see later). We believe that rapid differentiation in the B cell compartment of PRRSV-infected isolator piglets explains the hypergammaglobulinemia of all isotypes (**Figure 1**). Such a rapid differentiation process would seem to leave little time for effective germinal center (GC) activity in lymph nodes that require virus-specific helper T cells to select B cells with high affinity BCRs for PRRSV epitopes. The polyclonal expansion of the major Vβ families suggests that the extraordinary B cell expansion must be is driven by non-specific helper T cells rather than the few that are virus-specific (34).

Although the number of lymph node GC has not been quantified or characterized in PRRS, the scenario we describe predicts that antibody repertoire development in PRRSV-infected piglet would be poor or retarded since their Repertoire Diversification Index (RDI) is indistinguishable from that of fetal and germfree piglets [(35); **Figure 3A**]. Thus, germline B cell populations that differentiate to AFC cells do so with limited selection for antigen specificity. This is supported by comparative spectratypic studies of the CDR3 region of heavy chain variable region genes (HVCDR3). These show that the HVCDR3 spectrum in PRRSV-infected piglets resembles the unselected spectrum of germfree piglets whereas that for SIV and PCV-2 infected piglets shows selection of specific clones (34). Analyses of VDJ sequences from PRRSV-infected piglets display the strongly hydrophobic characteristic of an undiversified antibody repertoire [(36, 37); **Figure 3B**]. An analysis of >415 HVCDR3 sequences showed that when examined in a hydropathicity profile, 92 sequences from PRRSV-infected piglet gave peaks at 0.4 and 0.7 which most resembled newborn piglets whereas in adults and SIV-infected controls, the index shifted to 0.1–0.3

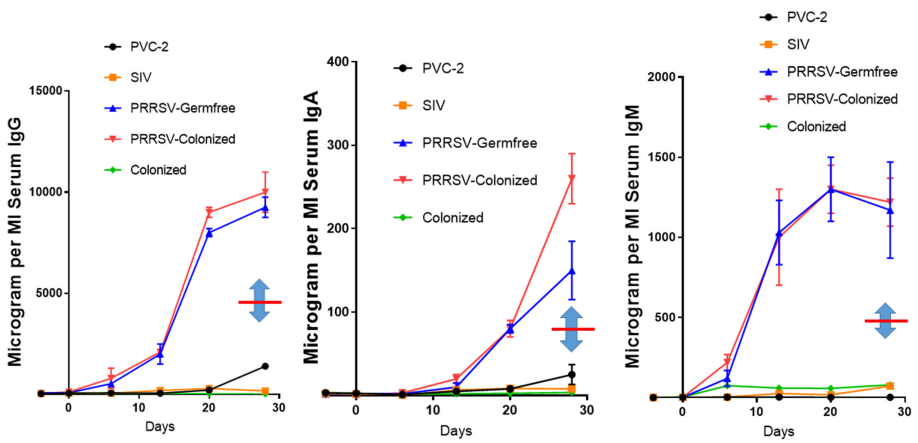

FIGURE 1 | PRRSV-induced hypergammaglobulinemia in isolator piglets. Serum IgG, IgA, and IgM levels during 4 weeks post infection in isolator piglets infected with low pathogenic PRRSV strain VR-2332, PCV-2, SIV, and germfree controls. Also shown are levels in PRRSV-infected isolator piglets that were colonized with benign *E. coli*. Double arrows indicate the mean Ig levels at 28 days postpartum in conventionally-reared piglets. Error bars are SEM. Those for PCV-2 and SIV are often smaller than the symbol and were therefore omitted. Legend is on the figure.

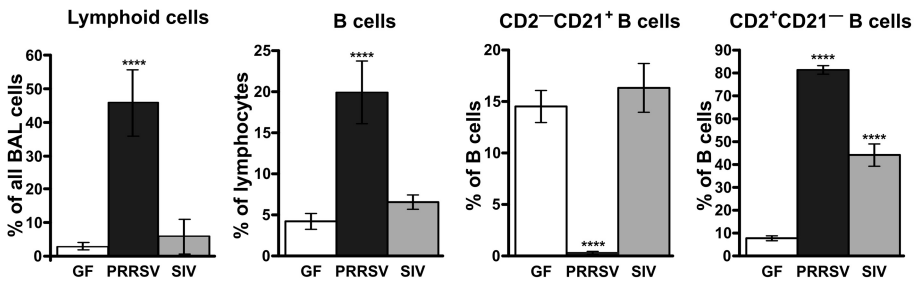

FIGURE 2 | Analysis of lymphoid cells and B lymphocyte subsets from the bronchio-alveolar lavage following infections of isolator piglets with PRRSV VR-2332 strain and SIV. Cell suspensions were analyzed according to phenotype using flow cytometry. The $CD2^{-}CD21^{+}$ subpopulation is comprised of primed/activated while $CD2^{+}CD21^{-}$ are memory/plasma cells. The functional role of these subpopulations has been described (32, 33). Statistically significant difference from GF animals are indicated by asterisks.

with a loss of clones in the 0.5–0.9 range. In the case of PRRS, the hydrophobicity appears dependent on the use of RF3 of DHA (HVD1) and many transcripts display the AMVLV motif. Thus, antibodies with hydopathicities of 0.4 and 0.7 are products of B cells that like those in newborns, have not diversified their repertoire under pressure from antigen and antigen-specific helper T cells.

In a polar environment, antibodies with hydrophobic binding sites may result in aggregation and give rise to what some call hydrophobic immune complexes that bind to ELISA plates even in the presence of Tween 20 (38, 39). Whether these are indeed immune complexes or IgG aggregates has not been tested. In any case, they are also deposited in the vasculature and kidney (9). Authentic autoantibodies are also a feature of PRRS (9) and LDV in mice (40) and include antinuclear antibodies and those directed to the Golgi. Whether aggregates or true autoantibodies, both phenomena are signs of immune dysregulation. Further support for immune dysregulation is that IDEXX tests indicate that <1% of IgG in PRRSV-infected isolator piglets is specific to PRRSV and are merely the consequence of non-specific B cell activity and may be of little virus-protective value (9).

The hypergammaglobulinemia seen in PRRSV-infected isolator piglets was a striking distraction in swine immunology until it was realized that especially polyclonal B cell activation and sometimes hypergammaglobulinemia, are common in numerous viral, bacterial and parasitic infections (41). While lymphopenia, lack of VN antibodies and hypergammaglobulinemia are symptoms of immune dysregulation, these alone are unlikely to be the cause of viral persistence. Rather there is a more compelling feature of PRRSV pathology which dates to the earliest observations on PRRSV-induced pathology that identified the thymus as one of the target organs (8, 22) and in extreme cases, reported its complete absence (41, 42). This correlated with a delayed antibody response and a decrease in helper cell-associated IL-4 (42). Thymus atrophy (**Figures 4A,C**) can explain PRRS-related lymphopenia (27, 28, 30, 42) and its severity is directly correlated with strain virulence (44, 46). Immunohistochemical studies indicate that thymocytes are

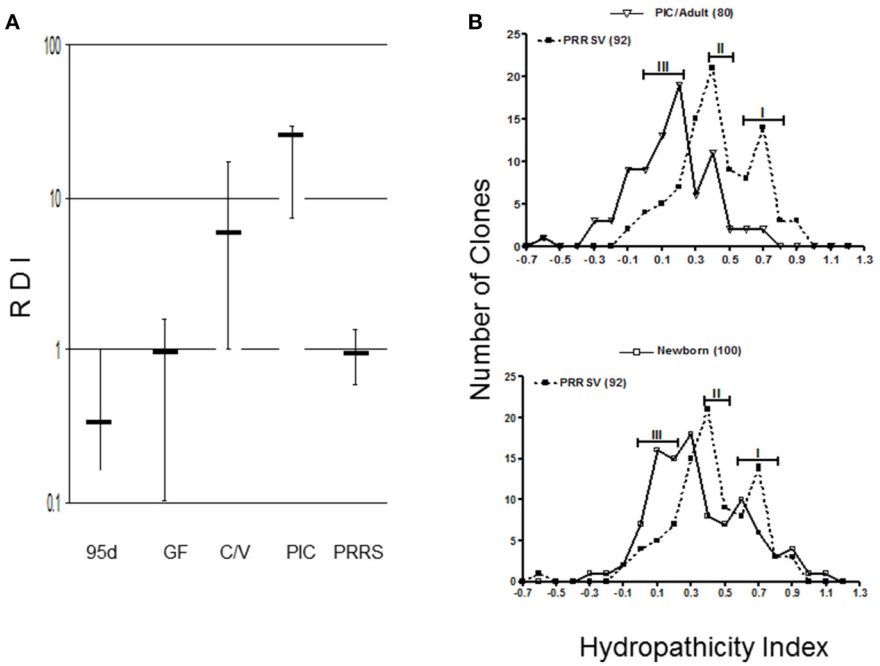

FIGURE 3 | Antibody repertoire development in PRRSV-infected isolator piglets. **(A)** Repertoire development measured as a repertoire diversification index (RDI) for various piglet groups in which error bars represent the SEM. PIC, antigenized adults; C/V, colonized SIV-infected piglets; 95d, fetal piglets at 95 days of gestation. **(B)** Hydropathicity profiles for HVCDR3 of PRRSV strain VR-2332 -infected piglets compared to antigenized adults (PIC) or GF newborn piglets. Numbers in parentheses indicate the number of clones sequenced. [From Butler et al. (35)].

undergoing apoptosis (**Figure 4F**) and flow cytometric studies show that DP thymocytes are depleted (**Figures 5A,B**). Depletion of DP thymocytes is greatest with the highly virulent HuN4 strain (**Figure 5B**) which explains why the relative proportion of immature $CD4^+$ and $CD8^+$ cells in the thymus is elevated (44). Histological studies show that the PRRSV nuclear antigen is localized to $CD14^+$ thymic cells [**Figure 4G**; (45)]. The latter observation is not surprising since PRRSV infects monocyte lineage cells and there is no evidence that cells other than TAPCs are involved in thymocyte development (53, 54). DP thymocytes are a focal point in the process of T cell "selection and education" so that damaging or deleting them through interaction with infected TAPCs would almost certainly affect the emerging T cell repertoire and its ability to recognize foreign epitopes including those of viral and other pathogens. **Figure 5C** shows that thymocyte depletion in PRRSV-infected piglets does indeed produces "holes" in the T cell repertoire. Thus, a deficiency of peripheral helper T cells due to loss of precursors $CD4^+CD8^+$ thymocytes, even if random, could explain the delay in the appearance of high affinity antibodies that can neutralize PRRSV. Interestingly there are no reports of thymic atrophy or lymph node adenopathy in EAV and this arterivirus infection is typically resolved without persistence in contrast to PRRS (55). There are no reports of thymic atrophy in PCV-2 and SIV and as shown in **Figure 1**, these infection in isolator piglets are not associated with hypergammaglobulinemia.

In studies using isolator piglets, the level of $CD4^+CD8^-$ α/β cells in blood gradually decreases in piglets infected with the mildly pathogenic PRRSV VR-2332 compared to littermates infected with SIV and PCV-2 (34). This decrease is also seen in PRRSV-infected conventionally-reared piglets (28, 29, 43) especially using highly pathogenic strains (HP-PRRSV). Infection with both mild and HP-PRRSV strains also results in a decrease in $CD8\alpha^+$ γ/δ T cells. In both PRRS isolator piglets and conventional piglets, there is a sharp rise in $CD4^+CD8^+$ α/β T cells after 21–28 dpi. These peripheral DP cells, that express CD8α, have been regarded as either "activated" or "memory" helper T cells. The kinetics of the reciprocal decrease in $CD4^+$ and increase in these DP α/β T cells might suggest this is merely a phenotypic/differentiation event in the same $CD4^+$ T cells which may reflects a change in function. The increase in DP helper T cells parallels the increase in $CD2^+CD21^-$ AFC in the BAL suggesting they may drive terminal differentiation of B cells at this site, resulting primarily in IgA^+ cells (34).

Discussion of thymic atrophy and thymocyte deletion also needs to consider the concept of central immune tolerance. During the Critical Window of Immunological Development (13), the offspring's immune system makes numerous decisions regarding how to respond to environmental and self-antigens and these depend heavily on the action of T cells. Therefore, any impairment of T cell development can impact both antibody and CTL development and function. There are several scenarios. First, PRRSV-infected TAPCs mediate random apoptosis of developing DP thymocytes including those that recognize all foreign epitopes including those of PRRSV and other pathogens. A second possibility is that the infected TAPCs present PRRSV

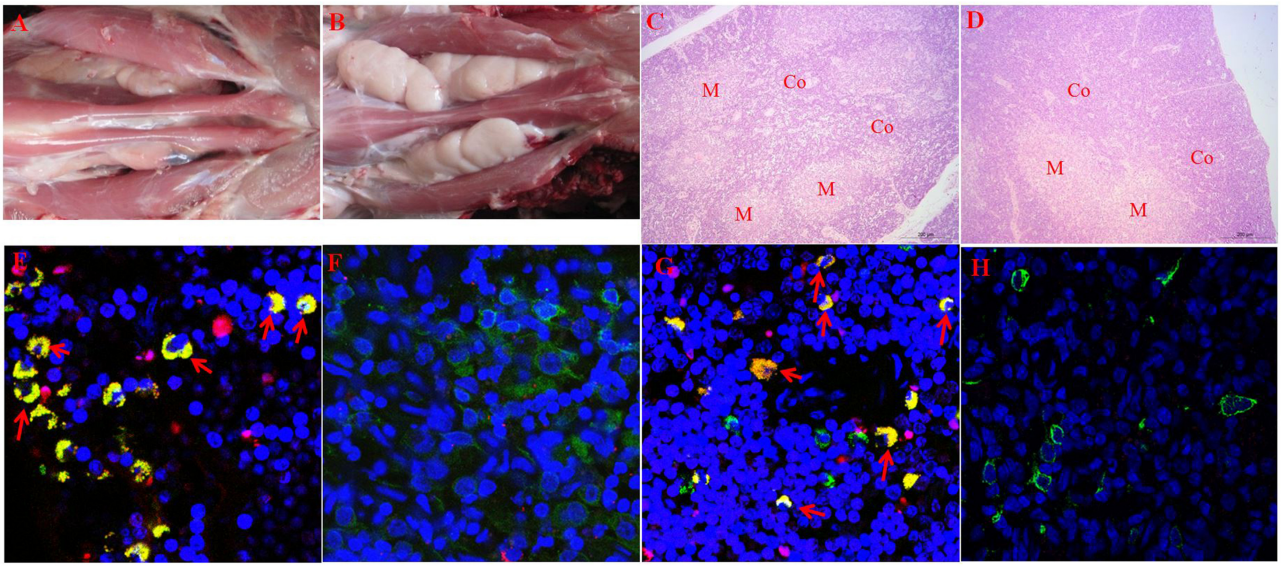

FIGURE 4 | Thymic atrophy and localization of PRRSV in thymic APCs. **(A–D)** (upper tier). Macroscopic and histological evidence of thymus atrophy in which **(A,C)** are from infected piglets. Thymocytes in the cortex (Co) are depleted and replaced by granulocytes. M, medulla. **(E–H)** (Lower tier). Immunohistology of infected and control thymi. In all sections, blue, nuclei stained with DAPI. **(E,G)** are from piglets infected with the high path HuN4 strain while **(F,H)** are from control piglets. In **(E,F)**, apoptotic cells are red, CD3+ cells are green and double-strained cells (green + red) are yellow. In sections **(G,H)**, CD14+ APC are green, those containing the PRRSV N protein are red so that infected APCs are yellow. [From Wang et al. (43), He et al. (44), and Li et al. (45)].

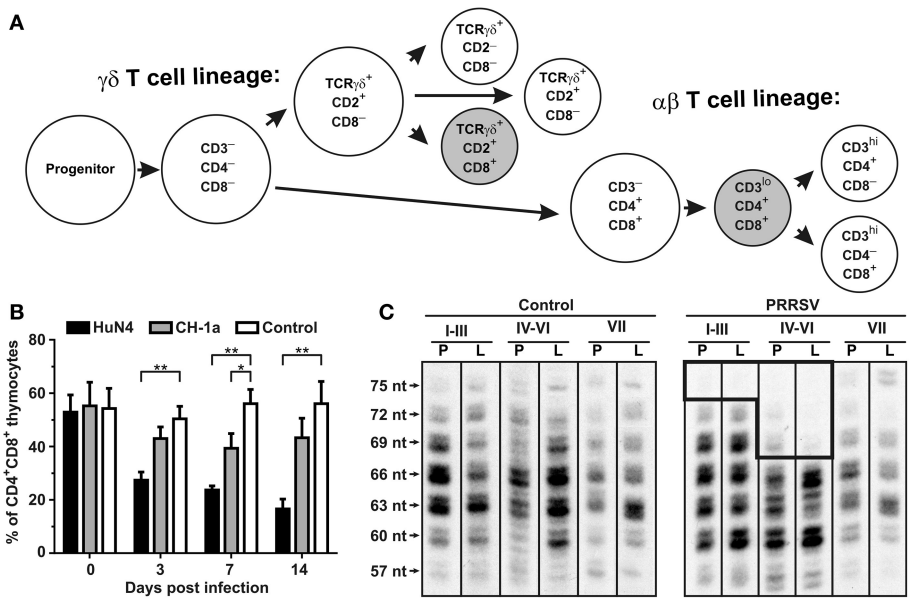

FIGURE 5 | Consequence of PRRSV infection in the porcine thymus and periphery. **(A)** Differentiation pathways of αβ and γδ thymocytes in swine (47–51). Shaded subsets are those which are significantly decreased during infection with low pathogenic VR-2332. **(B)** Flow cytometric comparison of non-infected (control) and PRRSV infected pigs with high-pathogenic strain HuN4 and low-pathogenic strain CD-1a shows that $CD4^{+}CD8^{+}$ thymocytes of αβ lineage are depleted after PRRSV infection depending on their pathogenicity (44). Asterisks (* and **) denote significance at the 0.05 and 0.01 levels, respectively. **(C)** Analysis of peripheral αβ T cells by CDR3 length analysis (52) of T cell repertoire (TCRBV) isolated from peripheral blood (indicated by P) and Broncho alveolar lavage (indicated by L) from piglets infected with the VR-2332 strain is also shown. Analysis done for Vβ I–Vβ III families (I–III), Vβ IV–Vβ VI families (IV–VI), and Vβ VII family (VII) (47). The hole in TCRβ repertoire in PRRSV infected animals is boxed. Lengths of CDR3 are indicated on left and include number of nucleotides (nt) from the 3′end of V segment to the 3′end of J segment (34).

epitopes as self-peptides to DP thymocytes triggering their apoptosis and thus eliminating them from the developing T cell repertoire. The mechanisms of DP elimination is the same as used in central tolerance induction. Such thymocytes deletion would be selective and dependent on the affinity of their TCR for particular PRRSV epitopes. A third possibility is that some elements of both mechanisms operate simultaneously to impair the ability of developing piglets to recognize PRRSV and other pathogens.

Both models can explain the persistence of PRRSV infections, the low levels of IL-4 and the CD4+ lymphopenia. The random depletion model is consistent with the increased susceptibility of piglets to other pathogens (14–17), and can explain why there are sufficient non-specific T cells to aid polyclonal B cell activation (9, 34). However, it cannot easily explain why pan-specific and anti-nucleocapsid (NC) responses are normal (23, 56) while VN antibody responses are consistently delayed (57). The last pattern is a better fit for the second scenario in that thymocytes with TCRs that tightly bind VN epitopes are deleted but not those to NC epitopes and others which bind poorly. It is well known that thymocytes with low affinity TCRs survive "thymic education." In normal individuals, these comprise the autoreactive T cell subset. In our hypothesis and scenario, they are the DP thymocytes that bind poorly to NP T cell epitopes. The third scenario is a "fail-safe" argument which includes the central tolerance scenario, and can explain all available data.

In contrast to piglets, PRRSV induced depletion of DP thymocytes in adult swine would not prevent the production of the effective VN antibodies that can transfer protection (11, 12). Adult animals, not infected with PRRSV, fetally or neonatally, would have experienced normal, undisturbed thymus development and therefore, should have developed a normal peripheral T cell repertoire. This includes T cells able to help in the selection and proliferation of B cells with high affinity BCRs for VN epitopes. If thymocyte loss occurs in adult animals, it would be too late to seriously impair the T cell repertoire. Thus, there would be sufficient peripheral T cells to recognize PRRSV epitopes including those needed for the production of high affinity VN antibodies and those of other pathogens.

Since our hypothesis revolves around thymic atrophy, we need to mention that thymic atrophy occurs in many infectious diseases and often results in apoptosis of DP thymocytes. These typically comprise 80% of all thymocytes in mice and are under heavy selective pressure in the healthy thymus so that apoptotic cells are a normal feature of thymocyte development even in normal individuals. However, thymic atrophy and apoptosis is increased in AIDS, rabies, hepatitis, pestiviruses in cattle and swine and especially parasitic diseases (58–62). Infection of the mouse thymus by highly virulent influenza can also cause thymic atrophy (63). Similar to PRRS, thymic atrophy is positively correlated with virulence but interestingly in Chagas disease, a non-virulent strain of the parasite does not induce thymic atrophy (64). In most cases, the thymic epithelium is infected or damaged and elements of the extra-cellular matrix, e.g., laminin, collagen, etc. are deposited in higher than normal amounts. In parasitic infections and AIDS, macrophages and DCs are infected, similar to what is described for the TAPCs in PRRS. It appears that a number of infectious agents target the thymus, presumably to knock-out or dampen the host's specific immune recognition system and thereby allow the pathogen to thrive. Different pathogens may use somewhat different mechanisms to attack different elements of T cell development, but all with the same overall objective.

If thymic atrophy and interference with T cell development is common to so many infectious agents, why have PRRS researchers not examined this issue given that much older studies in mice showed that *in utero* infection with LCMV and hepatitis B lead to loss of virus-specific T cells (65, 66)? Since >25 years of PRRS research has failed to identify the immune pathology of the PRRS pandemic, we chose to remind investigators of the thymic atrophy which occurs in PRRS and to emphasize its effect on development of the T cell repertoire.

Much like thymic atrophy, polyclonal B cell activation and hypergammaglobulinemia are features of many viral infections including choriomeningitis virus (LCMV), LDV and HIV-1 (41, 67, 68). As with PRRS, only a small proportion of the excessive amount of IgG is specific for the virus (9). While this has not been measured for IgM and IgA, the lack of variable region diversity in PRRS (34, 36, 37) predicts it would affect all isotypes. The phenomenon seems to be the work of non-specific T cells including those promoting isotype switch (67) and has been observed for other viruses (68–70). While perhaps driven by LCMV, HIV-1, trypanosomes and PRRSV, class-switch recombination in swine occurs even during mid-gestation in the absence of environmental antigen or infection (71). In both PRRSV and HIV-1, infection results in a peripheral T cell deficiency. Either directly or indirectly, hypergammaglobulinemia and its ensuing events rely on some form of T cell, since TCR$\beta^{-/-}$ athymic mice and those lacking CD40L, do not develop hypergammaglobulinemia.

Numerous polyclonal B cell activators have been described including parasite proteins, Staphylococcal protein A, gp120 of HIV, envelope glycoproteins of LDV and various PAMPs acting through TLRs (41). While no candidate has been described for PRRS, unpublished reports that killed PRRSV can also activate B cells, and the virus presents a B cell superantigen, may supports the latter. Naturally cytokines are involved and since PRRSV infects macrophages, IL-6 is an obvious candidate. In IL-6 deficient mice infected with murine cytomegalovirus (MCMV), polyclonal B cell activation is reduced (72). In trypanosome-induced polyclonal B cell activation, stimulation of CD11b+ cells results in production of IL-6, IL-10, and BAFF (73). The consensus view in infectious diseases is that B cell differentiation is dependent on IL-6 and IL-1 derived from macrophages and dendritic cells. IL-15 may also be involved (74).

The polyclonal B cell activation that we observed in PRRSV-infected isolator piglets has another feature similar to what is seen with HIV-1. In HIV-1, GC formation is delayed or absent in gut-associated lymphoid tissues [GALT; (67)] so that B cell development proceeds without antigen selection in the mucosal immune compartment. Unfortunately, the current literature provides no quantitative or qualitative information about lymph node GC in PRRSV-infected piglets or adult swine, the latter which develop sterilizing immunity. Of interest is that LCMV

which causes thymic atrophy and polyclonal B cell activation, is also associated with a delay in appearance of VN antibodies from 70 to 200 days (26) reminiscent of events in PRRS (24, 25).

Since polyclonal B cell activation is a common feature of various viral diseases and was pronounced in isolator piglets infected with PRRSV (**Figure 1**), it is worthwhile to ask whether it provides some protection to the host, favors the infectious virus or is just a distractive by-stander event. This subject was treated by Montes et al. (68) and the phenomenon summarized below. On the negative side, polyclonal B cell activation can be a distractive mechanism triggered by pathogens to lower the probability for pathogens to encounter a pathogen-specific B cell. On the positive side, it causes the production of natural antibodies that have a broad range of specificities, although their affinity for any particular pathogen might be low (37). Either scenario requires the host to expend energy to produce antibodies that are poorly designed to neutralize or eliminate the pathogen. Since polyclonal B cell activation appears to parallel a deficiency of antigen-specific T cells, it suggests that the phenomenon reflects a kind of "desperation" by the host, or "all-out-war" in hopes that the pathogenic threat can be handled using the "brute force" of natural antibodies.

A "dark side" feature of polyclonal activation is the appearance of autoantibodies. When secreted in large amounts, these can have pathological consequences. During "normal" immunological development of lymphocytes in fetal and neonatal vertebrates, autoreactive T cells are selected against during thymocyte development, an event which leads to *central tolerance*. One characteristic of arteriviruses is the production of autoantibodies to NP and the Golgi apparatus (9, 40). Establishing central tolerance depends on thymic TAPCs which in PRRS, are virus-infected. Hence, their ability to present antigen to the developing DP thymocytes may be impaired, allowing self-reactive T cells to leave the thymus along with those that consider PRRSV as "self." Self-reactive B cells are de-selected in bone marrow during B cell lymphogenesis but unlike T cells, can be somatically generated throughout life. Nevertheless, their expansion and differentiation still depends on antigen-specific T cells. A low level of autoreactive T and B cells is normal and only foster autoimmune disease when their numbers are abnormally elevated by high concentrations of self-antigens, which may explain their detection in PRRS.

While investigators studying PRRSV infections in conventional piglets regularly report polyclonal B cell activation and lymph node adenopathy (75), none report the hypergammaglobulinemia seen in isolator piglets (**Figure 1**). Rather, limited and unpublished data suggest that IgG levels in PRRS after 4 weeks are similar to the norm reported for healthy piglets of the same age (**Figure 1**; see double arrows). The paucity of data on this point may be because investigators decided that hypergammaglobulinemia would be masked in conventionally reared piglets that ingested a bolus of maternal colostrum. This would be true if measurements were made before 25 days after birth but would no longer be true 4 weeks postpartum (PP) when >95% of serum Ig in piglets is of *de novo* origin (**Figure 6**). The alternative and more plausible

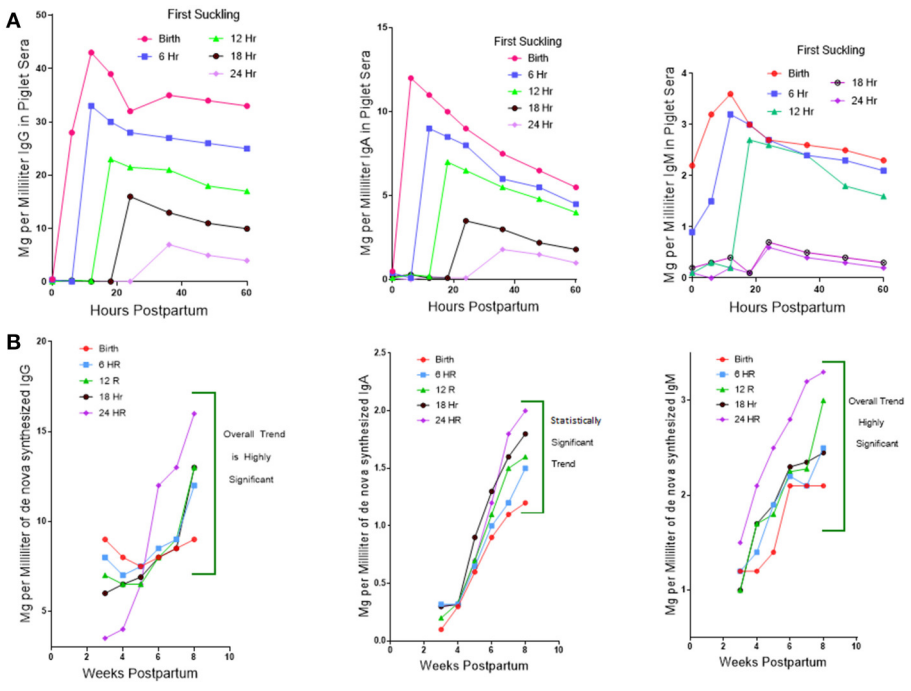

FIGURE 6 | Regulation of *de novo* Ig synthesis in suckling piglets by IgG of maternal origin. **(A)** (Top). Serum IgG levels in piglets for which suckling was delayed in 6 h interval for up to 24 h. postpartum (PP). Legend on figure. Error bars eliminated to remove clutter. **(B)** (Bottom). The level of *de novo* synthesis of IgG, IgM, and IgA 4–8 weeks PP in piglets in which suckling was delayed at 6 h intervals for up to 24 h. Error bars removed to avoid clutter.

explanation is that hypergammaglobulinemia is weak, absent or easily overlooked in PRRSV-infected conventionally-reared piglets. Unlike isolator piglets, they receive colostrum. Therefore, it is less interesting to speculate on what causes polyclonal B cell activation in PRRSV-infected isolator piglets and in other infections, than to address the question as to why polyclonal B cell activation does not progress to hypergammaglobulinemia in PRRSV-infected conventionally-reared piglets. This question is the basis of our second hypothesis.

A clue as to why hypergammaglobulinemia has not been reported in conventionally-reared piglets comes from work done 30–40 year ago (76). In these older studies, delaying suckling at 6 h intervals during the first 24 h. Postpartum (PP) resulted in a progressive decrease in the amount of maternal Igs that enter the blood of newborn specific pathogen free (SPF) piglets (**Figure 6A**). This occurs because gut closure starts at birth and progressively increases so by 24 h. PP only fragments of maternal IgG can be found in serum (77). Over the same period, the concentration of Igs in porcine colostrum progressively decreases from >90 mg/ml at birth to< 20 mg/ml at 24 h (78). In SPF piglets given a bovine-based milk replacer (MR) *de novo* Ig synthesis is spontaneous, apparently due to non-pathogenic environmental stimuli. At day 20 PP, 50% of serum IgG is of *de novo* origin, and this rises to 81% on day 25 PP and >95% on day 30 PP. Hence, at 4 weeks PP, virtually all serum Igs are of *de novo* origin. **Figure 6B** shows that *de novo* synthesis of IgG, IgM, and IgA after 4 weeks PP in suckling SPF piglets is inversely proportional to the amount of maternal IgG absorbed from colostrum (76). Since other factors in colostrum might explain this results, SPF piglets were reared in an autosow facility and raised on maternal colostrum or a bovine-based milk replacer (MR) to which purified swine IgG was added in various amounts. **Figure 7** shows that the level of serum IgG after 8 weeks in piglets that received only the MR were two-fold higher that animals receiving colostrum and that administration of just 3 g total of purified swine IgG, reduced the level of *de novo* synthesis to that seen in piglets receiving colostrum [(76); **Figure 6A** vs. **B**]. Three grams is only 20% of the amount of IgG that is provided in colostrum, yet it is enough to suppress *de novo* synthesis to the level seen in piglets receiving porcine colostrum. The spontaneous increase in *de novo* IgG synthesis in piglets receiving only the MR was not associated with any clinical disease. IgG dependent down-regulation of B cell activity is well-documented (79, 80) and has been explained as idiotypic network regulation (81–84). The T15 idiotypic system has been described for those wishing to test the idiotypic regulation hypothesis in swine (85). It is noteworthy that piglets reared on the MR were ingesting and absorbing large amounts of all bovine Igs (86), yet this bovine IgG did not suppress *de novo* Ig synthesis in these piglets, an observation consistent with the view that few idiotypes cross species lines.

In addition to the effect of maternal IgG on *de novo* IgG synthesis in suckling piglets, it was also observed that colostrum stored at −20 C for 1 month to 8 years, prior to use in rearing SPF piglets in the autosow facility, resulted in substantial loss of down-regulatory capacity [(86); **Figure 8**]. Immunoglobulin levels were unaffected by storage over any time period. While

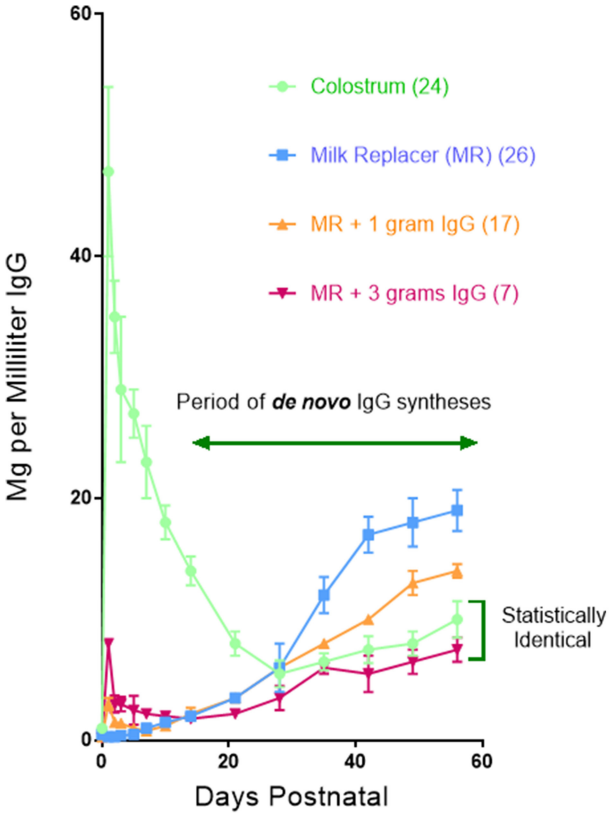

FIGURE 7 | The concentration of IgG in the sera of piglets reared in an autosow facility. Piglets were reared on porcine colostrum or a bovine-based milk replacer (MR) to which each piglet received either 1 or 3 g of purified swine IgG during the first day. Legend is on the figure. Numbers in parentheses indicate the number of piglets in each group. Error bars are SEM. From Klobasa et al. (76).

storage has no significant effect 6–7 weeks PP on *de novo* IgM synthesis, it suppressive effect 2 weeks PP was striking (**Figure 8**). Loss of down-regulation at the time was ascribed to labile unidentified regulatory factors.

It was not until the period from the 1990s, that reports began to surface on the relatively high levels of cytokines in lacteal secretions of a number of species (33). Those in highest concentrations were TGFβ, IL-10, CSF, and EGF. All are major modulators of T cell activity and are delivered in large amounts to the newborn where they mediate the transformation of helper T cells into regulatory T cells (Tregs). Once referred to as "suppressor T cells," these Tregs secrete both IL-10 and TGFβ that control B cell activation and expansion. These and other cytokines in porcine colostrum are absorbed into the sera of suckling piglets (33). These investigators also showed that TGFβ significantly reduced the ability of LPS to generate Ig secreting cells *in vitro*. In human infants these can dampen the host response to beneficial members of the gut microbiome and to food antigens like maternal milk proteins for which little central tolerance is developed. In the veterinary world, cows forced to "hold their milk" develop local edema which then forces milk proteins to enter the blood where they are recognized

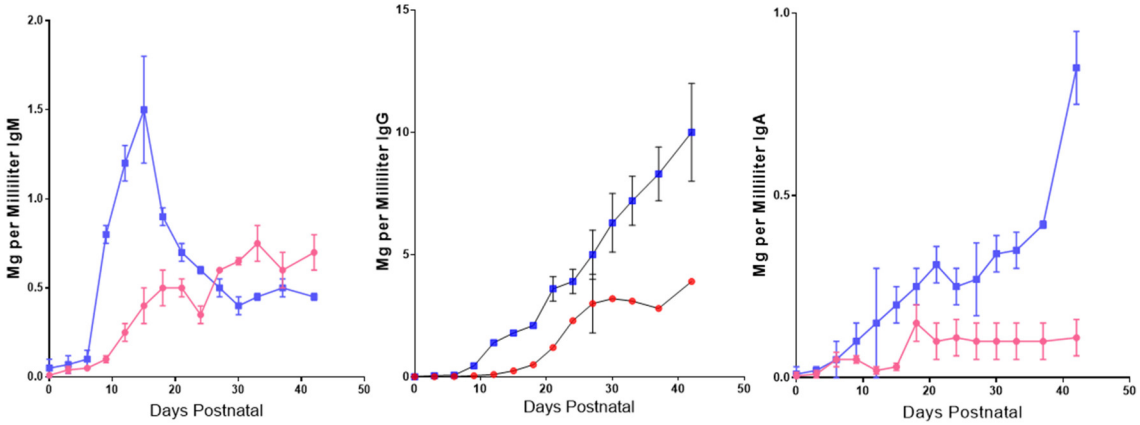

FIGURE 8 | Effect of labile factors in colostrum on *de novo* Ig synthesis in piglets. Piglets were reared in an autosow facility on fresh colostrum or colostrum frozen −20 C for 1–8 years. Length of storage had no effect so data from all three storage times were pooled. ■ = stored ($n = 24$) ● = fresh ($n = 9$). Error bars are SEM. Differences after 12 days PP for IgG and IgA were highly significant ($p < 0.05$) For IgM, differences were significant from 9 to 23 days PP ($p < 0.05$). From Klobasa et al. (86).

as foreign and can produce lethal anaphylactic shock (87). All four of the immune regulatory factors mentioned above are directly or indirectly immunosuppressive. Porcine, bovine and human colostrum deliver 40–400 micrograms of TGFβ daily to the newborn gastrointestinal tract (GIT). Porcine colostrum contains 1.5 mg/ml of EGF and when delivered experimentally, promotes the development of Tregs and also drives IgA switch recombination in the mucosal immune system (88). These regulatory factors have been shown to be important in pediatrics medicine and have been used in arguments supporting the importance of breast-feeding (89, 90).

In summary we believe the suppressive effect of colostrum (**Figure 6**) can be attributed to IgG (**Figure 7**) as well as to labile colostral factors (**Figure 8**) including cytokines like TGFβ and IL-10. These colostral factors can collectively explain why hypergammaglobulinemia has not been reported in conventionally-reared PRRSV-infected piglets.

This hypothesis article has mostly focused on the immunological pathway that normally results in VN antibodies which in turn leads to the establishment of sterilizing immunity. Our emphasis on the antibody aspect is because the delay in forming VN antibodies is a widely-cited feature by investigators and because almost every study on PRRS involves some measurement of antibody activity. However, any PRRSV-induced deficiency in the T cell repertoire would also cause a deficiency of the virus-specific CTLs that are needed to eliminate virus-infected cells. While less discussed, a CTL deficiency would equally contribute to persistence of the infection.

The purpose of this article has been to assimilate observations made in the past 25 years in an effort to develop a testable hypothesis that could move PRRS research forward and to encourage investigators to test it. Currently, investigators appear stuck on the very first step of the scientific method, i.e., the accumulation of phenomena such as thymic atrophy. We believed that construction of a testable hypothesis could help others to characterize the mechanism of PRRS-induced immune dysregulation and pathogenesis. We believe that the continued development of subunit vaccines or those based on attenuated virus, will remain a partial fix until the mechanism of immune dysregulation is known. Thus, we encourage PRRS investigators to design and perform experiments like those described in the next section of this article that can address critical tenets of our hypothesis. Should our hypothesis be confirmed, namely that the PRRSV interferes with development of the T cell repertoire in a manner that prevents the piglet from recognizing neonatal pathogens, it could shift emphasis to development of vaccines or other treatments that block this interference. Given that older animals develop sterilizing immunity, "holding the block" on the CD163 receptor on TAPCs or disrupting it until the piglet can complete development of their normal T cell repertoire, would be a step in the right direction.

MATERIALS AND METHODS

Previously Published Data

With exception of some new data presented in **Figure 5**, all of the methods employed and materials used in obtaining the data presented are provided in the cited publications. In regard to **Figure 5**, samples collected during previously published experiment (34) from animals infected by PRRSV strain VR-2332 were used as a starting material. Frozen material included cDNA prepared using random hexamer primers on total RNA from cell suspensions isolated using TRI Reagent according to a protocol recommended by the manufacturer (Sigma-Aldrich). Analysis of these samples are described below.

RNA Isolation, PCR Amplification and CDR3 Length Analysis

Each cDNA preparation was amplified in three concurrent analyses for one of three Vβ super-families (VβI–VβIII families, VβIV–VβVI families, and VβVII family) (34, 47). The 1st round

PCR targeted the original cDNA preparation while the 2nd round PCR targeted the 1st round PCR products. After checking PCR product on 1.5% agarose gels stained by GelRed, the diversity of the Vβ CDR3 regions was inspected by CDR3 length analyses. Technically, the second round of PCR products for each Vβ superfamily was subjected to the 3rd round of PCR that involved incorporation of radioactive adenosine 5'-ATP γ-32P triphosphate nucleotide labeled Cβ primer (34). The products were separated on sequencing gels that were subsequently dried and their radioactive images were obtained by Storage Phosphor Screens BAS-IP MS scanned in fluorescent Image Analyser FLA-7000 (Fujifilm Corporation, Yokyo, Japan). All primers and PCR conditions used for amplifications were published earlier (34).

CONFIRMING OBSERVATIONS AND TESTING HYPOTHESES

Verification of Basic Observations

Figures 4, **5** summarize key observations that underlie our major hypothesis. Before proceeding to undertake major and perhaps costly experiments to test it, we encourage others to confirm and extend our observations. Those with existing tissue specimens might compare the number of GCs in PRRSV-infected vs. a variety of control piglets. Such additional observations may help to justify more defined studies like those described below. Verification studies should also focus on establishing a more definitive phenotype for the cells we have referred to as TAPCs and which are positive for the PRRSV NC.

Testing the Hypotheses

Described below are four studies that test tenets of our major hypothesis plus one that tests our secondary hypothesis.

1. PRRSV infection reduces the size of the specific T cell repertoire.

Construct a series of tetramer assays using T cell epitopes for PRRSV, SIV, and ovalbumin (OVA). The latter can be adapted from murine experiments. Infect groups of conventional and/or isolator piglets with moderately virulent PRRSV or SIV. Two to 3 weeks later, immunize half of each group plus uninfected controls with OVA in Freund's adjuvant. After boosting, determine for each group/subgroup the proportion of T cells recovered from various sites that recognize PRRSV, SIV, or OVA in tetramer assays. We predict that a lower proportion of T cells recognize PRRSV than SIV and that PRRSV infection, but not infection with SIV, significantly reduces the number of OVA-specific T cells.

2. Loss of T cells in PRRSV-infected piglets is selective.

Should it be shown in the above experiment that thymic atrophy is associated with a reduced functional T cell repertoire, it is important to determine whether this has been selective for PRRSV epitopes. Using the same tetramer methods or something equivalent, the T cell repertoire of infected piglets and control piglets should be compared using a spectrum of candidate T cell epitopes such as those for NC and GP5 and others considered important for providing help in production of VN antibodies. We predict that deletion of T cells from the repertoire will be selective and may favor deletion of those involved in the production of VN antibodies.

3. Helper T cell-rich germinal centers (GCs) are greatly reduced in PRRS.

Newborn SPF piglets should be infected with PRRSV or SIV, and sacrificed 20 dpi or at 30 dpi if challenged with virus or vaccine. Immunohistochemical analyses of peripheral lymphoid tissues, especially including the tracheal bronchial lymph nodes, can them be examined for germinal centers using AID as a marker and appropriate mAbs to test for co-localization of DP, activated T cells.

4. Non-neutralizing antibodies in PRRS are of low affinity.

Using several purified PRRSV B cell epitopes especially recognized VN epitopes, develop a BiaCore or modified ELISA assay to measure absolute and/or relative affinity of IgG antibodies produced by conventional PRRSV-infected piglets. Develop similar assays for SIV. We predict that the antibodies to VN epitopes of PRRSV will be of lower affinity than those to SIV and when used in *in vitro* VN assays, they will behave poorly compared to those against SIV.

5. Colostral factors reduce hypergammaglobulinemia in PRRSV-infected piglets.

This experiment is designed to test our secondary hypothesis that colostral factors down-regulate B cell activity in newborn piglets. Recover two or more litters of colostrum-deprived, Caesarian derived (CDCD) piglets from genetically diverse backgrounds and rear them under SPF conditions. Allow a mixture of half to suckle a surrogate sow. Infect half of the piglets in the suckling group and half in the non-suckling group with a mildly pathogenic PRRSV. Measure serum IgG levels on a daily/weekly schedule. We predict that serum IgG levels 30 days postpartum in PRRSV-infected piglets allowed to suckle will be significantly lower than in PRRSV-infected piglets denied colostrum. This experiments allows for numerous permutation and advanced studies that are not discussed here.

AUTHOR CONTRIBUTIONS

GW, YL, and XC contributed and organized **Figures 4**, **5** (in part). JB drafted the manuscript and contributed **Figures 1**, **3**, **6**, **7**, **8**. MS and KS provided the data summarized in **Figures 2**, **5** and its interpretation.

FUNDING

Work in the Peoples Republic of China was supported by grants to GW from State Key Laboratory of Veterinary Biotechnology Foundation [grant number SKLVBP2018002], and the Heilongjiang Province Natural Science Foundation of China [grant number C2016068]. Work from the Czech

Republic was supported by the Czech Science Foundation Grant 16-09296S and acknowledges contributions from Miroslav Toman (Brno) where data shown in **Figure 5** was collected. Work reviewed by JB was supported by the National Pork Board and the National Science Foundation of the USA [MCB 0077237].

REFERENCES

1. Allende R, Laegieid WW, Kutish GF, Galesta JA, Wills RW, Ososrio FA. Porcine reproductive and respiratory syndrome virus: description of persistence in individual pigs upon experimental infection. *J Virol*. (2000) 74:10834–7. doi: 10.1128/JVI.74.22.10834-10837.2000
2. Calvert JG, Slade DE, Shields SL, Jolie R, Mannan RM, Ankenbauer RG, et al. CD163 expression confers susceptibility to porcine reproductive and respiratory syndrome viruses. *J Virol*. (2007) 81:7371–9. doi: 10.1128/JVI.00513-07
3. Whitworth KM, Rowland RR, Ewen CL, Trible BR, Kerrigan MA, Cino-Ozuna AG, et al. Gene-edited pigs are protected from porcine reproductive and respiratory syndrome virus. *Nat Biotechnol*. (2006) 34:20–2. doi: 10.1038/nbt.3434
4. Butler JE. Immunoglobulins of the mammary secretions. In: Larson BL, Smith V, editors. *Lactation, a Comprehensive Treatise*. New York, NY: Academic Press (1974). p. 217–55.
5. Butler JE, Wertz N, Sinkora M. Antibody repertoire development in swine. *Annu Rev Anim Biosci*. (2017) 5:255–79. doi: 10.1146/annurev-animal-022516-022818
6. Kristiansen M, Graversen JH, Jacobsen C, Sonne O, Hoffman HJ, Law SK, et al. Identification of the haemoglobin scavenger receptor. *Nature*. (2001) 409:198–201. doi: 10.1038/35051594
7. Novakovic, P, Harding JC, Al-Dissi AN, Detmer SE. Type 2 porcine reproductive and respiratory syndrome virus infection increase apoptosis at the maternal-fetal interface in late gestation pregnant gilts. *PLoS ONE*. (2017) 12:e0173360. doi: 10.1371/journal.pone.0173360
8. Rowland RRR, Lawson S, Rossow K, Benfield DA. Lymphotropism of porcine reproductive and respiratory syndrome virus replication during persistent infection of pigs originally exposed to virus *in utero*. *Vet Microbiol*. (2003) 96:219–35. doi: 10.1016/S0378-1135(03)00246-3
9. Lemke CD, Haynes JS, Spaete R, Adolphson D, Vorwald A, Lager K, et al. Lymphoid hyperplasia resulting in immune dysregulation is caused by porcine reproductive and respiratory syndrome virus infection in neonatal pigs. *J Immunol*. (2004) 172:1916–25. doi: 10.4049/jimmunol.172.3.1916
10. Sun X-Z, Lager KM, Tobin G, Nara P, Butler JE. Antibody repertoire development in fetal and neonatal piglets. XXIII. Fetal piglets infected with a vaccine strain of PRRS virus display the same immune dysregulation seen in isolator piglets. *Vaccine*. (2012) 30:3646–52. doi: 10.1016/j.vaccine.2012.03.038
11. Robinson S, Schwartz J, Murtaugh M. Humoral response to porcine reproductive and respiratory syndrome virus. *10th International Veterinary Immunology Symposium (IVIS)* Abstract P05.17, Milan (2013). p. 82.
12. Osorio FA, Galeota JA, Nelson E, Brodersen B, Doster A, Wills R, et al. Passive transfer of virus-specific antibodies confer protection against reproductive failure induced by a virulent strain of porcine reproductive and respiratory syndrome virus and establishes sterilizing immunity. *Virology*. (2002) 301:9–20. doi: 10.1006/viro.2002.1612
13. Butler JE, Sinkora M, Wertz N, Holtmeier W, Lemke CD. Development of the neonatal B- and T-cell repertoire in swine: implications for comparative and veterinary immunology. *Vet Res*. (2006) 37:417–41. doi: 10.1051/vetres:2006009
14. Done SH, Paton DJ. Porcine reproductive and respiratory syndrome: clinical disease, pathology and immunosuppression. *Vet Rec*. (1995) 136:32–5. doi: 10.1136/vr.136.2.32
15. Van Reeth K, Nauwynck H, Pensaert M. Dual infections of feeder pigs with porcine reproductive and respiratory syndrome virus followed by porcine respiratory coronavirus or swine influenza virus: a clinical and virological study. *Vet Microbiol*. (1996) S48:325–35. doi: 10.1016/0378-1135(95)00145-X
16. Wills RW, Gray JT, Fedorka-Cray PJ, Yoon KJ, Ladely S, Zimmerman JJ. Synergism between porcine reproductive and respiratory syndrome virus (PRRSV) and Salmonella choleraesuis in swine. *Vet Microbiol*. (2000) 71:177–92. doi: 10.1016/S0378-1135(99)00175-3
17. Feng W, Laster SM, Tompkins M, Brown T, Xu JS, Altier C, et al. *In utero* infection by porcine reproductive and respiratory syndrome virus is sufficient to increase susceptibility of piglets to challenge by *Streptococcus suis* type II. *J Virol*. (2001) 75:4889–95. doi: 10.1128/JVI.75.10.4889-4895.2001
18. Niederwerder MC, Bawa B, Serao NVL, Trible BR, Kerrigan MA, Lunney JK, et al. Vaccination with a porcine reproductive and respiratory syndrome (PRRS) modified live virus vaccine followed by challenge with PRRS virus and porcine circovirus Type 2 (PCV2) protects against PRRS but enhances PCV2 replication and pathogenesis compared to results for non-vaccinated co-challenged controls. *Clin Vaccine Immunol*. (2015) 22:1244–54. doi: 10.1128/CVI.00434-15
19. Chand RJ, Trible BR, Rowlands RR. Pathogenesis of porcine reproductive and respiratory syndrome virus. *Curr Opin Virol*. (2012) 2:256–63. doi: 10.1016/j.coviro.2012.02.002
20. Renukaradhya GJ, Alekseev K, Jong K, Fang Y, Saif LJ. Porcine reproductive and respiratory syndrome virus-induced suppression exacerbates the inflammatory response to porcine respiratory coronavirus in pigs. *Viral Immunol*. (2010) 23:457–66 doi: 10.1089/vim.2010.0051
21. Salines ME, Barnaud E, Andraud M, Eono F, Renson R, Bourry O, et al. Hepatitis E virus chronic infection of swine co-infected with porcine reproductive and respiratory syndrome virus. *Vet Res*. (2015) 46:55. doi: 10.1186/s13567-015-0207-y
22. Feng W-H, Tompkins MB, Xu J-S, Brown TT, Laster SM, Xhang H-X, et al. Thymocyte and peripheral blood T lymphocyte subpopulation changes in piglets following *in utero* infection with porcine reproductive and respiratory syndrome virus. *Virology*. (2002) 302:363–72. doi: 10.1006/viro.2002.1650
23. Labarque GG, Nauwynck HJ, Van Reeth K, Pensaert MB. Effect of cellular changes and onset of humoral immunity on the replication of porcine reproductive and respiratory syndrome virus in the lungs of pigs. *J Gen Virol*. (2000) 81:1327–34. doi: 10.1099/0022-1317-81-5-1327
24. Lopez OJ, Osorio FA. Role of neutralizing antibodies in PRRSV protective immunity. *Vet Immunol Immunopath*. (2004) 102:155–63. doi: 10.1016/j.vetimm.2004.09.005
25. Diaz I, Darwich L, Pappatera G, Pujola J, Mateu, E. Immune response of pigs after experimental infection with a European strain of porcine reproductive and respiratory syndrome virus. *J Gen Virol*. (2006) 86:1943–51. doi: 10.1099/vir.0.80959-0
26. Eschuli B, Zellweger RM, Wepf A, Lang KS, Quirin K, Weber J, et al. Early antibodies specific for the neutralizing epitopes on the receptor binding subunit of the lymphocyte choriomeningitis virus glycoprotein fail to neutralize the virus. *J Virol*. (2007) 81:11650–7. doi: 10.1128/JVI.00955-07
27. Christianson WT, Choi CS, Collins JE, Molitor TW, Morrison RB, Joo HS. Pathogenesis of porcine reproductive and respiratory syndrome virus infection in mid-gestation sows and fetuses. *Can J Vet Res*. (1993) 57:262–8.
28. Ladinig A, Gerner W, Saalmueller A, Lunney JK, Ashley C, Harding JCS. Changes in leukocyte subsets of pregnant gilts experimentally infected with porcine reproductive and respiratory syndrome virus and relationship with viral load and fetal outcome. *Vet Res*. (2014) 45:128–40. doi: 10.1186/s13567-014-0128-1
29. Ferrari L, Canelli E, de Angelis E, Catella A, Ferrari G, Ogno G, et al. A highly pathogenic porcine reproductive and respiratory syndrome virus type 1 (PRRSV-1) strongly modulates cellular innate and adaptive immune subsets upon experimental infection. *Vet Microbiol*. (2018) 216:85–92. doi: 10.1016/j.vetmic.2018.02.001

30. Nielsen J, Botner A. Hematological and immunological parameters of 4 1/2-month old pigs infected with PRRS virus. *Vet Microbiol*. (1997) 55:289–94. doi: 10.1016/S0378-1135(96)01334-X
31. Butler JE, Weber P, Sinkora M, Baker D, Schoenherr A, Mayer B, et al. Antibody repertoire development in fetal and neonatal piglets. VIII. Colonization is required for newborn piglets to make serum antibodies to T-dependent and type 2 T-independent antigens. *J Immunol*. (2002) 169:6822–30. doi: 10.4049/jimmunol.169.12.6822
32. Butler JE, Rainard P, Lippolis J, Salmon H, Kacskovics I. The mammary gland in mucosal and regional immunity. In: Mestechy J, Strober W, Russell MW, Kelsall BL, Cheroutre H, Lambrecht BN, editors. *Mucosal Immunology*. Amsterdam; Boston, MA: Elsevier/Academic Press (2015). p. 2269–306.
33. Nguyen TV, Yuan L, Azevedo MSP, Jeong K, Gonzalez A-M, Saif LJ. Transfer of maternal cytokines to suckling piglets: *in vivo* and *in vitro* models with implications for immunomodulation of neonatal immunity. *Vet Immunol Immunopath*. (2007) 117:236–48. doi: 10.1016/j.vetimm.2007.02.013
34. Sinkora M, Butler JE, Lager KM, Potockova H, Sinkorova J. The comparative profile of lymphoid cells and the T and B cell spectratype of germ-free piglets infected with viruses SIV, PRRSV or PCV2. *Vet Res*. (2014) 45:91. doi: 10.1186/s13567-014-0091-x
35. Butler JE, Lager KM, Golde W, Faaberg KS, Sinkora M, Loving C, et al. Porcine reproductive and respiratory syndrome (PRRS): an immune dysregulatory pandemics. *Immunol Res*. (2014) 59:81–108. doi: 10.1007/s12026-014-8549-5
36. Butler JE, Lemke CD, Weber P, Sinkora M, Lager KM. Antibody repertoire development in fetal and neonatal piglets. XIX. Undiversified B cells with hydrophobic HCDR3s preferentially proliferate in PRRS. *J Immunol*. (2007) 178:6320–31. doi: 10.4049/jimmunol.178.10.6320
37. Butler JE, Weber P, Wertz N, Lager KM. Porcine reproductive and respiratory syndrome virus (PRRSV) subverts development of adaptive immunity by proliferation of germline-encoded B cells with hydrophobic HCDR3s. *J Immunol*. (2008) 180:2347–56. doi: 10.4049/jimmunol.180.4.2347
38. Even C, Hu B, Erickson L, Plagemann PG. Correlation between levels of immunoglobulins and immune complexes in plasma of C57BL6 and C57L/J mice infected with MAIDS retrovirus. *Viral Immunol*. (1992) 5:39–50. doi: 10.1089/vim.1992.5.39
39. Plagemann PG, Rowland RR, Cafruny WA. Polyclonal hypergammaglobulinemia and formation of hydrophobic immune complexes in porcine reproductive and respiratory syndrome virus-infected and uninfected piglets. *Viral Immunol*. (2005) 18:138–47. doi: 10.1089/vim.2005.18.138
40. Weiland E, Weiland F. Autoantibodies against Golgi apparatus induced by Arteriviruses. *Cell Mol Biol*. (2002) 48:279–84.
41. Ozuna AG, Rowland RR, Nietfeld JC, Kerrigan MA, Dekkers JC, Wyatt CR. Preliminary findings of a previously unrecognized porcine primary immunodeficiency disorder. *Vet Path*. (2013) 50:144–6. doi: 10.1177/0300985812457790
42. Wang G, Song T, Tu Y, Liu Y, Shi W, Wang S, et al. Immune responses in piglets infected with highly pathogenic porcine reproductive and respiratory syndrome virus. *Vet Immunol Immunopath*. (2011) 142:170–8. doi: 10.1016/j.vetimm.2011.05.004
43. Wang G, Yu Y, Zhang C, Tu Y, Tong J, Liu Y, et al. Immune response to modified live virus vaccines developed from classical or highly pathogenic PRRSV following change with a highly pathogenic PRRSV strain. *Develop Comp Immunol*. (2016) 62:1–7. doi: 10.1016/j.dci.2016.04.019
44. He Y, Wang G, Liu Y, Shi W, Han Z, Wu J, et al. Characterization of thymus atrophy in piglets infected with highly pathogenic porcine reproductive and respiratory syndrome virus. *Vet Microbiol*. (2012) 160:455–62. doi: 10.1016/j.vetmic.2012.05.040
45. Li Y, Wang G, Liu Y, Tu Y, He Y, Han Z, et al. Identification of apoptotic cells in the thymus of piglets infected with highly pathogenic porcine reproductive and respiratory syndrome virus. *Virus Res*. (2014) 189:29–33. doi: 10.1016/j.virusres.2014.04.011
46. Amarilla SP, Gomez-Laguna J, Carrasco L, Rodriquez-Gomez IM, Caridad JM, Ocerin Y, et al. Thymic depletion of lymphocytes is associated with virulence of PRRSV-1 strains. *Vet Microbiol*. (2016) 188:47–58. doi: 10.1016/j.vetmic.2016.04.005
47. Butler JE, Wertz N, Sun J, Sacco RE. Comparison of the expressed porcine Vβ and Jβ repertoire of thymocytes and peripheral T cells. *Immunology*. (2005) 114:184–93. doi: 10.1111/j.1365-2567.2004.02072.x
48. Sinkora M, Stepanova K, Sinkorova J. Different anti-CD21 antibodies can be used to discriminate developmentally and functionally different subsets of B lymphocytes in circulation of pigs. *Dev Comp Immunol*. (2013) 39:409–18. doi: 10.1016/j.dci.2012.10.010
49. Sinkora M, Sinkorova J, Holtmeier W. Development of gamma delta thymocyte subsets during prenatal and postnatal ontogeny. *Immunology*. (2005) 115:544–55. doi: 10.1111/j.1365-2567.2005.02194.x
50. Sinkora M, Sinkorova J, Cimburek Z, Holtmeier W. Two groups of porcine TCRγδ$^+$ thymocytes behave and diverge differently. *J Immunol*. (2007) 17:711–9. doi: 10.4049/jimmunol.178.2.711
51. Stepanova K, Sinkora M. The expression of CD25, CD11b, SWC1, SWC7, MHC-II, and family of CD45 molecules can be used to characterize different stages of γδ T lymphocytes in pigs. *Dev Comp Immunol*. (2012) 36:728–40. doi: 10.1016/j.dci.2011.11.003
52. Sinkora M, Sinkorova J, Stepanova K. Ig light chain precedes heavy chain gene rearrangement during development of B cells in swine. *J Immunol*. (2017) 198:1543–52. doi: 10.4049/jimmunol.1601035
53. Proietto AI, van Dommelen S, Wu L. The imprint of circulating dendritic cells on the development and differentiation of thymocytes. *Immunol Cell Biol*. (2009) 87:39–45. doi: 10.1038/icb.2008.86
54. Nunes-Alves C, Nobrega C, Behar SM, Correia-Neves M. Tolerance has its limits: how the thymus copes with infection. *Trends Immunol*. (2013) 34:502–10. doi: 10.1016/j.it.2013.06.004
55. Carossino M, Loynachan AT, Canisso IF, Cook RF, Campos JR, Nam B, et al. Equine arteritis virus has specific tropism for stromal cells and CD8+ T and CD21+ B lymphocytes but not for glandular epithelium at the primary site of persistent infection in the stallion reproductive tract. *J Virol*. (2017) 13:e00418-17 doi: 10.1128/JVI.00418-17
56. Loemba HD, Mounir S, Mardassi D, Archarabault D, Dea S. Kinetics and humoral immune response to major structural proteins of porcine reproductive and respiratory syndrome virus. *Arch Virol*. (1996) 141:751–61. doi: 10.1007/BF01718333
57. Lopez OJ, Oliveira MF, Alvarez-Garcia E, Kwon BJ, Doster A, Osoria FA. Protection against porcine reproductive and respiratory syndrome virus (PRRSV) infection through passive transfer of PRRSV-neutralizing antibodies is dose dependent. *Clin Vac Immunol*. (2007) 14:269–75. doi: 10.1128/CVI.00304-06
58. Savino, W. The thymus is a common target organ in infectious disease. *PLoS Pathog*. (2006) 2:e62. doi: 10.1371/journal.ppat.0020062
59. Markovistz R, Bertho AL, Matos DC. Relationship between apoptosis and thymocyte depletion in rabies-infected mice. *Braz J Med Bio Res*. (1994) 27:1599–603.
60. Ito M, Nishiyama K, Hyodo S, Shigeta S, Ito T. Weight reduction of thymus and depletion of lymphocytes of T-dependent areas in peripheral lymphoid tissues of mice infected with *Francicella tularensis*. *Infect Immun*. (1985) 49:812–8.
61. Falkenburg SM, Johnson C, Bauermann FV, McGill J, Palmer MV, Sacco RE, et al. Changes observed in the thymus and lymph nodes of 14 days after exposures to BVDV field strains of enhanced or typical virulence in neonatal calves. *Vet Immunol Immunopath*. (2014) 160:70–80. doi: 10.1016/j.vetimm.2014.03.018
62. Raya AI, Gomez-Villamandos JC, Bautista MJ. Role of thymic epithelial cells in lymphoid depletion after experimental infection with non-cytopathic BVDVI strain 7443. *Vet Path*. (2015) 52:291–4. doi: 10.1177/0300985814535610
63. Vogel AB, Haasbach E, Reiling SJ, Droebner K, Klingel K, Planz O. Highly pathogenic infection of the thymus interferes with T cell development. *J Immunol*. (2010) 158:4824–34. doi: 10.4049/jimmunol.0903631
64. Verinaud L, Cruz-Hoefling MA, Sakurada JK, Rangel HA, Vassalla J, Wakelin D, et al Immunodepression induced by *Trypanosome cruzi* and mouse hepatitis type 3 virus is associated with thymic apoptosis. *Clin Diag Lab Immunol*. (1998) 5:186–91.

65. Jamieson BD, Ahmed R. T cell tolerance: exposure to virus *in utero* does not cause permanent deletion of specific T cells. *Proc Natl Acad Sci USA*. (1988) 85:2265–8. doi: 10.1073/pnas.85.7.2265
66. Milich DR, Jones JE, Hughes JL, Price J, Raney AK, McLachlan A. Is a function of the secreted hepatitis Be antigen to induce immunologic tolerance *in utero*? *Proc Natl Acad Sci USA*. (1990) 87:6599–603. doi: 10.1073/pnas.87.17.6599
67. Levesque MC, Moody MA, Hwang KK, Marshall DJ, Whitesides JF, Amos JD, et al. Polyclonal B cell differentiation and loss of gastrointestinal tract germinal centers in earliest stages of HIV-1 infection. *PLoS Med*. (2009) 6:e1000107. doi: 10.1371/journal.pmed.1000107
68. Montes, CL, Acosta-Rodriquez EV, MerinoMC, Bermejo DA, Grupp A. Polyclonal B cell activation in infections: infectious agents devilry or defense mechanism of the host? *J Leuk Biol*. (2007) 82:1027–32. doi: 10.1189/jlb.0407214
69. Reina-San-Martin, B, Cosson A, Minoprio P. Lymphocyte polyclonal activation: a pitfall for vaccine design against infectious agents. *Parasitol Today*. (2000) 16:62–7. doi: 10.1016/S0169-4758(99)01591-4
70. Gao W, Wortis H, Pereira MA. The *Trypanosoma cruzi* trans-sialidase is a T cell-independent B cell mitogen and an inducers of non-specific Ig secretion. *Int Immunol*. (2002) 14:299–308. doi: 10.1093/intimm/14.3.299
71. Butler JE, Sun J, Weber P, Ford SP, Rehakova Z, Sinkora J, et al. Antibody repertoire development in fetal and neonatal piglets. IV. Switch recombination, primarily in fetal thymus occurs independent of environmental antigen and is only weakly associated with repertoire diversification. *J Immunol*. (2001) 167:3239–49. doi: 10.4049/jimmunol.167.6.3239
72. Karupiah G, Sacks TE, Klinman DM, Fredrickson TN, Hartley JW, Chan JH, et al. Murine cytolomegalo virus infection-induced polyclonal B cell activation is independent of CD4+ T cells and CD40. *Virology*. (1998) 240:162–72. doi: 10.1006/viro.1997.8900
73. Montes CL, Acosta-Rodriguez EV, Mucci J, Zuriga EI, Competell O, Grupp A. A *Trypanosome cruzi* antigen signals CD11b+ cells to secrete cytokines that promote B cell proliferation and differentiation into antibody-secreting cells. *Eur J Immunnol*. (2006) 36:1474–85. doi: 10.1002/eji.200535537
74. Kacani L, Sprinzl GM, Erdei A, Dierich MP. Interleukin-15 enhances HIV-1 driven polyclonal B cell responses *in vitro*. *Exp Clin Immunogenet*. (1999) 16:162–72. doi: 10.1159/000019108
75. Lamontague L, Page C, Larochelle R, Magar R. Polyclonal activation of B cells occurs in lymphoid organs from porcine reproductive and respiratory syndrome virus (PRRSV)-induced pigs. *Vet Immunol Immunopath*. (2003) 82:165–82. doi: 10.1016/S0165-2427(01)00335-X
76. Klobasa F, Werhahn E, Butler JE. Regulation of humoral immunity in the piglet by immunoglobulins of maternal origin. *Res Vet Sci*. (1981) 31:195–206. doi: 10.1016/S0034-5288(18)32494-9
77. Werhahn E, Klobasa F, Butler JE. Investigations of some factors which influence the absorption of IgG by neonatal piglets. *Vet Immunol Immunopath*. (1981) 2:35–51. doi: 10.1016/0165-2427(81)90037-4
78. Klobasa F, Werhahn E, Butler JE. Composition of sow milk during lactation. *J Anim Sci*. (1987) 64:1458–66. doi: 10.2527/jas1987.6451458x
79. Setcavage TM, Kim VB. Inhibition of the immune response by membrane bound antibody. *J Immunol*. (1978) 121:1706–17.
80. Jarrett E, Hall E. Selective suppression of IgE antibody responsiveness by maternal influences. *Nature*. (1979) 280:145–7. doi: 10.1038/280145a0
81. Jerne NK. Toward a network theory of the immune system. *Annal Immun*. (1974) 125C:373–89.
82. Wikler M, Demeur C, Dewasme G, Urbain J. Immunoregulatory role of maternal idiotypes. Ontogeny of immune networks. *J Exp Med*. (1980) 152:1024–35. doi: 10.1084/jem.152.4.1024
83. Baz A, Hernandez A, Dematteis S, Caro H, Nieto A. Idiotypic modulation of the antibody response of mice to *Echinococcus granulosus* antigens. *Immunology*. (1995) 84:350–4.
84. Geha RS. Presence of circulating anti-idiotypic bearing cells after booster immunization with tetanus toxoid (TT) and inhibition of anti-TT antibody synthesis by auto-anti-idiotypeic antibodies. *J Immunol*. (1983) 130: 1634–9.
85. Butler JE, Cambier JC, Klobasa F. Identification and characterization of a hapten-modifiable TEPC 15 cross-reactive idiotype in swine. *Mol Immunol*. (1985) 22:1159–68. doi: 10.1016/0161-5890(85)90004-5
86. Klobasa F, Butler JE, Habe F. Maternal-neonatal immunoregulation: suppression of *de novo* immunoglobulin synthesis of IgG and IgA, but not IgM, in neonatal piglets by bovine colostrum, is lost upon storage. *Am J Vet Res*. (1990) 51:1407–12.
87. Campbell SG. Milk allergy, an autoallergic disease in cattle. *Cornell Vet*. (1970) 60:684–721.
88. DeDoare K, Bellis K, Faal A, Birt J, Munbilt D, Humphries H, et al. SIgA, TGFβ1, IL-10 and TNFα in colostrum are associated with infant Group B Streptococcus colonization. *Front Immunol*. (2017) 8:1269. doi: 10.3389/fimmu.2017.01269
89. Marek A, Zagierski M, Liberek A, Aleksandrowicz E, Korzon M, Krzykowski G, et al. TGF-beta (1), IL-10 and IL-4 in colostrum of allergic and nonallergic mothers. *Acta Biochim Pol*. (2009) 56:411–4. doi: 10.18388/abp.2009_2474
90. Kainonen E, Rautava S, Isolauri E. Immunological programming by breast milk creates an anti-inflammatory cytokine milieu in breast-fed infants compared to formula-fed infants. *Br J Nutr*. (2013) 109:1962–70. doi: 10.1017/S0007114512004229

Conflict of Interest Statement: The authors declare that the research was conducted in the absence of any commercial or financial relationships that could be construed as a potential conflict of interest.

frontiers in Immunology

ORIGINAL RESEARCH
published: 18 June 2019
doi: 10.3389/fimmu.2019.01380

Porcine Invariant Natural Killer T Cells: Functional Profiling and Dynamics in Steady State and Viral Infections

*Alexander Schäfer[1], Jane Hühr[1], Theresa Schwaiger[2], Anca Dorhoi[1], Thomas C. Mettenleiter[3], Sandra Blome[4], Charlotte Schröder[2] and Ulrike Blohm[1]**

[1] Institute of Immunology, Friedrich-Loeffler-Institut, Greifswald-Insel Riems, Germany, [2] Department of Experimental Animal Facilities and Biorisk Management, Friedrich-Loeffler-Institut, Greifswald-Insel Riems, Germany, [3] Institute of Molecular Virology and Cell Biology, Friedrich-Loeffler-Institut, Greifswald-Insel Riems, Germany, [4] Institute of Diagnostic Virology, Friedrich-Loeffler-Institut, Greifswald-Insel Riems, Germany

OPEN ACCESS

Edited by:
John E. Butler,
University of Iowa, United States

Reviewed by:
Nicolas Bertho,
INRA Biologie, Épidémiologie et Analyse de Risque en santé animale (BIOEPAR), France
Sankar Renu,
The Ohio State University, United States

***Correspondence:**
Ulrike Blohm
ulrike.blohm@fli.de

Specialty section:
This article was submitted to Comparative Immunology, a section of the journal Frontiers in Immunology

Received: 29 October 2018
Accepted: 31 May 2019
Published: 18 June 2019

Citation:
Schäfer A, Hühr J, Schwaiger T, Dorhoi A, Mettenleiter TC, Blome S, Schröder C and Blohm U (2019) Porcine Invariant Natural Killer T Cells: Functional Profiling and Dynamics in Steady State and Viral Infections. Front. Immunol. 10:1380. doi: 10.3389/fimmu.2019.01380

Pigs are important livestock and comprehensive understanding of their immune responses in infections is critical to improve vaccines and therapies. Moreover, similarities between human and swine physiology suggest that pigs are a superior animal model for immunological studies. However, paucity of experimental tools for a systematic analysis of the immune responses in pigs represent a major disadvantage. To evaluate the pig as a biomedical model and additionally expand the knowledge of rare immune cell populations in swine, we established a multicolor flow cytometry analysis platform of surface marker expression and cellular responses for porcine invariant Natural Killer T cells (iNKT). In humans, iNKT cells are among the first line defenders in various tissues, respond to CD1d-restricted antigens and become rapidly activated. Naïve porcine iNKT cells were $CD3^+/CD4^-/CD8^+$ or $CD3^+/CD4^-/CD8^-$ and displayed an effector- or memory-like phenotype ($CD25^+/ICOS^+/CD5^{hi}/CD45RA^-/CCR7^{\pm}/CD27^+$). Based on their expression of the transcription factors T bet and the iNKT cell-specific promyelocytic leukemia zinc finger protein (PLZF), porcine iNKT cells were differentiated into functional subsets. Analogous to human iNKT cells, *in vitro* stimulation of porcine leukocytes with the CD1d ligand α-galactosylceramide resulted in rapid iNKT cell proliferation, evidenced by an increase in frequency and Ki-67 expression. Moreover, this approach revealed CD25, CD5, ICOS, and the major histocompatibility complex class II (MHC II) as activation markers on porcine iNKT cells. Activated iNKT cells also expressed interferon-γ, upregulated perforin expression, and displayed degranulation. In steady state, iNKT cell frequency was highest in newborn piglets and decreased with age. Upon infection with two viruses of high relevance to swine and humans, iNKT cells expanded. Animals infected with African swine fever virus displayed an increase of iNKT cell frequency in peripheral blood, regional lymph nodes, and lungs. During Influenza A virus infection, iNKT cell percentage increased in blood, lung lymph nodes, and broncho-alveolar lavage.

Our in-depth characterization of porcine iNKT cells contributes to a better understanding of porcine immune responses, thereby facilitating the design of innovative interventions against infectious diseases. Moreover, we provide new evidence that endorses the suitability of the pig as a biomedical model for iNKT cell research.

Keywords: iNKT cells, T cells, pig, biomedical model, influenza A virus, African swine fever virus

INTRODUCTION

Biomedical research is in need of large animal models that reflect human infectious diseases better than current rodent models (1, 2). Because of the striking resemblances between porcine and human immune system and physiology, pigs could be a superior model species (3–10). In order to establish pigs as a new biomedical model species, a more detailed understanding of porcine immune responses and leukocyte subsets is strongly needed.

Leukocytes at systemic and peripheral sites are eminently important for control of microbial colonization and defense against infections by induction of protective immunity (11). One of those leukocyte subsets are invariant Natural Killer T (iNKT) cells. These cells bridge and orchestrate both untargeted innate and specific adaptive responses, which are crucial for pathogen clearance and survival. In contrast to the vast heterogeneity of T cell receptors (TCR) among conventional $CD3^+$ T cells (cTC), iNKT cells possess a semi-invariant TCR. This TCR is restricted to the non-classical major histocompatibility complex (MHC) class I-related CD1d, presenting lipid or glycolipid antigens. iNKT cells can be activated antigen-dependently with glycolipids derived from microbes or the host by TCR-CD1d interactions or antigen-independently via cytokines, mainly interleukin-(IL-)12 and IL-18 or type I interferons (IFN). The induction of cytokine expression in iNKT cells does not require classical co-stimulation, whereas iNKT cell proliferation depends on co-stimulatory signals by B7/CD28 or CD40/CD40L (12). Additionally, effector cytokines are present as immediately available preformed mRNA transcripts in iNKT cells (13). Therefore, iNKT cells rapidly proliferate and secrete effector molecules like IFNγ, IL-17 or granulocyte-macrophage colony-stimulating factor after activation (14). Moreover, they are able to lyse infected cells by perforin and Fas/FasL interaction (15–18). iNKT cells also augment B cell responses, class switching and affinity maturation independently of classical helper cells (19, 20). Several iNKT cell subsets have been identified by their expression of different transcription factors, like promyelocytic leukemia zinc finger protein (PLZF) and T-bet, most notably in mice, where they are primarily differentiated into iNKT1 ($T\text{-}bet^+/PLZF^+$), iNKT2 ($T\text{-}bet^-/PLZF^{hi}$), and iNKT17 ($T\text{-}bet^-/PLZF^{lo}$) (21–26). Differentiated subsets of human iNKT cells are not as well-defined as in mice (27).

At present, most studies focusing on porcine iNKT cells investigated the potential use of the cognate CD1d ligand α-galactosyl-C16-ceramide (αGC) as an adjuvant for vaccines against Influenza A virus (IAV) and other infectious diseases (28–32). Knowledge about phenotype, response kinetics, and functional aspects of iNKT cell responses in pigs is scarce. The antigen presentation molecules of the CD1 family are of particular importance for iNKT cells. In addition to CD1d, there are four other members in the CD1 family, CD1a, CD1b, CD1c, and CD1e. All of these molecules are expressed in pigs as well as in humans, while mice lack proteins other than CD1d (33). It has been shown that expression of CD1d on thymocytes is required for iNKT cell development, in mice (34) as well as in pigs (35). Murine CD1d tetramers loaded with the αGC analog PBS57 have been shown to detect porcine iNKT cells (7, 36). Their frequency is typically between 0.01 and 1% among $CD3^+$ T cells, thereby resembling human iNKT cell frequencies (7, 28). Porcine iNKT cells are $CD8\alpha^+$ or $CD8\alpha^-$ but lack expression of CD4 in most tissues (28, 29, 37). In contrast to human and murine iNKT cells, naïve porcine iNKT cells express high levels of CD44, as most lymphocytes in swine (38, 39). Moreover, the iNKT cell-specific transcription factor PLZF is highly expressed in porcine iNKT cells (36). Some evidence indicates that iNKT cells expand upon stimulation of porcine PBMC with αGC (29, 36). Using next generation sequencing, it has recently been shown that porcine iNKT cells predominantly use Vα and Jα segments homologous to the Vα24-Jα18 and Vα14-Jα18 rearrangements used in humans and mice, respectively (40). Moreover, molecular investigations demonstrated that the antigen-binding domain of the invariant α-chain, CDR1α, is conserved between pigs and humans (40). This indicates that responses of porcine iNKT cells mimic responses of human iNKT cells, thereby further underlining the suitability of the pig as a biomedical model species for human iNKT cells.

In order to comprehensively understand porcine iNKT cells and advance research, we investigated their phenotype, dynamics and functional responses in-depth in steady state and during IAV and African swine fever virus (ASFV) infection.

MATERIALS AND METHODS

Pigs and Biological Samples

In total 13 German landrace pigs for IAV and 12 for ASFV experiments were obtained from a commercial breeding unit (BHZP-Basiszuchtbetrieb Garlitz-Langenheide, Germany) with high biosecurity standards and hygiene (free of IAV and Porcine reproductive and respiratory syndrome virus among others). Samples for the investigation of age-dependent changes in iNKT cell frequency were obtained during routine veterinary check-ups from the same commercial breeding unit (BHZP-Basiszuchtbetrieb Garlitz-Langenheide, Germany).

Swine (Danish landrace/Danish Large White/Danish Duroc hybrid) used for *in vitro* experiments involving PBMC, were kept at the Friedrich-Loeffler-Institut (FLI), Greifswald-Insel Riems under conventional conditions.

Viruses and Infection Experiments

Influenza virus A/Bayern/74/2009 was propagated on Madin-Darby canine kidney cells (MDCKII) cells in MEM supplemented with 0.56% bovine serum albumin, 100 U/ml Penicillin, 100 μg/ml Streptomycin and 2 μg/ml L-1-Tosylamide-2-phenylethyl chloromethyl ketone (TPCK)-treated trypsin (Sigma-Aldrich, USA). For viral titration by $TCID_{50}$ assay, serial 10-fold dilutions of virus suspensions were prepared, added to MDCKII cells in 96-well plates, and incubated for 3 days at 37°C and 5% CO_2. Cytopathic effect was microscopically evaluated. Titers were calculated according to Spearman-Kärber (41, 42). Four-week-old piglets were obtained from a commercial breeding facility directly after weaning. Absence of acute IAV infection of pigs used for the IAV study was confirmed by real-time PCR (AgPath.IDTM One-Step RT-PCR Kit, Applied Biosystems, USA) of nasal swabs prior to transport to the FLI (modified from Spackman et al. (43)). IAV infection was performed 3 weeks after transport to our facility by intranasal administration of 2 ml virus suspension (10^6 $TCID_{50}$/ml) using mucosal atomization devices (Wolfe Tory Medical, USA).

ASFV Armenia08 was propagated and titrated using mature porcine PBMC-derived macrophages as previously described (44). For back titration, virus hemadsorption test was performed by endpoint titration of the diluted inoculation virus. In brief, 100 μl virus dilution were incubated for 24 h on PBMC-derived macrophages in 96-well plates. Thereafter, 20 μl of a 1% homolog erythrocyte suspension were added and hemadsorption read after 24 and 48 h. All samples were tested in quadruplicates. Hemadsorbing units (HAU) were used for read-out. For infection, 2 ml macrophage culture supernatant containing $10^{6.25}$ HAU ASFV Armenia08 were inoculated oro-nasally. All work involving ASFV was done in the high containment facility ($L3^+$) at the Friedrich-Loeffler-Institut.

Cell Isolation and Culture

For isolation of peripheral blood mononuclear cells (PBMC), whole blood was separated by density gradient centrifugation using Pancoll (PAN-Biotech, Germany). PBMC were collected and washed with PBS-EDTA (1 mM; used for all analyses). Cell count was determined using Neubauer improved haemocytometer. Single cell suspensions from spleen and lymph nodes were prepared by mechanically disrupting tissue with a sieve. Lymphocytes from liver were isolated following a modified protocol previously described (45). In brief, liver samples were perfused with ice-cold PBS-EDTA. Perfused regions were minced with sterile scissors, resuspended in PBS-EDTA supplemented with 100 μM $CaCl_2$, and digested with Collagenase D (1 mg/ml; Sigma-Aldrich) for 40 min at 37°C. Remaining tissue was removed by short centrifugation. Cell pellet was resuspended in PBS-EDTA and used for flow cytometry. Lymphocytes from lung tissue were isolated by mincing non-perfused lung tissue, followed by enzymatic digestion as described for liver samples. Lung tissue was additionally mashed through a cell strainer with the plunger of a syringe after digestion. Unless otherwise stated, cells were cultured in Ham's F12/IMDM (1:1), supplemented with 10% fetal calf serum (FCS), 2-mercaptoethanol (50 μM), 100 U/ml penicillin, and 100 μg/ml streptomycin.

Cell Stimulation

For iNKT cell stimulation, freshly isolated PBMC were seed into round-bottom 96-well plates at a density of 10^7 PBMC/ml. αGC (Toronto Research Chemicals, Canada) dissolved in dimethyl sulfoxide (DMSO; Sigma-Aldrich, USA) or DMSO as vehicle control diluted in cell culture media were added. αGC was used at 0.1 μg/ml (low-dose) and 1 μg/ml (high-dose). Cells were incubated at 38.5°C, 5% CO_2 for the indicated time. After incubation, cells were harvested, washed with PBS-EDTA, and analyzed by flow cytometry.

For detection of IFNγ and perforin, cells were stimulated as previously described (46). After 4 days, fresh medium with αGC in the corresponding concentrations was added to the cells. After another 2 h incubation, Brefeldin A (10 μg/ml, Biolegend, USA) was added to enable intracellular accumulation of target proteins. Cells were incubated for 4 h and then stained and analyzed by flow cytometry.

For analysis of CD107a surface expression as a marker of degranulation, cells were treated as previously described (47). Briefly, freshly isolated PBMC were seed into 96-well plates at a density of 10^7 PBMC/ml and rested overnight. For antigenic stimulation, αGC was added for a final concentration of 0.1 μg/ml or 1 μg/ml. As unspecific inducers, Phorbol-12-myristat-13-acetat (PMA; Sigma-Aldrich, USA) and ionomycin (Sigma-Aldrich, USA) were added for final concentrations of 50 ng/ml and 1 μg/ml, respectively. The cells were stimulated in the presence of anti-CD107a antibodies (clone 4E9/11, Bio-Rad, USA; 4 μg/ml). After 1 h incubation, Brefeldin A (10 μg/ml), and Monensin (4 μM, Biolegend, USA) were added and the cells were incubated for another 5 h and then stained and analyzed by flow cytometry. Specific degranulation was calculated as the difference in surface expression of stimulated and control cells and is given as ΔCD107a.

For *in vitro* activation assays, porcine $CD172a^+$ cells were purified using monoclonal antibodies (cone 74-22-15) and magnetic anti-mouse IgG1 beads (BD Bioscience, USA). $CD172a^+$ cells were infected with IAV (MOI 1) or ASFV (MOI 0.1) for 48 h. Then, supernatants were collected, cleared of debris by centrifugation, and stored at −80°C until further use. Freshly isolated porcine PBMC were stimulated with the respective supernatants or 1 μg/ml αGC as a positive control for 4 days and then stained and analyzed by flow cytometry.

Cell Proliferation Assay

Freshly isolated PBMC were stained using Tag-it Violet Proliferation and Cell Tracking Dye (Biolegend, USA) according to the manufacturer's instructions. Briefly, total PBMC were

adjusted to 1×10^7 cells/ml in PBS and incubated with the Tag-it Violet Proliferation and Cell Tracking Dye at a concentration of 5 μM. Cells were incubated for 20 min at 37°C in the dark. Quenching was done by addition of cell culture media supplemented with 10% FCS. After washing, stained cells were used for visualization of iNKT cell proliferation after stimulation with αGC.

Flow Cytometry

Stainings for flow cytometry were performed using either single cell suspensions or whole blood. All incubation steps were carried out for 15 min at 4°C in the dark, unless otherwise stated. Antibodies used for flow cytometry are shown in **Supplementary Table 1**. For iNKT cell staining, first tetramers were added at the predetermined concentration (1:500) and incubated at room temperature in the dark for 30 min. Antibodies for staining of additional surface markers were added without washing and incubated with the tetramers for another 15 min. After washing, antibody staining was proceeded. Unconjugated antibodies were detected by isotype-specific fluorochrome-conjugated secondary antibodies. When whole blood or tissue samples containing erythrocytes were stained, erythrocytes were lysed after surface staining prior to fixation by lysis buffer (1.55 M NH_4Cl, 100 mM $KHCO_3$, 12.7 mM Na_4EDTA, pH 7.4, in A.dest.). For intracellular staining, cells were fixed after surface staining using the True-Nuclear Transcription Factor Buffer Set (Biolegend, USA) according to the manufacturer's instructions. Murine CD1d tetramers, empty or loaded with PBS57, were obtained from the NIH Tetramer Core Facility.

Doublets were excluded by consecutive gating FSC-W/FSC-H and SSC-W/SSC-H. Living lymphocytes were gated based on their forward-scatter (FSC) and side-scatter (SSC) properties. Live, single lymphocytes were further separated in conventional T cells (cTC; $CD3^+$/CD1d-Tet^-) and iNKT cells ($CD3^+$/CD1d-Tet^+) for subsequent analysis.

Per sample, at least 1×10^5 single cTC were recorded. BD FACS Canto II or BD LSRFortessa with FACS DIVA Software (all BD Bioscience, USA) and FlowJo V10 (Treestar, USA) were used for all analyses.

Statistical Analysis

GraphPad Prism 7 (Graphpad Software Inc., USA) was used for statistical analysis and graph creation. Normality was tested with the Shapiro-Wilk normality test. Subsequent analysis was performed with either parametric tests for normally distributed data sets or non-parametric tests for non-normally distributed data sets. For analysis of data sets with three or more groups, Repeated-measures one-way ANOVA was used to investigate statistically significant differences between the groups. Multiple comparisons were performed for differences between iNKT cells and cTC subsets, respectively. No statistical analyses were performed for differences between iNKT cells and cTC. Holm-Sidak's *post-hoc* test was used for correction of multiple comparisons. For analysis of data from the IAV and ASFV trial, ordinary one-way ANOVA with Holm-Sidak's *post-hoc* test for correction of multiple comparisons was used. For analysis of data sets of two groups, paired *t*-tests were used. Unless indicated otherwise, data is shown as mean (SD). Statistical significance was defined as $^*p < 0.05$, $^{**}p < 0.01$, $^{***}p < 0.001$, and $^{****}p < 0.0001$.

RESULTS

Naïve Peripheral Porcine iNKT Cells Are Mostly $CD8\alpha^+$ and Display an Effector- and Memory-Like Phenotype

To investigate porcine iNKT cells in peripheral blood by flow cytometry, we used murine CD1d tetramers loaded with the αGC analog PBS57 (PBS57 Tet) as previously described (7, 36). After exclusion of doublet cells, live cTC were gated as $CD3^+$/PBS57 Tet^- cells and iNKT cells were defined as $CD3^+$/PBS57 Tet^+ among the lymphocyte gate [**Figure 1A** (48)]. In healthy animals, the average iNKT cell frequency was 0.5%, comparable to frequencies in blood published earlier (36, 37). Most naïve iNKT cells expressed CD8α, while only a small amount was $CD4^+$, although a considerable proportion of iNKT cells expressed low levels of CD4 (**Figures 1B,C**). Thereby, we confirmed previous findings showing similar results (36, 37). iNKT cells expressed neither CD8β nor γδTCR (**Figure 1B**). For differentiation of iNKT cell subsets, expression of the classical T cell markers CD8α and CD4 was analyzed. The subsets were gated according to the respective expression of these markers on cTC. The major subset of peripheral iNKT cells in swine was $CD8\alpha^+/CD4^-$ ($73.7 \pm 11.9\%$; **Figure 1C**). There was no distinct $CD4^+$ population; however, a minor fraction of iNKT cells was $CD8\alpha^+/CD4^{lo}$ (DP; $3.6 \pm 1.9\%$). Moreover, there was a considerable $CD8^-/CD4^-$ (DN) population ($21.5 \pm 10.8\%$).

For further differentiation, we investigated steady state expression of surface markers that are frequently associated with an effector phenotype in mice and humans, i.e., CD5 (49), CD25 [IL-2Rα (50)], CD278 [Inducible T-cell co-stimulator, ICOS (51)], and the major histocompatibility complex class II [MHC II (52)] in naïve iNKT cells and cTC. All iNKT cells were positive for CD5 whereas only around 60% of cTC showed CD5 expression (**Figure 2A**). Around half of all iNKT cells expressed CD25 at low levels on their surface, while cTC displayed only a minor $CD25^{hi}$ fraction (**Figure 2A**). ICOS was expressed on virtually all iNKT cells, while only on a minor fraction of cTC (**Figure 2A**). MHC II was expressed on most iNKT cells at medium or high levels (**Figure 2A**). In contrast, cTC were mostly MHC II^- but the MHC II^+ fraction expressed it at comparable levels (**Figure 2A**). Because CD25 and MHC II were not expressed by all iNKT cells, we investigated which iNKT cell subset expressed the proteins (**Figure 2B**). Differential staining with CD8α revealed that both proteins were predominantly expressed on $CD8\alpha^+$ iNKT cells. DN iNKT cells showed no or low expression of CD25 and MHC II.

To investigate the functional differentiation of porcine iNKT cells, we analyzed the expression of markers regularly associated with antigen experience and memory status, CD45RA, C-C

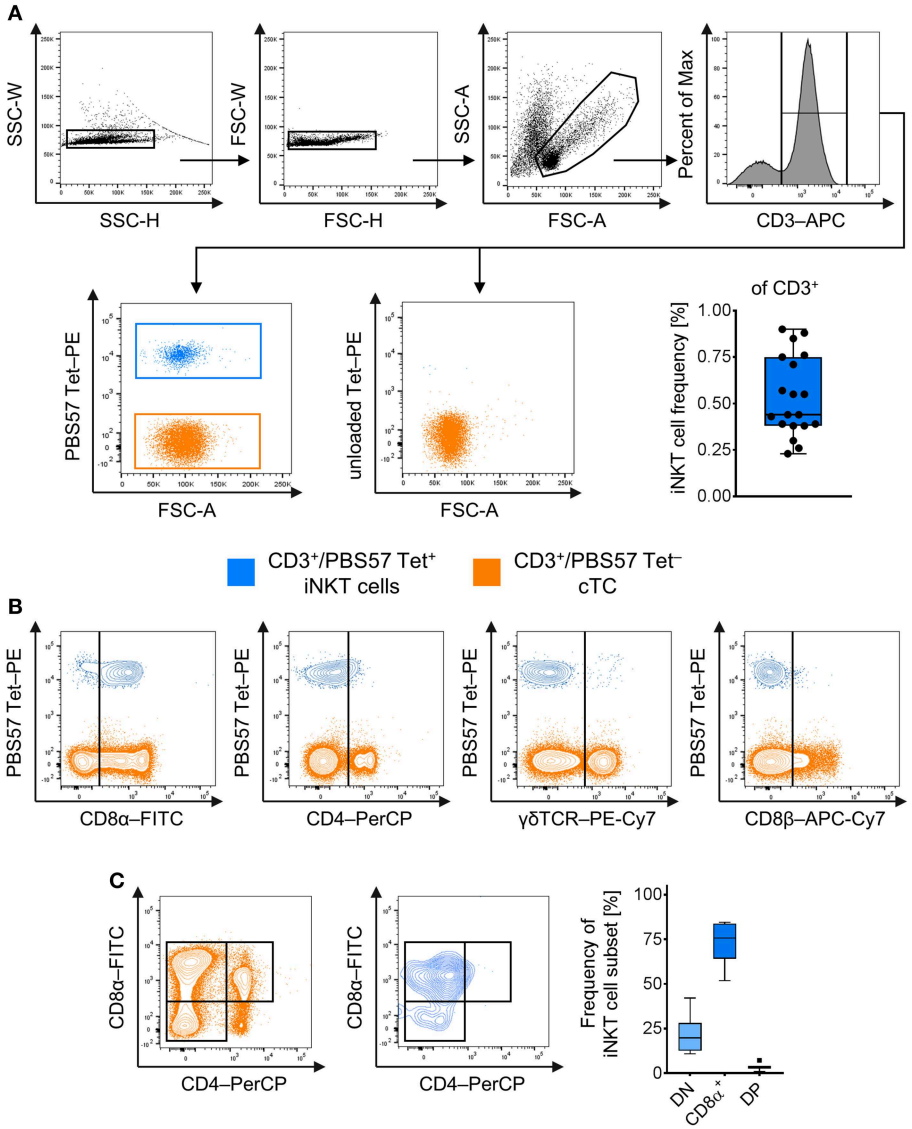

FIGURE 1 | Identification and phenotype of naïve peripheral porcine iNKT cells**.** Expression of surface markers was analyzed by flow cytometry. **(A)** Doublets were excluded by SSC-W vs. SSC-H gates, followed by FSC-W vs. FSC-H gates. Live lymphocytes were identified according to their FSC/SSC characteristics. All T cells were identified using antibodies against CD3. $CD3^+$ T cells stained with the PBS57-loaded CD1d tetramer (left plot) were defined as invariant Natural Killer T cells (iNKT; blue), tetramer-negative cells were defined as conventional T cells (cTC; orange). Unloaded tetramers served as control (right plot). Frequency of iNKT cells in peripheral blood among $CD3^+$ lymphocytes shown as Tukey box plot ($n = 19$). **(B)** Evaluation of expression of CD8α, CD4, γδTCR, and CD8β on iNKT cells and cTC. Representative plots of at least four experiments are shown. **(C)** Representative plots of CD8α and CD4 co-expression by cTC and iNKT cells. $CD8\alpha^-/CD4^-$ (DN; light blue), $CD8\alpha^+/CD4^-$ ($CD8\alpha^+$, blue), and $CD8\alpha^+/CD4^+$ (DP; dark blue) subsets among iNKT cells were identified according to their expression pattern in cTC. Frequency of iNKT cell subsets shown as Tukey box plots ($n = 7$).

chemokine receptor type 7 (CCR7), and CD27 (53–56). cTC displayed a minor fraction of naïve $CD45RA^+$ cells, while the larger fraction consisted of antigen-experienced $CD45RA^-$ cells (**Figure 2C**). $CD45RA^-$ cTC were further divided into $CD27^+/CCR7^+$ central memory cells, $CD27^+/CCR7^-$ transitional memory cells and $CD27^-/CCR7^-$ effector memory cells. There was only a minor population of $CD27^-/CCR7^+$ activated effector memory cells (**Figure 2C**). All iNKT cells were $CD45RA^-$ and thus displayed an antigen-experienced phenotype. Most iNKT cells were $CD27^+/CCR7^+$, resembling central memory cells. A second major fraction expressed CD27 but was $CCR7^-$, similar to transitional memory cells. About a third of iNKT cells was $CD27^-$ and could further be divided into equal fractions of $CCR7^-$ and $CCR7^+$, thereby differentiating subsets comparable to resting and activated effector memory cells, respectively (**Figure 2C**). Expression of CD27 and CCR7 was also investigated for co-expression with $CD8\alpha^+$. Most $CD8\alpha^+$ iNKT cells expressed CCR7 as well as CD27 (**Figure 2D**).

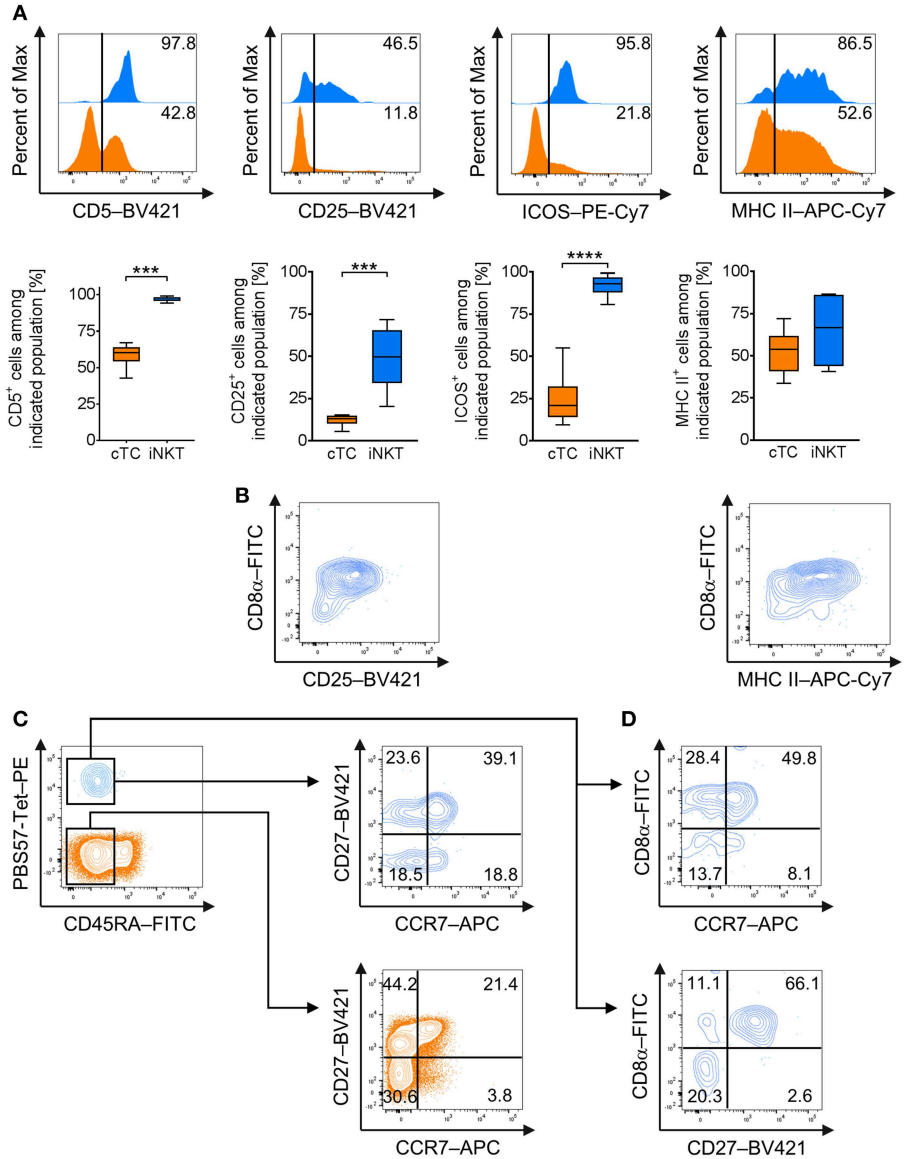

FIGURE 2 | Expression of effector and memory cell-associated markers on naïve porcine iNKT cells. Expression of surface markers associated with effector functions and memory status on naïve peripheral iNKT cells was analyzed by flow cytometry. **(A)** Representative flow cytometric plots of CD5, CD25, MHC II, and ICOS expression by iNKT cells (blue) and cTC (orange). Summarized data show frequencies of iNKT cells or cTC expressing CD5, CD25, MHC II, and ICOS (mean (SD), $n = 6$). **(B)** Representative flow cytometric plots showing differential expression of CD8a and CD25 or MHC II on iNKT cells. **(C)** Expression of CD45RA (left) on iNKT cells and cTC. CD45RA$^-$ cTC (middle) and iNKT cells (right) were further investigated for expression of CD27 and CCR7 and divided into CD27$^+$/CCR7$^+$ central memory cells, CD27$^+$/CCR7$^-$ transitional memory cells, CD27$^-$/CCR7$^-$ effector memory cells, and CD27$^-$/CCR7$^+$ activated effector memory cells. **(D)** Differential expression of CD8α and CCR7 or CD27. Representative plots and histograms of at least three experiments are shown. ***$p < 0.001$, ****$p < 0.0001$, paired t-test.

DN iNKT cells were negative for CD27 while a fraction expressed CCR7 (**Figure 2D**).

In mice, intracellular staining of transcription factors, including T-bet and PLZF, is used to define functional iNKT cell subsets iNKT1 (T-bet$^+$/PLZF$^+$), iNKT2 (T-bet$^-$/PLZF^{hi}), and iNKT17 (T-bet$^-$/PLZF^{lo}) resembling the T-helper cell populations Th1, Th2, and Th17, respectively (21–26). Currently, there is no such differentiation available for porcine iNKT cells. Therefore, we investigated the expression of T-bet and PLZF in porcine iNKT cells. We confirmed that porcine iNKT cells express higher levels of PLZF than cTC (**Figure 3A**). Moreover, we detected expression of T-bet in a subset of porcine iNKT cells (**Figure 3A**). Co-expression of T-bet and PLZF was used to define iNKT cell subsets corresponding to the ones described in other species (**Figures 3B–E**). In naïve swine, the largest iNKT cell subset had a T-bet$^+$/PLZF$^+$ phenotype and was therefore defined as iNKT1 (49.8 ± 14.8%). The second major group was T-bet$^-$/PLZF^{hi}, thereby resembling

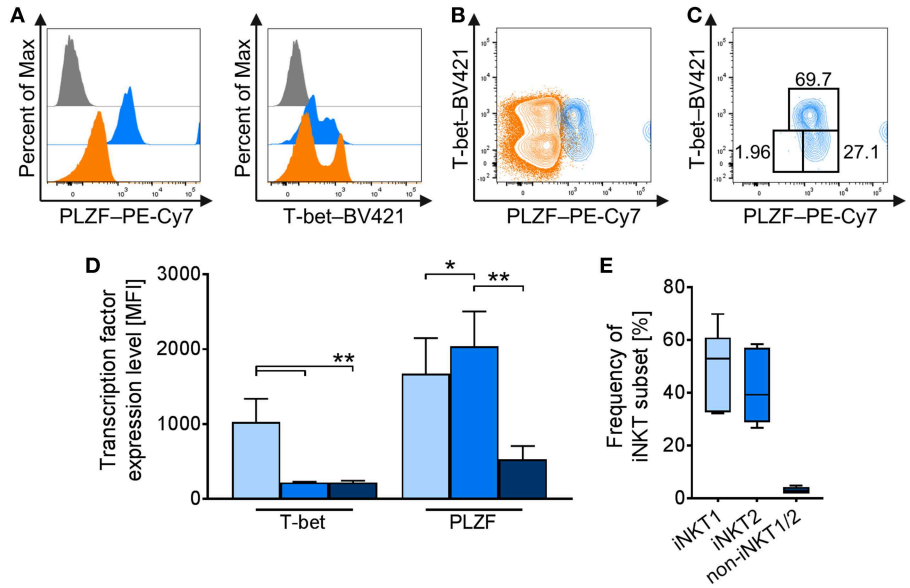

FIGURE 3 | Differential profiling of naïve porcine iNKT cells. Peripheral iNKT cells were differentiated by flow cytometry according to their expression of the transcription factors PLZF and T-bet. **(A)** Representative flow cytometric histograms of PLZF (left) and T-bet (right) expression in iNKT cells (blue) and cTC (orange). Control stainings are shown in gray. **(B)** Representative flow cytometric plot showing co-expression of T-bet and PLZF in iNKT cells and cTC. **(C)** Differential gating of iNKT cells according to their T-bet and PLZF expression. iNKT1 were defined as T-bet^{+}/PLZF^{+} (light blue), iNKT2 as T-bet^{-}/PLZF^{hi} (blue), and non-iNKT1/2 as T-bet^{-}/PLZF^{lo} (dark blue). **(D)** Expression profiles of T-bet and PLZF in iNKT1 (light blue), iNKT2 (blue), and non-iNKT1/2 (dark blue) ($n = 6$). **(E)** Frequency of iNKT subsets in naïve swine shown as Tukey box plots ($n = 6$). *$p < 0.05$, **$p < 0.01$, repeated-measures one-way ANOVA with Holm-Sidak's *post-hoc* test for multiple comparisons.

iNKT2 (41.7 ± 13.3%). A small fraction was T-bet^{-}/PLZF^{lo} (3.1 ± 1.2%) and was defined as non-iNKT1/non-iNKT2 (non-iNKT1/2) because additional differentiating markers were not available. Appropriate differentiation was confirmed by analysis of T-bet and PLZF expression levels in the iNKT cell subsets. T-bet expression in iNKT1 was significantly higher than in iNKT2 and non-iNKT1/2 (**Figure 3D**). PLZF expression level was the highest in iNKT2 and the lowest in non-iNKT1/2 (**Figure 3D**).

Taken together, we confirmed the phenotype of naïve iNKT cells from peripheral blood of healthy pigs to be predominantly CD3^{+}/CD4^{-}/CD8^{+} or CD3^{+}/DN. All iNKT cells expressed the αβTCR but not the CD8 β-chain. Moreover, we showed that naïve porcine iNKT cells display an effector-like (CD5^{hi}/CD25^{+}/MHC II^{+}/ICOS^{+}) and memory-like phenotype (CD45RA^{-}/CCR7^{+}/CD27^{+}). The CD8α subset expressed higher levels of CD25 and MHC II, as well as higher levels of CCR7 and CD27. Additionally, analogous to classifications in rodents, we were able to divide peripheral iNKT cells into three subsets, iNKT1, iNKT2, and non-iNKT1/2, according to their respective T-bet and PLZF expression.

Antigenic Activation Induces Strong Proliferation in Porcine iNKT Cells

A major feature of iNKT cells is their ability to proliferate rapidly upon activation. For porcine iNKT cells, data regarding responses after antigenic activation is limited. Therefore, we investigated the proliferative ability by quantifying iNKT frequency among CD3^{+} lymphocytes and expression of the proliferation marker Ki-67 after stimulation of porcine PBMC with low-dose (0.1 μg/ml) and high-dose (1 μg/ml) αGC or DMSO as vehicle control for 4 days. We also visualized cell divisions by staining with a fluorescent cell tracking dye. Upon stimulation with αGC, iNKT cell frequency among CD3^{+} lymphocytes strikingly increased. After 4 days of stimulation with low-dose αGC, iNKT cells accounted for about 9.7 ± 7.9% of CD3^{+} T cells, a 20-fold increase. High-dose αGC stimulation resulted in a 30-fold increase, leading to an iNKT cell frequency of 16.9 ± 9% among CD3^{+} lymphocytes (**Figure 4A**). To verify that this increase was due to proliferation, we investigated the expression of Ki-67, a widely used marker specific for proliferating cells (57). Most iNKT cells were Ki-67^{+} after stimulation (85.3 ± 10.6% and 91.7 ± 8.7% after low- and high-dose αGC stimulation, respectively), thereby demonstrating that the majority of iNKT cells were proliferating (**Figure 4B**). Expression of Ki-67 in cTC remained on a low level of background activation, proving the specific activation of iNKT cells by αGC (**Figure 4B**). Staining of PBMC with a fluorescent cell tracking dye (Tag-it Violet) before stimulation allows for detection of single proliferation steps upon activation. Again, nearly all iNKT cells were in a highly proliferative state and up to seven proliferation steps were detectable (**Figure 4C**). There was no detectable difference between both αGC doses. cTC demonstrated no proliferation over background level upon αGC stimulation.

Taken together, we demonstrated the rapid proliferative abilities of peripheral porcine iNKT cells in response to antigenic stimulation.

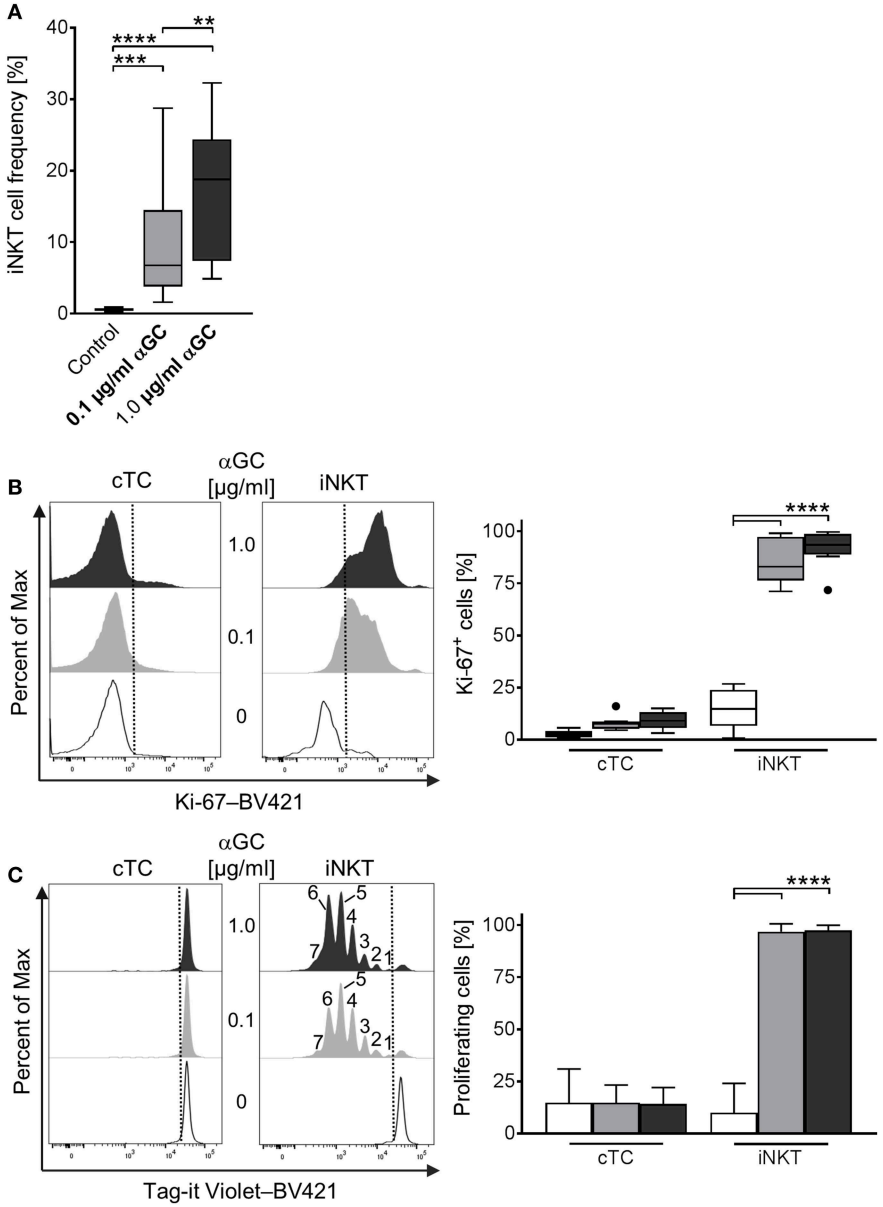

FIGURE 4 | Proliferative activity of porcine iNKT cells upon antigenic activation. **(A)** PBMC were cultivated in the presence of 0.1 μg/ml (gray) or 1 μg/ml (black) αGC or DMSO as vehicle control (white) for 4 days. Proliferation measured as iNKT cell frequency among $CD3^+$ lymphocytes shown as Tukey box plots ($n = 17$). **(B)** Cell proliferation was investigated by measuring Ki-67 expression in cTC and iNKT cells. Representative histograms showing expression of Ki-67 in cTC (left) and iNKT cells (right). Dotted lines indicate the threshold according to the control staining. Frequency of proliferating, Ki-67^+ iNKT cells and cTC ($n = 6$). **(C)** Porcine PBMC were stained with Tag-it Violet and cultivated in the presence of 0.1 μg/ml (gray) or 1 μg/ml (black) αGC or DMSO as vehicle control (white) for 4 days. Proliferating cells were defined as Tag-it $Violet^{lo}$. Representative histograms showing proliferating, Tag-it $Violet^{lo}$ cells in cTC and iNKT cells. Dotted lines indicate the threshold according to the control staining. Numbers indicate individual proliferation steps. Frequency of proliferating, Tag-it $Violet^{lo}$ cTC and iNKT cells (mean (SD), $n = 3$). $^{**}p < 0.01$, $^{***}p < 0.001$, $^{****}p < 0.0001$, repeated-measures one-way ANOVA with Holm-Sidak's *post-hoc* test for multiple comparisons.

Porcine iNKT Cells Upregulate Expression of CD25, MHC II, ICOS, and CD5 and Differentiate Into iNKT1 Upon Antigenic Stimulation

Whereas several iNKT cell activation markers are known in mice and humans, for porcine iNKT cells, no markers have been described to investigate their immune response or differentiation status. We therefore analyzed low- and high-dose αGC-stimulated porcine PBMC for activation-dependent changes in expression of multiple surface and intracellular markers. Among the established activation markers used for human and murine T cells are CD25 (50), MHC II (52), ICOS (51), and CD5 (49). Multicolor flow cytometry revealed that the

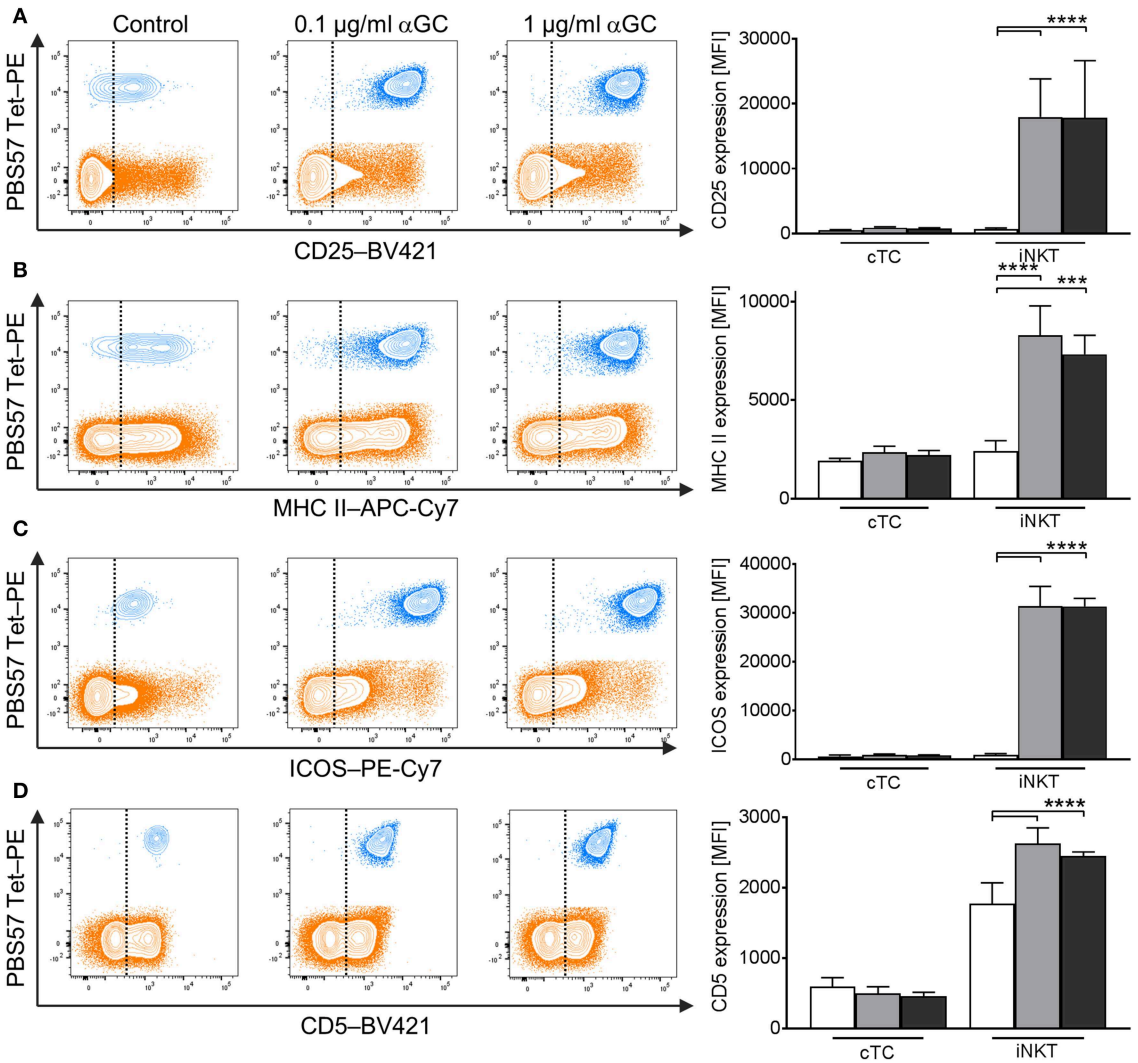

FIGURE 5 | Changes in surface marker expression on porcine iNKT cells upon antigenic activation. Porcine PBMC were incubated in the presence of 0.1 µg/ml or 1 µg/ml αGC or DMSO as vehicle control for 4 days. Representative flow cytometric plots showing expression of **(A)** CD25, **(B)** MHC II, **(C)** ICOS, and **(D)** CD5 on cTC (orange) and iNKT cells (blue). Expression level of control cells (white) and cells stimulated with 0.1 µg/ml (gray) and 1 µg/ml αGC (black) are shown (n = 3-4). Dotted lines show threshold according to marker expression by cTC. Data shown as mean (SD), ***$p < 0.001$, ****$p < 0.0001$, repeated-measures one-way ANOVA with Holm-Sidak's *post-hoc* test for multiple comparisons.

expression of these markers on the surface of cTC did not change significantly irrespective of stimulus or dose. In contrast, upon activation, iNKT cells significantly upregulated the expression of all investigated surface markers. Since most naïve iNKT cells were already positive for MHC II, ICOS, and CD5, the percentage of cells positive for the respective markers did not change. Only the frequency of $CD25^+$ iNKT cells increased significantly after stimulation. However, the expression level of all markers on the surface of iNKT cells increased significantly upon αGC stimulation, as evidenced by heightened MFI. CD25 expression (**Figure 5A**) increased from controls (MFI: 591 ± 106) to low-dose and high-dose αGC-stimulated iNKT cells (MFI: 15,427 ± 3,717; 13,593 ± 2,568, respectively). MHC II (**Figure 5B**) was markedly upregulated between controls (MFI: 2,341 ± 1,248) to low-dose (MFI: 9,653 ± 1,527) and high-dose αGC-stimulated iNKT cells (MFI: 8,159 ± 1,215). ICOS expression (**Figure 5C**) rose from controls (MFI: 849 ± 678) to low-dose (MFI: 35,309 ± 2,548) and high-dose αGC-stimulated iNKT cells (MFI: 31,366 ± 4,013). Expression levels of CD5 (**Figure 5D**) increased from controls (MFI: 1,776 ± 294) to low-dose (MFI: 2,626 ± 170) and high-dose αGC-stimulated iNKT cells (MFI: 2,448 ± 59). There were no significant differences in the expression levels of CD25, MHC II, ICOS, and CD5 on cTC after stimulation with low or high concentrations of αGC.

In mice, activated iNKT cells have been shown to regulate the expression of T-bet and PLZF, depending on the type of activating stimulus (21–26). Comparable data for swine is missing. To investigate the differentiation status of αGC-activated porcine

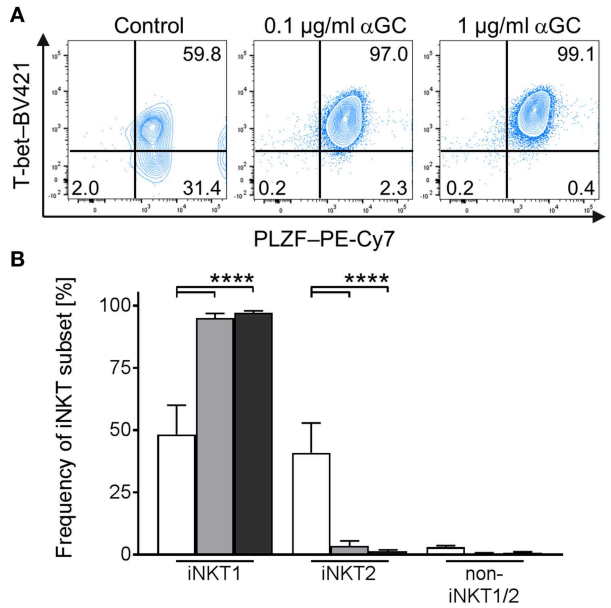

FIGURE 6 | Differentiation of activated porcine iNKT cells. Porcine PBMC were cultivated in the presence of αGC or DMSO as vehicle control. Intracellular expression of T-bet and PLZF was analyzed by flow cytometry after stimulation for 4 days. **(A)** Representative plots of T-bet/PLZF co-expression in untreated control iNKT cells (left) and iNKT cells stimulated with 0.1 µg/ml (middle) or 1 µg/ml (right) αGC. **(B)** Frequency of iNKT1, iNKT2, and non-iNKT1/2 upon stimulation with 0.1 µg/ml (gray) or 1 µg/ml (black) αGC or DMSO as vehicle control (white) ($n = 6$). Data shown as mean (SD), ****$p < 0.0001$, repeated-measures one-way ANOVA with Holm-Sidak's *post-hoc* test for multiple comparisons.

iNKT cells, we used the differential staining of T-bet and PLZF established in this study. While PLZF expression was not regulated in iNKT cells (**Figure 6A**), T-bet expression increased in iNKT cells after stimulation with low- and high-dose αGC (**Figure 6A**). Co-expression analysis revealed that all αGC-activated iNKT cells were T-bet$^+$/PLZF$^+$ iNKT1 (**Figure 6B**). There was no difference between low- and high-dose stimulated iNKT cells.

In short, we established a stimulation protocol for porcine iNKT cells. Activation by αGC results in strong upregulation of CD5, CD25, ICOS, and MHC II on iNKT cells and differentiation into T-bet$^+$/PLZF$^+$ iNKT1.

Porcine iNKT Cells Upregulate CD8 and CD4 Expression Upon Antigenic Stimulation

Naïve porcine iNKT cells were mostly CD8α$^+$ or DN and did not display a distinct CD4$^+$ population. However, after stimulation with αGC, frequencies of iNKT cell subsets changed significantly: DN iNKT decreased from 21.5 ± 10.8% in controls to 4.1 ± 3.6% in low-dose and 4.0 ± 2.8% in high-dose αGC-stimulated samples (**Figures 7A,B**). At the same time, the frequency of CD8α$^+$ iNKT cells increased from 73.7 ± 11.9% in controls to 84.1 ± 6.5% in low-dose and 79.6 ± 6.2% in high-dose stimulated samples (**Figures 7A,B**). Stimulation of porcine iNKT cells with αGC resulted in a significant increase of DP iNKT cells. In controls, only 3.6 ± 1.9% of all iNKT cells were DP. Stimulated iNKT cells upregulated CD4 expression, resulting in 11.2 ± 4.4% DP iNKT cells in low-dose and 15.5 ± 5.2% DP iNKT cells in high-dose αGC-stimulated samples (**Figures 7A,B**). Whether these subsets have functional implications was analyzed by investigation of CD25, ICOS, and MHC II expression on DN, CD8α$^+$ and DP iNKT cells. All three proteins tended to be expressed in higher levels on CD8α$^+$ and DP iNKT cells, while expression levels on DN iNKT cells were always the lowest (**Figure 7C**). However, this was statistically significant only for ICOS expression.

Porcine iNKT Cells Express IFNγ, Upregulate Perforin, and Display Fast Degranulation Upon Antigenic Activation

Among the effector mechanisms of iNKT cells are the secretion of effector cytokines and cytotoxicity. Porcine iNKT cells have been shown to secrete IFNγ upon unspecific stimulation with phorbol myristate acetate (PMA) and ionomycin (36, 37). Knowledge about antigen-specific induction of effector molecule production in porcine iNKT cells is missing. Therefore, we investigated expression of IFNγ and perforin and the cytolytic capacities of cTC and iNKT cells after stimulation of porcine PBMC with αGC.

iNKT cells showed a dose-dependent increase of IFNγ expression. Treatment of PBMC with low-dose αGC resulted in 8.4% IFNγ$^+$ iNKT cells, while high-dose αGC resulted in 15.9% IFNγ$^+$ iNKT cells (**Figure 8A**). Perforin expression (**Figure 8B**) increased significantly in iNKT cells upon treatment with both low- and high-dose αGC (MFI: 822.3 ± 280.3 vs. 1,095 ± 175, respectively) in contrast to naïve cells (MFI: 294 ± 33). In contrast, cTC did not express IFNγ (**Figure 8A**) after stimulation with low- and high-dose αGC. There was, however, an increased frequency of perforin$^+$ cTC (**Figure 8B**) after stimulation with αGC. Porcine iNKT cells also displayed cytolytic capacities in response to αGC stimulation. While low-dose αGC did not result in significant changes in CD107a expression on iNKT cells or cTC, high-dose αGC resulted in a significantly higher frequency of CD107a$^+$ iNKT cells (**Figure 8C**). Unspecific stimulation with PMA/ionomycin resulted in an even higher frequency of CD107a$^+$ iNKT cells. However, cTC did not show significant changes of CD107a expression. Thus, we demonstrated antigen-specific induction of the effector molecules IFNγ and perforin and degranulation of porcine iNKT cells.

iNKT Cell Frequency in Swine Decreases With Age

Previous studies in humans indicated an important role for iNKT cells in early stages of life, evidenced by a higher percentage of iNKT cells in young individuals. To investigate whether the iNKT cell frequency in swine is also age-dependent, we analyzed the percentage of CD3$^+$ cells among lymphocytes (**Figure 9A**) and iNKT cells among CD3$^+$ lymphocytes (**Figure 9B**) in blood of healthy pigs two-weeks, four-weeks, 10-12-weeks, 16-weeks, and 25-weeks of age. There was no difference in the frequency of

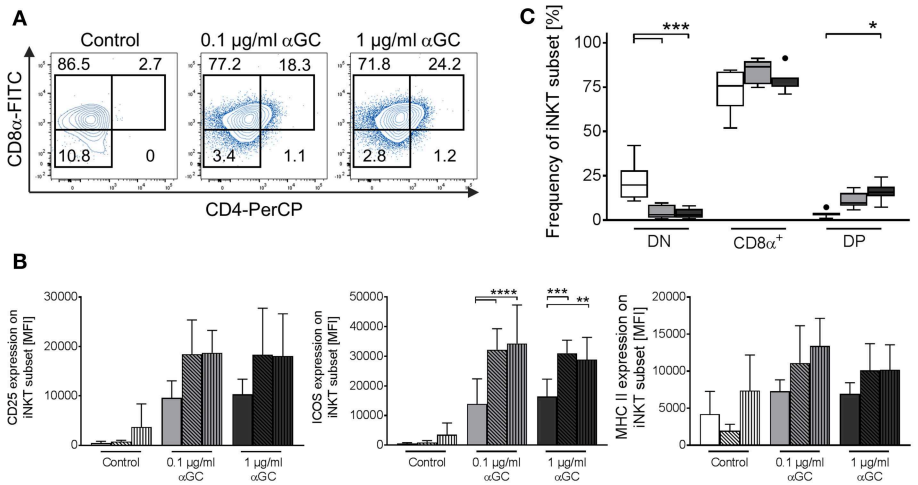

FIGURE 7 | Changes in iNKT cell subset frequency upon antigenic activation. Porcine PBMC were incubated in the presence of of 0.1 µg/ml or 1 µg/ml αGC or DMSO as vehicle control for 4 days. **(A)** Expression of CD8α and CD4 on iNKT cells was investigated. Representative flow cytometric plots of controls (left plot), low-dose (middle plot), and high-dose αGC (right plot) stimulated iNKT cells are shown. $CD8\alpha^-/CD4^-$ (DN), $CD8\alpha^+/CD4^-$ ($CD8\alpha^+$), and $CD8\alpha^+/CD4^+$ (DP) subsets in iNKT cells were identified as previously shown. Numbers in the plot show the frequencies of the respective gate. **(B)** Frequency of iNKT cell subsets in controls (white) and after stimulation with 0.1 µg/ml (gray) or 1 µg/ml αGC (black) shown as Tukey box plots ($n = 7$). **(C)** Expression level of CD25 (left graph), ICOS (middle graph), and MHC II (right graph) on DN (empty bars), $CD8\alpha^+$ (diagonal black hatching), and DP (vertical black stripes) iNKT cells was investigated in control cells (white) and cells stimulated with 0.1 µg/ml (gray) or 1 µg/ml (black) αGC (mean (SD), $n = 4$). $^*p < 0.05$, $^{**}p < 0.01$, $^{***}p < 0.001$, $^{****}p < 0.0001$, repeated-measures one-way ANOVA with Holm-Sidak's *post-hoc* test for multiple comparisons.

$CD3^+$ cells among the different groups. In contrast, we found the frequency of iNKT cells in 2-week-old piglets (1.1% ± 0.19) to be significantly higher than in all other groups. iNKT cell frequency declined rapidly with increasing age. Four-week-old piglets still displayed significantly higher proportions of iNKT cells (0.48% ± 0.25) than older animals. The frequency of iNKT cells was still elevated, but not statistically significant, in 10–12 week-old pigs (0.24% ± 0.1) compared to older animals. In comparison to 2-week-old piglets, iNKT cell frequency was markedly reduced. In 16-week-old and 25-week-old pigs, iNKT cell frequency remained on a comparable low level (0.09% ± 0.06, 0.08% ± 0.04, respectively).

Virus-Infected Swine Display Increasing Frequencies of iNKT Cells in Disease-Related Tissues

iNKT cells are among the first responders after microbial infection. In pigs, iNKT cell dynamics upon infection have not been investigated so far. Hence, we measured iNKT cell frequency in viral infections of either high zoonotic potential, i.e., IAV (H1N1; **Figure 10A**), or of high veterinary and economic importance, i.e., ASFV strain Armenia08 (**Figure 10B**). Over the course of the study, IAV-infected animals showed no clinical signs of disease. However, during subclinical IAV infection (**Figure 10A**), we found a significant increase in iNKT cell frequency in lung lymph nodes (*Nodus lymphaticus tracheobronchales inferiores*) at 4 days post infection (dpi), which decreased until 7 dpi to levels still higher than in control animals. In line with this finding, iNKT cell frequencies tended to increase non-significantly in peripheral blood, broncho-alveolar lavage (BAL), and lung at 4 dpi, which returned to control levels at 7 dpi in all tissues. In spleen, iNKT cell frequency peaked at 7 dpi. There were no changes in iNKT cell frequency in the gut. In contrast to IAV, ASFV-infected swine showed typical clinical signs of severe disease. ASFV infection was fatal in all animals in this study. During ASFV infection, we detected a significant increase in iNKT cell frequency in blood and lung at 5 dpi. In the lung, frequency dropped to control levels at 7 dpi, while they remained elevated, although not significantly, in blood. iNKT cell frequency was also increased in liver and one of the liver lymph nodes (*Nodi lymphatici hepatici*) 5 dpi but was on control levels again at 7 dpi. We therefore described the first iNKT cell dynamics in virus-infected swine.

To further evaluate the role of porcine iNKT cells in the aforementioned viral infections and to test our findings with the synthetic CD1d ligand αGC, we stimulated porcine PBMC with supernatant of $CD172a^+$ cells infected with IAV or ASFV. We found a small but significant increase of $CD25^+$, $ICOS^+$, and Ki-67^+ iNKT cells after stimulation with IAV-conditioned supernatant (**Figure 11A**). For ASFV, there was no detectable activation of iNKT cells (**Figure 11B**).

DISCUSSION

iNKT cells are a subset of innate lymphocytes located at potential pathogen entry sites at mucosal surfaces and lymphoid tissues. Even though they are a rare population in the vast pool of lymphocytes, they are pivotal orchestrators of innate and adaptive responses (58–60). Because of this central role in immunity, iNKT cells and their cellular responses have

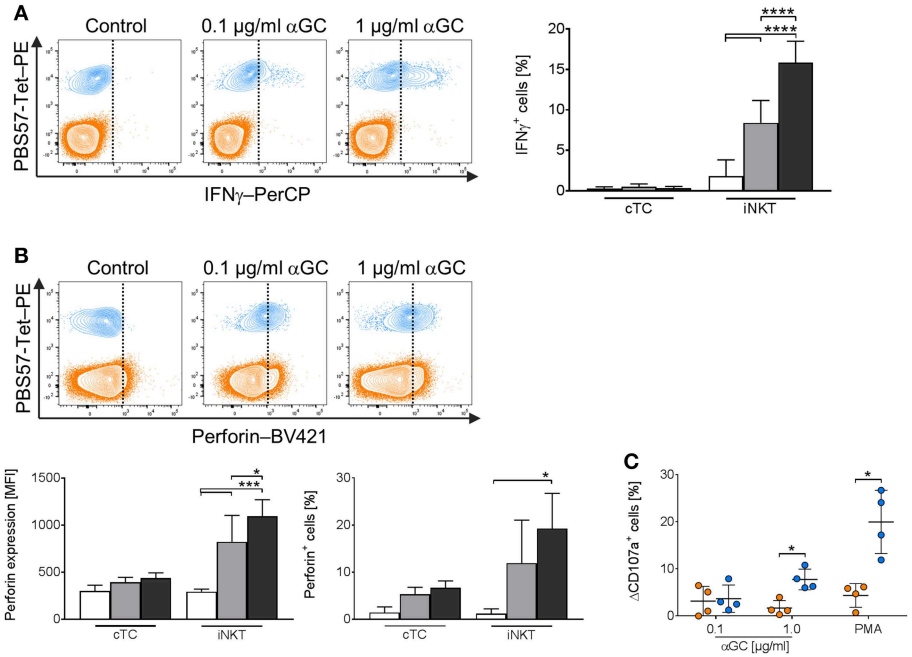

FIGURE 8 | Expression of IFNγ and perforin and degranulation of activated porcine iNKT cells upon antigenic activation. Porcine PBMC were cultivated in the presence of 0.1 µg/ml (gray) or 1 µg/ml αGC (black) or DMSO (white) as a control for 4 days. At day 4, the cells were restimulated with medium containing the respective treatment. 2 h later, Brefeldin A was added and the cells were incubated for another 4 h. Intracellular expression of IFNg and perforin in iNKT cells (blue) and cTC (orange) was analyzed by flow cytometry. **(A)** Representative flow cytometric plots showing IFNγ expression in iNKT cells and cTC (vertical line indicates threshold based on expression level in controls). Frequency of IFNγ-expressing iNKT cells and cTC in controls and after stimulation with 0.1 µg/ml or 1 µg/ml αGC (n = 5-7). **(B)** Representative flow cytometric plots showing perforin expression (vertical line indicates threshold based on expression level in controls). Expression level of perforin in iNKT cells and cTC in controls and after antigenic stimulation. Perforin$^+$ iNKT cells and cTC after antigenic stimulation (n = 4). **(C)** CD107a surface expression on iNKT cells and cTC after stimulation with 0.1 µg/ml or 1 µg/ml αGC and PMA/ionomycin. Specific degranulation was calculated as the difference in surface expression of stimulated and control cells and is given as ΔCD107a (n = 4). Data shown as mean (SD), $^*p < 0.05$, $^{***}p < 0.001$, $^{****}p < 0.0001$, repeated-measures one-way ANOVA with Holm-Sidak's *post-hoc* test for multiple comparisons.

been investigated extensively in mice and humans. However, a large animal model for immunological research in general and iNKT cell research in specific is still needed. Because of their physiological and immunological similarities with humans, pigs exhibit high potential as a biomedical model for infectious diseases (3–10). Moreover, because pigs are of high veterinary and economic importance, understanding of their immune system has an invaluable relevance exceeding mere scientific modeling.

We comprehensively characterized peripheral porcine iNKT cells and provided evidence for similarities with their human and murine counterparts. Naïve peripheral iNKT cells in swine were predominantly CD8α$^+$ and did not display a distinct CD4$^+$ population, which confirms earlier data (36, 37). These characteristics are comparable to human peripheral iNKT cells, which are predominantly CD8α$^+$ or DN, and in contrast to murine iNKT cells, which are mostly CD4$^+$ and lack CD8 surface expression (61). CD8α$^+$ iNKT cells in swine and humans are principally CD8αα$^+$ but do not express the CD8 β-chain (61). Differences in the study design in various species may hamper accurate comparative analysis of iNKT. Human and murine iNKT are often expanded *in vitro* before experimental investigations, resulting in significant changes of the subset distribution (61, 62). Therefore, some authors question the reliability of functional classifications of CD4/CD8 subsets in iNKT. We investigated freshly isolated iNKT. Hence, the described characteristics of iNKT subsets in this study are largely unaffected by *ex vivo* sample processing.

Porcine iNKT cells displayed an antigen-experienced phenotype, indicated by lack of CD45RA expression on the cell surface. Applying the characterization of human memory T cells to swine, porcine CCR7$^+$/CD27$^+$ iNKT cells represent a subset functionally similar to central memory cells, while CCR$^-$/CD27$^+$ and CCR$^-$/CD27$^-$ iNKT cells resemble transitional memory cells and effector memory cells, respectively (56). Upon activation, central memory cells produce IL-2 and rapidly proliferate. After differentiation into effector memory cells, they express cytokines, including IFNγ (55). An elevated fraction of CD27$^-$/CCR7$^+$ iNKT cells, probably representing activated effector cells with *de novo* expression of CCR7 (63), further strengthens our hypothesis that iNKT cells exhibit a preactivated phenotype in naïve animals. A comparable phenotype has been shown in human and murine iNKT cells as well (13, 64–66). This preactivation is discussed as the result of a lower activation threshold of iNKT cells in comparison to cTC (67) or exposition to endogenous ligands (68). Either

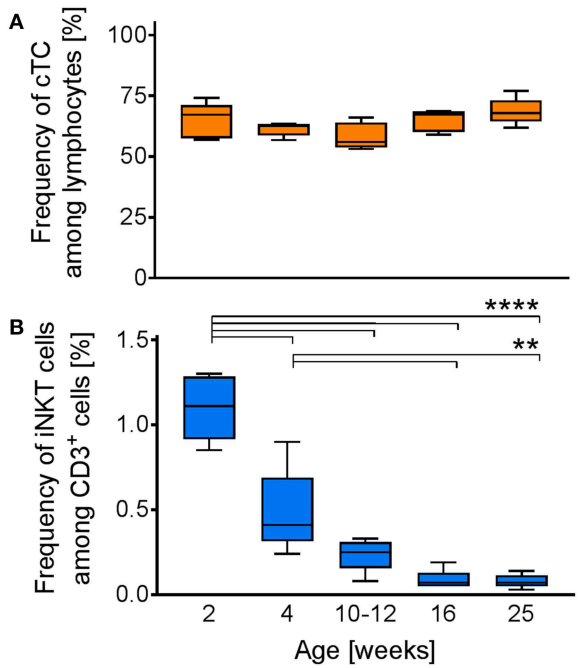

FIGURE 9 | Age-dependent changes in iNKT cell frequency. Whole blood from swine of the indicated age ($n = 5$) was investigated for the frequencies of iNKT cells and cTC among $CD3^+$ lymphocytes. Box plots showing the frequency of **(A)** $CD3^+$ cells among lymphocytes and **(B)** iNKT cells among $CD3^+$ cells. $^{**}p < 0.01$, $^{****}p < 0.0001$, ordinary one-way ANOVA with Holm-Sidak's *post-hoc* test for multiple comparisons.

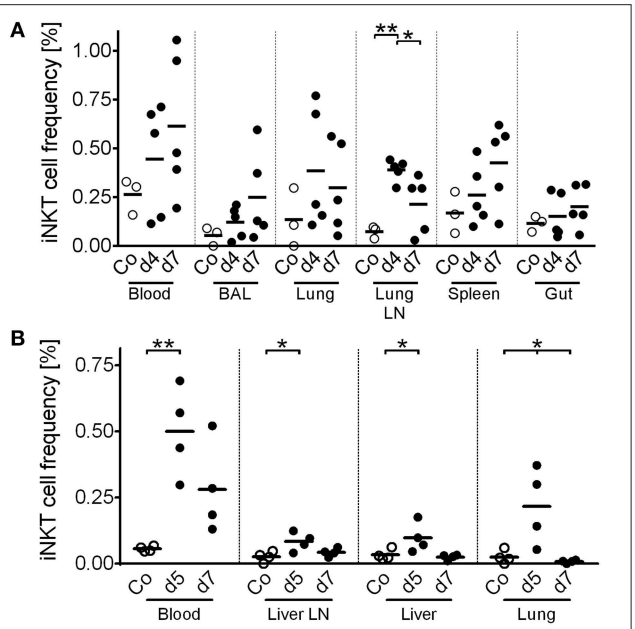

FIGURE 10 | *In vivo* dynamics of porcine iNKT cells during viral infections. Pigs were experimentally infected with **(A)** IAV ($n = 3$-5) or **(B)** ASFV ($n = 4$). At the indicated time after infection, animals were euthanized and lymphocytes of the indicated tissues were isolated. Frequency of iNKT among $CD3^+$ lymphocytes was then investigated using flow cytometry. Open circles show uninfected control animals (Co). Closed circles show infected animals at the indicated time post infection. Each symbol represents an individual animal with a line indicating mean. BAL, Broncho alveolar lavage. Lung LN, lung lymph node (*Nodi lymphatici tracheobronchales inferiores*). Liver LN, liver lymph node (*Nodi lymphatici hepatici*). $^{*}p < 0.05$, $^{**}p < 0.01$, ordinary one-way ANOVA with Holm-Sidak's *post-hoc* test for multiple comparisons.

way, preactivation of iNKT cells *in vivo*, in line with preformed cytokine mRNA (13), additionally emphasizes the ability of iNKT cells to respond immediately to stimuli (66). About half of all porcine iNKT cells expressed CCR7, which is critical for T cell extravasation and migration into T cell areas of secondary lymphoid tissues (69). CCR7 expression on porcine peripheral iNKT cells could therefore also explain the significant *in vivo* increases of iNKT cell frequencies in regional lymph nodes during infection with IAV (H1N1) as well as with ASFV strain Armenia08. Functional CCR7 expression, i.e., chemotactic migration to CCR7 ligands, has been shown for peripheral murine and human iNKT cells (70, 71). Moreover, CCR7 seems to be pivotal for the differentiation into effector subsets in the periphery (71). This indicates that porcine $CCR7^+$ iNKT cells are licensed to early migration from peripheral blood to secondary lymphoid tissues as well. Additionally, we found high levels of CD27 on porcine $CD8\alpha^+$ iNKT cells but not on DN iNKT cells. CD27 is essential for survival of $CD8^+$ effector cells, especially after multiple rounds of cell division (72, 73). Ligand-binding of CD27 on $CD8^+$ cells induces proliferation even in the absence of *bona fide* stimuli such as IL-2 (74). Cumulatively, our results emphasize that porcine iNKT cells display an effector-memory phenotype and that activation of porcine $CD8\alpha^+$ iNKT cells may occur in the absence of co-stimulation by other cells.

Our phenotypic characterization further indicated the presence of two main iNKT subsets, iNKT1 and iNKT2, and a minor subset, non-iNKT1/2. According to studies in mice, these subsets differ not only phenotypically but also functionally. iNKT1 exhibit properties associated with Th1 cells, like production of IFNγ, while iNKT2 produce the Th2 cytokine IL-4. The non-iNKT1/2 fraction may contain several other iNKT cell subsets, which at present cannot be further investigated in swine due to lack of detection systems. Among the possible iNKT subsets are iNKT17, producing IL-17, and regulatory and follicular helper iNKT cells. Different regulatory iNKT cells have been identified by the expression of FoxP3 or E4BP4 in mice (75, 76), follicular helper iNKT have been described as $Bcl\text{-}6^+$ (19). A recent study has provided evidence indicating that porcine iNKT cells also provide non-cognate B cell help (32), indicating that follicular helper iNKT cells exist in pigs as well. In humans, $CD4^+$ iNKT cells are the most efficient B cell helpers (77). Upregulation of CD4 and MHC II in activated porcine iNKT cells suggests that $CD4^+$ iNKT cells in swine have similar functions. MHC II expression by human cTC and iNKT cells is also upregulated upon activation during viral infections (78, 79). Both cell types may act as effective Antigen-presenting cells (APC) (52). Expression of MHC II on the surface of T lymphocytes has also been shown for a variety of other species, including rats, canine, bovine, and equine

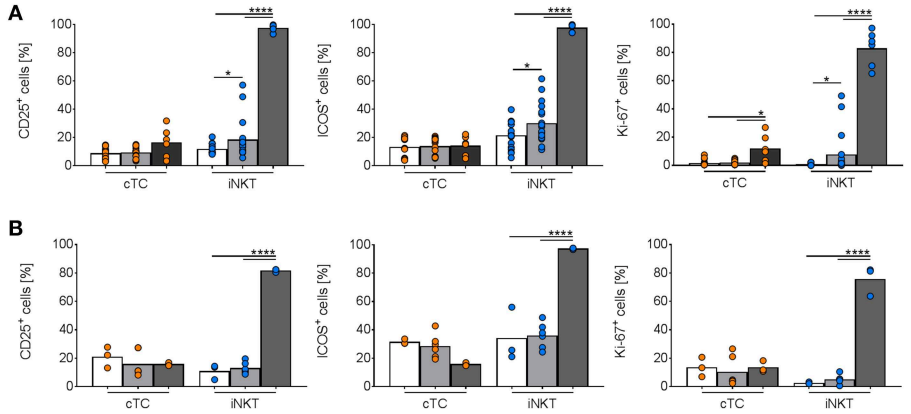

FIGURE 11 | *In vitro* activation of porcine iNKT cells during viral infections. Freshly isolated porcine PBMC were incubated without stimulation (white bars) or in the presence of supernatant of purified CD172a$^+$ cells infected with **(A)** IAV (MOI 1; gray) or **(B)** ASFV (MOI 0.1; gray), or 1 μg/ml αGC (black) for 4 days. Frequencies of iNKT cells (blue circles) and cTC (orange circles) positive for CD25, ICOS, and Ki-67 are shown. Pooled data of two experiments with six individual pigs for IAV and three individual pigs for ASFV shown as mean (SD), $^*p < 0.05$, $^{****}p < 0.0001$, ordinary one-way ANOVA with Holm-Sidak's *post-hoc* test for multiple comparisons.

(52). Murine T cells, unlike cells from other mammals, do not express MHC II on their own but rather acquire it from other cells (52). We found that activation of porcine iNKT cells with αGC leads to abundant cell surface expression of MHC II. Thus, porcine iNKT cells reflect human iNKT cells better than murine iNKT cells. However, the role of MHC II$^+$ iNKT cells is not entirely understood. Earlier studies indicated that interaction of MHC II and CD4 on CD4$^+$ iNKT cells could boost previous TCR-dependent activation by *trans*-interaction of MHC II$^+$ and CD4$^+$ iNKT cells, respectively (80). Upregulation of CD4 as well as MHC II by activated porcine iNKT cells indicates that such a process may occur in swine as well.

Human as well as murine iNKT cells primarily display an effector phenotype (61). We showed that porcine iNKT cells have similar characteristics. Naïve porcine iNKT cells abundantly expressed CD5 and were positive for CD25, MHC II, and ICOS. These markers are associated with effector cells (49–52). Expression of CD25 on naïve iNKT cells has also been shown in humans and mice (81, 82), ensuring prompt iNKT cell responsiveness (83). Expression of CD5 is upregulated by human cTC upon activation (49). We observed a corresponding increase of CD5 on the surface of activated porcine iNKT cells, thereby demonstrating highly activated cells (49). However, the role of CD5 on cTC and iNKT cells is not entirely understood. Molecular studies with human CD5 indicate that homophilic interactions with CD5 on other T cells or APC in *trans* or on the same cell in *cis* are needed for the regulation of T cell immunity (84). CD5 could also be used for regulation of iNKT cell responses, because expression of CD5 has been shown to inhibit TCR-dependent cell activation (49). Therefore, the high levels of CD5 on activated iNKT cells could limit further activation and possible immunopathology. Responses of iNKT cells are further regulated by ICOS. Interaction of ICOS with ICOSL, expressed exclusively on APC (85), is essential for homeostasis, activation, and survival of iNKT cells (51, 86, 87). Expression of ICOS, along with the receptors for IL-12 and IL-18, is induced by PLFZ, thereby shaping the ability of iNKT cells to respond to stimuli (88). This underlines the importance of ICOS for iNKT cell functionality. Some studies indicate that ICOS expression is associated with a Th1-based response, because ICOS expression on iNKT cells correlates with a pro-inflammatory phenotype and expression of IFNγ (86, 87). Other studies suggest that ICOS is not linked to a certain Th-subset differentiation but rather identifies cells in an effector state (89). Thus, ICOS expression on porcine iNKT cells does not necessarily indicate differentiation of iNKT cells into iNKT1. However, in context with the expression of other markers, such as CD25 or CD5, their shift to a T-bet$^+$ iNKT1 phenotype, and their expression of IFNγ and perforin, it seems accurate that αGC-stimulated porcine iNKT cells differentiate primarily into Th1/iNKT1.

In this study, we observed a higher expression of activation and effector markers, like CD25 and MHC II, on CD8α$^+$ iNKT cells than on CD8α$^-$ iNKT cells. Moreover, CD8α$^+$ iNKT cells were the primary subset we detected during Th1-biased iNKT cell responses. Comparable results have been described in earlier studies, where CD8α$^+$ iNKT cells produced higher amounts of IFNγ during unspecific activation with PMA/ionomycin (37). CD8α has also been described as an activation marker on another population of unconventional porcine lymphocytes, γδ T cells (90). This indicates that CD8α also acts as a marker of maturation and effector functions on porcine iNKT cells. Additionally, since activation resulted in a loss of DN iNKT cells and an increase of DP and CD8α$^+$ iNKT cells, both with a significantly higher ICOS expression than DN iNKT cells, CD8α$^+$ and DP iNKT cells might represent highly differentiated effector subsets. The high expression of effector markers even in steady state indicates that porcine iNKT cells are also licensed for rapid responses. Overall, porcine iNKT cells phenotypically mimic human iNKT cells significantly better than murine iNKT cells.

Porcine iNKT cells upregulated perforin expression and displayed degranulation as shown by increased CD107a surface expression upon antigenic stimulation. This feature is shared with iNKT cells in mice and humans (17, 91–93). Cytotoxicity, including perforin production, is induced independent of TCR stimulation by pro-inflammatory cytokines like IL-12 or IL-18 secreted by APC (91, 94). How iNKT cells precisely mediate cytotoxicity is still under discussion. Perforin-mediated lysis was described in viral infections and cancer models (15, 16, 91), while other studies suggested rather Fas/FasL-dependent lysis of target cells by iNKT cells (18, 94). Both pathways are CD1d-dependent, although CD1d-independent lysis mediated by NKG2D has also been described (95). Which of these pathways prevails in a specific context likely depends on the activation mode and availability of relevant molecules on the surface of target cells (14). Deciphering activation and mode of porcine iNKT cell cytotoxicity require in-depth analysis. Our phenotypic and functional characterization paves ways for such studies. The increase of perforin-expressing cTC we saw in our studies is likely due to direct and indirect effects on cTC during iNKT cell activation. IFNγ, highly expressed by activated iNKT cells, is known to enhance the cytotoxic activity of T cells by autocrine and paracrine stimulation (96). Moreover, IFNγ has been shown to induce the expression of the high-affinity IL-12 receptor (97). This enables cTC to react to IL-12, secreted by APC during αGC stimulation. IL-12 in turn is known to enhance perforin responses (98). This bystander activation provides further protection during ongoing immune responses and demonstrates the linkage of both early iNKT cell and subsequent cTC responses.

Interestingly, we only saw significant differences between the effects of the two concentrations of αGC in three cases. High-dose αGC resulted in heightened proliferation, increased perforin expression, and increased frequencies of IFNγ-producing iNKT cells. As iNKT cells do not require co-stimulation for cytokine-production (12, 13), dose-dependent effects are explained by interaction loops between APC and iNKT cells. Activated iNKT cells readily produce cytokines, like IFNγ, and induce maturation of dendritic cells, which in turn increase production of iNKT cell-stimulating cytokines, like IL-12 (99). Notably, αGC is a highly potent antigen with a high affinity to the iNKT cell TCR and a long half-life (100). Therefore, αGC likely induces stronger responses in iNKT cells than activation with natural ligands (27). The distinctive phenotype of *in vitro*-stimulated porcine iNKT cells requires *in vitro* verification with other CD1d ligands or bacterial/viral antigens and, most importantly, *in vivo* validation in infection studies.

We found a rapid age-dependent decrease in iNKT cell percentage during the first 12 weeks of life. In animals older than 12 weeks, iNKT cells maintained the same abundance. Since the frequency of $CD3^+$ lymphocytes did not change, the drop in iNKT cell frequency cannot be explained by changes in the overall T cell frequency. The high iNKT cell frequencies in young individuals indicate that iNKT cells play a critical role for immunological responses in the first weeks of life. Similar age-dependent decreases are known in humans as well (101, 102). The frequency of iNKT cells in swine investigated for age-related changes was lower than in swine investigated in other experiments. This might be explained by different housing conditions of the pigs used for different experiments. The samples for investigation of age-dependent iNKT cell frequency were obtained from a pig farm with strict biosafety standards, limiting contact with pathogenic microorganisms. In contrast, animals for other experiments were kept at our institute under conventional conditions, enabling microbial colonization. In mice, iNKT cell frequencies decrease if animals are kept under germ-free conditions (103, 104). This indicates that iNKT cell homeostasis in swine is also at least partially dependent on the microbiome of the respective animal.

We described the first iNKT cell kinetics in pigs in two viral infections, IAV and ASFV. We observed increases in iNKT cell frequency in blood and mucosal tissues at early time points during both infections, in line with the well-documented relevance of this lymphocyte population at the onset of infection (58, 105). However, iNKT cell dynamics changed at later stages of infection and their frequencies decreased over time. Moreover, we detected small but significant activation of iNKT cells in *in vitro* assays using IAV-conditioned supernatant. A host-beneficial expansion of iNKT cells with antiviral properties during IAV infection has been described in other species as well [reviewed in Crosby and Kronenberg (27)]. Mechanistically, iNKT cells act in various ways during IAV infection. Via secreted IFNγ, iNKT cells activate multiple bystander cells and induce protective adaptive responses. Moreover, iNKT cells facilitate conventional antiviral $CD8^+$ T cell responses (106), inhibit immunosuppression by myeloid-derived suppressor cells (107), and produce cytokines critical for mucosal immunity and integrity, like IL-22 (108). The iNKT cell influx during IAV infection in swine peaked significantly in the lung lymph nodes and non-significantly in lung and broncho-alveolar lavage in our study. Comparable expansions of iNKT populations in these tissues were shown during IAV infection in humans (27). This, in connection with our *in vitro* data, indicates that iNKT cells in swine may play a similar role during respiratory infections as in humans. Future studies will clarify precisely how iNKT cells are involved in antiviral immunity against IAV in swine. In response to ASFV infections, $CD8^+$ T cells seem to play a major role (109). Moreover, higher IFNγ production correlated with higher protection from ASFV challenge (110). A role for iNKT cell-like cells in the immunity against ASFV infection has been discussed earlier, as cells with a NKT-like phenotype ($CD3^+/CD4^-/CD8^+/CD5^{\pm}/CD6^-/CD11b^+/CD16^+$) expanded after co-culture of porcine PBMC with ASFV *in vitro* (110). However, as others and we showed, the phenotype of these cells resembled real iNKT cells only rudimentarily. It is therefore questionable whether the described expansion and effects are attributable to iNKT cells. Contrary to the changes *in vivo*, we did not see any ASFV-induced iNKT cell activation *in vitro*. This might be explained by immune evasion mechanisms used by pathogenic ASFV strains, that were recently been shown to block type I IFN responses in infected cells (111). Since type I IFN are potent inductors of iNKT cell activation (14), blockage of type I IFN expression would impair iNKT cell activation. However, these evasion mechanisms might at least partially be counteracted

in vivo, which cannot be simulated *in vitro*. Our *in vivo* data still indicates that iNKT cells are involved in the immune response against ASFV because the iNKT cell frequency increased locally in affected tissues and systemically in peripheral blood. However, an immunopathological role of iNKT cells during ASFV infection cannot be excluded. Overactivation of iNKT cells may result in a cytokine storm, which further weakens the animals and contributes to morbidity (112, 113). Furthermore, excessive local responses result in immunopathology, like liver damage (114, 115), as typically seen in animals succumbed to ASFV infection. The role of porcine iNKT cells in ASFV infections has to be evaluated in future studies.

iNKT cells are increasingly coming to the fore as target cells for novel vaccine adjuvants. New and more effective vaccines against infectious diseases are needed for swine as well as for humans. This is especially true for zoonotic diseases, like IAV, for which humans and swine are susceptible. αGC or αGC-analogs have been shown to induce high IgG and IgA titers against co-administered proteins in mice (116) as well as in swine (28, 29, 31). Expression of IFNγ by iNKT cells is crucial for B cell help and induction of class switch (20). We observed IFNγ expression by porcine iNKT cells upon antigenic stimulation, which indicates that pathways similar to those in mice are used by porcine iNKT cells to help B cells. αGC-adjuvanted vaccines also prime and potentiate cytotoxic CD8 T cell responses in mice (116, 117) and non-human primates (118). Targeting iNKT cells during vaccination represents a promising new way to increase vaccine efficacy. However, cellular and molecular interactions of porcine iNKT cells with effector cells of the adaptive immune system need further evaluation.

Taken together, we established a multicolor flow cytometry platform for analysis of porcine iNKT cells. Our study pioneered detailed phenotyping and differentiation of porcine iNKT cells and their effector molecules. Moreover, we provided first insights into the relevance of iNKT cells in viral diseases in pigs. We demonstrated that porcine iNKT cells display striking phenotypic and functional similarities to human but less to murine iNKT cells. Therefore, pigs were shown to be a valuable large animal model for immunological studies, especially for, but not limited to, iNKT cell research.

ETHICS STATEMENT

All animal experiments were approved by the ethics committee of the State Office for Agriculture, Food Safety and Fishery in Mecklenburg-Western Pomerania (LALFF M-V) with reference numbers 7221.3-1-035/17 for IAV and 7221.3-1.1-064/17 for ASFV. All applicable animal welfare regulations, including EU Directive 2010/63/EC and institutional guidelines, were taken into consideration.

AUTHOR CONTRIBUTIONS

AS and UB: conceived and designed *in vitro* experiments. TS, TM, SB, CS, and UB: conceived and designed animal experiments. AS, JH, TS, SB, and CS: acquired animal samples. AS: performed *in vitro* experiments. AS, AD, TM, and UB: data analysis and interpretation. AS and UB: manuscript preparation. All authors reviewed and approved the final version of the manuscript.

FUNDING

This study was funded by Federal Excellence Initiative of Mecklenburg Western Pomerania and European Social Fund (ESF) Grant KoInfekt (ESF_14-BM-A55-00xx_16).

ACKNOWLEDGMENTS

The authors thank Stefanie Knöfel and Silke Rehbein for outstanding technical assistance. For excellent care of animals, we thank the veterinarians and animal keepers of the FLI. The CD1d tetramer was thankfully provided by the NIH Tetramer Core Facility.

SUPPLEMENTARY MATERIAL

The Supplementary Material for this article can be found online at: https://www.frontiersin.org/articles/10.3389/fimmu.2019.01380/full#supplementary-material

Supplementary Table 1 | Antibodies used in this study.

REFERENCES

1. Gutierrez K, Dicks N, Glanzner WG, Agellon LB, Bordignon V. Efficacy of the porcine species in biomedical research. *Front Genet*. (2015) 6:293. doi: 10.3389/fgene.2015.00293
2. Seok J, Warren HS, Cuenca AG, Mindrinos MN, Baker HV, Xu W, et al. Genomic responses in mouse models poorly mimic human inflammatory diseases. *Proc Natl Acad Sci USA*. (2013) 110:3507–12. doi: 10.1073/pnas.1222878110
3. Fairbairn L, Kapetanovic R, Sester DP, Hume DA. The mononuclear phagocyte system of the pig as a model for understanding human innate immunity and disease. *J Leukoc Biol*. (2011) 89:855–71. doi: 10.1189/jlb.1110607
4. Giraud S, Favreau F, Chatauret N, Thuillier R, Maiga S, Hauet T. Contribution of large pig for renal ischemia-reperfusion and transplantation studies: the preclinical model. *J Biomed Biotechnol*. (2011) 2011:532127. doi: 10.1155/2011/532127
5. Mair KH, Sedlak C, Kaser T, Pasternak A, Levast B, Gerner W, et al. The porcine innate immune system: an update. *Dev Comp Immunol*. (2014) 45:321–43. doi: 10.1016/j.dci.2014.03.022
6. Swindle MM, Makin A, Herron AJ, Clubb FJ Jr., Frazier KS. Swine as models in biomedical research and toxicology testing. *Vet Pathol*. (2012) 49:344–56. doi: 10.1177/0300985811402846
7. Renukaradhya GJ, Manickam C, Khatri M, Rauf A, Li X, Tsuji M, et al. Functional invariant NKT cells in pig lungs regulate the airway hyperreactivity: a potential animal model. *J Clin Immunol*. (2011) 31:228–39. doi: 10.1007/s10875-010-9476-4
8. Ugolini M, Gerhard J, Burkert S, Jensen KJ, Georg P, Ebner F, et al. Recognition of microbial viability via TLR8 drives TFH cell differentiation and vaccine responses. *Nat Immunol*. (2018) 19:386–96. doi: 10.1038/s41590-018-0068-4

9. Maisonnasse P, Bouguyon E, Piton G, Ezquerra A, Urien C, Deloizy C, et al. The respiratory DC/macrophage network at steady-state and upon influenza infection in the swine biomedical model. *Mucosal Immunol*. (2016) 9:835–49. doi: 10.1038/mi.2015.105
10. Meurens F, Summerfield A, Nauwynck H, Saif L, Gerdts V. The pig: a model for human infectious diseases. *Trends Microbiol*. (2012) 20:50–7. doi: 10.1016/j.tim.2011.11.002
11. Iwasaki A, Foxman EF, Molony RD. Early local immune defences in the respiratory tract. *Nat Rev Immunol*. (2017) 17:7–20. doi: 10.1038/nri.2016.117
12. Uldrich AP, Crowe NY, Kyparissoudis K, Pellicci DG, Zhan Y, Lew AM, et al. NKT cell stimulation with glycolipid antigen *in vivo*: costimulation-dependent expansion, Bim-dependent contraction, and hyporesponsiveness to further antigenic challenge. *J Immunol*. (2005) 175:3092–101. doi: 10.4049/jimmunol.175.5.3092
13. Stetson DB, Mohrs M, Reinhardt RL, Baron JL, Wang ZE, Gapin L, et al. Constitutive cytokine mRNAs mark natural killer (NK) and NK T cells poised for rapid effector function. *J Exp Med*. (2003) 198:1069–76. doi: 10.1084/jem.20030630
14. Kohlgruber AC, Donado CA, LaMarche NM, Brenner MB, Brennan PJ. Activation strategies for invariant natural killer T cells. *Immunogenetics*. (2016) 68:649–63. doi: 10.1007/s00251-016-0944-8
15. Bassiri H, Das R, Guan P, Barrett DM, Brennan PJ, Banerjee PP, et al. iNKT cell cytotoxic responses control T-lymphoma growth *in vitro* and *in vivo*. *Cancer Immunol Res*. (2014) 2:59–69. doi: 10.1158/2326-6066.CIR-13-0104
16. Bassiri H, Das R, Nichols KE. Invariant NKT cells: killers and conspirators against cancer. *Oncoimmunology*. (2013) 2:e27440. doi: 10.4161/onci.27440
17. Gumperz JE, Miyake S, Yamamura T, Brenner MB. Functionally distinct subsets of CD1d-restricted natural killer T cells revealed by CD1d tetramer staining. *J Exp Med*. (2002) 195:625–36. doi: 10.1084/jem.20011786
18. Wingender G, Krebs P, Beutler B, Kronenberg M. Antigen-specific cytotoxicity by invariant NKT cells *in vivo* is CD95/CD178-dependent and is correlated with antigenic potency. *J Immunol*. (2010) 185:2721–9. doi: 10.4049/jimmunol.1001018
19. Chang PP, Barral P, Fitch J, Pratama A, Ma CS, Kallies A, et al. Identification of Bcl-6-dependent follicular helper NKT cells that provide cognate help for B cell responses. *Nat Immunol*. (2011) 13:35–43. doi: 10.1038/ni.2166
20. Doherty DG, Melo AM, Moreno-Olivera A, Solomos AC. Activation and regulation of B cell responses by invariant natural killer T cells. *Front Immunol*. (2018) 9:1360. doi: 10.3389/fimmu.2018.01360
21. Benlagha K, Kyin T, Beavis A, Teyton L, Bendelac A. A thymic precursor to the NK T cell lineage. *Science*. (2002) 296:553–5. doi: 10.1126/science.1069017
22. Constantinides MG, Bendelac A. Transcriptional regulation of the NKT cell lineage. *Curr Opin Immunol*. (2013) 25:161–7. doi: 10.1016/j.coi.2013.01.003
23. Lee YJ, Holzapfel KL, Zhu J, Jameson SC, Hogquist KA. Steady-state production of IL-4 modulates immunity in mouse strains and is determined by lineage diversity of iNKT cells. *Nat Immunol*. (2013) 14:1146–54. doi: 10.1038/ni.2731
24. McNab FW, Berzins SP, Pellicci DG, Kyparissoudis K, Field K, Smyth MJ, et al. The influence of CD1d in postselection NKT cell maturation and homeostasis. *J Immunol*. (2005) 175:3762–8. doi: 10.4049/jimmunol.175.6.3762
25. Strong BS, Newkold TJ, Lee AE, Turner LE, Alhajjat AM, Heusel JW, et al. Extrinsic allospecific signals of hematopoietic origin dictate iNKT cell lineage-fate decisions during development. *Sci Rep*. (2016) 6:28837. doi: 10.1038/srep28837
26. Watarai H, Sekine-Kondo E, Shigeura T, Motomura Y, Yasuda T, Satoh R, et al. Development and function of invariant natural killer T cells producing T(h)2- and T(h)17-cytokines. *PLoS Biol*. (2012) 10:e1001255. doi: 10.1371/journal.pbio.1001255
27. Crosby CM, Kronenberg M. Tissue-specific functions of invariant natural killer T cells. *Nat Rev Immunol*. (2018) 18:559–74. doi: 10.1038/s41577-018-0034-2
28. Artiaga BL, Whitener RL, Staples CR, Driver JP. Adjuvant effects of therapeutic glycolipids administered to a cohort of NKT cell-diverse pigs. *Vet Immunol Immunopathol*. (2014) 162:1–13. doi: 10.1016/j.vetimm.2014.09.006
29. Artiaga BL, Yang G, Hackmann TJ, Liu Q, Richt JA, Salek-Ardakani S, et al. α-Galactosylceramide protects swine against influenza infection when administered as a vaccine adjuvant. *Sci Rep*. (2016) 6:23593. doi: 10.1038/srep23593
30. Artiaga BL, Yang G, Hutchinson TE, Loeb JC, Richt JA, Lednicky JA, et al. Rapid control of pandemic H1N1 influenza by targeting NKT-cells. *Sci Rep*. (2016) 6:37999. doi: 10.1038/srep37999
31. Dwivedi V, Manickam C, Dhakal S, Binjawadagi B, Ouyang K, Hiremath J, et al. Adjuvant effects of invariant NKT cell ligand potentiates the innate and adaptive immunity to an inactivated H1N1 swine influenza virus vaccine in pigs. *Vet Microbiol*. (2016) 186:157–63. doi: 10.1016/j.vetmic.2016.02.028
32. Renu S, Dhakal S, Kim E, Goodman J, Lakshmanappa YS, Wannemuehler MJ, et al. Intranasal delivery of influenza antigen by nanoparticles, but not NKT-cell adjuvant differentially induces the expression of B-cell activation factors in mice and swine. *Cell Immunol*. (2018) 329:27–30. doi: 10.1016/j.cellimm.2018.04.005
33. Eguchi-Ogawa T, Morozumi T, Tanaka M, Shinkai H, Okumura N, Suzuki K, et al. Analysis of the genomic structure of the porcine CD1 gene cluster. *Genomics*. (2007) 89:248–61. doi: 10.1016/j.ygeno.2006.10.003
34. Bendelac A. Positive selection of mouse NK1+ T cells by CD1-expressing cortical thymocytes. *J Exp Med*. (1995) 182:2091–6. doi: 10.1084/jem.182.6.2091
35. Yang G, Artiaga BL, Hackmann TJ, Samuel MS, Walters EM, Salek-Ardakani S, et al. Targeted disruption of CD1d prevents NKT cell development in pigs. *Mamm Genome*. (2015) 26:264–70. doi: 10.1007/s00335-015-9564-0
36. Thierry A, Robin A, Giraud S, Minouflet S, Barra A, Bridoux F, et al. Identification of invariant natural killer T cells in porcine peripheral blood. *Vet Immunol Immunopathol*. (2012) 149:272–9. doi: 10.1016/j.vetimm.2012.06.023
37. Yang G, Artiaga BL, Lewis ST, Driver JP. Characterizing porcine invariant natural killer T cells: a comparative study with NK cells and T cells. *Dev Comp Immunol*. (2017) 76:343–51. doi: 10.1016/j.dci.2017.07.006
38. Yang G, Richt JA, Driver JP. Harnessing invariant NKT cells to improve influenza vaccines: a pig perspective. *Int J Mol Sci*. (2017) 19:68. doi: 10.3390/ijms19010068
39. Yang H, Binns RM. Expression and regulation of the porcine CD44 molecule. *Cell Immunol*. (1993) 149:117–29. doi: 10.1006/cimm.1993.1141
40. Yang G, Artiaga BL, Lomelino CL, Jayaprakash AD, Sachidanandam R, McKenna R, et al. Next generation sequencing of the pig alphabeta TCR repertoire identifies the porcine invariant NKT cell receptor. *J Immunol*. (2019) 202:1981–91. doi: 10.4049/jimmunol.1801171
41. Spearman C. The method of "right and wrong cases" (constant stimuli) without Gauss's formula. *Br J Psychol*. (1908) 2:227–42. doi: 10.1111/j.2044-8295.1908.tb00176.x
42. Kärber G. Beitrag zur kollektiven Behandlung pharmakologischer Reihenversuche. *Naunyn Schmiedebergs Arch Exp Pathol Pharmakol*. (1931) 162:480–3. doi: 10.1007/BF01863914
43. Spackman E, Senne DA, Myers TJ, Bulaga LL, Garber LP, Perdue ML, et al. Development of a real-time reverse transcriptase PCR assay for type A influenza virus and the avian H5 and H7 hemagglutinin subtypes. *J Clin Microbiol*. (2002) 40:3256–60. doi: 10.1128/JCM.40.9.3256-3260.2002
44. Pietschmann J, Guinat C, Beer M, Pronin V, Tauscher K, Petrov A, et al. Course and transmission characteristics of oral low-dose infection of domestic pigs and European wild boar with a Caucasian African swine fever virus isolate. *Arch Virol*. (2015) 160:1657–67. doi: 10.1007/s00705-015-2430-2
45. Kitani H, Yoshioka M, Takenouchi T, Sato M, Yamanaka N. Characterization of the liver-macrophages isolated from a mixed primary culture of neonatal swine hepatocytes. *Results Immunol*. (2014) 4:1–7. doi: 10.1016/j.rinim.2014.01.001
46. Fernandez CS, Cameron G, Godfrey DI, Kent SJ. *Ex-vivo* α-galactosylceramide activation of NKT cells in humans and macaques. *J Immunol Methods*. (2012) 382:150–9. doi: 10.1016/j.jim.2012.05.019
47. Singh D, Ghate M, Godbole S, Kulkarni S, Thakar M. Functional invariant natural killer T cells secreting cytokines are associated with non-progressive human immunodeficiency virus-1 infection but not with suppressive anti-retroviral treatment. *Front Immunol*. (2018) 9:1152. doi: 10.3389/fimmu.2018.01152

48. Zekavat G, Mozaffari R, Arias VJ, Rostami SY, Badkerhanian A, Tenner AJ, et al. A novel CD93 polymorphism in non-obese diabetic. (NOD) and NZB/W F1 mice is linked to a CD4+ iNKT cell deficient state. *Immunogenetics*. (2010) 62:397–407. doi: 10.1007/s00251-010-0442-3
49. Domingues RG, Lago-Baldaia I, Pereira-Castro I, Fachini JM, Oliveira L, Drpic D, et al. CD5 expression is regulated during human T-cell activation by alternative polyadenylation, PTBP1, and miR-204. *Eur J Immunol*. (2016) 46:1490–503. doi: 10.1002/eji.201545663
50. Waldmann TA. The multi-subunit interleukin-2 receptor. *Annu Rev Biochem*. (1989) 58:875–911. doi: 10.1146/annurev.biochem.58.1.875
51. Dong C, Juedes AE, Temann UA, Shresta S, Allison JP, Ruddle NH, et al. ICOS co-stimulatory receptor is essential for T-cell activation and function. *Nature*. (2001) 409:97–101. doi: 10.1038/35051100
52. Holling TM, Schooten E, van Den Elsen PJ. Function and regulation of MHC class II molecules in T-lymphocytes: of mice and men. *Hum Immunol*. (2004) 65:282–90. doi: 10.1016/j.humimm.2004.01.005
53. Larbi A, Fulop T. From "truly naive" to "exhausted senescent" T cells: when markers predict functionality. *Cytometry A*. (2014) 85:25–35. doi: 10.1002/cyto.a.22351
54. Okada R, Kondo T, Matsuki F, Takata H, Takiguchi M. Phenotypic classification of human CD4+ T cell subsets and their differentiation. *Int Immunol*. (2008) 20:1189–99. doi: 10.1093/intimm/dxn075
55. Sallusto F, Geginat J, Lanzavecchia A. Central memory and effector memory T cell subsets: function, generation, and maintenance. *Annu Rev Immunol*. (2004) 22:745–63. doi: 10.1146/annurev.immunol.22.012703.104702
56. Mahnke YD, Brodie TM, Sallusto F, Roederer M, Lugli E. The who's who of T-cell differentiation: human memory T-cell subsets. *Eur J Immunol*. (2013) 43:2797–809. doi: 10.1002/eji.201343751
57. Soares A, Govender L, Hughes J, Mavakla W, de Kock M, Barnard C, et al. Novel application of Ki67 to quantify antigen-specific *in vitro* lymphoproliferation. *J Immunol Methods*. (2010) 362:43–50. doi: 10.1016/j.jim.2010.08.007
58. Brigl M, Bry L, Kent SC, Gumperz JE, Brenner MB. Mechanism of CD1d-restricted natural killer T cell activation during microbial infection. *Nat Immunol*. (2003) 4:1230–7. doi: 10.1038/ni1002
59. Liew PX, Kubes P. Intravital imaging - dynamic insights into natural killer T cell biology. *Front Immunol*. (2015) 6:240. doi: 10.3389/fimmu.2015.00240
60. Metelitsa LS. Anti-tumor potential of type-I NKT cells against CD1d-positive and CD1d-negative tumors in humans. *Clin Immunol*. (2011) 140:119–29. doi: 10.1016/j.clim.2010.10.005
61. Garner LC, Klenerman P, Provine NM. Insights into mucosal-associated invariant T cell biology from studies of invariant natural killer T cells. *Front Immunol*. (2018) 9:1478. doi: 10.3389/fimmu.2018.01478
62. Chan AC, Leeansyah E, Cochrane A, d'Udekem d'Acoz Y, Mittag D, Harrison LC, et al. *Ex-vivo* analysis of human natural killer T cells demonstrates heterogeneity between tissues and within established CD4(+) and CD4(-) subsets. *Clin Exp Immunol*. (2013) 172:129–37. doi: 10.1111/cei.12045
63. Sallusto F, Kremmer E, Palermo B, Hoy A, Ponath P, Qin S, et al. Switch in chemokine receptor expression upon TCR stimulation reveals novel homing potential for recently activated T cells. *Eur J Immunol*. (1999) 29:2037–45. doi: 10.1002/(SICI)1521-4141(199906)29:06<2037::AID-IMMU2037>3.0.CO;2-V
64. D'Andrea A, Goux D, De Lalla C, Koezuka Y, Montagna D, Moretta A, et al. Neonatal invariant Vα24+ NKT lymphocytes are activated memory cells. *Eur J Immunol*. (2000) 30:1544–50. doi: 10.1002/1521-4141(200006)30:6<1544::AID-IMMU1544>3.0.CO;2-I
65. Park SH, Benlagha K, Lee D, Balish E, Bendelac A. Unaltered phenotype, tissue distribution and function of Vα14(+) NKT cells in germ-free mice. *Eur J Immunol*. (2000) 30:620–5. doi: 10.1002/1521-4141(200002)30:2<620::AID-IMMU620>3.0.CO;2-4
66. Cole SL, Benam KH, McMichael AJ, Ho LP. Involvement of the 4–1BB/4–1BBL pathway in control of monocyte numbers by invariant NKT cells. *J Immunol*. (2014) 192:3898–907. doi: 10.4049/jimmunol.1302385
67. van den Heuvel MJ, Garg N, Van Kaer L, Haeryfar SM. NKT cell costimulation: experimental progress and therapeutic promise. *Trends Mol Med*. (2011) 17:65–77. doi: 10.1016/j.molmed.2010.10.007
68. Van Rhijn I, Kasmar A, de Jong A, Gras S, Bhati M, Doorenspleet ME, et al. A conserved human T cell population targets mycobacterial antigens presented by CD1b. *Nat Immunol*. (2013) 14:706–13. doi: 10.1038/ni.2630
69. Kim CH, Johnston B, Butcher EC. Trafficking machinery of NKT cells: shared and differential chemokine receptor expression among Vα24+Vβ11+ NKT cell subsets with distinct cytokine-producing capacity. *Blood*. (2002) 100:11–6. doi: 10.1182/blood-2001-12-0196
70. Johnston B, Kim CH, Soler D, Emoto M, Butcher EC. Differential chemokine responses and homing patterns of murine TCRαβ NKT cell subsets. *J Immunol*. (2003) 171:2960–9. doi: 10.4049/jimmunol.171.6.2960
71. Wang H, Hogquist KA. CCR7 defines a precursor for murine iNKT cells in thymus and periphery. *Elife*. (2018) 7:e34793. doi: 10.7554/eLife.34793
72. Hendriks J, Gravestein LA, Tesselaar K, van Lier RA, Schumacher TN, Borst J. CD27 is required for generation and long-term maintenance of T cell immunity. *Nat Immunol*. (2000) 1:433–40. doi: 10.1038/80877
73. Hendriks J, Xiao Y, Borst J. CD27 promotes survival of activated T cells and complements CD28 in generation and establishment of the effector T cell pool. *J Exp Med*. (2003) 198:1369–80. doi: 10.1084/jem.20030916
74. Carr JM, Carrasco MJ, Thaventhiran JE, Bambrough PJ, Kraman M, Edwards AD, et al. CD27 mediates interleukin-2-independent clonal expansion of the CD8+ T cell without effector differentiation. *Proc Natl Acad Sci USA*. (2006) 103:19454–9. doi: 10.1073/pnas.0609706104
75. Lynch L, Michelet X, Zhang S, Brennan PJ, Moseman A, Lester C, et al. Regulatory iNKT cells lack expression of the transcription factor PLZF and control the homeostasis of T(reg) cells and macrophages in adipose tissue. *Nat Immunol*. (2015) 16:85–95. doi: 10.1038/ni.3047
76. Monteiro M, Almeida CF, Caridade M, Ribot JC, Duarte J, Agua-Doce A, et al. Identification of regulatory Foxp3+ invariant NKT cells induced by TGF-β. *J Immunol*. (2010) 185:2157–63. doi: 10.4049/jimmunol.1000359
77. Zeng SG, Ghnewa YG, O'Reilly VP, Lyons VG, Atzberger A, Hogan AE, et al. Human invariant NKT cell subsets differentially promote differentiation, antibody production, and T cell stimulation by B cells *in vitro*. *J Immunol*. (2013) 191:1666–76. doi: 10.4049/jimmunol.1202223
78. Ibarrondo FJ, Wilson SB, Hultin LE, Shih R, Hausner MA, Hultin PM, et al. Preferential depletion of gut CD4-expressing iNKT cells contributes to systemic immune activation in HIV-1 infection. *Mucosal Immunol*. (2013) 6:591–600. doi: 10.1038/mi.2012.101
79. Montoya CJ, Catano JC, Ramirez Z, Rugeles MT, Wilson SB, Landay AL. Invariant NKT cells from HIV-1 or Mycobacterium tuberculosis-infected patients express an activated phenotype. *Clin Immunol*. (2008) 127:1–6. doi: 10.1016/j.clim.2007.12.006
80. Thedrez A, de Lalla C, Allain S, Zaccagnino L, Sidobre S, Garavaglia C, et al. CD4 engagement by CD1d potentiates activation of CD4+ invariant NKT cells. *Blood*. (2007) 110:251–8. doi: 10.1182/blood-2007-01-066217
81. Jukes JP, Wood KJ, Jones ND. Bystander activation of iNKT cells occurs during conventional T-cell alloresponses. *Am J Transplant*. (2012) 12:590–9. doi: 10.1111/j.1600-6143.2011.03847.x
82. Schneiders FL, Prodohl J, Ruben JM, O'Toole T, Scheper RJ, Bonneville M, et al. CD1d-restricted antigen presentation by Vgamma9Vdelta2-T cells requires trogocytosis. *Cancer Immunol Res*. (2014) 2:732–40. doi: 10.1158/2326-6066.CIR-13-0167
83. Ladd M, Sharma A, Huang Q, Wang AY, Xu L, Genowati I, et al. Natural killer T cells constitutively expressing the interleukin-2 receptor alpha chain early in life are primed to respond to lower antigenic stimulation. *Immunology*. (2010) 131:289–99. doi: 10.1111/j.1365-2567.2010.03304.x
84. Brown MH, Lacey E. A ligand for CD5 is CD5. *J Immunol*. (2010) 185:6068–74. doi: 10.4049/jimmunol.0903823
85. Wikenheiser DJ, Stumhofer JS. ICOS co-stimulation: friend or foe? *Front Immunol*. (2016) 7:304. doi: 10.3389/fimmu.2016.00304
86. Akbari O, Stock P, Meyer EH, Freeman GJ, Sharpe AH, Umetsu DT, et al. ICOS/ICOSL interaction is required for CD4+ invariant NKT cell function and homeostatic survival. *J Immunol*. (2008) 180:5448–56. doi: 10.4049/jimmunol.180.8.5448
87. Kaneda H, Takeda K, Ota T, Kaduka Y, Akiba H, Ikarashi Y, et al. ICOS costimulates invariant NKT cell activation. *Biochem Biophys Res Commun*. (2005) 327:201–7. doi: 10.1016/j.bbrc.2004.12.004

88. Gleimer M, von Boehmer H, Kreslavsky T. PLZF controls the expression of a limited number of genes essential for NKT cell function. *Front Immunol*. (2012) 3:374. doi: 10.3389/fimmu.2012.00374
89. Burmeister Y, Lischke T, Dahler AC, Mages HW, Lam KP, Coyle AJ, et al. ICOS controls the pool size of effector-memory and regulatory T cells. *J Immunol*. (2008) 180:774–82. doi: 10.4049/jimmunol.180.2.774
90. Stepanova K, Sinkora M. The expression of CD25, CD11b, SWC1, SWC7, MHC-II, and family of CD45 molecules can be used to characterize different stages of gammadelta T lymphocytes in pigs. *Dev Comp Immunol*. (2012) 36:728–40. doi: 10.1016/j.dci.2011.11.003
91. Dao T, Mehal WZ, Crispe IN. IL-18 augments perforin-dependent cytotoxicity of liver NK-T cells. *J Immunol*. (1998) 161:2217–22.
92. Ichikawa T, Negishi Y, Shimizu M, Takeshita T, Takahashi H. α-Galactosylceramide-activated murine NK1.1(+) invariant-NKT cells in the myometrium induce miscarriages in mice. *Eur J Immunol*. (2016) 46:1867–77. doi: 10.1002/eji.201545923
93. Van Der Vliet HJ, Nishi N, Koezuka Y, Peyrat MA, Von Blomberg BM, Van Den Eertwegh AJ, et al. Effects of alpha-galactosylceramide. (KRN7000), interleukin-12 and interleukin-7 on phenotype and cytokine profile of human Vα24+ Vβ11+ T cells. *Immunology*. (1999) 98:557–63. doi: 10.1046/j.1365-2567.1999.00920.x
94. Leite-De-Moraes MC, Hameg A, Arnould A, Machavoine F, Koezuka Y, Schneider E, et al. A distinct IL-18-induced pathway to fully activate NK T lymphocytes independently from TCR engagement. *J Immunol*. (1999) 163:5871–6.
95. Kuylenstierna C, Bjorkstrom NK, Andersson SK, Sahlstrom P, Bosnjak L, Paquin-Proulx D, et al. NKG2D performs two functions in invariant NKT cells: direct TCR-independent activation of NK-like cytolysis and co-stimulation of activation by CD1d. *Eur J Immunol*. (2011) 41:1913–23. doi: 10.1002/eji.200940278
96. Bhat P, Leggatt G, Waterhouse N, Frazer IH. Interferon-gamma derived from cytotoxic lymphocytes directly enhances their motility and cytotoxicity. *Cell Death Dis*. (2017) 8:e2836. doi: 10.1038/cddis.2017.67
97. Gollob JA, Kawasaki H, Ritz J. Interferon-gamma and interleukin-4 regulate T cell interleukin-12 responsiveness through the differential modulation of high-affinity interleukin-12 receptor expression. *Eur J Immunol*. (1997) 27:647–52. doi: 10.1002/eji.1830270311
98. Ebert EC. Interleukin-12 up-regulates perforin- and Fas-mediated lymphokine-activated killer activity by intestinal intraepithelial lymphocytes. *Clin Exp Immunol*. (2004) 138:259–65. doi: 10.1111/j.1365-2249.2004.02614.x
99. Gottschalk C, Mettke E, Kurts C. The role of invariant natural killer T cells in dendritic cell licensing, cross-priming, and memory CD8(+) T cell generation. *Front Immunol*. (2015) 6:379. doi: 10.3389/fimmu.2015.00379
100. Cerundolo V, Silk JD, Masri SH, Salio M. Harnessing invariant NKT cells in vaccination strategies. *Nat Rev Immunol*. (2009) 9:28. doi: 10.1038/nri2451
101. Jing Y, Gravenstein S, Chaganty NR, Chen N, Lyerly KH, Joyce S, et al. Aging is associated with a rapid decline in frequency, alterations in subset composition, and enhanced Th2 response in CD1d-restricted NKT cells from human peripheral blood. *Exp Gerontol*. (2007) 42:719–32. doi: 10.1016/j.exger.2007.01.009
102. Patin E, Hasan M, Bergstedt J, Rouilly V, Libri V, Urrutia A, et al. Natural variation in the parameters of innate immune cells is preferentially driven by genetic factors. *Nat Immunol*. (2018) 19:302–14. doi: 10.1038/s41590-018-0049-7
103. Wei B, Wingender G, Fujiwara D, Chen DY, McPherson M, Brewer S, et al. Commensal microbiota and CD8+ T cells shape the formation of invariant NKT cells. *J Immunol*. (2010) 184:1218–26. doi: 10.4049/jimmunol.0902620
104. Wingender G, Stepniak D, Krebs P, Lin L, McBride S, Wei B, et al. Intestinal microbes affect phenotypes and functions of invariant natural killer T cells in mice. *Gastroenterology*. (2012) 143:418–28. doi: 10.1053/j.gastro.2012.04.017
105. Crosby CM, Kronenberg M. Invariant natural killer T cells: front line fighters in the war against pathogenic microbes. *Immunogenetics*. (2016) 68:639–48. doi: 10.1007/s00251-016-0933-y
106. Paget C, Ivanov S, Fontaine J, Blanc F, Pichavant M, Renneson J, et al. Potential role of invariant NKT cells in the control of pulmonary inflammation and CD8+ T cell response during acute influenza A virus H3N2 pneumonia. *J Immunol*. (2011) 186:5590–602. doi: 10.4049/jimmunol.1002348
107. De Santo C, Salio M, Masri SH, Lee LY, Dong T, Speak AO, et al. Invariant NKT cells reduce the immunosuppressive activity of influenza A virus-induced myeloid-derived suppressor cells in mice and humans. *J Clin Invest*. (2008) 118:4036–48. doi: 10.1172/JCI36264
108. Paget C, Ivanov S, Fontaine J, Renneson J, Blanc F, Pichavant M, et al. Interleukin-22 is produced by invariant natural killer T lymphocytes during influenza A virus infection: potential role in protection against lung epithelial damages. *J Biol Chem*. (2012) 287:8816–29. doi: 10.1074/jbc.M111.304758
109. Oura CA, Denyer MS, Takamatsu H, Parkhouse RM. *In vivo* depletion of CD8+ T lymphocytes abrogates protective immunity to African swine fever virus. *J Gen Virol*. (2005) 86:2445–50. doi: 10.1099/vir.0.81038-0
110. Takamatsu HH, Denyer MS, Lacasta A, Stirling CM, Argilaguet JM, Netherton CL, et al. Cellular immunity in ASFV responses. *Virus Res*. (2013) 173:110–21. doi: 10.1016/j.virusres.2012.11.009
111. Garcia-Belmonte R, Perez-Nunez D, Pittau M, Richt JA, Revilla Y. African swine fever virus Armenia/07 virulent strain controls IFN-beta production through cGAS-STING pathway. *J Virol*. (2019). doi: 10.1128/JVI.02298-18
112. Scheuplein F, Thariath A, Macdonald S, Truneh A, Mashal R, Schaub R. A humanized monoclonal antibody specific for invariant Natural Killer T. (iNKT) cells for *in vivo* depletion. *PLoS ONE*. (2013) 8:e76692. doi: 10.1371/journal.pone.0076692
113. Van Kaer L, Parekh VV, Wu L. The response of CD1d-restricted invariant NKT cells to microbial pathogens and their products. *Front Immunol*. (2015) 6:226. doi: 10.3389/fimmu.2015.00226
114. Osman Y, Kawamura T, Naito T, Takeda K, Van Kaer L, Okumura K, et al. Activation of hepatic NKT cells and subsequent liver injury following administration of α-galactosylceramide. *Eur J Immunol*. (2000) 30:1919–28. doi: 10.1002/1521-4141(200007)30:7<1919::AID-IMMU1919>3.0.CO;2-3
115. Takeda K, Hayakawa Y, Van Kaer L, Matsuda H, Yagita H, Okumura K. Critical contribution of liver natural killer T cells to a murine model of hepatitis. *Proc Natl Acad Sci USA*. (2000) 97:5498–503. doi: 10.1073/pnas.040566697
116. Lee YS, Lee KA, Lee JY, Kang MH, Song YC, Baek DJ, et al. An alpha-GalCer analogue with branched acyl chain enhances protective immune responses in a nasal influenza vaccine. *Vaccine*. (2011) 29:417–25. doi: 10.1016/j.vaccine.2010.11.005
117. Venkataswamy MM, Baena A, Goldberg MF, Bricard G, Im JS, Chan J, et al. Incorporation of NKT cell-activating glycolipids enhances immunogenicity and vaccine efficacy of *Mycobacterium bovis bacillus* Calmette-Guerin. *J Immunol*. (2009) 183:1644–56. doi: 10.4049/jimmunol.0900858
118. Padte NN, Boente-Carrera M, Andrews CD, McManus J, Grasperge BF, Gettie A, et al. A glycolipid adjuvant, 7DW8-5, enhances CD8+ T cell responses induced by an adenovirus-vectored malaria vaccine in non-human primates. *PLoS ONE*. (2013) 8:e78407. doi: 10.1371/journal.pone.0078407

Conflict of Interest Statement: The authors declare that the research was conducted in the absence of any commercial or financial relationships that could be construed as a potential conflict of interest.

frontiers in Immunology

ORIGINAL RESEARCH
published: 06 August 2019
doi: 10.3389/fimmu.2019.01689

Dynamics and Differences in Systemic and Local Immune Responses After Vaccination With Inactivated and Live Commercial Vaccines and Subsequent Subclinical Infection With PRRS Virus

Miroslav Toman[1], Vladimir Celer[2], Lenka Kavanová[1], Lenka Levá[1], Jitka Frolichova[2], Petra Ondráčková[1], Hana Kudláčková[1], Kateřina Nechvátalová[1], Jiri Salat[3] and Martin Faldyna[1]*

[1] Department of Immunology, Veterinary Research Institute, Brno, Czechia, [2] Faculty of Veterinary Medicine, University of Veterinary and Pharmaceutical Sciences, Brno, Czechia, [3] Department of Virology, Veterinary Research Institute, Brno, Czechia

OPEN ACCESS

Edited by:
John E. Butler, University of Iowa, United States

Reviewed by:
Jinhai Huang, Tianjin University, China
Lorenzo Fraile, Universitat de Lleida, Spain

***Correspondence:**
Miroslav Toman
toman@vri.cz

Specialty section:
This article was submitted to Comparative Immunology, a section of the journal Frontiers in Immunology

Received: *14 November 2018*
Accepted: *04 July 2019*
Published: *06 August 2019*

Citation:
Toman M, Celer V, Kavanová L, Levá L, Frolichova J, Ondráčková P, Kudláčková H, Nechvátalová K, Salat J and Faldyna M (2019) Dynamics and Differences in Systemic and Local Immune Responses After Vaccination With Inactivated and Live Commercial Vaccines and Subsequent Subclinical Infection With PRRS Virus. Front. Immunol. 10:1689. doi: 10.3389/fimmu.2019.01689

The goals of our study were to compare the immune response to different killed and modified live vaccines against PRRS virus and to monitor the antibody production and the cell mediated immunity both at the systemic and local level. In the experiment, we immunized four groups of piglets with two commercial inactivated (A1—Progressis, A2—Suivac) and two modified live vaccines (B3—Amervac, B4—Porcilis). Twenty-one days after the final vaccination, all piglets, including the control non-immunized group (C5), were i.n., infected with the Lelystad strain of PRRS virus. The serum antibody response (IgM and IgG) was the strongest in group A1 followed by two MLV (B3 and B4) groups. Locally, we demonstrated the highest level of IgG antibodies in bronchoalveolar lavages (BALF), and saliva in group A1, whereas low IgA antibody responses in BALF and feces were detected in all groups. We have found virus neutralization antibody at DPV 21 (days post vaccination) and higher levels in all groups including the control at DPI 21 (days post infection). Positive antigen specific cell-mediated response in lymphocyte transformation test (LTT) was observed in groups B3 and B4 at DPV 7 and in group B4 at DPV 21 and in all intervals after infection. The IFN-γ producing lymphocytes after antigen stimulation were found in $CD4^{-}CD8^{+}$ and $CD4^{+}CD8^{+}$ subsets of all immunized groups 7 days after infection. After infection, there were obvious differences in virus excretion. The virus was detected in all groups of piglets in serum, saliva, and occasionally in feces at DPI 3. Significantly lower virus load was found in groups A1 and B3 at DPI 21. Negative samples appeared at DPI 21 in B3 group in saliva. It can be concluded that antibodies after immunization and infection, and the virus after infection can be detected in all the compartments monitored. Immunization with inactivated vaccine A1—Progressis

induces high levels of antibodies produced both systemically and locally. Immunization with MLV-vaccines (Amervac and Porcilis) produces sufficient antibody levels and also cell-mediated immunity. After infection virus secretion gradually decreases in group B3, indicating tendency to induce sterile immunity.

Keywords: porcine reproductive and respiratory syndrome, virus, antibody, cell-mediated immunity, inactive vaccine, modified-live vaccine

INTRODUCTION

Porcine reproductive and respiratory syndrome (PRRS) is the most economically significant infectious disease currently affecting swine worldwide. Typical clinical symptoms of PRRS are mild to severe respiratory disease in infected newborn and growing pigs, and reproductive failure in pregnant sows. Two genotypes of the PRRS virus (PRRSV) have been identified: European (type 1) and North American (type 2). There are considerable genetic and virulence differences between and within PRRSV genotypes (1–3) correlated with a lack of cross-protection by vaccines (4–8). Highly pathogenic strains of PRRSV (HP-PRRSV) have been identified within both genotypes (9–11). Depending on viral strain and immune status of the host, some swine farms may have pigs subclinically infected, whereas others experience severe reproductive, and/or respiratory disease. Infection with both "classical" and highly pathogenic strains is associated with aberrant host immune response (9, 12).

Swine are the only known natural host of PRRSV and the primary target cells for replication of PRRSV are porcine alveolar macrophages (PAMs) (13). The first stage is represented by acute infection, resulting in viremia 6–12 h post-infection (PI), and lasting for several weeks despite the presence of circulating antibodies. In the second, persistent stage of infection, the virus is no longer detected in blood and lungs, and pigs no longer exhibit signs of clinical disease. In this stage, viral replication is primarily localized in lymphoid organs, including tonsils, and lymph nodes (14).

Infection with PRRSV elicit poor innate and adaptive immune responses associated with immune modulation and incomplete viral clearance in most of the pigs, depending on their age, and immune status (12, 15–17). Infection with certain PRRSV strains induced significant suppression of NK cell cytotoxic activity (18). The quantity of pro-inflammatory cytokines is significantly lower than in other viral infections and is strain dependent (19). PRRSV is also a poor inducer of IFN-α. Infection with PRRSV induces an antibody response (production) by 7–9 DPI but with no evidence of protection against PRRSV infection; serum neutralizing antibodies appear only later, typically ≥28 days PI (20). The virus also evades host cell-mediated immunity most likely by the promotion of immunosuppressive cytokines IL-10 and TGF-β resulting in delayed onset of Th1 immune response (18). Similarly, an immunosuppressive function of PRRSV was shown to probably be mediated by the cytokines IL-10 and TGF-β and action of Treg (21–23). Immunosuppression induced by PRRSV facilitates other viral and bacterial infections (18, 24, 25).

Vaccination is the principal means used to control and treat PRRSV infection. Several comprehensive review articles have been published recently. They critically evaluate different vaccination approaches against the PRRS virus and indicate the main weaknesses of current vaccines and vaccination strategies (26–29). Among others the problem are caused by high heterogeneity and occurrence of highly pathogenic strains and therefore efforts have been made to develop vaccines with a broad spectrum of effects (4, 5, 7, 30–33). However, the opinion still prevails that vaccination is more cost-beneficial over other health interventions (34–36).

Our study had the following three aims:

1) to establish complex immune response characteristics using several methodological approaches;
2) to monitor the dynamics in different compartments and in a time-dependent manner after vaccination and the challenging infection;
3) to compare the types of immune responses after vaccination with inactivated or live attenuated vaccines and subsequent challenge using a homologous strain.

MATERIALS AND METHODS

Animals

Twenty-five weaned piglets aged 8 weeks and weighing 8–12 kg of the Large White breed from a PRRSV negative herd were used. The negative status of the animals was confirmed by serology using commercial ELISA kit (Idexx Labs). The use of animals was approved by the Branch Commission for Animal Welfare of Ministry of Agriculture of the Czech Republic (approval protocol No. MZe-1487) as a part of project as a part of project Respig (QJ1210120).

Vaccines

Four commercial vaccines were used. Their characteristics are in **Table 1**.

Challenge Virus

Lelystad strain PRRSV (CAPM V-490) was obtained from the collection of animal pathogenic microorganisms (CAPM) at the Veterinary Research Institute (Brno, Czech Republic). The virus was propagated on the MARC-145 cell line and maintained in Dulbecco's Modified Eagle's Medium (DMEM) (Invitrogen) supplemented with 10% fetal bovine serum (FBS) (Thermo Scientific), 1% antibiotics (Antibiotic Antimycotic Solution 100x: 10,000 units penicillin, 10 mg streptomycin, and 25 μg amphotericin B per mL; Sigma-Aldrich) at 37°C and 5% CO_2.

TABLE 1 | Characteristics of vaccines used in the experiment.

Name	Producer	Type	Group of animals	Virus strain	Adjuvans
Progressis	Merial	Inactivated	A1	P120	Water in oil
Suivac PRRS-In	Dyntec	Inactivated	A2	VD-E1, -E2, -A1	Water in oil saponin
Amervac PRRS	Hipra	Modified live	B3	VP-046BIS	Diluent A3 levamisole
Porcilis PRRS	Intervet	Modified live	B4	DV	Diluent Diluvac forte

The virus was clarified by centrifugation, and its concentration was determined by plaque assay. The concentration of stock virus used in experiments was 5×10^6 plaque forming units per mL.

Experiment Design

Twenty-five piglets were used in the experiment. The piglets were assigned to five groups of five animals each according to weight and gender. The animals were housed in BSL2 isolation rooms, keeping animals from only one experimental group in each room. The animals were left to acclimate for 14 days after stocking. All piglets were clinically healthy at the time the experiment started. On day 0 (D0) two groups of piglets (A1 and A2) were immunized. Each animal was administered 2 ml of inactivated vaccine by an intramuscular (i.m.) injection. After 21 days (D21), piglets in these groups were revaccinated with the same dose, and piglets from the other two groups (B3 and B4) were immunized with 2 ml of a MLV vaccine. The health status of piglets was monitored on a regular basis, including temperature measurements, and samples of blood and other body fluids were taken for respective examinations at pre-set time intervals. After an additional 21 days (D42), all pigs, including control group (C5), were infected with 2 ml of the live PRRS virus. The piglets were monitored for another 21 days and then slaughtered (D63). Euthanasia was performed by exsanguination after combined anesthesia with a TKX (Telazol-Ketamin-Xylazin) mixture containing 12.5 mg/mL tiletamine and 12.5 mg/mL zolazepam (Telazol, Virbac, Carros, France), 12.5 mg/mL ketamine (Vetoquinol, Lure, France), and 12.5 mg/mL xylazine (Bioveta, Ivanovice na Hane, Czech Republic), administered intramuscularly in a final volume of 0.2 mL/kg body weight. As well as collection of blood and other body fluids (intestinal contents, bronchoalveolar lavage), an autopsy was performed and organs (lung parenchyma, spleen, lymph nodes,...) were collected for virological examination.

Sampling

Blood samples for serum and heparin-treated blood samples were taken from the jugular vein. Group saline samples were collected using ropes which were left in the hutch for 3 h. Individual fecal samples were collected when handling the animals.

Bronchoalveolar lavage fluid (BALF) sampling was performed for the first time on live animals and for the second time after slaughter. The intravital lavage was performed with the animals under general anesthesia (a mixture of Xylazine and Ketamin) without the use of an endoscope by a method described earlier (37). Pigs were positioned in the sternal recumbency. An endotracheal tube was inserted into the trachea and 20 ml of sterile PBS (pH 7.2) was injected into the distal parts of the airways, toward the bronchus. About 60% of the infused saline was recovered as BALF aspirate and was filtered and centrifuged for 15 min at 200 g. Supernatant was stored at -20°C prior to serological analyses.

Quantitative RT-PCR for Viral Load Detection

Total RNA from experimental samples of sera, oral fluids, and BAL (100 μL) was extracted using a NucleoSpin® RNA II kit (MACHEREY-NAGEL), in accordance with the manufacturer's instructions (protocol for total RNA preparation from biological fluids). The RNA obtained was eluted in 60 μL RNase-free water and immediately used for qRT-PCR amplification. Remaining RNA was frozen at −80°C for subsequent use.

Isolated RNA was used for qRT-PCR amplification by EZ-PRRSV™ MPX 4.0 Real Time RT-PCR kit (Tetracore), in accordance with the manufacturer's instructions. Quantification of the virus genome copies was based on quantification standards included in the kit.

Serology Evaluation

For the evaluation of systemic and local antibody production two ELISA methods were used.

All swine sera tested were examined by commercially available ELISA test INGEZIM PRRS UNIVERSAL (Ingenasa), in accordance with the manufacturer's instructions, to examine for the presence of N protein specific IgG antibodies.

All swine sera, oral fluids, and BAL tested were examined by home-made indirect ELISA test based on recombinant nucleocapsid protein N of PRRS virus (developed previously in our department) for detection of specific IgM, IgG, and IgA antibodies.

Optimal antigen, serum, and antibodies concentrations were determined by checkerboard titration of positive and negative porcine sera. The cut-off value was determined by defining the upper prediction limit based on the upper tail of the t-distribution of negative control OD readings, at a confidence level of 99.5%. Positive serum with an absorbance corresponding to the calculated cut-off was included in all test plates.

The recombinant N protein diluted in 50 mM Bicarbonate-Carbonate Buffer pH 9.6 to a final concentration of 1.5 μg/mL was coated on 96-well-microtiter plates (Maxisorp II® Immunoplates, Nunc, Denmark) overnight at 26°C. The wells were then blocked with 3% skimmed milk in PBS for 90 min

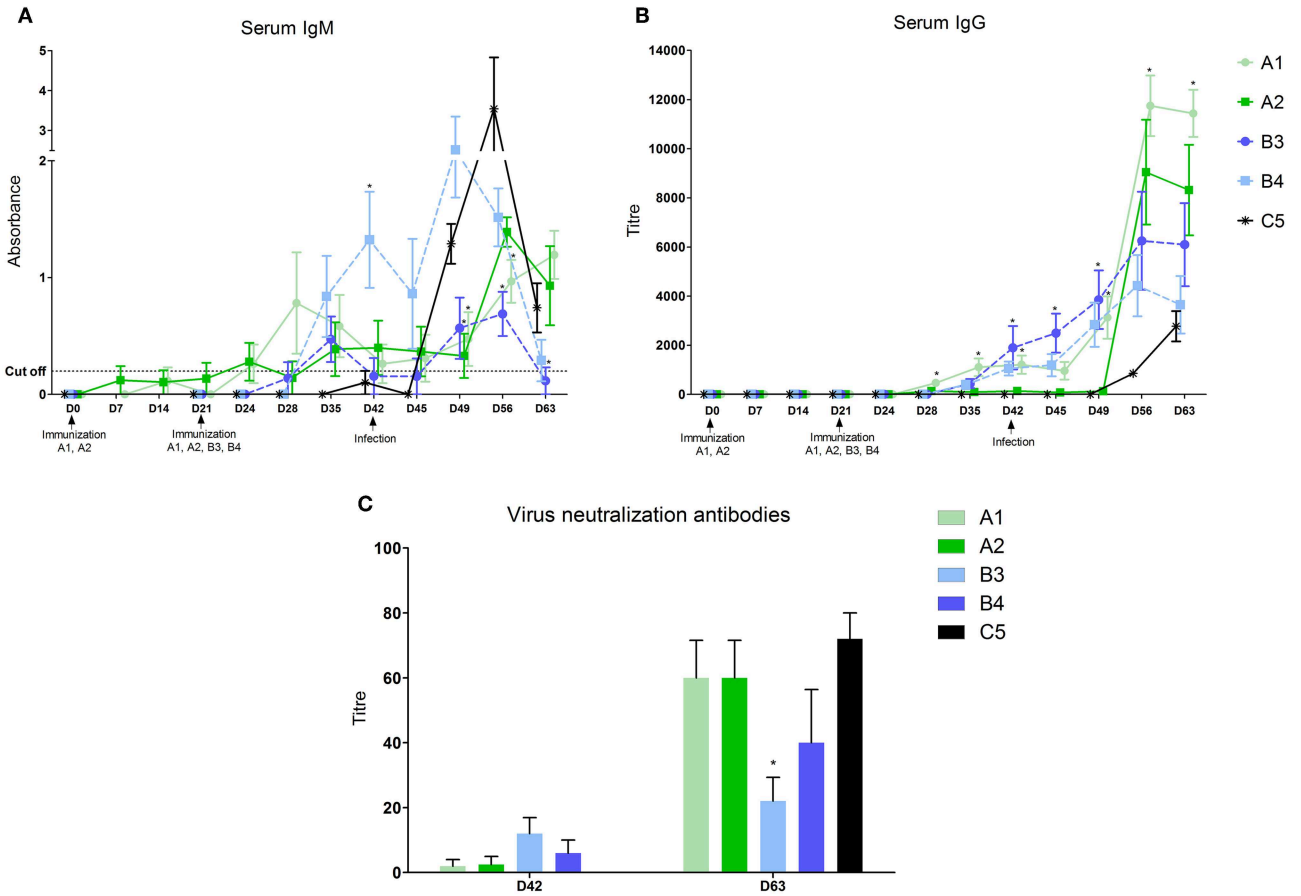

FIGURE 1 | Levels of antibodies in sera. Levels of antibodies were measured in sera with home-made ELISA (**A**–IgM) or the commercial ELISA test Ingezim PRRS universal (**B**–IgG) Levels of virus neutralization antibodies 21 days after vaccination and 21 days after infection **(C)**. *statistically significant difference ($p < 0.05$) from control group.

at 37°C and then washed with PBS. Positive and negative controls were included in each test plate. Each sample diluted in 3% skimmed milk in T-PBS (PBS with 0.1% Tween 20 and 0.5 M NaCl) was added in duplicates on antigen-coated wells with some differences among different types of samples. One hundred microliters of serum samples diluted 1:40 (for detection of IgM antibodies) or 100 μL of non-diluted samples of BAL (for detection of IgG and IgA antibodies) were incubated for 60 min at 37°C. Two hundred and fifty microliters of oral fluids diluted 1:2 were incubated 16 h at 4°C (for detection of IgG antibodies). Subsequently the plates were washed three times with T-PBS and antibody binding was detected by incubation for 60 min at 37°C with 100 μL of anti-Pig IgM peroxidase conjugate (1:10,000, Bethyl), anti-Pig IgG peroxidase conjugate (1:30,000, Sigma), or with anti-Pig IgA peroxidase conjugate (1:3,000, Bethyl) separately (diluted in T-PBS with 3% skimmed milk). After washing the plates as described above, 100 μL per well of the TMB-Complete (TEST-LINE) substrate was added. The optical density (OD) was measured at 450 nm after an incubation time of 5–10 min at room temperature.

Virus Neutralization Test

The virus neutralization test for detection of PRRSV neutralization antibodies was performed as follows. Samples of sera were diluted 1:4 in DMEM medium (Sigma–Aldrich) supplemented with 3% FBS. Then, heat inactivated sera (56°C for 60 min) were diluted 2-fold serially in flat-bottom 96-well-microplate (NUNC). Next, equal volume (50 μL) of media containing 50 PRRSV PFU (Lelystad—CAPM V-490) was added to each well. Following incubation (60 min at 37°C) MARC-145 cells were added to each well (3×10^4 per well) in 100 μL media per well. After 5 days of cultivation (37°C, 5% CO_2), the cytopathic effect (CPE) of PRRSV on MARC-145 was evaluated by optical microscopy. The reciprocal value of the last sera dilution causing 50% reduction of CPE was defined as virus neutralization antibody titer.

Lymphocyte Transformation Test

The lymphocyte transformation test was performed according to the method published earlier (38). Peripheral blood mononuclear cells (PBMC) were obtained by gradient centrifugation

TABLE 2 | Summary of immune responses and virus excretion of individual vaccines used in the experiment.

	Parameters	Time	A1—inactivated (Progressis)			A2—inactivated (Suivac)			B3—mlv (Amervac)			B4—mlv (Porcilis)		
ANTIBODY PRODUCTION														
Serum	Dynamics: IgM	D24	+			+			−			−		
		D28	++			+			−			−		
		D35	++			+			++			+		
	Dynamics: IgG	D28	++			+			−			−		
		D35	++			+			++			++		
		D49	++			+			++			++		
		D63	+++			+++			++			++		
	Virus neutralization Ab	D42	±			±			++			+		
		D63	+++			+++			+			++		
Local response	Saliva IgG	D35	+			−			−			−		
		D49	++			−			+			−		
		D63	+++			++			++			++		
	BALF IgG	D35	+++			+			+			−		
		D63	++			++			+			+		
	BALF IgA	D35	++			++			++			+		
		D63	−			+			+			+		
CELL MEDIATED IMMUNITY														
	LTT: non-stimulated cells	All	+++			+++			++			−		
	LTT: stimulated cells (SI)	All	not evalable			not evaluable			+ at D28			++ at D28, D42, D49, D63		
	IFNγ in Ag–stimulated subsets	D49	positive $CD4^{-}CD8^{+}$cells			positive $CD4^{-}CD8^{+}$cells			positive $CD4^{-}CD8^{+}$cells			positive $CD4^{-}CD8^{+}$cells		
			positive $CD4^{+}CD8^{+}$cells			positive $CD4^{+}CD8^{+}$cells			positive $CD4^{+}CD8^{+}$cells			positive $CD4^{+}CD8^{+}$cells		
	Elispot IFNγ	D63	positive			positive			positive			positive		
VIRUS LOAD														
			serum	saliva	feces	serum	saliva	feces	serum	saliva	feces	serum	saliva	feces
	Post immunization	D24	−	−	−	−	−	−	++	++	−	++	++	−
		D42	−	−	−	−	−	−	+++	++	−	++	−	++
	Post infection	D45	++	++	+++	+++	−	+++	+++	++	+++	+++	++	+++
		D56	+	++	−	++	−	+	++	−	++	++	++	++
	The end of experiment	D63	+	++	++	+	++	+++	±	−	+	+	++	+

post vaccination (D0-D42) + + + positive (high); ++ positive (mid); + positive (low); ± positive in some animals.

post infection (D45-D63) –negative.

All All intervals.

Groups of 5 piglets were immunized i.m with inactivated vaccine A1 (Progressis) or A2 (Suivac PRRS-In) at intervals D0 and D21. Groups of 5 piglets were immunized i.m with modified live vaccine B3 (Amervac PRRS) or B4 (Porcilis PRRS) at interval D21. All animals were infected with a challenge virus on D42, including the group of control non-immunized piglets (C5). All levels or activities after vaccination or infection are expressed as – (negative) or + to + + + as positive at different intensity.

(Histopaque-1077, Sigma–Aldrich). Concentration of the cells was adjusted to 200,000 cells in 200 μL of RPMI-1640 medium supplemented with 10% of autologous serum, 100 IU/mL penicillin, 100 μg/mL streptomycin, and 4 μg/mL gentamicin). They were incubated with the 20 μg of optimal concentration of the specific antigen (MOI 1.0) for 5 days at 37°C in 5% CO_2. Negative controls were incubated with RPMI-1640 medium only. All samples were evaluated in triplicate. ^{3}H-thymidine was added on the last day of cultivation. Subsequently, the cells were harvested (FilterMate Harvestor, Packard Bioscience Company, USA), and ^{3}H-thymidine incorporation was measured by a microplate scintillation and luminescence counter (TopCount NXT^{TM}, Packard Bioscience Company) in counts per minute (CPM). The results were expressed in terms of stimulation indexes (SI), which were calculated as the ratio of CPM in stimulated samples vs. CPM in non-stimulated controls.

ELISpot (for IFN-γ Production)

The number of IFN-γ producing cells was calculated by ELISpot techniques. Commercially available Porcine IFN-γ ELISpot kit (3130-4HPW-10, MABTECH) was used in accordance with the manufacturer's instructions. The number of cells used in the test was 5×10^5/well. PRRSV was used for stimulation of the antigen-specific response in multiplicity of infection (MOI) 0.5. Mitogen ConA at a concentration 66 μg/mL was used as a positive control. Cells without stimulation were used as a negative control. Incubation lasted for 20 h. Spots were detected using ELISpot reader system ELRO7TL (AID, Germany). The results were recalculated to the number of $CD3^+$ lymphocytes.

Identification of Lymphocyte Subpopulation Producing IFN-γ After Antigen Stimulation

The 5×10^5 of PBMC per well was stimulated with PRRS virus in MOI 0.5 for 20 h. The 5×10^5 of cultured PBMC were pelleted and 20 μL of primary monoclonal antibody cocktail containing anti-CD4 (IgG2b, clone 74-12-4, WSU, Monoclonal Antibody Center, USA), anti-CD8 (IgG2a, clone 76-2-11, WSU, USA), and anti-γδ TCR (IgG1, clone PGBL22A, WSU, USA) and 20 μL of heat-inactivated goat serum was added. The cells were incubated for 20 min at 4°C and then rinsed twice with cell washing solution. Then, 50 μL of goat anti-mouse secondary antibody cocktail (anti-IgG2b: DyLight 405, anti-IgG2a: Alexa Fluor 647, and anti-IgG1: PE-Cy7) was added and the cells were incubated for another 20 min at 4°C. The cells were rinsed and then 70 μL of anti-CD3 antibody (IgG1, clone PPT3, Southern Biotech, pre-stained with Alexa Fluor 488 dye using Zenon Antibody Labeling Kit, Invitrogen) was added and the cells were incubated, rinsed twice, and fixation and permeabilization for subsequent intracellular staining was performed by solutions A and B of Intra Stain Kit (DAKO Cytomation, USA) (39). Finally, 5 μL of RPE-conjugated anti-IFN-γ antibody (clone CC302, AbD Serotec UK) was added and the cells were incubated for 30 min. The cells were measured as soon as possible using BD LSR Fortessa flow cytometer (Becton-Dickinson, USA). At least 100,000 events were acquired. The post-acquisition analysis of data was performed using the FACS Diva software (Becton-Dickinson, USA). The following lymphocyte subpopulations were identified: ($CD3^+$) $\gamma\delta^+CD8^+$, ($CD3^+$) $\gamma\delta^+CD8^-$, ($CD3^+\gamma\delta^-$) $CD4^+CD8^+$, ($CD3^+\gamma\delta^-$) $CD4^-CD8^+$, ($CD3^+\gamma\delta^-$) $CD4^+CD8^-$, ($CD3^+\gamma\delta^-$) $CD4^-CD8^-$, and $CD3^-CD8^+$. The percentage of IFN-γ-positive cells was established for each subpopulation.

Statistical Analysis

The normality of data distribution were confirmed. Experimental groups were compared using non-parametric Man-Whitney test. Data from different dates were compared using non-parametric Wilcoxon test for paired samples.

Legend on the Figure

Groups of five piglets were immunized i.m. with inactivated vaccine A1 (Progressis) or A2 (Suivac PRRS-In) at intervals D0 and D21. Groups of five piglets were immunized i.m. with modified live vaccine B3 (Amervac PRRS) or B4 (Porcilis PRRS) at interval D21. All animals were infected with a challenge virus on D42, including the group of control non-immunized piglets (C5).

RESULTS

Detection of Antibody Levels in Sera

After vaccination with inactivated vaccines (A1 and A2) the first IgM in the serum started to appear 14 days after the first dose in some piglets, and 7 days after the second dose in all animals of the A1 group (**Figure 1A** and **Table 2**). IgG antibodies appeared in all animals of both groups 7 days after the second dose (**Figure 1B**). The level of antibodies in the A1 group was significantly higher than in the group given the A2 vaccine. In groups of piglets vaccinated with MLV vaccines (B3 and B4), both IgM and IgG antibodies appeared 14 days after vaccination. On day 21 after immunization, their antibody responses were comparable to that of the A1 group.

After infection, we identified a further increase in antibodies in the vaccinated groups. For the A1 group, a further increase in serum IgG antibodies was observed after 1 week and especially at 14 and 21 days after infection, when this antibody level significantly exceeded the values in the MLV immunized groups (B3 and B4) and the control one (C5). The A2 group showed a sharp increase on post infection days 14 and 21, and the level of serum IgG antibodies at these intervals was comparable to A1. In groups immunized with MLV (B3 and B4), serum IgG levels increased after 7, 14, and 21 days post infection, but did not reach the A1 group values. In the control, non-immunized group, the first IgM antibodies appeared 3 days after infection, with a significant increase on day 7 and 14. IgG antibody levels appeared 14 and 21 days after infection but were lower than in the immunized groups.

The virus neutralization antibody was detected in sera of animals 21 days after vaccination (**Figure 1C**). These antibodies were detected in some animals in the groups A1 and A2 only. At the end of experiment (D63, 21 days post-infection) the high

level of virus neutralization antibodies were detected in all groups except B3 group, in which significantly lower level was found (**Figure 1C**).

Detection of Antibody Levels in Other Compartments

Local antibodies in the BALF performed 14 days post vaccination we detected low levels of IgA in all immunized groups (**Figure 2A**) and IgG in A1, A2, and B3 (none in B4) with the level in the A1 group being significantly higher (**Figure 2B**). 21 days after infection we detected low levels of IgA antibodies in A2, B3, B4, and control group (C5) and low levels of IgG antibodies in all immunized groups (none in C5). Local antibodies were detected in the saliva of the A1 group in low concentrations 14 and 21 days after the second vaccination and in all groups after infection with variability in individual intervals and with no statistically significant between-group difference (**Figure 2C**). In the feces, local antibodies (IgA) were detected from 1 week after the second immunization dose in groups A1 and A2, and from 1 week after MLV immunization in groups B3 and B4 (**Figure 2D**) Increased levels of antibody were detected in all groups including control after infection with no statistically significant between-group difference.

Cell Mediated Immune Response

A positive cell-mediated response after lymphocyte stimulation with specific antigen *in vitro* (stimulation index in LTT above 3) was observed in the B4 group after 7 and 21 days post vaccination and 7 and 21 days post-infection (**Figure 3**). A positive stimulation index was detected in the B3 group at 7 days post vaccination only as a non-specific basal stimulation occurred from 21 days post vaccination in this group (**Figure 3A**).

Groups immunized with inactivated vaccines A1 and A2 showed a marked non-specific stimulation of cells even without using antigen (**Figure 3A**) and, therefore, it was impossible to demonstrate the effect of antigen addition and thus cell-mediated immune response.

Cell-mediated immune response after challenge infection was positive in all vaccinated groups and in the control group after 21 days post infection, using ELISpot in PBMC from bronchoalveolar lavages. The results were recalculated to the number of $CD3^+$ lymphocytes. The differences between individual animals, but no significant differences between groups were detected (**Figure 3D**).

We detected IFN-γ producing lymphocytes after PRRS antigen stimulation. The most marked differences from control were found in $CD4^-CD8^+$ and $CD4^+CD8^+$ (and partly also in $CD3^-8^+$ and $\gamma\delta^+8^+$) subsets of all immunized groups 7 days after infection.

Virus Load and Clinical Signs

In the groups vaccinated with live vaccines (B3 and B4), the virus load was demonstrated in serum and saliva from day 3 after immunization, in BALF 14 days after immunization (the only time point when the lavage was taken), and in feces occasionally 7 days after vaccination, then in all piglets 14 days after immunization (data not shown).

No clinical signs were observed in piglets after infection. Elevated body temperature was occasionally found in the first 2 days, independent of the experimental group.

However, viral shedding was noted, with between-group differences. The virus appeared in serum, saliva, and feces in all groups including the control group 3 days after infection (**Figures 4A,B,D**). The virus was detected in BALF 21 days after infection in A1, A2, and C5 groups (**Figure 4C**). Virus shedding was decreased in immunized groups 14 and 21 days after infection with the level in the A1 and B3 group being significantly lower compared to control group 21 days after infection. Negative samples appeared 21 days after infection in saliva (in B3 group) and in feces (B3 and B4 groups).

DISCUSSION

The goals of our study were (1) to establish comprehensive immune response characteristics using several methodological approaches and monitor the dynamics in different compartments and in a time-dependent manner after vaccination and the challenging infection and (2) to compare the immune response to different killed and modified live vaccines against PRRS using these methodological tools. In order to compare the immune response after vaccination with different vaccines, we used a model of vaccinations of young piglets (beginning at 8 weeks of age) and given vaccination intervals and subsequent infections, regardless of the fact that manufacturers' recommendations were different (especially in Progressis).

There are only a few papers published providing a comprehensive picture of immune response after vaccination against PRRSV (40–43) because the majority of the existing studies are based mainly on the evaluation of the vaccination effectiveness by monitoring the immune responses found in the blood (5, 30, 33, 44–46). Our results show that antibodies after immunization and infection, and the virus after infection, can be detected in all the monitored compartments (blood, respiratory tract, intestine). By repeated sampling and simultaneous monitoring of the antibody and cell-mediated immunity and virus shedding systematically and locally, we have managed to get comprehensive information about the dynamics of the immune response after vaccination or PRRS virus infection.

In practical diagnostics of field samples is an effort to seek simple approaches to obtain tentative information on the epidemiological situation of the herd. One current trend is the monitoring of antibody levels and shedding of the virus in the oral fluid (41–43). In our experiment, the antibody detection rate in the oral fluid collected with ropes in pens was sufficient. The levels of antibodies detected after vaccination were low, but they increased after challenge infection. These findings confirms the possibility of using this approach for preliminary characteristics in the herd. It was interesting to observe the dynamics of antibody levels and viral shedding in feces too. This is an approach which is not often used for PRRSV infection monitoring but is used in other situations where feces samples are more readily available than samples from other sources (47,

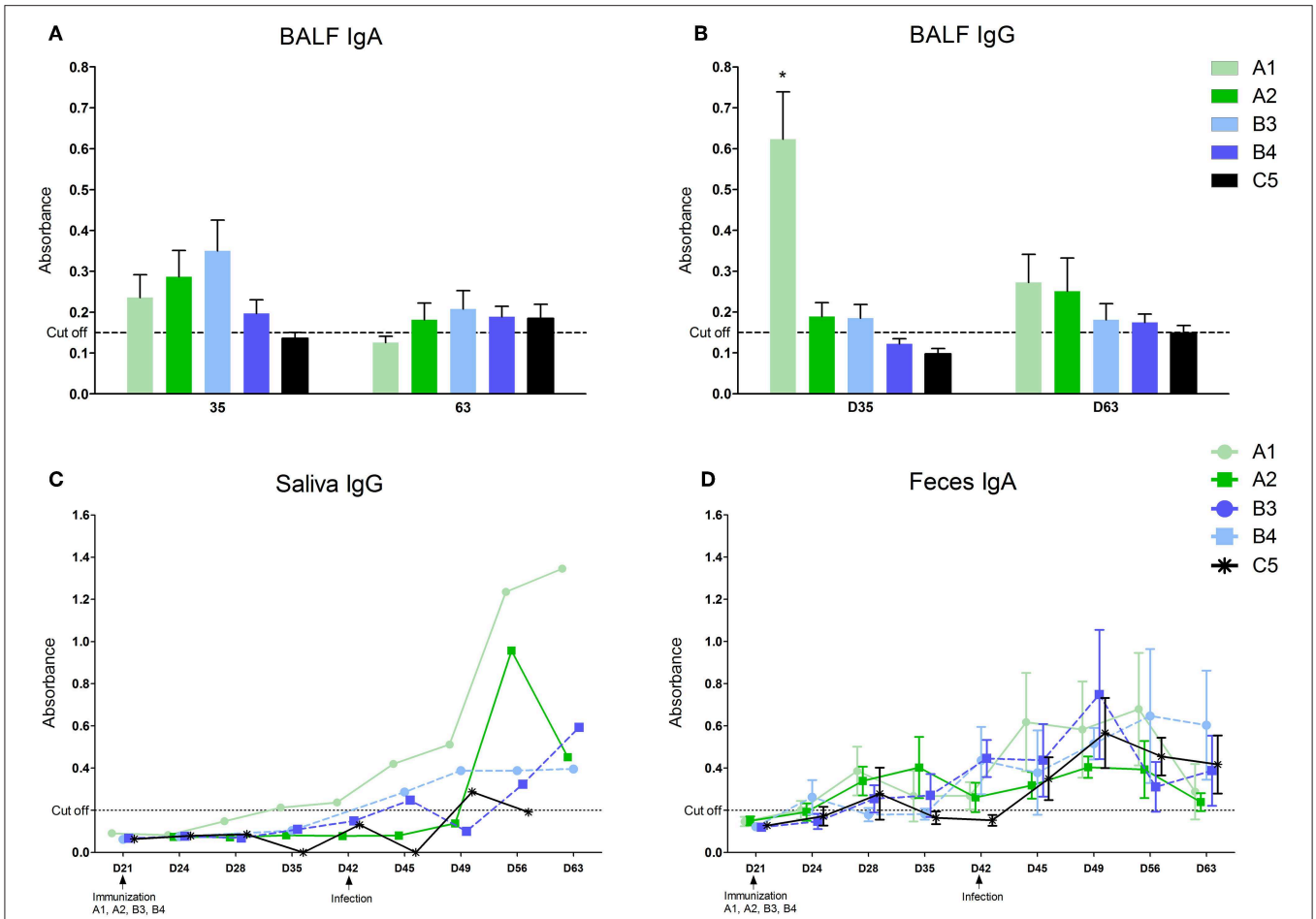

FIGURE 2 | Levels of antibodies in different compartments. Levels of antibodies were measured in oral fluids **(A)**, fluid from bronchoalveolar lavages (**B**–IgG, **C**–IgA), and feces (**D**–IgA) with home-made ELISA. *statistically significant difference ($p < 0.05$) from control group.

48). We were wondering, among other things, to what extent infections occurring systemically, or locally in the respiratory tract occur in this remote compartment. Our findings show that fecal samples can also be used for PRRSV infection monitoring. Detection of both the viruses and antibodies is not entirely consistent, because they appear in individual animals, and cease at later intervals, therefore, it is necessary to consider these findings as approximate. They can be used for herd- or pen- level testing, but not for establishing a diagnosis in individual animals.

It appeared to be technically difficult to demonstrate specific cell-mediated immunity. The partial results were provided by each of the three methods used and a comprehensive picture could be obtained by compiling this information. Therefore, it was not possible to use only data of IFN-γ production in ELISpot, although it is currently the most commonly used method for CMI (5, 29, 37, 38, 49, 50). A positive cell-mediated response after lymphocyte stimulation with specific antigen *in vitro* (in lymphocyte transformation test) was observed in MLV groups and especially in the B4 group as a non-specific basal stimulation occurred from 21 days post-vaccination in B3 group. The strong non-specific stimulation of PBMC without specific antigen were detected in groups A1 and A2 immunized with inactive types of vaccine. This non-specific stimulation of cells *in vivo* masks the overall picture, and thus specific cell-mediated immunity cannot be demonstrated. This effect is attributed to the use of strong adjuvants in inactivated types of vaccines. In the test of IFN-γ production and detection with ELISpot, which is very often used to identify CMI both in experimental studies (5, 37), and in the field (49, 50), we have shown an increase in both blood and cells acquired by lavage, but the individual variability among the animals was too high and, consequently, there were no differences found between the groups under study. We detected also IFN-γ producing lymphocytes after PRRS antigen stimulation in all immunized groups 7 days after infection. The most marked differences from control were found in $CD4^{-}CD8^{+}$ and $CD4^{+}CD8^{+}$ (and partly also in $CD3^{-}CD8^{+}$ and $\gamma\delta^{+}CD8^{+}$) subsets of lymphocytes. The $CD4^{-}CD8^{+}$ subpopulation belongs to cytotoxic groups of cells, $CD4^{+}CD8^{+}$ is considered a group of Th1 memory cells (51). In another study the expression of cytotoxic $CD4^{+}CD8^{+}$ and $CD4^{+}CD8^{-}$ was described which help to recover from PRRS infection (52).

There were qualitative and quantitative differences in the immune responses to the inactivated vaccines and to MLV ones.

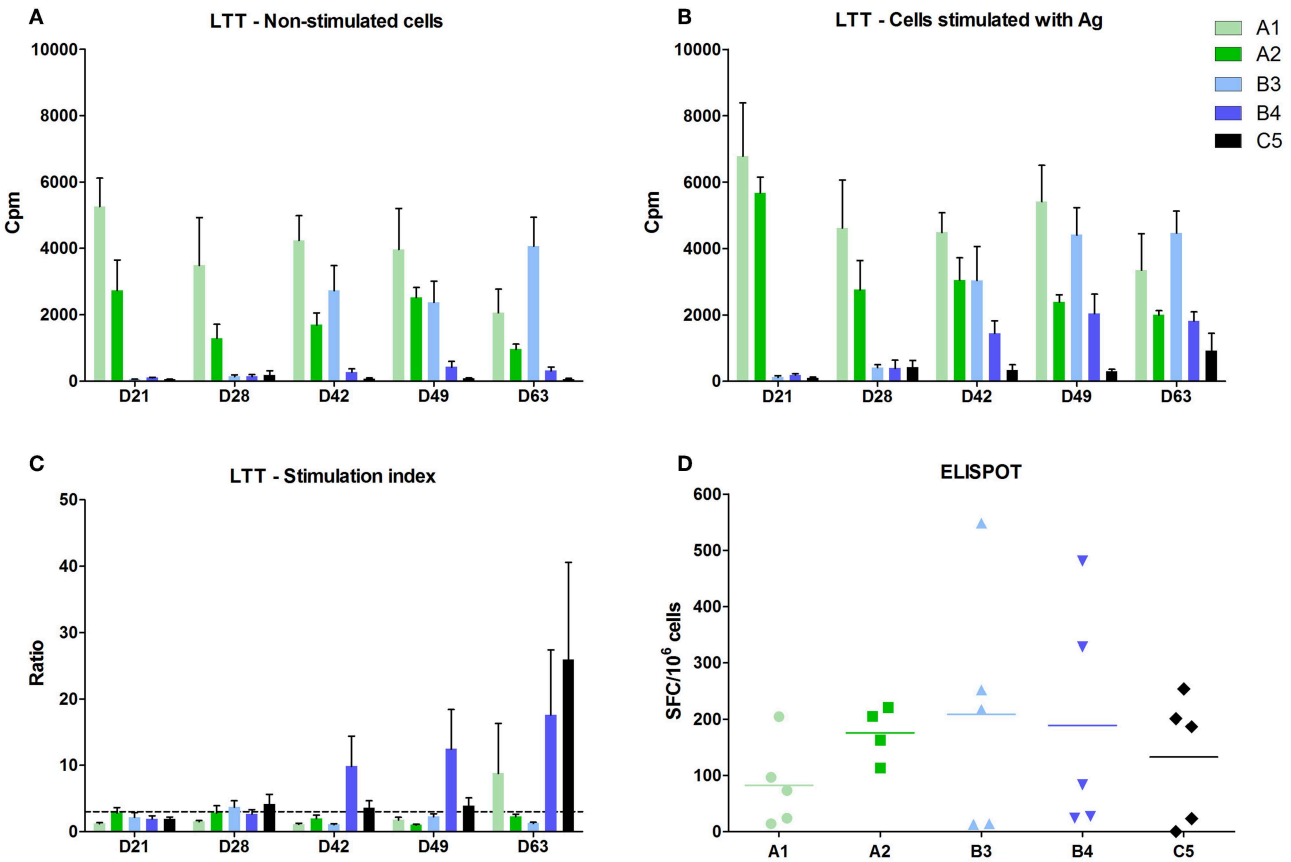

FIGURE 3 | Cell mediated immunity. The activity of blood lymphocytes was measured in the lymphoblast transformation test (LTT) using 5-day cultivation of cells. **(A)** Control, activity of non-stimulated cells. **(B)** Activity of cells stimulated with PRRSV antigen. The activities were measured after adding ^{3}H-thymidine and counted as counts per minute (CPM) in a beta-counter. **(C)** Ratio the ratio of stimulated to non-stimulated cells (stimulating index—SI). **(D)** ELISPOT. The number of IFN-γ producing cells was calculated in cells from bronchoalveolar lavage fluid (BALF) on D63, i.e. 21 days after the challenge infection. The results were recalculated to the number of $CD3^{+}$ lymphocytes.

After immunization with the inactivated vaccine (especially A1—Progressis), high levels of antibodies were produced generally (serum), which were mostly of the IgM, and IgG isotypes, and also locally (saliva, BALF), both IgG and IgA. Nevertheless it should be noted that we have applied Progressis to piglets in our study, while the manufacturers declare the use of this vaccine for gilts and sows. Cell-mediated immunity was detected only after infection, high non-specific cell stimulation was detected after vaccination and therefore any specific response could not be demonstrated in these intervals. The antigen specific cell mediated immunity after inactivated vaccine is rarely described (50). Most work describes low or no CMI after vaccination with inactivated vaccine.

After immunization with MLV vaccines, sufficient levels of antibodies in serum and BALF (IgG) were also produced, but lower than after the inactivated vaccine administration. The levels of IgA antibodies in BALF were comparable but low. Low levels of virus neutralization antibodies after vaccination can be explained by a short interval between vaccination and infection, since neutralizing antibodies after vaccination or PRRS infection occur within 28 days (42).

The dynamics of virus shedding after vaccination and infection is often used for monitoring vaccine efficacy (30, 40, 49). The decrease in virus secretion was observed 14 days after MLV immunization and disappearance in 28 days (42). In another study the excretion of virus was described still for 21 days after vaccination with for Porcilis or Amervac vaccine (53). Demonstration of cell-mediated immunity and reduction in viral load correlate with studies by other authors and support the preferred use of MLV vaccines in the control of PRRS infection (29, 46).

The question is to what extent these results are influenced by the composition of vaccines from different manufacturers and to what extent different types of vaccines (inactivated vs. live attenuated). There was an obvious difference in the quality between the inactivated vaccines, whereas the character of the immune response to both MLV vaccines was similar with only partial differences in the time-related response dynamics. The vaccine B3 (Amervac) showed a more pronounced decrease

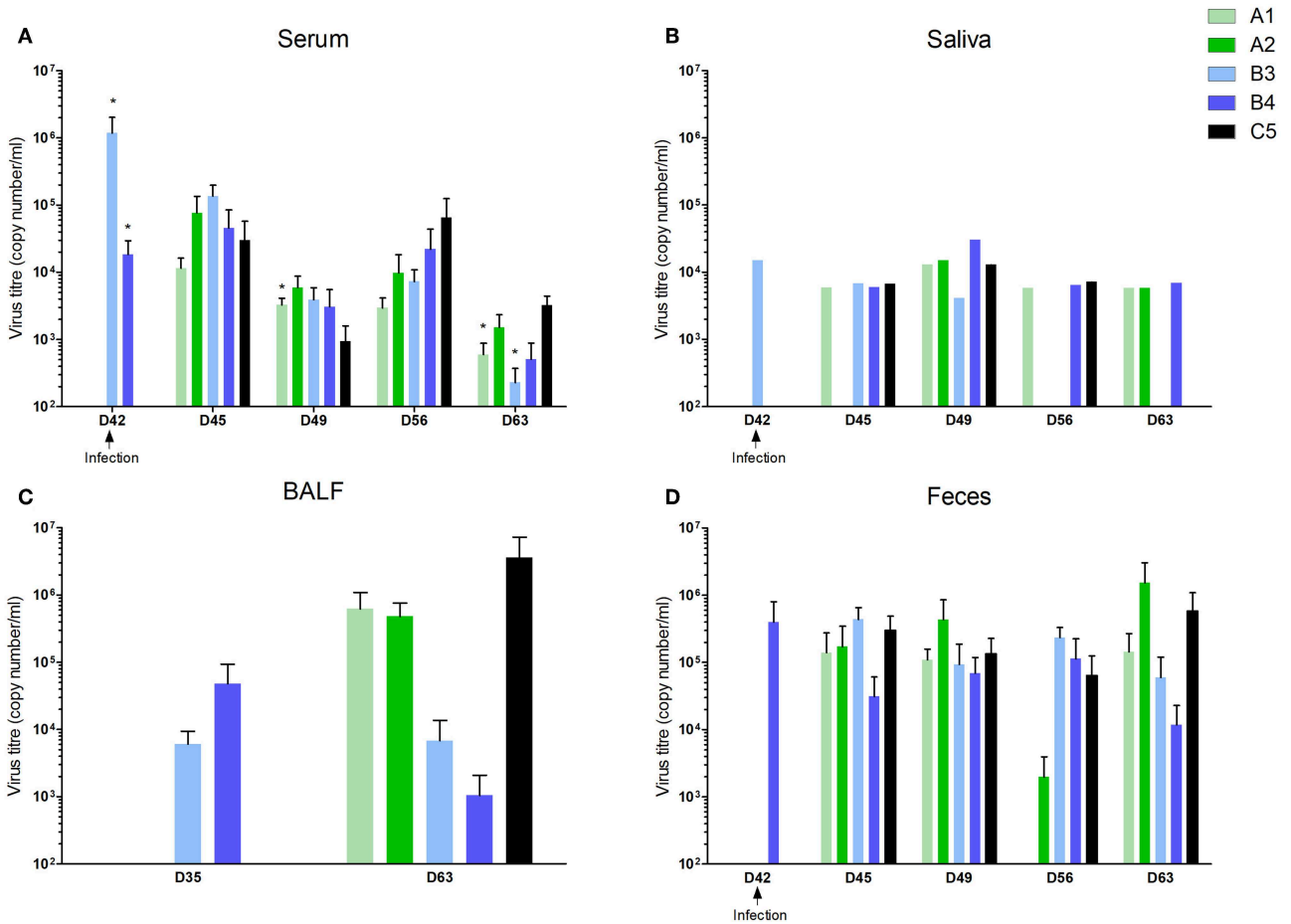

FIGURE 4 | Viral load in different compartments. Groups of 5 piglets were immunized i.m with inactivated vaccine A1 (Progressis) or A2 (Suivac PRRS-In) at intervals D0 and D21. Groups of 5 piglets were immunized i.m with modified live vaccine B3 (Amervac PRRS) or B4 (Porcilis PRRS) at interval D21. All animals were infected with a challenge virus on D42, including the group of control non-immunized piglets (C5). Viral load was measured by quantitative real-time-PCR. **(A)** Viral load in sera, **(B)** oral fluids, **(C)** fluid from bronchoalveolar lavages, and **(D)** feces. *statistically significant difference ($p < 0.05$) from control group.

in virus secretion and a tendency to induce sterile immunity, while B4 (Porcilis) vaccine had a more pronounced of CMI in lymphocyte transformation test. It should be noted that the strain used in Porcilis had a higher genetic link with the Lelystad strain compared to the strain of Amervac (54, 55) which, however, probably did not significantly affect the above characteristics.

Despite the fact that many studies focused on PRRS immunoprophylaxis have already been published and many procedures are implemented in the agricultural industry, a universal model does not yet exist (46–60). The use of live attenuated vaccines is generally preferred as was also confirmed in our field study (61). In this study, we controlled the infection by a repeated blanket immunization with MLV vaccine (Porcilis), followed by targeted immunization of gilts, and sows. The success of the strategy selected and evidence of virus eradication from the given herd were demonstrated by introducing sentinel animals into a fattening herd. Based on this result, we believe that control programs can be adopted even in herds with continual throughput housing without interrupting production. However, in this case, vaccination is only one of the necessary preconditions and the introduction of very strict principles of good biosecurity is of no less importance.

ETHICS STATEMENT

The use of animals was approved by the Branch Commission for Animal Welfare of Ministry of Agriculture of the Czech Republic (approval protocol No. MZe 1487) as a part of project as a part of project Respig (QJ1210120).

AUTHOR CONTRIBUTIONS

MT, VC, JS, and MF designed the study. MT, LL, JS, and KN performed the experiments. LL, HK, LK, PO, and JF performed the lab work and analyzed the data. LK produced the figures and statistical analysis. MT wrote the manuscript. JS and MF participated in manuscript preparation. All authors read and approved the final manuscript.

FUNDING

The study was supported by Projects No. QJ1210120, QJ1510108, and RO0518 of the Ministry of Agriculture of the Czech Republic and by project LO1218 with financial support from the Ministry of Education, Youth, and Sports of the Czech Republic under the NPU I program.

REFERENCES

1. Stadejek T, Oleksiewicz MB, Potapchuk D, Podgorska K. Porcine reproductive and respiratory syndrome virus strains of exceptional diversity in Eastern Europe support the definition of new genetic subtypes. *J Gen Virol.* (2006) 87:1835–41. doi: 10.1099/vir.0.81782-0
2. Stadejek T, Oleksiewicz MB, Potapchuk D, Scherbakov AV, Timina AM, Krabbe JS, et al. Definition of subtypes in the European genotype of porcine reproductive and respiratory syndrome virus: nucleocapsid characteristics and geographical distribution in Europe. *Arch.Virol.* (2008) 153:1479–88. doi: 10.1007/s00705-008-0146-2
3. Darwich L, Gimeno M, Sibila M, Diaz I, de la Torre E, Dotti S, et al. Genetic and immunobiological diversities of porcine reproductive and respiratory syndrome genotype I strains. *Vet Microbiol.* (2011) 150:49–62. doi: 10.1016/j.vetmic.2011.01.008
4. Mengeling WL, Lager KM, Vorwald AC, Koehler KJ. Strain specificity of the immune response of pigs following vaccination with various strains of porcine reproductive and respiratory syndrome virus. *Vet Microbiol.* (2003) 93:13–24. doi: 10.1016/S0378-1135(02)00427-3
5. Park CH, Seo HW, Han K, Kang I, Chae CH. Evaluation of the efficacy of a new modified live porcine reproductive and respiratory syndrome virus (PRRSV) vaccine (Fostera PRRS) against heterologous PRRSV challenge. *Vet Microbiol.* (2014) 172:432–44. doi: 10.1016/j.vetmic.2014.05.030
6. Geldhof MF, Vanhee M, Van Breedam W, Van Doorsselaere J, Karniychuk U, Nauwynck, HJ. Comparison of the efficacy of autogenous inactivated porcine reproductive and respiratory syndrome virus (PRRSV) vaccines with that of commercial vaccines against homologous and heterologous challenges. *BMC Vet Res.* (2012) 8:182. doi: 10.1186/1746-6148-8-182
7. Choi K, Park CH, Jeong J, Chae CH. Comparison of protection provided by type 1 and 2 porcine reproductive and respiratory syndrome field viruses against homologous and heterologous challenge. *Vet Microbiol.* (2016) 1191:72–81. doi: 10.1016/j.vetmic.2016.06.003
8. Correas I, Osorio FA, Stefen D, Pattnaik AK, Vu HLX. Cross efficacy of immune responses to porcine reproductive and respiratory syndrome virus infection. *Vaccine.* (2017) 35:782–8. doi: 10.1016/j.vaccine.2016.12.040
9. Xiao S, Mo D, Wang Q, Jia JY, Qin LM, Yu XC, et al. Aberrant host immune response induced by highly virulent PRRSV identified by digital gene expression tag profiling. *BMC Genomics.* (2010) 11:544. doi: 10.1186/1471-2164-11-544
10. Karniychuk U, Geldhof M, Vanhee M, Van Doorsselaere J, Saveleva TA, Nauwynck, HJ. Pathogenesis and antigenic characterization of a new East European subtype 3 porcine reproductive and respiratory syndrome virus isolate. *BMC Vet Res.* (2010) 6:30. doi: 10.1186/1746-6148-6-30
11. Han J, Zhou L, Ge X, Guo X, Yang H. Pathogenesis and control of the Chinese highly pathogenic porcine reproductive and respiratory syndrome virus. *Vet Microbiol.* (2017) 209:2017. doi: 10.1016/j.vetmic.2017.02.020
12. Loving CL, Osorio FA, Murtough MP, Zuckermann, FA. Innate and adaptive immunity against porcine reproductive and respiratory syndrome virus. *Vet Immunol Immunopathol.* (2015) 167:1–14. doi: 10.1016/j.vetimm.2015.07.003
13. Duan X, Nauwynck, HJ, Pensaert MB. Effects of origin and state of differentiation and activation of monocytes/macrophages on their susceptibility to porcine reproductive and respiratory syndrome virus (PRRSV). *Arch Virol.* (1997) 142:2483–97. doi: 10.1007/s007050050256
14. Allende R, Laegreid WW, Kutish GF, Galeota JA, Willis RW, Osorio FA. Porcine reproductive and respiratory syndrome virus: description of persistence in individual pigs upon experimental infection. *J Virol.* (2000) 80:3994–4004. doi: 10.1128/jvi.74.22.10834-10837.2000
15. Mateu E, Diaz I. The challenge of PRRS imunology. *Vet J.* (2008) 177:345–51. doi: 10.1016/j.tvjl.2007.05.022
16. Gomez-Laguna J, Salguero FJ, Pallares FJ, Carraso L. Immunopathogenesis of porcine reproductive and respiratory syndrome in the respiratory tract of pigs. *Vet J.* (2013) 195:148–55. doi: 10.1016/j.tvjl.2012.11.012
17. Lunney JK, Fang Y, Ladinig A, Chen N, Yanhua L, Rowland B, et al. Porcine reproductive and respiratory syndrome virus (PRRSV): pathogenesis and interaction with the immune system. *Annu Rev Anim Bosci.* (2016) 4:129–54. doi: 10.1146/annurev-animal-022114-111025
18. Renukaradhya GJ, Aleksejev K, Jung K, Fang Y, Saif LJ. Porcine reproductive and respiratory syndrome virus-induced immunosuppression exacerbates the inflammatory response to porcine respiratory coronavirus. *Viral Immunol.* (2010) 23:457–66. doi: 10.1089/vim.2010.0051
19. Van Reeth K, Labarque G, Nauwynck H, Pensaert M. Differential production of proinflammatory cytokines in the pig lung during different respiratory virus infections: correlation with pathogenicity. *Res Vet Sci.* (1999) 67:47–52. doi: 10.1053/rvsc.1998.0277
20. Yoon IJ, Joo HS, Goyal SM, Molitor TW. A modified serum neutralization test for the detection of antibody to porcine reproductive and respiratory syndrome virus in swine sera. *J Vet Diagnost Invest.* (1994) 6:289–92. doi: 10.1177/104063879400600326
21. Johnsen CK, Botner A, Kastrup S, Lind P, Nielsen J. Cytokine mRNA profiles in bronchoalveolar cells of piglets experimentally infected with porcine reproductive and respiratory syndrome virus: association of sustained expression of IFN-γ and IL-10 after viral clearance. *Viral Immunol.* (2002) 15:549–56. doi: 10.1089/088282402320914494
22. Suradhat S, Thanawoghuwech R, Poovoran Y. Upregulation of Il-10 gene expression in peripheral blood mononuclear cells by porcine reproductive and respiratory syndrome virus. *J Gen Virol.* (2003) 84:453–9. doi: 10.1099/vir.0.18698-0
23. Diaz I, Darwich I, Pappatera G, Pujols J, Mateu E. Immune response of pigs after experimental infection with European strain of porcine reproductive and respiratory syndrome virus. *J Gen Virol.* (2005) 89:1943–51. doi: 10.1099/vir.0.80959-0
24. Kavanova L, Prodelalova J, Nedbalcova K, Matiasovic J, Volf J, Faldyna M, et al. Immune response of porcine alveolar macrophages to a concurrent infection with porcine reproductive and respiratory syndrome virus and *Haemophilus parasuis in vitro*. *Vet Microbiol.* (2015) 180:28–35. doi: 10.1016/j.vetmic.2015.08.026
25. Kavanova L, Matiašková K, Levá L, Nedbalcová K, Matiašovic J, Faldyna M, et al. Current infection of monocyte-derived macrophages and with porcine reproductive and respiratory syndrome virus and *Haemophilus parasuis*: a role of IFNα in pathogenesis of co-infections. *Vet Microbiol.* (2018) 225:64–71. doi: 10.1016/j.vetmic.2018.09.016
26. Kimman TJ, Cornelissen LA, Moormann RJ, Rebel JMJ, Stockhofe-Zurwieden N. Challenges for porcine reproductive and respiratory syndrome virus(PRRSV) vaccinology. *Vaccine.* (2009) 27:3704–18. doi: 10.1016/j.vaccine.2009.04.022
27. Murtaugh MP, Genzow M. Immunological solutions for treatment and prevention of porcine reproductive and respiratory syndrome (PRRS). *Vaccine.* (2011) 29:8192–204. doi: 10.1016/j.vaccine.2011.09.013
28. Renukaradhya GJ, Meng XJ, Calvert JG, Roof M, Lager, KM. Inactivated and subunit vaccines against porcine reproductive and respiratory syndrome: current status and future direction. *Vaccine.* (2015) 33:4069–80. doi: 10.1016/j.vaccine.2015.06.092
29. Renukaradhya GJ, Meng XJ, Calvert JG, Roof M, Lager, KM. Live porcine reproductive and respiratory syndrome virus vaccines: current status and future direction. *Vaccine.* (2015) 33:3065–72. doi: 10.1016/j.vaccine.2015.04.102
30. Diaz I, Gimeno M, Callen J, Pujols J, Lopez S, Charreyre C, et al. Comparison of different vaccination schedules for sustaining immune response against porcine reproductive and respiratory syndrome virus. *Vet J.* (2013) 197:438–44. doi: 10.1016/j.tvjl.2013.02.008
31. Bonckaert C, Van der Meulen K, Rodriguez-Bellara I, Pedrazuela Sanz R, Martinez MF, Nauwynck HJ. Modified-live PRRSV subtype 1 vaccine UNISTRAIN PRRS provides a partial clinical and virological protection upon

challenge with East European subtype 3 PRRSV strain Lena. *Porcine Health Manag.* (2016) 2:12. doi: 10.1186/s40813-016-0029-y
32. Kristensen CHS, Kvisgaard LK, Pawlowski M, Holmgaard Carlsen S, Hjulsager CK, Heegaard PMH, et al. Efficacy and safety of simultaneous vaccination with two modified live virus vaccine against porcine reproductive and respiratory syndrome virus types 1 and 2 in pigs. *Vaccine.* (2018) 36:227–36. doi: 10.1016/j.vaccine.2017.11.059
33. Sun H, Workman A, Osorio FA, Steffen D, Vu HLX. Development of a broadly protective modified-live vaccine candidate against porcine reproductive and respiratory syndrome virus. *Vaccine.* (2018) 36:66–73. doi: 10.1016/j.vaccine.2017.11.028
34. Linhares DCL, Johnson C, Morrison RB. Economic analysis of vaccination strategies for PRRS control. *PloS ONE.* (2015) 10:e0144265. doi: 10.1371/journal.pone.0144265
35. Pileri E, Mateu E. Review on the transmission porcine reproductive and respiratory syndrome virus between pigs and farms and impact on vaccination. *Vet Res.* (2016) 47:108. doi: 10.1186/s13567-016-0391-4
36. Nathues H, Alarcon P, Rushton J, Jolie R, Fiebig K, Jimenez M, et al. Cost of porcine reproductive and respiratory syndrome virus at farm level – an economic model. *Prev Vet Med.* (2017) 142:16–29. doi: 10.1016/j.prevetmed.2017.04.006
37. Nechvatalova K, Knotigova P, Krejci J, Faldyna M, Gopfert E, Satran P, et al. Significance of different types and levels of antigen-specific immunity to *Actinobacillus pleuropneumoniae* infection in piglets. *Vet Med Czech.* (2005) 50:47–59. doi: 10.17221/5596-VETMED
38. Stepanova H, Pavlova B, Stromerova N, Matiasovic J, Kaevska M, Pavlik I, Faldyna M. Cell-mediated immune response in swine infected with *Mycobacterium avium* subsp. *Avium Vet Immunol Immunopathol.* (2011) 142:107–12. doi: 10.1016/j.vetimm.2011.04.005
39. Zelnickova P, Faldyna M, Stepanova H, Ondracek J, Kovaru F. Intracellular cytokine detection by flow cytometry in pigs: fixation, permeabilization and cell surface staining. *J Immunol Methods.* (2007) 327:18–29. doi: 10.1016/j.jim.2007.07.006
40. Zuckermann FA, Garcia EA, Luque ID, Christopher-Hennings J, Doster A, Brito M, et al. Assessment of the efficacy of commercial porcine reproductive and respiratory syndrome virus (PRRSV) vaccines based on measurement of serologic response, frequency of gamma-IFN-producing cells and virological parameters upon challenge. *Vet Microbiol.* (2007) 123:69–85. doi: 10.1016/j.vetmic.2007.02.009
41. Kuiek AM, Ooi PT, Yong CK, Chi FN. Comparison of serum and oral fluid antibody responses after vaccination with modified live (MLV) porcine reproductive and respiratory syndrome virus (PRRSV) vaccine in PRRS endemic farms. *Trop Anim Health Prod.* (2015) 47:1337–42. doi: 10.1007/s11250-015-0868-6
42. Rotolo ML, Gimenez-Lirola L, Ji J, Magtoto R, Henao-Diaz YA, Wang CH, et al. Detection of porcine reproductive and respiratory syndrome virus (PRRSV)-specific IgM-IgA in oral fluid samples reveals PRRSV infection in the presence of maternal antibody. *Vet Microbiol.* (2018) 214:13–20. doi: 10.1016/j.vetmic.2017.11.011
43. Woonwong Y, Kedkovid R, Arunorat J, Sirisereewan CH, Nedumpun T, Poonsuk K, et al. Oral fluid samples used for PRRSV acclimatization program and sow performance monitoring in endemic PRRS-positive farms. *Trop Anim Health Prod.* (2018) 50:291–8. doi: 10.1007/s11250-017-1428-z
44. Sattler T, Pikalo J, Wodak E, Schmoll F. Ability of ELISAs to detect antibodies against porcine reproductive and respiratory syndrome virus in serum of pigs after inactivated vaccination and subsequent challenge. *BMC Vet Res.* (2016) 12:259. doi: 10.1186/s12917-016-0888-0
45. Madapong A, Temeeya G, Sang-chuto K, Tripipat T, Navasakuljinda W, Boonsoongnern A, et al. Humoral immune response and viral shedding following vaccination with modified live porcine reproductive and respiratory syndrome virus vaccines. *Arch Virol.* (2017) 162:139–46. doi: 10.1007/s00705-016-3084-4
46. Kroll J, Piontkowski M, Rathkjen PH, Orveillon FX, Kraft CH, Duran OG. Long duration of immunity against a type 1 heterologous PRRS virus challenge in pigs immunised with novel PRRS MLV vaccine: a randomised controlled study. *Porcine Health Manag.* (2018) 4:11. doi: 10.1186/s40813-018-0087-4
47. Hrazdilova K, Dadakova E, Brozova K, Modry D, Vodicka R, Celer V. New species of Torque Teno miniviruses infecting gorillas and chimpanzees. *Virology.* (2016) 487:207–14. doi: 10.1016/j.virol.2015.10.016
48. Dadakova E, Brozova K, Piel AK, Steward FA, Modry D, Celer V, et al. Adenovirus infection in savanna chimpanzees *(Pan troglodytes schweinfurthii)* in the Issa Valley, Tanzania. *Arch Virol.* (2018) 163:191–6. doi: 10.1007/s00705-017-3576-x
49. Stadler J, Naderer L, Beffort L, Ritzmann M, Fiebig K, Saalmüller A, et al. Safety and immune response after intradermal application of Porcilis PRRS in either neck or the perianal region. *PloS ONE.* (2018) 13:e0203560. doi: 10.1371/journal.pone.0203560
50. Piras F, Bolard S, Laval F, Joisel F, Reynaud G, Charreyre C, et al. Porcine reproductive and respiratory syndrome (PRRS) virus-specific Interferon-γ^+ T-cell responses after PRRS virus infection or vaccination with inactivated PRRS vaccine. *Virol Immunol.* (2005) 18:381–9. doi: 10.1089/vim.2005.18.381
51. Saalmuller A, Verner T, Fachinger V. T-helper cells from naive to commited. *Vet Immunol Immunopathol.* (2002) 87:137–45. doi: 10.1016/S0165-2427(02)00045-4
52. Chung CHJ, Cho SH, Grimm AL, Ajithdoss D, Rzepka J, Chung G, et al. Pig that recover porcine reproduction and respiratory syndrome virus infection develop cytotoxic $CD4^+CD8^+$ and $CD4^+CD8^-$ T-cells that kill virus infected cells. *PloS ONE.* (2018) 13:0203482. doi: 10.1371/journal.pone.0203482
53. Martinez-Lobo FJ, de Lome LC, Diez-Fuertes F, Segales J, Garcia-Artiga C, Simarro I, et al. Safety of reproductive and respire syndrome modified live virus (MLV) vaccine strains in a young pig infection model. *Vet Res.* (2013) 44:115. doi: 10.1186/1297-9716-44-115
54. Shi M, Lam TTY, Hon CH, Hui RK, Faaberg KS, Vennblom T, et al. Molecular epidemiology of PRRSV: a phylogenetic perspective. *Vet Res.* (2010) 154:7–17. doi: 10.1016/j.virusres.2010.08.014
55. Wang X, Yang X, Rong Z, Zhou L, Ge X, Guo X. Genomic characterization and pathogenicity of a strain of type 1 porcine reproductive and respiratory syndrome virus. *Virus Res.* (2016) 225:40–9. doi: 10.1016/j.virusres.2016.09.006
56. Heller P, Schagemann G, Schroder C, Stampa E, Ohlinger V, Wendt M. Elimination of PRRS virus (EU-type) from farrow-to finish breeding farm by vaccination with Ingel-vac ® PRRS MLV under unfavourable conditions. *Praktische Tierarzt.* (2011) 92:416–20.
57. Zhao Z, Qin Y, Lai Z, Peng L, Cai X, Wang L, et al. Microbial ecology of swine farms and PRRS vaccine vaccination strategies. *Vet Microbiol.* (2012) 155:247–56. doi: 10.1016/j.vetmic.2011.09.028
58. Werdeling F, Mues G, Offenberg S, Zantz S, Fiebig K. Development and control of an acute PRRS field virus infection in an endemic PRRS breeding herd after vaccination with modified live vaccine. *Praktische Tierarzt.* (2012) 93:722–7.
59. Cheah ZH, Ooi PT, Phang LY, Chua V, Low SE, Cheah HC, et al. Different porcine reproductive and respiratory syndrome (PRRS) vaccine regimes and its effect on pig immunity status at South Asia pig farms. *Trop Biomed.* (2017) 34:388–95.
60. Jeong J, Kim S, Park KH, Kang I, Park SJ, Park CH, et al. Evaluation of the effect of a porcine reproductive and respiratory syndrome (PRRS) modified-live virus vaccine on sow reproductive performance in endemic PRRS farm. *Vet Microbiol.* (2017) 208:47–52. doi: 10.1016/j.vetmic.2017.07.016
61. Toman, M, Celer V, Smola J. Successful elimination of PRRS virus from an infected farrow-to-finish herd by vaccination. *Vet Med Czech.* (2017) 62:553–8. doi: 10.17221/68/2017-VETMED

Conflict of Interest Statement: The authors declare that the research was conducted in the absence of any commercial or financial relationships that could be construed as a potential conflict of interest.

frontiers in Immunology

REVIEW
published: 27 September 2019
doi: 10.3389/fimmu.2019.02258

Porcine Anti-viral Immunity: How Important Is It?

Kelly M. Lager and Alexandra C. Buckley*

Virus and Prion Research Unit, United States Department of Agriculture, National Animal Disease Center, Agricultural Research Service, Ames, IA, United States

Pork has become the number one meat consumed worldwide. Meeting the demand for pork has forced the revolution of swine production from traditional husbandry practices that involved a few pigs or small herds to intensive concentration of swine raised in multisite production systems. This dramatic change has made the production of pork very efficient, but it has also changed the ecology of many swine diseases, may encourage the emergence of new diseases, and amplifies the economic impact of swine diseases. Sustained treatment of diseases in livestock production is not feasible making prevention of disease a priority. Prevention of livestock diseases involves eliminating exposure to pathogens and anti-viral strategies to prevent or reduce clinical disease. For some swine diseases, efficacious vaccines can be made, however, for other diseases the host/pathogen relationship is more complex and efficacious vaccines are not available. Given the increasing demand for pork, the development of new approaches to improve swine anti-viral immunity is critical. Rate-limiting steps to improving vaccines are understanding how the pathogen interacts with the host's immune system, any immunopathology resulting from such interactions and how the host's immune system resolves the infection. Solving this puzzle will require sustained research and may require new technologies to battle contemporary diseases now wreaking havoc in swine production systems around the world. This Special Issue will focus on current swine viral diseases that are the most challenging to the global production of pork with contributions focusing on anti-viral immunity.

Keywords: swine, virus, disease, immunology, vaccine

OPEN ACCESS

Edited by:
Anastasia N. Vlasova, The Ohio State University, United States

Reviewed by:
Julio Villena, CONICET Centro de Referencia para Lactobacilos (CERELA), Argentina
Ralph A. Tripp, University System of Georgia, United States
Alexander Zakhartchouk, University of Saskatchewan, Canada

****Correspondence:***
Kelly M. Lager
kelly.lager@ars.usda.gov

Specialty section:
This article was submitted to Viral Immunology, a section of the journal Frontiers in Immunology

Received: *27 June 2019*
Accepted: *06 September 2019*
Published: *27 September 2019*

Citation:
Lager KM and Buckley AC (2019) Porcine Anti-viral Immunity: How Important Is It? Front. Immunol. 10:2258. doi: 10.3389/fimmu.2019.02258

The quest for food is primal, and for most of mankind's existence, a daily struggle for all. About 15,000 years ago agriculture began to develop with the cultivation of crops and domestication of animals. This lessened the daily burden of searching for food and began providing time for creativity which has led to unimaginable technologic achievements, and to exponential growth in the human population. Despite all contemporary technology, the stability of our food supply is still vulnerable to many challenges that have existed since the beginning of agriculture, and to new ones that are associated with modern agriculture practices that produce massive amounts of food. Although, there are many challenges to meeting our absolute need for food, this review focuses on just one aspect of modern agriculture, the production of pork.

In the twenty first century, agriculture reflects a broad spectrum from subsistence farming to single-commodity production systems producing meat, milk, grains, fruits, and vegetables on an unprecedented scale. The increasingly efficient production of pork has made it more readily available and it has become the number one meat consumed worldwide (1). Meeting the demand for pork has forced the evolution of swine production from traditional inefficient husbandry practices involving a few pigs or small herds to an intensive concentration of swine that is divided

into stages of production housed at different sites often far apart. This dramatic change has made the production of pork very efficient, but it has also changed the ecology of many swine diseases. Moreover, this style of production may encourage the emergence of new diseases, and amplifies their economic impact.

Control strategies for swine diseases are driven by the economic impact of the respective disease and the diseases can be divided into two broad categories: those that warrant interdiction and those that do not. There are many swine viruses that have been infrequently associated with disease; sometimes one or just a few animals are affected, other times the disease may spontaneously reach a high incidence in the herd, and then just as quickly, it dissipates. In general, these viruses can be economically insignificant to a regional or national swine herd and will not be further discussed. However, this group of viruses is still important since the reasons for when a sporadic viral disease might flare up in a herd, and then "burn out," are poorly understood. It is still prudent to investigate the epidemiology of these "insignificant" viruses since they might 1 day become significant. Swine viruses causing, or that potentially could cause, significant economic disease in a herd are similar around the world and these viruses are the focus of this Special Topics review (**Table 1**). For a more comprehensive review of swine viral diseases, the reader is encouraged to read *Diseases of Swine*, 11th edition (2) and *Porcine Viruses: From Pathogenesis to Strategies for Control* (3). General information from these books about specific diseases is used extensively throughout this manuscript, and will not be cited repetitively.

Successful pork production is dependent upon many variables of which animal health may be the most volatile. For example, just one biosecurity mistake in protocols designed to mitigate herd health risks can produce long-term health consequences for the herd and financial ruin for the producer. An economic loss of this nature for one producer can be exponentially amplified if such a mistake would cause a country to lose its export market. For example, about 25% of the US pork produced each year is exported making the US swine industry quite vulnerable since any pandemic of local or foreign origin could induce a ban on the importation of US pork for fear of transmitting the disease. Following the emergence of the 2009 influenza pandemic, such a ban or threat of a ban was enacted by more than 27 countries that produced an immediate loss of market. Although, it only took a few months to refute the ban, the industry still lost an estimated 1.5 billion dollars (4).

Vaccines can increase the resistance of an animal to infection making them an increasingly important tool in the health management of swine herds. Although, many vaccines are efficacious, continual pathogen mutation and the emergence of new virus threats drives a constant need for new and improved vaccines. Not surprisingly, many of the significant-economic-disease viruses are viruses for which there are no vaccine, or the current vaccine has limited efficacy. Any solution to the current swine vaccine problem will involve a better understanding of the pig's immune response to these pathogens with the hope of applying this knowledge toward the development and improvement of vaccines, and other more rapid responses to new diseases in the future.

TABLE 1 | Swine viral pathogens of economic or zoonotic importance.

Virus[a]	Economic[b]	Vaccine[c]	Zoonotic[d]
ASFV	++++	No	–
FMDV	++++	Yes	–
CSFV	+++	Yes	–
ADV	++	Yes	–
PRRSV	++++	Yes	–
IVA-S	++	Yes	+++
PCV2	+	Yes	–
PEDV	+	Yes	–
SVA	+	No	–
JEV	+	Yes	++
HEV	+	No	++
Nipah virus	+	No	+++
EMCV	+	No	+
Menangle virus	+	No	+
VSV	+	No	+
VESV	+	No	+

[a] *ASFV, African swine fever virus; FMDV, foot and mouth disease virus; CSFV, classical swine fever virus; ADV, Aujeszky's disease virus; PRRSV, porcine reproductive and respiratory syndrome virus; IVA-S, influenza virus A- swine; PCV2, porcine circovirus type 2; PEDV, porcine epidemic diarrhea virus; SVA, Senecavirus A; JEV, Japanese encephalitis virus; HEV, Hepatitis E virus; EMCV, encephalomyocarditis virus; VSV, Vesicular stomatitis virus; VESV, Vesicular exanthema of swine virus.*

[b] *Economic impact ranging from + (infrequent/mild) to ++++ (frequent/severe).*

[c] *Vaccine available to aid in control and prevention: yes or no.*

[d] *Zoonotic potential ranging from + (infrequent/mild) to ++++ (frequent/severe).*

Porcine reproductive and respiratory syndrome virus (PRRSV), a previously unknown swine virus, emerged in the late 1980s and spread around the world within a few years becoming the first of several swine pandemics that would occur over the next 30 years. PRRSV quickly became the number one health problem in major swine producing countries because it is able to affect all stages of production, is highly infectious, has a prolonged shedding duration, and perhaps most importantly, is able to dysregulate the pig's immune response. The economic impact of this virus is substantial, e.g., in 2013 PRRSV was estimated to cost just the US swine industry alone 660 M a year (5). A number of inactivated and attenuated vaccines are available in most countries with attenuated vaccines reported as superior to inactivated virus vaccines, suggesting the importance of the mucosal response for clinical protection. Despite being derived from various field viruses, attenuated virus vaccines are able to induce homologous protection, but only variable heterologous protection (6). The nature of this sometimes poor cross-protection is not understood and is a major obstacle to improving PRRSV vaccines.

Foot and mouth disease virus (FMDV) is a highly infectious virus that affects cloven-hooved animals causing vesicular lesions involving the feet and oral cavity resulting in a crippling disease and loss of production to the extent that this virus is the most important disease concern for livestock producers around the world. Once FMDV has been eradicated from a country, substantial resources are committed to keeping the country FMDV-free that include the regulated movement of

livestock, substantial diagnostic testing, and the quest for safe and efficacious vaccines. Similar to PRRSV, FMDV vaccines are available, however, they are serotype specific and lack cross-protection among the 7 FMDV serotypes (7). Moreover, there can be variation within a subtype to a degree where the subtype-specific vaccine may not provide adequate protection. Although, a properly matched subtype vaccine can be used in control and eradication programs, it is prohibitively expensive to maintain a vaccine bank for all potential serotypes. There is a dramatic need for more cross-protective FMDV vaccines to help resolve FMDV epidemics when they occur, and maintain FMDV-free countries.

The control of influenza A viruses in swine (IAV-S) exemplifies the challenges of passively acquired maternal immunity in modern swine production. In the late 1990s, a novel IAV-S H3 subtype was first detected in the United States, and similar to the then endemic North American H1 subtype, the new virus caused respiratory disease in fattening hogs and sows (8). In response to this new H3 subtype lineage, specific inactivated vaccines were produced and combined with H1 vaccines to form new polyvalent vaccines that were efficacious in naïve older swine when administered prior to the onset of disease. However, as the intensification of swine production expanded, the ecology of IAV-S began to change with younger pigs becoming clinically affected which supported strategies to immunize the sows to provide passive immunity to their piglets. This was helpful, but the practice also jeopardized the ability to vaccinate young pigs to protect them against disease in later stages of production illustrating the passive immunity conundrum when using inactivated vaccines given intramuscularly to young pigs. Recently, an attenuated IAV-S vaccine has been released for sale in the US that is given intranasally to neonatal pigs to circumvent passively acquired immunity. It is reported to provide protection to young pigs and induce a broader protective immune response when compared to inactivated vaccines given intramuscularly (9).

IAV-S is a swine virus with zoonotic potential (**Table 1**). It is ubiquitous in swine producing regions around the world, and with variable frequency, swine-to-human transmission does occur. Fortunately, most transmission events are limited in scope of disease and subsequent human-to-human transmission. However, the 2009 influenza pandemic is a stark reminder of the potential for influenza viruses to jump species and become a pandemic. Reverse zoonosis, IAV transmission from people to swine, is being detected with similar frequency. This phenomenon is an important mechanism for transferring human viruses into swine where the virus can adapt to swine and be maintained as a potential reservoir of human-like IAV that could jump back to humans. Other zoonotic swine viruses are more regional in distribution and usually are not considered to cause significant economic loss. Crossover events with these viruses are much less frequent when compared to IAV-S; however, they can have a higher case fatality rate in people (Japanese encephalitis virus, Hepatitis E virus). Most zoonotic swine virus crossover events are very rare and typically cause minimal human disease, however, in 1998, Nipah virus, a previously unknown virus, emerged in swine in Malaysia. It caused a respiratory infection with high morbidity in all ages of swine on several farms. Sick pigs transmitted the virus to farm workers causing a severe illness with a Case Fatality Rate of about 40% in the initial outbreak (10). The disease was eradicated from the affected farms within months, and with the discovery that bats were the reservoir for this virus, precautions could be taken to prevent future infections which have been successful to date.

In 2013, porcine epidemic diarrhea virus (PEDV), one of the swine enteric coronaviruses that causes severe diarrhea in neonatal pigs, was discovered in the Western Hemisphere for the first time. Within 6 months of entry into the US, the virus had spread through all swine dense regions killing about 10% of the pig crop that year. Although, swine can mount a rapid protective immune response to PEDV, young pigs are unable to survive the disease long enough to develop a protective response which makes protecting young pigs the most important step to controlling this disease. The only option to protect the pigs is to provide passive maternal immunity to the suckling pig via colostrum/milk, a strategy that can work but is dependent on the sow having adequate exposure to PEDV to induce mucosal immunity. Although, wild-type PEDV might induce the best lactogenic and colostral immunity for the piglet, immunizing the sow herd with wild-type PEDV has serious safety concerns demonstrating the need for improved PEDV vaccines.

Beginning in late 2014 and into 2015, there were outbreaks of idiopathic vesicular disease in Brazil followed by similar outbreaks in the United States. Disease was most often recognized in market-weight swine and sows, and samples from these cases tested positive for Senecavirus A (SVA). Subsequently, the virus has also been identified in Canada, China, Colombia, and Thailand (11). Although, the clinical disease is mild in most animals, and the incidence is low when compared to most economically important swine diseases, vesicular lesions from SVA infection are indistinguishable from FMDV infection. Foot and mouth disease is the number one disease concern for livestock producers around the world which makes understanding the pathogenesis and immunology of any virus that may confound FMDV diagnostic investigations important. Recent SVA studies have demonstrated fulfillment of Koch's postulates, documented pathogenesis, and shown that contemporary isolates are closely related. Sterile protective immunity was demonstrated in piglets exposed to wild-type SVA and then challenged with the same isolate 7 weeks later (12). This preliminary research indicates pigs can develop a protective immune response and there is potential for the use of vaccines. There are still many questions about the ecology and epidemiology of this virus including (1) why these "mini-epidemics" occurred in different countries with similar viruses (over 94% nucleotide identity among contemporary isolates), (2) the apparent seasonality to the clinical expression of the disease, (3) prevalence of the virus, and (4) field reports suggest there may be a long-term or persistent infection with the potential for acute recrudescence of clinical disease post transport/stress.

The economic loss from the introduction of a foreign animal disease is multidimensional ranging from the acute direct losses to livestock producers to a chronic loss of production that can diminish an entire industry for extended periods of time, and perhaps permanently. In addition, the increased costs of food and reduced availability of once common products can lead to social instability. In 2018, African Swine Fever virus (ASFV)

emerged for the first time in China, the largest producer of pork in the world accounting for over 50% of all production. African Swine Fever was first described in Africa in 1921 causing a fulminating disease in domestic swine (13). Wild swine found outside the continent of Africa are also quite susceptible, but in the African continent wild swine have co-evolved with ASFV developing some tolerance to the virus. Since its discovery, there have been sporadic regional epidemics in countries outside of Africa and only through heroic efforts could the virus be eradicated. In 2007, an ASFV epidemic began in Georgia in the Caucasus region that slowly, but steadily spread into Russia and then Europe (14). Although, the Chinese transmission event is unknown, this same lineage of virus jumped to China in mid-2018 and within 6 months had spread to all swine producing regions (15). The ASFV state-of-the-art control strategy is to depopulate the affected herd, and all pigs in potential contact with it. This strategy can be devastating in current production systems as occurred in Romania in August of 2018 when over 140,000 pigs were euthanized in an attempt to stop the spread of ASFV in that region (16). Currently, there is no vaccine for use in the control and prevention of ASFV which makes research in this area a top priority as the virus is now spreading in countries contiguous with China. An ASFV-positive status in just one pig (domestic or wild), immediately restricts the movement of domestic pigs and pork products within and from that country. Depending on regulatory infrastructure, some countries that have only had ASFV-infection in wild swine may have some export restrictions reduced, but the economic impact on disrupted markets is still substantial. The ASFV-pig interaction is very complicated and despite extensive research, the correlates of protection are poorly defined and current technology is inadequate to produce a safe and efficacious vaccine.

The constant need for more food in the world requires each agriculture commodity to be more efficiently produced which includes a perpetual battle against disease in crops and livestock. In the case of swine, the continual evolution of viruses requires sustained research into the basic immunology against these pathogens to provide new mechanistic insights into how pigs, and perhaps other species, respond to pathogens and enable the production of safer and more efficacious vaccines and anti-viral approaches. This knowledge may enable the application of novel technologies that could modulate the pig's immune response in the fight against disease, and ensure the availability of safe and wholesome pork around the globe. In response to the title, it is VERY important to study viral immunity in swine as well as livestock and poultry because more efficient production of meat protein is essential to the quest for more food.

AUTHOR CONTRIBUTIONS

KL and AB contributed to and wrote the manuscript.

FUNDING

KL and AB were funded by the USDA Agricultural Research Service.

REFERENCES

1. United States Department of Agriculture Foreign Agricultural Service. *Livestock and Poultry: World Markets and Trade* (2019).
2. Zimmerman JJ, Karriker LA, Ramirez A, Schwartz KJ, Stevenson GW, Zhang J. *Diseases of Swine, 11th Edn*. Hoboken, NJ: John Wiley and Sons, Inc. (2019). doi: 10.1002/9781119350927
3. Zakaryan H. *Porcine Viruses: From Pathogenesis to Strategies for Contol*. Poole; Norfolk: Caister Academic Press (2019).
4. Vincent AL, Lager KM, Harland M, Lorusso A, Zanella E, Ciacci-Zanella JR, et al. Absence of 2009 pandemic H1N1 influenza A virus in fresh pork. *PLoS ONE*. (2009) 4:e8367. doi: 10.1371/journal.pone.0008367
5. Holtkamp DJ, Kliebenstein JB, Neumann L, Zimmerman JJ, Rotto H, Yoder TK, et al. Assessment of the economic impact of porcine reproductive and respiratory syndrome virus on United States pork producers. *J Swine Health Prod*. (2013) 21:72–84. doi: 10.31274/ans_air-180814-28
6. Nan Y, Wu C, Gu G, Sun W, Zhang YJ, Zhou EM. Improved vaccine against PRRSV: current progress and future perspective. *Front Microbiol*. (2017) 8:1635. doi: 10.3389/fmicb.2017.01635
7. Mahapatra M, Parida S. Foot and mouth disease vaccine strain selection: current approaches and future perspectives. *Expert Rev Vaccines*. (2018) 17:577–91. doi: 10.1080/14760584.2018.1492378
8. Zhou NN, Senne DA, Landgraf JS, Swenson SL, Erickson G, Rossow K, et al. Genetic reassortment of avian, swine, and human influenza A viruses in American pigs. *J Virol*. (1999) 73:8851–6.
9. Eichmeyer MA, Johnson W, Vaughn E, Roof MB, Hayes PW. Development of ingelvac provenza: a new tool against IAV-S. In: *49th Annual Meeting of the American Association of Swine Veterinarians*. San Diego, CA (2018).
10. Chua KB, Bellini WJ, Rota PA, Harcourt BH, Tamin A, Lam SK, et al. Nipah virus: a recently emergent deadly paramyxovirus. *Science*. (2000) 288:1432–5. doi: 10.1126/science.288.5470.1432
11. Zhang X, Zhu Z, Yang F, Cao W, Tian H, Zhang K, et al. Review of Seneca valley virus: a call for increased surveillance and research. *Front Microbiol*. (2018) 9:940. doi: 10.3389/fmicb.2018.00940
12. Buckley A, Montiel N, Kulshreshtha V, van Geelen A, Guo B, Hoang H, et al. Demonstration of Senecavirus A protective immunity in a pig model. In: *International Pig Veterinary Society*. Dublin (2016).
13. Montgomery RE. On a form of swine fever occurring in British East Africa (Kenya Colony). *J Comp Pathol Ther*. (1921) 34:159–91. doi: 10.1016/S0368-1742(21)80031-4
14. Rowlands RJ, Michaud V, Heath L, Hutchings G, Oura C, Vosloo W, et al. African swine fever virus isolate, Georgia, 2007. *Emerg Infect Dis*. (2008) 14:1870–4. doi: 10.3201/eid1412.080591
15. Schmidhuber J. African swine fever: challenges for some, opportunities for others? In: *FAO 2019 Food Outlook - Biannual Report on Global Food Markets*. (2019). Available online at: http://www.fao.org/3/ca4526en/ca4526en.pdf
16. OIE. African swine fever, Romania. In: *Disease Alerts*. (2018). Available online at: https://www.oie.int/wahis_2/public/wahid.php/Reviewreport/Review?page_refer=MapFullEventReportandreportid=27687External~Link

Conflict of Interest: The authors declare that the research was conducted in the absence of any commercial or financial relationships that could be construed as a potential conflict of interest.

frontiers in Immunology

ORIGINAL RESEARCH
published: 26 November 2019
doi: 10.3389/fimmu.2019.02660

A Novel Live Attenuated Vaccine Candidate Protects Against Heterologous *Senecavirus A* Challenge

Bishwas Sharma[1,2†], *Maureen H. V. Fernandes*[1,2,3†], *Marcelo de Lima*[1,4], *Lok R. Joshi*[1,2,3], *Steve Lawson*[1] *and Diego G. Diel*[1,2,3*]

[1] *Animal Disease Research and Diagnostic Laboratory, Department of Veterinary and Biomedical Sciences, South Dakota State University, Brookings, SD, United States,* [2] *Center for Biologics Research and Commercialization, South Dakota State University, Brookings, SD, United States,* [3] *Department of Population Medicine and Diagnostic Sciences, Animal Health Diagnostic Center, College of Veterinary Medicine, Cornell University, Ithaca, NY, United States,* [4] *Laboratório de Virologia e Imunologia Animal, Faculdade de Veterinária, Universidade Federal de Pelotas, Pelotas, Brazil*

OPEN ACCESS

Edited by:
Anastasia N. Vlasova, The Ohio State University, United States

Reviewed by:
Laura Nicoleta Burga, University of Otago, New Zealand
Jun Zhao, Henan Agricultural University, China
Alexandra Buckley, Virus Prion Research Unit, Agricultural Research Service (USDA), United States

***Correspondence:**
Diego G. Diel
dgdiel@cornell.edu

[†]*These authors have contributed equally to this work*

Specialty section:
This article was submitted to Viral Immunology, a section of the journal Frontiers in Immunology

Received: *27 July 2019*
Accepted: *28 October 2019*
Published: *26 November 2019*

Citation:
Sharma B, Fernandes MHV, de Lima M, Joshi LR, Lawson S and Diel DG (2019) A Novel Live Attenuated Vaccine Candidate Protects Against Heterologous Senecavirus A Challenge. Front. Immunol. 10:2660. doi: 10.3389/fimmu.2019.02660

Senecavirus A (SVA) is an emerging picornavirus causing vesicular disease (VD) clinically indistinguishable from foot-and-mouth disease (FMD) in pigs. Currently there are no vaccines currently available for SVA. Here we developed a recombinant SVA strain (rSVAm SacII) using reverse genetics and assessed its immunogenicity and protective efficacy in pigs. *In vivo* characterization of the rSVAm SacII strain demonstrated that the virus is attenuated, as evidenced by absence of lesions, decreased viremia and virus shedding in inoculated animals. Notably, while attenuated, rSVA mSacII virus retained its immunogenicity as high neutralizing antibody (NA) responses were detected in inoculated animals. To assess the immunogenicity and protective efficacy of rSVA mSacII, 4-week-old piglets were sham-immunized or immunized with inactivated or live rSVA mSacII virus-based formulations. A single immunization with live rSVA mSacII virus via the intramuscular (IM) and intranasal (IN) routes resulted in robust NA responses with antibodies being detected between days 3–7 pi. Neutralizing antibody responses in animals immunized with the inactivated virus via the IM route were delayed and only detected after a booster on day 21 pi. Immunization with live virus resulted in recall T cell proliferation ($CD4^+$, $CD8^+$, and $CD4^+/CD8^+$ T cells), demonstrating efficient stimulation of cellular immunity. Notably, a single dose of the live attenuated vaccine candidate resulted in protection against heterologous SVA challenge, as demonstrated by absence of overt disease and reduced viremia, virus shedding and viral load in tissues. The live attenuated vaccine candidate developed here represents a promising alternative to prevent and control SVA in swine.

Keywords: *Senecavirus A*, Seneca Valley virus, recombinant virus, live attenuated vaccine, inactivated vaccine

INTRODUCTION

Senecavirus A (SVA) is a vesicular disease (VD)-causing pathogen of pigs and the only species of the genus *Senecavirus* in the family *Picornaviridae* (1). SVA is a non-enveloped, icosahedral virus with a single-stranded positive sense RNA genome with ∼7.2 kb. The SVA genome encodes a unique open reading frame (ORF), which is proteolytically processed in four structural proteins (VP1-VP4) and eight non-structural proteins (L, 2A−2B−2C−3A−3B−3C−3D) (2). The virus genome is organized in a central coding region (ORF1) flanked by 5′- and 3′-untranslated regions (UTRs) and a poly(A) tail following the 3′-UTR (2).

Senecavirus A was first identified as a contaminant of human fetal retinal cells (PER.C6) in the US in 2002 (3). Retrospective sequencing of archived picorna-like viruses at the United States Department of Agriculture National Veterinary Service Laboratories (NVSL), revealed the circulation of SVA in the US swine population since at least 1988 (3). Since its first description in 2002, SVA has been explored as an oncolytic agent for cancer treatment in humans (4–6). Recently the virus gained importance in the veterinary field due to the increased incidence of SVA-induced VD in pigs. Since 2014, SVA has been associated with VD outbreaks in swine in Canada (7), the US (2, 8–10), Brazil (9, 11, 12), Colombia (13), China (14), Thailand (15), and Vietnam (16). Pigs are thought to be the main reservoir for SVA; however, the virus has been also isolated from mice, and its nucleic acid has been detected in houseflies collected in SVA affected and non-affected farms (9). Additionally, neutralizing antibodies against SVA have been detected in pigs, cattle and mice (3). The importance of these species for the epidemiology of SVA, however, remains unknown. The protein Anthrax Toxin Receptor 1 (ANTXR1) has been identified as a potential receptor for SVA and shown to interact with the virus capsid during infection of human H446 cancer cells (17), however, the contribution of this molecule to SVA infection in swine await experimental confirmation.

The clinical relevance of SVA, lies on its similarity with other high-consequence VDs of swine, including FMD, swine vesicular disease (SVD), vesicular stomatitis (VS) and vesicular exanthema of swine (VES) (12). Infection with SVA likely occurs via the oral and/or respiratory routes and after an incubation period of 3–5 days, clinical signs including lethargy and lameness are observed. The clinical signs are followed by development of vesicles on the snout and/or feet (dewclaw, interdigital space coronary band and sole) of affected animals (18). The lesions are characterized by cutaneous hyperemia which progresses into fluid-filled vesicles. As the disease progresses, the vesicles rupture and evolve into skin erosions that eventually scab and resolve within 12–16 days post-infection (pi) (18–20). A short-term viremia (1–10 days post-infection, pi) occurs in infected animals and the levels of viremia decline as serum neutralizing antibody (NA) levels rise (19).

The immune responses to SVA are characterized by the development of early and robust NA titers (18, 19, 21), which are strongly correlated with VP2- and VP3-specific IgM responses within the first week of infection (19). Notably, NA levels parallel with decreased viremia and resolution of the disease (19). Analysis of the major porcine T cell subsets revealed that during the acute/clinical phase of SVA infection (14 days pi) T cell responses are characterized by an increased frequency of αβ T cells, especially $CD4^+$ T cells that are initially detected by day 7 pi and increase in frequency until day 14 pi. Additionally, the frequency of $CD8^+$ and double-positive $CD4^+CD8^+$ T cells (effector/memory T cells) expressing IFN-γ or proliferating in response to recall SVA stimulation increases after day 10 pi (19). These observations indicate that SVA elicits B and T cell activation early upon infection, with IgM antibody levels being associated with early neutralizing activity against the virus and peak B and T-cell responses paralleling with clinical resolution of the disease, suggesting that both arms of the immune system may contribute to the control of SVA infection. Importantly, there is only one known serotype of SVA (2, 22) and genetically diverse viral strains present cross neutralizing- and cross T-cell responses (22).

Currently there are no vaccines available for SVA. A recent study assessed the immunogenicity of an inactivated SVA vaccine candidate, demonstrating protection against homologous virus challenge (23). The most effective picornavirus vaccines consist of inactivated or live attenuated vaccines. Most vaccines used for FMDV, for example, are inactivated; however, they fail to induce long-term protection requiring annual re-vaccinations (24). Poliovirus (PV) vaccines long used in humans, leading to the eradication of wild type poliovirus, were either inactivated poliovirus vaccine (IPV) or live oral poliovirus vaccine (OPV). The live OPV induces long-lasting mucosal immunity against PV. In this study we generated a recombinant attenuated SVA strain based on a contemporary SVA isolate (18) and assessed the immunogenicity and protective efficacy of inactivated or live virus formulations against heterologous SVA challenge.

MATERIALS AND METHODS

Viruses and Cells

H1299 and BHK-21 cells were obtained from the American Type Culture Collection (ATCC-CRL 5803 and CCL-10, respectively). PK-15 cells were obtained from the Virology section at the Animal Disease Research and Diagnostic Laboratory (ADRDL). H1299 and PK-15 BHK-21 cells were maintained at 37°C with 5% CO_2 in RPMI-1640 or MEM (Corning, NY), respectively, supplemented with 10% fetal bovine serum (VWR, Chicago, IL) and 2 mM L-Glutamine (Corning, NY). Penicillin (100 U/mL) and streptomycin (100 μg/mL) were also added to culture media.

SVA strain SD15-26 was isolated from swine presenting vesicular disease and has been previously characterized (18, 19). The challenge virus, SVA strain MN15-84-22, was isolated from swine presenting vesicular disease (9). For both wild type SVA strains, low-passage (passage 4) viral stocks were amplified and titrated in H1299 cells and used in experiments described below. Recombinant rSVA mSacII virus was rescued in BHK-21 and H1299 cells and amplified in PK15 cells as described below.

Generation, Rescue, and Amplification of rSVA mSacII Virus

An infectious virulent cDNA clone of SVA strain SD15-26 (pBrick-FLSVA-SD15-26) containing the full length SVA genome under control of a T7 RNA polymerase promoter was recently developed in our laboratory (Fernandes et al., unpublished data). The pBrickA-FLSVA-SD15-26 was constructed using a strategy combining: i. synthesis of cDNA fragments corresponding to the 5′- and 3′ ends of the SVA genome and ii. PCR amplification of the central region of the SVA genome, followed by restriction digestion and cloning. The clone was used as a backbone to construct the rSVA mSacII virus here. In the rSVA mSacII clone, four nucleotide changes were introduced in the virus genome. Three of those changes are in the 5′UTR (c→t, positions 29, 31 and 32) and the fourth change consists of a silent nucleotide change (c→a) at position 942 (VP4 coding region) of the rSVA genome (added to delete a SacII restriction endonuclease site). A synthetic DNA fragment (GenScript) containing these specific nucleotide changes was cloned into the backbone of the rSVA plasmid (virus described above; pBrick-FLSVA-SD15-26) using unique restriction endonucleases (NheI and SfiI) and standard cloning techniques. The resultant recombinant SacII mutant clone (pBRICK-rSVA mSacII) was amplified in Stable 2 cells (Life Technologies) and the purified plasmid DNA was linearized with NotI-HF (NEB) restriction enzyme, which digests the cDNA clone after the poly A tail. The linear pBRICK-rSVA mSacII DNA was used as template in *in vitro* transcription reactions using the MEGAscript™ T7 Transcription Kit (ThermoFisher Scientific) following the manufacturer's instructions. Full-length viral genomic RNA was purified using standard phenol:chloroform purification and ethanol precipitation, and ∼1 μg of viral RNA was transfected in BHK-21 cells using Lipofectamine™ RNAiMAX transfection reagent (ThermoFisher Scientific) according to the manufacturer's instructions. At 48 h post-transfection cells were subjected to three freeze-and-thaw cycles and the virus passaged two more times in H1299 cells. When cytopathic effect was observed, cells were fixed and rescue of rSVA mSacII virus was confirmed by immunofluorescence (IFA) using a rabbit polyclonal antibody against SVA.

The identity of the rSVA mSacII virus was confirmed by RT-PCR amplification of a fragment in the 5′ end of the SVA genome (primers sequences available upon request) followed by SacII restriction digestion of the PCR amplicon. Restriction digestion reactions were analyzed by agarose gel electrophoresis and the identity of rSVA mSacII was determined by lack of SacII digestion in the rSVA mSacII virus PCR amplicon. A PCR amplicon of wt rSVA SD15-26 was used as control. Additionally, complete genome sequencing of rSVA mSacII virus was used to confirm the identity and integrity of the virus genome using the Illumina MiSeq sequencing platform (18). Stocks of rSVA mSacII (p. 4) were produced in PK15 cells. Semi-confluent monolayers of PK15 cells were inoculated with a low MOI (∼0.1) of rSVA mSacII and incubated at 37°C for 72 h until complete SVA CPE was observed in inoculated monolayers. Cells were subjected to three freeze-and-thaw cycles and virus stocks were cleared by centrifugation, aliquoted (1 ml), and stored at −80°C until used in the experiments described below.

Growth Curves

Replication kinetics of wt SVA SD15-26 and rSVA mSacII were assessed *in vitro*. H1299 cells were cultured in six-well plates, infected with both viruses at a multiplicity of infection (MOI) of 0.1 (multi-step growth curve) or 10 (single-step growth curve), and harvested at various time points post-infection (2, 4, 8, 12, and 24 h post-infection). Virus titers were determined using end-point dilution and the Spearman and Karber's calculation method and expressed as $TCID_{50}$/ml.

Western Blots

Western blot was performed to assess protein expression by the rSVA mSacII virus in comparison with wt SVA virus. For this, H1299 cells were infected with both viruses at a MOI of 10 and harvested at different time points post-infection (0, 2, 4, 8, 12, and 24 h). Cells were lysed with M-PER mammalian protein extraction reagent (ThermoFisher Scientific) containing protease inhibitors. Approximately, 100 μg total protein extracts were mixed with Laemmli Buffer (Bio-Rad, Hercules, CA) containing 5% β-mercaptoethanol and denatured at 95°C for 10 min then loaded in 10% SDS-PAGE gel. Electrophoresis was performed at 90 volts for 90 min and proteins were transferred to nitrocellulose membranes and blocked with 5% skim-milk in 1 × phosphate-buffered saline (PBS) overnight at 4°C. Nitrocellulose membranes were washed three times in 1 × PBS containing 0.05% Tween 20 (PBST) and incubated with anti-VP1 and anti-VP2 mouse monoclonal antibodies (kindly provided by Dr. Steve Lawson, SDSU) (1:1,000) in 0.05% PBST for 2 h at RT. Membranes were washed three times with 0.05% PBST. Secondary IRDye® 800CW Goat anti-Mouse IgG (H+L) (LI-COR Biosciences, Lincoln, NE) antibody was added to the membranes (1:15,000 on 1% skim-milk on 0.05% PBST) and incubated for 1 h at RT. Membranes were washed three times with PBST 0.05% and blots developed using a LI-COR® Odyssey® Fc Imaging system (LI-COR Biosciences, Lincoln, NE).

The antigen load in both inactivated and live rSVA mSacII vaccine formulations was also assessed by western blots. For this, 20 μL of each vaccine formulation containing the rSVA mSacII virus suspension at 10^6 $TCID_{50}$/mL were mixed with Laemmli Buffer (Bio-Rad, Hercules, CA) and subjected to SDS-PAGE and immunoblotting as described above.

Animal Pathogenesis Study

The pathogenicity of the rSVA mSacII virus was investigated in pigs. For this, twelve 15-week old SVA-negative finishing pigs weighing ∼60 kg were randomly allocated in two experimental groups as follows: Group 1, wt SVA SD15-26- inoculated group ($n = 6$), and rSVA mSacII-inoculated group ($n = 6$). Animals from both groups were inoculated with virus suspensions containing $10^{8.5}$ $TCID_{50}$ via the oronasal route (5 mL orally and 5 mL intranasally [half into each nostril]). Animals were

challenged on arrival at SDSU Animal Resource Wing (ARW). Animals received food and water *ad libitum* for the duration of the 14-day experiment.

Animals were monitored daily after inoculation for characteristic SVA clinical signs and lesions. Clinical signs and lesions were recorded, and individual daily lesion scores were attributed to each animal (22) and total daily scores were calculated. Swabs (oral, nasal and rectal) and blood samples (serum and whole heparinized blood) were collected on days 0, 1, 3, 7, 10, and 14 pi. At necropsy on day 14 pi, tissues including heart, lungs, kidney, liver, small intestine, large intestine, thymus, spleen, mediastinal lymph node, mesenteric lymph node, and tonsil were collected and stored at−80°C. Animal experiments were revised and approved by the SDSU Institutional Animal Care and Use Committee (approval number 16-002A).

Immunization-Challenge Experiment

The immunogenicity and protective efficacy of rSVA mSacII virus were evaluated in 3-week-old SVA-negative piglets. Animals were randomly allocated in four experimental groups: control (G1, received RPMI 1640, IM; $n = 6$), inactivated (G2, received BEI-inactivated rSVA mSacII vaccine; $n = 6$), live IM (G3, receiving rSVA mSacII by IM route; $n = 6$) and live IN (G4, received rSVA mSacII by IN route; $n = 6$). After a week of acclimation, animals were immunized with the corresponding candidate vaccines (2 mL) via the immunization routes described above and presented in **Table 1**. Inactivation of rSVA mSacII virus by BEI was performed as previously described (25), and a water-in-oil-in-water (W/O/W) emulsion was produced by shear-mixing equal volume of the MONTANIDE^{TM} ISA 201 VG oil adjuvant (1 mL, Seppic SA, Paris) with BEI inactivated virus (1 mL; 10^6 $TCID_{50}$) at 31°C using syringes joined by a lure lock connector as recommended by the adjuvant manufacturer. The live rSVA mSacII vaccine consisted of 2 ml virus suspension (10^6 $TCID_{50}$) in RPMI 1640 medium. Animals in control and inactivated groups were immunized on day 0 and boosted on day 21 post-primary immunization, whereas animals in the live IM and live IN groups were immunized with a single vaccine dose on day 0.

Animals were monitored daily for signs and lesions throughout the experiment. Oral, nasal, and rectal swabs were collected on days 0, 3, 7, 14, and 21 pi. Blood was collected on days 0, 3, 5, 7, 14, 21, 28, and 35 pi. Serum separation and PBMC isolation were performed as previously described (19).

A heterologous SVA isolate (SVA MN15-84-22; 97% nt identity with SVA SD15-26) (9) was used as challenge virus and animals in all groups were challenged on day 42 pi (or day 0 post-challenge; pc). Blood and swabs (oral, nasal, and rectal) were collected on days 0, 3, 7, 10, and 14 pc and processed and stored as above. All animals were euthanized on day 14 pc at the Animal Disease Research and Diagnostic Laboratory (ADRDL), SDSU. Tissues including tonsil and mediastinal and mesenteric lymph nodes were collected and stored at −80°C. Animal immunization-challenge experiments were reviewed and approved by the SDSU Institutional Animal Care and Use Committee (approval number 18-032A).

TABLE 1 | Animal immunization/challenge experimental design.

Group (*n*)	Treatment	Dose	Route	Immunization day	Virus challenge[b]
1 ($n = 6$)	Control	2 mL RPMI	IM	0 and 21	SVA MN15-84-22 $10^{8.5}$ $TCID_{50}$ at 42 dpi
2 ($n = 6$)	Inactivated (BEI) SVA[a]	10^6 $TCID_{50}$ in 2 mL	IM	0 and 21	
3 ($n = 6$)	Live attenuated rSVA mSacII	10^6 $TCID_{50}$ in 2 mL	IM	0	
4 ($n = 6$)	Live attenuated rSVA mSacII	10^6 $TCID_{50}$ in 2 mL	IN	0	

aAdjuvant: Seppic Montanide^{TM} ISA 201 (1:1).
bAnimals were challenged oronasally with 10 mL of virus inoculum (18).

RNA Extraction and Real-Time Reverse Transcriptase PCR (RT-qPCR)

Nucleic acid was extracted from serum, swabs, and tissue samples using the Cador® Pathogen 96 kit (Indical Bioscience) and the QIAcube® HT (Qiagen) automated extractor following the manufacturer's instructions. Swab samples were vortexed and cleared by centrifugation (10,000 × g for 5 min) and 200 μL of cleared supernatant was used for nucleic acid extraction. Two hundred μL of serum were used for nucleic acid extraction. For tissues, ∼0.5 g of each tissue was minced using sterile scalpel, re-suspended in RPMI 1640 medium (10% w/v) and homogenized using a stomacher (2 cycles of 60 s). Homogenized samples were then centrifuged at 14,000 × g for 2 min at room temperature and 200 μL of cleared supernatant was used for nucleic acid extraction using automated QIAcube HT (Qiagen). The presence of SVA RNA in samples was assessed using the SensiFAST^{TM} Probe LO-ROX One-Step kit (Bioline-Meridian Bioscience, MA, USA) and custom designed primers and probe (PrimeTime qPCR probe assays, Integrated DNA Technologies Inc., USA) targeting the SVA 3D gene. Primers and probe were designed using the PrimerQuest Tool (Integrated DNA Technologies Inc., USA). The probe and primers sequence are 5'-/56-FAM/CAGGAACAC/ZEN/TACT CGAGAAGCTGCAA/3IABkFQ/-3′, 5′- GAAGCCATGCTCTC CTACTTC-3′ and 5′- GGGTGCATCAATCTATCATATTCT TC-3′ respectively. Amplification and detection were performed with an Applied Biosystems 7500 real time PCR system under following conditions: 10 min at 45°C for reverse transcription, 2 min at 95°C for polymerase activation and 40 cycles of 5 s at 95°C for denaturation and 30 s at 60°C for annealing and extension. A standard curve was established by using a SVA SD15-26 virus suspension containing $10^{7.88}$ TCID50/mL and preparing 10-fold serial dilutions from 10^{-1} to 10^{-10}. Relative viral genome copy numbers were calculated based on the standard curve determined

using the four- parameter logistic regression model function within MasterPlex Readerfit 2010 software (Hitachi Software Engineering America, Ltd., San Francisco, CA). The amount of viral RNA detected in samples were expressed as $\log_{10}$ (genome copy number)/mL.

Neutralization Assays

Neutralizing antibody (NA) responses elicited by the vaccine candidates and post-challenge (pc) infection were assessed using a virus neutralization assay as previously described (18, 19). Neutralization assays were performed using the parental SVA SD15-26 and the challenge MN15-84-22 virus. NA titers were expressed as $\log_2$ (reciprocal of highest serum dilution capable of completely inhibiting SVA infection). All assays were performed in triplicate and included positive and negative controls in all test plates.

PBMC Recall Stimulation and Flow Cytometry

PBMC recall stimulation was performed as previously described (19). Briefly, PBMCs were thawed and stained with 2.5 μM carboxyfluorescein succinimidyl ester (CFSE; in PBS) according to the manufacturer's instruction (BD Biosciences). CFSE-stained cells were seeded at a density of 5×10^5 cells/well in 96-well plates, rested for 4 h and stimulated as follows: UV-inactivated SVA SD15-26 [multiplicity of infection [MOI] = 2] and recombinant purified VP2 protein (1 μg/mL). Concanavalin A (ConA; 5 μg/mL) plus phytohemagglutinin (PHA; 5 μg/mL) (both from Sigma-Aldrich, St. Louis, MO), or cRPMI alone were used as positive and negative controls in all assays, respectively. After stimulation, the cells were incubated for 5 days at 37°C with 5% CO_2.

Antigen-specific T-cell responses were assessed by flow cytometric analysis. T-cell phenotypes were determined using the various swine-specific antibodies as previously described (19). Single-stain and fluorescence-minus-one (FMO) controls were included in all assays. All flow cytometry data were acquired with an Attune NxT flow cytometer (Thermo Fisher Scientific) and analyzed using FlowJo v.10 software (TreeStar, San Carlos, CA). The percentage of responding cells was calculated as the percentage of total T cells (live $CD3^+$ cells).

Statistical Analysis

Statistical analysis was performed by analysis of variance (ANOVA) followed by Tukey's multiple comparison test. Normality was checked before performing any tests. To assess the association of neutralizing antibody titers and/or T-cell responses between levels of viremia, virus shedding and viral load in tissues, Spearman rank correlation was used. Statistical analysis and data visualization were performed using GraphPAD Prism 8.0.1(244) software (GraphPAD Software Inc., La Jolla, CA).

RESULTS

Generation and *in vitro* Characterization of Recombinant SVA

Recently we have developed a cDNA clone for SVA strain SD15-26 (Fernandes et al., unpublished data), which was used here to develop a second recombinant SVA, originally designed to facilitate the differentiation of the rSVA virus from the parental wt SVA strain. In this clone, we introduced four additional nucleotide changes in the rSVA genome. Three changes are located in the 5′UTR (c→ t, positions 29, 31, and 32) and the fourth change consists of a silent nucleotide change (c→ a) at position 942 (VP4 coding region) of the rSVA genome (added to delete a SacII restriction endonuclease site). The identity of the rSVA mSacII was confirmed by sequencing (data not shown) and restriction digestion with SacII (**Figure 1A**) and its replication properties were compared to the wt SVA virus *in vitro*. Multi-step growth curves revealed a lower replication ability of the rSVA mSacII virus when compared to wt SVA, as evidenced by lower viral yields in rSVA mSacII infected cells (∼1 log) between 8 and 12 h post-inoculation ($P < 0.001$) (**Figures 1D,E**). Additionally, expression levels of two of the main SVA capsid proteins (VP1 and VP2) were compared between wt SVA and rSVA mSacII viruses. As shown in **Figures 1B,C**, the levels of VP1 and VP2 protein detected in rSVA mSacII infected cells were markedly lower when compared to the levels of those proteins detected in wt SVA infected cells.

The rSVA mSacII Virus Is Attenuated but Retains Its Immunogenicity in Pigs

The pathogenicity of the rSVA mSacII virus was compared to that of the wt SVA strain in pigs. Notably, while all pigs inoculated with the wt SVA strain SD15-26 presented characteristic clinical signs (lethargy, lameness) and lesions (vesicles on the snout and/or foot) of SVA infection, none of the rSVA mSacII-inoculated animals developed overt clinical disease (**Figures 2A,B**).

Viremia, virus shedding (oral and nasal secretions and feces) and viral load in tissues were also evaluated. Levels of viremia and virus shedding were significantly lower in rSVA mSacII -inoculated animals when compared to wt SVA-inoculated animals (**Figures 2C–F**). Additionally, viral load in tissues was reduced in rSVA mSacII-inoculated animals when compared to wt SVA-inoculated animals (**Figure 3A**). Notably, NA responses were similar in rSVA mSacII- and wt SVA-inoculated animals (**Figure 3B**), indicating that the attenuated rSVA mSacII virus retained its immunogenicity in pigs.

Clinical and Virological Findings Following Immunization With Inactivated or Live rSVA mSacII Virus

Clinical and virological parameters were evaluated following immunization of weaned piglets with inactivated or live attenuated rSVA mSacII virus. Western blot analysis of the vaccine candidate preparations demonstrated similar antigen loads for two of the major SVA capsid proteins VP1

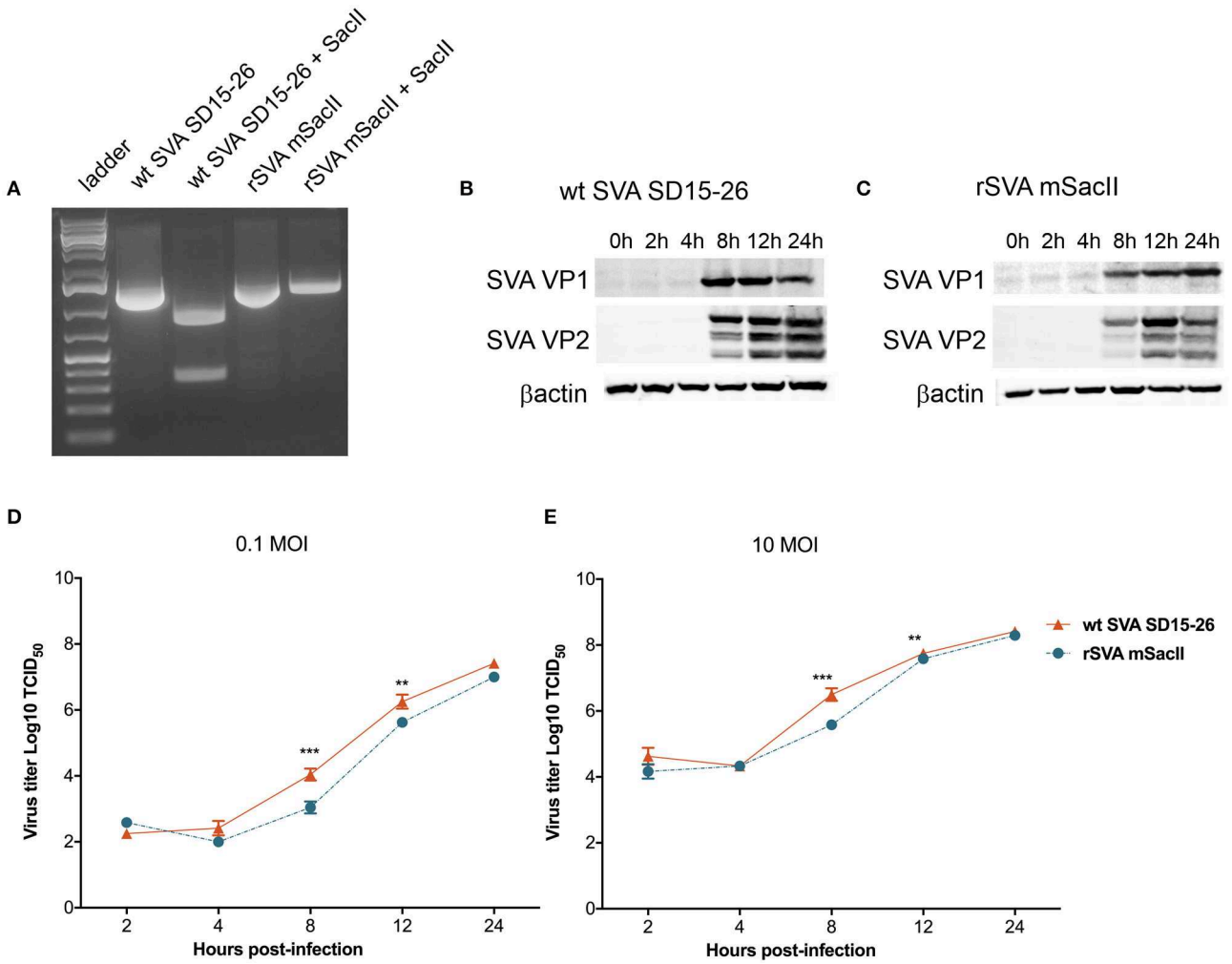

FIGURE 1 | Characterization of the recombinant rSVA mSacII virus *in vitro*. **(A)** Restriction digestion with SacII enzyme of PCR amplicon of the P1 region of SVA genome. Agarose gel image shows digestion of P1-amplicon in wt SVA SD15-26 but not in rSVA mSacII. Undigested PCR products were used as controls. **(B)** Western blot to assess SVA-VP1 and VP2 protein expression in **(B)** wt SVA SD15-26 and **(C)** rSVA mSacII infected cells. H1299 cells were infected with an MOI of 10 of each virus harvested on the indicated time points and subjected to western blots using a VP1- or VP2-specific mAb. **(D)** Multi-step or **(E)** single-step growth curves. H1299 cells were infected with **(D)** 0.1 and **(E)** 10 MOI of wt SVA SD15-26 and rSVA mSacII and virus titers were determined at 2, 4, 8, 12, and 24 h post-infection; Error bars represent SEM calculated based on results of four independent experiments (*P*-values were determined by unpaired *t*-test; $^{**}P < 0.01$; $^{***}P < 0.001$).

and VP2 in both inactivated and live attenuated virus preparations (**Figure 4**). Following immunization, all animals were monitored daily for characteristic SVA clinical signs and vesicular lesions (22). No clinical signs nor lesions were observed in any of the immunized animals (**Figure 5A**). As no gross lesions were observed, clinical scores remained 0 for all groups during the post-immunization (pi) phase of the experiment (**Figure 5B**).

The levels of viremia were assessed in serum samples collected on days 0, 3, 5, 7, 14, and 21 pi by using a SVA real-time reverse transcriptase PCR (RT-qPCR). No viremia was detected in control (G1) and inactivated rSVA mSacII (G2)-immunized animals (**Figure 5C**). Whereas, SVA RNA was detected in serum from both live rSVA mSacII IM (G3) and IN (G4) immunized groups. Animals in G3 and G4 presented viremia between days 3 and 7 pi with all animals being negative from day 14 pi onwards (**Figure 5C**).

Virus shedding was assessed in oral and nasal secretions and feces. Oral, nasal and rectal swabs collected on days 0, 3, 5, 7, 14, and 21 pi were tested by RT-qPCR. Virus shedding was detected up to day 14 pi on oral secretions or up to day 14–21 pi on nasal secretions and feces of animals in the live IM (G3) and live IN (G4)-vaccine groups, respectively (**Figures 5D–F**). No virus excretion was detected on control (G1) and inactivated (G2) groups (**Figures 5D–F**).

Immunogenicity of Inactivated or Live rSVA mSacII Virus in Pigs

The immunogenicity of inactivated or live rSVA mSacII virus was evaluated. Humoral immune responses were assessed by virus

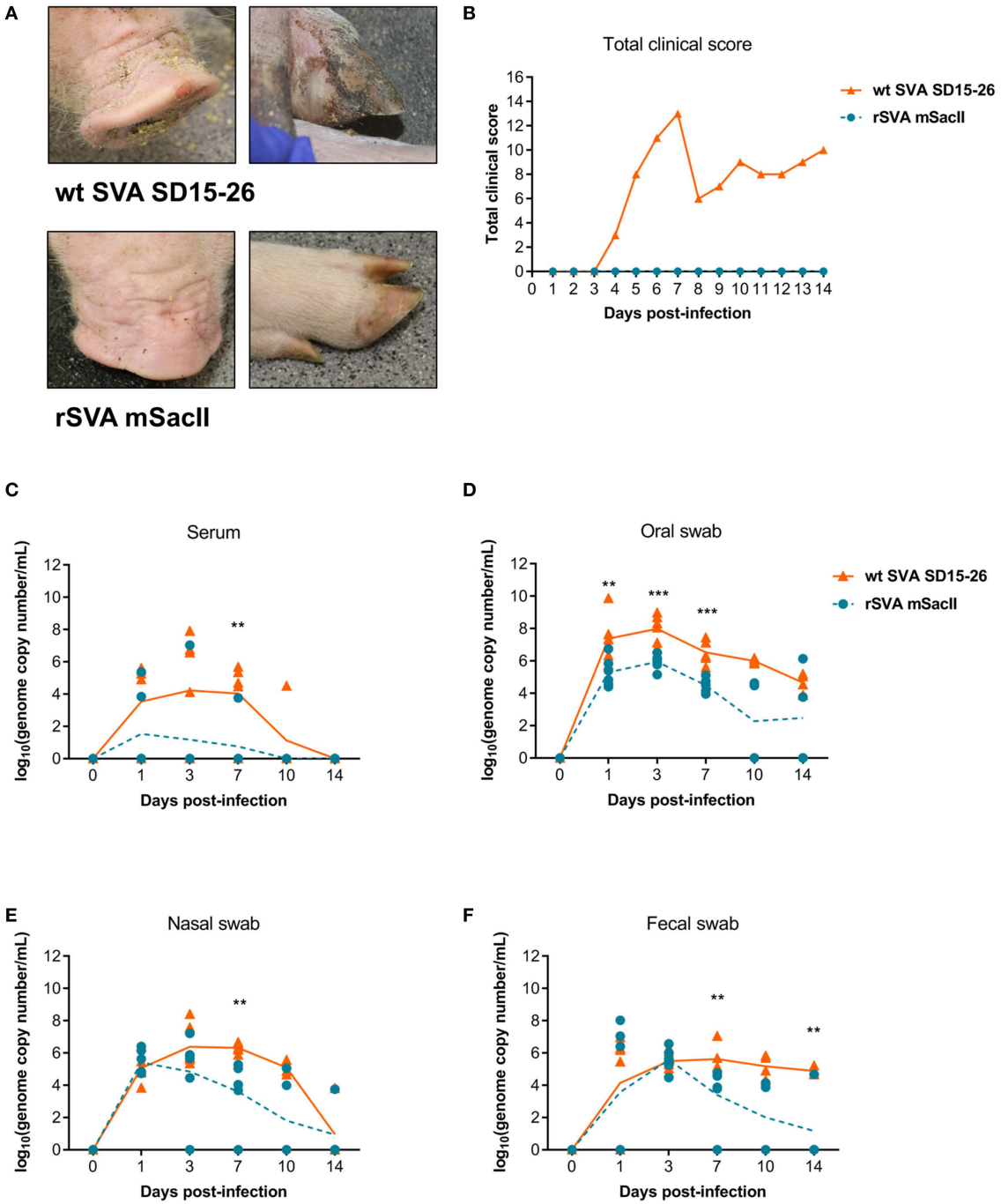

FIGURE 2 | The recombinant rSVA mSacII is attenuated in swine. **(A)** Clinical outcome post-inoculation of wt SVA SD15-26 or rSVA mSacII viruses. Vesicular lesions were observed on the snout and feet of animals infected with wt SVA SD15-26 but not in animals infected with rSVA mSacII. **(B)** Total daily clinical scores post-infection in pigs. A score of 1 was attributed daily to each feet or snout presenting vesicular lesions for a total score of 5 per animal per day. **(C)** Viremia levels as determined by RT-qPCR in serum samples collected at the indicated times post-infection. Virus shedding in oral secretions **(D)**, nasal secretions **(E)** or feces **(F)** as determined by RT-qPCR on swabs collected on indicated times post-infection (*P*-values were determined by unpaired *t*-test; $^{**}P < 0.01$; $^{***}P < 0.001$).

neutralization assays (9, 19) in serum samples collected on days 0, 3, 5, 7, 14, 21, 28, and 35 pi. Immunization with live rSVA mSacII virus via the IM (G2) and IN (G3) routes, elicited robust NA responses with high antibody titers being detected as early as day 3 pi in animals in the live IM group (G3) (**Figures 6A,B**). Interestingly, early NA titers elicited by live IM immunization were significantly higher than antibody titers elicited by IN immunization (day 5–7 pi; $P < 0.01$), whereas no differences in

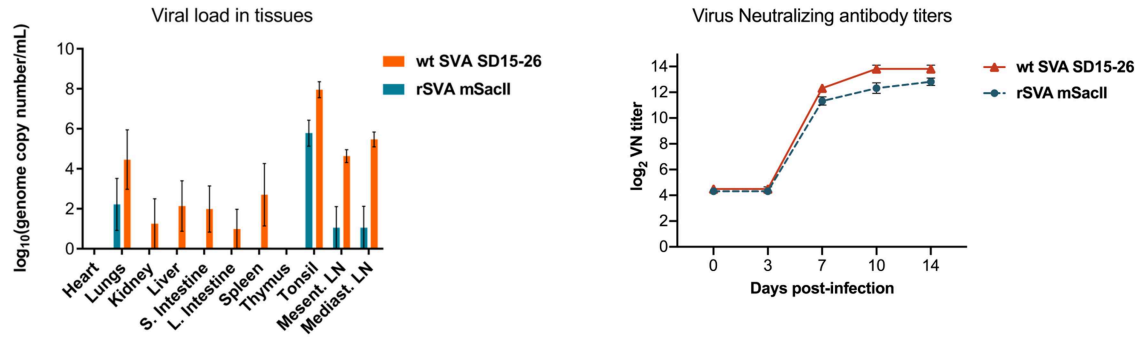

FIGURE 3 | Viral load in tissues and serological responses post-infection in swine. **(A)** Viral load in tissues was determined by RT-qPCR in several tissues collected on day 14 post-infection. **(B)** Neutralizing antibody titers in both virus infected groups (Data represent group means ± SEMs).

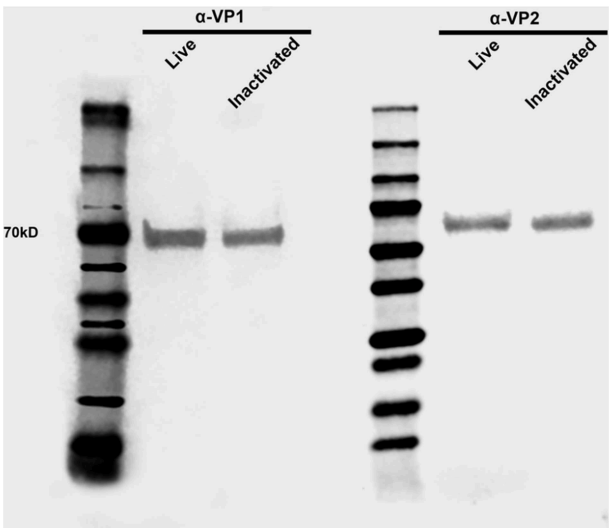

FIGURE 4 | Antigen load in live and inactivated vaccine formulations. Western blot demonstrating similar levels of capsid VP1 and VP2 proteins in both live and inactivated vaccines. After dilution to a virus suspension containing 10^6 TCID50/ml, approximately 20 μl of each vaccine preparation were subjected SDS-PAGE, transferred to a nitrocellulose membrane and probed with anti-SVA-VP1 and -VP2 specific monoclonal antibodies.

NA titers in the live IM and IN immunized groups were observed after day 14 pi (**Figures 6A,B**). Notably, a single dose of the live rSVA mSacII administered either by the IM or IN routes resulted in significantly higher NA responses when compared to immunization with the inactivated virus formulation, even after the booster immunization on day 21 pi (**Figures 6A,B**, days 3–35 pi; $P < 0.01$). No NA antibodies were detected in control sham-immunized animals (G1) prior to challenge infection (days 0–35 pi) (**Figures 6A,B**).

T cell responses elicited by immunization with rSVA mSacII virus were evaluated by lymphocyte proliferation assays. Peripheral blood mononuclear cells (PBMCs) collected on day 42 pi (day of challenge) were subjected to *in vitro* recall stimulation with SVA or with recombinant SVA-VP2 protein as previously described (19). Interestingly, significant recall T cell ($CD3^+$) proliferation was detected in animals immunized with live rSVA mSacII via the IM (G3) and IN (G4) routes ($P < 0.05$) (**Figure 6C**). Additionally, proliferative recall responses of individual T cell subsets, including CD4+, $CD8^+$, double positive $CD4^+/CD8^+$ and γδ T cells (double negative $CD4^-/CD8^-$ cells) were also significantly higher in animals in the live IM (G3) and live IN (G4) groups ($P < 0.05$) (**Figure 6C**). A similar trend in recall T cell proliferation was observed in animals immunized with live virus and re-stimulated with recombinant VP2 protein (**Figure 6D**).

Immunization With rSVA mSacII Protects Against Heterologous SVA Challenge

The protective efficacy of inactivated or live rSVA mSacII virus were evaluated following challenge infection with a heterologous contemporary SVA strain. All immunized animals were challenged oronasally with a virulent SVA strain SVA MN15-84-22 (9) on day 42 post-immunization (**Table 1**). All animals in control sham-immunized G1 presented clinical signs and/or lesions of SVA starting on day 4 post-challenge (pc). Animals presented lethargy and lameness and four of six animals (4/6; 66.6%) displayed characteristic vesicular lesions (**Figure 7A**). Additionally, 3/6 (50%) animals in the inactivated G2 developed lameness and characteristic VD (**Figure 7A**). Similar to control animals, G2 animals developed lesions on or after day 4 pc (**Figures 7A,B**). Notably, a single dose of the live rSVA mSacII via the IM (G3) or the IN (G4) routes resulted in protection from clinical SVA, as no clinical signs nor lesions were observed in immunized animals (**Figures 7A,B**). Peak clinical scores were observed on day 6 pc in control animals or on day 8 pc in the inactivated vaccine group (**Figure 7B**). As no gross lesions were observed in both live vaccine groups (G3 and G4) (**Figure 7A**), clinical scores for these groups remained 0 throughout the challenge phase of the experiment (**Figure 7B**).

The levels of viremia were also assessed post-challenge infection. Serum samples collected on days 0, 3, 7, 10, and 14 pc

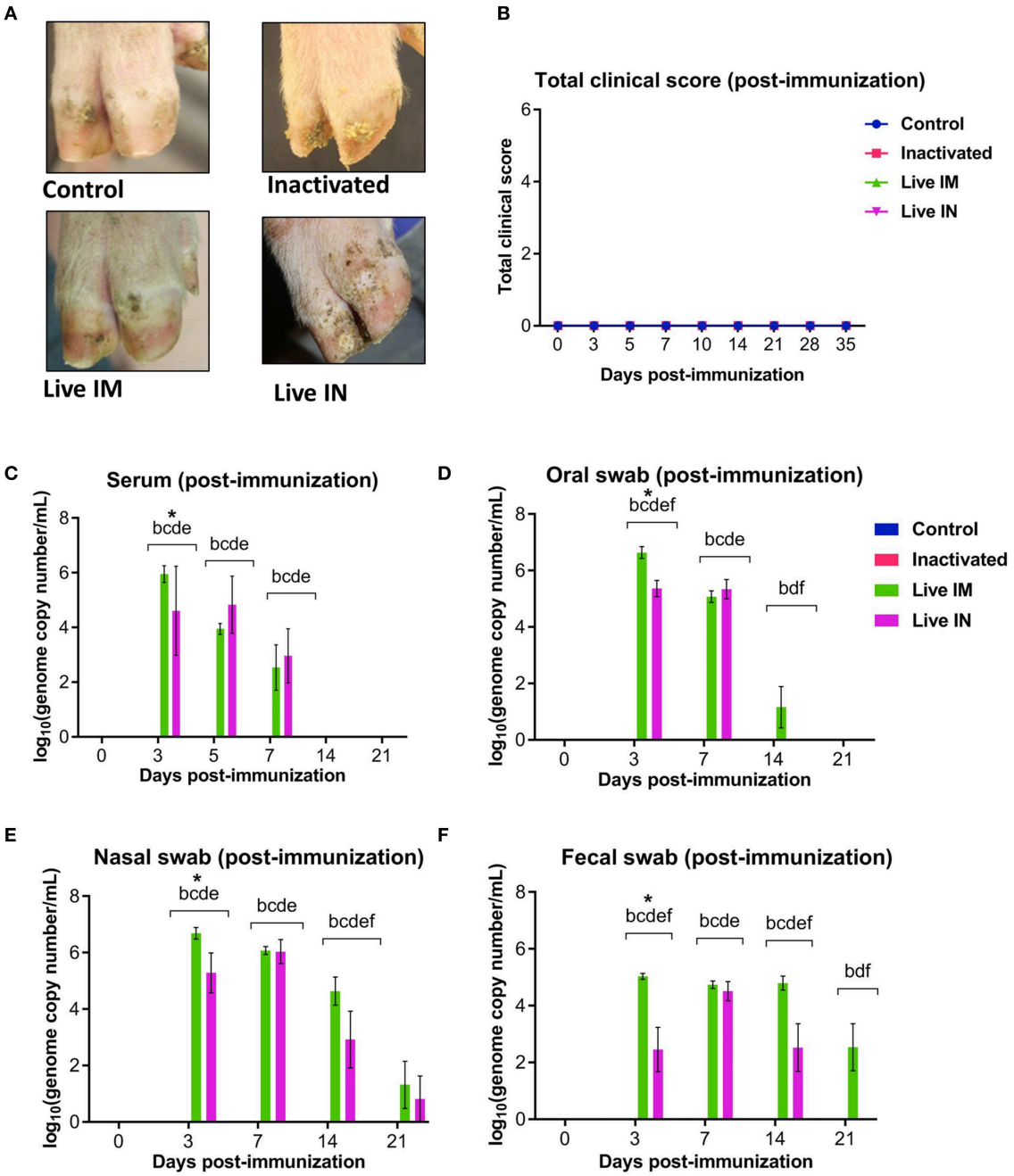

FIGURE 5 | Clinical and virologic outcomes after immunization. Twenty-four 4-week old piglets were randomly allocated to four experimental groups ($n = 6$) and sham-immunized or immunized with inactivated or live (IM or IN) rSVA mSacII vaccine formulations. **(A)** Clinical outcome following immunization showing no lesions in immunized animals. **(B)** Total clinical scores following immunization. **(C)** Viremia levels determined in sera as determined by RT-qPCR at the indicated time points post-immunization. Virus shedding in oral secretions **(D)**, nasal secretions **(E)** and feces **(F)** as determined by RT-qPCR collected from immunized animals at the indicated times post-immunization. *a, b, c, d, e, f indicates significant difference between groups as follows: a. Control vs. Inactivated, b. Control vs. Live IM, c. Control vs. Live IN, d. Inactivated vs. Live IM, e. Inactivated vs. Live IN and f. Live IM vs. Live IN at $P < 0.05$ (Data represent group means ± SEMs. *P*-values were determined by Tukey's multiple comparison test).

were tested for SVA RNA by RT-qPCR. SVA viremia was detected in control sham-immunized (G1) and in the inactivated group (G2) animals between days 3 and 10 pc (**Figure 7C**). The levels of viremia in animals immunized with live rSVA mSacII IM and IN were significantly lower than in control- and inactivated rSVA mSacII-immunized animals (**Figure 7C**, $P < 0.01$). In fact,

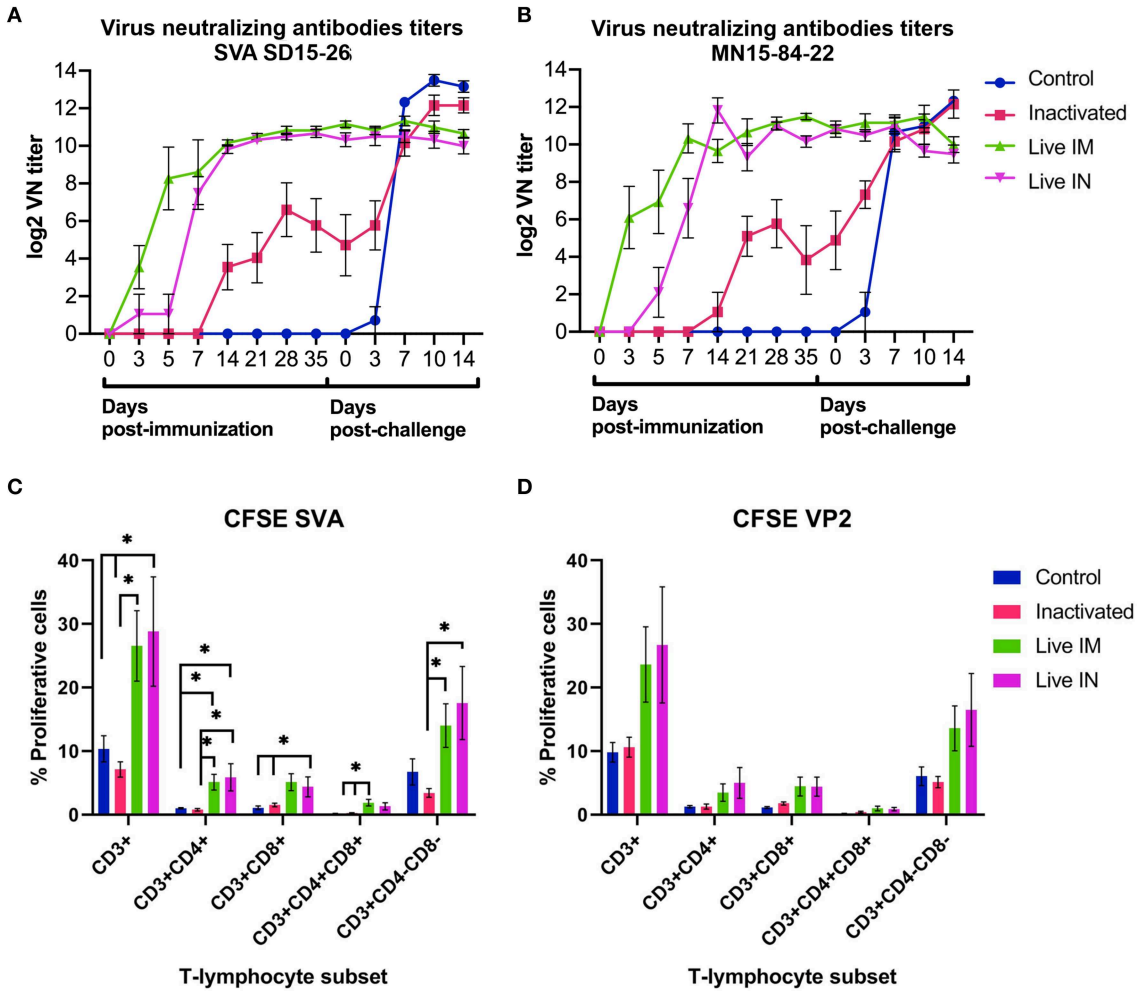

FIGURE 6 | Immune responses elicited by immunization and/or challenge infection. **(A,B)** Virus neutralizing antibody responses against SVA strain SD15-26 **(A)** or MN15-84-22 **(B)** as determined by VN assays performed in serum samples collected at the indicated times post-immunization and post-challenge. **(C)** Carboxyfluorescein succinimidyl ester (*CFSE*) proliferation assay performed in PBMCs obtained on day 42 pi (day of challenge). Cells were stimulated with UV-inactivated SVA (MOI = 1) for 5 days and proliferative responses of major swine T cell subsets were determined by flow cytometry. **(D)** CFSE proliferation assay performed in PBMCs obtained on day 42 pi (day of challenge). Cells stimulated with recombinant SVA VP2 protein (1 μg/mL) for 5 days and proliferative responses of major swine T cell subsets were determined by flow cytometry. Proliferative T cells were expressed as percent of total $CD3^+$ T cells on each sample (Data represent group means ± SEMs. *P*-values were determined by Tukey's multiple comparison; $^*P < 0.05$).

only 2/6 animals immunized with live rSVA mSacII IM and 3/6 immunized IN presented viremia on day 3 or 7 pc, respectively (data not shown).

Virus shedding was assessed in oral and nasal secretions and feces in swabs collected on days 0, 3, 7, 10, and 14 pc by RT-qPCR. High levels of virus excretion were detected between days 3 and 14 pc in animals from the control (G1) and inactivated-vaccine groups (G2) (**Figures 7D–F**). Virus shedding was significantly lower in animals from live IM (G3)- and live IN (G4) groups ($P < 0.01$) when compared to both control (G1) and inactivated (G2) groups in oral and nasal secretions (**Figures 7D,E**). Interestingly, no virus shedding was detected in feces in the live IM (G3)- and live IN (G4) group animals (**Figure 7F**).

The association of NA responses (day 42 pi/0 pc) and levels of viremia/virus shedding were evaluated in samples collected from control and immunized animals. Data points used in the correlation analysis included samples from day 1 through 14 pc. A high negative correlation between NA levels and levels of viremia ($r = -0.856$, 95% CI = −0.938 to −0.685, $P < 0.001$), virus shedding in oral ($r = -0.744$, 95% CI = −0.885 to −0.478, $P < 0.001$), nasal secretions ($r = -0.756$, 95% CI = −0.891 to −0.497, $P < 0.001$), and feces ($r = -0.797$, 95% CI = −0.910 to −0.571, $P < 0.001$) was observed (**Figure 8A**). We also assessed the correlations between T-cell responses and levels viremia/virus shedding. Low to moderate negative correlation between proliferative $CD4^+$ and $CD8^+$ T cell responses

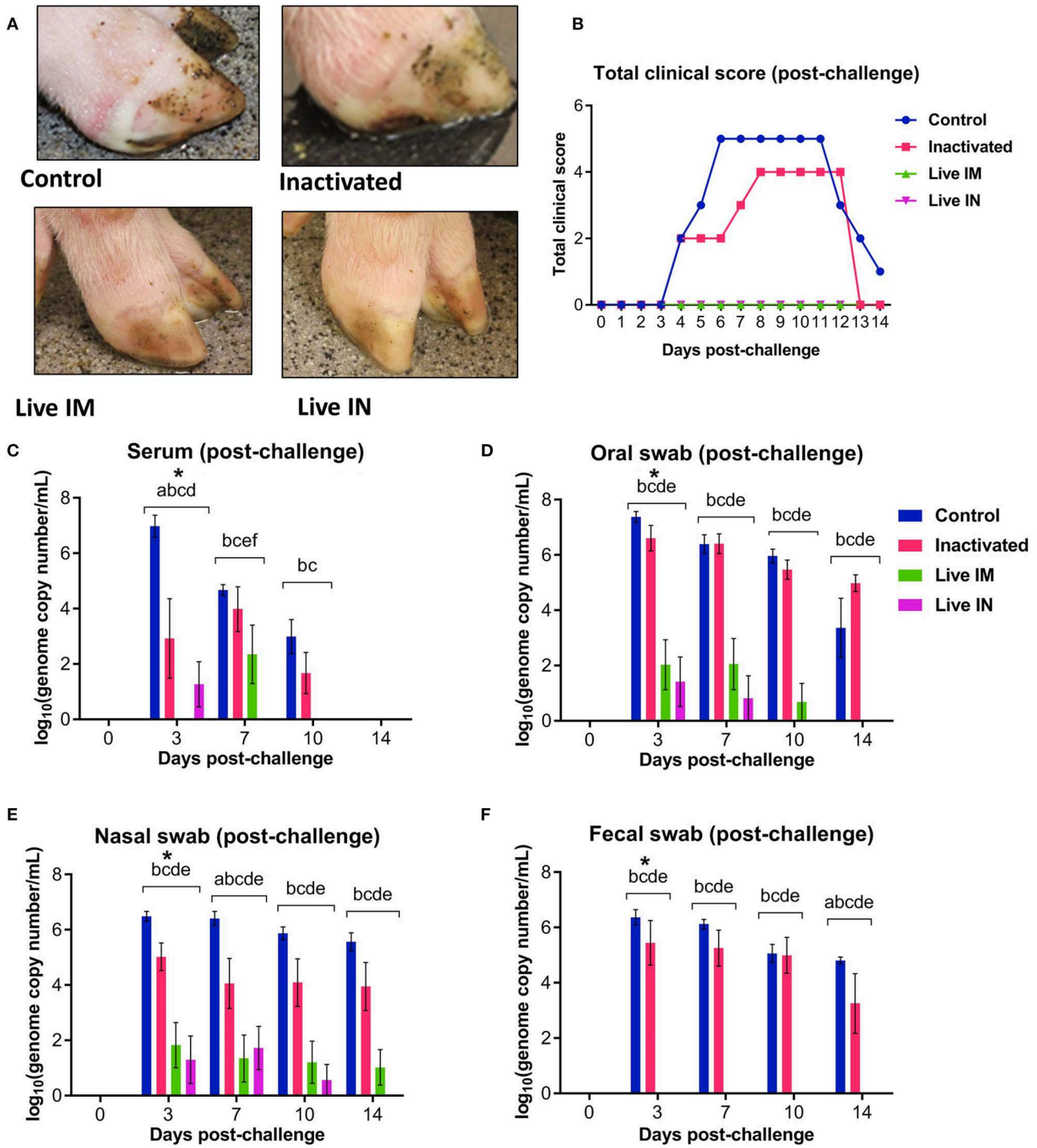

FIGURE 7 | Clinical and virologic outcomes after heterologous SVA challenge. Animals in all groups were challenged oronasally with SVA MN15-84-22 ($10^{8.5}$ $TCID_{50}$). **(A)** Clinical outcome following immunization showing no lesions in immunized animals. **(B)** Total clinical scores following immunization. **(C)** Viremia levels determined in sera by RT-qPCR at the indicated time points post-immunization. Virus shedding in oral secretions **(D)**, nasal secretions **(E)** and feces **(F)** as determined by RT-qPCR at the indicated times post-challenge. *a, b, c, d, e, f indicates significant differences between groups as follows: a. Control vs. Inactivated, b. Control vs. Live IM, c. Control vs. Live IN, d. Inactivated vs. Live IM, e. Inactivated vs. Live IN and f. Live IM vs. Live IN at $P < 0.05$ (Data represent group means ± SEMs. *P*-values were determined by Tukey's multiple comparison).

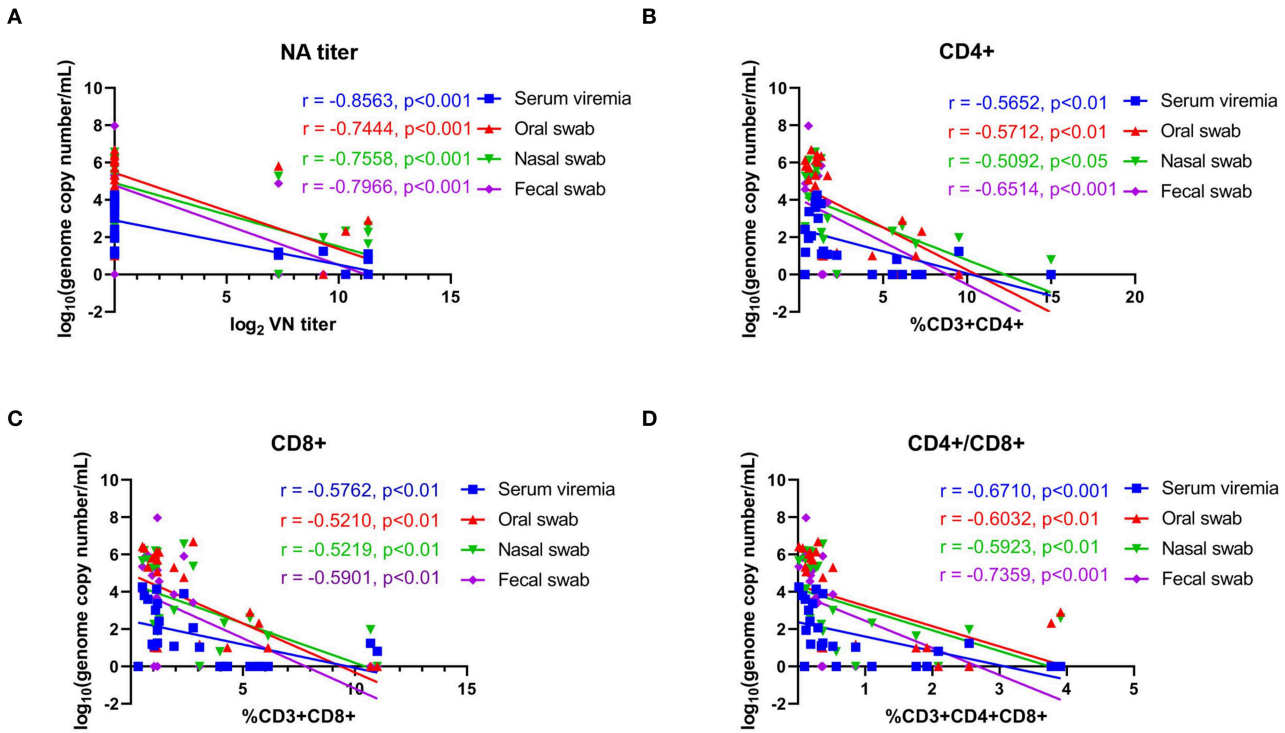

FIGURE 8 | Correlations between neutralizing antibody titers and proliferative T-cell responses with viremia and virus shedding. **(A)** Correlation between the levels of neutralizing antibody (NA) titers at day 42 pi (day of challenge) with levels of viremia, virus shedding in oral secretions, nasal secretions and feces with post challenge infection (days 43–63 pi). **(B)** Correlation of CD4+ T-cell proliferation at day 42 pi (day of challenge) with levels of viremia, virus shedding in oral secretions, nasal secretions and feces post challenge infection (days 43–63 pi). **(C)** Correlation of $CD8^+$ T-cell proliferation at day 42 pi (day of challenge) with the levels of viremia, virus shedding in oral secretion, nasal secretion and fecal swab post challenge infection (days 43–63 pi). **(D)** Correlation of $CD4^+CD8^+$ T-cell proliferation at day 42 pi (day of challenge) with the levels of viremia, virus shedding in oral secretions, nasal secretions and feces post challenge infection (days 43–63 pi). Groups included in the analysis are Control, Live IN, Live IN, and Inactivated. Correlation coefficient (R) values and statistics for each correlation are shown in the graphs (95% CI).

and levels of viremia/virus shedding (oral, nasal and fecal) was observed (**Figure 8B**). Additionally, moderate to high negative correlation between proliferative double positive $CD4^+CD8^+$ T cell responses and viremia/virus shedding was detected (**Figures 8B–D**).

Neutralizing Antibody Responses Post-challenge Infection

The serological responses post-challenge infection was evaluated by VN assays. Serum samples collected on days 0, 3, 7, and 14 pc were tested by VN assays. As shown in **Figures 6A,B**, all animals in control (G1) and inactivated (G2) groups seroconverted post-SVA challenge infection, presenting an anamnestic increase in NA antibody titers. Levels of NA detected in control animals on days 7, 10, and 14 pc were significantly higher than in inactivated (G2), live IM (G3), and live IN (G4) groups (**Figures 6A,B**). Notably, no increase in NA titers were detected in animals from the live IM (G3) and live IN (G4) groups after challenge infection (**Figures 6A,B**).

Protective Responses Elicited by Immunization With rSVA mSacII Lead to Decreased Viral Load in Tissues

Viral load was assessed in lymphoid tissues (tonsil, mediastinal and mesenteric lymph nodes) following challenge infection (day 14 pc) using RT-qPCR. Immunization with inactivated or live rSVA mSacII virus led to a marked decrease in viral load in all tissues tested (**Figure 9**). Significantly lower SVA genome copy numbers were detected in the tonsil of animals immunized with inactivated (G2, $P < 0.05$)-, live IM (G3, $P < 0.05$), or live IN (G4, $P < 0.05$) rSVA mSacII virus, when compared to control animals (G1) (**Figure 9A**). No significant differences in SVA RNA copy number was observed between inactivated (G2)-, live IM (G3)-, live IN (G4)- rSVA mSacII immunized animals (**Figure 9A**). Viral load in mediastinal or mesenteric lymph nodes were significantly lower in live IM (G3; $P < 0.05$)-, live IN (G4, $P < 0.001$)- rSVA mSacII immunized animals when compared to control animals (G1) (**Figures 9B,C**). The levels of SVA load in tissues of animals in the live IN (G4) group were lower with fewer animals being positive in all three tissues when compared to animals in G2 and G3 (**Figure 9**).

The association between NA- and T cell responses with viral load in tissues (day 14 pc) was evaluated. Moderate-to-high negative correlations between NA levels and vial load in the tonsil ($r = -0.569$, 95% CI = −0.795 to −0.202, $P < 0.01$), mediastinal LN ($r = -0.711$, 95% CI = −0.869 to −0.422, $P < 0.001$), and mesenteric LN ($r = -0.761$, 95% CI = −0.894 to −0.507, $P < 0.001$) were observed (**Figure 10A**). We also observed an association between T cell responses and tissue viral load. Moderate negative correlation between CD8+ and CD4+CD8+ double positive T cells were observed (**Figures 10B,C**).

DISCUSSION

Here we generated an attenuated rSVA strain and assessed its safety and efficacy when administered as an inactivated/adjuvanted or live attenuated vaccine against heterologous SVA challenge in pigs. The rSVA mSacII was generated using reverse genetics and engineered to contain three nucleotide changes in the 5′UTR region (C→ T) of the genome and one silent nt change (C→ A) in the P1/VP4 coding region. The three nucleotides substitutions in the 5′UTR region (C→ T) were derived from the low virulence SVA strain SVV001, while the change in the P1/VP4 region (position 942) was inserted to delete a SacII restriction site from the virus genome.

Although originally designed with the intent of rescuing a virulent rSVA strain, *in vitro* characterization of the rSVA mSacII virus demonstrated lower viral yields and protein expression in infected cells when compared to the wt SVA SD15-26 virus. Most importantly, inoculation of finishing pigs with the rSVA mSacII virus did not result in overt VD, and inoculated animals presented lower levels of viremia and virus shedding in oral, nasal secretions and feces when compared to animals inoculated the wt SVA SD15-26 virus. These findings indicated that the rSVA mSacII virus was attenuated in pigs. The mechanism(s) of attenuation of rSVA mSacII was/were not investigated in our study, however, it is possible that the nucleotide changes introduced in the 5′UTR and/or in the P1 coding region may have affected the conformation of RNA secondary structures present in these regions of the virus genome [e.g., internal ribosomal entry site [IRES] or cis-active RNA elements [CRE], respectively] (26–28). Changes affecting the conformation of these RNA structures have been linked to impaired protein expression and/or picornavirus replication, thus resulting in decreased virus virulence and attenuated disease phenotype (29–31). Results here showing lower viral yields and reduced protein expression levels in rSVA mSacII infected cells support this hypothesis. However, additional studies are needed to dissect the precise molecular determinants that led to attenuation of the rSVA mSacII virus in pigs. Notably, despite its attenuated phenotype no significant differences in the levels of NA were observed between animals inoculated with rSVA mSacII or with the parental wt SVA SD15-26, demonstrating that rSVA mSacII virus retained its immunogenicity.

Given the attenuated phenotype and the immunogenicity of the rSVA mSacII in pigs, the next step of our study was to assess the potential of this viral strain as a vaccine candidate for SVA. Previously we have shown that both antibody- and T cell responses are correlated with the control of SVA infection and peak antibody and T cell responses parallel with disease resolution (19). Thus, here we assessed the efficacy of inactivated- or live rSVA mSacII vaccine formulations against a heterologous SVA challenge. Following immunization none of the animals presented clinical signs nor lesions of SVA, confirming efficient inactivation- (G2) and, most importantly, attenuation of the rSVA mSacII virus (G3 and G4). As expected, animals immunized with the live rSVA mSacII via the IM or IN routes excreted virus in

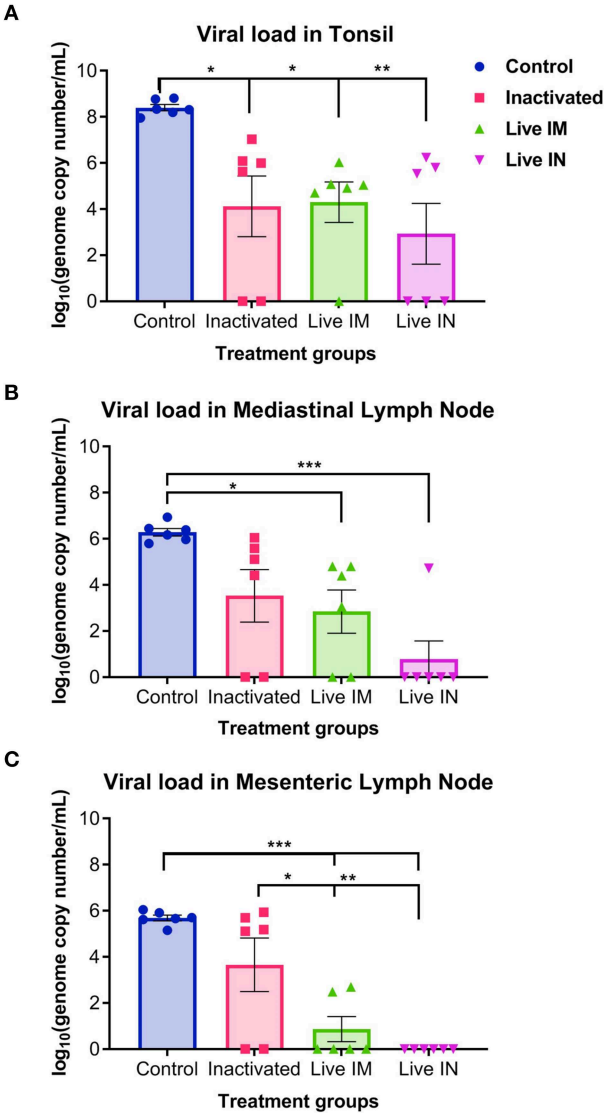

FIGURE 9 | Viral load in tissues. Virus load in the **(A)** tonsil, **(B)** mediastinal lymph node, and **(C)** mesenteric lymph node as determined by RT-qPCR on tissues collected at necropsy on day 14 post-challenge (Data represent group means ± SEMs. *P*-values were determined by Tukey's multiple comparison; **P* < 0.05; ***P* < 0.01; ****P* < 0.001).

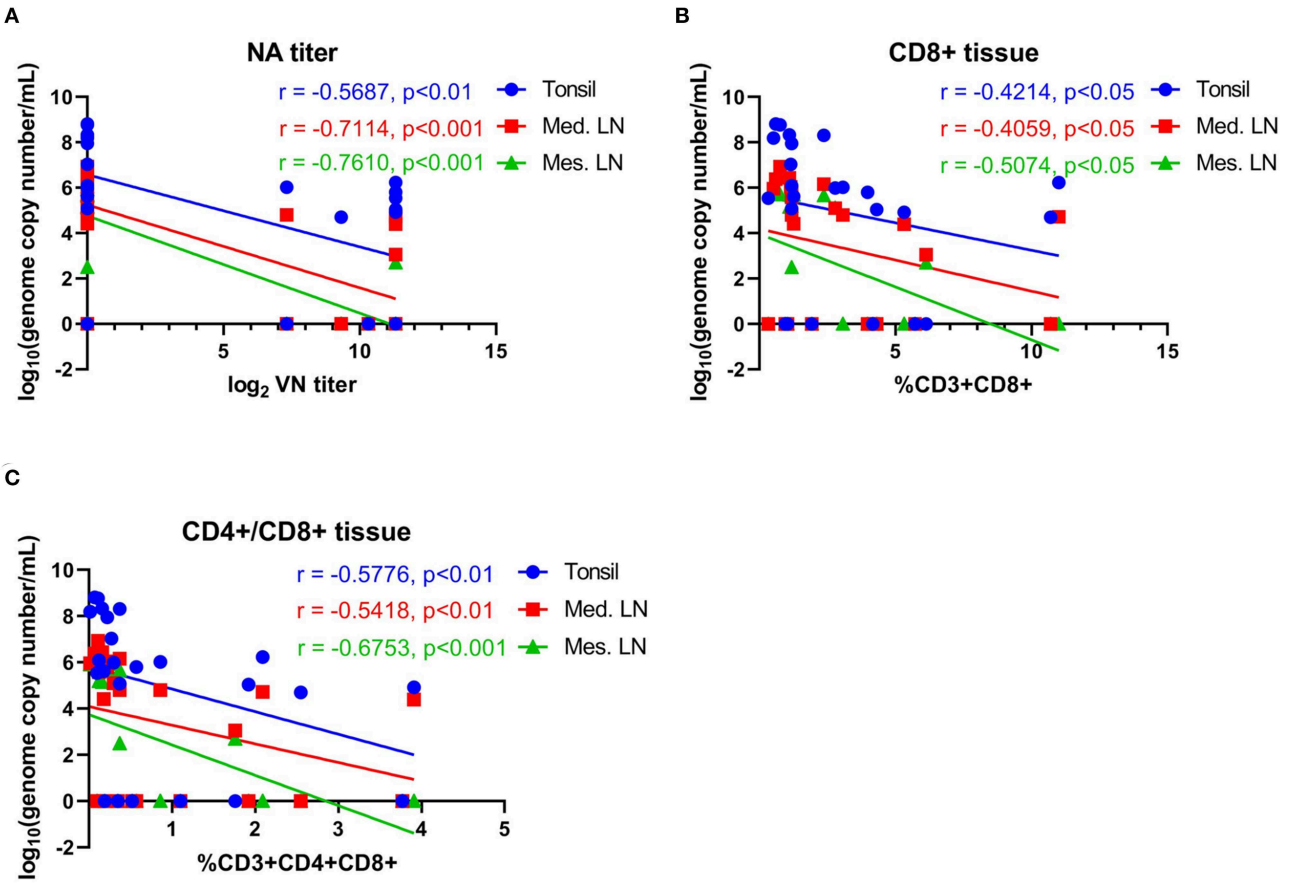

FIGURE 10 | Correlations between neutralizing antibody titers and T-cell responses with viral load in tissues. **(A)** Correlation between NA antibody titers at day 42 pi (day of challenge) with viral load in tonsil, mediastinal lymph node and mesenteric lymph node measured on day 63 pi (day of necropsy). **(B)** Correlation of $CD8^+$ T-cell proliferation at day 42 pi (day of challenge) with viral load in tonsil, mediastinal lymph node and mesenteric lymph node on day 63 pi (day of necropsy). **(C)** Correlation of $CD4^+CD8^+$ T-cell proliferation at day 42 pi (day of challenge) with viral load in tonsil, mediastinal lymph node, and mesenteric lymph node on day 63 pi (day of necropsy). Groups included in the analysis are Control, Live IN, Live IN, and Inactivated. Correlation coefficient (R) value and statistics for each correlation are shown in the graphs (95% CI).

nasal and oral secretions and in feces for 7–21 days post-immunization. Restriction enzyme (Sac II) analysis of the P1 region from PCR amplicons obtained directly from serum and/or nasal secretions from immunized animals on day 3 post-immunization confirmed the identity of the rSVA mSacII sequences during replication of the vaccine virus in pigs (data not shown). These results indicate that rSVA mSacII is a good vaccine candidate to prevent SVA in swine. Additional studies are required, however, to evaluate the genetic stability of this virus after passage/transmission among a cohort of immunized/commingled animals.

The immune responses elicited by immunization with inactivated or live rSVA mSacII vaccine formulations were also evaluated. Notably, while robust neutralizing antibody responses were detected in all animals immunized with a single dose of the live rSVA mSAcII via the IM and the IN routes, animals immunized with the inactivated vaccine formulation presented a delayed NA response with several animals only seroconverting after the booster immunization on day 21 pi. Importantly, one dose of the live rSVA mSacII virus elicited significantly higher NA responses against SVA, than two doses of the inactivated rSVA mSacII vaccine formulation. Although a secondary humoral immune response was observed after the booster immunization with the inactivated rSVA mSacII vaccine, NA titers never reached the levels elicited by immunization with the live virus. This is likely a result of antigen amplification during replication of the live attenuated virus in immunized animals leading to a broader and more efficient stimulation of the immune system. This was also evident at the T cell level, as recall stimulation of PBMCs from animals immunized with the live rSVA mSacII led to robust proliferative responses of $CD4^+$, $CD8^+$, $CD4^+CD8^+$, and γδ- T cells ($CD4^-CD8^-$).

The association between the capacity of picornavirus vaccines to elicit virus-specific immune responses and protection against challenge infection has been reported for several picornaviruses

(23, 24, 32, 33). Neutralizing antibodies seem to be correlated with protection against most picornaviruses (23, 33–35), while the role of T cell responses is debatable with some studies showing the contribution of T cells to protection (36), while others demonstrate only partial protection (37). The protective efficacy of the rSVA mSacII vaccine formulations and the immune responses elicited by immunization with these vaccine candidates was investigated here following challenge of immunized animals with a virulent heterologous SVA strain (MN15-84-22 at $10^{8.5}$ $TCID_{50}$; day 42 post-immunization) (**Table 1**). While 4 out of 6 (4/6) animals in the control group and 3/6 animals in the inactivated vaccine group presented characteristic SVA lesions, none of the animals in the live IM and IN groups presented clinical signs or lesions compatible with SVA infection. Consistent with the clinical outcome post-challenge, the magnitude and extent of viremia and virus shedding in nasal and oral secretions and feces was significantly lower in animals immunized with the live rSVA mSacII virus via the IM or IN routes. Notably, no fecal excretion was detected in the live IM and IN groups following challenge infection. Additionally, no anamnestic serological responses were detected in animals in the IM and IN after the challenge infection, whereas control animals and animals in the inactivated vaccine group seroconverted to the challenge virus. Together, these findings demonstrate solid protection of animals immunized with the live attenuated rSVA mSacII virus against heterologous virus challenge. Immunization with the inactivated rSVA mSacII formulation, on the other hand, only elicited partial protection. These contrasting protective efficacies may potentially reflect significant differences in the levels of neutralizing antibodies and/or T cell responses elicited by live or inactivated virus immunization (**Figure 6**).

Recently the immunogenicity and protective efficacy of a cell culture derived inactivated SVA vaccine candidate was evaluated in pigs (23). This study demonstrated that animals immunized with a 2 μg-dose of the vaccine formulation developed higher titers of NA antibodies and were protected against homologous SVA challenge (23). Animals that received 1/3 or 1/9 of the vaccine dose, however, developed lower levels of NA antibodies and were only partially protected against challenge infection (23). Although a parallel between the levels/titers of neutralizing antibodies elicited by immunization and protection was observed in the present study and in the study by Yang and collaborators (23), studies with other picornaviruses, including FMDV, have shown that this correlation is not precise (23, 34, 37). While some animals presenting low NA titers can resist challenge infection, others will succumb and develop overt clinical disease (23, 34). Thus, defining protective antibody levels for picornaviruses is complex and it is complicated by the role of antibodies in opsonization and phagocytosis and by the potential involvement of T cells in protection against virus infection (23, 38).

Viral load in tissues was also evaluated in our study as a measure of vaccine elicited protection. For this, SVA RNA present in lymphoid tissues, including tonsil and mediastinal- and mesenteric lymph nodes was quantified by RT-qPCR. These tissues have been shown to harbor SVA with the tonsil potentially serving as one of the primary sites for virus replication (18, 22). Results here show low amounts of SVA RNA in tonsil and mediastinal and mesenteric lymph nodes in animals from the live vaccine groups (**Figure 9**). Some animals did not present detectable levels of SVA RNA in the tonsil and many animals did not present detectable viral RNA in the lymph nodes. A lower frequency of positive animals was detected in the group immunized with the live rSVA mSacII via the IN route, suggesting a more effective role of local mucosal immunity in protection against SVA challenge when compared to systemic immunity elicited by parenteral administration of the inactivated or live vaccine formulations. The lower amounts of virus detected in tissues of animals in the live IM or live IN vaccine groups when compared to the viral load detected in inactivated group, may also be a result of increased T cell activity and virus clearance elicited by the live virus vaccine. Additional studies are needed, however, to characterize local mucosal immunity following IN immunization with SVA and to dissect the function of T cells in protection against SVA.

This study describes the development of an effective live attenuated rSVA vaccine candidate capable of providing solid protection against heterologous SVA challenge in pigs. A single dose of the live attenuated vaccine candidate administered via the IM or IN routes elicited protection to challenge with a virulent SVA strain, as evidenced by lack of clinical signs and lower levels of viremia, virus shedding and viral load in tissues. Given that currently there is only one known SVA serotype circulating in the swine population worldwide (22), the live attenuated vaccine candidate developed here may represent a valuable tool to prevent and control SVA outbreaks.

DATA AVAILABILITY STATEMENT

All datasets generated for this study are included in the manuscript.

ETHICS STATEMENT

All animal studies were carried out in accordance with the principles of the Animal Welfare Act, and the recommendations of the Guide for the Care and Use of Agricultural Animals in Research and Teaching. The protocols were approved by the SDSU IACUC (16-002A and 18-032A).

AUTHOR CONTRIBUTIONS

BS, MF, and DD contributed conception and design of the study, and data analysis. ML contributed in the design of the vaccine candidate. BS and LJ performed critical experiments and statistical analysis. SL contributed with animal experiments. BS and DD wrote the manuscript. All authors

contributed to manuscript revision, read, and approved the submitted version.

FUNDING

The work was funded in part by the SD Governor's Office for Economic Development through a grant to the Center for Biologics Research and Commercialization (CBRC) and by the USDA National Institute of Food and Agriculture Hatch project SD00H517-14, Multi-state project SD00R518-14, and foundational project 2018-06740.

ACKNOWLEDGMENTS

We thank the staff of the SDSU Animal Resource Wing (ARW) for their help and care for animals. MHV Fernandes is recipient of the MorriSTONE graduate scholarship, a kind gift provided by Pipestone Veterinary Services.

REFERENCES

1. ICTV. *Virus Taxonomy: 2018 Release*. Washington, DC (2018) Available online at: https://talk.ictvonline.org/ictv-reports/ictv_online_report/positive-sense-rna-viruses/picornavirales/w/picornaviridae/702/genus-senecavirus (accessed January 8, 2019).
2. Hales LM, Knowles NJ, Reddy PS, Xu L, Hay C, Hallenbeck PL. Complete genome sequence analysis of Seneca Valley virus-001, a novel oncolytic picornavirus. *J Gen Virol.* (2008) 89:1265–75. doi: 10.1099/vir.0.83570-0
3. Knowles NJ, Hales LM, Jones BH, Landgraf JG, House JA, et al. Epidemiology of Seneca Valley virus: identification and characterization of isolates from pigs in the United States. In: *XIVth Meeting of the European Study Group on Molecular Biology of Picornaviruses*. Saariselka (2006). p. G2.
4. Rudin CM, Poirier JT, Senzer NN, Stephenson J, Loesch D, Burroughs KD, et al. Phase I clinical Study of Seneca Valley Virus (SVV-001), a replication-competent picornavirus, in advanced solid tumors with neuroendocrine features. *Clin Cancer Res.* (2011) 17:888–95. doi: 10.1158/1078-0432.CCR-10-1706
5. Liu Z, Zhao X, Mao H, Baxter PA, Huang Y, Yu L, et al. Intravenous injection of oncolytic picornavirus SVV-001 prolongs animal survival in a panel of primary tumor-based orthotopic xenograft mouse models of pediatric glioma. *Neuro Oncol.* (2013) 15:1173–85. doi: 10.1093/neuonc/not065
6. Poirier JT, Dobromilskaya I, Moriarty WF, Peacock CD, Hann CL, Rudin CM. Selective tropism of Seneca Valley virus for variant subtype small cell lung cancer. *J Natl Cancer Inst.* (2013) 105:1059–65. doi: 10.1093/jnci/djt130
7. Xu W, Hole K, Goolia M, Pickering B, Salo T, Lung O, et al. Genome wide analysis of the evolution of *Senecavirus A* from swine clinical material and assembly yard environmental samples. *PLoS ONE.* (2017) 12:e0176964. doi: 10.1371/journal.pone.0176964
8. Corner SSK. Seneca valley virus and vesicular lesions in a pig with idiopathic vesicular disease. *J Vet Sci Technol.* (2012) 03:3–5. doi: 10.4172/2157-7579.1000123
9. Joshi LR, Mohr KA, Clement T, Hain KS, Myers B, Yaros J, et al. Detection of the emerging picornavirus *Senecavirus A* in pigs, mice, and houseflies. *J Clin Microbiol.* (2016) 54:1536–45. doi: 10.1128/JCM.03390-15
10. Hause BM, Myers O, Duff J, Hesse RA. *Senecavirus A* in pigs, United States, 2015. *Emerg Infect Dis.* (2016) 22:1323–5. doi: 10.3201/eid2207.151591
11. Vannucci FA, Linhares DCL, Barcellos DESN, Lam HC, Collins J, Marthaler D. Identification and complete genome of seneca valley virus in vesicular fluid and sera of pigs affected with idiopathic vesicular disease, Brazil. *Transbound Emerg Dis.* (2015) 62:589–93. doi: 10.1111/tbed.12410
12. Leme RA, Zotti E, Alcântara BK, Oliveira M V, Freitas LA, Alfieri AF, et al. *Senecavirus A*: an emerging vesicular infection in brazilian pig herds. *Transbound Emerg Dis.* (2015) 62:603–11. doi: 10.1111/tbed.12430
13. Sun D, Vannucci F, Knutson TP, Corzo C, Marthaler DG. Emergence and whole-genome sequence of *Senecavirus A* in Colombia. *Transbound Emerg Dis.* (2017) 64:1346–9. doi: 10.1111/tbed.12669
14. Wu Q, Zhao X, Bai Y, Sun B, Xie Q, Ma J. The First Identification and complete genome of *Senecavirus A* affecting pig with idiopathic vesicular disease in China. *Transbound Emerg Dis.* (2017) 64:1633–40. doi: 10.1111/tbed.12557
15. Saeng-chuto K, Rodtian P, Temeeyasen G, Wegner M, Nilubol D. The first detection of *Senecavirus A* in pigs in Thailand, 2016. *Transbound Emerg Dis.* (2018) 65:285–8. doi: 10.1111/tbed.12654
16. Arzt J, Bertram MR, Vu LT, Pauszek SJ, Hartwig EJ, Smoliga GR, et al. First detection and genome sequence of *Senecavirus A* in Vietnam. *Microbiol Resour Announc.* (2019) 8:e01247-18. doi: 10.1128/MRA.01247-18
17. Miles LA, Burga LN, Gardner EE, Bostina M, Poirier JT, Rudin CM. Anthrax toxin receptor 1 is the cellular receptor for Seneca Valley virus. *J Clin Invest.* (2017) 127:2957–67. doi: 10.1172/JCI93472
18. Joshi LR, Fernandes MHV, Clement T, Lawson S, Pillatzki A, Resende TP, et al. Pathogenesis of *Senecavirus A* infection in finishing pigs. *J Gen Virol.* (2016) 97:3267–79. doi: 10.1099/jgv.0.000631
19. Maggioli MF, Lawson S, de Lima M, Joshi LR, Faccin TC, Bauermann FV, et al. Adaptive immune responses following *Senecavirus A* infection in pigs. *J Virol.* (2018) 92:e01717-17. doi: 10.1128/JVI.01717-17
20. Montiel N, Buckley A, Guo B, Kulshreshtha V, VanGeelen A, Hoang H, et al. Vesicular disease in 9-week-old pigs experimentally infected with *Senecavirus A*. *Emerg Infect Dis.* (2016) 22:1246–8. doi: 10.3201/eid2207.151863
21. Yang M, van Bruggen R, Xu W. Generation and diagnostic application of monoclonal antibodies against Seneca Valley virus. *J Vet Diagn Invest.* (2012) 24:42–50. doi: 10.1177/1040638711426323
22. Fernandes MHV, Maggioli MF, Joshi LR, Clement T, Faccin TC, Rauh R, et al. Pathogenicity and cross-reactive immune responses of a historical and a contemporary *Senecavirus A* strains in pigs. *Virology.* (2018) 522:147–57. doi: 10.1016/j.virol.2018.06.003
23. Yang F, Zhu Z, Cao W, Liu H, Zhang K, Tian H, et al. Immunogenicity and protective efficacy of an inactivated cell culture-derived Seneca Valley virus vaccine in pigs. *Vaccine.* (2018) 36:841–6. doi: 10.1016/j.vaccine.2017.12.055
24. Rodriguez LL, Grubman MJ. Foot and mouth disease virus vaccines. *Vaccine.* (2009) 27:D90–4. doi: 10.1016/j.vaccine.2009.08.039
25. Bahnemann HG. Inactivation of viral antigens for vaccine preparation with particular reference to the application of binary ethylenimine. *Vaccine.* (1990) 8:299–303. doi: 10.1016/0264-410X(90)90083-X
26. Steil BP, Barton DJ. Cis-active RNA elements (CREs) and Picornavirus RNA Replication. *Virus Res.* (2009) 139:240–52. doi: 10.1016/j.virusres.2008.07.027
27. Kloc A, Rai DK, Rieder E. The roles of Picornavirus untranslated regions in infection and innate immunity. *Front Microbiol.* (2018) 9:485. doi: 10.3389/fmicb.2018.00485
28. Willcocks MM, Locker N, Gomwalk Z, Royall E, Bakhshesh M, Belsham GJ, et al. Structural features of the Seneca Valley virus internal ribosome entry site (IRES) element: a picornavirus with a pestivirus-like IRES. *J Virol.* (2011) 85:4452–61. doi: 10.1128/JVI.01107-10
29. Sun C, Yang D, Gao R, Liang T, Wang H, Zhou G, et al. Modification of the internal ribosome entry site element impairs the growth of foot-and-mouth disease virus in porcine-derived cells. *J Gen Virol.* (2016) 97:901–11. doi: 10.1099/jgv.0.000406
30. García-Nuñez S, Gismondi MI, König G, Berinstein A, Taboga O, Rieder E, et al. Enhanced IRES activity by the 3′UTR element determines the virulence of FMDV isolates. *Virology.* (2014) 448:303–13. doi: 10.1016/j.virol.2013.10.027
31. Li R, Zou Q, Chen L, Zhang H, Wang Y. Molecular analysis of virulent determinants of enterovirus 71. *PLoS ONE.* (2011) 6:e26237. doi: 10.1371/journal.pone.0026237
32. de Costa F, Yendo ACA, Cibulski SP, Fleck JD, Roehe PM, Spilki FR, et al. Alternative inactivated poliovirus vaccines adjuvanted with Quillaja brasiliensis or Quil-a saponins are equally effective in

inducing specific immune responses. *PLoS ONE.* (2014) 9:e105374. doi: 10.1371/journal.pone.0105374
33. Brehm KE, Kumar N, Thulke H-H, Haas B. High potency vaccines induce protection against heterologous challenge with foot-and-mouth disease virus. *Vaccine.* (2008) 26:1681–7. doi: 10.1016/j.vaccine.2008.01.038
34. Mayr GA, O'Donnell V, Chinsangaram J, Mason PW, Grubman MJ. Immune responses and protection against foot-and-mouth disease virus (FMDV) challenge in swine vaccinated with adenovirus-FMDV constructs. *Vaccine.* (2001) 19:2152–62. doi: 10.1016/S0264-410X(00)00384-4
35. Dotzauer A, Kraemer L. Innate and adaptive immune responses against picornaviruses and their counteractions: an overview. *World J Virol.* (2012) 1:91–107. doi: 10.5501/wjv.v1.i3.91
36. Neal ZC, Splitter GA. Picornavirus-specific CD4+ T lymphocytes possessing cytolytic activity confer protection in the absence of prophylactic antibodies. *J Virol.* (1995) 69:4914–23.
37. Sanz-Parra A, Jimenez-Clavero MA, Garcia-Briones MM, Blanco E, Sobrino F, Ley V. Recombinant viruses expressing the foot-and-mouth disease virus capsid precursor Polypeptide (P1) induce cellular but not humoral antiviral immunity and partial protection in pigs. *Virology.* (1999) 259:129–34. doi: 10.1006/viro.1999.9717
38. Stenfeldt C, Eschbaumer M, Smoliga GR, Rodriguez LL, Zhu J, Arzt J. Clearance of a persistent picornavirus infection is associated with enhanced pro-apoptotic and cellular immune responses. *Sci Rep.* (2017) 7:17800. doi: 10.1038/s41598-017-18112-4

Conflict of Interest: A provisional patent application has been submitted to the United States Patent and Trademark Office for this the vaccine candidate (US serial no. 62/874,094).

The authors declare that the research was conducted in the absence of any commercial or financial relationships that could be construed as a potential conflict of interest.

frontiers in Immunology

ORIGINAL RESEARCH
published: 08 January 2020
doi: 10.3389/fimmu.2019.02995

Illumination of PRRSV Cytotoxic T Lymphocyte Epitopes by the Three-Dimensional Structure and Peptidome of Swine Lymphocyte Antigen Class I (SLA-I)

Xiaocheng Pan[1,2†], *Nianzhi Zhang*[1†], *Xiaohui Wei*[1], *Yinan Jiang*[1], *Rong Chen*[1], *Qirun Li*[1], *Ruiying Liang*[1], *Lijie Zhang*[1], *Lizhen Ma*[1] *and Chun Xia*[1,3*]

[1] *Department of Microbiology and Immunology, College of Veterinary Medicine, China Agricultural University, Beijing, China,* [2] *Institute of Animal Husbandry and Veterinary Science, Anhui Academy of Agricultural Science, Hefei, China,* [3] *Key Laboratory of Animal Epidemiology of the Ministry of Agriculture, China Agricultural University, Beijing, China*

OPEN ACCESS

Edited by:
Anastasia N. Vlasova, The Ohio State University, United States

Reviewed by:
Scott P. Kenney, The Ohio State University, United States
Zhihao Jia, Purdue University, United States

***Correspondence:**
Chun Xia
xiachun@cau.edu.cn

†These authors have contributed equally to this work

Specialty section:
This article was submitted to Comparative Immunology, a section of the journal Frontiers in Immunology

Received: *11 December 2018*
Accepted: *05 December 2019*
Published: *08 January 2020*

Citation:
Pan X, Zhang N, Wei X, Jiang Y, Chen R, Li Q, Liang R, Zhang L, Ma L and Xia C (2020) Illumination of PRRSV Cytotoxic T Lymphocyte Epitopes by the Three-Dimensional Structure and Peptidome of Swine Lymphocyte Antigen Class I (SLA-I). Front. Immunol. 10:2995. doi: 10.3389/fimmu.2019.02995

To investigate CTL epitope applications in swine, SLA-1*1502-restricted peptide epitopes matching porcine reproductive and respiratory syndrome virus (PRRSV) strains were explored by crystallography, biochemistry, and the specific pathogen-free (SPF) swine experiments. First, nine predicted PRRSV peptides were tested by assembly of the peptide-SLA-1*1502 (pSLA-1*1502) complexes, and the crystal structure of the SLA-1*1502 complex with one peptide (NSP9-TMP9) was determined. The NSP9-TMP9 peptide conformation presented by pSLA-1*1502 is different from that of the peptides presented by the known pSLA-1*0401 and pSLA-3*hs0202 complexes. Two consecutive Pro residues make the turn between P3 and P4 of NSP9-TMP9 much sharper. The D pocket of pSLA-1*1502 is unique and is important for peptide binding. Next, the potential SLA-1*1502-restricted peptide epitopes matching four typical genetic PRRSV strains were identified based on the peptide-binding motif of SLA-1*1502 determined by structural analysis and alanine scanning of the NSP9-TMP9 peptide. The tetrameric complex of SLA-1*1502 and NSP9-TMP9 was constructed and examined. Finally, taking NSP9-TMP9 as an example, the CTL immunogenicity of the identified PRRSV peptide epitope was evaluated. The SPF swine expressing the SLA-1*1502 alleles were divided into three groups: modified live vaccine (MLV), MLV+NSP9-TMP9, and the blank control group. NSP9-TMP9 was determined as a PRRSV CTL epitope with strong immunogenicity by flow cytometry and IFN-γ expression. Our study developed an integrated approach to identify SLA-I-restricted CTL epitopes from various important viruses and is helpful in designing and applying effective peptide-based vaccines for swine.

Keywords: SLA, structure, CTL, epitope, PRRSV, vaccine

INTRODUCTION

The development of new viral vaccines should be increasingly focused on biosafety, especially to remove the viral genetic material and to avoid the possibility of recombinant viruses developing due to the use of vaccines. In view of this central idea, diverse viral vaccines, such as cytotoxic T lymphocyte (CTL) and B cell epitope vaccines, have been experimentally researched in animals for the ongoing control of viral diseases and immunological deficiency diseases (1). Porcine reproductive and respiratory syndrome virus (PRRSV) is one of the most important swine pathogens and has caused significant economic losses in the swine industry worldwide for two decades (2). PRRSV is an enveloped positive-strand RNA virus with a viral genome of ∼15 kb in length and contains 11 open reading frames (ORFs) (3). ORFs 1a and 1b are situated 5′-proximal to the polycistronic genome and encode two large non-structural replicase polyproteins, pp1a, and pp1b, which are processed into at least 14 non-structural proteins (nsps). Eight relatively small genes following ORF1 in the 5′ to 3′ direction encode four membrane-associated glycoproteins, three membrane proteins, and a nucleocapsid protein. Progress has been made in identifying nsp function related to RNA synthesis (nsp9 and nsp10), subgenomic mRNA synthesis regulation (nsp1), membrane-rearrangement (nsp2 and nsp3), replicative endonuclease (nsp11), major virulence factors (nsp3–8), and viral pathogenesis and host immunity (nsp1, nsp2, nsp4, nsp7, and nsp11) (4). The frequent mutation and recombination of the PRRSV RNA genome have resulted in the emergence of numerous variants (5, 6). These phenomena can cause the emergence of some virulent strains, such as the highly pathogenic PRRSVs that are causing enormous economic losses in Asia (7), and have led to the failure of vaccines against new emerging PRRSVs. There are considerable challenges and specific requirements in the development of novel vaccines to prevent PRRS, such as the CTL-epitope vaccine (8, 9).

The greatest challenge is that PRRSV can markedly suppress the swine immune defense system (10). The current evaluation of the PRRSV vaccine is based on its induced antibody response. Although high antibody titers can be produced after immunization, protection is not ideal because the key neutralizing antibodies (NAbs) against PRRSV appear late, typically >28 days post-infection (dpi), and usually at low levels (11). Furthermore, NAbs are usually specific for the homologous PRRSV strain and confer little cross-protection against heterologous strains (12, 13). Regarding CTL-mediated immunity, specific CTL responses have been observed in PRRSV (10, 14, 15). The virulent type 1 (Lena) PRRSV resulted in increased IL-1α production and a higher percentage of CD8+ T cells and IFNγ-producing cells compared with controls. Cross-reactivity against divergent PRRSV is also associated with cytotoxic CD8+IFNγ and CD8–IFNγ+ cells to a different extent (9). PRRSV-specific T cells could be observed as early as 2 weeks after infection, with the viral loads decreasing in persistent infection (13). Modified live vaccines (MLVs) could induce CTL immune responses and confer better protection against heterologous PRRSV strains than inactivated PRRS vaccines (16). These findings indicate that specific $CD8^+$ CTL immunity may play an important role in controlling PRRSV infection. However, there is limited clear and direct evidence of CTLs eliminating PRRSV infection, and more basic immune reagents, such as the tetramer of swine major histocompatibility complex (MHC) class I with PRRSV peptide epitope, are required to address these important issues (9).

Swine MHC class I has been referred to as swine lymphocyte antigen (SLA-I). There are three classical SLA-I loci (SLA-1, SLA-2, and SLA-3) in the swine genome, and all are dominantly expressed (17). SLA-I molecules can present viral peptide epitopes to swine $CD8^+$ T cells and induce the CTL response to kill the infected cells (18). Similar to human MHC (also known as human leukocyte antigen, HLA), SLA-I molecules are a highly polymorphic gene superfamily whose peptide-binding specificities are significantly influenced by highly variable sites (17). Thus, far, more than 100 SLA-I genes have been cloned (IPD; http://www.ebi.ac.uk/ipd/index.html), and two three-dimensional (3D) structures of peptide-SLA-I (p/SLA-I) molecules have been determined, revealing the peptide presentation characteristics of SLA-I molecules in swine (19, 20). Thus, the situation is favorable for the design and development of a novel viral CTL vaccine against swine PRRS based on these 3D structures of SLA-I molecules.

In an attempt to identify anti-PRRSV CTL epitopes in this study, first, predicted peptide epitopes derived from PRRSV were synthesized, and a trimolecular complex, the structure of the epitope from PRRSV-NSP9 (TMPPGFELY, termed NSP9-TMP9)-bound SLA-1*1502 (pSLA-1*1502), was solved. Next, the potential SLA-1*1502-restricted peptide epitopes matching four typical genetic PRRSV strains were identified. Finally, the immunogenicity of the CTL epitope was identified. Our results provide a novel strategy, i.e., the use of the MHC-restricted structural mechanism, to identify and validate CTL epitopes that could be used to develop a peptide-based vaccine against swine PRRS.

MATERIALS AND METHODS

Prediction and Synthesis of PRRSV Peptides

Peptide epitopes were predicted by the NetMHCpan 4.0 Server (http://www.cbs.dtu.dk/services/NetMHCpan/) based on the whole protein sequences of four typical PRRSV strains (VR2332, GenBank accession no. EF536003.1; HB-13.9, GenBank accession no. EU360130.1; JXwn06, GenBank accession no. EF641008.1; and CHsx1401, GenBank accession No. KP861625.1). These potential non-apeptides were predicted using the SLA-1*1502 allele (GenBank accession no. HQ909439) and purified to >90% purity by analytical reverse-phase high-performance liquid chromatography (HPLC) (SciLight Biotechnology) (**Table 1**). These peptides were stored in lyophilized aliquots at −20 or −80°C after synthesis and were dissolved in dimethyl sulfoxide (DMSO) before use.

Refolding of the SLA-1*1502 Complex

To assemble the pSLA-1*1502 complexes with each non-apeptide (**Table 1**), SLA-1*1502 heavy chain (HC) and swine β2m(sβ2m) inclusion bodies were refolded (in a 1:1:1 molar ratio) via the gradual dilution method we described previously (21, 22). The SLA-1*1502 HC and sβ2m inclusion bodies were also refolded without peptides or with non-combined peptides as negative controls. In addition, the SLA-1*0401 HC and sβ2m inclusion bodies were refolded with a positive peptide (amino acid sequence NSDTVGWSW) as a positive control. After 48 h of incubation at 4°C, the remaining soluble portion of the complex was concentrated and then purified via chromatography in a Superdex200 16/60 column, followed by Resource-Q anion-exchange chromatography (GE Healthcare), as previously described (21).

Crystallization and Data Collection of pSLA-1*1502

The purified complex (44 kDa) of pSLA-1*1502 with the NSP9-TMP9 peptide (amino acid sequence TMPPGFELY, derived from residues 198–206 of the PRRSV non-structural protein) was dialyzed against crystallization buffer (20 mM Tris–HCl pH 8.0, 50 mM NaCl) and concentrated to 12 mg/mL. The sample was then mixed with reservoir buffer at a 1:1 ratio and crystallized via the hanging-drop vapor diffusion technique at 277 and 291 K. Index Kits (Hampton Research, Riverside, CA) were employed to screen the crystals. With a protein concentration of 12 mg/mL, crystals of pSLA-1*1502 were obtained in 10–14 days from index solution No. 65 (0.1 M Bis-Tris pH 5.5, 0.1 M ammonium acetate, 17% PEG 10 000) at 4°C. Diffraction data were collected at a resolution of 2.2 Å (pSLA-1*1502) with an in-house X-ray source (Rigaku Micro-Max007 desktop rotating anode X-ray generator with a Cu target operated at 40 kV and 30 mA) and an R-AXIS IV^{++} imaging plate detector at a wavelength of 1.5418 Å. The crystals were first soaked in reservoir solution containing 25% glycerol as a cryoprotectant and then flash-cooled in a stream of gaseous nitrogen at −173°C (23). The collected intensities were indexed, integrated, corrected for absorption, scaled, and merged by using the HKL2000 package (24).

Structural Determination and Refinement of pSLA-1*1502

The structures of pSLA-1*1502 with NSP9-TMP9 were solved via molecular replacement using the MOLREP program with HLA-A*1101 (PDB code, 1Q94) as the search model. Extensive model building was performed by hand with COOT (25), and restrained refinement was performed with REFMAC5. Additional rounds of refinement were conducted by using the phenix.refine program implemented in the PHENIX package (26) with isotropic atomic displacement parameter (ADP) refinement and bulk solvent modeling. The stereochemical quality of the final model was assessed with the PROCHECK program (27). Data collection and refinement statistics are listed in **Table 2**.

Determination of the Circular Dichroism Spectra and Thermal Unfolding of pSLA-1*1502

The thermostability of SLA-1*1502 with six mutant peptides was examined via circular dichroism (CD) spectroscopy. CD spectra were measured at 20°C in a Jasco J-810 spectropolarimeter equipped with a water-circulating cell holder. Far-UV CD spectra (180–260 nm) were collected at a protein concentration of 0.2 mg/ml in 20 mM Tris (pH 8.0) buffer in a cuvette with a length of 1 mm at 0.1-nm spectral resolution. The ellipticity at 218 nm was continuously recorded during heating. Thermal denaturation curves were obtained by monitoring the CD value at 218 nm in a cell with an optical path length of 1 mm as the temperature was raised from 25 to 90°C at a rate of 1°C/min. The temperature of the sample solution was directly measured with a thermistor. The fraction of unfolded protein was calculated from the mean residue ellipticity (θ) by the standard method: the unfolded fraction (%) is expressed as $(\theta–\theta_N)/(\theta_U-\theta_N)$, where θ_N and θ_U are the mean residue ellipticity values in the fully folded

TABLE 1 | Predicted peptides from PRRSV and influenza virus and their binding to SLA-1*1502 evaluated via *in vitro* refolding.

Name	Sequence	Derived protein	Position	%Random[a]	Stability[b]
PP1	SSSHLQLIY	PRRSV-GP5	34–41	0.388	++
PP2	IFLNCAFTF	PRRSV-M	48–56	0.473	++
PP3	LMLSSCLFY	PRRSV-GP4	96–104	0.592	++
PP4	IFLCCGFLY	PRRSV-GP3	9–17	0.538	++
PP5	SSAAAIPPY	PRRSV-NSP2	940–948	0.260	+
PP6	RWFAANLLY	PRRSV-NSP9	404–412	0.703	++
PP7	TMPPGFELY	PRRSV-NSP9	198–216	0.540	++
PP8	RTAIGTPVY	PRRSV-GP4	69–77	0.416	+
PP9	ISAVFQTYY	PRRSV-GP3	160–168	0.327	+
IP1	NSDTVGWSW	SI-NA	449–457	0.246	–

[a] *% Random is a base value for estimation of the binding affinities of peptides by the NetMHCpan 4.0 Server (http://www.cbs.dtu.dk/services/NetMHCpan/); the Rank threshold for strongly binding peptides is 0.100, and the rank threshold for weakly binding peptides is 1.000.*

[b] *Stability is the capacity for peptide binding to SLA-1*1502. ++, peptide binds strongly and can tolerate anion-exchange chromatography; –, peptide does not bind SLA-1*1502; +, peptide binds SLA-1*1502 but cannot tolerate anion-exchange chromatography.*

TABLE 2 | X-ray diffraction data processing and refinement statistics.

Parameter	SLA-1*1502-NSP9-TMP9
Data processing	
Space group	$P2_12_12_1$
Unit cell parameters (Å)	a = 66.058, b = 74.059, c = 98.596 α = 90.00, β = 90.00, γ = 90.00
Resolution range (Å)	50.00-2.20 (2.20–2.28)[a]
Total reflections	197,524
Unique reflections	24,678
Avg redundancy	7.9 (7.9)
Completeness (%)	99.5 (98.9)
R_{merge} (%)[b]	8.3 (28.6)
Avg I/σ (I)	27.366 (7.517)
Refinement	
Resolution (Å)	29.607-2.199
R_{factor} (%)[c]	20.0
R_{free} (%)	24.3
R M S Deviations	
Bonds (Å)	0.014
Angles (°)	1.140
Average B factor	26.602
Ramachandran plot quality	
Most favored region (%)	91.5
Allowed region (%)	8.5
Disallowed region (%)	0.0

[a] *Values in parentheses are for the highest-resolution shell.*

[b] $R_{merge} = \Sigma_{hkl} \Sigma_i |I_i(hkl) - \langle I(hkl) \rangle| / \Sigma_{hkl} \Sigma_i I_i(hkl)$, *where* $I_i(hkl)$ *is the observed intensity and* $\langle I(hkl) \rangle$ *is the average intensity from multiple measurements.*

[c] $R = \Sigma_{hkl} || F_{obs} | - k | Fcalc | | / \Sigma_{hkl} | F_{obs} |$, *where* R_{free} *is calculated for a random chosen 5% of reflections, and* R_{work} *is calculated for the remaining 95% of reflections employed for structural refinement.*

and fully unfolded states. The midpoint transition temperature (Tm) was determined by fitting the data to the denaturation curves by using the Origin 8.0 program (OriginLab), as described previously (28).

Tetramer Preparation

The tetrameric pSLA-1*1502 complex was constructed according to a previously described method (29). Briefly, a sequence containing a BirA enzymatic biotinylation site was added to the C-terminus of the SLA-1*1502 HC via PCR. The PCR primers and conditions were as described previously (30). Then, the entire construct was cloned into the pET-21a(+) vector, which was subsequently transfected into *Escherichia coli* strain BL21(DE3) for protein expression. The inclusion bodies of recombinant SLA-1*1502 HC containing the BirA site and of sβ2m were refolded with the NSP9-TMP9 peptide as described above. The pSLA-1*1502 complex was then purified and biotinylated by using the BirA enzyme (Avidity Aurora, CO). Finally, the complex was purified and tetramerized by mixing pSLA-1*1502-BSP with PE-labeled streptavidin (BioSource International, Camarillo, CA) at a molar ratio of 4:1, after which the samples were separated by using 100 KDa Millipore tubes. SDS-PAGE electrophoresis was used to determine the efficiency of tetramerization.

Evaluation of the Immunogenicity of NSP9-TMP9 in Swine

A total of nine specific pathogen-free (SPF) swine (15 kg, 8–9 weeks old). Beijing Center of SPF Swine Breeding and Management) expressing the SLA-1*1502 alleles were divided into three groups: MLV, MLV+NSP9-TMP9, and a blank control group. For initial immunization, the MLV and MLV+NSP9-TMP9 groups were injected with an attenuated PRRSV vaccine according to the manufacturer's instructions (Boehringer-Ingelheim, Ingelvac). After seven days, for the second immunization, the MLV + NSP9-TMP9 group was injected with the NSP9-TMP9 peptide mixed with complete Freund's adjuvant (CFA, 1:3 emulsification). The MLV group was injected with the MLV peptide mixed with CFA. Seven days later, peptide mixed with incomplete Freund's adjuvant (IFA, 1:3 emulsification) was injected into the MLV+NSP9-TMP9 group. The MLV group was injected with MLV mixed with IFA. The immune dose of the peptide was 0.1 mg/kg body weight. The control group was injected with phosphate-buffered saline (PBS), deionized water mixed with CFA (1:3 emulsification), and deionized water mixed with IFA (1:3 emulsification) at the same time as the immunization group. Equivalent volumes were used in the immunization group and the control group. Blood was collected from the anterior vena cava, and peripheral blood mononuclear cells (PBMCs) were isolated by the kit according to the manufacturer's instructions (Solarbio). The PBMCs were incubated for 30 min at 37°C in staining buffer (PBS with 0.1% BSA and 0.1% sodium azide) containing the PE-labeled tetrameric complex and the FITC-labeled anti-CD8 monoclonal antibody. The cells were then washed once with staining buffer and detected via flow cytometry. More than 10^6 cell events were acquired for each sample. Cells stained with PE-labeled tetramers and a FITC-labeled anti-CD8 monoclonal antibody were counted as CTL response cells (31). The results for fluorescence-activated cell sorting (FACS) data are presented as the mean ± standard error of the mean (SEM) for the three animals in each group. Statistical analysis was performed using GraphPad Prism 7 (https://www.graphpad.com) for Windows. Significant differences ($P < 0.01$) between means were tested by two-tailed Student's t-test.

Production of IFN-γ in Swine After Immunization With NSP9-TMP9

One week after immunization with NSP9-TMP9 or deionized water, PBMCs were collected from immunized and control groups. These PBMCs were stimulated with NSP9-TMP9 peptide at a concentration of 2 μg/ml. PHA was added at the same concentration to each positive control group, while an equivalent volume of PBS was added to the negative groups. Swine IFN-γ in the supernatant was detected via an ELISA kit according to the manufacturer's instructions (Invitrogen) after the cells had been incubated at 37°C for 18 h.

RESULTS

PRRSV Peptide Prediction and Verification of SLA-1*1502

Six SLA-I alleles were cloned from Landrace pigs. SLA-1*1502 showed better PRRSV peptide-binding ability than the others (**Table S1**) according to *in silico* prediction (http://www.cbs.dtu.dk/services/NetMHCpan). Nine PRRSV peptides, all of which could be presented by SLA-1*1502, were synthesized to test this prediction (**Table 1**). All nine peptides could form complexes with SLA-1*1502 and swine β2m (pSLA-1*1502) by *in vitro* refolding. The stable pSLA-1*1502 complexes were further used to screen the crystal structures.

3D Structure of pSLA-1*1502

SLA-1*1502 in complex with NSP9-TMP9 was crystallized in the $P2_12_12_1$ space group with a high resolution of 2.20 Å (**Table 2**). One asymmetric unit contains only one SLA-1*1502 molecule. The pSLA-1*1502 complex displays a canonical p/MHC I structure, including the α1, α2, and α3 domains of the HC and the light chain sβ2m. NSP9-TMP9 is located in the peptide-binding groove (PBG) formed by the α1 and α2 domains (**Figure 1A**). The root mean square differences (RMSDs) between SLA-1*1502 and two other solved p/SLA I structures (SLA-1*0401, PDB code: 3QQ3; SLA-3*hs0202, PDB code: 5H94) were found to be 0.446 and 0.592, respectively, indicating similarities among the overall structures of the p/SLA I molecules. The NSP9-TMP9 peptide is fixed by 15 hydrogen bonds with residues in the N- and C-termini of the PBG, and no hydrogen bonds were observed in the middle portion (P3–P7) (**Figure 1B**). Based on the surface model, the P4 and P8 residues are located outside the PBG, and their side chains are solvent accessible, especially the P8 residue, which is at the top position of the NSP9-TMP9 peptide conformation (**Figure 1C**).

Pocket Composition of pSLA-1*1502 Bound to NSP9-TMP9 Peptide

The compositions and polarities of the six pockets of pSLA-1*1502 are shown in **Figure 2**, and the interactions between the NSP9-TMP9 peptide and these pockets are listed in **Table 3**. The pockets of pSLA-1*1502, p/SLA-1*0401, and p/SLA-3*hs0202 are compared in **Figure 3**. The A pocket of pSLA-1*1502, composed of Leu^5, Tyr^7, Phe^{33}, Tyr^{59}, Glu^{63}, Tyr^{159}, Leu^{163}, Ser^{167}, and Tyr^{171}, fixes P1-Thr via hydrogen bonds and strong van der Waals forces (VDWs) (**Figure 2A**; **Table 3**). The residues forming the A pockets of SLA I molecules, including Ser^{167}, are highly conserved (**Figure 3**). In most MHC I molecules of other

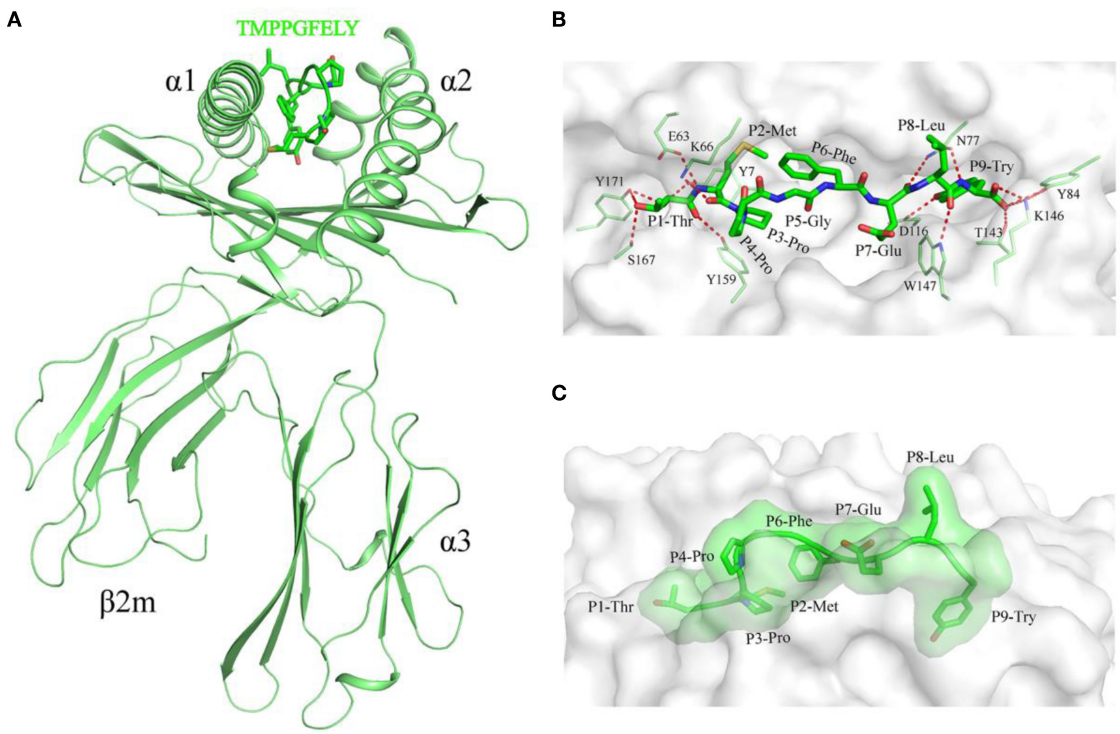

FIGURE 1 | Structural overview and NSP9-TMP9 peptide presentation in pSLA-1*1502. **(A)** Overall structure of SLA-1*1502 in complex with the NSP9-TMP9 peptide. The non-apeptide is shown in stick representation between the α1 domain and α2 domain of pSLA-1*1502. **(B)** Interactions between the NSP9-TMP9 peptide and residues in the PBG. The hydrogen bonds are represented as red dashes. **(C)** Surface model of NSP9-TMP9. Most regions of P4-Pro and P8-Leu are located outside the PBG.

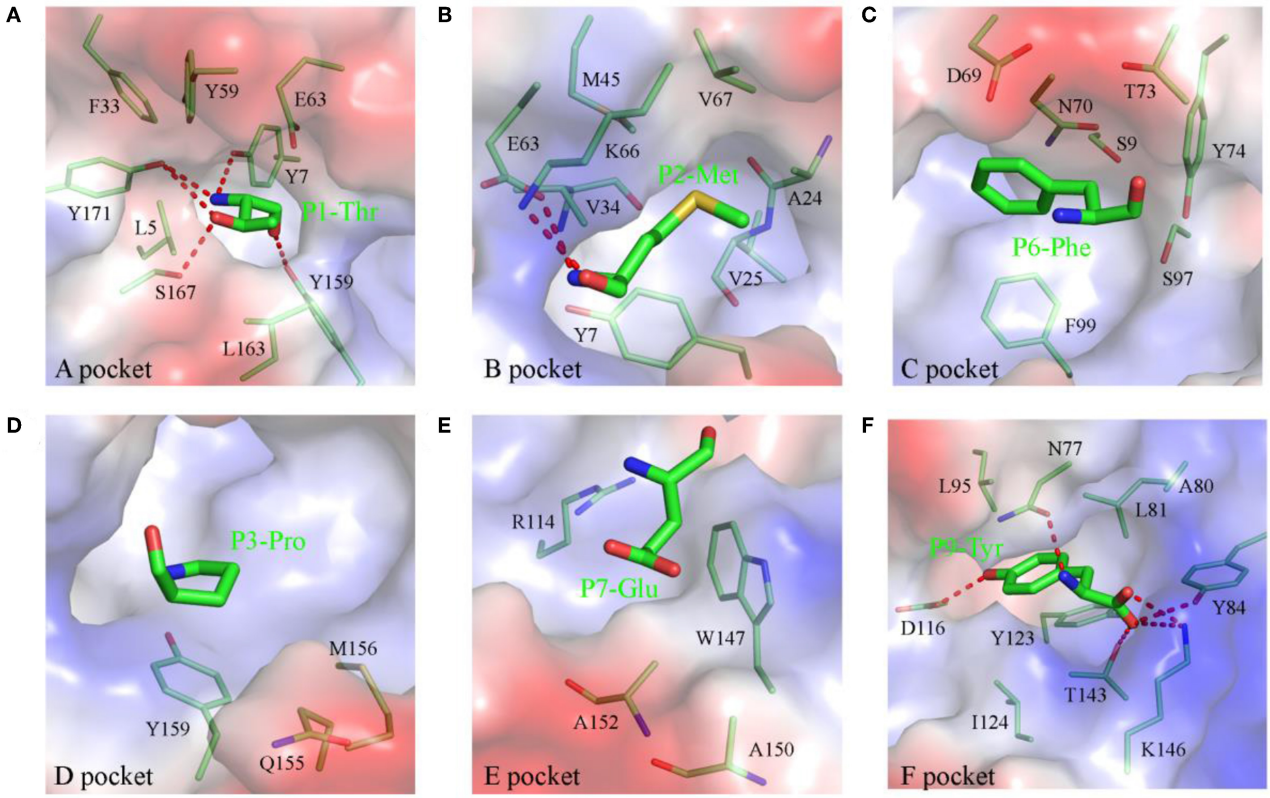

FIGURE 2 | Composition and polarities of the six pockets of pSLA-1*1502 bound to NSP9-TMP9 peptide. The pockets are shown in surface representation with their polarities colored as follows: red, negatively charged; white, non-polar; and blue, positively charged. The residues forming these pockets (light green) and the bound peptide (C, green; N, blue; O, red) are labeled. The hydrogen bonds between peptides and the red complex are shown with dashes. **(A)** Pocket A with residue P1 (Thr). **(B)** Pocket B with residue P2 (Met). **(C)** Pocket C with residue P6 (Phe). **(D)** Pocket D with residue P3 (Pro). **(E)** Pocket E with residue P7 (Glu). **(F)** Pocket F with residue P9 (Tyr).

species, the residue at position 167 is Trp (32). Due to the small Ser^{167} residue, the N-terminus of the PBG of SLA I molecules appears to be more open than in other MHC I molecules.

The B pocket consists of Tyr^{7}, Ala^{24}, Val^{25}, Val^{34}, Met^{45}, Glu^{63}, Lys^{66}, and Val^{67} (**Figure 2B**). The charged Glu^{63} and Lys^{66} residues at the top of the B pocket can form two hydrogen bonds with the main chain of P2-Met. The hydrophobic B pocket accommodates the non-polar side chain of P2-Met via the VDWs provided by the surrounding residues (**Figure 2B**; **Table 3**). The residue composition of SLA-1*1502 is similar to that of SLA-1*0401, and only the residue at position 66 (Lys/Val) is different (**Figure 3**).

The C, D, and E pockets usually form a large cavity in the middle portion of the PBG. The amino acid compositions of these three pockets in SLA-1*1502 are shown in **Figures 2C–E**. No hydrogen bonds or salt bridges were found in these structures; instead, many VDWs were observed between the three pockets and the NSP9-TMP9 peptide (**Table 3**). The D pocket is critical for the peptide selection of SLA-1*0401 and SLA-3*hs0202 because of the charged residue at position 156 (19, 20). The non-polar Met^{156} causes the D pocket of SLA-1*1502 to be hydrophobic, in contrast to the charged D pocket of SLA-1*0401 or SLA-3*hs0202 (**Figure 3**).

The F pocket of pSLA-1*1502 consists of Asn^{77}, Ala^{80}, Leu^{81}, Tyr^{84}, Leu^{95}, Asp^{116}, Tyr^{123}, Ile^{124} Thr143, and Lys^{146} and shows numerous interactions with P9-Tyr, reflecting a key anchoring site (**Figure 2F**). P9-Tyr can form 6 hydrogen bonds and many VDWs with the residues of the F pocket (**Table 3**). The F pockets of both pSLA-1*1502 and p/SLA-1*0401 can accommodate P9-Tyr, and only two different residues (Asn/Gly^{77} and Ala/Thr^{80}) were found between the two F pockets (**Figure 3**).

The NSP9-TMP9 peptide conformation presented by SLA-1*1502 is different from that of the peptides presented by SLA-1*0401 and SLA-3*hs0202 (**Figure 4**). Because of the two consecutive Pro residues, the turn between P3 and P4 of the NSP9-TMP9 peptide is much sharper than that in the other two peptides (**Figures 4A,B**). Previous studies on SLA-1*0401 and SLA-3*hs0202 showed that the residue at position 156 plays a key role in peptide binding by fixing the P3 residue with a salt bridge or hydrogen bond (**Figures 4C,D**). In contrast, no salt bridge or hydrogen bond forms between the P3-Pro of NSP9-TMP9 and Met^{156} of SLA-1*1502.

Analysis of the Peptide-Binding Motif of pSLA-1*1502

To determine the peptide-binding motif of SLA-1*1502, the peptide NSP9-TMP9 was mutated by alanine scanning (19), and CD spectra were used to test the stability of pSLA-1*1502 complexes with these mutant peptides (**Figure 5**). The *in vitro* refolding and CD results showed that the binding stabilities of P2-Ala, P3-Ala, and P9-Ala mutant peptides are significantly lower than that of the wild-type NSP9-TMP9 peptide. Although P3-Pro cannot form a hydrogen bond or salt bridge with the D pocket of SLA-1*1502, its Ala mutant still impairs the stability of the pSLA-1*1502 complex. According to these results, the P2, P3, and P9 residues are the primary anchor residues of the epitope peptides presented by SLA-1*1502. The B, D and F pockets accommodate these primary anchor residues and determine the peptide-binding motif of SLA-1*1502, similar to SLA-1*0401 and SLA-3*hs0202.

The B and F pockets accommodate the P2 and P9 anchor residues of the binding peptide, respectively, and their preference for P2 and P9 anchor residues is determined by their amino acid composition. **Figure 2** shows the pocket composition of SLA-1*1502. **Figure 3** shows that the amino acid composition of the B and F pockets of SLA-1*1502 is very similar to that of SLA-1*0401. Differential amino acids are found only at one or two individual sites and do not form direct contacts with the side chains of the P2 or P9 residues of the binding peptide. Because of the similar B and F pockets, the P2 and P9 residues of the SLA-1*1502-binding peptides should be the same as in the SLA-1*0401 peptides. The SLA-1*0401 binding peptide (20) and the SLA-1*1502 binding peptide have a large overlap at the P2 and P9 residues (**Table 1**). The B pocket of SLA-1*1502 accommodates multiple uncharged residues, while the F pocket mainly binds Phe, Tyr and Trp. The *in vitro* refolding results for the peptides supported this reasonable speculation (**Table 1**). The uncharged D pocket of SLA-1*1502 might accommodate various uncharged P3 residues, unlike those of SLA-1*0401 and SLA-3*hs0202. Peptides with P3-Ala cannot provide sufficient affinity, unlike larger amino acids, such as L, M, F, S, N, and P (**Table 1**). In summary, the preliminary peptide-binding motif of SLA-1*1502 is expected to contain the following combination: X-(S/M/F/W/T/V/I/L)-(L/P/M/F/S/N)-X-X-X-X-X-(F/Y/W).

TABLE 3 | Hydrogen bonds and van der Waals interactions between the NSP9-TMP9 peptides and complexes.

Complex	Peptide		Hydrogen bond partner		Van der Waals contact residues[a]
	Residue	Atom	Residue	Atom	
SLA-1*1502 /sβ2m/TY9	P1-Thr	N	Tyr^{7}	OH	Leu^{5}, Tyr^{7}, Phe^{33}, Tyr^{59}, Glu^{63}, Tyr^{159}, Leu^{163}, Ser^{167}, Tyr^{171}
			Tyr^{171}	OH	
		O	Tyr^{159}	OH	
		OG1	Ser^{167}	OG	
			Tyr^{171}	OH	
	P2-Met	N	Glu^{63}	OE1	Tyr^{7}, Ala^{24}, Val^{25}, Val^{34}, Met^{45}, Glu^{63}, Lys^{66}, Val^{67}
		O	Lys^{66}	NZ	
	P3-Pro				Gln^{155}, Met^{156}, Tyr^{159}
	P4-Pro				
	P5-Gly				
	P6-Phe				Ser^{9}, Asp^{69}, Asn^{70}, Thr^{73}, Tyr^{74},Ser^{97}, Phe^{99}
	P7-Glu	O	Asn^{77}	ND2	Arg^{114}, Trp^{147}, Ala^{150}, Ala^{152}
	P8-Leu	O	Trp^{147}	NE1	Thr^{73}, Asn^{77}, Trp^{147}
	P9-Tyr	N	Asn^{77}	OD1	Asn^{77}, Ala^{80}, Leu^{81}, Tyr^{84},
		O	Lys^{146}	NZ	Leu^{95}, Asp^{116}, Tyr^{123}, Ile^{124},
		OH	Asp^{116}	OD1	Thr^{143}, Lys^{146}
		OXT	Tyr^{84}	OH	
			Thr^{143}	OG1	
			Lys^{146}	NZ	
		O	Tyr^{84}	OH	
			Thr^{143}	OG1	
		OXT	Tyr^{84}	OH	
			Lys^{146}	NZ	

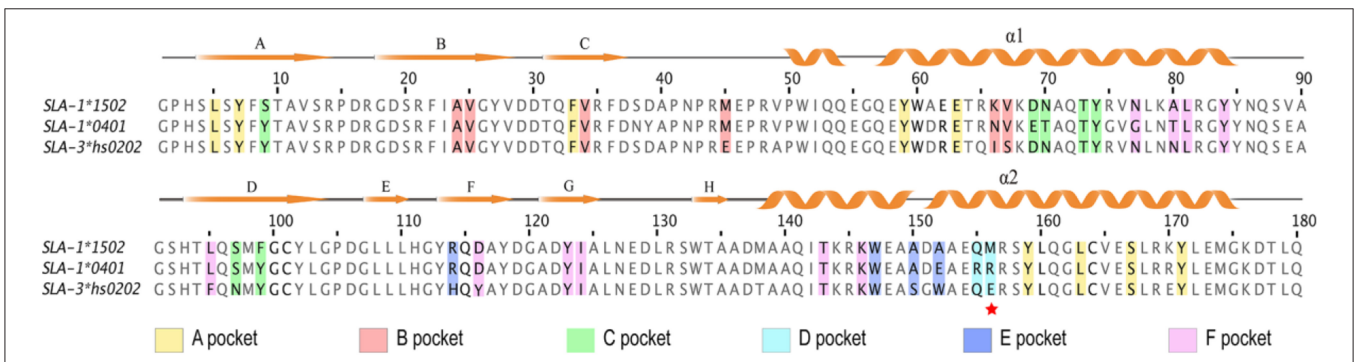

FIGURE 3 | Structure-based amino acid sequence alignment of SLA-1*1502, SLA-1*0401, and SLA-3*hs0202 alleles. The amino acid sequences of the PBGs of SLA-1*1502, SLA-1*0401, and SLA-3*hs0202 were aligned, and the secondary structural elements are indicated above the sequences. Orange arrows indicate β-strands, and orange cylinders denote α-helices. The residues in pockets A-F are highlighted with different colors. The residues at position 156 in the D pocket are indicated with a red star.

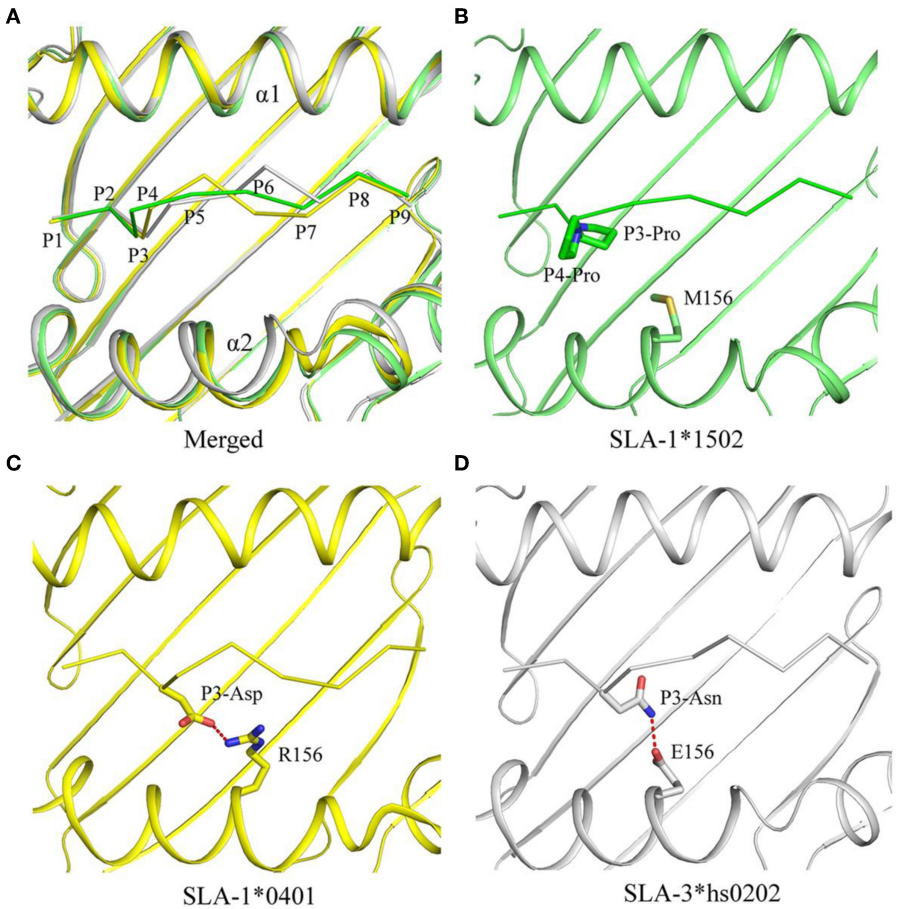

FIGURE 4 | Comparison of NSP9-TMP9 and dissimilar peptide conformations and interactions among the three solved SLA I structures. The superposition of the structures of pSLA-1*1502 (green), p/SLA-1*0401 (yellow), and p/SLA-3*hs0202 (white). **(A)** The peptide conformations in these three structures are different. **(B–D)** Interactions between residue 156 and non-apeptide in the three p/SLA complexes. The salt bridge between the peptide and SLA I is represented by red dashes.

Identification of Peptide-Binding Maps for the SLA-1*1502 Allele Derived From Four Typical PRRSV Strains

The predicted peptide epitopes derived from whole protein sequences of four typical PRRSV strains were screened: the first isolated strain, VR2332; the low-virulence strain HB-13.9; the highly pathogenic strain JXwn06; and the CHsx1401 strain, which was responsible for a recent epidemic in China (**Figure 6**). Most SLA-1*1502-restricted PRRSV peptides are located in the non-structural protein and the RNA-dependent RNA polymerase (RDRP) encoded by ORF1a and 1b. Although numerous 9-mer SLA-1*1502-binding peptides exist in each of these four PRRSV strains (∼90 peptides), only 30 peptides were found to be completely conserved in all four strains (**Table S2**). RDRP contains 13 conserved peptides, which is a much greater number than in the other proteins.

Identification of NSP9-TMP9 as the CTL Epitope by Using the Tetramer Technique and the Detection of Swine IFN-γ

The tetrameric pSLA-1*1502 complex was constructed (**Figures 7A–C**) (33). Six Landrace pigs expressing the SLA-1*1502 genes were used to check the immunogenicity of NSP9-TMP9 peptide (**Figure 8**). A total of 10,000 events were recorded by the flow. The ratio of pSLA-1*1502 tetramer and CD8 double-positive cells was at a rate of ∼0.5–1% in the MLV+NSP9-TMP9-immunized group, which was significantly higher than in the control group ($P = 0.0305$). The MLV-immunized group was significantly higher than in the control group ($P = 0.0355$); however, there was no significant difference between the MLV+NSP9-TMP9-immunized group and the MLV-immunized group ($P = 0.0538$) (**Figure 8B**). Additionally, swine IFN-γ expression in the peripheral blood of each pig was

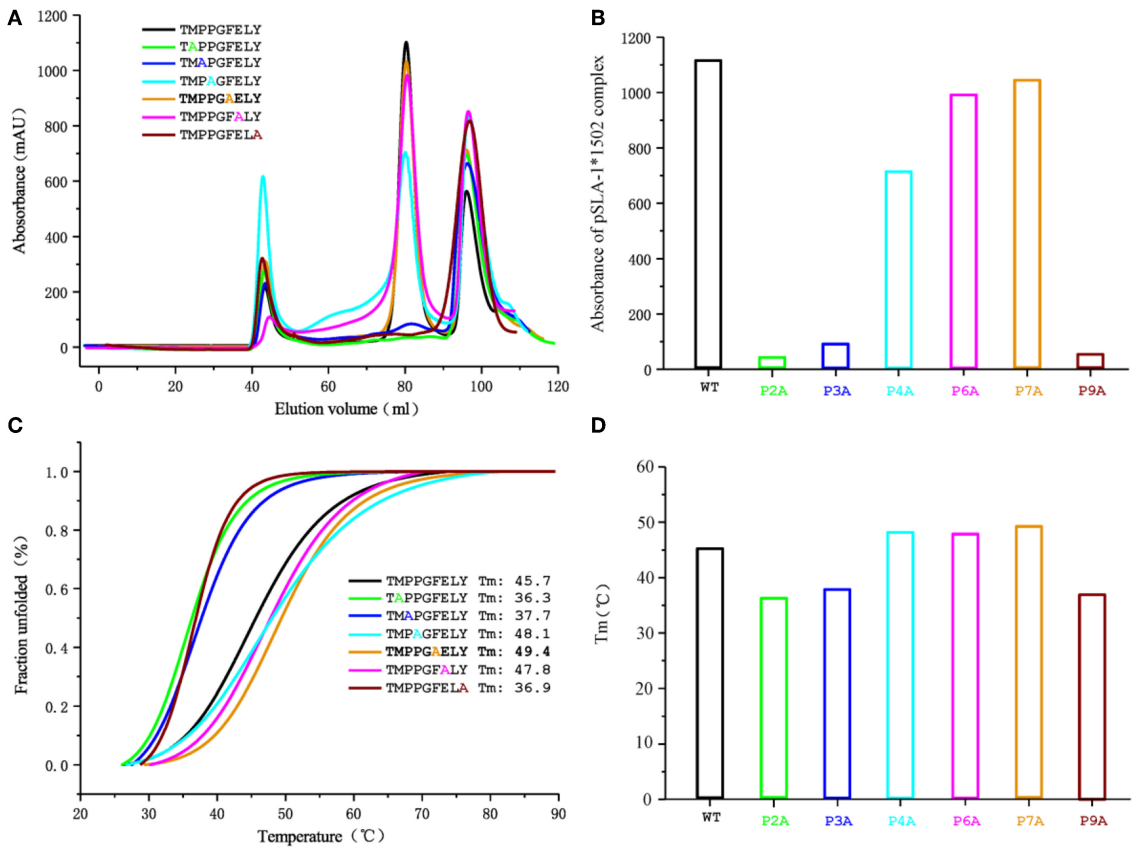

FIGURE 5 | Gel filtration chromatogram and CD spectra of the NSP9-TMP9 peptide and its mutants. The elution curves and CD spectra of the complexes with different peptides are indicated in different colors. **(A)** Gel filtration chromatograms of the refolded products obtained with a Superdex 200 10/300 GL column (GE Healthcare). The aggregated H chain, the correctly refolded pSLA-1*1502 complex (~45 kDa), and excess β2m are indicated by three peaks appearing in order. The efficiency of refolding is represented by the height of the pSLA-1*1502 complex peak. A higher peak indicates better efficiency of the peptide in promoting the renaturation of SLA I. **(B)** Bar graph of the peak absorbance of the pSLA-1*1502 complex. Bars with different colors show the differences in the refolding efficiencies of the pSLA-1*1502 complex with alanine scanning peptides. **(C)** Thermostability of the pSLA-1*1502 complex with the NSP9-TMP9 peptide and the peptide harboring substitutions (alanine screening of NSP9-TMP9). CD spectra were utilized to assess the thermostability of purified pSLA-1*1502 complexes. Denaturation was monitored at 218 nm as the temperature was ramped up from 25 to 90°C at 1°C/min. The fitting data for the denaturation curves obtained using Origin 9.1 (OriginLab) are shown. The Tms of different peptides (when 50% of the fraction was unfolded) are indicated by the gray line. **(D)** Bar graph of the thermostability of the pSLA-1*1502 complex. Bars with different colors show the Tm values of the pSLA-1*1502 complex with alanine scanning peptides more clearly.

detected according to the methods used by Kumar and Walker (34, 35). Secreted IFN-γ was detectable in all of the immunized pigs but was lower than the lowest detectable limit in all control pigs (**Figure 8C**). These data indicated that NSP9-TMP9, as the CTL epitope, could stimulate specific CTL immunity in swine.

DISCUSSION

CTL epitopes might be a requirement of optimal PRRSV immunity for the control and treatment of PRRSV infection (36, 37). In our study, a novel approach was used to select PRRSV CTL epitopes, i.e., starting from a computer prediction for PRRSV peptides, followed by *in vitro* complex refolding with SLA-1*1502, the analysis of the complex crystal structure, the identification of SLA-1*1502-restricted potential epitopes from whole genomes of different PRRSV strains, and finally, verification of the immunogenicity of SLA-1*1502-restricted PRRSV epitope.

The crystal structure of SLA-1*1502 is the third to be solved for an SLA-I allele. The crystal structure of SLA-1*1502 exhibits the typical structural characteristics of an MHC I complex. The structure of SLA-1*1502 is very similar to those of SLA-1*0401 and SLA-3*hs0202, indicating that the overall combination of heavy chains, light chains, and peptides in the swine SLA-I complex is highly conserved. However, in terms of peptide binding, the SLA-1*1502 structure not only reflects the common features of SLA-I alleles but also exhibits unique allelic-specific characteristics. Similar to the previously resolved SLA-1*0401 and SLA-3*hs0202, the N-terminus of the SLA-1*1502 PBG is open because the amino acid at position 167 of the A pocket is a small Ser (**Figure 2A**), but in other species such as humans and mice, the amino acid at this position is a large Trp (19, 20). The peptide-binding motif of SLA-1*1502, like that of SLA-1*0401

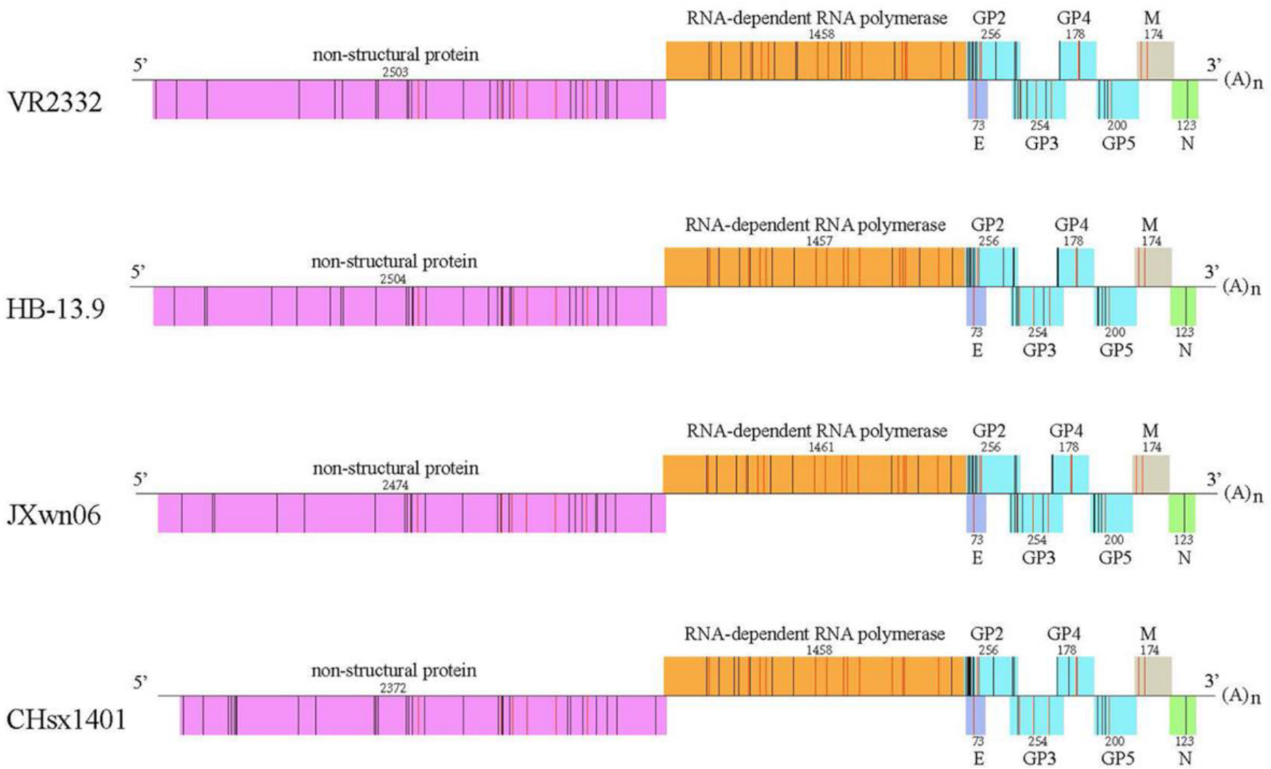

FIGURE 6 | Peptide predictions from different PRRSV strains according to the binding motifs of the pSLA-1*1502 complex. Genome-wide scanning results for peptides matching the following motifs of the pSLA-1*1502 complex: X-(S/M/F/W/T/V/I/L)-(L/P/M/F/S/N)-X-X-X-X-(F/Y/W). Different proteins are indicated by different colors. The number above indicates the sequence length of each protein. The non-apeptides matching the motifs of the pSLA-1*1502 complex from different proteins are indicated by bars, and red indicates the conserved peptides in four PRRSV strains, including the first isolated strain VR2332 (GenBank accession # EF536003.1); the low-virulence strain HB-13.9 (GenBank accession # EU360130.1); the highly pathogenic strain JXwn06 (GenBank accession # EF641008.1); and the CHsx1401 strain, which was responsible for a recent epidemic in China (GenBank accession # KP861625.1).

and SLA-3*hs0202, is determined by the three pockets B, D and F together, while the HLA-I molecule is mostly determined by the two pockets B and F. These common characteristics indicate that SLA-I has its own unique species features in binding peptides. In the B and F pocket composition, SLA-1*1502 and SLA-1*0401 are very similar, and only the non-critical amino acids in the individual positions are different (**Figure 3**), resulting in a large overlap of the anchoring residues accommodated in their B and F pockets (20). In the structures of SLA-1*0401 and SLA-3*hs0202, the D pocket plays a key role in fixing the bound peptides, with a strong salt bridge between the charged residue 156 and the P3 residue of the peptides (19, 20). The uncharged Met^{156} of SLA-1* 1502 cannot form strong charge interactions with P3 residues similar to those observed for SLA-1*0401 and SLA-3*hs0202 (**Figure 4**). Nevertheless, the D pocket is still important in determining the peptide binding of SLA-1*1502 and prefers uncharged residues of a certain size to form sufficient VDWs. The three p/SLA I structures indicate that regardless of its properties, the D pocket is critical in determining the peptide-binding motif of SLA-I, and this phenomenon is expected to be a common feature among different SLA-I alleles.

SLA-1*1502 was predicted *in silico* to present more PRRSV peptide epitopes than other SLA-I alleles cloned from Landrace pigs, and the *in vitro* refolding results confirmed that most of the predicted PRRSV peptides could be bound by SLA-1*1502. Four typical PRRSV strains of the North American genotype were used to screen SLA-1*1502-restricted binding peptides. According to the summarized peptide-binding motifs, approximately 90 peptides in each PRRSV strain could be presented by SLA-1*1502. These peptides are unevenly distributed in different regions, with the NSP3/4/5 proteins encoded by ORF1a, NSP9/10/11 encoded by ORF1b and GP2/3 exhibiting most of the candidate peptide epitopes. Approximately one out of three peptides are conserved among the four PRRSV strains, and approximately half of these peptides are encoded by ORF1b of RDRP. CTL-epitope-based vaccines present advantages in terms of safety, specificity, and usability and are successfully used to control many viruses, such as HIV, HPV, and dengue virus (38–41). Although studies aimed at developing an anti-PRRSV epitope-based vaccine have been performed, no mature product is currently available (42–44). Our data indicated that RDRP (especially NSP9/10/11) may be the best target for developing a PRRSV vaccine to induce a CTL response to genetically heterologous strains.

Tetramers of p/MHC I alleles are basic reagents that are used in immunological studies (11, 45, 46). However, the

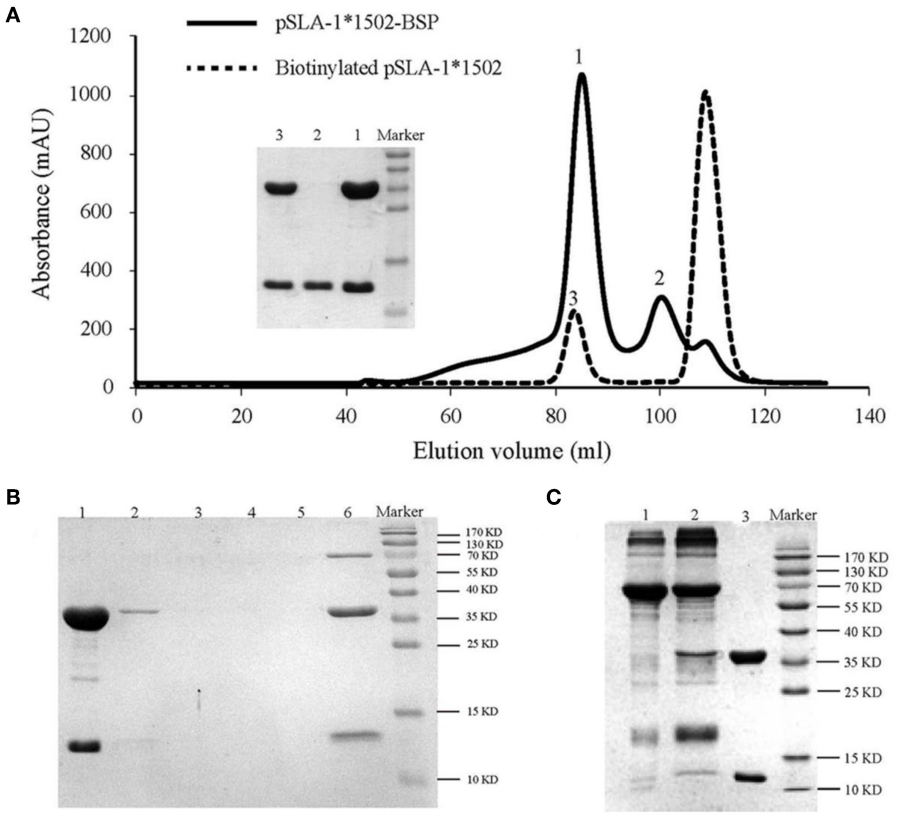

FIGURE 7 | Production of the SLA−1*1502 tetramer. **(A)** The pSLA-1*1502-BSP complex with the NSP9-TMP9 peptide (solid line) and the biotinylated pSLA-1*1502-BSP complex obtained by using the BirA enzyme (dashed line) were purified via chromatography with a Superdex 200 size-exclusion column. The efficiency of purification for the complex was tested via SDS-PAGE. The pSLA-1*1502-BSP complex is shown in lane 1; sβ2m is shown in lane 2; and biotinylated pSLA-1*1502 is shown in lane 3. **(B)** SDS-PAGE analysis of the effect of pSLA-1*1502-BSP biotinylation. The biotinylated pSLA-1*1502-BSP was mixed with streptavidin MagneSpheres. Lane 1 contains the supernatant from biotinylated pSLA-1*1502-BSP that had reacted with streptavidin MagneSpheres. Lanes 2, 3, 4, and 5 contain the supernatants from the first, second, third, and fourth washings of the streptavidin MagneSpheres, respectively. Lane 6 contains the supernatant of streptavidin MagneSpheres boiled after washing the sample four times. **(C)** SDS-PAGE analysis of purified tetramers. Biotinylated pSLA-1*1502-BSP was mixed with PE-labeled streptavidin and filtered with a 100 kDa Millipore tube. Lane 1, PE-labeled streptavidin; Lane 2, pSLA-1*1502-BSP tetramer >100 kDa; and Lane 3, biotinylated pSLA-1*1502-BSP monomer.

absence of SLA-I tetramers limits effective and convincing research on swine antiviral CTL responses, especially regarding accurate quantitative research. In this study, the crystallized NSP9-TMP9 peptide was used to produce the tetramer for evaluating SLA-1*1502-restricted CTL responses. The NSP9-TMP9 epitope could induce CD8 and tetramer double-positive CTLs at a rate of ∼0.5–1% in MLV+NSP-TMP9-immunized pigs, similar to the results obtained for other known efficiently protective viral CTL epitopes found in humans and mice by FACS (47–49). Our results also showed that the MLV used (produced by the VR2332 strain) could induce a CTL response specific to PRRS. Somewhat disappointingly, we do not have live PRRSV with which to challenge these swine groups and evaluate the protection of MLV and NSP-TMP9 epitope. However, NSP9-TMP9 was identified as an immunogenic epitope that could stimulate the proliferation of specific $CD8^+$ CTLs and the expression of IFN-γ in SPF Landrace pigs bearing SLA-1*1502 alleles. Immunization enhancement with NSP9-TMP9 produces a specific CTL response similar to that of immunization with MLV, indicating that the peptide vaccine can produce effective immunoprotection and thus that it is feasible to develop an effective PRRSV polypeptide epitope vaccine.

In conclusion, we solved the crystal structure of SLA-1*1502 and described its PRRSV peptide-binding map according to its preliminary peptide-binding motif determined via biochemical analyses. Using the tetramer of SLA-1*1502, the immunogenicity of NSP9-TMP9 was identified by FACS and the expression of IFN-γ. The results increase our understanding of how to acquire a viral CTL vaccine against swine PRRS disease. In addition, this study provides a complete and credible method for identifying SLA-I-restricted viral epitopes, demonstrating the feasibility of peptide vaccines in antiviral immunity of swine. Based on our experimental results, we encourage and promote the development of a safe peptide vaccine that can effectively activate CTL immune protection, solve the safety problems

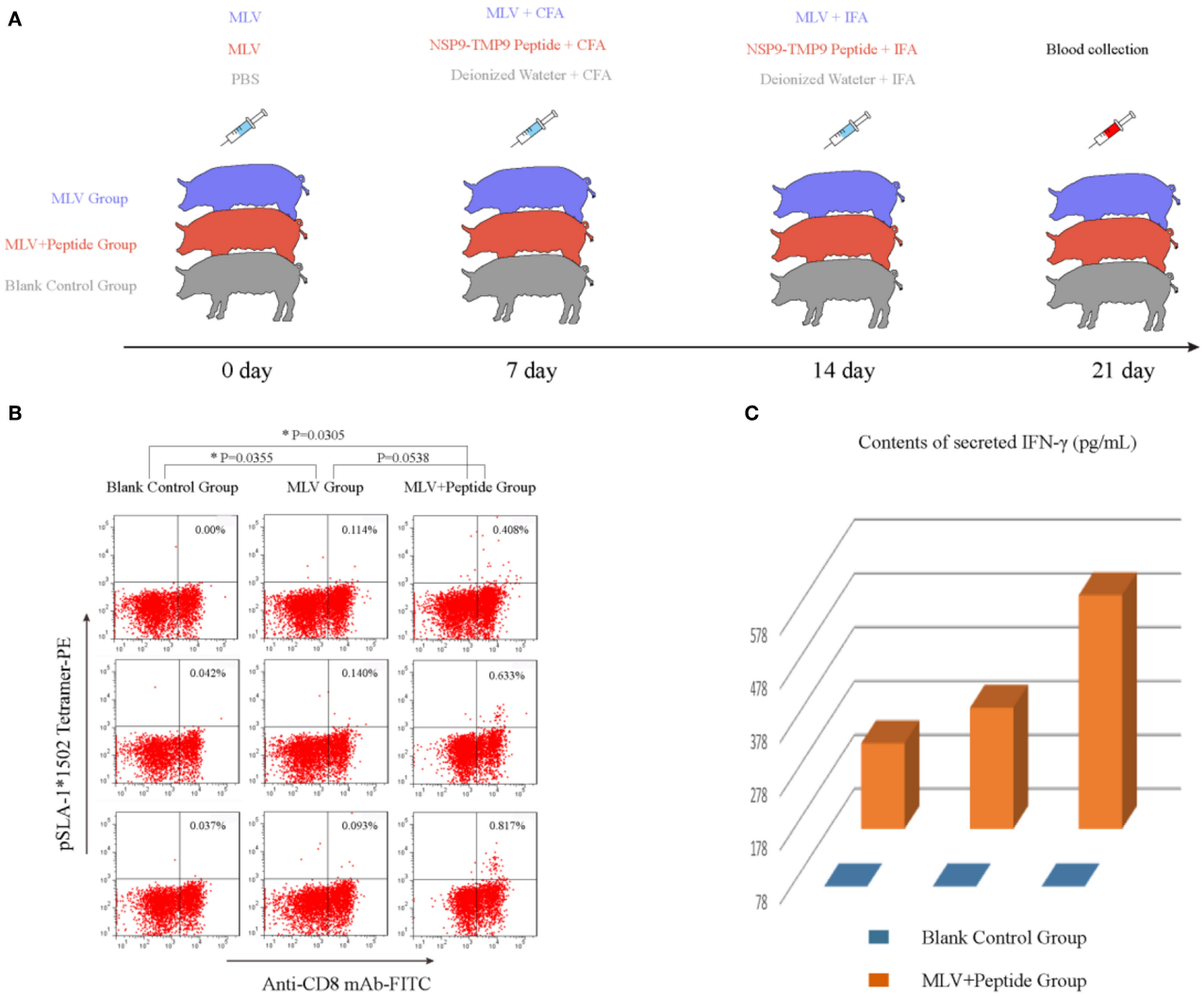

FIGURE 8 | Identification of the functional NSP9-TMP9 CTL epitope. **(A)** Immunization program for SPF pigs. Nine pigs expressing SLA-1*1502 were divided into three groups: the MLV group, MLV+Peptide group and blank control group. The MLV and MLV+Peptide groups were injected with an attenuated PRRSV vaccine as the first immunization. Seven days later, the MLV+Peptide group was injected with the NSP9-TMP9 peptide mixed with CFA, and the MLV group was injected with MLV mixed with CFA as the second immunization. At day 14, the MLV+Peptide group was injected with the NSP9-TMP9 peptide mixed with IFA, and the MLV group was injected with MLV mixed with IFA as the third immunization. Pigs in control group were injected with PBS, deionized water mixed with CFA, and deionized water mixed with IFA. **(B)** NSP9-TMP9-specific CTLs stained with PE-labeled SLA-1*1502 tetramer and FITC-labeled anti-CD8 monoclonal antibody were detected via flow cytometry. **(C)** The secreted IFN-γ contents of the control group and immunized group were measured via ELISA kit. The secreted IFN-γ content of the control group was less than the lowest detectable limit (78 pg/mL).

caused by conventional attenuated vaccines, and provide new ideas for controlling not only PRRS but also the extent of African swine fever.

DATA AVAILABILITY STATEMENT

The coordinates and structural characteristics of pSLA-1*1502 have been deposited in the Protein Data Bank under accession number 5YLX; the sequence of SLA-1*1502 is available at the National Center for Biotechnology Information (NCBI) database under accession number HQ909439.

ETHICS STATEMENT

The animal trials in this study were performed according to the Chinese Regulations for Laboratory Animals-The Guidelines for the Care of Laboratory Animals (Ministry of Science and Technology of People's Republic of China) and Laboratory Animal Requirements for Environment and Housing Facilities (GB14925-2010, National Laboratory Animal Standardization Technical Committee). The license number associated with this research protocol is CAU20140305-2, which was approved by The Laboratory Animal Ethics Committee of China Agricultural

University. The protocol adhered to the recommendations in the Institute for Laboratory Animal Research's Guide for the Care and Use of Laboratory Animals.

AUTHOR CONTRIBUTIONS

CX: design of the study. XP and NZ: data collection. XP, YJ, and QL: analysis and interpretation of data. CX, NZ, and XW: drafting the article. CX, XP, RL, LZ, and LM: critical revision of the article. XP, NZ, XW, YJ, RC, QL, RL, LZ, LM, and CX: final approval of the version to be published.

FUNDING

This work was supported by the 863 Project of the China Ministry of Science and Technology (Grant no. 2013AA102503), the National Natural Science Foundation of China (Grant no. 31201887), the 973 Project of the China Ministry of Science and Technology (Grant no. 2013CB835302), the Beijing Natural Science Foundation (Grant no. 6182029), and the Science and Technology Program of Anhui Province (Grant no. 1704A07020066).

ACKNOWLEDGMENTS

We thank the Shanghai Synchrotron Radiation Facility (SSRF), Shanghai, People's Republic of China, for the crystal diffraction data. We thank Dr. Lei Zhou for his help in collecting information on PRRSV strains. We thank Prof. George F. Gao of the Chinese Academy of Sciences.

SUPPLEMENTARY MATERIAL

The Supplementary Material for this article can be found online at: https://www.frontiersin.org/articles/10.3389/fimmu.2019.02995/full#supplementary-material

REFERENCES

1. Blanco E, Guerra B, de la Torre BG, Defaus S, Dekker A, Andreu D, et al. Full protection of swine against foot-and-mouth disease by a bivalent B-cell epitope dendrimer peptide. *Antiviral Res*. (2016) 129:74–80. doi: 10.1016/j.antiviral.2016.03.005
2. Neumann EJ, Kliebenstein JB, Johnson CD, Mabry JW, Bush EJ, Seitzinger AH, et al. Assessment of the economic impact of porcine reproductive and respiratory syndrome on swine production in the United States. *J Am Vet Med Assoc*. (2005) 227:385–92. doi: 10.2460/javma.2005.227.385
3. Dokland T. The structural biology of PRRSV. *Virus Res*. (2010) 154:86–97. doi: 10.1016/j.virusres.2010.07.029
4. Fang Y, Snijder EJ. The PRRSV replicase: exploring the multifunctionality of an intriguing set of nonstructural proteins. *Virus Res*. (2010) 154:61–76. doi: 10.1016/j.virusres.2010.07.030
5. Martin-Valls GE, Kvisgaard LK, Tello M, Darwich L, Cortey M, Burgara-Estrella AJ, et al. Analysis of ORF5 and full-length genome sequences of porcine reproductive and respiratory syndrome virus isolates of genotypes 1 and 2 retrieved worldwide provides evidence that recombination is a common phenomenon and may produce mosaic isolates. *J Virol*. (2014) 88:3170–81. doi: 10.1128/JVI.02858-13
6. Wenhui L, Zhongyan W, Guanqun Z, Zhili L, JingYun M, Qingmei X, et al. Complete genome sequence of a novel variant porcine reproductive and respiratory syndrome virus (PRRSV) strain: evidence for recombination between vaccine and wild-type PRRSV strains. *J Virol*. (2012) 86:9543. doi: 10.1128/JVI.01341-12
7. Yu L, Zhao P, Dong J, Liu Y, Zhang L, Liang P, et al. Genetic characterization of 11 porcine reproductive and respiratory syndrome virus isolates in South China from 2014 to 2015. *Virol J*. (2017) 14:139. doi: 10.1186/s12985-017-0807-4
8. Tian K, Yu X, Zhao T, Feng Y, Cao Z, Wang C, et al. Emergence of fatal PRRSV variants: unparalleled outbreaks of atypical PRRS in China and molecular dissection of the unique hallmark. *PLoS ONE*. (2007) 2:e526. doi: 10.1371/journal.pone.0000526
9. Meng XJ. Heterogeneity of porcine reproductive and respiratory syndrome virus: implications for current vaccine efficacy and future vaccine development. *Vet Microbiol*. (2000) 74:309–29. doi: 10.1016/S0378-1135(00)00196-6
10. Lunney JK, Fang Y, Ladinig A, Chen N, Li Y, Rowland B, et al. Porcine Reproductive and Respiratory Syndrome Virus (PRRSV): pathogenesis and interaction with the immune system. *Annu Rev Anim Biosci*. (2016) 4:129–54. doi: 10.1146/annurev-animal-022114-111025
11. Loving CL, Osorio FA, Murtaugh MP, Zuckermann FA. Innate and adaptive immunity against porcine reproductive and respiratory syndrome virus. *Vet Immunol Immunopathol*. (2015) 167:1–14. doi: 10.1016/j.vetimm.2015.07.003
12. Vu HL, Kwon B, Yoon KJ, Laegreid WW, Pattnaik AK, Osorio FA. Immune evasion of porcine reproductive and respiratory syndrome virus through glycan shielding involves both glycoprotein 5 as well as glycoprotein 3. *J Virol*. (2011) 85:5555–64. doi: 10.1128/JVI.00189-11
13. Zhou L, Ni YY, Pineyro P, Sanford BJ, Cossaboom CM, Dryman BA, et al. DNA shuffling of the GP3 genes of porcine reproductive and respiratory syndrome virus (PRRSV) produces a chimeric virus with an improved cross-neutralizing ability against a heterologous PRRSV strain. *Virology*. (2012) 434:96–109. doi: 10.1016/j.virol.2012.09.005
14. Xiao Z, Batista L, Dee S, Halbur P, Murtaugh MP. The level of virus-specific T-cell and macrophage recruitment in porcine reproductive and respiratory syndrome virus infection in pigs is independent of virus load. *J Virol*. (2004) 78:5923–33. doi: 10.1128/JVI.78.11.5923-5933.2004
15. Ferrari L, Martelli P, Saleri R, De Angelis E, Cavalli V, Bresaola M, et al. Lymphocyte activation as cytokine gene expression and secretion is related to the porcine reproductive and respiratory syndrome virus (PRRSV) isolate after *in vitro* homologous and heterologous recall of peripheral blood mononuclear cells (PBMC) from pigs vaccinated and exposed to natural infection. *Vet Immunol Immunopathol*. (2013) 151:193–206. doi: 10.1016/j.vetimm.2012.11.006
16. Charerntantanakul W. Porcine reproductive and respiratory syndrome virus vaccines: Immunogenicity, efficacy and safety aspects. *World J Virol*. (2012) 1:23–30. doi: 10.5501/wjv.v1.i1.23
17. Fan S, Wang Y, Wang S, Wang X, Wu Y, Li Z, et al. Polymorphism and peptide-binding specificities of porcine major histocompatibility complex (MHC) class I molecules. *Mol Immunol*. (2017) 93: 236–45. doi: 10.1016/j.molimm.2017.06.024
18. Lunney JK, Ho CS, Wysocki M, Smith DM. Molecular genetics of the swine major histocompatibility complex, the SLA complex. *Dev Comp Immunol*. (2009) 33:362–74. doi: 10.1016/j.dci.2008.07.002
19. Fan S, Wu Y, Wang S, Wang Z, Jiang B, Liu Y, et al. Structural and biochemical analyses of swine major histocompatibility complex class i complexes and prediction of the epitope map of important influenza a virus strains. *J Virol*. (2016) 90:6625–41. doi: 10.1128/JVI.00119-16
20. Zhang N, Qi J, Feng S, Gao F, Liu J, Pan X, et al. Crystal structure of swine major histocompatibility complex class I SLA-1 0401 and identification of 2009 pandemic swine-origin influenza A H1N1 virus cytotoxic T lymphocyte epitope peptides. *J Virol*. (2011) 85:11709–24. doi: 10.1128/JVI.05040-11
21. Chu F, Lou Z, Gao B, Bell JI, Rao Z, Gao GF. Complex assembly, crystallization and preliminary X-ray crystallographic studies of rhesus macaque MHC

Mamu-A*01 complexed with an immunodominant SIV-Gag nonapeptide. *Acta crystallogr Section F*. (2005) 61:614–6. doi: 10.1107/S1744309105016453
22. Zhou M, Xu Y, Lou Z, Cole DK, Li X, Liu Y, et al. Complex assembly, crystallization and preliminary X-ray crystallographic studies of MHC H-2Kd complexed with an HBV-core nonapeptide. *Acta Crystallogr D Biol Crystallogr*. (2004) 60:1473–5. doi: 10.1107/S0907444904013587
23. Harp JM, Timm DE, Bunick GJ. Macromolecular crystal annealing: overcoming increased mosaicity associated with cryocrystallography. *Acta Crystallogr D Biol Crystallogr*. (1998) 54:622–8. doi: 10.1107/S0907444997019008
24. Jensen LH. Refinement and reliability of macromolecular models based on X-ray diffraction data. *Methods Enzymol*. (1997) 277:353–66. doi: 10.1016/S0076-6879(97)77020-4
25. Emsley P, Cowtan K. Coot: model-building tools for molecular graphics. *Acta Crystallogr D Biol Crystallogr*. (2004) 60:2126–32. doi: 10.1107/S0907444904019158
26. Adams PD, Afonine PV, Bunkoczi G, Chen VB, Echols N, Headd JJ, et al. The Phenix software for automated determination of macromolecular structures. *Methods*. (2011) 55:94–106. doi: 10.1016/j.ymeth.2011.07.005
27. Laskowski RA, Moss DS, Thornton JM. Main-chain bond lengths and bond angles in protein structures. *J Mol Biol*. (1993) 231:1049–67. doi: 10.1006/jmbi.1993.1351
28. Tobita T, Oda M, Morii H, Kuroda M, Yoshino A, Azuma T, et al. A role for the P1 anchor residue in the thermal stability of MHC class II molecule I-Ab. *Immunol Lett*. (2003) 85:47–52. doi: 10.1016/S0165-2478(02)00206-7
29. Zhou M, Xu D, Li X, Li H, Shan M, Tang J, et al. Screening and identification of severe acute respiratory syndrome-associated coronavirus-specific CTL epitopes. *J Immunol*. (2006) 177:2138–45. doi: 10.4049/jimmunol.177.4.2138
30. Altman JD, Moss PA, Goulder PJ, Barouch DH, McHeyzer-Williams MG, Bell JI, et al. Phenotypic analysis of antigen-specific T lymphocytes. *Science*. (1996) 274:94–6. doi: 10.1126/science.274.5284.94
31. Tsao YP, Lin JY, Jan JT, Leng CH, Chu CC, Yang YC, et al. HLA-A*0201 T-cell epitopes in severe acute respiratory syndrome (SARS) coronavirus nucleocapsid and spike proteins. Biochem Biophys Res Commun. (2006) 344:63–71. doi: 10.1016/j.bbrc.2006.03.152
32. Liang R, Sun Y, Liu Y, Wang J, Wu Y, Li Z, et al. Major histocompatibility complex class I (FLA-E*01801) molecular structure in domestic cats demonstrates species-specific characteristics in presenting viral antigen peptides. *J virol*. (2018) 92: e01631–17. doi: 10.1128/JVI.01631-17
33. Bousso P. Generation of MHC-peptide tetramers: a new opportunity for dissecting T-cell immune responses. *Microbes Infect*. (2000) 2:425–9. doi: 10.1016/S1286-4579(00)00324-5
34. Kumar D, Chernenko S, Moussa G, Cobos I, Manuel O, Preiksaitis J, et al. Cell-mediated immunity to predict cytomegalovirus disease in high-risk solid organ transplant recipients. *Am J Transplant*. (2009) 9:1214–22. doi: 10.1111/j.1600-6143.2009.02618.x
35. Walker S, Fazou C, Crough T, Holdsworth R, Kiely P, Veale M, et al. *Ex vivo* monitoring of human cytomegalovirus-specific CD8+ T-cell responses using QuantiFERON-CMV. *Transpl Infect Dis*. (2007) 9:165–70. doi: 10.1111/j.1399-3062.2006.00199.x
36. Liao YC, Lin HH, Lin CH, Chung WB. Identification of cytotoxic T lymphocyte epitopes on swine viruses: multi-epitope design for universal T cell vaccine. *PLoS ONE*. (2013) 8:e84443. doi: 10.1371/journal.pone.0084443
37. Zhang W, Lin Y, Bai Y, Tong T, Wang Q, Liu N, et al. Identification of CD8+ cytotoxic T lymphocyte epitopes from porcine reproductive and respiratory syndrome virus matrix protein in BALB/c mice. *Virol J*. (2011) 8:263. doi: 10.1186/1743-422X-8-263
38. Li S, Peng L, Zhao W, Zhong H, Zhang F, Yan Z, et al. Synthetic peptides containing B- and T-cell epitope of dengue virus-2 E domain III provoked B- and T-cell responses. *Vaccine*. (2011) 29:3695–702. doi: 10.1016/j.vaccine.2011.03.002
39. Muderspach L, Wilczynski S, Roman L, Bade L, Felix J, Small LA, et al. A phase I trial of a human papillomavirus (HPV) peptide vaccine for women with high-grade cervical and vulvar intraepithelial neoplasia who are HPV 16 positive. *Clin Cancer Res*. (2000) 6:3406–16.
40. Spearman P, Kalams S, Elizaga M, Metch B, Chiu YL, Allen M, et al. Safety and immunogenicity of a CTL multiepitope peptide vaccine for HIV with or without GM-CSF in a phase I trial. *Vaccine*. (2009) 27:243–9. doi: 10.1016/j.vaccine.2008.10.051
41. Strohmaier K, Franze R, Adam KH. Location and characterization of the antigenic portion of the FMDV immunizing protein. *J Gen Virol*. (1982) 59:295–306. doi: 10.1099/0022-1317-59-2-295
42. Zuckermann FA, Garcia EA, Luque ID, Christopher-Hennings J, Doster A, Brito M, et al. Assessment of the efficacy of commercial porcine reproductive and respiratory syndrome virus (PRRSV) vaccines based on measurement of serologic response, frequency of gamma-IFN-producing cells and virological parameters of protection upon challenge. *Vet Microbiol*. (2007) 123:69–85. doi: 10.1016/j.vetmic.2007.02.009
43. Ellingson JS, Wang Y, Layton S, Ciacci-Zanella J, Roof MB, Faaberg KS. Vaccine efficacy of porcine reproductive and respiratory syndrome virus chimeras. *Vaccine*. (2010) 28:2679–86. doi: 10.1016/j.vaccine.2009.12.073
44. Martelli P, Gozio S, Ferrari L, Rosina S, De Angelis E, Quintavalla C, et al. Efficacy of a modified live porcine reproductive and respiratory syndrome virus (PRRSV) vaccine in pigs naturally exposed to a heterologous European (Italian cluster) field strain: clinical protection and cell-mediated immunity. *Vaccine*. (2009) 27:3788–99. doi: 10.1016/j.vaccine.2009.03.028
45. Altman JD, Davis MM. MHC-Peptide Tetramers to Visualize Antigen-Specific T Cells. *Curr protocols immunol*. (2016) 115:17.3.1–17.3.44. doi: 10.1002/cpim.14
46. Doherty PC. The numbers game for virus-specific CD8+ T cells. *Science*. (1998) 280:227. doi: 10.1126/science.280.5361.227
47. Aoshi T, Nagata T, Suzuki M, Uchijima M, Hashimoto D, Rafiei A, et al. Identification of an HLA-A*0201-restricted T-cell epitope on the MPT51 protein, a major secreted protein derived from *Mycobacterium tuberculosis*, by MPT51 overlapping peptide screening. *Infect Immun*. (2008) 76:1565–71. doi: 10.1128/IAI.01381-07
48. Huang J, Zeng X, Sigal N, Lund PJ, Su LF, Huang H, et al. Detection, phenotyping, and quantification of antigen-specific T cells using a peptide-MHC dodecamer. *Proc Natl Acad Sci USA*. (2016) 113:E1890–7. doi: 10.1073/pnas.1602488113
49. Sun Y, Liu J, Yang M, Gao F, Zhou J, Kitamura Y, et al. Identification and structural definition of H5-specific CTL epitopes restricted by HLA-A*0201 derived from the H5N1 subtype of influenza A viruses. *J. gen virol*. (2010) 91:919–30. doi: 10.1099/vir.0.016766-0

Conflict of Interest: The authors declare that the research was conducted in the absence of any commercial or financial relationships that could be construed as a potential conflict of interest.

Advantages of publishing in Frontiers

OPEN ACCESS
Articles are free to read for greatest visibility and readership

FAST PUBLICATION
Around 90 days from submission to decision

HIGH QUALITY PEER-REVIEW
Rigorous, collaborative, and constructive peer-review

TRANSPARENT PEER-REVIEW
Editors and reviewers acknowledged by name on published articles

Frontiers
Avenue du Tribunal-Fédéral 34
1005 Lausanne | Switzerland

Visit us: www.frontiersin.org
Contact us: info@frontiersin.org | +41 21 510 17 00

REPRODUCIBILITY OF RESEARCH
Support open data and methods to enhance research reproducibility

DIGITAL PUBLISHING
Articles designed for optimal readership across devices

FOLLOW US
@frontiersin

IMPACT METRICS
Advanced article metrics track visibility across digital media

EXTENSIVE PROMOTION
Marketing and promotion of impactful research

LOOP RESEARCH NETWORK
Our network increases your article's readership